+ A

300/

401

The quantum theory of light

RODNEY LOUDON

The quantum theory of light

530

SECOND EDITION

…ITY LIBRARY
…AO - GOA
…No. 160
… S·V
Amonkar

CLARENDON PRESS · OXFORD
1983

GOA UNIVERSITY LIBRARY
This book is …

Oxford University Press, Walton Street, Oxford OX2 6DP
London Glasgow New York Toronto
Delhi Bombay Calcutta Madras Karachi
Kuala Lumpur Singapore Hong Kong Tokyo
Nairobi Dar es Salaam Cape Town
Melbourne Auckland
and associates in
Beirut Berlin Ibadan Mexico City Nicosia

Oxford is a trade mark of Oxford University Press

Published in the United States
by Oxford University Press, New York

© *Oxford University Press* 1973, 1983
First edition 1973
Second edition 1983

All rights reserved. No part of this publication may be reproduced, stored in a retrieval system, or transmitted, in any form or by any means, electronic, mechanical, photocopying, recording, or otherwise, without the prior permission of Oxford University Press

This book is sold subject to the condition that it shall not, by way of trade or otherwise, be lent, re-sold, hired out or otherwise circulated without the publisher's prior consent in any form of binding or cover other than that in which it is published and without a similar condition including this condition being imposed on the subsequent purchaser

British Library Cataloguing in Publication Data

Loudon, Rodney
The quantum theory of light.—2nd ed
1. Quantum optics
I. Title
535'.15 QC446.2

ISBN 0-19-851152-3
ISBN 0-19-851155-8 Pbk

Library of Congress Cataloging in Publication Data

Loudon, Rodney.
The quantum theory of light.

Includes bibliographies and index.
1. Quantum optics. I. Title.
QC446.2.L68 1983 535'.15 83–4045
ISBN 0-19-851152-3
ISBN 0-19-851155-8 (pbk.)

Printed in Great Britain by
St Edmundsbury Press, Bury St Edmunds, Suffolk

We all *know* what light is; but it is not easy to *tell* what it is.
Samuel Johnson, from Vol. 3 of Boswell's *Life*

Preface

THE purpose of this book is to provide a detailed account of the basic theory required for an understanding of the properties of light and its interaction with atoms. The material is intended to bridge the gap between the more formal development of quantum electrodynamics and the application of the theory to the explanation of experimental results. The choice of theoretical topics is accordingly governed by the needs of experimental interpretation, but only a few representative experiments are discussed in any detail and the reader must look elsewhere for more complete accounts of the observational aspects.

The aim throughout is to give the simplest and most direct treatment of the theory, and many of the changes from the first edition result from attempts to provide more lucid derivations. The main changes are made however in response to the development of the subject during the past ten years. There has for example been increasing progress in the study of optical processes that are not interpretable in terms of any classical theory, where only the quantum theory of light gives adequate descriptions of the observed effects. Some of this work involves the investigation of the resonant fluorescence scattering of narrow-band incident light, where it is necessary to use the optical Bloch equations for the motion of the coupled atom–radiation system. An account of these equations is now included in addition to the rate equations for broad-band illumination covered in the first edition. The main applications of the theory are grouped as before in the last four chapters, which discuss photon optics, the generation and amplification of light, resonance fluorescence and light scattering, and nonlinear optics.

The reader is assumed to have the usual undergraduate background knowledge of quantum mechanics, electromagnetic theory, and statistical mechanics. The material of the first half of the book is derived from notes for lecture courses given to final-year undergraduates and to first-year postgraduates. The level of the second half is appropriate to more advanced graduate students and to research workers with a more specialized interest in the topics covered

This is intended to serve as a textbook rather than a monograph and, while it is hoped that the student will find adequate references for more detailed study of particular topics, there has been no serious attempt to cite all the original sources of the theoretical derivations. Over 90 problems are distributed through the text to provide the student with some practice in using the theory. The calculations use SI units throughout.

The scope of the material is restricted in various ways, but most importantly in the frequency range of the electromagnetic radiation for which the results are generally valid. We concentrate particularly on the theoretical requirements of experiments that use visible light. However, the approximations appropriate to the visible region embrace a more extended range of the frequency spectrum. The lower end of the range is determined by the requirement that the photons should be sufficiently energetic that no significant thermal excitation occurs at room temperature. This sets a lower limit on the frequency of about 10^{13} Hz, in the far infrared.

The highest frequencies contemplated are such that the photons cannot give sufficient energy to electrons with which they interact to cause the electron velocity to approach the velocity of light. If the electron velocity is to be less than one-tenth that of light, then the photon frequency must be smaller than about 10^{18} Hz. We shall loosely use the terms 'visible light' and 'optical frequencies' to cover the range 10^{13} to 10^{18} Hz, although only a narrow band of frequencies in the region of 5×10^{14} Hz is strictly visible.

The scope is further restricted by the nature of the matter with which the light is considered to interact. It is assumed throughout that the atoms or molecules are randomly oriented in a gaseous or fluid state. In particular, there is no treatment of the important changes that occur in some of the optical effects when the atoms are arranged in a regular crystal structure. The choice of topics, particularly for the final chapters, is also arbitrary to some extent. It would, for example, have been possible to include treatments of pulse effects, such as photon echoes, self-induced transparency, and superradiant emission. However, space limitations require some selection to be made, and many of the omitted topics are well covered by other books (for pulse effects, see Allen, L. and Eberly, J. H. (1975). *Optical resonance and two-level atoms*. Wiley, New York).

Finally, a comment on the use made of classical and quantum theory. The book contains calculations in the so-called semiclassical theory, where the light is treated classically but the atoms are treated quantum-mechanically, and in the full quantum theory, where quantum mechanics is used for both light and atoms. The semiclassical theory is used particularly in the earlier chapters of the book. Such calculations have the advantage that they sometimes enable radiative processes to be treated in terms of easily visualized classical models, and they often give the same results as completely quantum-mechanical calculations. However, we take the view that the properties of light can only be reliably investigated in terms of a theory where the electromagnetic field is formally quantized. Most of the book accordingly uses the quantized field theory, and there is some emphasis in the later chapters on those phenomena for which the classical field theory has proved to be inadequate.

East Bergholt, Suffolk R.L.
1982

Acknowledgements

THE author is grateful to Dr M. Babiker, Dr E. Jakeman, Dr P. L. Knight, Dr E. R. Pike, Professor E. A. Power, Dr T. J. Shepherd, and Dr R. G. Woolley for most helpful advice on some of the material included in the book. Mrs Silvia Sussmann very kindly carried out a computer calculation and Mrs Mary Loudon performed a numerical integration. The typescript has been carefully prepared by Mrs Mary Loudon, whose help and encouragement in the production of the book are deeply appreciated.

Permission to reproduce or adapt tables and diagrams was generously granted by the following authors and publishers: Fig. 1.17, Dr J. L. Picqué and North-Holland Publishing Company; Fig. 2.8, Dr D. T. Pegg and North-Holland Publishing Company; Fig. 2.11, Professor H. A. Haus and the American Institute of Physics; Fig. 3.13, Professor R. Hanbury Brown and the Royal Society; Fig. 3.16, Dr L. Mandel and the Institute of Physics; Fig. 6.3, Professor F. T. Arecchi and North-Holland Publishing Company; Figs. 6.7 and 6.8, Dr E. R. Pike and the Institute of Physics; Fig. 8.6, Professor S. Ezekiel and the American Institute of Physics; Fig. 8.9, Dr L. Mandel and the American Institute of Physics; Figs. 8.11 and 8.12, Professor M. Gavrila and the American Institute of Physics; Figs. 8.14 and 8.15, Professor D. L. Mills and the American Institute of Physics; Fig. 8.17, Dr J. F. Clauser and the American Institute of Physics; Fig. 9.3, Professor F. Bassani and the American Institute of Physics; Fig. 9.5, Dr H. P. Weber and the Institute of Electrical and Electronic Engineers. Figs. 3.11, 6.2, 6.4, 8.4, 8.16, and 8.18 are adapted from the author's (1980) article 'Nonclassical effects in the statistical properties of light'. *Rep. Prog. Phys.* **43**, 913.

Contents

1. PLANCK'S RADIATION LAW AND THE EINSTEIN COEFFICIENTS 1
- 1.1. Density of field modes in a cavity 2
- 1.2. Quantization of the field energy 5
- 1.3. Planck's law 8
- 1.4. Fluctuations in photon number 11
- 1.5. Einstein's *A* and *B* coefficients 13
- 1.6. The case of thermal equilibrium 15
- 1.7. Theory of simple optical processes 17
- 1.8. Properties of the microscopic processes 18
- 1.9. Optical excitation of atoms 22
- 1.10. Macroscopic theory of absorption 24
- 1.11. Microscopic theory of absorption 26
- 1.12. Population inversion: the laser 30
- 1.13. Radiation pressure 33

2. QUANTUM MECHANICS OF THE ATOM–RADIATION INTERACTION 39
- 2.1. Time-dependent quantum mechanics 40
- 2.2. Form of the interaction Hamiltonian 42
- 2.3. The transition rate 45
- 2.4. Expression for the *B* coefficient 50
- 2.5. The Dirac delta-function 52
- 2.6. The optical Bloch equations 54
- 2.7. Rabi oscillations 56
- 2.8. Radiative broadening 59
- 2.9. Power broadening 63
- 2.10. Rabi oscillations with radiative damping 65
- 2.11. Collision broadening 70
- 2.12. Doppler broadening 72
- 2.13. Composite absorption lineshape 74
- 2.14. Bloch equations and rate equations 78

3. FLUCTUATION PROPERTIES OF CHAOTIC LIGHT 82
- 3.1. Spectrum of a fluctuating light beam 83
- 3.2. Model of a collision-broadened light source 85
- 3.3. First-order coherence and frequency spectrum 90
- 3.4. Young's interference fringes 92
- 3.5. Degree of first-order coherence 96
- 3.6. Intensity fluctuations of chaotic light 101
- 3.7. Degree of second-order coherence 105
- 3.8. Second-order coherence of chaotic light 107
- 3.9. Experiment of Hanbury Brown and Twiss 111
- 3.10. Higher-order coherence and polarization effects 116

4. THE QUANTIZED RADIATION FIELD 120
- 4.1. Potential theory for the classical electromagnetic field 121
- 4.2. The Coulomb gauge 123
- 4.3. The free classical field 126
- 4.4. The quantum-mechanical harmonic oscillator 129
- 4.5. Quantization of the field 134
- 4.6. Field commutation properties 137
- 4.7. The zero-point energy 139
- 4.8. The mode phase operators 141
- 4.9. Physical properties of the single-mode number states 144
- 4.10. The coherent photon states 146
- 4.11. Physical properties of the single-mode coherent states 148
- 4.12. The radiative density operator 152
- 4.13. Density operators for pure states 155
- 4.14. Statistical mixture states of the radiation field 157

5. INTERACTION OF THE QUANTIZED FIELD WITH ATOMS 162
- 5.1. Atomic multipole moments 162
- 5.2. The multipolar interaction Hamiltonian 166
- 5.3. The electric-dipole approximation 169
- 5.4. Second quantization of the atomic Hamiltonian 172
- 5.5. Photon absorption and emission rates 175
- 5.6. The photoelectric effect 178
- 5.7. The photon intensity operator 184
- 5.8. Transformation to the Schrödinger representation 187

- 5.9. General expression for radiative transition rates 191
- 5.10. Time-dependent perturbation theory 193
- 5.11. The Heisenberg representation 197
- 5.12. Time dependence of the atom–radiation system 199
- 5.13. The source-field expression 202
- 5.14. The interaction representation 206

6. PHOTON OPTICS 211
- 6.1. Quantum theory of Young's interference experiment 211
- 6.2. Quantum degree of first-order coherence 216
- 6.3. Quantum degree of second-order coherence 219
- 6.4. Hanbury Brown and Twiss experiment with photons 222
- 6.5. Photon bunching and antibunching 226
- 6.6. Photon counting 229
- 6.7. Photon-count distributions for coherent and chaotic light 232
- 6.8. Quantum-mechanical photon-count distribution 238
- 6.9. Photon counting in the Michelson interferometer 242
- 6.10. Higher-order coherence and polarization effects 247

7. GENERATION AND AMPLIFICATION OF LIGHT 251
- 7.1. Single-mode photon rate equations 251
- 7.2. Steady-state solutions 255
- 7.3. Photon statistics of attenuated light 257
- 7.4. Photon statistics of amplified light 261
- 7.5. Laser threshold condition 263
- 7.6. Rate equations for the atoms 267
- 7.7. Rate equations for the laser photons 271
- 7.8. The laser photon distribution 273
- 7.9. Fluctuations in laser light 278
- 7.10. Multimode emission by a driven atom 284

8. RESONANCE FLUORESCENCE AND LIGHT SCATTERING 290
- 8.1. The scattering cross-section 292
- 8.2. Single-atom resonance fluorescence 295
- 8.3. Weak incident beam 299
- 8.4. Exactly-resonant incident beam 303
- 8.5. Multiatom resonance fluorescence 308

8.6. The Kramers–Heisenberg formula 310
8.7. Elastic Rayleigh scattering 314
8.8. Inelastic Raman scattering 320
8.9. Two-photon cascade emission 326

9. NONLINEAR OPTICS 334
9.1. Double-beam two-photon absorption 335
9.2. Single-beam two-photon absorption 344
9.3. The nonlinear susceptibility 347
9.4. The stimulated Raman effect 351
9.5. Third-harmonic generation 357
9.6. Photon statistics and nonlinear optics 363
9.7. Photon statistics of double-beam two-photon absorption 366
9.8. Photon statistics of single-beam two-photon absorption 373
9.9. Photon statistics of the stimulated Raman effect 378
9.10. Conclusion 382

INDEX 385

1. Planck's radiation law and the Einstein coefficients

The quantum theory of light began in 1900 when Planck[1] found that he could account for measurements of the spectral distribution of the electromagnetic energy radiated by a thermal source by postulating that the energy of a harmonic oscillator is quantized. That is, a harmonic oscillator of angular frequency ω can only have energies that are integral multiples of the fundamental quantum $\hbar\omega$, where $\hbar = h/2\pi$ and h is Planck's original constant. In 1905, Einstein[2] showed how the photoelectric effect could be explained on the hypothesis of a corpuscularity of electromagnetic radiation. The quantum of radiation was named[3] a *photon* much later, in 1926. The work of Planck and Einstein initiated much of the development of quantum mechanics.

Another main stream in the early formulation of the quantum theory was concerned with the explanation of atomic spectral lines. The interaction of electromagnetic radiation with atoms was discussed by Einstein[4] in 1917. His theory of the absorption and emission of light by an atom depends upon simple phenomenological considerations but leads to correct predictions and is still frequently used. We begin our account of the quantum theory of light where the subject began historically, with the theories of Planck and Einstein.

The main topic of much of the later part of the book is the application of quantum mechanics to the theory of light. Thus in Chapter 4, where the electromagnetic field is quantized, it is shown that the electric and magnetic fields **E** and **B** must be represented by quantum-mechanical operators. However, it is possible to derive correct results for many features of light and its interaction with atoms from a classical theory of electromagnetic waves. The quantum hypothesis of Planck is then grafted onto the classical theory as an additional assumption in the calculation of the energy content of an electromagnetic field. We employ the classical description of the electric and magnetic fields based on Maxwell's equations for the first three chapters. The limitations of the classical theory of light are discussed in Chapter 6.

The main concerns of the present chapter are the thermal excitation of electromagnetic radiation and the basic kinds of interaction that can occur between radiation, or light, and atomic transitions. The theories of these phenomena are related since the absorption and emission of light by atoms provide the mechanisms by which the degree of excitation of the electromagnetic radiation can adjust to the conditions of thermal equilibrium. However, the Einstein theory of absorption and emission also applies to systems not in thermal equilibrium, where for example an atomic gas is illuminated by light from some external source. It is possible in this way to calculate the magnitude of a variety of effects that result from the interaction of light with atoms.

1.1. Density of field modes in a cavity

It is usually convenient to envisage the electromagnetic radiation as confined inside a cavity. Although some experiments with light do take place within a clearly defined optical cavity, it is often impossible to distinguish any real experimental cavity. Nevertheless, it is helpful to insert a cavity in theoretical treatments so as to limit the space considered to a finite region. This is just a theoretical artifice, and the end results of calculations are generally independent of the size, shape, and nature of the cavity assumed. To make calculations as simple as possible, we choose a cubic cavity of side L, and define axes as in Fig. 1.1. The walls of the cavity are assumed perfectly conducting, and the tangential component of the field $\mathbf{E}$ must accordingly vanish at the cavity boundaries.

Planck's law expresses the spectral distribution of the electromagnetic radiation in the interior of a cavity in thermal equilibrium at temperature T. The radiation is called black-body radiation; its frequency distribution is the same as that radiated by a perfectly black body at temperature T. The calculation of the frequency distribution breaks up into two distinct parts. We first consider the spatial dependence of the field in the cavity and derive an expression for the number of different modes of excitation of the field. In the second part, we consider the time dependence of the field and calculate the energy carried by each excitation mode at temperature T.

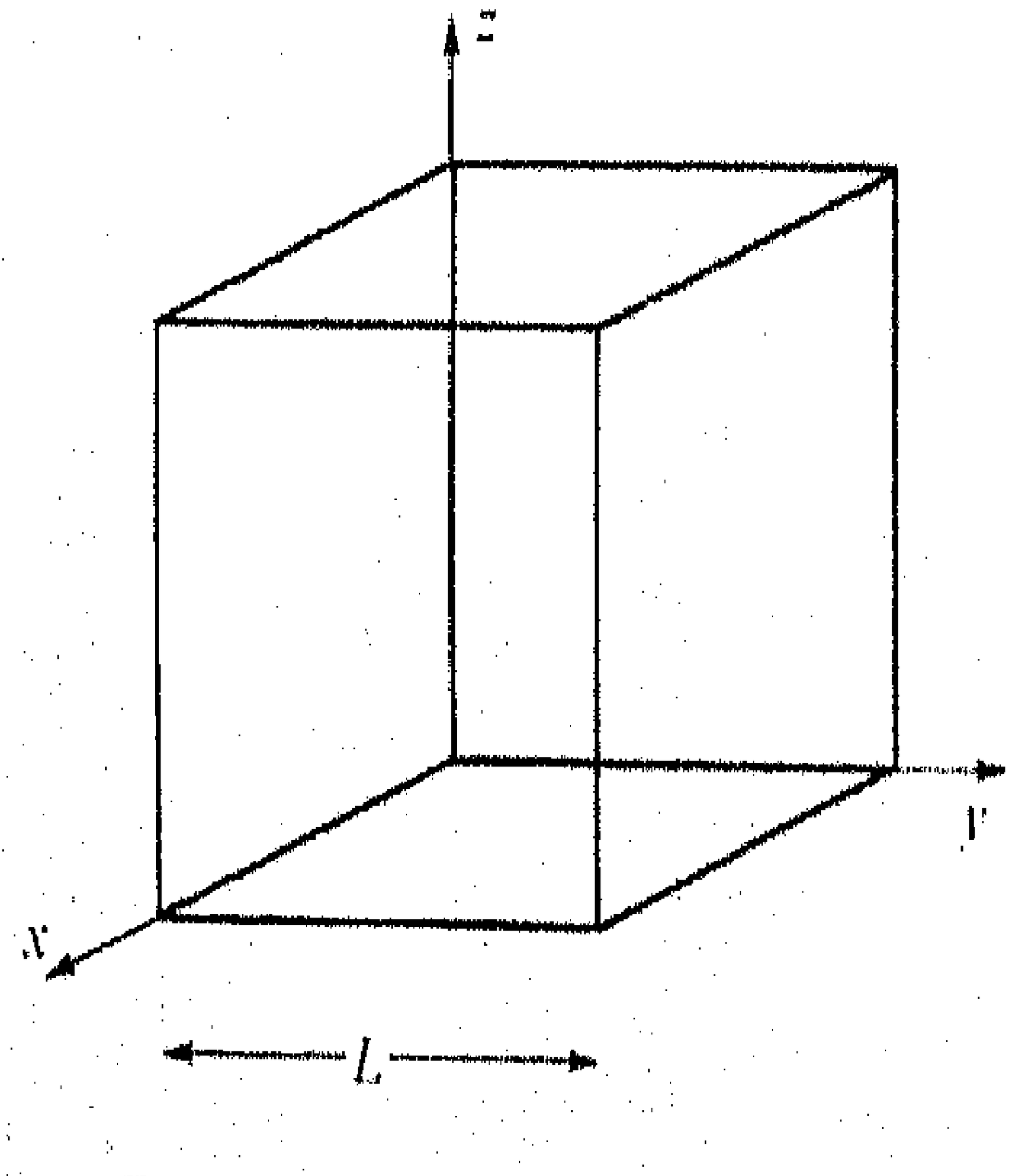

FIG. 1.1. Geometry of the optical cavity.

The first part of the calculation is entirely classical. The electric field in empty space must satisfy the wave equation

$$\nabla^2\mathbf{E} = \frac{1}{c^2}\frac{\partial^2\mathbf{E}}{\partial t^2} \tag{1.1}$$

where c is the velocity of light, together with the Maxwell equation

$$\nabla.\mathbf{E} = 0. \tag{1.2}$$

The solution that satisfies the boundary conditions has components

$$E_x(\mathbf{r}t) = E_x(t)\cos(k_x x)\sin(k_y y)\sin(k_z z),$$

$$E_y(\mathbf{r}t) = E_y(t)\sin(k_x x)\cos(k_y y)\sin(k_z z), \tag{1.3}$$

and

$$E_z(\mathbf{r}t) = E_z(t)\sin(k_x x)\sin(k_y y)\cos(k_z z),$$

where $\mathbf{E}(t)$ is independent of position, and the wavevector $\mathbf{k}$ has components

$$k_x = \pi\nu_x/L, \qquad k_y = \pi\nu_y/L, \qquad k_z = \pi\nu_z/L \tag{1.4}$$

with

$$\nu_x, \nu_y, \nu_z = 0, 1, 2, 3, \ldots. \tag{1.5}$$

The integers ν are further restricted, in that only one of them can be zero at a time since, if two or three are zero, $\mathbf{E}(\mathbf{r}t)$ is also zero and there is no electromagnetic field in the cavity.

It is easily verified that $\mathbf{E}(\mathbf{r}t)$ given by eqn (1.3) satisfies the boundary conditions at the cavity walls, for example, $E_x(\mathbf{r}t) = 0$ at $y = 0$ or L and at $z = 0$ or L. The boundary conditions could be equally well satisfied with the cosines replaced by sines, but it would not then be possible to satisfy the Maxwell equation (1.2) everywhere in the cavity. For the solution (1.3), this equation leads to the constraint

$$\mathbf{k}.\mathbf{E}(t) = 0. \tag{1.6}$$

This is just the condition for $\mathbf{E}(t)$ to be at right-angles to $\mathbf{k}$ and there are two independent directions of $\mathbf{E}(t)$ for each $\mathbf{k}$.

The boundary conditions force the wavevector components to take discrete values specified by the integers ν_x, ν_y, and ν_z. Each set of integers $(\nu_x\ \nu_y\ \nu_z)$ defines a mode of the radiation field in the cavity and corresponds to two degrees of freedom of the field when the two polarization directions are taken into account. Any excitation of the electromagnetic field can be expressed as a linear sum of these field modes. The allowed values of $\mathbf{k}$ can be plotted as a lattice of points in three dimensions, the lattice constant being π/L. Fig. 1.2

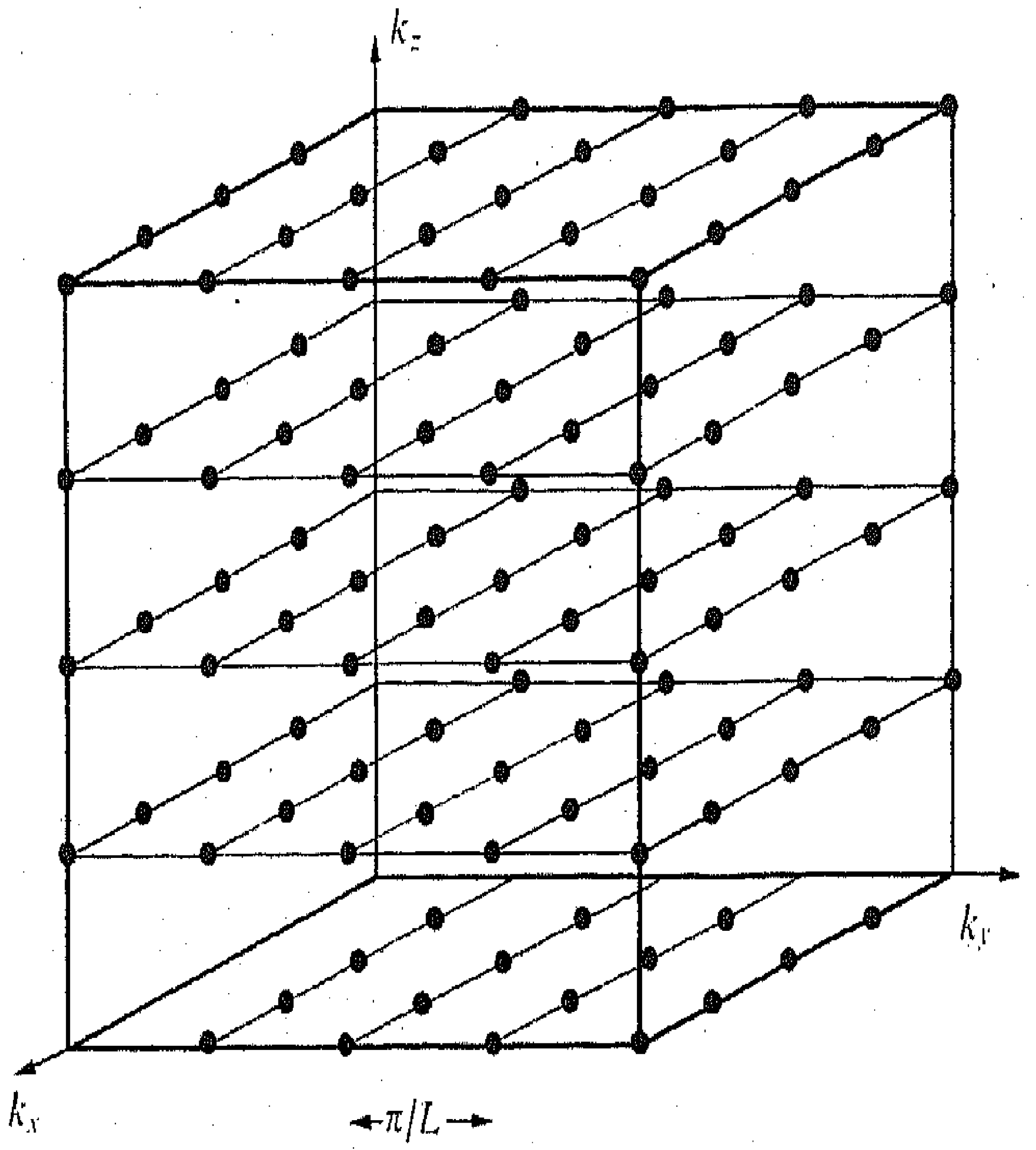

FIG. 1.2. The allowed wavevectors k for a cubic cavity of edge L. Note the absence of points for which two or three of the components would be zero.

shows the lattice with the values of ν_x, ν_y, and ν_z restricted to be less than or equal to 4.

We shall need an expression for the number of field modes having the magnitude of their wavevector between the values k and $k+\mathrm{d}k$. This is just the number of lattice points in the octant of a spherical shell bounded by radii k and $k+\mathrm{d}k$. Each lattice point is surrounded by an empty volume $(\pi/L)^3$, so assuming that the shell has a sufficiently large volume compared to $(\pi/L)^3$, the required number is

$$\tfrac{1}{8}(4\pi k^2\,\mathrm{d}k)(\pi/L)^{-3}\times 2, \tag{1.7}$$

where the final factor takes account of the two possible polarizations.

The density $\rho_k\,\mathrm{d}k$ of field modes is defined to be the number of modes per unit volume of cavity having their wavevector in the specified range. Thus from eqn (1.7)

$$\rho_k\,\mathrm{d}k = k^2\,\mathrm{d}k/\pi^2. \tag{1.8}$$

This result holds generally and is independent of the nature of the cavity used in its derivation. The angular frequency ω of a mode is related to its wavevector in the usual way by

$$\omega = ck. \tag{1.9}$$

Thus eqn (1.8) can be converted into an expression for the density $\rho_\omega\,\mathrm{d}\omega$ of modes having their frequency between ω and $\omega+\mathrm{d}\omega$,

$$\rho_\omega\,\mathrm{d}\omega = \omega^2\,\mathrm{d}\omega/\pi^2c^3. \tag{1.10}$$

In later chapters we shall encounter expressions that must be summed over the field modes. Using the mode densities of eqns (1.8) and (1.10) such summations can be converted to integrations over k or ω,

$$\sum_{\mathbf{k}} \rightarrow \int (Vk^2/\pi^2)\,\mathrm{d}k \rightarrow \int (V\omega^2/\pi^2c^3)\,\mathrm{d}\omega, \tag{1.11}$$

where V is the cavity volume and the summation on the left is understood to cover the two independent polarizations for each wavevector **k**.

1.2. Quantization of the field energy

So much for the spatial dependence of the electromagnetic field. The second stage of the calculation determines the amount of energy stored in each field mode at temperature T. An equation for the time dependence of the electric field is obtained by substituting the solution (1.3) into the wave equation (1.1), and using (1.9),

$$\partial^2\mathbf{E}(t)/\partial t^2 = -\omega^2\mathbf{E}(t). \tag{1.12}$$

This is a simple-harmonic-motion equation whose solution can be taken as

$$\mathbf{E}(t) = \mathbf{E}_0\exp(-\mathrm{i}\omega t), \tag{1.13}$$

where $\mathbf{E}_0$ is a constant vector which, in classical electromagnetic theory, can have any arbitrary magnitude.

According to classical theory, the energy contained in an electromagnetic field is given by the integral

$$\frac{1}{2}\int_{\text{cavity}} (\epsilon_0\mathbf{E}^2+\mu_0^{-1}\mathbf{B}^2)\,\mathrm{d}V, \tag{1.14}$$

where ϵ_0 and μ_0 are the electric permittivity and magnetic permeability of free space, related to the velocity of light by

$$c = (\epsilon_0\mu_0)^{-\frac{1}{2}}, \tag{1.15}$$

and **E** and **B** are the real electric and magnetic fields. For the field mode considered, the complex electric field is given by eqns (1.3) and (1.13). It is convenient to average the field energy over a cycle of oscillation, since the energy variation that occurs during a cycle is not usually susceptible to measurement. The cycle average is easily carried out by means of a theorem, which we here state in the form of a problem.

Problem 1.1. The cycle-average theorem. Show that if $\mathscr{A}$ and $\mathscr{B}$ are two complex quantities which both vary with time as $\exp(-\mathrm{i}\omega t)$ then the average over a cycle of the oscillation of the product of the real parts of $\mathscr{A}$ and $\mathscr{B}$ is given by

$$\overline{(\mathrm{Re}\,\mathscr{A})\times(\mathrm{Re}\,\mathscr{B})} = \tfrac{1}{2}\mathrm{Re}(\mathscr{A}\mathscr{B}^*), \qquad (1.16)$$

where the star denotes complex conjugation.

The cycle-average theorem can be applied to the energy expression (1.14) where the electric vector for the field mode considered is given by eqns (1.3) and (1.13). The corresponding magnetic vector is obtained from the Maxwell equation

$$\nabla\times\mathbf{E} = -\partial\mathbf{B}/\partial t. \qquad (1.17)$$

The detailed spatial dependence of the magnetic field is slightly different from that of the electric field, but the amplitudes B_0 and E_0 of the two fields are related by

$$B_0 = (k/\omega)E_0 = (\epsilon_0\mu_0)^{\frac{1}{2}}E_0. \qquad (1.18)$$

It follows that the electric and magnetic contributions in eqn (1.14) are equal, and the total average field energy is accordingly

$$\frac{1}{2}\int_{\text{cavity}} \epsilon_0|\mathbf{E}(\mathbf{r}t)|^2\,\mathrm{d}V. \qquad (1.19)$$

It is at this point that Planck's quantization hypothesis is introduced. In classical theory, the field energy given by eqn (1.19) can have any positive value, since $\mathbf{E}_0$ in eqn (1.13) can have any magnitude. However, the field $\mathbf{E}(t)$ satisfies the harmonic-oscillator equation (1.12), and if this equation is treated quantum-mechanically (the details are given in Chapter 4) rather than classically, then the energy of the oscillator can take only the discrete values

$$E_n = (n+\tfrac{1}{2})\hbar\omega, \qquad n = 0, 1, 2, 3, \ldots. \qquad (1.20)$$

We accordingly assign these allowed values to the electromagnetic energy of the mode as represented by eqn (1.19),

$$\frac{1}{2}\int_{\text{cavity}} \epsilon_0|\mathbf{E}(\mathbf{r}t)|^2\,\mathrm{d}V = (n+\tfrac{1}{2})\hbar\omega. \qquad (1.21)$$

Obviously this quantization condition puts restrictions on the possible magnitudes of the amplitude $\mathbf{E}_0$ in eqn (1.13). However, it is not necessary to consider these consequences for the present; we treat the fields as classical quantities and impose the quantization condition only on the field energy. At a deeper level one must treat the electromagnetic field as a quantum-mechanical system as in Chapter 4, but for many problems the semiclassical approach outlined above is adequate.

The essence of the quantum theory for the radiation field is thus the association of a quantum harmonic oscillator with each mode of the field. The energy levels of such an oscillator are shown in Fig. 1.3. When the mode energy is given by eqn (1.20), the corresponding oscillator is in its nth excited state. For $n = 0$ the oscillator is in its ground state, but a finite amount of energy $\frac{1}{2}\hbar\omega$ is still present in the field. This is the zero-point energy of the oscillator and its significance is discussed in §4.7. For most experiments the factor that governs the observations is the degree of excitation above the ground-state energy. In the state with energy E_n there are n quanta of energy $\hbar\omega$ in addition to the zero-point energy. These quanta are called photons, and one speaks of n photons being excited in the mode of the radiation field. A photon is said to have been created (destroyed) when the electromagnetic energy in the mode is increased (decreased) by a single quantum. Fig. 1.4 shows the lowest levels of the harmonic oscillators associated with the first ten field modes in order of increasing frequency. Note that there are two independently polarized modes for each of these oscillators.

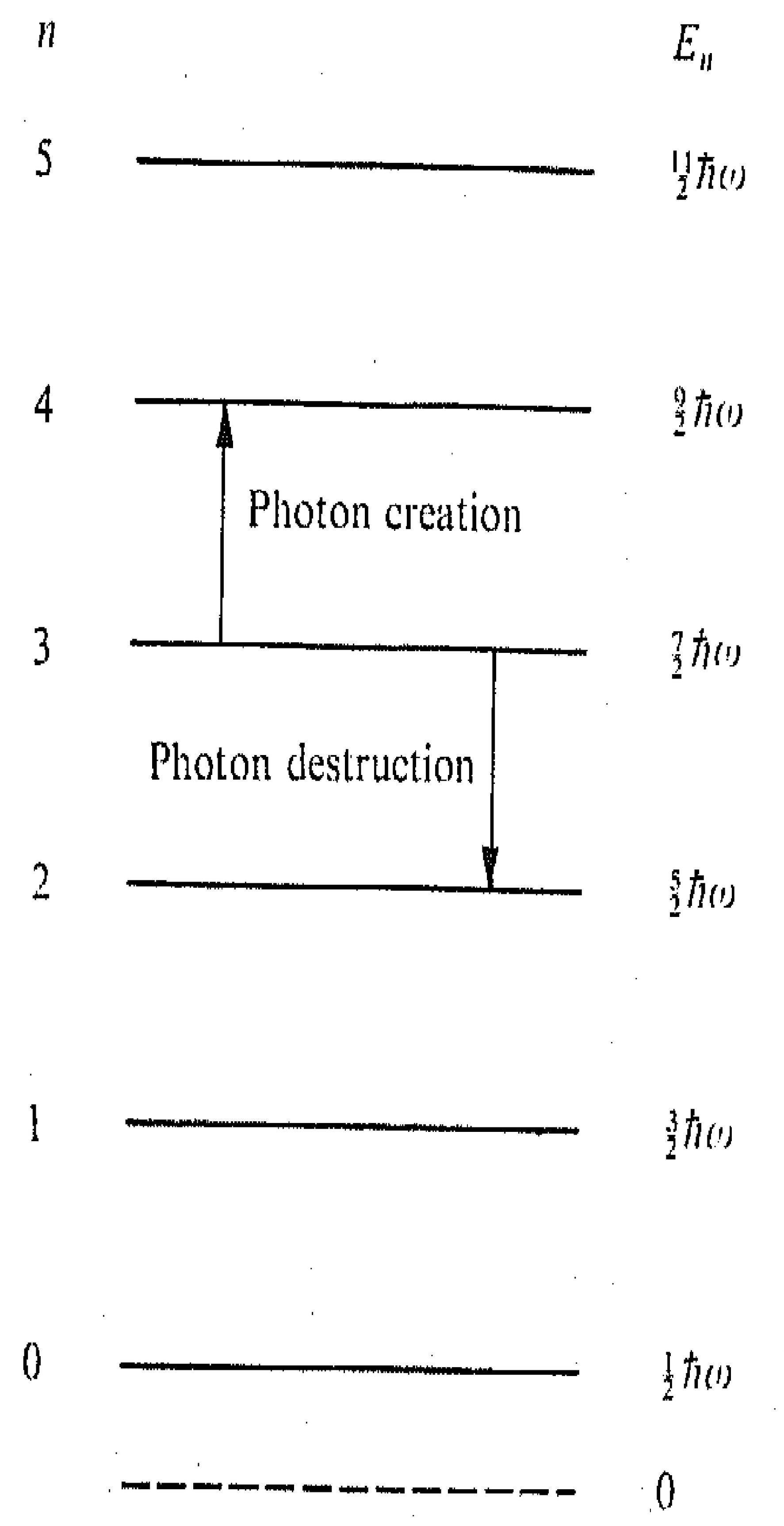

FIG. 1.3. The six lowest energy levels of a quantum harmonic oscillator.

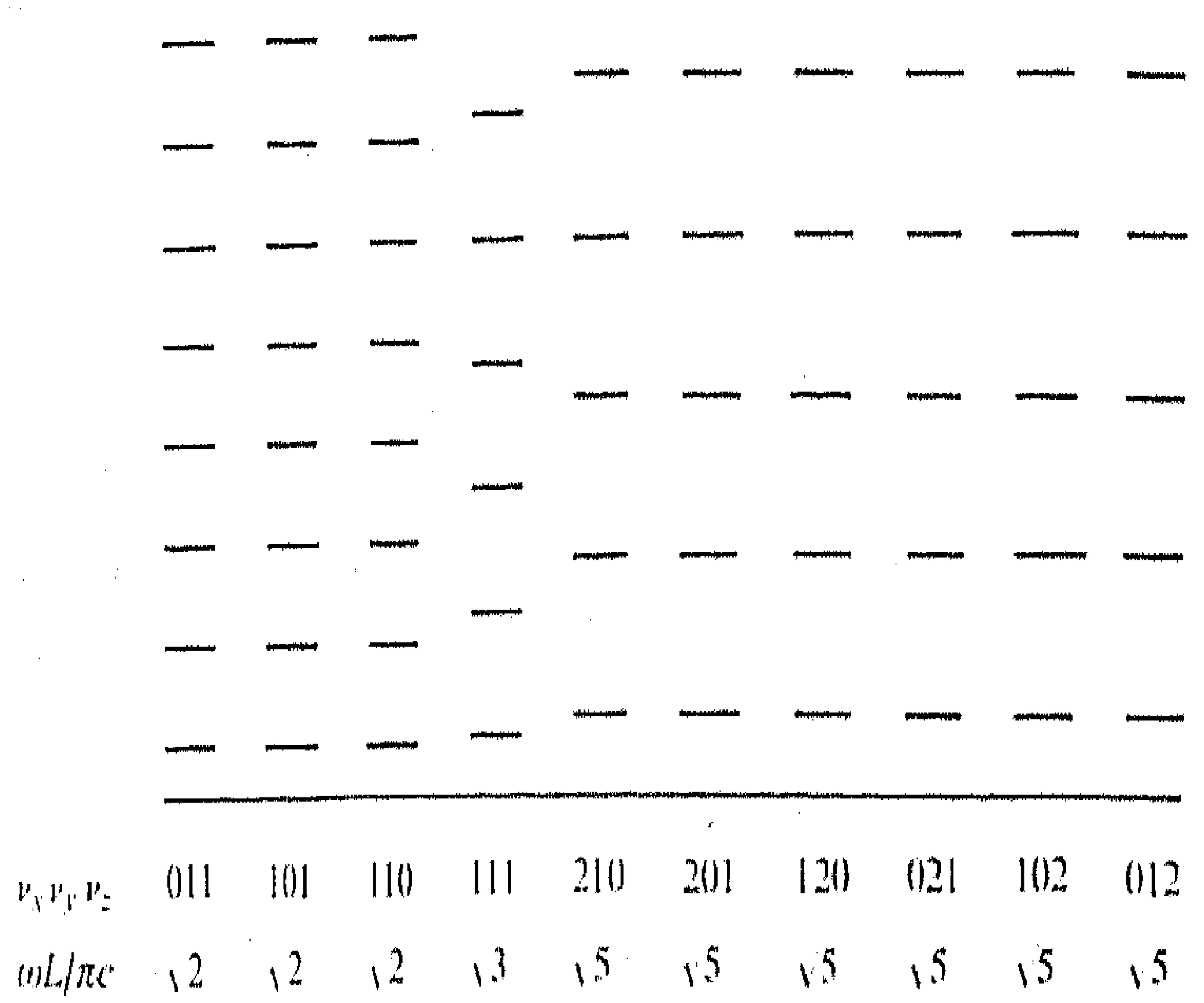
$\nu_x\nu_y\nu_z$
011 101 110 111 210 201 120 021 102 012
$\omega L/\pi c$
$\sqrt{2}$ $\sqrt{2}$ $\sqrt{2}$ $\sqrt{3}$ $\sqrt{5}$ $\sqrt{5}$ $\sqrt{5}$ $\sqrt{5}$ $\sqrt{5}$ $\sqrt{5}$

FIG. 1.4. Harmonic oscillator levels for the modes that correspond to the ten points closest to the origin in Fig. 1.2.

1.3. Planck's law

In thermal equilibrium at temperature T, the probability P_n that the mode oscillator is thermally excited to the nth excited state is given by the usual Boltzmann factor

$$P_n = \frac{\exp(-E_n/k_BT)}{\sum\limits_n \exp(-E_n/k_BT)}. \tag{1.22}$$

The zero-point energy cancels when the quantized energy expression (1.20) is substituted and, with the shorthand notation

$$U = \exp(-\hbar\omega/k_BT), \tag{1.23}$$

the thermal probability becomes

$$P_n = U^n \bigg/ \sum_n U^n. \tag{1.24}$$

The denominator is an easily-summed geometric series,

$$\sum_{n=0}^{\infty} U^n = 1/(1-U). \tag{1.25}$$

Hence

$$P_n = (1-U)U^n. \tag{1.26}$$

The mean number $\bar{n}$ of photons excited in the field mode at temperature T is therefore

$$\begin{aligned}\bar{n} &= \sum_n nP_n = (1-U)\sum_n nU^n \\ &= (1-U)U\,\partial/\partial U \sum_n U^n \\ &= U/(1-U),\end{aligned} \tag{1.27}$$

where eqns (1.25) and (1.26) have been used. Thus, with the help of eqn (1.23), the mean photon number is

$$\bar{n} = \frac{1}{\exp(\hbar\omega/k_BT)-1}. \tag{1.28}$$

This important result is the Planck thermal excitation function. It is plotted in Fig. 1.5 as a function of the oscillator or photon frequency ω.

The results (1.10) and (1.28) give, respectively, the number of radiation field modes per unit volume whose frequency is in the range ω to $\omega+d\omega$, and the mean energy $\bar{n}\hbar\omega$ in addition to the zero-point energy in each such mode at

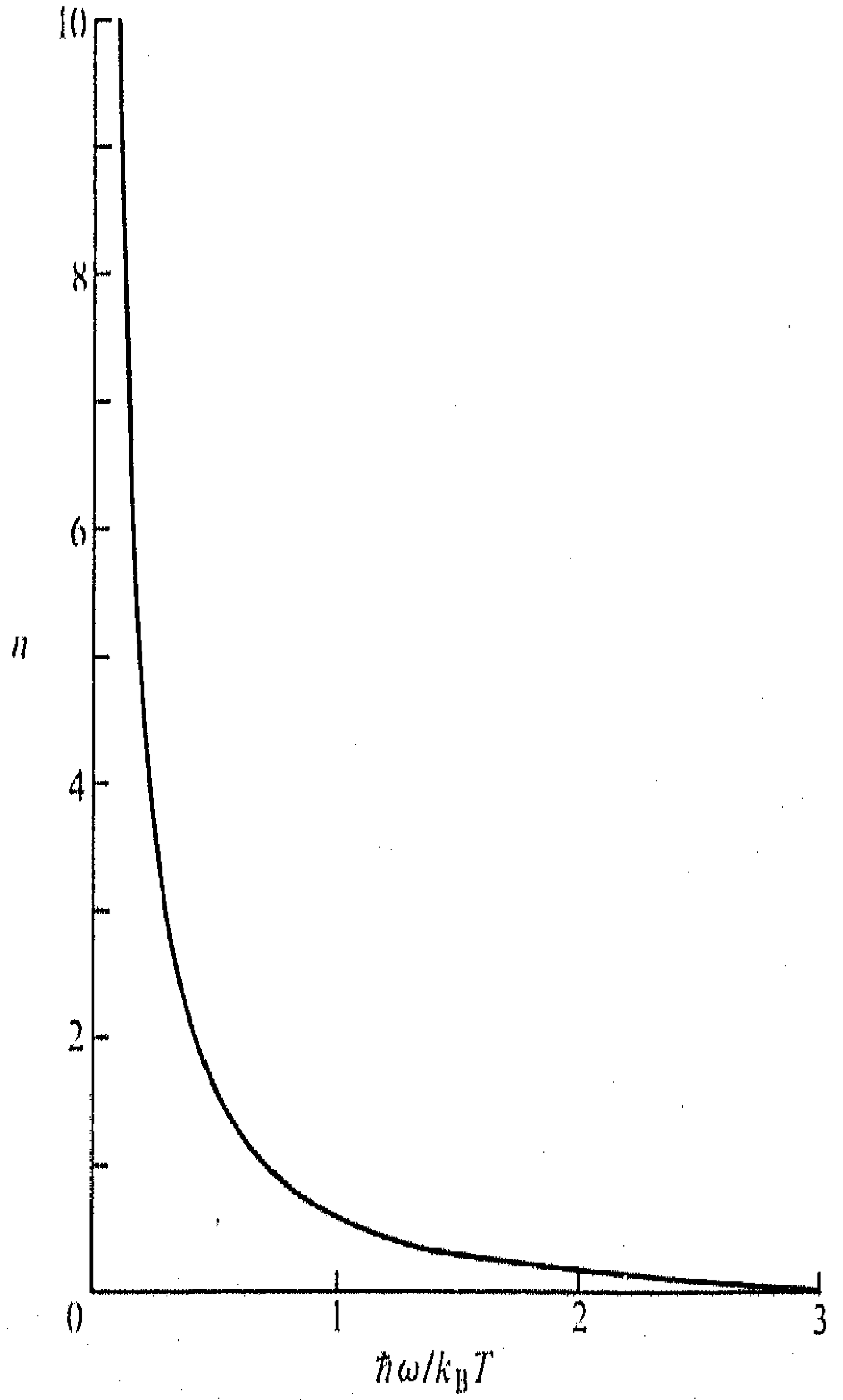

FIG. 1.5. Mean number $\bar{n}$ of photons of frequency ω that are thermally excited at temperature T.

temperature T. They can be combined to obtain the mean energy density $\bar{W}_T(\omega)\,\mathrm{d}\omega$ of the radiation in these modes at temperature T,

$$\bar{W}_T(\omega)\,\mathrm{d}\omega = \bar{n}\hbar\omega\rho_\omega\,\mathrm{d}\omega = \bar{n}\hbar\omega^3\,\mathrm{d}\omega/\pi^2c^3 = \frac{\hbar\omega^3}{\pi^2c^3}\frac{\mathrm{d}\omega}{\exp(\hbar\omega/k_BT)-1}. \tag{1.29}$$

This is Planck's law for the radiative energy density $\bar{W}_T(\omega)$. A plot of $\bar{W}_T(\omega)$ versus $\hbar\omega/k_BT$ is given in Fig. 1.6.

Planck's law takes on slightly simpler forms at high and low temperatures. For $k_BT \gg \hbar\omega$, the exponential can be expanded, to give

$$\bar{W}_T(\omega) \approx \omega^2k_BT/\pi^2c^3 \qquad (k_BT \gg \hbar\omega). \tag{1.30}$$

This form of radiation law was derived by Rayleigh[5] in 1900, shortly before Planck's formulation of the correct law. Rayleigh's law is the classical limit obtained by letting Planck's quantum constant $\hbar$ tend to zero.

At low temperatures where $k_BT \ll \hbar\omega$, the exponential is very large and eqn (1.29) reduces to Wien's formula[6]

$$\bar{W}_T(\omega) \approx (\hbar\omega^3/\pi^2c^3)\exp(-\hbar\omega/k_BT) \qquad (k_BT \ll \hbar\omega). \tag{1.31}$$

Both approximate forms of Planck's law break down when $\hbar\omega$ is comparable to k_BT.

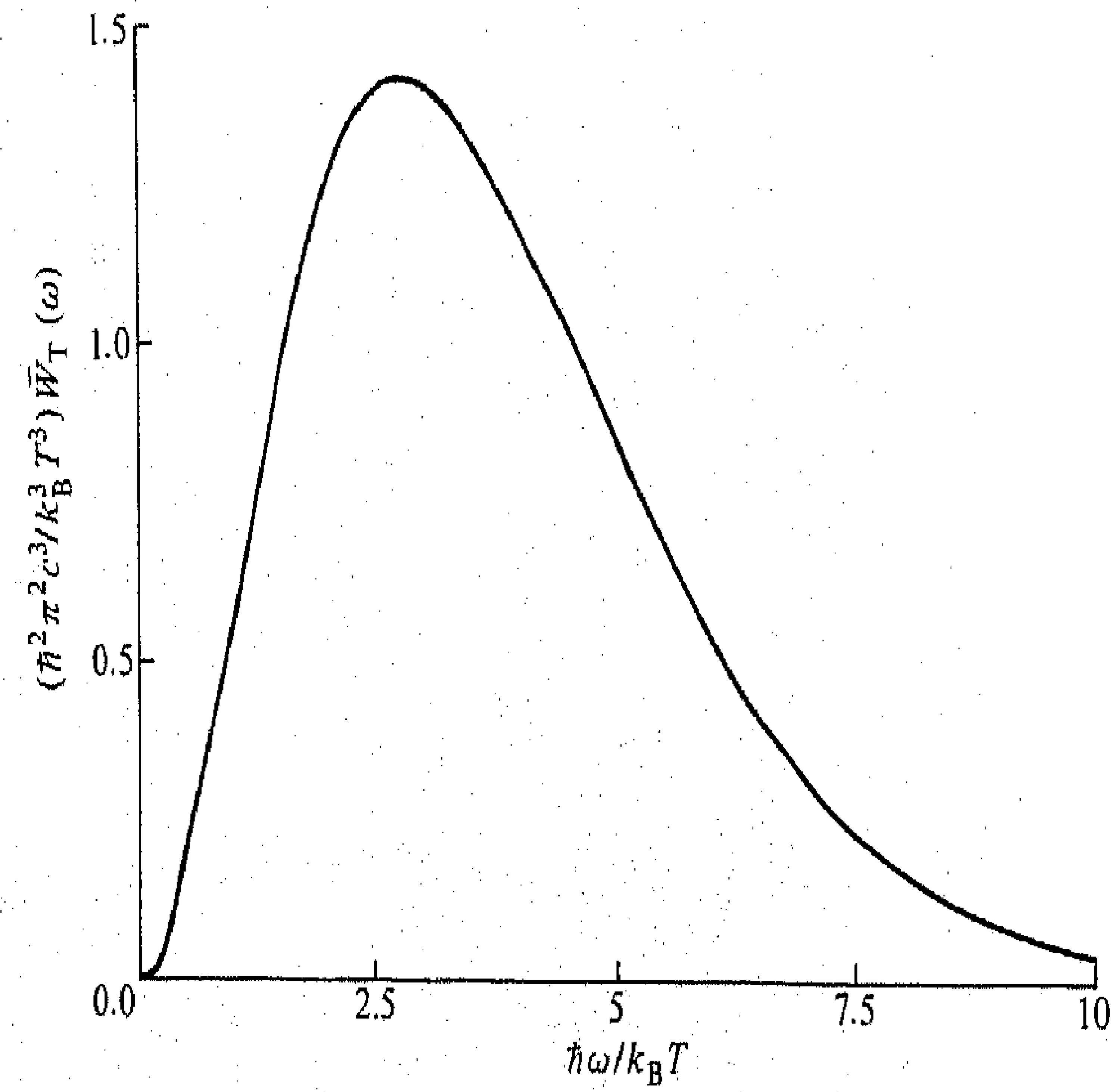

FIG. 1.6. Planck's law for the energy density of electromagnetic radiation at frequency ω and temperature T.

The maximum in the thermal distribution of the radiative energy occurs at a frequency $\omega_{\max}$ that can be found by differentiating eqn (1.29). The result obtained,

$$\hbar\omega_{\max} = 2.8k_BT, \tag{1.32}$$

is Wien's displacement law[7].

The total energy density of the photons in the cavity is obtained by integrating eqn (1.29),

$$\int_0^\infty \bar{W}_T(\omega)\,\mathrm{d}\omega = \frac{k_B^4T^4}{\pi^2c^3\hbar^3}\int_0^\infty \frac{x^3\,\mathrm{d}x}{\mathrm{e}^x-1} = \frac{\pi^2k_B^4T^4}{15c^3\hbar^3}, \tag{1.33}$$

where the value $\pi^4/15$ has been inserted for the definite integral. The proportionality of the total energy density to T^4 is the Stefan-Boltzmann radiation law, formulated in 1879. If $\mathbf{E}_T(\mathbf{r}t)$ is the total electric field that results from all the modes of the radiation field in a cavity at temperature T, then the total electromagnetic energy density can be alternatively expressed with the help of eqn (1.19) as

$$\int_0^\infty \bar{W}_T(\omega)\,\mathrm{d}\omega = (1/2V)\int_{\text{cavity}} \epsilon_0|\mathbf{E}_T(\mathbf{r}t)|^2\,\mathrm{d}V. \tag{1.34}$$

1.4. Fluctuations in photon number

The occurrence of photon absorption and emission processes causes the number of photons in each mode of the radiation field in the cavity to fluctuate. The fluctuation takes place with a characteristic time scale that is discussed in detail in Chapter 3. However, some average properties of the fluctuations can be deduced without any knowledge of the time scales involved. We make use of the ergodic theorem[8] of statistical mechanics, according to which time averages are equivalent to averages taken over a large number of exactly similar systems, each maintained in a fixed state. The fictitious collection of similar systems is called an ensemble; the systems in the ensemble are distributed among their various possible states in accordance with the appropriate probability distribution for the system considered..

For the case of photons in a particular field mode of a cavity, we must imagine an ensemble that consists of the same field mode in a large number of similar cavities. Each cavity mode in the ensemble has some fixed number of photons. The fraction of cavity modes that contain n photons is determined by the function P_n given in eqn (1.26). We have already evaluated the mean photon number $\bar{n}$ using eqn (1.27); the result of this calculation (eqn (1.28)) can equally well be regarded as an ensemble average, or as an average over time of the number of photons in the given mode of a real single cavity. The period over which the time average is taken must clearly be long compared to the characteristic time scale of the fluctuations. The two averages are equal according to the ergodic theorem, which is further discussed in Chapter 3.

The probability distribution P_n can also be used to determine the size of the fluctuations of n about the mean value $\bar{n}$. Let us first examine the form of P_n in greater detail. According to eqn (1.27)

$$U = \bar{n}/(1+\bar{n}). \tag{1.35}$$

Substitution in eqn (1.26) gives

$$P_n = (\bar{n})^n/(1+\bar{n})^{1+n}. \tag{1.36}$$

This is a convenient form for plotting P_n as a function of n for a given value of $\bar{n}$, and some examples are shown in Fig. 1.7. The probability P_n is the distribution of readings one would obtain from a large number of successive measurements of the number of photons in the selected field mode. It is seen that $n = 0$ always has the largest probability of occurrence, and P_n falls off monotonically with increasing n, a result of the decreasing Boltzmann probability of occupation for the higher levels of the mode harmonic oscillator. Note that the probability P_n shows no particular feature at $n = \bar{n}$.

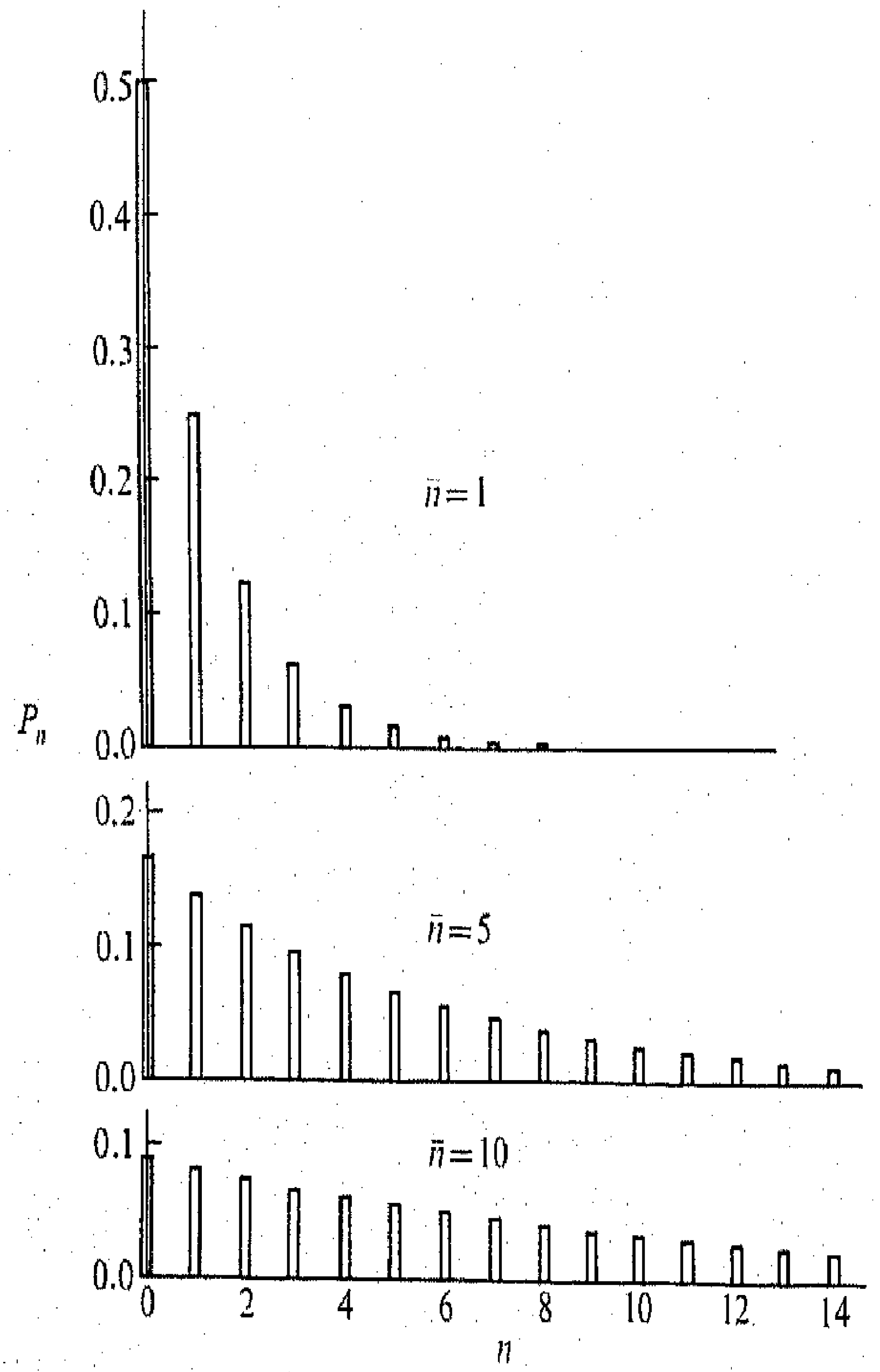

FIG. 1.7. Planck photon-number distributions for three values of the average number $\bar{n}$.

The Planck photon probability distribution P_n is sometimes called the thermal distribution or the geometric distribution. It is often useful to characterize the distribution by its factorial moments. The rth factorial moment is defined to be

$$\overline{n(n-1)(n-2)\ldots(n-r+1)} = \sum_n n(n-1)(n-2)\ldots(n-r+1)P_n, \tag{1.37}$$

where r is any positive integer. The first factorial moment is the same as the mean number of excited photons evaluated in eqn (1.27). The same differentiation method can be used to obtain the higher factorial moments.

Problem 1.2. Prove that the rth factorial moment of the Planck probability distribution, eqns (1.26) or (1.36), is

$$\overline{n(n-1)(n-2)\ldots(n-r+1)} = r!(\bar{n})^r. \tag{1.38}$$

The size of the fluctuation in photon number is characterized by the root-mean-square deviation Δn of the distribution. By definition

$$(\Delta n)^2 = \sum_n (n-\bar{n})^2 P_n = \overline{n^2} - (\bar{n})^2. \tag{1.39}$$

The second factorial moment obtained from eqn (1.38) gives

$$\overline{n^2} - \bar{n} = 2(\bar{n})^2, \tag{1.40}$$

and hence

$$\Delta n = \{(\bar{n})^2 + \bar{n}\}^{\frac{1}{2}}. \tag{1.41}$$

It is seen that the magnitude of the fluctuation in n is always larger than the mean value $\bar{n}$, in accordance with the large spread of the probability distribution shown in Fig. 1.7. For large $\bar{n}$, eqn (1.41) tends to

$$\Delta n = \bar{n} + \tfrac{1}{2} \qquad (\bar{n} \gg 1). \tag{1.42}$$

The theory of photon-counting experiments is described in detail in Chapter 6. It should be mentioned that the results obtained above using the ergodic theorem are strictly valid only for an idealized experiment where each individual measurement of the number of photons is made effectively instantaneously, that is in a time short compared to the characteristic time scale of the fluctuations. Any real measurement has a finite resolving time and the results obtained depend upon its size relative to the fluctuation time scale.

1.5. Einstein's *A* and *B* coefficients

The mechanism by which the number of photons in a cavity can change is the absorption or emission of photons by the atoms or molecules in the cavity walls. We now consider the basic interaction processes between the electromagnetic radiation and atoms. They can be treated by means of a simple phenomenological theory due to Einstein. The Einstein theory allows a qualitative understanding of a large variety of radiative processes, for example, the absorption and scattering of light by atoms and the amplification of light beams by lasers.

The Einstein theory is based on some physically reasonable postulates concerning the absorption and emission of photons by atoms. The postulates can all be rigorously justified by quantum-mechanical treatments of the interaction processes (see §5.5). However, no explicit quantum mechanics is used in the Einstein theory, except that the atomic energy levels are assumed discrete, and it is convenient (though not essential) to regard the electromagnetic field energy as quantized into photons.

It is simpler to consider the interaction of radiation, not with the atoms in the cavity walls, but with some atoms or molecules placed in the interior of the cavity. Suppose that a gas of N identical atoms is placed in the cavity, each atom having a pair of bound-state energy levels E_1 and E_2, and let

$$\hbar\omega = E_2 - E_1. \tag{1.43}$$

Energy-conserving processes are possible in which photons of frequency ω are emitted or absorbed by atoms that make transitions between the two states. We allow the two atomic levels to be multiplets, with degeneracies g_1 and g_2, but for simplicity we neglect all the other atomic energy levels. Let the numbers of atoms that have energies E_1 and E_2 be denoted by the level populations N_1 and N_2 respectively. The levels are shown in Fig. 1.8.

A closed cavity that contains atoms and thermally-excited radiation is not a very interesting system from an experimental point of view. To measure the interaction between atoms and radiation, we need to do something more sophisticated. For example, we might pass a beam of radiation at frequency ω through the cavity and measure the fraction of the beam intensity lost in the cavity. In a typical experiment, the cycle-averaged energy density of radiation at frequency ω exceeds the thermal part $\bar{W}_T(\omega)$ by an amount $\bar{W}_E(\omega)$ that represents the contribution from some external source of electromagnetic

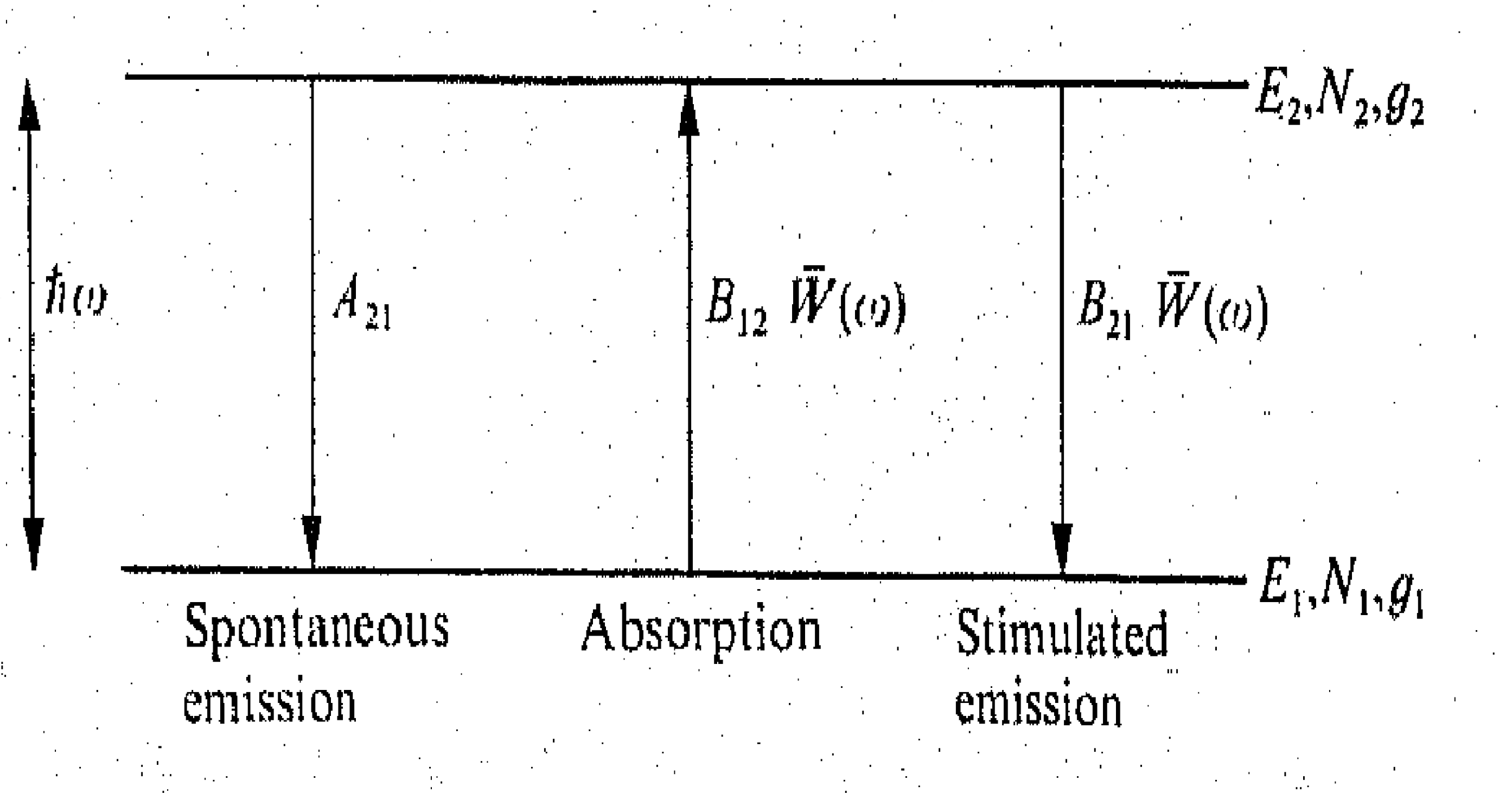

FIG. 1.8. The three basic kinds of radiative process.

radiation. The total energy density is thus

$$\bar{W}(\omega) = \bar{W}_T(\omega) + \bar{W}_E(\omega). \tag{1.44}$$

In general $\bar{W}_E(\omega)$ is a function of position in the cavity, and the external radiation does not have the spatially isotropic distribution of the thermal radiation, but let us ignore these features for the moment. It is however an essential requirement for the validity of the Einstein theory that the total energy density is a slowly-varying function of ω in the vicinity of the atomic transition frequency.

The probabilities of photon absorption and emission are defined as follows. Consider a single atom in state 2. There is a finite probability A_{21} per unit time that the atom will spontaneously fall into the lower state 1 and emit a photon of energy $\hbar\omega$.

Now consider an atom in state 1. In the absence of any radiation of frequency ω there is no way in which the atom can pass into state 2, since it is impossible to conserve energy in such a transition. However, in the presence of energy density $\bar{W}(\omega)$ of radiation, the upward transition $1 \rightarrow 2$ can proceed by absorption of a photon $\hbar\omega$. The transition rate is assumed proportional to $\bar{W}(\omega)$, with a coefficient of proportionality B_{12}.

These two processes are intuitively reasonable, but it is not so obvious that the presence of the radiation described by $\bar{W}(\omega)$ also enhances the rate of transition from the upper state to the lower state. However, we shall later prove that such an enhancement must take place, and we write the increase in transition rate $B_{21}\bar{W}(\omega)$. This third radiative process is called induced or stimulated emission of radiation. The transition rates for all three processes are shown in Fig. 1.8.

It should be emphasized that the three Einstein coefficients A_{21}, B_{12}, and B_{21} are defined to be independent of $\bar{W}(\omega)$. They depend only on the properties of the two atomic states involved, in a way determined by quantum mechanics (see §2.4). For the present, they are treated as phenomenological constants.

Consider the influence of the three transition rates on the level populations N_1 and N_2. It is assumed that N is a sufficiently large number for the individual absorptions and emissions to produce a smooth time dependence in N_1 and N_2. The rates of change of N_1 and N_2 are then

$$\mathrm{d}N_1/\mathrm{d}t = -\mathrm{d}N_2/\mathrm{d}t = N_2A_{21} - N_1B_{12}\bar{W}(\omega) + N_2B_{21}\bar{W}(\omega). \tag{1.45}$$

We solve this equation after we have considered the relations that exist between the Einstein coefficients.

1.6. The case of thermal equilibrium

The rate equation (1.45) holds generally, but some useful results can be obtained by consideration of the special case of thermal equilibrium. In any equilibrium condition the level populations are constant and eqn (1.45) gives

$$N_2A_{21}-N_1B_{12}\bar{W}(\omega)+N_2B_{21}\bar{W}(\omega) = 0. \tag{1.46}$$

For *thermal* equilibrium, with no external radiation introduced into the cavity, the energy density in eqn (1.46) is just the thermal contribution $\bar{W}_T(\omega)$, and solution for this quantity gives

$$\bar{W}_T(\omega) = \frac{A_{21}}{(N_1/N_2)B_{12}-B_{21}}. \tag{1.47}$$

The level populations N_1 and N_2 are related in thermal equilibrium by Boltzmann's law

$$N_1/N_2 = g_1\exp(-E_1/k_B T)/g_2\exp(-E_2/k_B T) = (g_1/g_2)\exp(\hbar\omega/k_B T). \tag{1.48}$$

Thus from eqn (1.47)

$$\bar{W}_T(\omega) = A_{21}/\{(g_1/g_2)\exp(\hbar\omega/k_BT)B_{12}-B_{21}\}. \tag{1.49}$$

This expression for $\bar{W}_T(\omega)$ follows from the definitions of the Einstein coefficients and an application of the Boltzmann distribution to the atomic level populations. However, the result must be consistent with Planck's law (eqn (1.29)) for the radiative energy density in thermal equilibrium. The two expressions are identical at all temperatures T only if

$$(g_1/g_2)B_{12} = B_{21}, \tag{1.50}$$

$$(\hbar\omega^3/\pi^2c^3)B_{21}= A_{21}. \tag{1.51}$$

The three Einstein coefficients are therefore interrelated, and the transition rates between a pair of levels can all be expressed in terms of a single coefficient. It is seen from eqn (1.49) that consistency between the Einstein theory and Planck's law could not have been achieved without the introduction of the stimulated emission process. It will be shown in §5.5 that this process arises naturally in the rigorous theory of photon emission.

Comparison of Planck's law (eqn (1.29)) with eqn (1.51) shows that in thermal equilibrium

$$B_{21}\bar{W}_T(\omega) = A_{21}\bar{n}. \tag{1.52}$$

That is, the thermally-stimulated emission rate is equal to the spontaneous emission rate multiplied by the mean number of photons in each radiation field mode at the transition frequency ω. The sum of the two emission rates is

$$B_{21}\bar{W}_T(\omega)+A_{21} = A_{21}(\bar{n}+1). \tag{1.53}$$

It is of interest to compare the magnitudes of the two emission rates as a function of the photon frequency ω. From eqns (1.28) and (1.52)

$$A_{21}/B_{21}\bar{W}_T(\omega) = 1/\bar{n} = \exp(\hbar\omega/k_BT)-1. \tag{1.54}$$

For a cavity maintained at room temperature ($T = 300$ K), the exponent $\hbar\omega/k_BT$ is equal to unity for radiation that has a wavelength

$$\lambda \approx 50\ \mu\text{m}, \tag{1.55}$$

corresponding to a frequency of about 6×10^{12} Hz in the far-infrared region of the spectrum. Hence for radiation having longer wavelength than this, corresponding to the microwave and radiofrequency regions,

$$\hbar\omega \ll k_BT \quad \text{and} \quad A_{21} \ll B_{21}\bar{W}_T(\omega), \tag{1.56}$$

while, for radiation in the near-infrared, visible, ultraviolet, or X-ray regions,

$$\hbar\omega \gg k_BT \quad \text{and} \quad A_{21} \gg B_{21}\bar{W}_T(\omega). \tag{1.57}$$

It is seen that for frequencies *small* compared to 6×10^{12} Hz the thermally-stimulated emission rate is much larger than the spontaneous emission rate, but for frequencies *large* compared to 6×10^{12} Hz the spontaneous emission rate far exceeds the thermally-stimulated emission rate.

Finally, we note another way of expressing the thermal photon probability distribution P_n. From eqns (1.23), (1.35), and (1.48)

$$\bar{n}/(1+\bar{n}) = g_1N_2/g_2N_1, \tag{1.58}$$

or

$$\bar{n} = g_1N_2/(g_2N_1-g_1N_2). \tag{1.59}$$

Thus eqn (1.36) can be written

$$P_n = \left(\frac{g_1N_2}{g_2N_1}\right)^n\left(1-\frac{g_1N_2}{g_2N_1}\right), \tag{1.60}$$

and the thermal-equilibrium photon distribution is expressed entirely in terms of quantities related to the atomic energy levels.

1.7. Theory of simple optical processes

A wide variety of radiative processes can be treated by solution of the rate equation (1.45), and using the relations (1.50) and (1.51) between the Einstein coefficients. The main concern of the book is with optical experiments that use electromagnetic radiation in the near-infrared, visible, and ultraviolet regions of the spectrum. The thermally excited energy density $\bar{W}_T(\omega)$ is of course very small for experiments at room temperature. The inequality (1.57) applies and the spontaneous emission rate is much higher than the rates of thermally-stimulated emission or of absorption of thermal radiation.

For frequencies of order 10^{13} Hz or higher, it is accordingly a very good approximation to ignore the thermal energy density. The total energy density $\bar{W}(\omega)$ in eqn (1.44) then represents just the contribution $\bar{W}_E(\omega)$ from external sources of light and the E subscript can be dropped. The radiative processes of interest involve the absorption and stimulated emission associated with the external sources.

Atomic excited states in the optical frequency region have negligible thermal populations at room temperature. We consider atoms that have a single low-lying state, the atomic ground state, and large numbers of optical excited states. With the lower level in Fig. 1.8 taken to be the ground state, we have $N_1 = N$ in thermal equilibrium. Selective excitation of a particular excited level E_2 can often be achieved by irradiation of the atoms with light from an external source whose frequencies ω satisfy the resonance condition (1.43) for only a single atomic transition. The system may then behave essentially as a two-level atom, and the level populations satisfy

$$N_1 + N_2 = N. \tag{1.61}$$

Less simple optical processes may involve three or four atomic energy levels, as in the laser system treated later in the present chapter.

The two-level case is particularly simple, and it becomes simpler still when both levels are nondegenerate ($g_1 = g_2 = 1$) so that the B coefficients are equal according to eqn (1.50). The subscripts on the A and B coefficients can then be omitted, and the rate equation (1.45) simplifies to

$$\mathrm{d}N_1/\mathrm{d}t = -\mathrm{d}N_2/\mathrm{d}t = N_2 A + (N_2 - N_1) B\bar{W}, \tag{1.62}$$

where $\bar{W}$ is tacitly understood to be the energy density at frequency ω. In most experiments $\bar{W}$ varies with position in the cavity, and we show later in the chapter how to treat this situation. If the position dependence is ignored, eqn (1.62) depends only on time, and can be solved by standard methods.

Problem 1.3. Prove that the general solution of eqn (1.62) subject to the condition (1.61) is

$$N_1 = \left\{N_1^0 - \frac{N(A+B\bar{W})}{A+2B\bar{W}}\right\}\exp(-(A+2B\bar{W})t) + \frac{N(A+B\bar{W})}{A+2B\bar{W}}, \tag{1.63}$$

where N_1^0 is the initial value of N_1 at time $t = 0$. The solution for N_2 easily follows from eqn (1.61).

We conclude the section with a comment on the validity of the relations (1.50) and (1.51) between the Einstein coefficients. The relations are derived by consideration of the thermal-equilibrium case where the radiative energy density $\bar{W}_T(\omega)$ is distributed isotropically in space. They hold generally for any spatially-isotropic distribution of radiative energy density. However, the external light beams used in experiments do not usually have this property; for example, the light is often in the form of a plane parallel beam. Nevertheless, the relations (1.50) and (1.51) continue to apply for the interaction of light with a gas or fluid of atoms or molecules whose orientations are randomly distributed. The interaction of the radiation with the gas as a whole is then isotropic, even though the interaction with a single atom or molecule may be anisotropic. The orientation-averaged B coefficients are independent of the geometry of the light beam used in an experiment. These remarks do not necessarily apply to the interaction of light with matter in the solid state, where the constituent atoms or molecules may be locked in a common orientation to give anisotropic optical properties. We treat here only atoms or molecules in a gas or fluid where optical isotropy prevails.

1.8. Properties of the microscopic processes

The remainder of the chapter is concerned with various optical processes that can occur when a beam of light is transmitted through a cavity filled with an atomic or molecular gas. It is first necessary to discuss in greater detail the properties of the three basic processes envisaged in the Einstein theory, and particularly the distinction between the two kinds of emission.

Consider an incident beam of light excited in a single well-defined mode of the cavity. We suppose that the frequency of the light is resonant with an atomic transition described by Einstein coefficients A and B. Fig. 1.9 illustrates the directional properties of the three processes that can occur. The most important feature is the fact that light produced by stimulated emission from excited atoms appears in the same cavity mode as that of the incident light that causes the emission to take place. The emitted light also has the same phase properties as the incident beam. Thus stimulated emission tends to amplify the intensity of the incident beam while maintaining its other properties unchanged. These features of the stimulated emission are proved in §§5.5 and 7.4.

On the other hand, light produced by spontaneous emission is completely independent of the incident beam and it can be in any mode of the cavity that satisfies energy conservation. The propagation direction of the spontaneously-emitted light thus has a random orientation with respect to the incident light beam. The phase of the emitted light is arbitrary.

When the light and the atoms have settled down in a steady equilibrium state, the mean numbers of atoms (N_1 and N_2) in the lower and upper states remain constant. As the light beam traverses the atomic gas, photons are removed steadily by absorption processes. The atoms thus excited eventually

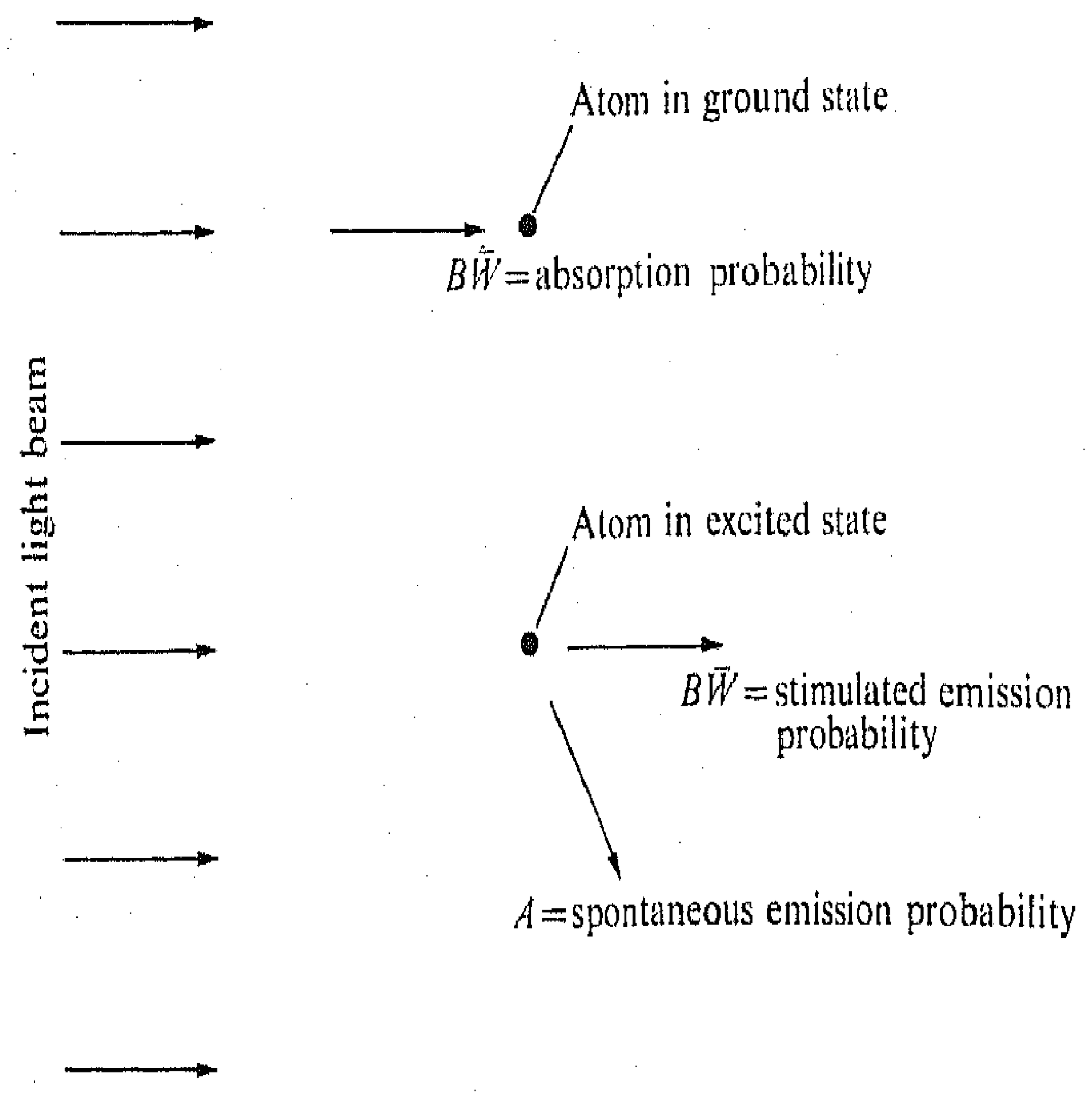
Atom in ground state
$B\bar{W}$ = absorption probability
Incident light beam
Atom in excited state
$B\bar{W}$ = stimulated emission probability
A = spontaneous emission probability

FIG. 1.9. Directional properties of the three radiative processes.

return to their ground states and can replace photons in the beam by stimulated emission. If only these two processes occurred, the beam would pass through the atoms with no change in intensity once a steady state had been achieved. However, since some of the atoms return to the ground state by spontaneous emission, a fraction

$$A/(A+B\bar{W}) = 1/\{1+(\pi^2c^3\bar{W}/\hbar\omega^3)\} \tag{1.64}$$

of the absorbed energy is re-emitted in random directions, only a small part being accidentally in the direction of the incident beam.

Spontaneous emission thus causes a scattering of light and a consequent attenuation of the incident beam. Such scattering is the microscopic source of the apparent absorption of a light beam during its passage through an atomic gas. It should be emphasized that despite the impression given by the word 'absorption', the energy lost by the incident beam in steady-state conditions is not absorbed by the atoms, but is scattered. The same basic phenomenon can be studied experimentally either by measurements of the absorption coefficient or by observations of the intensity of scattered light. The theory of the absorption coefficient is given later in the present chapter; the scattering of light is treated in detail in Chapter 8.

As shown in Fig. 1.9, the relative importance of the stimulated and spontaneous emission is governed by the size of the ratio $B\bar{W}/A$. For $B\bar{W}/A = 1$ the two emission rates are equal. Let us calculate some approximate numerical magnitudes for the intensity of the light beam. For visible light with a frequency in the region of 5×10^{14} Hz, we have

$$\omega \approx 3\times10^{15}\ \mathrm{s}^{-1}, \tag{1.65}$$

and each photon carries an amount of energy

$$\hbar\omega \approx 3\times10^{-19}\ \mathrm{J}. \tag{1.66}$$

The density of field modes given by eqn (1.10) is

$$\rho_\omega\,\mathrm{d}\omega = (\omega^2/\pi^2c^3)\,\mathrm{d}\omega \approx 3{\cdot}4\times10^4\,\mathrm{d}\omega\ \mathrm{m}^{-3}. \tag{1.67}$$

Thus for $B\bar{W}/A = 1$ the energy density of the light is

$$\bar{W}\,\mathrm{d}\omega = (A/B)\,\mathrm{d}\omega = (\hbar\omega^3/\pi^2c^3)\,\mathrm{d}\omega \approx 10^{-14}\,\mathrm{d}\omega\ \mathrm{Jm}^{-3}, \tag{1.68}$$

where eqn (1.51) has been used. The intensity of light beam required to equalize the rates of stimulated and spontaneous emission is obtained by multiplying eqn (1.68) by the velocity of light, as in eqn (1.97) below (we assume that the beam is in free space with unit refractive index), which gives

$$\bar{I}\,\mathrm{d}\omega \approx 3\times10^{-6}\,\mathrm{d}\omega\ \mathrm{W\,m}^{-2}. \tag{1.69}$$

A typical value for the frequency spread of a narrow emission line of an ordinary spectroscopic light source is about 10^{10} Hz, corresponding to a $\mathrm{d}\omega$ of $2\pi\ 10^{10}\ \mathrm{s}^{-1}$. The intensity required to achieve $B\bar{W} = A$ with a light beam of this spread is shown by eqn (1.69) to be about $2\times10^5\ \mathrm{W\,m}^{-2}$. This value can be put into perspective by reference to Table 1.1. It is seen that even the most powerful of conventional light sources, the mercury lamp, produces insufficient light intensity to equalize the rates of stimulated and spontaneous emission. For such light beams, almost all photons that are absorbed by the atoms are re-radiated by spontaneous emission, and are therefore scattered out of the incident beam. It is also seen from Table 1.1 that values of $B\bar{W}$ comparable to or greater than A can be achieved with laser light sources, particularly pulsed lasers. The stimulated emission is then important, and

TABLE 1.1

Rough orders of magnitude for the cycle-averaged intensity, electric-field amplitude, photon-number density, and number of photons in a single cavity mode for main types of light source.†

	$\bar{I}(\mathrm{W\,m}^{-2})$	$E(\mathrm{V\,m}^{-1})$	$n/V(\mathrm{m}^{-3})$	photons/mode
Mercury lamp	10^4	10^3	10^{14}	10^{-2}
Continuous laser	10^5	10^4	10^{15}	10^{10}
Pulsed laser	10^{13}	10^8	10^{23}	10^{18}

† The mercury lamp figures refer to the 253.7-nm emission line and represent upper limits on the outputs of conventional spectroscopic sources. The laser figures are typical values rather than upper limits.

the character of light propagation changes. The conditions $B\bar{W} \ll A$ and $B\bar{W} \gg A$ lead to different types of beam absorption or amplification, as discussed later in the chapter.

1.9. Optical excitation of atoms

As a preliminary to the derivation of a microscopic expression for the absorption coefficient, we consider the atomic level populations achieved by irradiation with a light beam. Suppose that N atoms are contained in a thin cavity so that the beam intensity changes by a negligible amount during passage through the atoms. Let a beam of constant energy density $\bar{W}$ be switched on at time $t = 0$ when all the atoms are in their ground state. Then, by eqns (1.61) and (1.63) the number of atoms in their excited states at a later time t is

$$N_2 = \frac{NB\bar{W}}{A+2B\bar{W}}\{1 - \exp(-(A + 2B\bar{W})t)\}. \tag{1.70}$$

The dependence of N_2 on time is shown in Fig. 1.10. For short times,

$$(A+2B\bar{W})t \ll 1, \tag{1.71}$$

the number of excited atoms grows linearly with t,

$$N_2 = NB\bar{W}t, \tag{1.72}$$

while for long times,

$$(A+2B\bar{W})t \gg 1, \tag{1.73}$$

the number of excited atoms approaches its steady-state value

$$N_2 = NB\bar{W}/(A+2B\bar{W}). \tag{1.74}$$

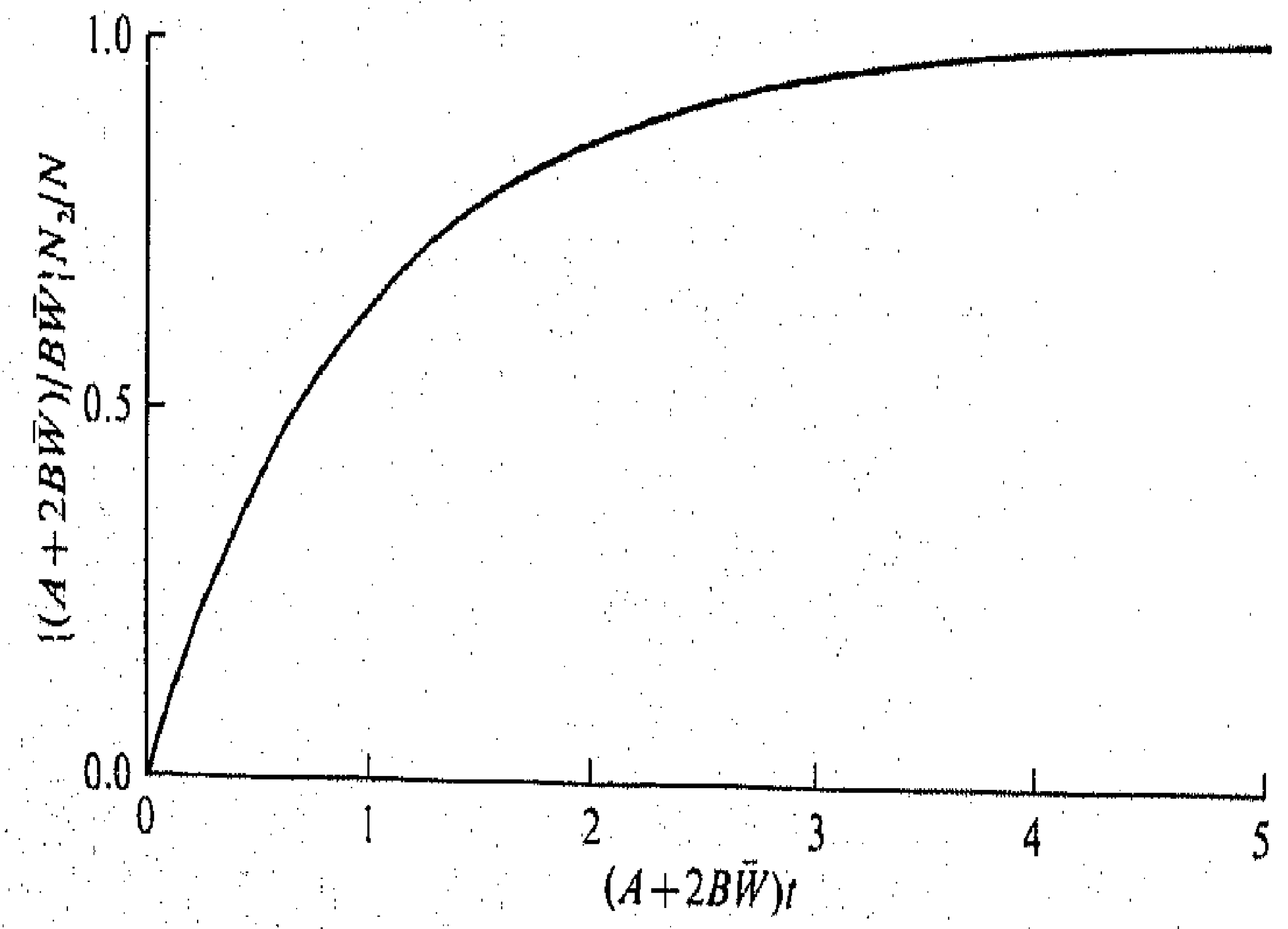

FIG. 1.10. Number of atoms in the excited state at time t.

When the light beam is first turned on, atoms are lifted into their excited states and energy is transferred from the light to the atoms. After the steady state is achieved, the atoms contain a constant amount of stored energy

$$N_2\hbar\omega = \frac{NB\bar{W}\hbar\omega}{A+2B\bar{W}} = \frac{N\bar{W}\hbar\omega}{(\hbar\omega^3/\pi^2c^3)+2\bar{W}}, \tag{1.75}$$

and the transfer of energy from the radiation ceases. The effect of the interaction between light and atoms is a redistribution of the spatial directions of the photons.

Fig. 1.11 shows the value of N_2 in the steady state. For ordinary light sources, where $B\bar{W} \ll A$, N_2 is much smaller than N and most of the atoms remain in their ground states. In this case, the second term in the denominator of eqn (1.74) can be neglected, and N_2 is proportional to the energy density of the incident light beam.

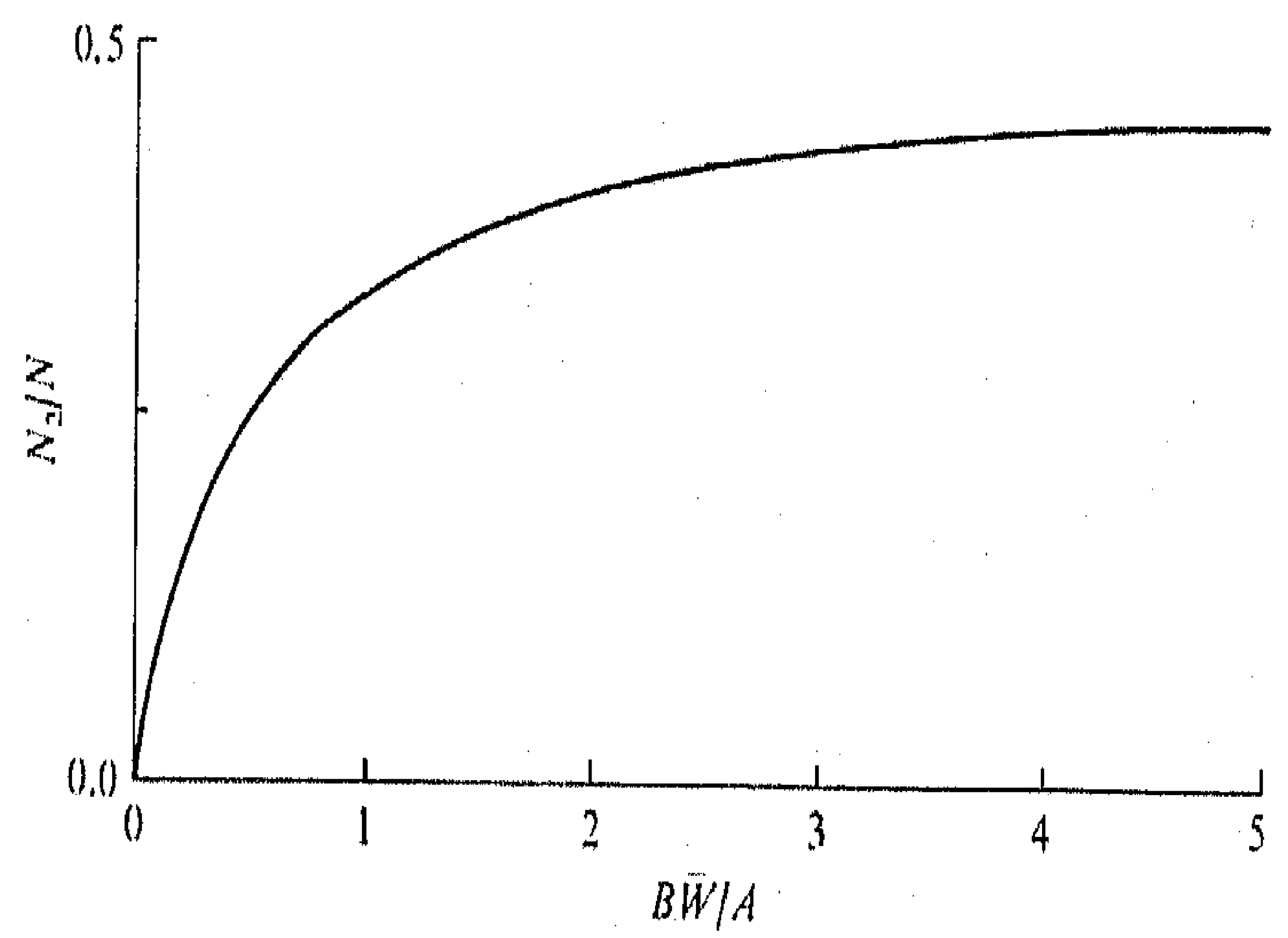

FIG. 1.11. Steady-state fraction of excited atoms as a function of light intensity.

For powerful laser sources, where $B\bar{W}$ approaches or exceeds A, the dependence of N_2 on the beam intensity becomes nonlinear, and the graph of N_2/N bends over to approach the value $\frac{1}{2}$ for $B\bar{W} \gg A$. The nonlinear behaviour is called *saturation* of the atomic transition. Saturation effects can usually be neglected for experiments using ordinary light beams, but they become important in the theories of experiments using laser light sources and in the theory of the operation of the laser itself. It is impossible to achieve the condition $N_2 > N_1$ in the type of experiment considered above.

If the incident beam is now turned off again, the excited atoms return to their ground states and the stored energy shown in eqn (1.75) is re-emitted as photons. Let N_2^0 be the steady-state excited-level population given by eqn (1.74) and let $t = 0$ be redefined as the instant at which the incident beam is removed. If the beam energy density $\bar{W}$ is set equal to zero in eqn (1.62), the rate equation becomes

$$\mathrm{d}N_2/\mathrm{d}t = -N_2A, \tag{1.76}$$

with solution

$$N_2 = N_2^0 \exp(-At). \tag{1.77}$$

Each decaying atom emits a quantum $\hbar\omega$, and the emitted light intensity also falls off as $\exp(-At)$. Observation of this fluorescent emission is an experimental means of measuring the Einstein A coefficient.

The reciprocal of A is denoted τ_R,

$$A = 1/\tau_R, \tag{1.78}$$

and is known as the fluorescent or radiative lifetime of the considered transition.

The results (1.70), (1.72), and (1.74) for N_2 refer to the mean population of the atomic excited state. Alternatively, N_2/N can be regarded as the probability of finding a selected atom in its excited state. Of course, a particular atom makes repeated upward and downward transitions as it absorbs and re-emits photons, these transitions occurring at random time intervals in accordance with the given absorption and emission probabilities. When the system achieves a steady state, N_2/N given by eqn (1.74) is the fraction of the time for which a particular atom is excited.

1.10. Macroscopic theory of absorption

Before we consider the microscopic nature of the optical attenuation process, it is convenient to summarize the relevant results of classical electromagnetic theory. A gas of atoms in a cavity can be regarded as a dielectric medium. We need the standard macroscopic theory of electromagnetic wave propagation through a dielectric.[9]

The presence of the dielectric leads to the generation of a polarization **P** by an applied electric field **E**. For electric fields that are not too strong, the polarization is proportional to the field,

$$\mathbf{P} = \epsilon_0\chi\mathbf{E}, \tag{1.79}$$

where χ is the linear electric susceptibility. The susceptibility is a function of the frequency ω of the applied field, whose form depends on the energy levels and wavefunctions of the atoms that make up the dielectric. Maxwell's equations still have wavelike solutions, but the relation between frequency and wavevector is generalized from eqn (1.9) to

$$(kc/\omega)^2 = 1+\chi, \tag{1.80}$$

which reduces to eqn (1.9) in the free-space limit $\chi = 0$. The quantity $1+\chi$ is known as the dielectric constant; of course, it is constant only in the sense of being independent of **E**, and its magnitude is a function of the frequency.

The susceptibility is generally a complex quantity and we write

$$\chi = \chi' + \mathrm{i}\chi''. \tag{1.81}$$

It is conventional to write the square root of eqn (1.80) as

$$kc/\omega = \eta + \mathrm{i}\kappa, \tag{1.82}$$

where η and κ defined in this way are, respectively, the refractive index and extinction coefficient. Comparison of the real and imaginary parts of eqn (1.80) after substitution of eqn (1.82) yields

$$\eta^2 - \kappa^2 = 1+\chi', \tag{1.83}$$

$$2\eta\kappa = \chi''. \tag{1.84}$$

These equations can be used to determine the frequency dependence of η and κ once the frequency-dependent susceptibility is known.

It is now convenient to consider travelling-wave solutions of Maxwell's equations rather than the standing waves of eqn (1.3). The space and time dependences of both **E** and **B** for a wave propagated in the z-direction are then given by

$$\exp \mathrm{i}(kz-\omega t) = \exp\left\{\mathrm{i}\omega\left(\frac{\eta z}{c}-t\right)-\frac{\omega\kappa z}{c}\right\}, \tag{1.85}$$

where eqn (1.82) has been used. The relation between the field amplitudes becomes

$$B_0 = (\epsilon_0\mu_0)^{\frac{1}{2}}(\eta+\mathrm{i}\kappa)E_0, \tag{1.86}$$

generalizing eqn (1.18). The cycle-averaged field energy density that is integrated in eqn (1.19) to obtain the total energy in the cavity is generalized to

$$\tfrac{1}{2}\epsilon_0\eta^2|\mathbf{E}(\mathbf{r}t)|^2 \tag{1.87}$$

by the presence of the dielectric.

The intensity **I** of the electromagnetic wave, defined as the energy crossing unit area in unit time, is given by the usual Poynting vector

$$\mathbf{I} = \mathbf{E}\times\mathbf{B}/\mu_0. \tag{1.88}$$

Thus according to eqn (1.16), the magnitude of the cycle-averaged Poynting vector is

$$\bar{I} = \tfrac{1}{2}\epsilon_0 c\eta|\mathbf{E}(\mathbf{r}t)|^2, \tag{1.89}$$

where eqn (1.86) has been used with the additional fact that **B** is at right angles to **E**. Since **E** varies with space and time in accordance with eqn (1.85), eqn

(1.89) shows that $\bar{I}$ depends only on position. If $\bar{I}_0$ is the cycle-averaged intensity at $z = 0$, we can write

$$\bar{I}(z) = \bar{I}_0 \exp(-Kz), \tag{1.90}$$

where

$$K = 2\omega\kappa/c. \tag{1.91}$$

The quantity K defined in this way is called the absorption coefficient; the intensity of an electromagnetic wave falls to $1/e$ of its initial value in a distance $1/K$.

1.11. Microscopic theory of absorption

We now consider from a microscopic viewpoint the same process of attenuation of a light beam during its passage through a gas of atoms contained in a thick cavity. The aim is to relate the attenuation rate, and hence the absorption coefficient, to the coefficients of the Einstein theory.

We suppose a steady state to have been reached, so that the rates of change (1.62) can be set equal to zero. There is however a small change in the rate equation necessitated by the presence of the dielectric. The Einstein B coefficients are defined in terms of an electromagnetic wave incident on a single atom in free space, where the energy density is related to the electric field as in eqns (1.19) or (1.34). If $\bar{W}$ is now taken to be the energy density in the dielectric, with the additional η^2 factor as in eqn (1.87), it is necessary to remove this factor from the rates of absorption and stimulated emission. The steady-state condition obtained from eqn (1.62) therefore reads

$$N_2 A = (N_1 - N_2)B\bar{W}/\eta^2. \tag{1.92}$$

The rate at which energy is scattered out of the beam by spontaneous emission is $N_2 A\hbar\omega$. The net rate of loss of energy from the beam is equal to the rate $N_1 B\bar{W}\hbar\omega/\eta^2$ at which energy is taken out of the beam by absorption, minus the rate $N_2 B\bar{W}\hbar\omega/\eta^2$ at which energy is put back in the beam by stimulated emission. In the steady state the two ways of computing the change in beam energy must be identical as in eqn. (1.92).

We use the right-hand side of eqn (1.92) to compute the rate of attenuation of the beam, but we must first refine the description of the atomic transitions. It has been assumed so far that all atoms have an identical sharply-defined transition frequency ω. However, as discussed in Chapter 2, there is always some statistical spread in the frequencies of photons that atoms can absorb or emit, even when the same pair of states is considered for each atom. Let $F(\omega)\,d\omega$ be the fraction of the transitions in which the photon frequency lies in a small range $d\omega$ about frequency ω. Fig. 1.12 shows the typical variation of $F(\omega)$ with frequency, the area under the curve being normalized to unity.

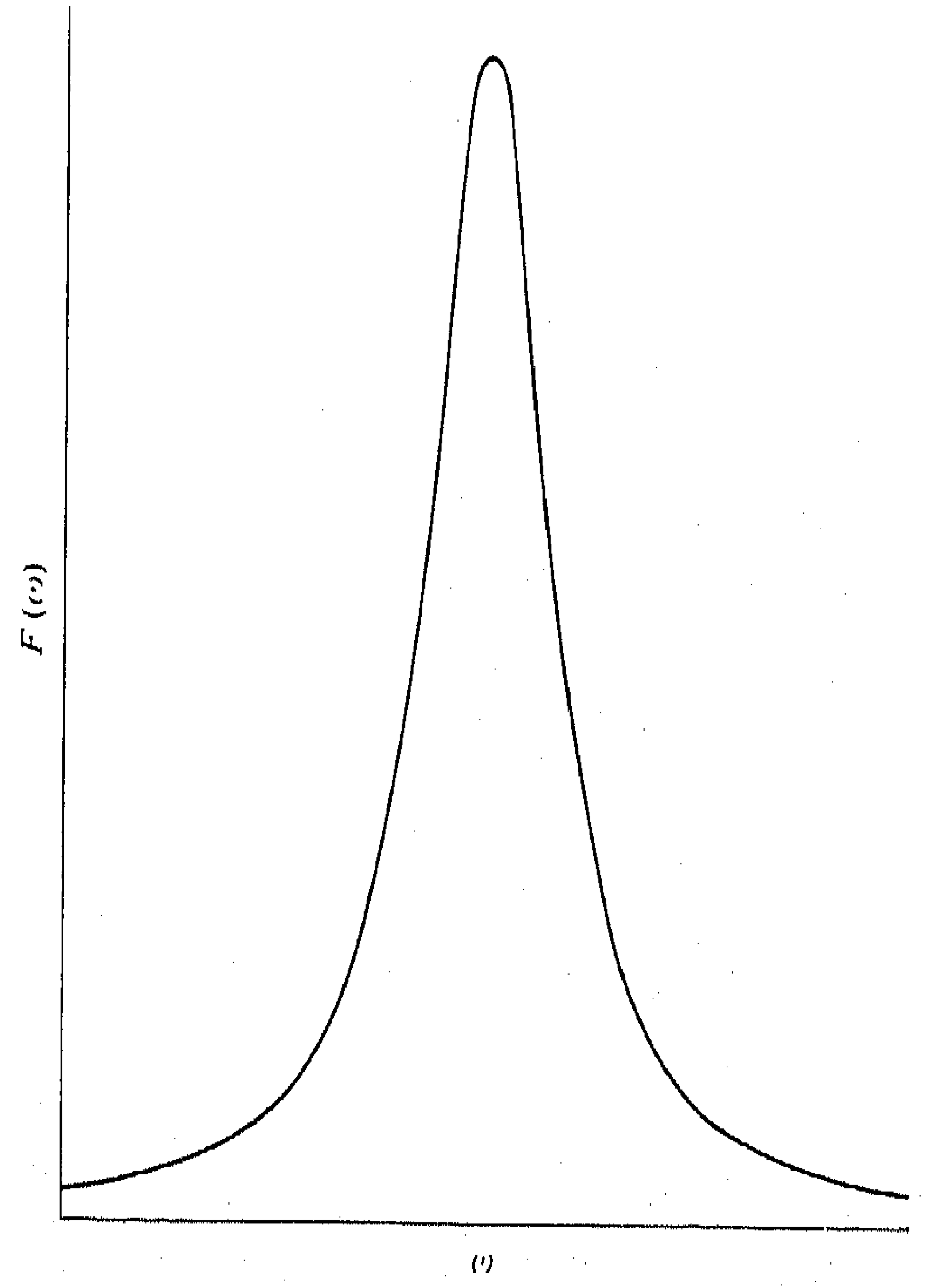

FIG. 1.12. Distribution of atomic transition frequencies.

Consider for the time being only those transitions for which the frequency ω lies in the specified range. In the steady state, where N_1 atoms are in the lower atomic level and N_2 are in the upper level, the rate of change of the beam energy in the frequency range $d\omega$ is equal to $-(N_1 - N_2)F(\omega)\,d\omega\; B\bar{W}\hbar\omega/\eta^2$.

Let the light beam be propagated parallel to the z-axis. The energy density $\bar{W}$ is a function of z owing to beam attenuation. Consider a thin slice of the cavity perpendicular to z, having thickness dz and cross-sectional area a, as illustrated in Fig. 1.13. The beam energy in the slice in the frequency range $d\omega$ is $\bar{W}\,d\omega a\,dz$, where $\bar{W}$ is assumed independent of position within the slice.

If V is the total cavity volume, then $a\,dz/V$ is the fractional number of atoms that are located in the slice considered. The condition for energy balance is

$$(\partial/\partial t)(\bar{W}\,d\omega a\,dz) = -(N_1 - N_2)F(\omega)\,d\omega B\bar{W}\hbar\omega(a\,dz/V\eta^2), \tag{1.93}$$

or, rearranging,

$$\partial\bar{W}/\partial t = -(N_1 - N_2)F(\omega)B\bar{W}\hbar\omega/V\eta^2. \tag{1.94}$$

The absorption coefficient K introduced in eqn (1.90) governs the spatial change of the beam *intensity* $\bar{I}$, whereas the Einstein theory leads to an

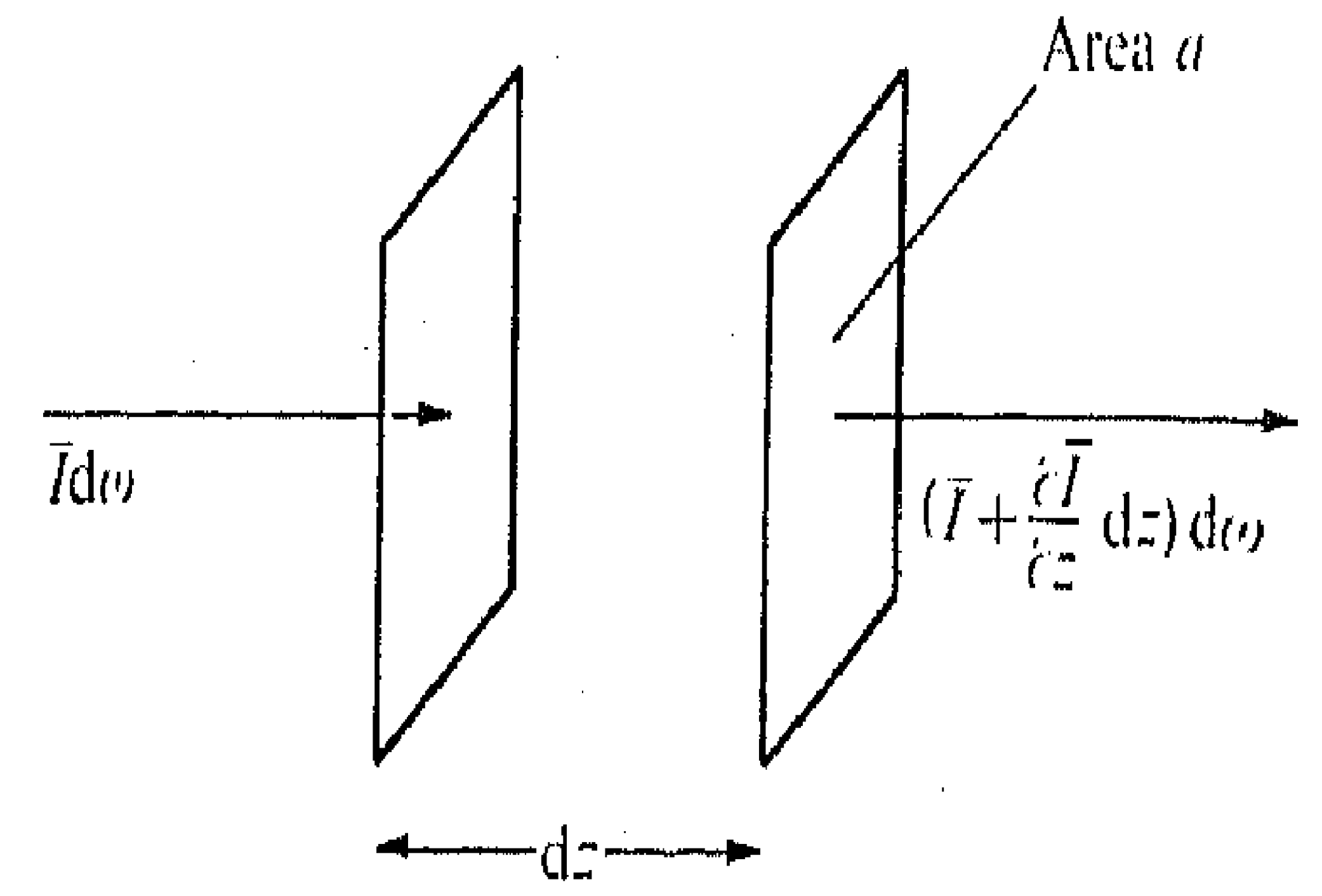
Area a
$\bar{I}\,\mathrm{d}\omega$
$(\bar{I}+\frac{\partial\bar{I}}{\partial z}\,\mathrm{d}z)\,\mathrm{d}\omega$
$\mathrm{d}z$

FIG. 1.13. Thin slice of cavity perpendicular to the beam direction.

equation for the time dependence of the beam *energy density* $\bar{W}$. Eqn (1.94) must be recast in terms of the intensity.

The left-hand side of eqn (1.94) can be converted by equating the rate of loss of energy within the slice, given by minus the left-hand side of eqn (1.93), to the net rate at which energy flows into the slice across its boundaries. If $\bar{I}\,\mathrm{d}\omega$ is the beam intensity between ω and $\omega+\mathrm{d}\omega$ then, by reference to Fig. 1.13,

$$-(\partial/\partial t)(\bar{W}\,\mathrm{d}\omega a\,\mathrm{d}z) = -a(\partial\bar{I}/\partial z)\,\mathrm{d}z\,\mathrm{d}\omega \tag{1.95}$$

or

$$\partial\bar{W}/\partial t = \partial\bar{I}/\partial z. \tag{1.96}$$

For conversion of the right-hand side of eqn (1.94), comparison of eqns (1.87) and (1.89) shows that

$$c\bar{W} = \eta\bar{I}. \tag{1.97}$$

Substitution of eqns (1.96) and (1.97) into eqn (1.94) yields the required equation for the spatial dependence of $\bar{I}$,

$$\partial\bar{I}/\partial z = -(N_1-N_2)F(\omega)(B\hbar\omega/Vc\eta)\bar{I}. \tag{1.98}$$

For degenerate energy levels, this equation is generalized by insertion of a factor g_2/g_1 which multiplies N_1. However, the subsequent discussion is restricted to the case $g_1 = g_2$ where the additional factor is equal to unity.

The solution of this equation is more complicated than at first appears because N_1 and N_2 themselves depend on $\bar{W}$ and hence on $\bar{I}$. According to eqns (1.74) and (1.97)

$$N_1-N_2 = NA/\{A+(2B\bar{W}/\eta^2)\} = NA/\{A+(2B\bar{I}/c\eta)\} \tag{1.99}$$

with the appropriate refractive index factors inserted. Thus eqn (1.98) can be written

$$\frac{1}{\bar{I}}\left(1+\frac{2B\bar{I}}{Ac\eta}\right)\frac{\partial\bar{I}}{\partial z} = -\frac{NB\hbar\omega F(\omega)}{Vc\eta}. \tag{1.100}$$

We consider the solution in two extreme cases.

For all ordinary light beams, the second term in the bracket on the left of eqn (1.100) (equal to $2B\bar{W}/\eta^2A$) is much smaller than unity, as discussed earlier in the chapter. If this term is neglected, which corresponds to neglect of the number N_2 of excited atoms, eqn (1.100) can be integrated to give

$$\bar{I}(z) = \bar{I}_0\exp(-Kz), \tag{1.101}$$

where

$$K = NB\hbar\omega F(\omega)/Vc\eta. \tag{1.102}$$

Eqn (1.101) is the same as eqn (1.90), and the absorption coefficient K defined by eqn (1.102) is the same absorption coefficient as defined in eqn (1.91). It is seen that K varies with frequency in a similar way to the distribution of atomic transition frequencies illustrated in Fig. 1.12, but multiplied by additional frequency-dependent factors.

With the factor $\hbar\omega/c\eta$ taken over to the left in eqn (1.102), integration of both sides over ω gives

$$\int(Kc\eta/\hbar\omega)\,\mathrm{d}\omega = NB/V, \tag{1.103}$$

where the normalization of the lineshape function $F(\omega)$ has been used. It is therefore possible to determine experimentally the value of B if K and η can be measured. For a dilute atomic gas, η is close to the free-space value of unity. Most absorption lines have widths that are small compared to the frequencies ω for which K is significantly large, and ω is nearly constant across the absorption line. In this case, B is directly proportional to the area under a graph of K as a function of ω. The functional form of K is discussed in Chapter 2.

The result (1.103) can be rewritten as an integral of the imaginary part χ'' of the susceptibility over the frequency spread of the absorption line considered,

$$\int\chi''\,\mathrm{d}\omega = \hbar NB/V, \tag{1.104}$$

where eqns (1.84) and (1.91) have been used.

We now consider the solution of eqn (1.100) in the other extreme case of a very intense light beam where $2B\bar{W}/A$ is much larger than unity and the dependence of the atomic populations on $\bar{W}$ becomes nonlinear, as discussed earlier. The first term in the bracket of eqn (1.100) can now be neglected, and the solution is

$$\bar{I}(z)-\bar{I}_0 = -(NA\hbar\omega F(\omega)/2V)z. \tag{1.105}$$

The beam intensity thus falls off linearly with distance through the cavity at a rate determined by the A coefficient, instead of the more rapid exponential fall-off determined by the B coefficient for low intensities.

The decrease in absorption as the atomic transition approaches saturation is due to the approach of the rate $N_2 A\hbar\omega$ of scattering of energy out of the beam to its maximum value $\frac{1}{2}NA\hbar\omega$. Any further increase in the beam intensity $\bar{I}$ cannot lead to a proportionate increase in the scattering rate, and the fractional change in $\bar{I}$ in traversing the gas decreases. The macroscopic theory of absorption based on Maxwell's equations does not apply in saturation conditions. Saturation must obviously be avoided in measurements of the absorption coefficient K if the results are to be interpreted in terms of the theory leading to eqn (1.103).

1.12. Population inversion: the laser

If the number N_2 of excited atoms can be made larger than the number N_1 of atoms in their ground states, eqn (1.98) shows that the beam intensity grows with distance through the atomic gas. The dependence is similar to eqn (1.101) except that the absorption coefficient is now negative. The condition $N_2 > N_1$ is known as population inversion, or sometimes as a negative-temperature condition since application of Boltzmann's law (eqn 1.48) implies T negative. More generally, for degenerate energy levels, the condition for a growing beam intensity is $N_2 > (g_2/g_1)N_1$.

Of course, population inversion can never occur in thermal equilibrium, and we have shown earlier that it cannot be achieved by resonant absorption of light at the transition frequency of the two states. However, population inversion can be achieved for levels 1 and 2 by experiments that make use of other energy levels of the atom. The simplest process makes use of three levels. Consider the case where all three levels are non-degenerate, to make the treatment as simple as possible. The refractive index η is also set equal to unity.

The arrangement of transitions is shown in Fig. 1.14. We now label the ground state as level 3, and levels 1 and 2 are the first and second excited states of the atom. A light beam of energy density $\bar{W}_P$ is used to excite the transition 3 → 2, so that a number N_2 of the atoms are in state 2. A light beam used in this way is called a pump. The fraction N_2/N of the total number of atoms pumped up in this way is usually fairly small, a figure of one in a million being typical, so that the transition 3 → 2 is far from the saturation condition.

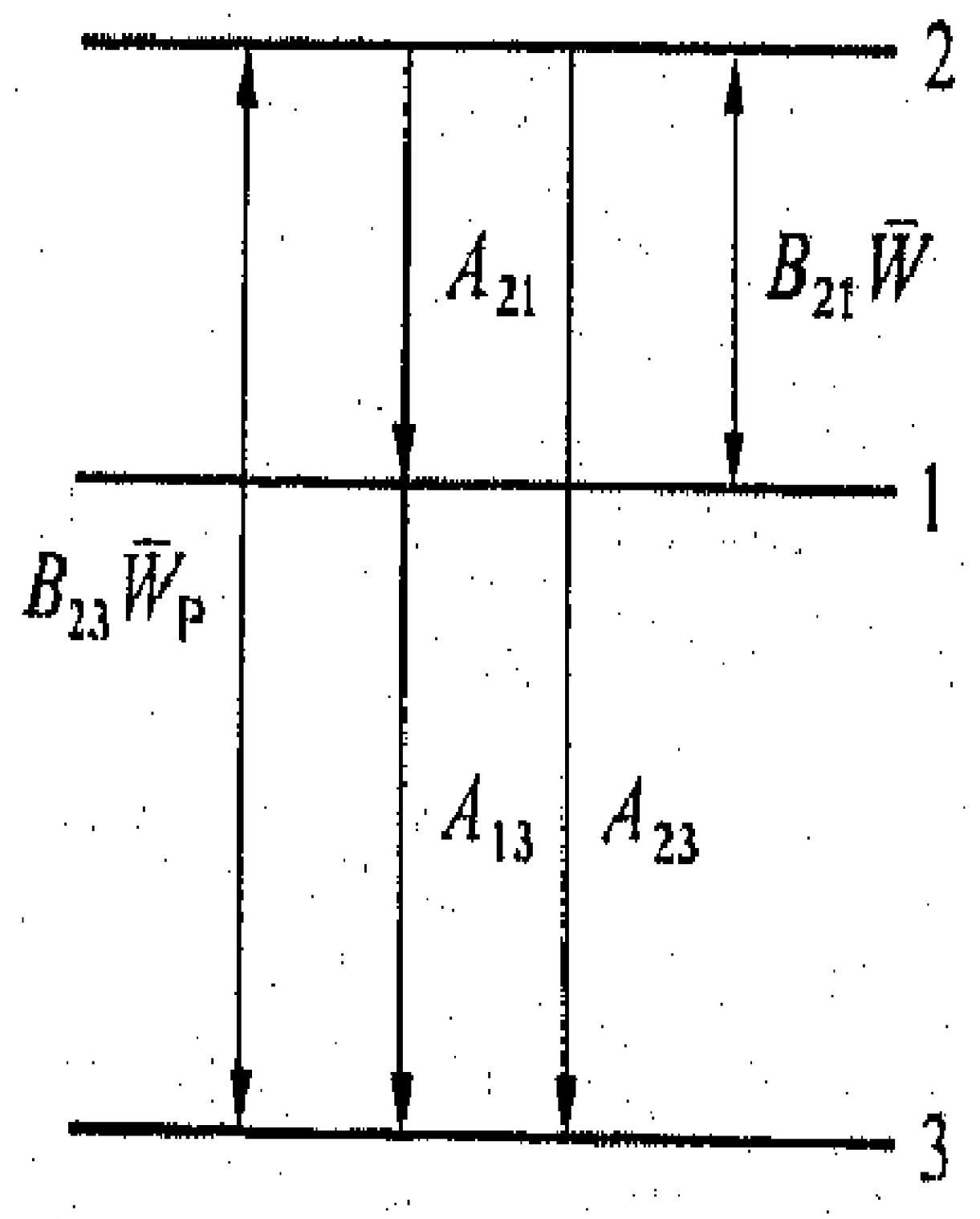

FIG. 1.14. Atomic energy levels and transition rates for a three-level laser.

An atom in level 2 can emit light by making downwards transitions 2 → 1 or 2 → 3; an atom in level 1 can decay back into the ground state 3. We show that for appropriate values of the Einstein coefficients, it is possible to achieve the condition $N_2 > N_1$ and thus amplify light of frequency $\omega = (E_2 - E_1)/\hbar$.

The equations that govern the transition rates for a three-level system are simple generalizations of the rate equations for a two-level system. The transition processes are all shown in Fig. 1.14. The Einstein coefficients must now be subscripted to show which levels they refer to. In addition to the radiative energy in the pump beam, we also assume that some light of energy density $\bar{W}$ is present at the frequency ω.

We assume that only the three atomic levels considered are populated, so that

$$N_1 + N_2 + N_3 = N. \tag{1.106}$$

The three rate equations are

$$\mathrm{d}N_2/\mathrm{d}t = -N_2 A_{21} - N_2 A_{23} + \bar{W}_P B_{23}(N_3 - N_2) - \bar{W} B_{21}(N_2 - N_1), \tag{1.107}$$

$$\mathrm{d}N_1/\mathrm{d}t = N_2 A_{21} - N_1 A_{13} + \bar{W} B_{21}(N_2 - N_1), \tag{1.108}$$

and

$$\mathrm{d}N_3/\mathrm{d}t = N_2 A_{23} + N_1 A_{13} - \bar{W}_P B_{23}(N_3 - N_2). \tag{1.109}$$

The sum of the three rates is zero in accordance with eqn (1.106)

All the time derivatives can be set equal to zero in the steady state. The resulting equations enable solutions to be found for the level populations N_1, N_2, and N_3 in terms of N, $\bar{W}$, and $\bar{W}_P$. The expressions are somewhat lengthy, and the main features of the steady-state solutions can be appreciated more easily by the following procedure. Let the pumping rate r be defined as

$$r = \bar{W}_P B_{23}(N_3 - N_2)/N, \tag{1.110}$$

so that Nr is the net rate at which atoms are promoted into state 2 by the pump. The steady-state conditions from eqns (1.108) and (1.109) are then

$$N_2(A_{21} + B_{21}\bar{W}) = N_1(A_{13} + B_{21}\bar{W}) \tag{1.111}$$

and

$$N_2 A_{23} + N_1 A_{13} = Nr. \tag{1.112}$$

It is immediately evident from eqn (1.111) that in order for N_2 to be larger than N_1, the condition

$$A_{21} < A_{13} \tag{1.113}$$

must be satisfied. In words, the atoms excited into state 2 must decay relatively slowly into state 1, from where they drop rapidly back into the ground state. The solutions of eqns (1.111) and (1.112) are

$$N_1 = \frac{N(A_{21}+B_{21}\bar{W})r}{A_{13}(A_{23}+A_{21})+B_{21}\bar{W}(A_{13}+A_{23})} \tag{1.114}$$

and

$$N_2 = \frac{N(A_{13}+B_{21}\bar{W})r}{A_{13}(A_{23}+A_{21})+B_{21}\bar{W}(A_{13}+A_{23})}. \tag{1.115}$$

A gas of atoms for which the condition (1.113) is satisfied is capable of amplifying the radiation of energy density $\bar{W}$. The theory is similar to that given above for the absorption of light, with some appropriate changes of sign. The structure of the expression for N_2-N_1 obtained from eqns (1.114) and (1.115) is similar to that for N_1-N_2 in the absorption case given by eqn (1.99). For low intensities of the beam to be amplified, eqns (1.114) and (1.115) show that N_2-N_1 is virtually independent of $\bar{W}$. For this case the beam intensity grows exponentially with distance through the gas. On the other hand, for high beam intensities N_2-N_1 is inversely proportional to the beam intensity, and the transition between levels 1 and 2 approaches saturation. In this case the amplification decreases and the beam intensity grows only linearly with distance. Detailed results for the two limits are given in the following problem.

Problem 1.4. Show that the analogue of eqn (1.100) for the case of amplification is

$$\frac{1}{\bar{I}}\left(1+\frac{\bar{I}}{I_c}\right)\frac{\partial \bar{I}}{\partial z} = G, \tag{1.116}$$

where

$$I_c = \frac{A_{13}(A_{23}+A_{21})}{A_{13}+A_{23}}\,\frac{c}{B_{21}} \tag{1.117}$$

and

$$G = \frac{r(A_{13}-A_{21})}{A_{13}(A_{23}+A_{21})}\,\frac{NB_{21}\hbar\omega F(\omega)}{Vc}. \tag{1.118}$$

The general solution is

$$\ln(\bar{I}/\bar{I}_0)+\{(\bar{I}-\bar{I}_0)/I_c\} = Gz \tag{1.119}$$

and leads in the limits of low and high intensities to

$$\bar{I}(z) = \bar{I}_0\exp(Gz) \qquad (\bar{I} \ll I_c) \tag{1.120}$$

and

$$\bar{I}(z) = \bar{I}_0+I_cGz \qquad (\bar{I} \gg I_c). \tag{1.121}$$

The general solution is plotted in Fig. 1.15 for two values of $\bar{I}_0$.

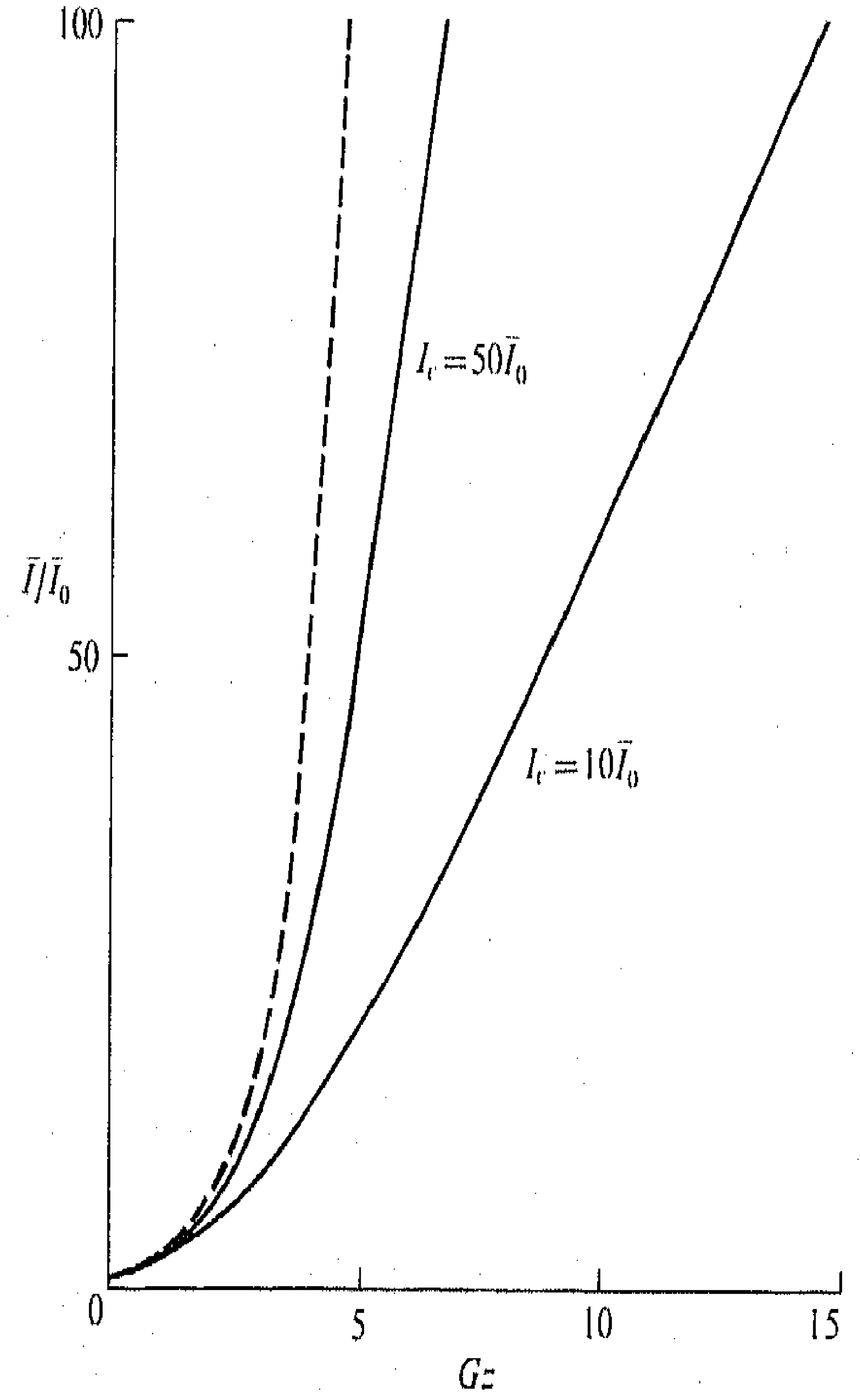

FIG. 1.15. Growth in intensity for a light beam in an amplifying medium for two values of $\bar{I}_0/I_c$. The regions of exponential and linear growth are clearly visible. The broken curve is a plot of eqn (1.120).

A light amplifier of the type described above is called a three-level laser. The laser can also act as a self-sustaining oscillator since even if no energy density $\bar{W}$ is present initially, some radiation at frequency ω can appear owing to the spontaneous emission rate A_{21}. Such an oscillator can produce light beams of very high intensity (see Table 1.1), and the nonlinear effects associated with the saturation of the active transition play an important role in determining the characteristics of the output beam. Other types of laser are possible in which more complicated atomic energy-level schemes are utilized. The three-level laser theory outlined above is considerably expanded in Chapter 7.

1.13. Radiation pressure

The photons that make up a travelling electromagnetic wave of wavevector **k** each carry a momentum $\hbar\mathbf{k}$. Their behaviour in this respect is similar to that of other particles in quantum mechanics, being governed by the de Broglie relation between particle wavelength and momentum. The total momentum is conserved in any interaction of photons with other particles. The reality of photon momentum was strikingly demonstrated by Compton, who, in 1922, observed the conservation of momentum in the scattering of photons by electrons. He used X-ray photons and free electrons, where the effects of photon momentum are particularly important. However, the photon momentum can lead to interesting consequences even in the interactions of lower-energy visible photons with relatively heavy atoms. The most accurate measurements of the momentum are currently made by determining the torsional force on a suspended mirror illuminated asymmetrically by a light beam[10]. The expression $\hbar\mathbf{k}$ for the momentum of a photon of wavevector $\mathbf{k}$ in vacuum has been verified to high accuracy, as has the modification of the momentum to $\eta\hbar\mathbf{k}$ in a medium of refractive index η (see also ref. 11).

Consider the effects of photon momentum on the three basic interactions of a beam of light with a gas of atoms, illustrated in Fig. 1.9. In an absorption process an amount of momentum $\hbar\mathbf{k}$ is transferred from the light beam to the absorbing atom, which acquires a velocity $\hbar\mathbf{k}/M$ parallel to the beam, where M is the atomic mass. If the excited atom subsequently decays by stimulated emission, the emitted photon carries away a momentum $\hbar\mathbf{k}$ parallel to the incident beam, and the atom loses the velocity it had previously gained.

If, however, the excited atom subsequently decays by spontaneous emission, the direction of the momentum carried away by the emitted photon may lie anywhere in the complete 4π solid angle centered on the atom. The atom thus acquires a recoil velocity in some *random* direction, and there is, on the average, no cancellation of the velocity component previously acquired by the atom in photon absorption.

It follows that each photon absorption that is followed by spontaneous emission transfers on average a momentum $\hbar\mathbf{k}$ from the photons to the atoms, in the direction of the light beam. This is true whether or not the atom-radiation system has reached a steady state, and contrasts with the transfer of excitation energies $\hbar\omega$ to the atoms, which ceases when a steady state is achieved, as emphasized in connection with eqn (1.75). The transfer of momentum to the atoms is equivalent to a pressure exerted on the gas by the radiation.

Suppose again that the number N of atoms is sufficiently large to produce smooth time dependences in the atomic populations. The rate of change of the total atomic momentum $\mathbf{\Pi}$, in the presence of radiative energy density $\bar{W}$ at a frequency ω that resonates with the transition between the atomic ground state and a single excited state, is proportional to the difference between the absorption and stimulated emission rates,

$$\mathrm{d}\mathbf{\Pi}/\mathrm{d}t = \hbar\mathbf{k}(N_1 - N_2)B\bar{W}. \tag{1.122}$$

This quantity is always positive for a two-level experiment, where $N_1 > N_2$, but it is possible to obtain negative momentum transfers[12] for transition schemes that use three or more levels, where N_2 can be greater than N_1. We treat here only the two-level case.

Problem 1.5. Evaluate the momentum transfer rate for the experiment envisaged in §1.9, where a light beam impinges on a gas of atoms in their ground states at the start of the experiment. Show that the atomic momentum at time t is

$$\mathbf{\Pi} = \frac{NB\bar{W}\hbar\mathbf{k}}{A+2B\bar{W}}\left\{At - \frac{2B\bar{W}}{A+2B\bar{W}}\left(\exp[-(A+2B\bar{W})t]-1\right)\right\}, \tag{1.123}$$

and discuss the limiting forms of the result at both short and long times.

In the steady state, where the number of excited atoms is given by eqn (1.74), the momentum transfer rate becomes

$$\mathrm{d}\mathbf{\Pi}/\mathrm{d}t = \hbar\mathbf{k}N_2A = \hbar\mathbf{k}NB\bar{W}A/(A+2B\bar{W}). \tag{1.124}$$

The transfer rate tends towards a saturation value

$$\mathrm{d}\mathbf{\Pi}/\mathrm{d}t = \hbar\mathbf{k}(N/2)A \qquad (B\bar{W} \gg A) \tag{1.125}$$

for very strong light beams. The dependence of the momentum transfer effect on the presence of the spontaneous emission process thus produces an upper limit to the transfer rate at beam strengths such that almost half the atoms are excited. Any increase of beam strength produces little change in the momentum transfer rate once the saturation region has been reached.

The steady-state momentum transfer rate (1.124) is equivalent to an average force acting on each atom of magnitude

$$F = \hbar kB\bar{W}A/(A+2B\bar{W}). \tag{1.126}$$

An applied light beam drives the atoms in a cavity parallel to the beam direction to give a higher atomic density at the light exit window than at the entrance window. If the z-axis is parallel to the beam and $N(z)$ is the atomic density at coordinate z, the distribution of atoms at temperature T has the form

$$N(z) = N(0)\exp(Fz/k_BT). \tag{1.127}$$

This spatial dependence has been verified[13] for a gas of sodium atoms placed in a tube with a beam of laser light directed along the length of the tube. The laser frequency resonated with the $3S_{\frac{1}{2}} \rightarrow 3P_{\frac{3}{2}}$ transition of sodium. Increases in the density of sodium atoms by as much as 50 per cent were observed between points in the laser beam separated by 200 mm.

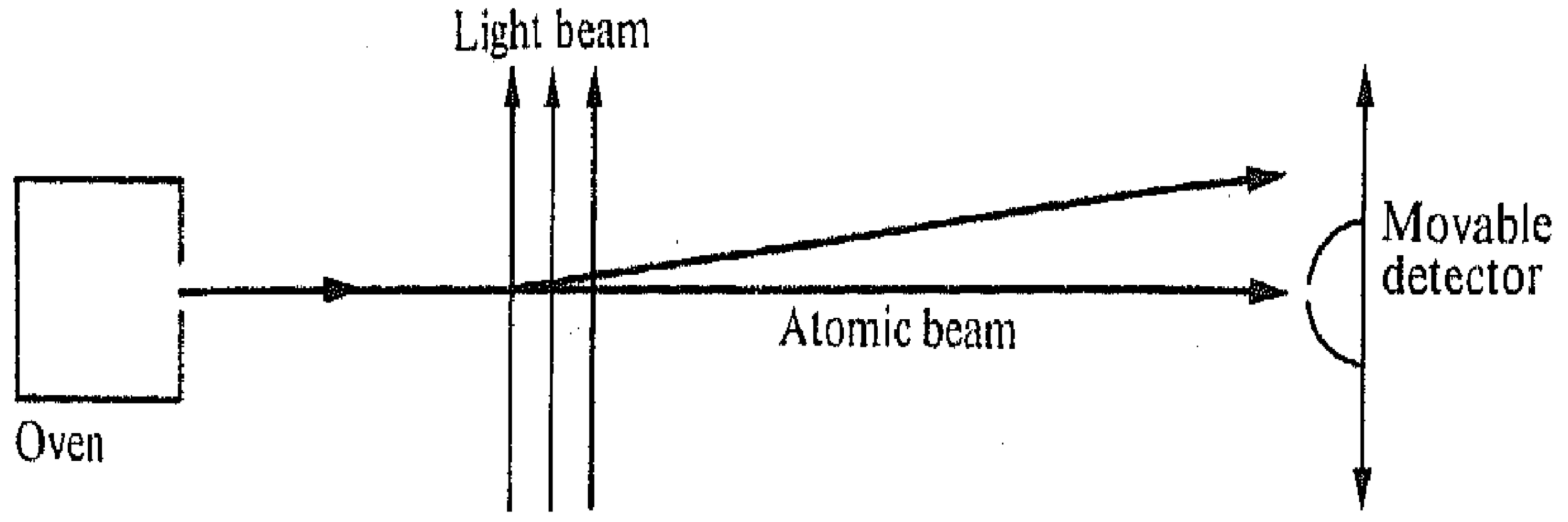

FIG. 1.16. Schematic arrangement for observation of the deflection of an atomic beam by interaction with a light beam.

Momentum transfer between photons and atoms leads to practical applications when the atoms are also in the form of a beam sent at right angles through a strong light beam[14]. The experimental arrangement is represented in Fig. 1.16. Those atoms that absorb photons are deflected from their original paths. Absorption followed by stimulated emission produces a small lateral shift in the atomic trajectory but no change in its direction. The main effect occurs as before for absorption followed by spontaneous emission, where the atom gains on average a momentum $\hbar\mathbf{k}$ perpendicular to its original path. The resulting deflection angle is typically of order 10^{-5} rad. Fig. 1.17 shows the distributions of the numbers of caesium atoms detected[15] as functions of distance perpendicular to the direction of the atomic beam. The average deflection corresponds to the absorption and spontaneous emission of about 6 photons by each atom during its passage through the light beam.

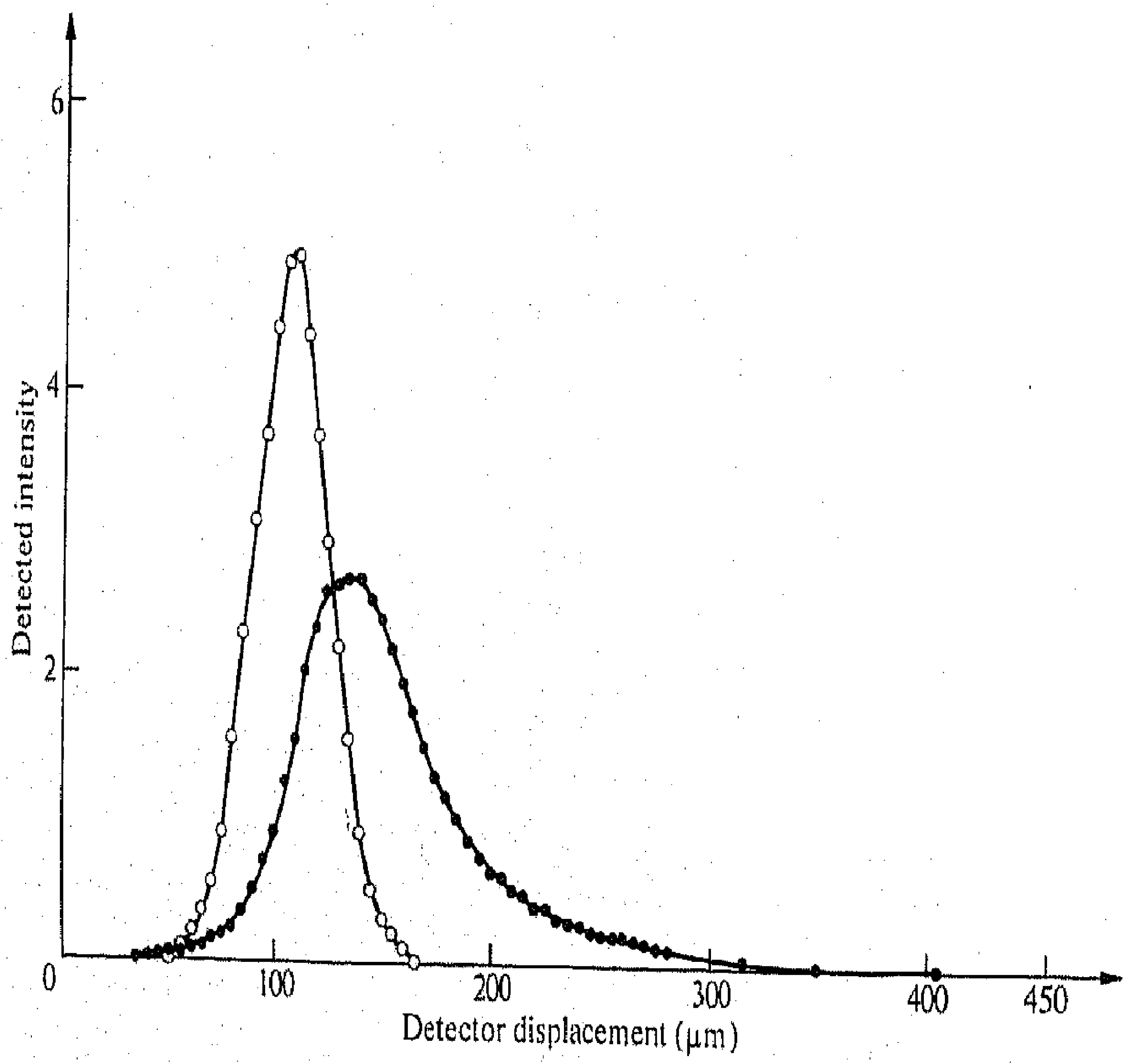

FIG. 1.17. Deflection of a beam of caesium atoms by light: ○ laser off, and ● laser turned on. (After J. L. Picqué and J. L. Vialle, ref. 15.)

It is possible, with the use of very strong light beams, to achieve a much larger number of photon absorptions and emissions per atom. Thus in the saturation region, where the rate of absorption/spontaneous emission events is of the order of one half the Einstein A coefficient, the number of such events is roughly $\frac{1}{2}A$ times the transit period of the atom through the light beam. This produces an average of 50 absorption/spontaneous emission events per atom for a light beam diameter of 5 mm, an atomic velocity of $5 \times 10^3\ \mathrm{m\,s^{-1}}$, and an A coefficient of $10^8\ \mathrm{s^{-1}}$ (see §2.4). Note that the saturation prevents the possibility of any significant increase in the number of spontaneous emissions for yet stronger light beams.

The electronic excitation energies of different isotopes of the same atom are in general slightly different, typically by about 1 part in 10^5. The frequency of the light beam in the arrangement of Fig. 1.16 can be tuned to resonate with a transition frequency of only one variety in a mixture of isotopes. The radiation pressure force then acts on only the one kind of isotope, which is deflected away from the remainder of the atomic beam. This method has been used for example to separate the various isotopes of barium[16]. It is of course advantageous to obtain the maximum spatial separation of the isotope of interest by the use of a light beam sufficiently strong to saturate the atomic transition. The radiation-pressure method is one of a range of optical techniques that can be used to separate isotopes[17].

References

1. Planck, M. (1900). *Verh. dt. phys. Ges.* **2,** 202 and 237.
2. Einstein, A. (1905). *Annln Phys.* **17,** 132.
3. Lewis, G. N. (1926). *Nature* **118,** 874.
4. Einstein, A. (1917). *Phys. Z.* **18,** 121.
   References 1, 2, and 4 are reprinted in English and discussed in detail by ter Haar, D. (1967). In *The old quantum theory.* Pergamon, Oxford.
5. Rayleigh, Lord (1900). *Phil. Mag.* **49,** 539.
6. Wien, W. (1896). *Annln. Phys.* **58,** 662.
7. Wien, W. (1893). *Ber. Berlin Akad. Wiss.* 9 Feb.
8. See, for example, Balescu, R. (1975). *Equilibrium and nonequilibrium statistical mechanics.* Wiley, New York. The equivalence of ensemble and time averages is discussed by Kittel, C. (1969). *Thermal physics,* p. 32. Wiley, New York.
9. See, for example, Reitz, J. R., Milford, F. J., and Christy, R. W. (1979). *Foundations of electromagnetic theory.* Addison-Wesley, Reading, Massachusetts.
10. Jones, R. V. and Leslie, B. (1978). *Proc. R. Soc.* **A360,** 347.
11. Gibson, A. F., Kimmitt, M. F., Koohian, A. O., Evans, D. E., and Levy, G. F. D. (1980). *Proc. R. Soc.* **A370,** 303.

12. COOK, R. J. (1980). *Optics Commun.* **32**, 235.
13. BJORKHOLM, J. E., ASHKIN, A., and PEARSON, D. B. (1975). *Appl. Phys. Lett.* **27**, 534.
14. ASHKIN, A. (1970) *Phys. Rev. Lett.* **25**, 1321.
15. PICQUÉ, J. L. and VIALLE, J. L. (1972). *Optics Commun.* **5**, 402.
16. BERNHARDT, A. F. (1976). *Appl. Phys.* **9**, 19.
17. ZARE, R. N. (Feb. 1977). *Sci. Amer.* **236**, 86.

2. Quantum mechanics of the atom–radiation interaction

THE calculations of the preceding chapter display some of the inadequacies of the Einstein theory of interaction of light with atoms. The theory itself gives no prescription for computing the values of the A and B coefficients appropriate to a given atomic transition. For this one must look to the quantum-mechanical theory of transition probabilities. More seriously, the Einstein theory is applicable only for broad-band illumination of the atom, where the frequencies in the incident light are distributed smoothly across the linewidth of the atomic transition. By contrast, many experiments with laser sources use light beams whose frequency distributions are narrower than atomic transition linewidths.

The present chapter begins with a quantum-mechanical calculation of the Einstein B coefficient. A semiclassical theory is used, with a classical representation of the electromagnetic field but a quantum-mechanical description of the atomic states. Identical results are obtained when both the light and the atom are treated quantum-mechanically (see Chapter 5). We assume that there is no thermal excitation of the atomic excited states, and that the only atomic states that need be considered are the ground state and a single excited state selected by the frequency of the light. The atoms can then be treated as effectively having just two levels, with consequent simplifications in the theory.

The interpretation of experiments with light beams of narrow frequency spread requires a more general theory of the effects of the atom–radiation interaction. Such a theory is provided by the optical Bloch equations, derived later in the chapter. It is shown that the behaviours of the atomic populations predicted by the optical Bloch equations agree with those of the Einstein theory in the limit of broad-band incident light. However, quite different behaviours occur for narrow-band incident light. It is also shown how various line-broadening mechanisms affect the theory of the atom–radiation interaction. These produce changes in the time dependences of the atomic-level populations and they generate characteristic shapes for the spectral lines seen in absorption or emission by atomic transitions.

2.1. Time-dependent quantum mechanics

The Einstein B coefficient describes the rate in time at which absorption and stimulated emission processes occur. The corresponding quantum-mechanical treatment must accordingly take as its starting point the time-dependent wave equation[1]

$$\hat{\mathscr{H}}\Psi = \mathrm{i}\hbar\,\mathrm{d}\Psi/\mathrm{d}t. \tag{2.1}$$

Here, $\hat{\mathscr{H}}$ is the quantum-mechanical Hamiltonian, in general time-dependent, and Ψ is the time-dependent wavefunction. A circumflex will be used throughout the book to signify quantities that are quantum-mechanical operators.

Consider first the problem of an isolated atom with no radiation present. The atomic Hamiltonian $\hat{\mathscr{H}}_{\mathrm{E}}$ contains the kinetic and potential energies of the constituent particles of the atom and has no explicit time dependence. It is shown in textbooks on quantum mechanics[2] that for a time-independent Hamiltonian like $\hat{\mathscr{H}}_{\mathrm{E}}$, the wave equation (2.1) has solutions of the form

$$\Psi_n(\mathbf{r}t) = \exp(-\mathrm{i}E_n t/\hbar)\psi_n(\mathbf{r}). \tag{2.2}$$

The time-dependent wavefunction Ψ splits into a product of a time-dependent phase factor and a wavefunction $\psi_n(\mathbf{r})$ which is independent of time and satisfies the energy eigenvalue equation

$$\hat{\mathscr{H}}_{\mathrm{E}}\psi_n(\mathbf{r}) = E_n\psi_n(\mathbf{r}). \tag{2.3}$$

In these equations n labels the different solutions and $\mathbf{r}$ symbolizes the coordinates of all the particles that form the atom. Obviously, eqn (2.3) is just the condition that the wavefunction of eqn (2.2) should satisfy the time-dependent wave equation (2.1) with $\hat{\mathscr{H}}_{\mathrm{E}}$ substituted for $\hat{\mathscr{H}}$.

The atomic states described by eqns (2.2) and (2.3) are known as stationary states. They have the property that, when the atom is in one of its stationary states, the average value of any observable is independent of time, provided that the operator representing the observable does not involve the time explicitly. A system put into one of the stationary states of its total Hamiltonian remains in the state for all subsequent times. For many purposes the time-dependent phase factor in eqn (2.2) can be ignored and the wavefunction taken as the spatial part $\psi_n(\mathbf{r})$ alone. The phase factors must, however, be retained for consideration of time-dependent processes like the absorption and emission of light by an atom.

For the calculation of the B coefficient we shall be concerned with only two energy eigenstates $\psi_1(\mathbf{r})$ and $\psi_2(\mathbf{r})$ of an atom, having energy eigenvalues E_1 and E_2,

$$\hat{\mathscr{H}}_{\mathrm{E}}\psi_1(\mathbf{r}) = E_1\psi_1(\mathbf{r})$$

and

$$\hat{\mathscr{H}}_{\mathrm{E}}\psi_2(\mathbf{r}) = E_2\psi_2(\mathbf{r}). \tag{2.4}$$

The corresponding time-dependent wavefunctions are

$$\Psi_1(\mathbf{r}t) = \exp(-\mathrm{i}E_1 t/\hbar)\psi_1(\mathbf{r})$$

and

$$\Psi_2(\mathbf{r}t) = \exp(-\mathrm{i}E_2 t/\hbar)\psi_2(\mathbf{r}). \tag{2.5}$$

The explicit functional dependence of Ψ and ψ will often be suppressed, with the understanding that the upper- or lower-case symbols imply that the time-dependent phase factor is or is not included in the wavefunction. The energy levels are as shown in Fig. 1.8, except that we now call the transition frequency ω_0,

$$\hbar\omega_0 = E_2 - E_1. \tag{2.6}$$

It will be assumed in the calculation that follows that ψ_1 and ψ_2 are known functions.

Now consider the effect on the atom of some electromagnetic radiation. An electromagnetic wave has associated electric and magnetic fields that vary with position and time. Their interaction with the atom causes it to have an additional electromagnetic energy which can be represented by an addition $\hat{\mathscr{H}}_{\mathrm{I}}$ to the Hamiltonian. The functional form of $\hat{\mathscr{H}}_{\mathrm{I}}$ will be discussed shortly; for the moment we treat it as a general operator that depends on $\mathbf{r}$ and t. The total Hamiltonian is

$$\hat{\mathscr{H}} = \hat{\mathscr{H}}_{\mathrm{E}} + \hat{\mathscr{H}}_{\mathrm{I}}. \tag{2.7}$$

Since $\hat{\mathscr{H}}$ depends explicitly on time, the wave equation (2.1) no longer has stationary-state solutions of the type given by eqns (2.2) and (2.3).

An expression for the Einstein coefficient B_{12} associated with the absorption of radiation can be derived as follows. We assume that at some instant of time the atom is in its state ψ_1. Owing to the presence of the term $\hat{\mathscr{H}}_{\mathrm{I}}$ in the Hamiltonian, ψ_1 is not a stationary state, and there is a finite probability that the atom will be found in state ψ_2 at a later time. This probability can be expressed as a rate of transition from state 1 to state 2, and hence related to the B coefficient. The required information is contained in the time-dependent wavefunction Ψ for the atom, obtained by solution of eqn (2.1).

If the frequency of the light is close to ω_0, only the two selected atomic states are involved in the radiative processes, and at any instant of time the wavefunction must be a linear superposition

$$\Psi(\mathbf{r}t) = C_1(t)\Psi_1(\mathbf{r}t) + C_2(t)\Psi_2(\mathbf{r}t). \tag{2.8}$$

The mixture of states varies with time but we may require $\Psi(\mathbf{r}t)$ to be normalized at all times

$$\int |\Psi(\mathbf{r}t)|^2\,\mathrm{d}V = |C_1(t)|^2 + |C_2(t)|^2 = 1, \tag{2.9}$$

where eqn (2.5) has been used and $\psi_1(\mathbf{r})$ and $\psi_2(\mathbf{r})$ have been assumed normalized and orthogonal. The coefficients C_1 and C_2 are independent of position.

Substitution of eqn (2.8) into eqn (2.1) leads to an equation for the coefficients C_1 and C_2 that can be simplified, with the help of eqns (2.4), (2.5), and (2.7), to

$$\hat{\mathscr{H}}_{\mathrm{I}}(C_1\Psi_1+C_2\Psi_2) = \mathrm{i}\hbar\left(\Psi_1\frac{\mathrm{d}C_1}{\mathrm{d}t}+\Psi_2\frac{\mathrm{d}C_2}{\mathrm{d}t}\right). \tag{2.10}$$

Multiplication from the left by the complex conjugate Ψ_1^*, followed by integration over all space leads to

$$C_1\int\psi_1^*\hat{\mathscr{H}}_{\mathrm{I}}\psi_1\,\mathrm{d}V+C_2\exp(-\mathrm{i}\omega_0 t)\int\psi_1^*\hat{\mathscr{H}}_{\mathrm{I}}\psi_2\,\mathrm{d}V = \mathrm{i}\hbar\,\mathrm{d}C_1/\mathrm{d}t, \tag{2.11}$$

where eqns (2.5) and (2.6) have been used. It is convenient to introduce a shorthand notation for the matrix elements of $\hat{\mathscr{H}}_{\mathrm{I}}$,

$$\hbar\mathscr{I}_{11} = \int\psi_1^*\hat{\mathscr{H}}_{\mathrm{I}}\psi_1\,\mathrm{d}V, \qquad \hbar\mathscr{I}_{12} = \int\psi_1^*\hat{\mathscr{H}}_{\mathrm{I}}\psi_2\,\mathrm{d}V, \text{ etc.,} \tag{2.12}$$

whereupon eqn (2.11) simplifies to

$$C_1\mathscr{I}_{11}+C_2\exp(-\mathrm{i}\omega_0 t)\mathscr{I}_{12} = \mathrm{i}\,\mathrm{d}C_1/\mathrm{d}t. \tag{2.13}$$

Similarly, multiplication of eqn (2.10) from the left by Ψ_2^* leads to

$$C_1\exp(\mathrm{i}\omega_0 t)\mathscr{I}_{21}+C_2\mathscr{I}_{22} = \mathrm{i}\,\mathrm{d}C_2/\mathrm{d}t. \tag{2.14}$$

Eqns (2.13) and (2.14) contain no position dependence and the matrix elements $\mathscr{I}$ are known functions of time once the functional form of $\hat{\mathscr{H}}_{\mathrm{I}}$ is specified. The equations can, in principle, be solved for C_1 and C_2 as functions of time, and the wavefunction $\Psi(\mathbf{r}t)$ is then determined by eqn (2.8).

2.2. Form of the interaction Hamiltonian

The complete form of the Hamiltonian for the interaction between the electromagnetic field and an atom is somewhat complicated, and a full discussion is deferred until Chapter 5. However, a knowledge of the main features of the interaction is sufficient for calculation of the B coefficient.

Consider the atom shown in Fig. 2.1, which consists of a nucleus of charge Ze surrounded by Z electrons each of charge $-e$. The atom interacts with a polarized electromagnetic wave having the electromagnetic field components shown in the figure, where the atomic nucleus is taken as the origin of coordinates. We use fields with real time-dependent parts in the present chapter. The magnitudes of the atomic electron radii are typified by the Bohr radius

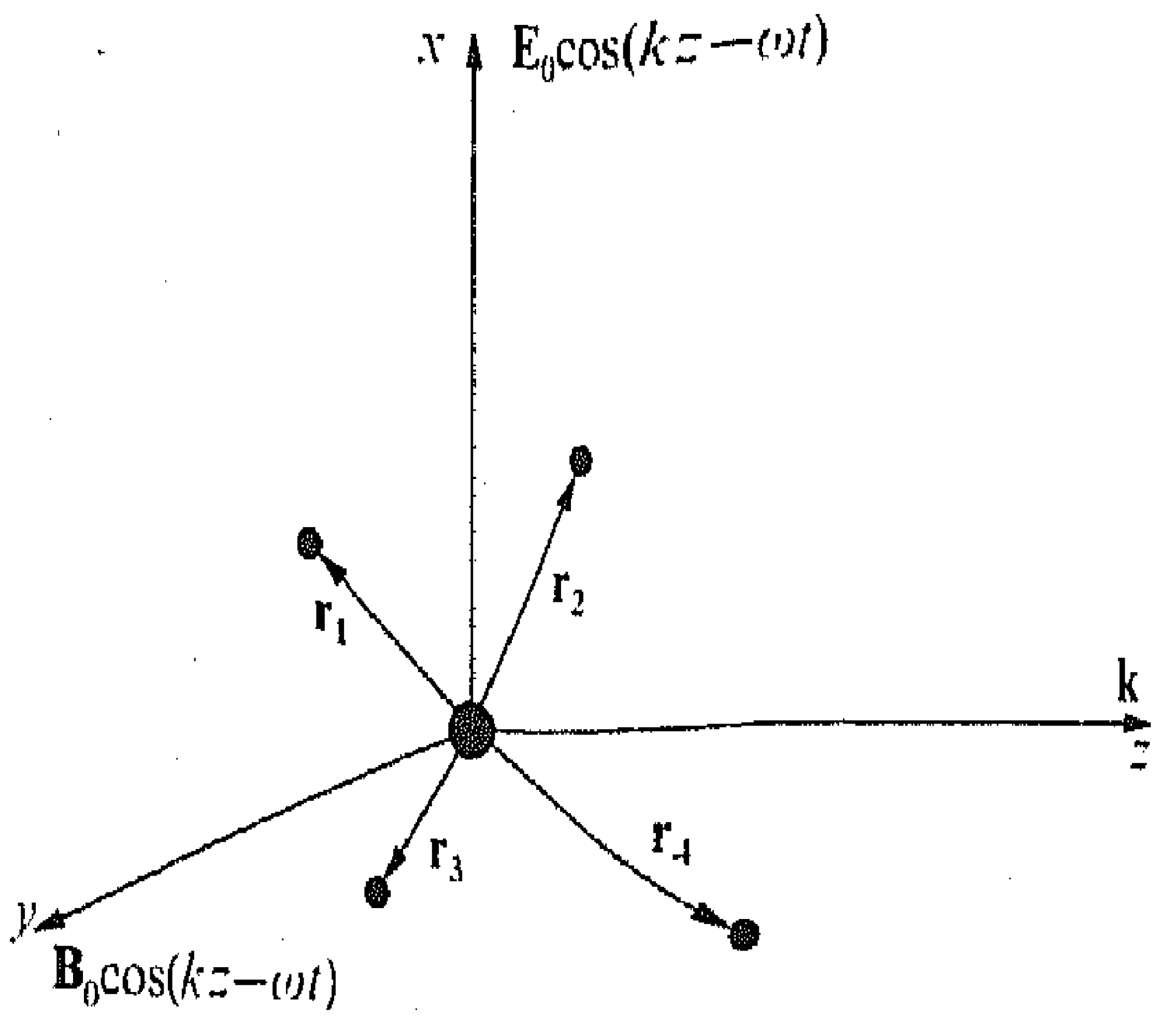
x
$\mathbf{E}_0\cos(kz-\omega t)$
$\mathbf{r}_1$
$\mathbf{r}_2$
$\mathbf{r}_3$
$\mathbf{r}_4$
k
z
y
$\mathbf{B}_0\cos(kz-\omega t)$

FIG. 2.1. Coordinate system for the atom and the electromagnetic wave.

$$a_0 = 4\pi\epsilon_0\hbar^2/me^2 \approx 5\times10^{-11}\ \mathrm{m}, \tag{2.15}$$

where m is the electron mass. The radius is much smaller than the wavelength of the electromagnetic wave, provided that the frequency is restricted to be smaller than about 10^{18} Hz. For such frequencies

$$ka_0 \ll 1, \tag{2.16}$$

and the spatial variation of the electric and magnetic fields across the dimensions of the atom is very small. It is then a good approximation to ignore the kz term in the cosine.

The total electric dipole moment of the atom can be written $-e\mathbf{D}$, where

$$\mathbf{D} = \sum_{j=1}^{Z}\mathbf{r}_j. \tag{2.17}$$

The main contribution to the interaction Hamiltonian arises from the potential energy of this electric dipole in the electric field $\mathbf{E}_0\cos\omega t$ and we can write

$$\hat{\mathscr{H}}_{\mathrm{I}} = e\mathbf{D}.\mathbf{E}_0\cos\omega t. \tag{2.18}$$

The other contributions to $\hat{\mathscr{H}}_{\mathrm{I}}$ are explicitly considered in §5.3 and shown to be much smaller than eqn (2.18).

The interaction Hamiltonian (eqn (2.18)) is real and has odd parity; that is $\hat{\mathscr{H}}_{\mathrm{I}}$ changes sign under inversion in the nucleus, when $\mathbf{r}_j$ is replaced by $-\mathbf{r}_j$. It follows that the integrands of the matrix elements $\mathscr{I}_{11}$ and $\mathscr{I}_{22}$ defined in eqn (2.12) are odd functions of position and the integrals must vanish,

$$\mathscr{I}_{11} = \mathscr{I}_{22} = 0. \tag{2.19}$$

Provided the atomic states ψ_1 and ψ_2 have opposite parity, the off-diagonal matrix elements $\mathscr{I}_{12}$ and $\mathscr{I}_{21}$ are not required to vanish, but according to eqn (2.12) they are related by

$$\mathscr{I}_{21} = \mathscr{I}_{12}^{*}. \tag{2.20}$$

Since $\mathbf{E}_0$ points in the x-direction in Fig. 2.1, the explicit form of the matrix element $\mathscr{I}_{12}$ is

$$\mathscr{I}_{12} = (eE_0X_{12}/\hbar)\cos\omega t, \tag{2.21}$$

where

$$X_{12} = \int \psi_1^{*} X \psi_2 \, \mathrm{d}V, \tag{2.22}$$

X is the x-component of $\mathbf{D}$, and the integration runs over all the electron coordinates. The matrix element $\mathscr{I}_{12}$ consists of the time-dependent term $\cos\omega t$ multiplied by a numerical factor for which it is convenient to have a simple notation. We define

$$\mathscr{V} = eE_0X_{12}/\hbar, \tag{2.23}$$

and eqn (2.21) becomes

$$\mathscr{I}_{12} = \mathscr{V}\cos\omega t. \tag{2.24}$$

Consider, for example, the 1S to 2P transition of atomic hydrogen. If account is taken of the electron-spin quantum-number, the ground 1S state is doubly degenerate and there are six degenerate 2P states. However, the spin quantum-number cannot change since the interaction Hamiltonian is independent of the electron spin. There are thus three accessible 2P states for a ground-state electron of given spin quantum-number. Also, for the x-polarized electromagnetic wave, the integral in $\mathscr{V}$ vanishes except for the $2\mathrm{P}_x$ state. The magnitude of $\mathscr{V}$ is calculated in the following problem.

Problem 2.1. For the hydrogen atom states

$$\psi_1 = \pi^{-\frac{1}{2}}a_0^{-\frac{3}{2}}\exp(-r/a_0) \tag{2.25}$$

$$\psi_2 = 2^{-\frac{5}{2}}\pi^{-\frac{1}{2}}a_0^{-\frac{5}{2}}x\exp(-r/2a_0), \tag{2.26}$$

prove that

$$\mathscr{V} = 2^{\frac{15}{2}}eE_0a_0/3^5\hbar. \tag{2.27}$$

The transition frequency is

$$\omega_0 = \tfrac{3}{4}\omega_\mathrm{R}, \tag{2.28}$$

where

$$\hbar\omega_\mathrm{R} = me^4/32\pi^2\epsilon_0^2\hbar^2. \tag{2.29}$$

Show that a field strength E_0 of order 3×10^{11} Vm^{-1} is required to make $\mathscr{V}$ equal to ω_0.

For the fields E_0 encountered in almost all light beams (see Table 1.1, p. 21),

$$\mathscr{V} \ll \omega_0. \tag{2.30}$$

Very powerful light beams required special treatment and are considered in Chapter 9.

2.3. The transition rate

The basic eqns (2.13) and (2.14) can now be simplified in the light of eqns (2.19), (2.20), and (2.24) to

$$\mathscr{V}\cos\omega t\,\exp(-\mathrm{i}\omega_0 t)C_2 = \mathrm{i}\,\mathrm{d}C_1/\mathrm{d}t \tag{2.31}$$

and

$$\mathscr{V}^{*}\cos\omega t\,\exp(\mathrm{i}\omega_0 t)C_1 = \mathrm{i}\,\mathrm{d}C_2/\mathrm{d}t. \tag{2.32}$$

These equations are exact within the restriction to a pair of atomic states.

Problem 2.2. Prove that $|C_1|^2+|C_2|^2$ does not change with time, thus ensuring that the normalization condition of eqn (2.9) remains valid throughout the time-dependent processes.

Problem 2.3. Consider the solution of eqns (2.31) and (2.32) for the special case $\omega = 0$ where the electric field applied to the atom is constant in time. Show that C_2 satisfies

$$\frac{\mathrm{d}^2C_2}{\mathrm{d}t^2}-\mathrm{i}\omega_0\frac{\mathrm{d}C_2}{\mathrm{d}t}+|\mathscr{V}|^2C_2 = 0, \tag{2.33}$$

and hence prove that, if the atom is in its lower state at time $t = 0$,

$$|C_2|^2 = \frac{4|\mathscr{V}|^2}{\omega_0^2+4|\mathscr{V}|^2}\sin^2\{(\omega_0^2+4|\mathscr{V}|^2)^{\frac{1}{2}}t/2\}; \tag{2.34}$$

$|C_1|^2$ can be found from the normalization condition (2.9).

The calculation of the Einstein B coefficient is similar in principle to the above problem, but eqns (2.31) and (2.32) must now be solved for a value of ω that is close to the transition frequency ω_0. The atom is again assumed to be in its lower state ψ_1 at time $t = 0$, and the boundary conditions are

$$C_1(0) = 1$$

and

$$C_2(0) = 0. \tag{2.35}$$

Again, $|C_2(t)|^2$ is the probability of finding the atom in its upper state ψ_2 at time t. The rate $|C_2(t)|^2/t$ at which the probability of finding the atom in its excited state grows is the quantum-mechanical transition rate. By comparison with the definition of B_{12} in Fig. 1.8, we must have

$$B_{12}\bar{W}(\omega) = |C_2(t)|^2/t, \tag{2.36}$$

where $\bar{W}(\omega)$ is the cycle-averaged radiative energy density associated with the electromagnetic wave in Fig. 2.1. Thus a calculation of $C_2(t)$ leads to the required quantum-mechanical expression for B_{12}.

Despite their simple forms eqns (2.31) and (2.32) are quite difficult to solve in general and it is necessary to look for approximate solutions. The inequality (2.30) suggests that it would be useful to obtain C_1 and C_2 as power series in $\mathscr{V}$. If the initial values (eqn (2.35)) of C_1 and C_2 are substituted on the left-hand sides of eqns (2.31) and (2.32), integration with respect to time gives a first approximation to the time dependence of C_1 and C_2. The results are

$$C_1(t) = 1$$

and

$$C_2(t) = \frac{\mathscr{V}^*}{2}\left\{\frac{1-\exp(\mathrm{i}(\omega_0+\omega)t)}{\omega_0+\omega}+\frac{1-\exp(\mathrm{i}(\omega_0-\omega)t)}{\omega_0-\omega}\right\}. \tag{2.37}$$

A second approximation can be obtained by substituting these solutions on the left-hand sides of eqns (2.31) and (2.32) and integrating again; $C_2(t)$ is unchanged, but the improved solution for $C_1(t)$ is of the form

$$C_1(t) = 1+|\mathscr{V}|^2\times(\text{function of } t). \tag{2.38}$$

A third approximation can now be obtained, and so on. In this way an iterative solution to the coupled equations is obtained. A series in even powers of $|\mathscr{V}|$ is obtained for $C_1(t)$, while $C_2(t)$ is expressed in a series of odd powers of $\mathscr{V}$ or $\mathscr{V}^*$.

According to eqn (2.23), the series can equally well be regarded as expansions in powers of the electric field strength E_0. The energy density in the wave is related to E_0 by

$$\frac{1}{2}\epsilon_0 E_0^2 = \int \bar{W}(\omega)\,\mathrm{d}\omega \tag{2.39}$$

similar to eqn (1.34), but with the volume integration carried out. Comparison of powers of E_0 on the two sides of eqn (2.36) shows that the required expression for B_{12} can be obtained if $C_2(t)$ is evaluated to first order in E_0, or equivalently $\mathscr{V}$. The first approximation (eqn (2.37)) is already adequate for this purpose. The Einstein theory of absorption and emission does not apply in situations where the terms of higher order in E_0 have an important effect.

The second term in the linear solution (eqn (2.37)) is much larger than the first. Consider light whose frequency ω is exactly equal to ω_0, where eqn (2.37) becomes

$$C_2(t) = -(\mathrm{i}\mathscr{V}^*/2\omega_0)(\exp(\mathrm{i}\omega_0 t)\sin\omega_0 t+\omega_0 t). \tag{2.40}$$

It will be found that the characteristic time spans t over which atomic transitions take place are typically of order 10^{-7} s or longer, whereas ω_0 from eqn (1.65) is typically of order $10^{15}\,\mathrm{s}^{-1}$. Thus the inequality

$$\omega_0 t \gg 1 \tag{2.41}$$

is very well satisfied for the times t of interest in the present calculation. In other words, many cycles of oscillation of the electromagnetic wave occur before there is a significant probability of atomic excitation. The second term in the bracket of eqn (2.40) is, therefore, much larger than the first, and this is still true when ω is close, but not exactly equal to ω_0.

It is, therefore, a good approximation to neglect the first term in the basic solution (eqn (2.37)), which then leads to

$$|C_2(t)|^2 = |\mathscr{V}|^2\,\frac{\sin^2\{(\omega_0-\omega)t/2\}}{(\omega_0-\omega)^2}. \tag{2.42}$$

When ω is exactly equal to ω_0, the excitation probability increases quadratically with time,

$$|C_2(t)|^2 = \tfrac{1}{4}|\mathscr{V}|^2 t^2, \qquad (\omega = \omega_0), \tag{2.43}$$

but an oscillatory behaviour in time occurs when ω is different from ω_0. This neglect of the first term in eqn (2.37) is known as the *rotating-wave approximation*. The term retained corresponds to phase angles ωt and $\omega_0 t$ for the light and the atomic transition that increase with time in the same sense, whereas the neglected term has phase angles that increase in magnitude but with opposite signs.

Fig. 2.2 shows the dependence of $|C_2(t)|^2$ on ω at a given time t. As t increases, the maximum in the curve moves upwards proportional to t^2, and the zeros of the function move in along the horizontal axis towards the origin.

Eqn (2.42) is the required solution for the probability that the atom has made a transition into its excited state by the time t. It is, however, necessary to carry out a further development of this result before it can be related to the measurable transition rate. We have assumed so far that the transition frequency ω_0 is a well-defined quantity that can be assigned a mathematically exact value. This does not correspond to the situation in any practicable experiment, where there is always some uncertainty in the value of ω_0. All spectroscopic equipment has finite resolution, such that the measured frequencies of spectral lines are undefined by some amount $\Delta\omega$. Even if one envisages an idealized experiment with perfect frequency-resolution, there is a more basic limitation in the intrinsic widths of spectral lines.

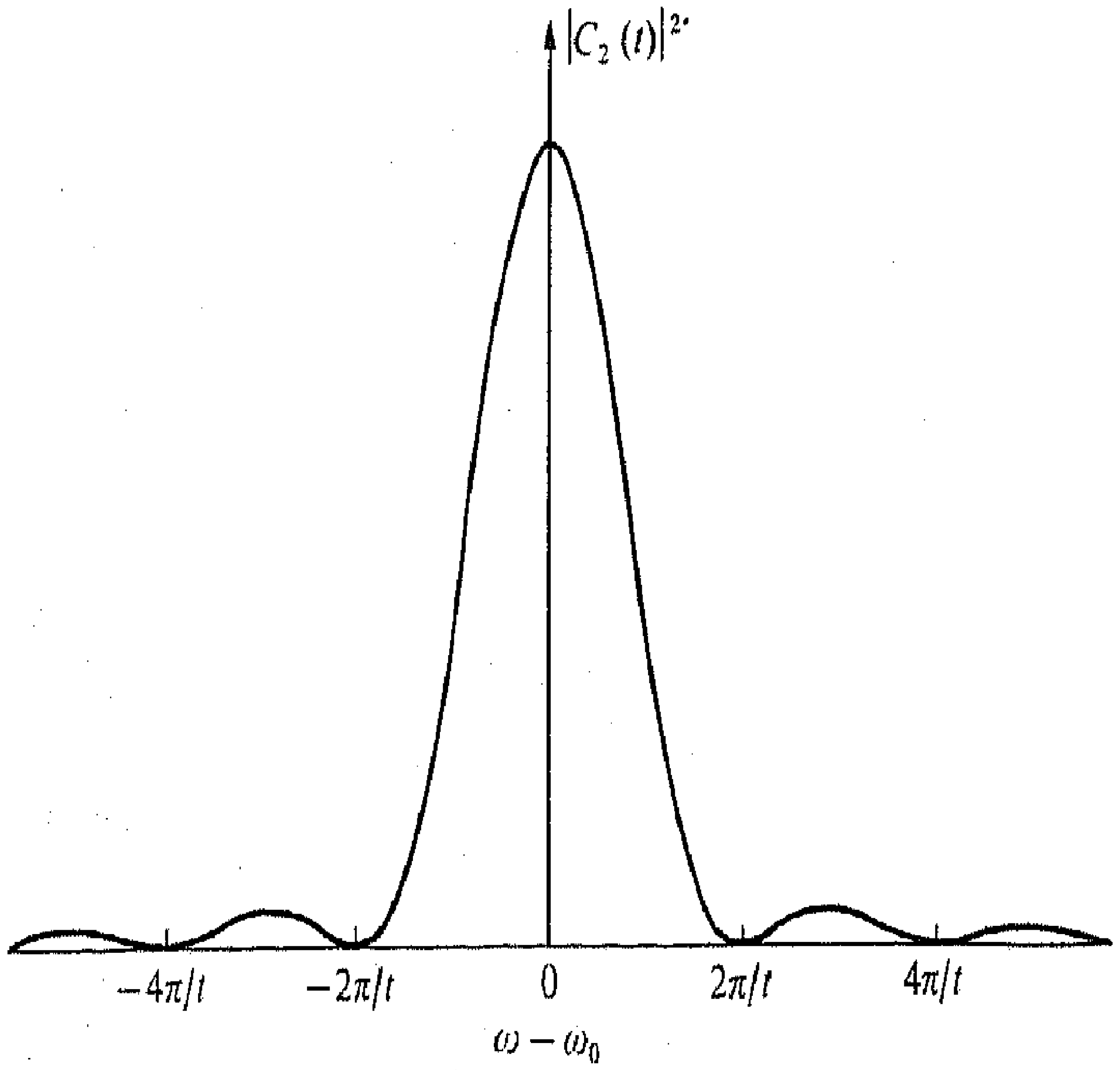

FIG. 2.2. The probability $|C_2|^2$ for the atom to be in its upper level at time t as a function of the frequency ω of the exciting light.

The uncertainty in the value of ω_0 can be taken account of by an integration of the expression for $|C_2(t)|^2$ over a range $\Delta\omega$. If ω_0 is now interpreted as the centre of the distribution of transition frequencies, eqn (2.42) can be written, with the use of eqns (2.23) and (2.39), as

$$|C_2(t)|^2 = \frac{2e^2|X_{12}|^2}{\epsilon_0\hbar^2}\int\limits_{\omega_0-\frac{1}{2}\Delta\omega}^{\omega_0+\frac{1}{2}\Delta\omega} \bar{W}(\omega)\,\frac{\sin^2\{(\omega_0-\omega)t/2\}}{(\omega_0-\omega)^2}\,\mathrm{d}\omega. \tag{2.44}$$

The assumption of broad-band illumination of the atom, basic to the Einstein theory, is now made in that the radiative energy density is taken to have a constant value $\bar{W}(\omega_0)$ over the range $\Delta\omega$. Then eqn (2.44) can be written

$$|C_2(t)|^2 = \{2e^2|X_{12}|^2\,\bar{W}(\omega_0)/\epsilon_0\hbar^2\}\mathrm{Int}, \tag{2.45}$$

where

$$\mathrm{Int} = \int\limits_{\omega_0-\frac{1}{2}\Delta\omega}^{\omega_0+\frac{1}{2}\Delta\omega} \frac{\sin^2\{(\omega_0-\omega)t/2\}}{(\omega_0-\omega)^2}\,\mathrm{d}\omega. \tag{2.46}$$

The way in which the value of this integral varies with $\Delta\omega$ and t is shown in Fig. 2.3. The two limiting values of the integral can be expressed analytically. For small $t\Delta\omega$, it is seen by reference to Fig. 2.2 that the integrand is almost constant, leading to

$$\mathrm{Int} = \tfrac{1}{4}t^2\Delta\omega \qquad (t\Delta\omega \ll 1). \tag{2.47}$$

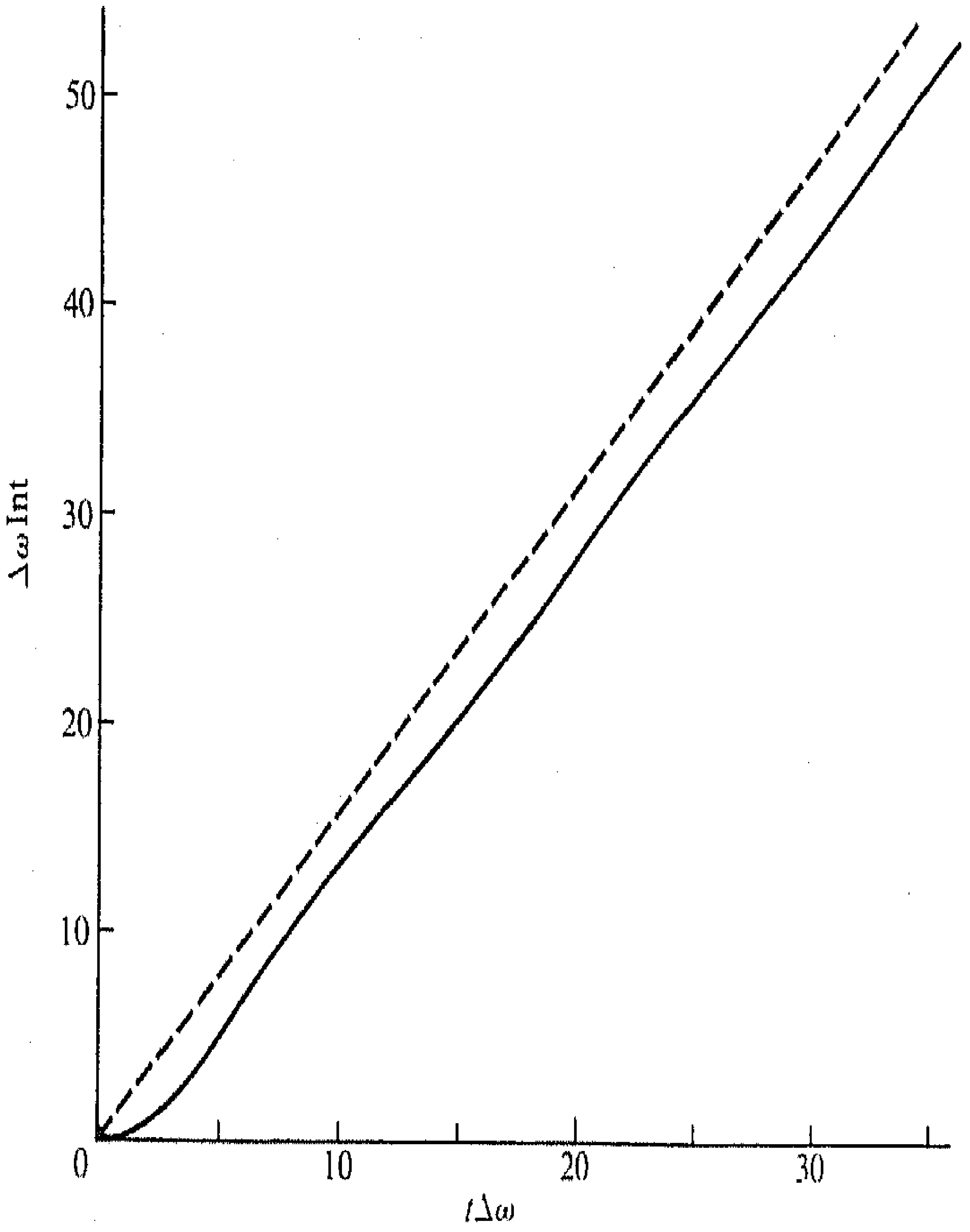

FIG. 2.3. The solid curve shows the value of the integral in eqn (2.46) as a function of t. The dashed line shows the approximation of eqn (2.48).

For large $t\Delta\omega$, the integration covers almost all the area under the curve in Fig. 2.2, and the limiting value is[3]

$$\mathrm{Int} = \tfrac{1}{2}\pi t \qquad (t\Delta\omega \gg 1). \tag{2.48}$$

This limiting behaviour, linear in t, is illustrated by the dashed line in Fig. 2.3. It can be seen that the exact value of Int is represented by a curve with slight undulations owing to the zeros of the function illustrated in Fig. 2.2, but the linear behaviour becomes a progressively better approximation for larger values of $t\Delta\omega$.

In accordance with eqn (2.36) the Einstein B coefficient is associated with a theory of absorption in which the probability of atomic excitation is proportional to the elapsed time t. This corresponds to the linear time behaviour shown in eqn (2.48) in the quantum theory of absorption. Combination of eqns (2.45) and (2.48) gives

$$|C_2(t)|^2 = \pi e^2|X_{12}|^2\,\bar{W}(\omega_0)t/\epsilon_0\hbar^2, \tag{2.49}$$

and this expression will be used below to obtain a quantum-mechanical expression for the B coefficient.

The linear approximation embodied in eqn (2.49) must clearly break down for times sufficiently long to make $|C_2(t)|^2$ greater than unity, contrary to the normalization condition (eqn (2.9)). However, the long-time behaviour of the degree of atomic excitation can be determined in the manner of eqns (1.70) – (1.74), once the magnitude of the B coefficient has been calculated.

2.4. Expression for the *B* coefficient

The calculation of the Einstein B coefficient is now in principle complete, but before writing down the result we must consider the generalization from the single atom considered to a gas of similar atoms.

Suppose that the interaction $\mathscr{H}_1$ is applied simultaneously to a large number N of identical atoms. At the time t each atom will have probability $|C_1|^2$ of being found in its lower state ψ_1, and probability $|C_2|^2$ of being found in its upper state ψ_2. The mean numbers of atoms in the two states are therefore

$$N_1 = N|C_1|^2$$

and

$$N_2 = N|C_2|^2. \tag{2.50}$$

The normalization condition (eqn (2.9)) then ensures that the level populations satisfy the conservation requirements of eqn (1.61). Eqn (2.50) can be used to relate the quantum-mechanical state amplitudes C_1 and C_2 calculated for a single atom to level populations for large numbers of identical atoms.

However, even in a gas of identical atoms or molecules, the spatial orientations of corresponding electronic states vary in a random way from one atom or molecule to the next. It is useful to quote a result for the B coefficient in which the random spatial orientations have been explicitly taken into account. Let $\boldsymbol{\varepsilon}$ be a unit vector in the direction of the electric field of the electromagnetic wave, taken as the x-axis in Fig. 2.1. The matrix element X_{12} can be written

$$X_{12} = \boldsymbol{\varepsilon}.\mathbf{D}_{12}, \tag{2.51}$$

where

$$\mathbf{D}_{12} = \int \psi_1^* \mathbf{D} \psi_2 \, \mathrm{d}V, \tag{2.52}$$

and $\mathbf{D}$ is defined in eqn (2.17).

For a given pair of states, ψ_1 and ψ_2, $\mathbf{D}_{12}$ points in a certain spatial direction, which varies randomly in the gas owing to the random atomic or molecular orientations. To obtain the B coefficient for a gas, using eqn (2.49), we need to average $|X_{12}|^2$ over the random orientations of $\mathbf{D}_{12}$. If θ is the angle between $\mathbf{D}_{12}$ and $\boldsymbol{\varepsilon}$, the required average involves the mean value of $\cos^2\theta$, given by

$$\overline{\cos^2\theta} = \tfrac{1}{3}, \tag{2.53}$$

and hence in eqn (2.49) we must make the replacement

$$|X_{12}|^2 \rightarrow \overline{|X_{12}|^2} = \tfrac{1}{3}|D_{12}|^2, \tag{2.54}$$

where D_{12} is the magnitude of the vector $\mathbf{D}_{12}$. Then comparison of eqns (2.36) and (2.49) gives the quantum-mechanical result for the Einstein coefficient as

$$B_{12} = \pi e^2 |D_{12}|^2 / 3\epsilon_0 \hbar^2. \tag{2.55}$$

In the absence of any incident electromagnetic wave $\mathscr{H}_1$ vanishes, and the states ψ_1 and ψ_2 again become stationary states of the total Hamiltonian which now reduces to $\mathscr{H}_E$ alone. No transitions can occur from state 1 to state 2, even if state 2 lies lower in energy than state 1. The semiclassical method of the present chapter does not embrace the spontaneous emission process, and a satisfactory treatment must use the quantum-mechanical radiation field. Such a treatment is given in §5.5. However, the correct expression for the A coefficient can be found by combination of the general relations shown in eqns (1.50) and (1.51) between the Einstein coefficients with the quantum-mechanical result for B_{12}, to give

$$A_{21} = \frac{\hbar\omega_0^3 g_1}{\pi^2 c^3 g_2} B_{12} = \frac{g_1 e^2 \omega_0^3 |D_{12}|^2}{3\pi\epsilon_0 g_2 \hbar c^3}. \tag{2.56}$$

The magnitudes of the A coefficients can be readily calculated for the case of atomic hydrogen. Consider the transitions between the 1S and 2P states. There are three 2P states having equal rates of transition from the 1S state, and the composite B_{12} coefficient has three times the value given by eqn (2.55), where D_{12} is the matrix element between 1S and any one of the three 2P states. We take $g_1 = 1$, $g_2 = 3$, and use eqns (2.15), (2.27), and (2.28) to obtain

$$A_{21} = \frac{e^2\omega_0^3|D_{12}|^2}{3\pi\epsilon_0\hbar c^3} = \frac{me^{10}}{3^8 4\pi^5 \epsilon_0^5 \hbar^6 c^3} = 6\times10^8\,\mathrm{s}^{-1}. \tag{2.57}$$

The radiative lifetime of the 2P state, defined as in eqn (1.78), is therefore 1.6×10^{-9} s. The 1S ↔ 2P emission or absorption line lies in the ultraviolet region. Rates for several hydrogen-atom transitions are shown in Fig. 2.4; note the trend to smaller transition rates with diminishing transition frequency, in accordance with the ω_0^3-dependence of the A coefficient.

For comparison with the rate of spontaneous emission given in eqn (2.57), the rate of stimulated emission by the same transition in a beam of intensity $10^4\,\mathrm{Wm}^{-2}$ and width $2\pi\, 10^{10}\,\mathrm{s}^{-1}$ (see Table 1.1) is

$$B_{21}\bar{W}(\omega) = 3\times10^7\,\mathrm{s}^{-1} \tag{2.58}$$

GOA UNIVERSITY LIBRARY
TALEGAO GOA

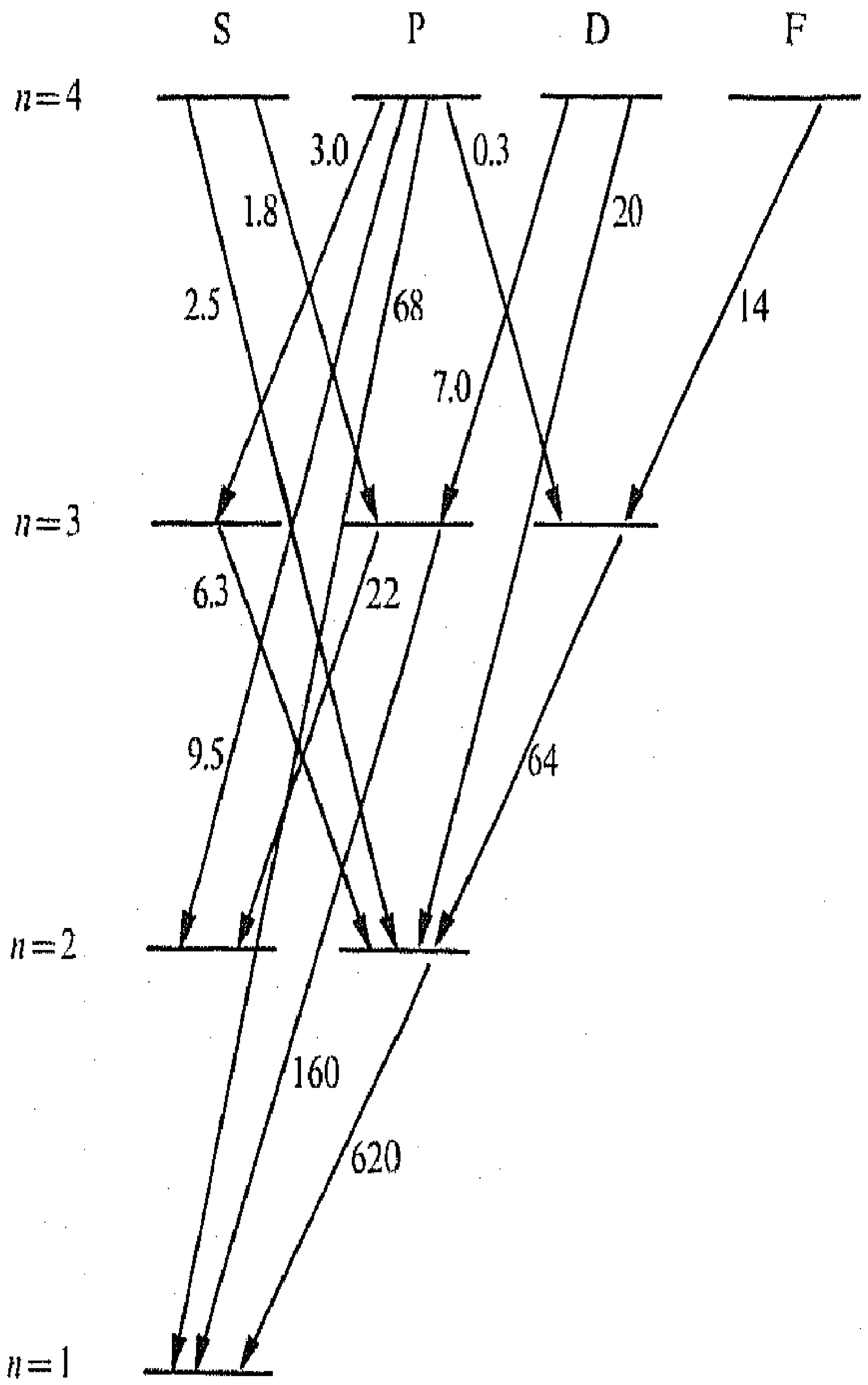

FIG. 2.4. Spontaneous transition rates between the lowest few levels of hydrogen in units of 10^6 s^{-1}. The values are taken from ref. 4.

2.5. The Dirac delta-function

The method used above to calculate the Einstein B coefficient has wide applicability, and it is useful to cast the result in a form that facilitates its application to other problems.

Consider the Dirac delta-function, which can be defined by

$$\delta(\omega_0-\omega) = \frac{2}{\pi} \operatorname*{Lt}_{t\to\infty} \frac{\sin^2\{(\omega_0-\omega)t/2\}}{(\omega_0-\omega)^2 t}. \tag{2.59}$$

According to eqn (2.48),

$$\int_{-\infty}^{\infty} \delta(\omega_0-\omega)\, d\omega = 1. \tag{2.60}$$

The delta function is illustrated by the limit of the curve plotted in Fig. 2.2 at infinite t, where the zeros all crowd in to the origin and the value at $\omega = \omega_0$ tends to infinity in such a way as to maintain a constant area under the curve.

All the area is concentrated at $\omega = \omega_0$ in the limit, and the delta function is zero everywhere else. Thus eqn (2.60) can be written more generally as

$$\begin{aligned}\int_{\omega_1}^{\omega_2} \delta(\omega_0-\omega)\, d\omega &= 1, \qquad \text{provided} \qquad \omega_1 < \omega_0 < \omega_2,\\ &= 0, \qquad \text{otherwise.}\end{aligned} \tag{2.61}$$

The definition given in eqn (2.59) can be used to prove the basic property of the delta function. Let $f(\omega)$ be any function of ω that is non-singular at $\omega = \omega_0$, and consider the integral

$$\int_{\omega_1}^{\omega_2} f(\omega)\,\delta(\omega_0-\omega)\, d\omega = \frac{2}{\pi} \operatorname*{Lt}_{t\to\infty} \int_{\omega_1}^{\omega_2} f(\omega) \frac{\sin^2\{(\omega_0-\omega)t/2\}}{(\omega_0-\omega)^2 t}\, d\omega. \tag{2.62}$$

Changing the variable of integration to $x = (\omega-\omega_0)t$ gives

$$\begin{aligned}\int_{\omega_1}^{\omega_2} f(\omega)\,\delta(\omega_0-\omega)\, d\omega &= \frac{2}{\pi} \operatorname*{Lt}_{t\to\infty} \int_{(\omega_1-\omega_0)t}^{(\omega_2-\omega_0)t} f\big((x/t)+\omega_0\big) \frac{\sin^2(x/2)}{x^2}\, dx\\ &= \frac{2}{\pi} f(\omega_0) \int_{-\infty}^{\infty} \frac{\sin^2(x/2)}{x^2}\, dx, \quad \text{provided} \quad \omega_1 < \omega_0 < \omega_2,\\ &= f(\omega_0).\end{aligned} \tag{2.63}$$

Inclusion of the delta function in an integral therefore picks out the value of the integrand at the point specified by the constant in the delta function.

There are alternative representations for the delta function, in addition to the particular limit given in eqn (2.59). The criterion for an acceptable representation of the delta function is that eqn (2.63) should be satisfied, and each representation must be justified by considering the integral on the left-hand side of eqn (2.62). Some examples are given in the following problem.

Problem 2.4. Prove that the following are acceptable representations of the Dirac delta-function

$$\begin{aligned}\delta(\omega_0-\omega) &= \frac{1}{2\pi} \operatorname*{Lt}_{T_1,T_2\to\infty} \int_{-T_1}^{T_2} \exp(i(\omega_0-\omega)t)\, dt\\ &= \operatorname*{Lt}_{T_1,T_2\to\infty} \frac{\exp(i(\omega_0-\omega)T_2)-\exp(-i(\omega_0-\omega)T_1)}{2\pi i(\omega_0-\omega)},\end{aligned} \tag{2.64}$$

with the special case

$$\delta(\omega_0-\omega) = \operatorname*{Lt}_{T\to\infty} \frac{\sin\{(\omega_0-\omega)T\}}{\pi(\omega_0-\omega)}, \tag{2.65}$$

and

$$\delta(\omega_0-\omega) = \frac{1}{\pi} \operatorname*{Lt}_{\varepsilon\to 0} \frac{\varepsilon}{(\omega_0-\omega)^2+\varepsilon^2}. \tag{2.66}$$

Some useful manipulative properties of the delta function can be established by examining the basic integral on the left of eqn (2.62). The most commonly used properties are given in the following problem.

Problem 2.5. Prove the following delta-function properties,

$$\delta(\omega-\omega_0) = \delta(\omega_0-\omega), \tag{2.67}$$

$$\delta(\omega_0-b\omega) = (1/|b|)\,\delta((\omega_0/b)-\omega), \tag{2.68}$$

and

$$\delta\{(\omega_1-\omega)(\omega_2-\omega)\} = \frac{\delta(\omega_1-\omega)+\delta(\omega_2-\omega)}{|\omega_1-\omega_2|}, \tag{2.69}$$

where b is a constant, and in each case the equality means that the two sides of the equation produce the same result when multiplied by some function and integrated.

In deriving an expression for the B coefficient, we took the solution given by eqn (2.48) for times t that are large compared with $1/\omega_0$ and $1/\Delta\omega$, the characteristic time spans that control the experimental observation of the absorption of light. In this large-time limit, it is appropriate to introduce the delta-function notation by eqn (2.59) and write eqn (2.42) in the form

$$|C_2(t)|^2 = (\pi|\mathcal{V}|^2 t/2)\,\delta(\omega_0-\omega). \tag{2.70}$$

The expression is more compact in this form and the integration over the frequency range $\Delta\omega$ is trivial to accomplish if eqn (2.63) is used. This result can be applied to any transition process where the time-dependent part of the Hamiltonian is proportional to $\cos\omega t$, and there is a continuous distribution of frequencies ω around the transition frequency ω_0; only the matrix element $\mathcal{V}$ is different for different processes. It should be emphasized that the highly-singular delta function can be physically meaningful only when its variable is to be integrated over. Thus in equations like (2.70) it is always understood that an integration will be performed before any physically measurable quantities are derived.

2.6. The optical Bloch equations

Eqns (2.31) and (2.32), together with the definition of the coefficients in eqn (2.8), provide an exact description of the state of a two-level atom in interaction with an oscillatory electric field. The discussion of §2.3 is concerned with the solution of eqns (2.31) and (2.32) for the case of a smooth distribution of oscillation frequencies in the vicinity of the atomic transition frequency. The solution is approximate in that only the terms of low order in $\mathcal{V}$ or E_0 were retained, and in addition the rotating-wave approximation was made in eqn (2.42).

We now look for more general solutions of eqns (2.31) and (2.32). The rotating-wave approximation will again be made, but we retain terms of all orders in $\mathcal{V}$ or E_0. Furthermore, the incident light is assumed to be monochromatic with an oscillatory electric field at the single frequency ω. The effect of a distribution of frequencies ω can then be found by an average of the results for monochromatic light.

In calculating the optical excitation of the atom, the quantity of interest is $|C_2|^2$ rather than the bare coefficient C_2. More generally the expectation values of any observables for the atom in state (2.8) depend upon products of the coefficients with complex conjugate coefficients. It is accordingly convenient to work directly with the bilinear products of the coefficients, and we define the four elements of the atomic density matrix ρ_{ij} to be

$$\rho_{11} = |C_1|^2 = N_1/N$$

$$\rho_{22} = |C_2|^2 = N_2/N \tag{2.71}$$

$$\rho_{12} = C_1C_2^*$$

$$\rho_{21} = C_2C_1^*. \tag{2.72}$$

The diagonal elements are clearly real and from eqn (2.9) they satisfy

$$\rho_{11}+\rho_{22} = 1 \tag{2.73}$$

at all times. For a collection of atoms they are connected with the average numbers in the two levels via eqn (2.50). The off-diagonal elements are generally complex and they satisfy

$$\rho_{21} = \rho_{12}^*. \tag{2.74}$$

Equations of motion for the density matrix elements are readily found from the equations of motion for the coefficients C_1 and C_2. Thus

$$\mathrm{d}\rho_{ij}/\mathrm{d}t = C_i(\mathrm{d}C_j^*/\mathrm{d}t)+C_j^*(\mathrm{d}C_i/\mathrm{d}t), \tag{2.75}$$

and with the substitution from eqns (2.31) and (2.32), it is easily shown that

$$\begin{aligned}\mathrm{d}\rho_{22}/\mathrm{d}t &= -\mathrm{d}\rho_{11}/\mathrm{d}t\\ &= -\mathrm{i}\cos\omega t\{\mathcal{V}^*\exp(\mathrm{i}\omega_0 t)\rho_{12}-\mathcal{V}\exp(-\mathrm{i}\omega_0 t)\rho_{21}\}\end{aligned} \tag{2.76}$$

$$\mathrm{d}\rho_{12}/\mathrm{d}t = \mathrm{d}\rho_{21}^*/\mathrm{d}t = i\mathcal{V}\cos\omega t\exp(-\mathrm{i}\omega_0 t)(\rho_{11}-\rho_{22}). \tag{2.77}$$

These are exact equations for the density matrix elements.

The solution of the equations is greatly facilitated if the rotating-wave approximation is made. With the same justification as for the similar approximation in eqn (2.42), the effect of the terms that oscillate at frequency $\omega_0+\omega$ is negligible compared to the effect of the terms that oscillate at frequency $\omega_0-\omega$, when ω is close to ω_0. Removal of the rapidly oscillating terms from eqns (2.76) and (2.77) produces the equations of motion

$$\begin{aligned} \mathrm{d}\rho_{22}/\mathrm{d}t &= -\mathrm{d}\rho_{11}/\mathrm{d}t \qquad (2.78)\\ &= -\tfrac{1}{2}\mathrm{i}\mathcal{V}^*\exp\{\mathrm{i}(\omega_0-\omega)t\}\rho_{12}+\tfrac{1}{2}\mathrm{i}\mathcal{V}\exp\{-\mathrm{i}(\omega_0-\omega)t\}\rho_{21} \end{aligned}$$

$$\mathrm{d}\rho_{12}/\mathrm{d}t = \mathrm{d}\rho_{21}^*/\mathrm{d}t = \tfrac{1}{2}\mathrm{i}\mathcal{V}\exp\{-\mathrm{i}(\omega_0-\omega)t\}(\rho_{11}-\rho_{22}). \qquad (2.79)$$

These are known as the optical Bloch equations. They are similar to equations derived by Bloch to describe the motion of a spin in an oscillatory magnetic field. The quantum mechanics of the two-level atom considered here is formally identical to that of a spin $\frac{1}{2}$ system. It is possible to draw many analogies between the influences of oscillatory fields on the two systems[5].

2.7. Rabi oscillations

Eqns (2.78) and (2.79) can be solved without any further approximations. They represent a set of four simultaneous equations for the four elements of the atomic density matrix. We take trial solutions of the forms

$$\begin{aligned} \rho_{11} &= \rho_{11}^{(0)}\exp(\lambda t)\\ \rho_{22} &= \rho_{22}^{(0)}\exp(\lambda t)\\ \rho_{12} &= \rho_{12}^{(0)}\exp\{-\mathrm{i}(\omega_0-\omega)t\}\exp(\lambda t)\\ \rho_{21} &= \rho_{21}^{(0)}\exp\{\mathrm{i}(\omega_0-\omega)t\}\exp(\lambda t), \qquad (2.80) \end{aligned}$$

where the $\rho_{ij}^{(0)}$ and λ are independent of the time. The four equations obtained by substitution of the trial solutions into eqns (2.78) and (2.79) can be written in matrix form as

$$\begin{bmatrix} -\lambda & 0 & \frac{1}{2}\mathrm{i}\mathcal{V}^* & -\frac{1}{2}\mathrm{i}\mathcal{V}\\ 0 & -\lambda & -\frac{1}{2}\mathrm{i}\mathcal{V}^* & \frac{1}{2}\mathrm{i}\mathcal{V}\\ \frac{1}{2}\mathrm{i}\mathcal{V} & -\frac{1}{2}\mathrm{i}\mathcal{V} & \mathrm{i}(\omega_0-\omega)-\lambda & 0\\ -\frac{1}{2}\mathrm{i}\mathcal{V}^* & \frac{1}{2}\mathrm{i}\mathcal{V}^* & 0 & -\mathrm{i}(\omega_0-\omega)-\lambda \end{bmatrix} \begin{bmatrix} \rho_{11}^{(0)}\\ \rho_{22}^{(0)}\\ \rho_{12}^{(0)}\\ \rho_{21}^{(0)} \end{bmatrix} = 0. \qquad (2.81)$$

The possible values of λ are the roots of the 4 × 4 matrix in eqn (2.81). The determinant of the coefficients yields the quartic equation

$$\lambda^2\{\lambda^2+(\omega_0-\omega)^2+|\mathcal{V}|^2\} = 0. \qquad (2.82)$$

The distinct roots are

$$\lambda_1 = 0, \qquad \lambda_2 = \mathrm{i}\Omega, \qquad \text{and} \qquad \lambda_3 = -\mathrm{i}\Omega, \qquad (2.83)$$

where

$$\Omega = \{(\omega_0-\omega)^2+|\mathcal{V}|^2\}^{\frac{1}{2}}. \qquad (2.84)$$

The most general solutions for the density matrix elements have the forms

$$\rho_{ij} = \rho_{ij}^{(1)}+\rho_{ij}^{(2)}\exp(\mathrm{i}\Omega t)+\rho_{ij}^{(3)}\exp(-\mathrm{i}\Omega t) \qquad (2.85)$$

with the additional oscillatory exponential factors for the off-diagonal elements from eqn (2.80). The constant coefficients are determined by substitution of eqn (2.85) into the optical Bloch equations. Together with the initial conditions at $t = 0$, these provide sufficient equations to determine all the coefficients in eqn (2.85).

The presence of $|\mathcal{V}|^2$ in the roots λ_2 and λ_3 produces changes in the frequencies of the coupled system of atom and light beam from their uncoupled values of ω_0 and ω respectively. Since $|\mathcal{V}|$ is proportional to the electric field amplitude of the oscillatory light beam, the shifts and splittings of the coupled frequencies are known as the dynamic Stark effect, by analogy with the shifts and splittings of atomic energy levels produced by application of a static electric field. The dynamic Stark splitting produces important observable effects in resonance fluorescent spectra, as described in §8.4.

The solutions of the optical Bloch equations are quite lengthy for arbitrary initial conditions and we therefore limit the discussion to a simple special case.

Problem 2.6. Show that solution of the optical Bloch equations (2.78) and (2.79) for the initial conditions

$$\rho_{22} = 0, \qquad \rho_{12} = 0 \qquad (2.86)$$

gives

$$\rho_{22} = (|\mathcal{V}|^2/\Omega^2)\sin^2(\tfrac{1}{2}\Omega t) \qquad (2.87)$$

$$\begin{aligned} \rho_{12} &= \exp\{-\mathrm{i}(\omega_0-\omega)t\}(\mathcal{V}/\Omega^2)\sin(\tfrac{1}{2}\Omega t)\\ &\quad\times\{-(\omega_0-\omega)\sin(\tfrac{1}{2}\Omega t)+\mathrm{i}\Omega\cos(\tfrac{1}{2}\Omega t)\}. \qquad (2.88) \end{aligned}$$

The time dependence of the degree of excitation ρ_{22} of the atom given by eqn (2.87) is illustrated in Fig. 2.5 for various values of the ratio of the detuning $\omega_0-\omega$ between the frequencies of incident light and atomic transition to the magnitude $|\mathcal{V}|$ of the transition matrix element. The degree of excitation oscillates between 0 and $|\mathcal{V}|^2/\Omega^2$. In the special case of zero detuning, $\omega_0 = \omega$, the results simplify to

$$\rho_{22} = \sin^2(\tfrac{1}{2}|\mathcal{V}|t) \qquad (2.89)$$

$$\rho_{12} = \mathrm{i}(\mathcal{V}/|\mathcal{V}|)\sin(\tfrac{1}{2}|\mathcal{V}|t)\cos(\tfrac{1}{2}|\mathcal{V}|t). \qquad (2.90)$$

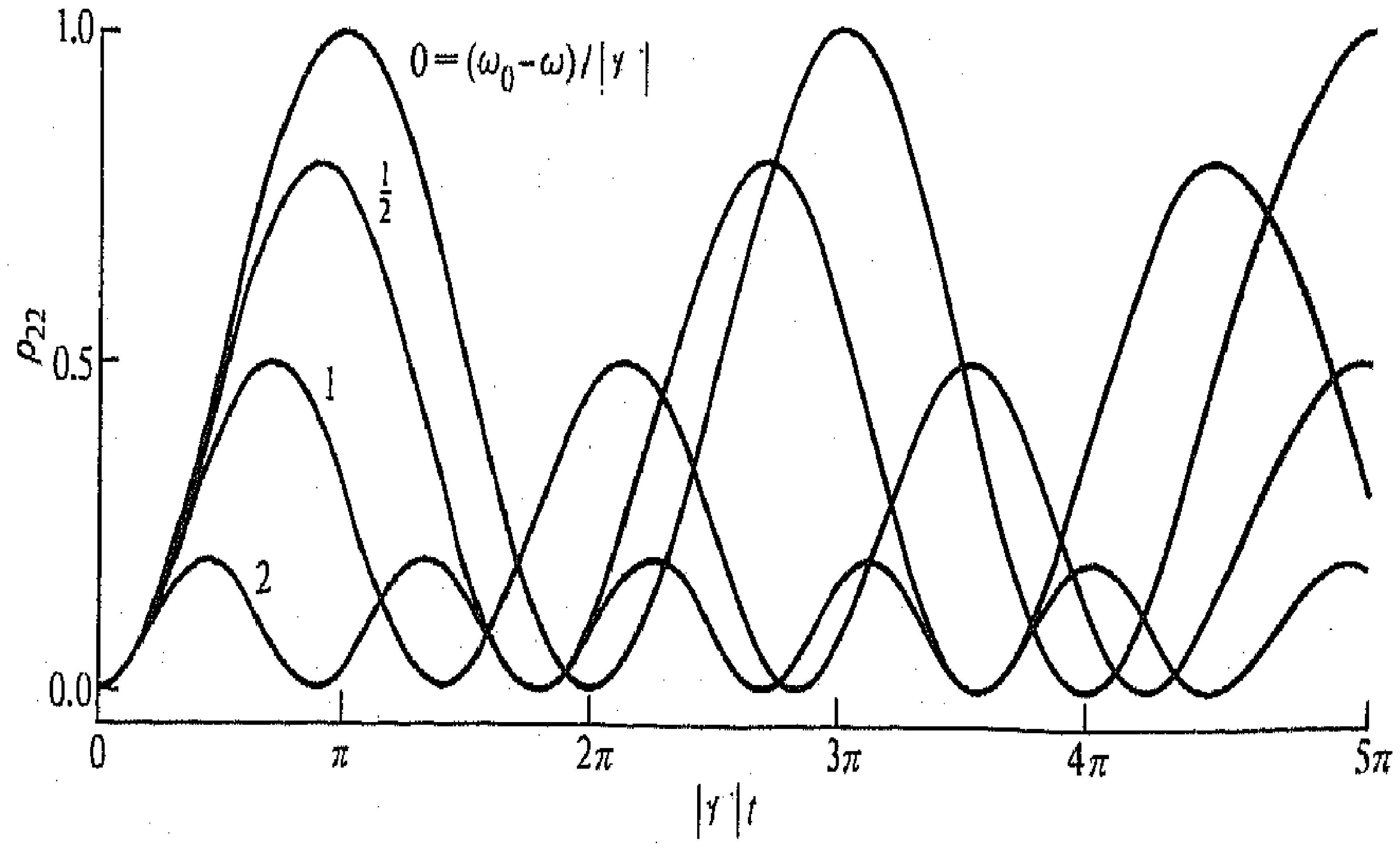

FIG. 2.5. Time dependences of the degree of atomic excitation ρ_{22} for the ratios of detuning $\omega_0-\omega$ to Rabi frequency $|\mathscr{V}|$ indicated against the curves.

The atom oscillates symmetrically between its ground and excited states in this case. These are known as Rabi oscillations and $|\mathscr{V}|$ is called the Rabi frequency, solutions similar to the above having been first obtained by Rabi[6] for the analogous problem of a spin subjected to an oscillatory magnetic field.

It must be emphasized that because the rotating-wave approximation is made in the optical Bloch equations, the solutions (2.87) and (2.88) are valid only when $\omega_0-\omega$ is very much smaller than $\omega_0+\omega$. It is therefore not possible to obtain the exact zero-frequency result (2.34) by setting $\omega = 0$ in eqn (2.87).

The solutions (2.87) and (2.88) refer to a strictly monochromatic incident beam of light with a single frequency ω of oscillation. In practice, the sinusoidal behaviours of ρ_{22} and ρ_{12} can only be observed experimentally with incident light whose frequency spread is small in comparison with the breadth of the distribution of atomic transition frequencies around ω_0. However, the processes that produce the broadening of the atomic transition frequencies also modify the optical Bloch equations and hence change the time dependences of the ρ_{ij}. These matters are discussed later in the chapter, and further consideration of the generation of Rabi oscillations is deferred until §2.10.

The opposite extreme case of a broad-band incident beam is the regime of the Einstein theory treated in Chapter 1 and the earlier part of the present chapter. The result (2.42) used in deriving the Einstein B coefficient is a special case of eqn (2.87), obtained by removing $|\mathscr{V}|$ from the frequency Ω defined in eqn (2.84). The derivation that extends from eqn (2.42) to the end result (2.55) remains valid if $|\mathscr{V}|$ is sufficiently small. Thus, the form of ρ_{22} illustrated in Fig. 2.2 is now strictly correct only if the abscissa represents Ω instead of $\omega-\omega_0$, but the required limiting value (2.48) for the area under the curve remains a good approximation if the additional condition

$$|\mathscr{V}|t \ll 1 \tag{2.91}$$

is satisfied. The condition essentially ensures that the incident light is not so strong as to produce any saturation of the atomic transition, and a consequent departure of the atomic excitation from the proportionality to the incident energy density assumed in the Einstein theory. The saturation effects included in the solutions to the optical Bloch equations are more fully discussed in §2.9.

2.8. Radiative broadening

The basic theory of absorption and emission already includes a line-broadening mechanism. The broadening arises from the spontaneous emission process and is known as radiative broadening. We include the effects of spontaneous emission in a quantum-mechanical derivation of the susceptibility of a gas of two-level atoms. The relation between susceptibility and absorption coefficient then provides an expression for the radiatively-broadened absorption lineshape.

Consider a gas of Z-electron atoms subjected to the perturbing effect of an electromagnetic wave whose frequency ω lies in the vicinity of an atomic transition frequency ω_0. As before we treat a single atom whose interaction with the electromagnetic wave is described by the Hamiltonian $\mathscr{H}_{\mathrm{I}}$ of eqn (2.18). The single-atom result is then suitably averaged to produce the analogous result for a gas of randomly oriented atoms or molecules.

The Hamiltonian $\mathscr{H}_{\mathrm{I}}$ represents the atomic perturbation produced by an applied electric field $E_0 \cos \omega t$, which contains frequency components at $+\omega$ and $-\omega$. We write the applied field as

$$E(t) = \tfrac{1}{2}E_0\{\exp(-\mathrm{i}\omega t)+\exp(\mathrm{i}\omega t)\}. \tag{2.92}$$

Application of this field to the atomic gas produces a polarization $P(t)$ proportional to the field as in eqn (1.79) with the linear susceptibility as the constant of proportionality. However, with a two-component field as in eqn (2.92) it is necessary to take account of the frequency dependence of the susceptibility $\chi(\omega)$, and eqn (1.79) is generalized to

$$P(t) = \tfrac{1}{2}\epsilon_0 E_0\{\chi(\omega)\exp(-\mathrm{i}\omega t)+\chi(-\omega)\exp(\mathrm{i}\omega t)\}. \tag{2.93}$$

The method of calculation is to compute $P(t)$ quantum-mechanically and then to determine $\chi(\omega)$ by comparison of the resulting expression with eqn (2.93).

Consider first the contribution to the polarization of the gas from a single representative atom. Suppose that the applied electric field points in the

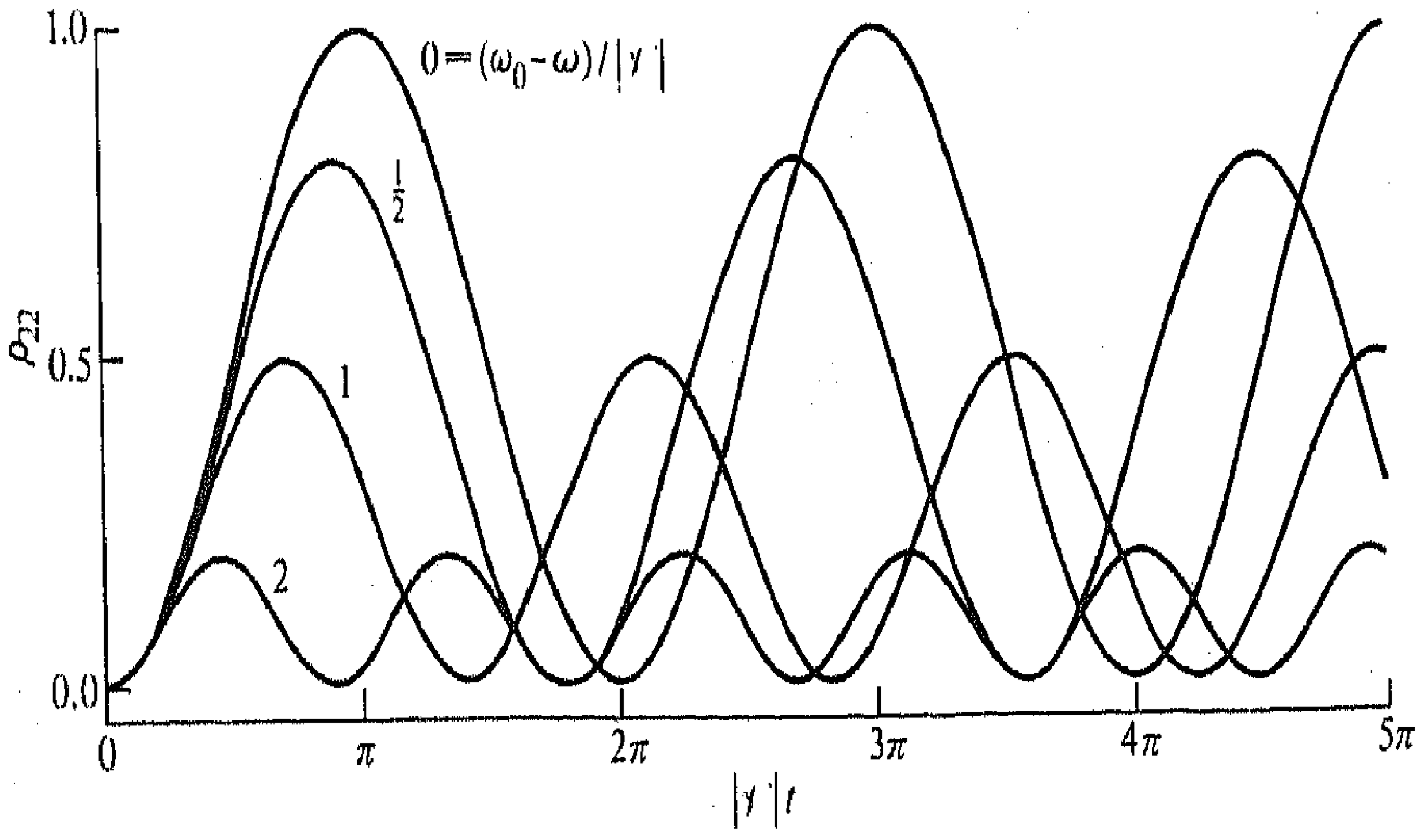

FIG. 2.5. Time dependences of the degree of atomic excitation ρ_{22} for the ratios of detuning $\omega_0-\omega$ to Rabi frequency $|\mathscr{V}|$ indicated against the curves.

The atom oscillates symmetrically between its ground and excited states in this case. These are known as Rabi oscillations and $|\mathscr{V}|$ is called the Rabi frequency, solutions similar to the above having been first obtained by Rabi[6] for the analogous problem of a spin subjected to an oscillatory magnetic field.

It must be emphasized that because the rotating-wave approximation is made in the optical Bloch equations, the solutions (2.87) and (2.88) are valid only when $\omega_0-\omega$ is very much smaller than $\omega_0+\omega$. It is therefore not possible to obtain the exact zero-frequency result (2.34) by setting $\omega = 0$ in eqn (2.87).

The solutions (2.87) and (2.88) refer to a strictly monochromatic incident beam of light with a single frequency ω of oscillation. In practice, the sinusoidal behaviours of ρ_{22} and ρ_{12} can only be observed experimentally with incident light whose frequency spread is small in comparison with the breadth of the distribution of atomic transition frequencies around ω_0. However, the processes that produce the broadening of the atomic transition frequencies also modify the optical Bloch equations and hence change the time dependences of the ρ_{ij}. These matters are discussed later in the chapter, and further consideration of the generation of Rabi oscillations is deferred until §2.10.

The opposite extreme case of a broad-band incident beam is the regime of the Einstein theory treated in Chapter 1 and the earlier part of the present chapter. The result (2.42) used in deriving the Einstein B coefficient is a special case of eqn (2.87), obtained by removing $|\mathscr{V}|$ from the frequency Ω defined in eqn (2.84). The derivation that extends from eqn (2.42) to the end result (2.55) remains valid if $|\mathscr{V}|$ is sufficiently small. Thus, the form of ρ_{22} illustrated in Fig. 2.2 is now strictly correct only if the abscissa represents Ω instead of $\omega-\omega_0$, but the required limiting value (2.48) for the area under the curve remains a good approximation if the additional condition

$$|\mathscr{V}|t \ll 1 \tag{2.91}$$

is satisfied. The condition essentially ensures that the incident light is not so strong as to produce any saturation of the atomic transition, and a consequent departure of the atomic excitation from the proportionality to the incident energy density assumed in the Einstein theory. The saturation effects included in the solutions to the optical Bloch equations are more fully discussed in §2.9.

2.8. Radiative broadening

The basic theory of absorption and emission already includes a line-broadening mechanism. The broadening arises from the spontaneous emission process and is known as radiative broadening. We include the effects of spontaneous emission in a quantum-mechanical derivation of the susceptibility of a gas of two-level atoms. The relation between susceptibility and absorption coefficient then provides an expression for the radiatively-broadened absorption lineshape.

Consider a gas of Z-electron atoms subjected to the perturbing effect of an electromagnetic wave whose frequency ω lies in the vicinity of an atomic transition frequency ω_0. As before we treat a single atom whose interaction with the electromagnetic wave is described by the Hamiltonian $\hat{\mathscr{H}}_I$ of eqn (2.18). The single-atom result is then suitably averaged to produce the analogous result for a gas of randomly oriented atoms or molecules.

The Hamiltonian $\hat{\mathscr{H}}_I$ represents the atomic perturbation produced by an applied electric field $E_0 \cos \omega t$, which contains frequency components at $+\omega$ and $-\omega$. We write the applied field as

$$E(t) = \tfrac{1}{2}E_0\{\exp(-\mathrm{i}\omega t)+\exp(\mathrm{i}\omega t)\}. \tag{2.92}$$

Application of this field to the atomic gas produces a polarization $P(t)$ proportional to the field as in eqn (1.79) with the linear susceptibility as the constant of proportionality. However, with a two-component field as in eqn (2.92) it is necessary to take account of the frequency dependence of the susceptibility $\chi(\omega)$, and eqn (1.79) is generalized to

$$P(t) = \tfrac{1}{2}\epsilon_0 E_0\{\chi(\omega)\exp(-\mathrm{i}\omega t)+\chi(-\omega)\exp(\mathrm{i}\omega t)\}. \tag{2.93}$$

The method of calculation is to compute $P(t)$ quantum-mechanically and then to determine $\chi(\omega)$ by comparison of the resulting expression with eqn (2.93).

Consider first the contribution to the polarization of the gas from a single representative atom. Suppose that the applied electric field points in the taken into account by making the same replacement (2.54) as in the calculation of the B coefficient. Then $d(t)$ given by the modified eqn (2.106) represents the averaged dipole moment per atom at time t, and the macroscopic polarization of the gas is simply

$$P(t) = Nd(t)/V. \tag{2.107}$$

The susceptibility obtained by comparison with eqn (2.93) is

$$\chi(\omega) = \frac{Ne^2|D_{12}|^2}{3\epsilon_0\hbar V}\left(\frac{1}{\omega_0-\omega-\mathrm{i}\gamma}+\frac{1}{\omega_0+\omega+\mathrm{i}\gamma}\right), \tag{2.108}$$

and the susceptibility at frequency $-\omega$ is given by a similar expression that satisfies

$$\chi(-\omega) = \chi^*(\omega). \tag{2.109}$$

The atomic absorption coefficient is related to the imaginary part of the susceptibility by

$$K = (\omega/c\eta)\chi''(\omega), \tag{2.110}$$

according to eqns (1.84) and (1.91). We consider a sufficiently dilute gas for the refractive index η to be close to unity at all frequencies. It is clear that the first term in the bracket of eqn (2.108) greatly exceeds the second term when ω is close to ω_0 and when γ is very much smaller than ω_0. We therefore neglect the second term, thereby making again the rotating-wave approximation first introduced in eqn (2.42). Then substitution of eqn (2.108) into (2.110) gives

$$K = \frac{\pi Ne^2|D_{12}|^2\omega_0}{3\epsilon_0\hbar cV}\,\frac{\gamma/\pi}{(\omega_0-\omega)^2+\gamma^2}, \tag{2.111}$$

where the narrowness of the absorption line allows ω to be replaced by ω_0 in the numerator.

The frequency dependence of the absorption coefficient is determined by the function

$$F_{\mathrm{L}}(\omega) = \frac{\gamma/\pi}{(\omega_0-\omega)^2+\gamma^2} \tag{2.112}$$

known as the Lorentzian lineshape and illustrated in Fig. 2.6. The constant in the numerator is chosen to produce the normalization

$$\int F_{\mathrm{L}}(\omega)\,\mathrm{d}\omega = 1. \tag{2.113}$$

As indicated in the figure, the full width of the line at half its maximum height is 2γ. Thus by eqn (2.102), the radiative broadening produces a linewidth equal to the spontaneous emission A coefficient for the transition.

For the decay of the hydrogen 2P state to the 1S state by spontaneous emission, eqn (2.57) shows that 2γ and A_{21} have a magnitude of $6\times10^8\ \mathrm{s}^{-1}$.

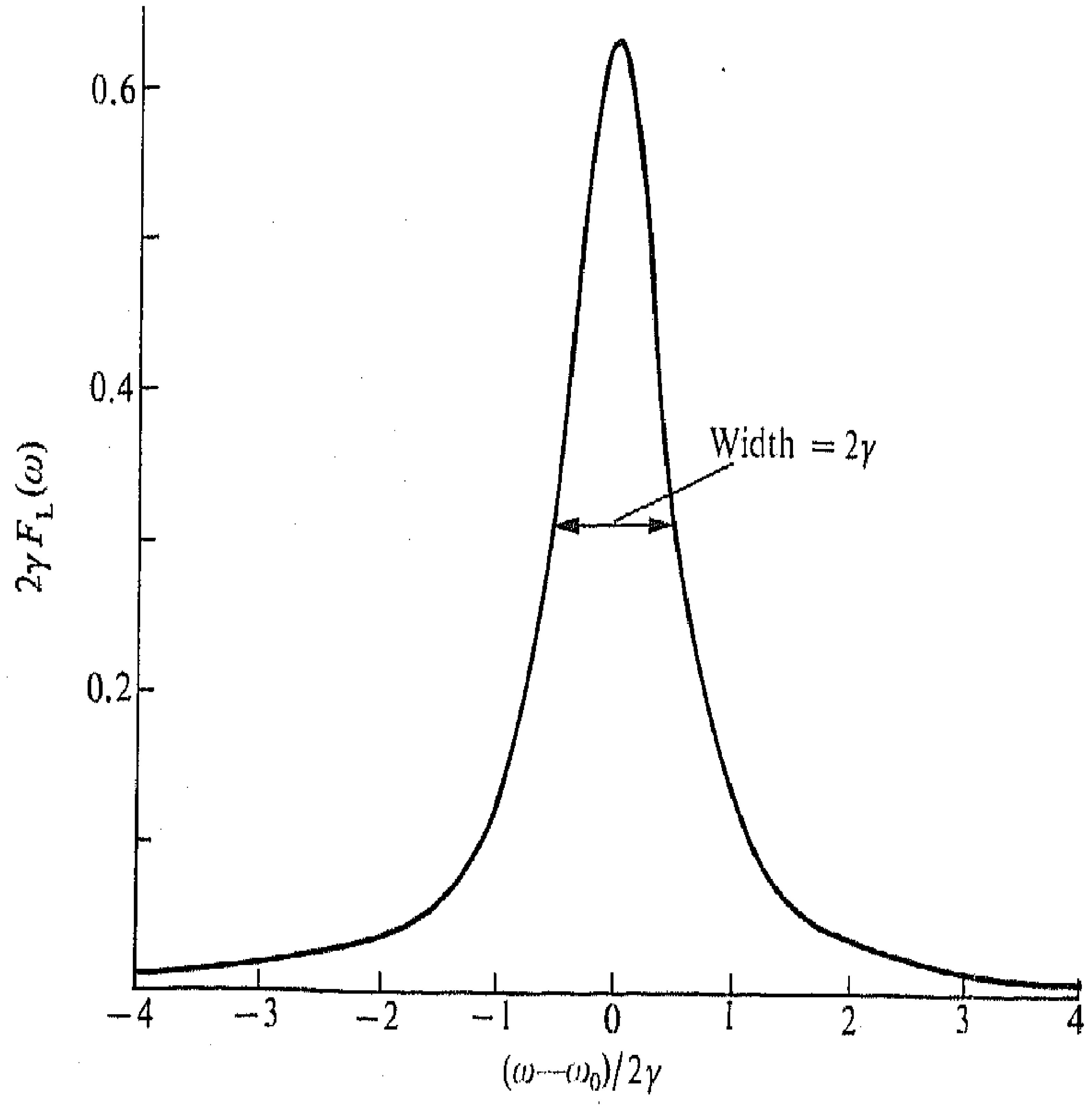

FIG. 2.6. The normalized Lorentzian lineshape function.

The corresponding absorption line thus has a width of about 10^8 Hz in frequency units (*not* angular frequency) owing to the existence of the spontaneous emission process. This is extremely narrow, and in most experiments the observed breadths of the atomic absorption lines are caused by other mechanisms, for example, the Doppler effect or atomic collisions discussed below. However, in principle, these additional broadening processes can always be reduced by some means, for example by cooling the gas or reducing its pressure. On the other hand, it is impossible to reduce the spontaneous emission rate, and the width A_{21} is the minimum possible breadth that can be achieved for a given transition. This spontaneous emission linewidth is accordingly called the natural linewidth of the spectral line. Note that this radiative width sets the minimum value for the spread $\Delta\omega$ of incident frequencies assumed in eqn (2.44) to derive the quantum expression for the Einstein B coefficient. The linear time dependence of the transition probability found in eqns (2.48) and (2.49) is valid only for t substantially longer than the radiative lifetime τ_{R}.

2.9. Power broadening

The susceptibility (2.108) is a correct result to the second order in the dipole matrix element X_{12} or D_{12} for the linear response of the atomic gas to the electric field of the incident light beam. A result that includes higher-order terms can be obtained by solution of the optical Bloch equations. The higher-order solution is made possible by the adoption of the rotating-wave approximation at the beginning of the calculation, as in the form of the optical Bloch equations (2.78) and (2.79). It is first necessary to generalize the equations by including the effects of spontaneous emission.

The Bloch equations with spontaneous emission included are calculated as in eqns (2.75)–(2.79) from the equations of motion for the coefficients C_1 and C_2. However, eqn (2.99) rather than eqn (2.32) is now used for the rate of change of C_2, while eqn (2.31) is retained for C_1. The resulting equations are

$$\mathrm{d}\rho_{22}/\mathrm{d}t = -\tfrac{1}{2}\mathrm{i}\mathscr{V}^* \exp\{\mathrm{i}(\omega_0-\omega)t\}\rho_{12}+\tfrac{1}{2}\mathrm{i}\mathscr{V} \exp\{-\mathrm{i}(\omega_0-\omega)t\}\rho_{21}-2\gamma\rho_{22} \tag{2.114}$$

$$\mathrm{d}\rho_{12}/\mathrm{d}t = \tfrac{1}{2}\mathrm{i}\mathscr{V} \exp\{-\mathrm{i}(\omega_0-\omega)t\}(\rho_{11}-\rho_{22})-\gamma\rho_{12}, \tag{2.115}$$

and the equations of motion for the other two density matrix elements are easily written down with the help of eqns (2.73) and (2.74). It is evident that this procedure for introducing γ is not entirely rigorous because eqn (2.31) ought also to be modified by spontaneous emission. However the optical Bloch equations (2.114) and (2.115) are the same as obtained by more rigorous calculations.

The spontaneous emission introduces damping terms into the optical Bloch equations. The solutions are no longer purely oscillatory as in eqns (2.87) and (2.88), but the system now settles down into a steady state after a sufficiently long period of time has elapsed. The steady-state solutions are found by first removing the oscillatory factors from eqns (2.114) and (2.115) by means of the substitutions

$$\tilde{\rho}_{12} = \exp\{\mathrm{i}(\omega_0-\omega)t\}\rho_{12}, \qquad \tilde{\rho}_{21} = \exp\{-\mathrm{i}(\omega_0-\omega)t\}\rho_{21}. \tag{2.116}$$

The equations then become

$$\mathrm{d}\rho_{22}/\mathrm{d}t = -\tfrac{1}{2}\mathrm{i}\mathscr{V}^*\tilde{\rho}_{12}+\tfrac{1}{2}\mathrm{i}\mathscr{V}\tilde{\rho}_{21}-2\gamma\rho_{22} \tag{2.117}$$

$$\mathrm{d}\tilde{\rho}_{12}/\mathrm{d}t = \tfrac{1}{2}\mathrm{i}\mathscr{V}(\rho_{11}-\rho_{22})-\gamma\tilde{\rho}_{12}+\mathrm{i}(\omega_0-\omega)\tilde{\rho}_{12}, \tag{2.118}$$

and the time derivative of $\tilde{\rho}_{21}$ is given by the complex conjugate of eqn (2.118). If these three rates of change are all set equal to zero, it is possible with the use of eqn (2.73) to solve for the steady-state density-matrix elements, and the results are

$$\rho_{22} = \frac{\tfrac{1}{4}|\mathscr{V}|^2}{(\omega_0-\omega)^2+\gamma^2+\tfrac{1}{2}|\mathscr{V}|^2} \tag{2.119}$$

$$\rho_{12} = -\exp\{-\mathrm{i}(\omega_0-\omega)t\}\,\frac{\tfrac{1}{2}\mathscr{V}(\omega_0-\omega-\mathrm{i}\gamma)}{(\omega_0-\omega)^2+\gamma^2+\tfrac{1}{2}|\mathscr{V}|^2}. \tag{2.120}$$

Consider first the effect of these more general expressions for the steady-state behaviour of the atoms on the expression for the susceptibility. The atomic dipole moment of eqn (2.96) is expressed in terms of density matrix elements with the help of eqn (2.72) as

$$\mathrm{d}(t) = -e\{\rho_{21}X_{12}\exp(-\mathrm{i}\omega_0 t)+\rho_{12}X_{21}\exp(\mathrm{i}\omega_0 t)\}. \tag{2.121}$$

Thus with substitution of eqn (2.120) and its complex conjugate, the same procedure as in eqns (2.106)–(2.108) produces a susceptibility

$$\chi(\omega) = \frac{Ne^2|D_{12}|^2}{3\epsilon_0\hbar V}\,\frac{\omega_0-\omega+\mathrm{i}\gamma}{(\omega_0-\omega)^2+\gamma^2+\tfrac{1}{2}|\mathscr{V}|^2}. \tag{2.122}$$

This is no longer a linear susceptibility because the field strength E_0 is contained in the quantity $|\mathscr{V}|$. The imaginary part of the susceptibility is the same as that given by the rotating-wave term in eqn (2.108) except for the additional contribution $\tfrac{1}{2}|\mathscr{V}|^2$ in the denominator.

The presence of the term $\tfrac{1}{2}|\mathscr{V}|^2$ in eqn (2.122) leads to saturation effects similar to those considered in Chapter 1. It clearly reduces the rate of absorption or attenuation of the incident light, and it corresponds to the same effect for monochromatic incident light as that for broad-band incident light discussed in the treatment of the microscopic theory of absorption. The linewidth of the atomic transition is increased from 2γ to

$$2(\gamma^2+\tfrac{1}{2}|\mathscr{V}|^2)^{\frac{1}{2}}; \tag{2.123}$$

the additional contribution to the linewidth is known as power broadening or saturation broadening.

2.10. Rabi oscillations with radiative damping

The susceptibility derived in the previous section is controlled by the steady-state off-diagonal density-matrix elements. The diagonal density-matrix elements provide the atomic populations in the two energy levels. The steady-state result (2.119) for the excited-state population produced by illumination with monochromatic light can be compared with the corresponding result (1.74) for illumination with broad-band light. The expressions differ in detail but have their more important features in common. Thus in the limit of very intense light, where $|\mathscr{V}|$ is much larger than the damping γ or the detuning $\omega_0-\omega$, eqn (2.119) tends to the limiting value $\tfrac{1}{2}$ in agreement with the saturation behaviour of eqn (1.74) illustrated in Fig. 1.11.

Again, in the limit of a weak beam of incident light, both expressions predict an atomic excitation proportional to the energy density of the light. Integration of eqn (2.119) gives

$$\int \rho_{22}\,\mathrm{d}\omega = \pi|\mathscr{V}|^2/4\gamma \qquad \text{for} \qquad |\mathscr{V}| \ll \gamma. \tag{2.124}$$

Now it can be shown from eqns (2.23), (2.39), and (2.55) that

$$\int B\bar{W}\,\mathrm{d}\omega = \pi|\mathscr{V}|^2/2. \tag{2.125}$$

Thus with the help of eqn (2.102), it is easily verified that in the weak-beam limit (1.74) agrees exactly with the broad-band result obtained by integrating eqn (2.119) over the absorption line.

The steady-state result (2.119) is independent of the initial atomic populations. For the variation of the atomic populations at shorter times, it is necessary to solve the Bloch equations (2.114) and (2.115) more generally with insertion of the initial conditions. It is unfortunately not possible to write down the general solutions of these equations in any very explicit form. We therefore consider two special cases that illustrate the form of the solutions, firstly assuming zero detuning ($\omega_0 = \omega$), and later assuming a weak beam of light with $|\mathscr{V}|$ much smaller than γ.

Problem 2.7. Show that solution of the optical Bloch equations (2.114) and (2.115) for $\omega_0 = \omega$ and the initial conditions

$$\rho_{22} = 0, \qquad \rho_{12} = 0$$

gives

$$\rho_{22} = \frac{\frac{1}{2}|\mathscr{V}|^2}{2\gamma^2+|\mathscr{V}|^2}\left\{1-\left[\cos\lambda t+\frac{3\gamma}{2\lambda}\sin\lambda t\right]\exp(-3\gamma t/2)\right\} \tag{2.126}$$

where

$$\lambda = (|\mathscr{V}|^2-\tfrac{1}{4}\gamma^2)^{\frac{1}{2}}. \tag{2.127}$$

Fig. 2.7 shows some examples of the time-dependent level of excitation obtained from eqn (2.126) for atoms initially in their ground states. The curve for zero radiative damping, $\gamma = 0$, reproduces the pure Rabi oscillations shown for zero detuning in Fig. 2.5, since in this case eqn (2.126) reduces to eqn (2.89). The curves for $\gamma \neq 0$ all tend to a steady-state limit given by the zero-detuning value of eqn (2.119). With increasing γ, the oscillations are damped out more and more rapidly and only a single maximum remains for $\gamma = |\mathscr{V}|/3$. Thus the incident light beam must be sufficiently strong for $|\mathscr{V}|$ to be much greater than 3γ in order for significant oscillations in the level populations to be generated.

The oscillatory behaviour of atomic excitation shown in Figs. 2.5 and 2.7 is known as *optical nutation*. The nutational frequency depends in general on the Rabi frequency $|\mathscr{V}|$, the detuning $\omega_0-\omega$, and the radiative damping γ. The frequencies given in eqns (2.84) and (2.127) apply respectively when γ and $\omega_0-\omega$ are set equal to zero, there being no simple analytical expression

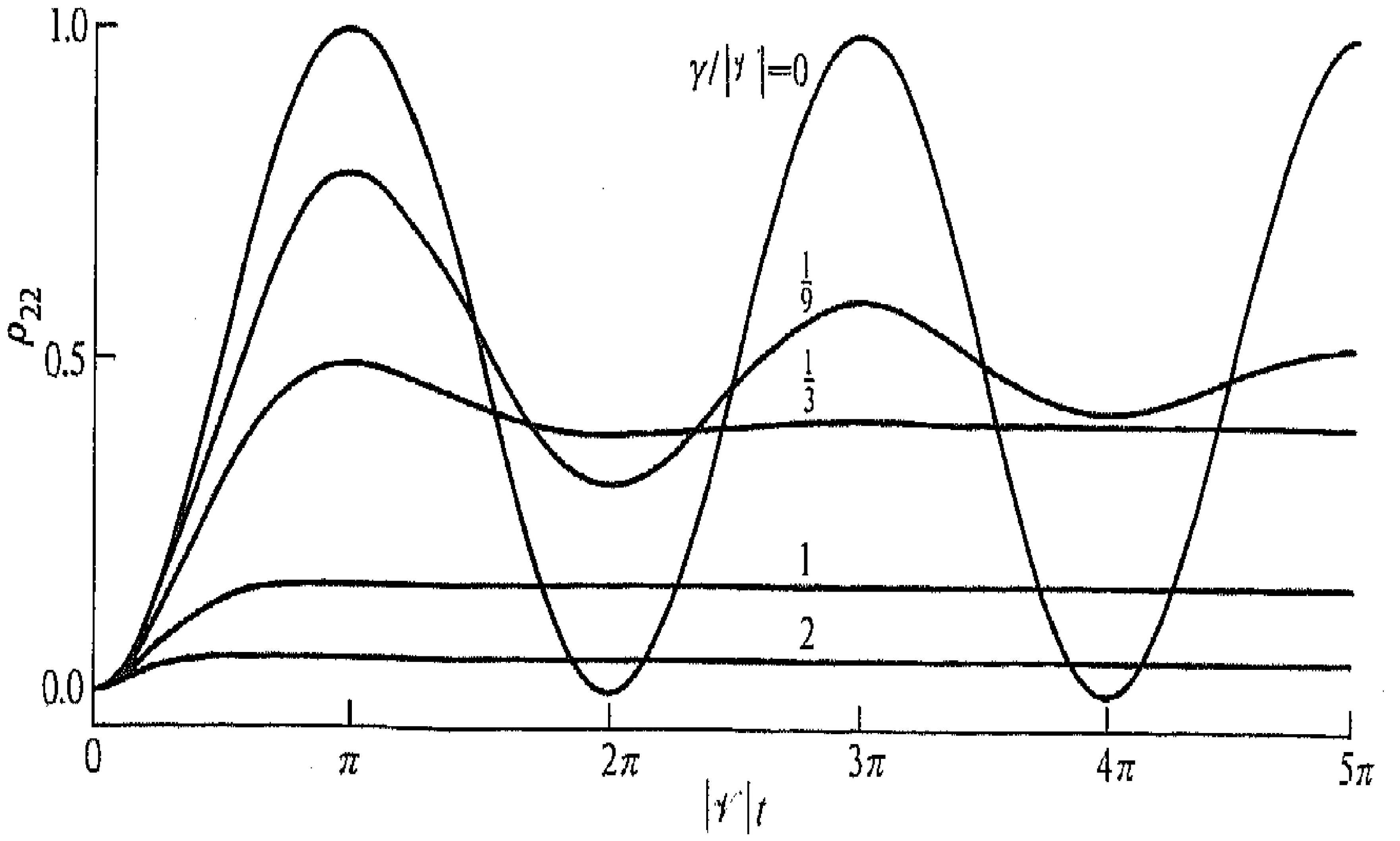

FIG. 2.7. Time dependences of the degree of atomic excitation ρ_{22} for zero detuning and the ratios of radiative damping γ to Rabi frequency $|\mathscr{V}|$ indicated against the curves.

for the nutational frequency in the general case. It is however always the case that significant oscillations occur only when the Rabi frequency is much greater than the radiative damping. The observation of optical nutation effects thus requires the use of intense exciting light, and laser sources are used in practice.

Consider the effect on the exciting beam of light of the changing level of atomic excitation. With the atoms initially in their ground states, the beam first suffers attenuation as energy is transferred to the atoms. However, as indicated in Figs. 2.5 and 2.7, for beams sufficiently intense that $|\mathscr{V}|$ is larger than the detuning and much larger than the damping, the excited-state component of the atomic wave-function eventually exceeds the ground-state component, and some of the atomic energy is radiated back into the light beam, producing an increase over its initial intensity. The optical nutation of the atoms is thus accompanied by corresponding oscillations in the intensity of the transmitted light. A detailed theory[7] of the time dependence of the transmitted light in a practical experiment must take account of other contributions to the optical linewidth, but the phenomenon is essentially a consequence of the oscillatory behaviour of the atomic excitation. Fig. 2.8 shows some experimental observations[8] of optical nutation effects in the D_2 transition of sodium; the Rabi frequency increases from $1{\cdot}27\times10^8\,\mathrm{s}^{-1}$ in trace (a) to $1{\cdot}80\times10^8\,\mathrm{s}^{-1}$ in trace (d), while the radiative damping parameter γ is approximately $3\times10^7\,\mathrm{s}^{-1}$. The reradiation of light by the atoms can in principle alter the cosine time dependence assumed for the incident light (see Chapter 7) but such effects can be ignored for an optically thin atomic vapour.

The second special case in which the Bloch equations can be easily solved is that of a weak beam of incident light where $|\mathscr{V}|$ is much smaller than the damping γ.

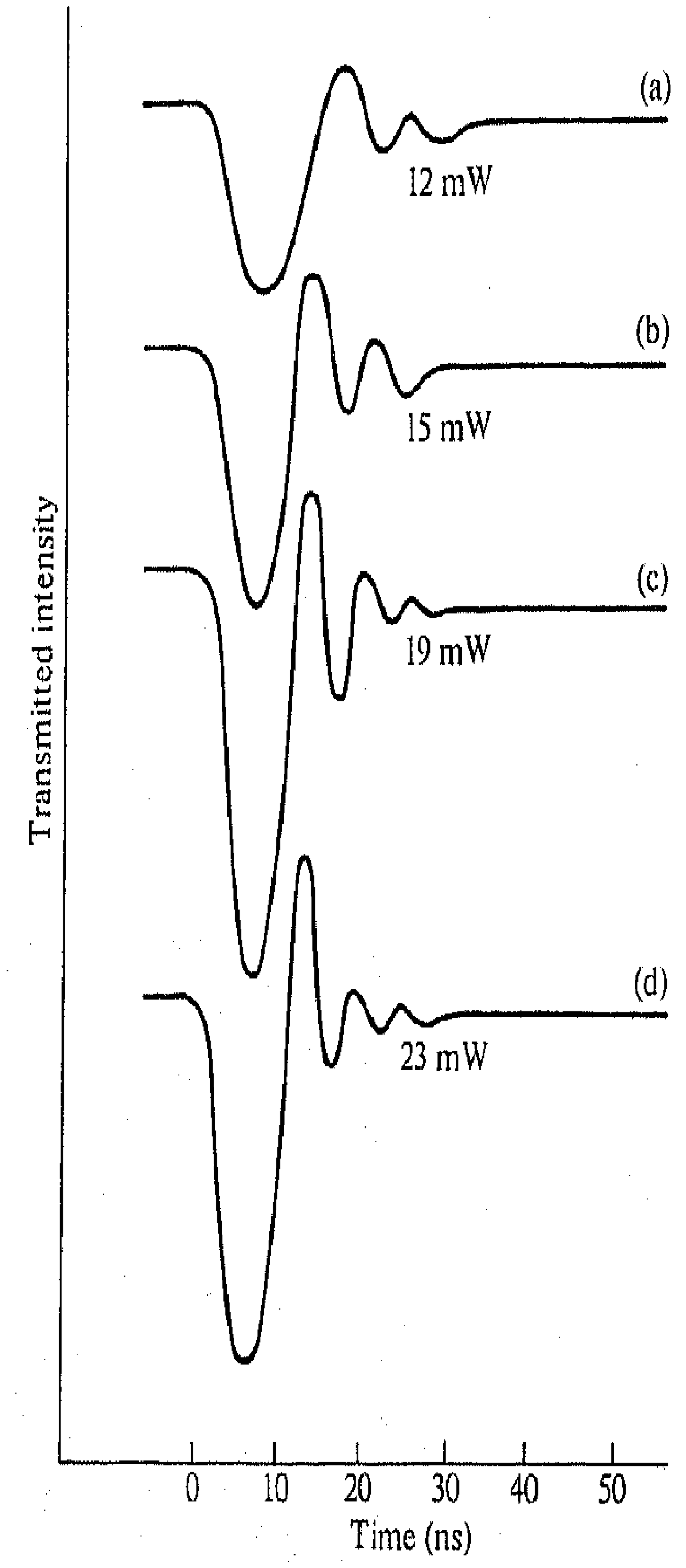

FIG. 2.8. Intensity of light transmitted through sodium vapour as a function of laser power. (After W. R. MacGillivray *et al.*, ref. 8.)

Problem 2.8. Show that solution of eqns (2.114) and (2.115) to lowest order in $|\mathscr{V}|$ in the limit $|\mathscr{V}| \ll \gamma$ for the same initial conditions as before gives

$$\rho_{22} = \frac{\frac{1}{4}|\mathscr{V}|^2}{(\omega_0-\omega)^2+\gamma^2}\{1+\exp(-2\gamma t)-2\cos[(\omega_0-\omega)t]\exp(-\gamma t)\}. \tag{2.128}$$

Fig. 2.9 shows the time dependence of the degree of atomic excitation in the weak-beam limit for several values of the detuning. This result generalizes eqn (2.42), to which it reduces in the limit of zero γ.

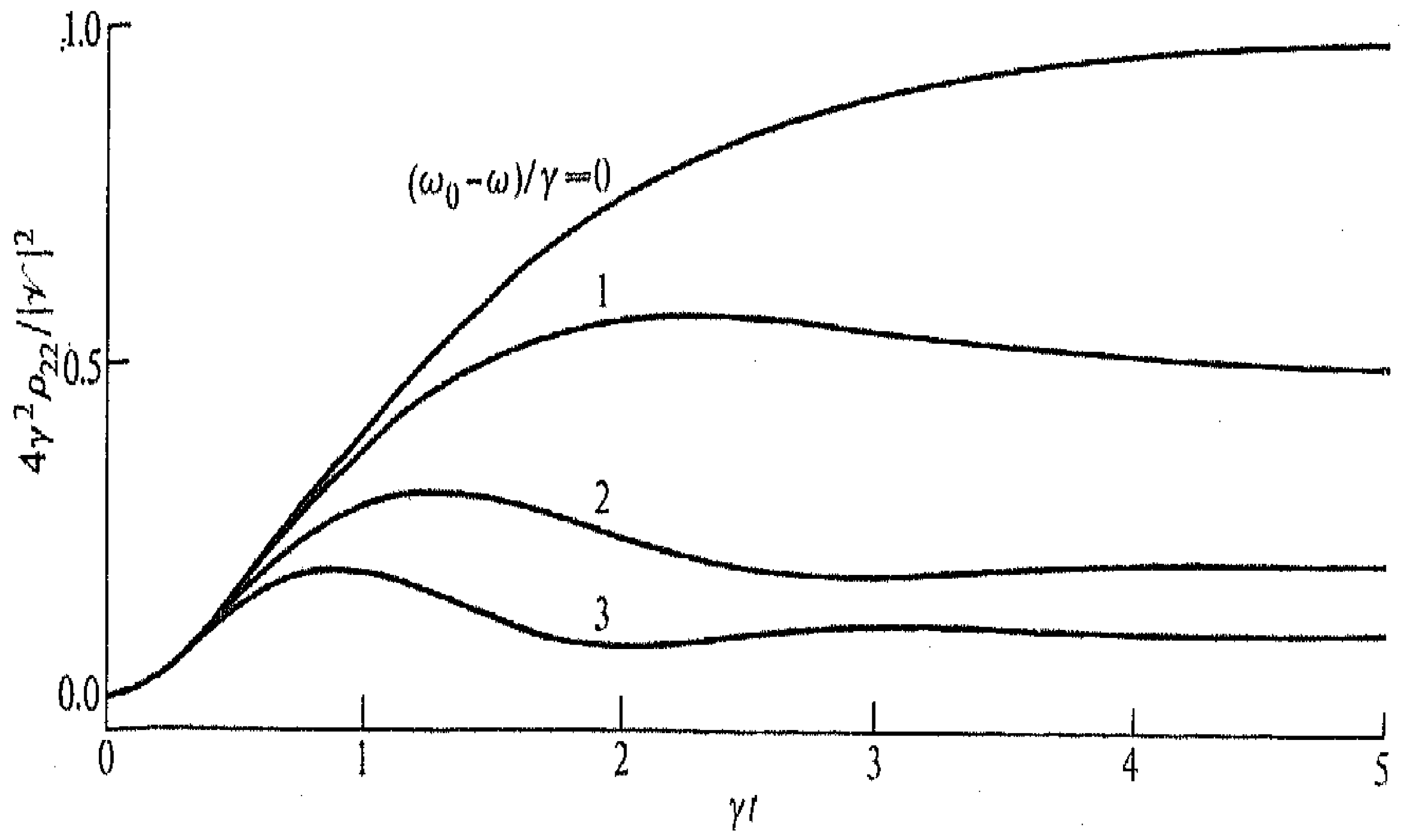

FIG. 2.9. Time dependences of the degree of atomic excitation ρ_{22} for a weak incident beam and the ratios of detuning $\omega_0-\omega$ to radiative damping γ indicated against the curves.

All of the curves in Figs. 2.5, 2.7, and 2.9 show the same initial quadratic dependence on time for $|\mathscr{V}|t \ll 1$. This property can be proved by a short-time expansion of the solutions of the optical Bloch equations.

Problem 2.9. Show that the lowest-order terms in the solution of the optical Bloch equations (2.114) and (2.115) for $|\mathscr{V}|t \ll 1$ and the initial conditions

$$\rho_{22} = 0, \qquad \rho_{12} = 0$$

give

$$\rho_{22} = \tfrac{1}{4}|\mathscr{V}|^2 t^2 \tag{2.129}$$

irrespective of the values of $\omega_0-\omega$ and γ.

This initial quadratic behaviour contrasts with the linear degree of atomic excitation for broad-band incident light. The broad-band result can be retrieved by integration of (2.128) over the radiatively broadened absorption line. Some simple contour integration gives

$$\int_{-\infty}^{\infty} \rho_{22}\,\mathrm{d}\omega = (\pi|\mathscr{V}|^2/4\gamma)\{1-\exp(-2\gamma t)\}. \tag{2.130}$$

This expression has the steady-state limit already found in eqn (2.124). With the help of eqn (2.125) it is seen that eqn (2.130) agrees exactly with the weak-beam limit of the broad-band result (1.70) derived in the Einstein theory of absorption and emission.

The explicit results derived in the present section give the time dependence of the degree of atomic excitation for the zero-detuning and weak-beam limits. More general solutions are most conveniently obtained by numerical integration of the optical Bloch equations[9].

2.11. Collision broadening

The radiative and power broadening discussed in §§2.8 and 2.9 are inescapable features of any atomic transition excited by an incident light beam. The importance of further line-broadening mechanisms depends upon the physical conditions of the atomic gas. The dominant effects, which result from the atomic motion, are the collision and Doppler broadening mechanisms discussed in this and the following section.

The theory of collision broadening is an extended field of study[10–13] and a thorough treatment would require a lengthy discussion. We here consider just enough detail of the process to illustrate the nature of the mechanism. The occurrence of collisions between the atoms in a gas is a random process. According to the kinetic theory of gases[14], the probability $p(\tau)\mathrm{d}\tau$ that an atom has a period of free flight between collisions lasting a length of time between τ and $\tau+\mathrm{d}\tau$ is

$$p(\tau)\,\mathrm{d}\tau = (1/\tau_0)\exp(-\tau/\tau_0)\,\mathrm{d}\tau, \tag{2.131}$$

where the mean period τ_0 of free flight can be expressed as

$$\frac{1}{\tau_0} = \frac{4d^2N}{V}\left(\frac{\pi k_B T}{M}\right)^{\frac{1}{2}}. \tag{2.132}$$

Here d is the distance between the centres of the atoms during a collision and M is the atomic mass.

The effect of a collision on the atomic energy levels and wavefunctions is quite complicated. The energy levels are shifted during a collision by the forces of interaction between the two colliding atoms, and the wavefunction becomes some linear combination of the wavefunctions of the unperturbed atom. If the duration of the collision is sufficiently brief, it is permissible to neglect any absorption or emission of light that occurs while the collision is taking place. The collisions then influence optical processes only via the changes in the atomic states from those preceding to those following the collision. We assume in what follows that the collision durations are indeed very short compared to the average time τ_0 of the periods of free flight during which the atomic states remain constant.

Two categories of collision can be distinguished. *Inelastic* collisions produce a change in the state of the atom from one energy level to another. Their effect can be represented by an additional decay rate for the atomic level populations and they appear in the optical Bloch equations via a suitable collisional addition to the radiative decay rate γ. *Elastic* collisions leave the atom in the same energy level as before and their effect is limited to changes in the phase of the atomic wavefunction. Changes of phase in C_1 and C_2 in eqn (2.8) change the off-diagonal elements (2.72) of the atomic density matrix but they produce no change in the diagonal elements (2.71). The elastic phase-interruption collisions thus introduce an additional decay rate into the off-diagonal optical Bloch equation (2.115) but the diagonal equation (2.114) is unchanged. We restrict attention to the elastic variety of collision; these have the dominant line-broadening effect for a wide range of physical conditions and they also provide a very convenient model for the discussion of time-dependent properties of light in Chapter 3.

The off-diagonal decay rate caused by the elastic collisions is denoted γ_{coll}. This quantity is clearly proportional to the collision rate $1/\tau_0$ and it is shown in §3.3 that in fact

$$\gamma_{\text{coll}} = 1/\tau_0; \tag{2.133}$$

the factor of 2 difference between this and the analogous relation (2.102) for radiative broadening should be noted. With collisions included, the off-diagonal optical Bloch equation (2.115) becomes

$$\mathrm{d}\rho_{12}/\mathrm{d}t = \tfrac{1}{2}\mathrm{i}\mathcal{V}\exp\{-\mathrm{i}(\omega_0-\omega)t\}(\rho_{11}-\rho_{22})-\gamma'\rho_{12}, \tag{2.134}$$

where

$$\gamma' = \gamma+\gamma_{\text{coll}}. \tag{2.135}$$

The results (2.119) and (2.120) for the steady-state density-matrix elements are generalized to

$$\rho_{22} = \frac{\frac{1}{4}(\gamma'/\gamma)|\mathcal{V}|^2}{(\omega_0-\omega)^2+\gamma'^2+\frac{1}{2}(\gamma'/\gamma)|\mathcal{V}|^2} \tag{2.136}$$

$$\rho_{12} = -\exp\{-\mathrm{i}(\omega_0-\omega)t\}\frac{\frac{1}{2}\mathcal{V}(\omega_0-\omega-\mathrm{i}\gamma')}{(\omega_0-\omega)^2+\gamma'^2+\frac{1}{2}(\gamma'/\gamma)|\mathcal{V}|^2}. \tag{2.137}$$

It is now straightforward to rederive the susceptibility, and the generalization of eqn (2.122) is

$$\chi(\omega) = \frac{Ne^2|D_{12}|^2}{3\epsilon_0\hbar V}\,\frac{\omega_0-\omega+\mathrm{i}\gamma'}{(\omega_0-\omega)^2+\gamma'^2+\frac{1}{2}(\gamma'/\gamma)|\mathcal{V}|^2}. \tag{2.138}$$

The linewidth of the atomic transition with inclusion of radiative, power, and collision broadening is thus

$$2\{\gamma'^2+\tfrac{1}{2}(\gamma'/\gamma)|\mathcal{V}|^2\}^{\frac{1}{2}}, \tag{2.139}$$

generalizing eqn (2.123).

Most of the subsequent discussion refers to fairly weak light beams where the power broadening is negligible and eqn (2.139) reduces to

$$2\gamma+2\gamma_{\text{coll}}. \tag{2.140}$$

The absorption line has a Lorentzian shape in this case and its width is obtained from a simple sum of the radiative and collisional contributions. A typical value of the collision time at a gas density corresponding to a pressure of 10^5 Pa at room temperature is

$$\tau_0 \approx 3\times 10^{-11}\,\mathrm{s}. \tag{2.141}$$

The collision linewidth for this value is about 100 times the natural or radiative linewidth derived from the *A*-coefficient magnitude of eqn (2.57).

2.12. Doppler broadening

The atoms in a gas have a spread in their velocities that leads via the Doppler effect to a corresponding distribution in the frequencies at which they can absorb or emit light. Let us ignore for the present all other sources of line broadening and consider the absorption of light of frequency ω propagated parallel to the *z*-axis. Suppose that an atom in its lower energy level E_1 has velocity $\mathbf{v}_1$ before the absorption takes place. Absorption of a photon of energy $\hbar\omega$ promotes the atom into its excited energy level E_2. The photon has a momentum $\hbar\mathbf{k}$, where $k = \omega/c$, and its absorption causes a recoil of the atom to a new velocity $\mathbf{v}_2$. The total momenta before and after the absorption must be equal,

$$M\mathbf{v}_1+\hbar\mathbf{k} = M\mathbf{v}_2, \tag{2.142}$$

where M is the atomic mass. The energy conservation condition is

$$E_1+\tfrac{1}{2}Mv_1^2+\hbar\omega = E_2+\tfrac{1}{2}Mv_2^2. \tag{2.143}$$

An atom with zero velocity before and after the absorption could absorb only light of frequency ω_0 given by

$$\hbar\omega_0 = E_2-E_1. \tag{2.144}$$

Elimination of v_2 from eqn (2.143) with the help of eqns (2.142) and (2.144) gives

$$\hbar\omega_0 = \hbar\omega-\hbar\mathbf{v}_1.\mathbf{k}-(\hbar^2k^2/2M), \tag{2.145}$$

or

$$\omega_0 = \omega-(\omega v_1^z/c)-(\hbar\omega^2/2Mc^2), \tag{2.146}$$

since $\mathbf{k}$ points in the *z*-direction. Typical orders of magnitude for some quantities on the right of eqn (2.146) are

$$v_1^z/c \approx 10^{-5}, \qquad \hbar\omega/2Mc^2 \approx 10^{-9}. \tag{2.147}$$

Thus ω differs only slightly from ω_0 and the final term on the right can be neglected altogether, so that

$$\omega = \frac{\omega_0}{1-(v_1^z/c)} \approx \omega_0\left(1+\frac{v_1^z}{c}\right). \tag{2.148}$$

The light can be absorbed only if its frequency ω differs from ω_0 by the Doppler shift appropriate to the initial atomic velocity.

The distribution of absorption frequencies for all the atoms in the gas therefore mirrors their velocity distribution. According to the Maxwellian velocity distribution[15], the relative probability that an atom in a gas at temperature T has the *z*-component of its velocity between v^z and $v^z+\mathrm{d}v^z$ is

$$\exp(-M(v^z)^2/2k_\mathrm{B}T)\,\mathrm{d}v^z = \exp\{-Mc^2(\omega-\omega_0)^2/2\omega_0^2k_\mathrm{B}T\}(c/\omega_0)\,\mathrm{d}\omega, \tag{2.149}$$

where eqn (2.148) has been used. The expression on the right is the frequency distribution of the absorbed light and is known as the Gaussian lineshape.

The peak of the Gaussian line is at $\omega = \omega_0$ and the line has half its maximum intensity at the frequencies that satisfy

$$\tfrac{1}{2} = \exp\{-Mc^2(\omega-\omega_0)^2/2\omega_0^2k_\mathrm{B}T\}. \tag{2.150}$$

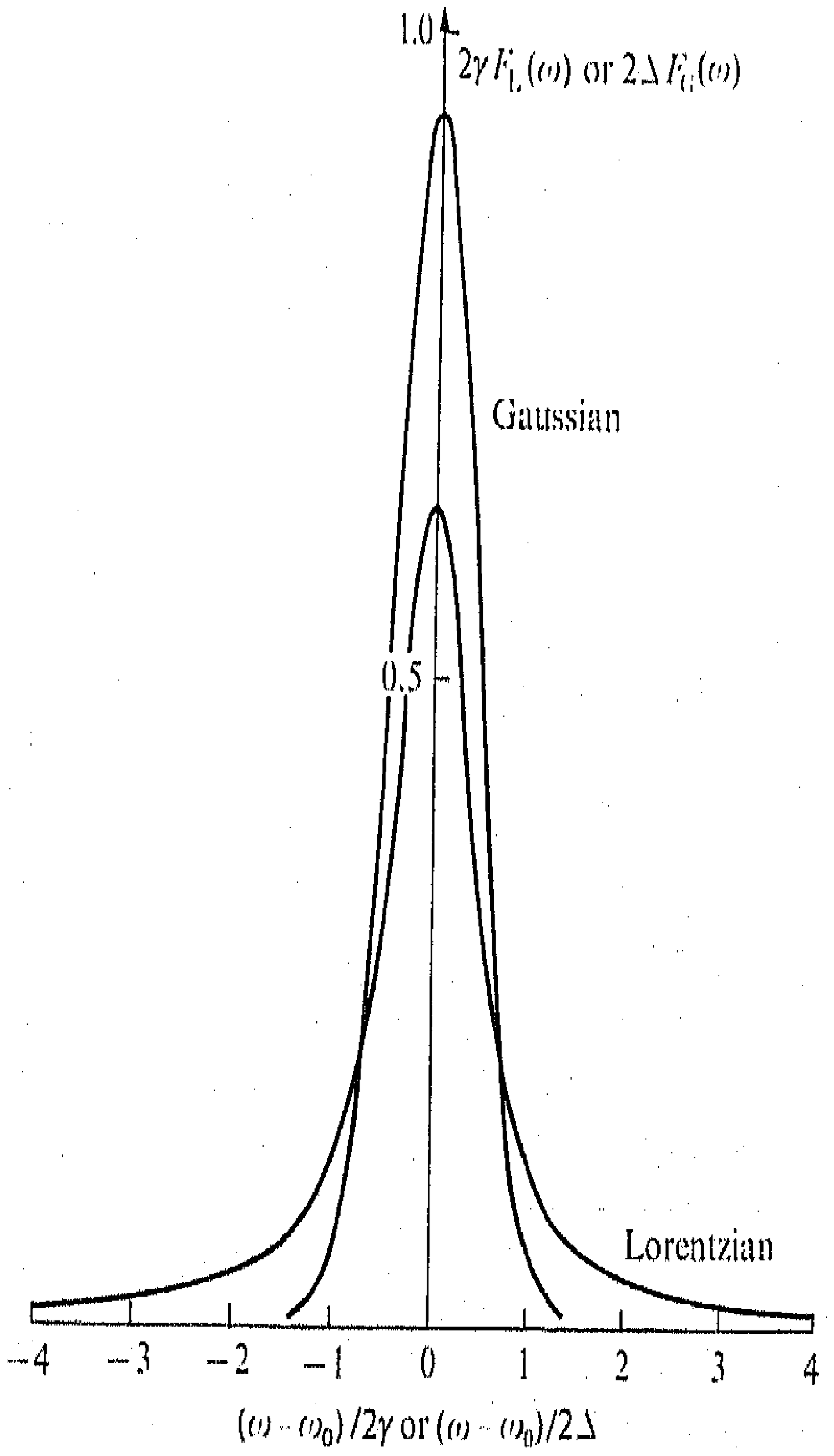

FIG. 2.10. Comparison of the Gaussian and Lorentzian normalized lineshape functions. The functions are shown with the same width, equal to one unit on the horizontal scale.

The full width of the Doppler-broadened line at half its maximum height is thus

$$2\Delta = 2\omega_0(2k_BT\ln 2/Mc^2)^{\frac{1}{2}}. \tag{2.151}$$

The breadth of the line can alternatively be expressed in terms of the root-mean-square spread δ of the Gaussian distribution. It is not hard to show that

$$\delta = \omega_0(k_BT/Mc^2)^{\frac{1}{2}} = \Delta/(2\ln 2)^{\frac{1}{2}} \approx \Delta/1{\cdot}18. \tag{2.152}$$

The Doppler width is approximately equal to the collisional width for the parameter values used in eqn (2.141).

It is convenient to define the Gaussian lineshape function as

$$F_G(\omega) = (2\pi\delta^2)^{-\frac{1}{2}}\exp\{-(\omega-\omega_0)^2/2\delta^2\}, \tag{2.153}$$

where the constant in front of the exponential factor ensures normalization

$$\int F_G(\omega)\,d\omega = 1. \tag{2.154}$$

The Gaussian lineshape function $F_G(\omega)$ and the Lorentzian function $F_L(\omega)$ defined in eqn (2.112) are plotted for comparison in Fig. 2.10. Both lines are drawn with the same width at half height, that is $2\Delta = 2\gamma$, and enclose equal unit areas. It is seen that the Gaussian line is the more sharply peaked and it falls off very rapidly away from the central region. In contrast, the Lorentzian line has tails that extend some way from the region of the peak.

2.13. Composite absorption lineshape

The expressions (2.132) and (2.151) show explicitly how the collision and Doppler widths can be made arbitrarily small by adjustment of experimental parameters. Both widths are proportional to the square root of the temperature, and the collision width is also proportional to the gas density or, equivalently, to the gas pressure. Collision broadening is sometimes called pressure broadening for this reason. It is in principle possible to observe an absorption line with only its unavoidable radiative line broadening by the use of a gas maintained at a sufficiently low temperature. In addition, by adjustment of the gas pressure, it is possible to vary the collision width relative to the Doppler and radiative widths.

Fig. 2.11 shows some experimental results[16] for the linewidth of a CO_2 transition at a wavelength of 10·6 μm as a function of the gas pressure. The expected linear contribution of the collision width is clearly observed, and the magnitude of the other linewidth contributions is determined by the zero-pressure intercept. The residual width in this case mainly arises from Doppler broadening, the radiative width being small owing to the low frequency of the transition. The collision width is also much smaller than that given by eqn (2.141) owing to the low pressures and correspondingly low densities used (15 Torr $\approx 2\times10^3$ Pa).

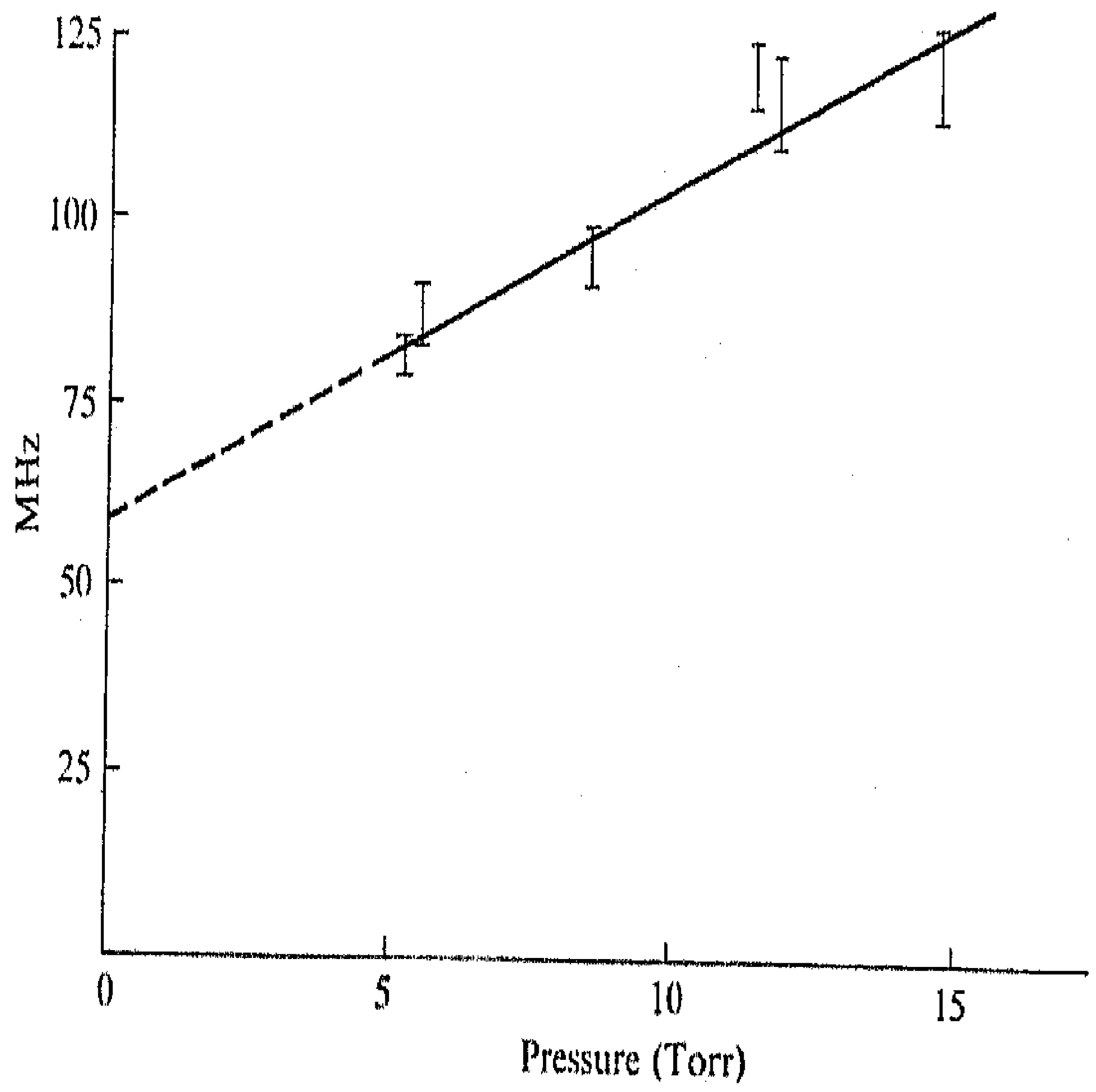

FIG. 2.11. Variation with pressure of the width of a laser transition in CO_2. (After T. J. Bridges *et al.*, ref. 16.)

When the Doppler, collision, and possibly also the radiative contributions to the linewidth are of comparable magnitude, it is necessary to determine the composite lineshape that results from the three processes (we assume a weak incident beam and negligible power broadening). Consider first the combination of two line-broadening mechanisms that individually generate normalized lineshape functions $F_1(\omega)$ and $F_2(\omega)$. The composite lineshape is

$$F(\omega) = \int_{-\infty}^{\infty} F_1(\nu)F_2(\omega+\omega_0-\nu)\,d\nu, \tag{2.155}$$

where ω_0 is the common central frequency of the two distributions. In words, the integration associates with each frequency component of the shape F_1 a broadened distribution appropriate to the mechanism that generates the shape F_2.

Clearly, any number of line-broadening mechanisms can be combined by repeated applications of eqn (2.155). Note also that the final shape is independent of the order in which the contributions are combined, and that the value of the integral in eqn (2.155) is invariant under interchange of F_1 and

F_2. Some applications of eqn (2.155) lead to simple results, as expressed in the following problems.

Problem 2.10. If the sources of broadening both lead to Lorentzian lineshapes with widths $2\gamma_1$ and $2\gamma_2$, prove that the composite line is also Lorentzian and has a width

$$2\gamma = 2\gamma_1 + 2\gamma_2. \tag{2.156}$$

The combined linewidth for radiative and collision broadening established in eqn (2.140) is a special case of this general result.

Problem 2.11. Carry out a similar calculation for the case of two Gaussian line-broadening mechanisms and show that the composite line is also Gaussian with a width 2Δ where

$$\Delta^2 = \Delta_1^2 + \Delta_2^2, \tag{2.157}$$

and $2\Delta_1$ and $2\Delta_2$ are the individual widths.

The case where one lineshape is Lorentzian and the other is Gaussian leads to the more complicated integral

$$\begin{aligned} F(\omega) &= \frac{\gamma}{2^{\frac{1}{2}}\pi^{\frac{3}{2}}\,\delta}\int\limits_{-\infty}^{\infty}\frac{\exp\{-(\omega-\nu)^2/2\,\delta^2\}}{(\omega_0-\nu)^2+\gamma^2}\,\mathrm{d}\nu \\ &= \frac{1}{(2\pi)^{\frac{1}{2}}\,\delta}\,\mathrm{Re}\,w\left(\frac{\omega_0-\omega+i\gamma}{2^{\frac{1}{2}}\,\delta}\right), \end{aligned} \tag{2.158}$$

where w is a form of complex error function[17]. There is no simple analytical expression for the linewidth in this case, but useful numerical tabulations of w are available[17,18]. The shape is named after Voigt and is intermediate between the Lorentzian and Gaussian shapes, to which it reduces in the limits $\delta \to 0$ and $\gamma \to 0$, respectively. The Voigt lineshape is important since it occurs in the common situation where Doppler and collision broadening are both significant, provided that the two mechanisms are assumed to contribute independently to the combined lineshape. Fig. 2.12 shows how the purely Gaussian lineshape is modified by combination with increasing amounts of Lorentzian line-broadening.

Line-broadening processes can be divided into two broad categories that are characterized by different qualitative properties and are associated with the two basic lineshapes. One category contains those sources of line broadening where different atoms absorb or emit light at somewhat different frequencies because of a statistical distribution in some parameter that determines the transition frequency. Such line-broadening processes generally produce a Gaussian lineshape. The Doppler broadening belongs to this category, the atomic velocity being the relevant statistical parameter. The atoms that absorb at a particular frequency are, in principle, distinguishable from the rest by their component of velocity parallel to the absorbed light beam. Another example occurs for absorption by atoms embedded in a crystal, where variations in the local strain can produce shifts in atomic transition frequency. These effects belong to the category of *inhomogeneous* broadening mechanisms.

The Lorentzian lineshape occurs for *homogeneous* broadening mechanisms, where each absorbing or emitting atom is identical to the rest. For example, in the radiative and collision broadening processes, there is, in principle, no experimental way of associating light of a certain frequency with a particular

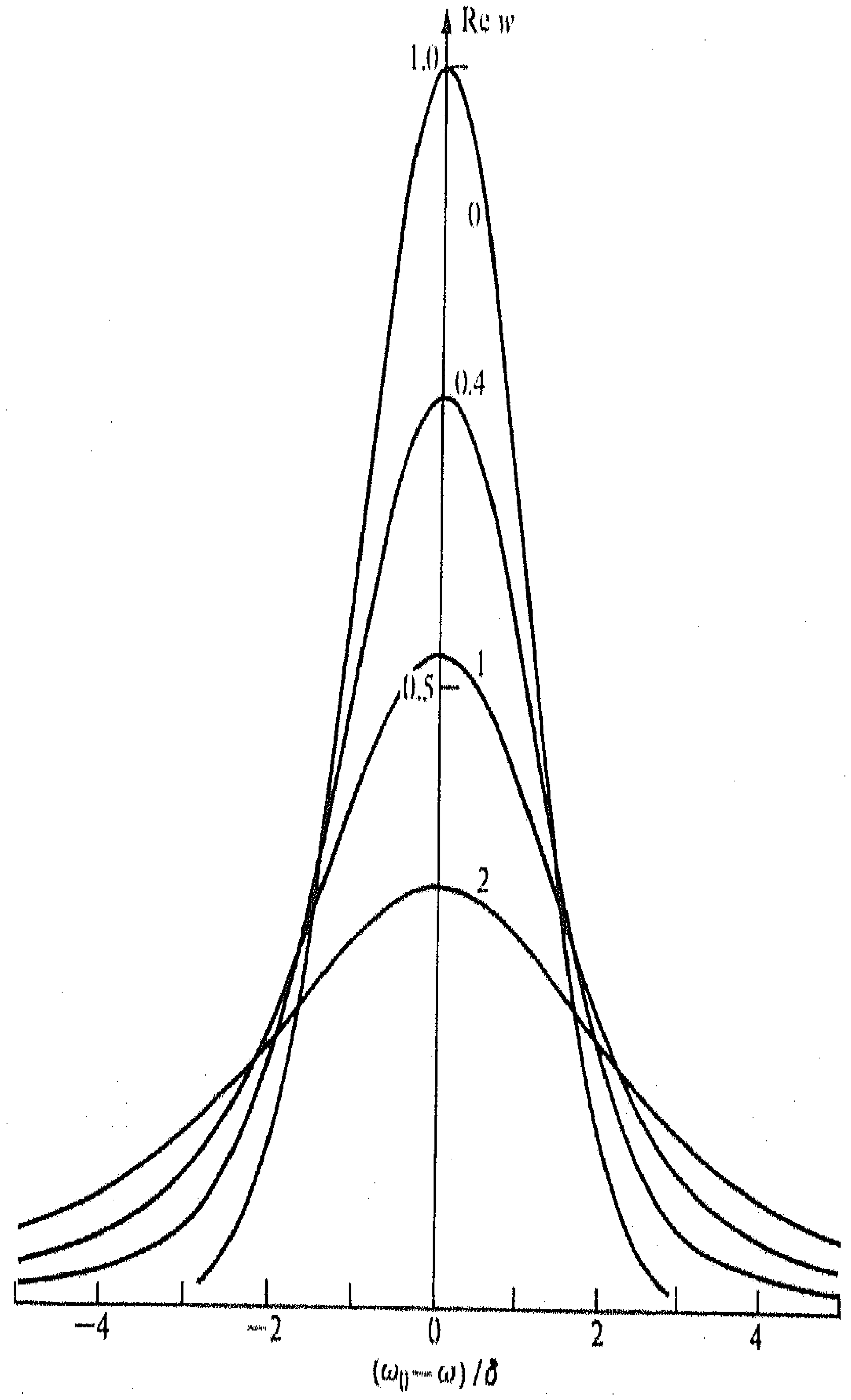

FIG. 2.12. Real part of the complex error function in eqn (2.158) for values of the ratio γ/δ indicated against the curves. The curve for $\gamma/\delta = 0$ is a Gaussian lineshape, while the remaining curves are Voigt lineshapes.

group of atoms. The width $\Delta\omega$ in these cases is a consequence of a finite mean length of time Δt for which the atomic state is undisturbed. According to the quantum-mechanical uncertainty principle, or the properties of Fourier transforms,

$$\Delta\omega\,\Delta t \geqslant 1, \tag{2.159}$$

in agreement with the explicit results for the radiative and collision processes.

Further details of spectral lineshape theory and the interplay between theory and experiment can be found in more specialized books and articles[11,13]. The main concern of the treatment given above is the provision of sufficient basis for the discussion of time-dependent fluctuation properties of light beams that forms the main topic of Chapter 3. Another related aspect not considered here is the effect of collision and Doppler broadening on the Rabi oscillations in the excitation of atoms subjected to monochromatic incident light; full discussions are available in the literature[19].

2.14. Bloch equations and rate equations

We conclude the chapter with a more detailed discussion of the relation between the optical Bloch equations and the simpler rate equations for atomic populations. The basic rate equation for two-level atoms is (1.45), and this has been used in Chapter 1 to treat a range of optical processes.

The most general optical Bloch equations derived in the present chapter are given by eqns (2.114) and (2.134). With

$$\tilde{\rho}_{12} = \exp\{\mathrm{i}(\omega_0-\omega)t\}\rho_{12} \qquad \text{and} \qquad \tilde{\rho}_{21} = \exp\{-\mathrm{i}(\omega_0-\omega)t\}\rho_{21}, \tag{2.160}$$

as in (2.116), the equations are

$$\mathrm{d}\rho_{22}/\mathrm{d}t = -\tfrac{1}{2}\mathrm{i}\mathscr{V}^*\tilde{\rho}_{12}+\tfrac{1}{2}\mathrm{i}\mathscr{V}\tilde{\rho}_{21}-2\gamma\rho_{22} \tag{2.161}$$

$$\mathrm{d}\tilde{\rho}_{12}/\mathrm{d}t = \tfrac{1}{2}\mathrm{i}\mathscr{V}(\rho_{11}-\rho_{22})+[\mathrm{i}(\omega_0-\omega)-\gamma']\tilde{\rho}_{12}. \tag{2.162}$$

Here γ is the radiative damping rate, while γ' is the sum of radiative and collision rates, as in eqn (2.135). By analogy with the Bloch equations for a spin in a magnetic field, the damping constants are sometimes expressed in the forms[5]

$$2\gamma = 1/T_1 \qquad \text{and} \qquad \gamma' = 1/T_2, \tag{2.163}$$

where T_1 and T_2 are known respectively as the longitudinal and transverse relaxation times.

The connections between the rate equations and the optical Bloch equations are most easily studied in the limit of low beam intensity where $|\mathscr{V}|$ is much smaller than γ. Then with the same initial conditions (2.86) as assumed before, solution of eqns (2.161) and (2.162) to the lowest order in $|\mathscr{V}|$ gives

$$\rho_{22} = \tfrac{1}{4}|\mathscr{V}|^2\Bigg\{\frac{\gamma'/\gamma}{(\omega_0-\omega)^2+\gamma'^2}+\frac{(2\gamma-\gamma')/\gamma}{(\omega_0-\omega)^2+(2\gamma-\gamma')^2}\exp(-2\gamma t)$$
$$-\frac{2[(\omega_0-\omega)^2+\gamma'(2\gamma-\gamma')]\cos[(\omega_0-\omega)t]+4(\omega_0-\omega)(\gamma'-\gamma)\sin[(\omega_0-\omega)t]}{[(\omega_0-\omega)^2+\gamma'^2][(\omega_0-\omega)^2+(2\gamma-\gamma')^2]}$$
$$\times\exp(-\gamma' t)\Bigg\}. \tag{2.164}$$

In the absence of collision broadening, where $\gamma' = \gamma$, this reduces to the result (2.128) derived previously. The off-diagonal density matrix element is not needed for the present discussion, but for use in Chapter 8 we give here the solution to lowest order in $|\mathscr{V}|$ for a somewhat less restrictive initial condition in which ρ_{22} vanishes but ρ_{12} has an arbitrary initial value $\rho_{12}(0)$,

$$\rho_{12} = \frac{\tfrac{1}{2}\mathrm{i}\mathscr{V}}{\mathrm{i}(\omega_0-\omega)-\gamma'}\{\exp(-\gamma' t)-\exp[-\mathrm{i}(\omega_0-\omega)t]\}+\rho_{12}(0)\exp(-\gamma' t). \tag{2.165}$$

There are two distinct regimes in which the diagonal solution (2.164) resembles the time dependence of the excited-state population obtained from the rate equations, where eqn (1.70) gives

$$N_2 = (NB\bar{W}/A)\{1-\exp(-At)\} \tag{2.166}$$

in the limit of a weak incident beam. The first regime is that of broad-band incident light, whose frequency spread exceeds the linewidth $2\gamma'$ of the atomic transition.

Problem 2.12. Prove by contour integration of (2.164) that

$$\int_{-\infty}^{\infty}\rho_{22}\,\mathrm{d}\omega = (\pi|\mathscr{V}|^2/4\gamma)\{1-\exp(-2\gamma t)\} \tag{2.167}$$

valid whether γ' is greater or smaller than 2γ.

This is exactly the same as eqn (2.130), and the result applies for all values, including zero, of the collision broadening. The broad-band limit, represented schematically on the left of Fig. 2.13, has already been mentioned several times.

The second regime is that of large collision broadening, where γ' is much greater than γ. Then for times t comparable to $1/\gamma$, the inequality $t \gg 1/\gamma'$ is satisfied, and the general solution (2.164) reduces to

$$\rho_{22} = \frac{|\mathscr{V}|^2\gamma'/4\gamma}{(\omega_0-\omega)^2+\gamma'^2}\{1-\exp(-2\gamma t)\} \qquad (\gamma' \gg \gamma). \tag{2.168}$$

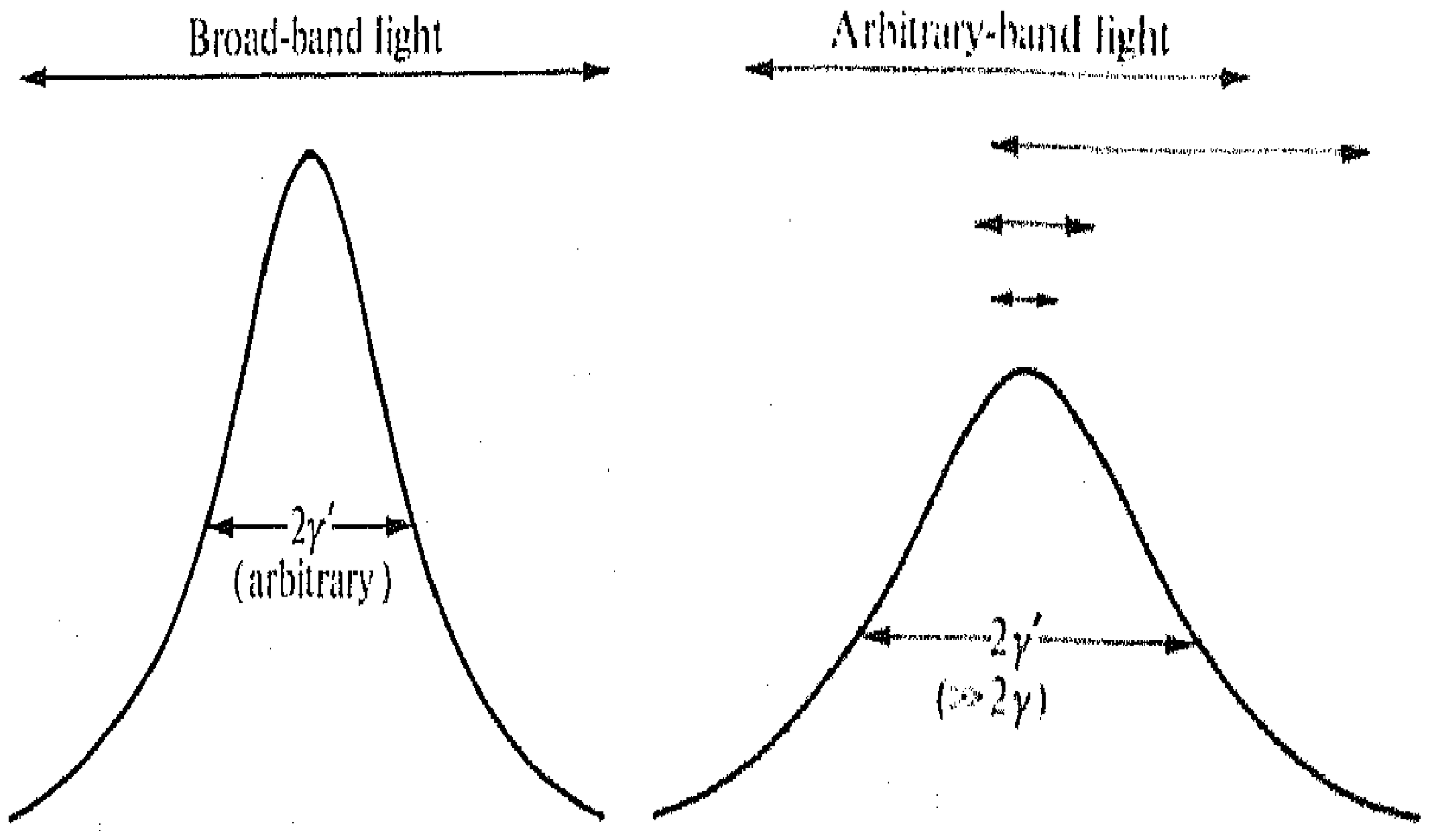

FIG. 2.13. Representations of the two regimes in which the optical Bloch equations reproduce the same atomic level populations as the Einstein-coefficient rate equations.

If we define a quantity

$$r = \tfrac{1}{2}|\mathscr{V}|^2\gamma'/[(\omega_0-\omega)^2+\gamma'^2], \qquad (2.169)$$

then the rate equation

$$\mathrm{d}\rho_{22}/\mathrm{d}t = r - 2\gamma\rho_{22} \qquad (2.170)$$

has a solution

$$\rho_{22} = (r/2\gamma)\{1-\exp(-2\gamma t)\} \qquad (2.171)$$

identical to eqn (2.168). The time dependence of eqns (2.168) or (2.171) is again the same as that in the weak-beam solution (2.166) of the basic rate equation. The equivalence of the Bloch equation and rate equation solutions in this second regime, shown schematically on the right of Fig. 2.13, holds for any bandwidth of the incident light.

The rate equation (2.170) that is equivalent to the optical Bloch equations in the $\gamma' \gg \gamma$ limit shows that the excited-state population is determined by the competition between an excitation rate r and the radiative decay rate 2γ. It is seen from eqn (2.169) that the excitation rate has a dependence on incident frequency ω that follows the collision-broadened Lorentzian lineshape of the atomic transition. The rate r has the same kind of physical significance as the pumping rate from level 3 to level 2 in the laser theory of §1.12.

The above discussion is based on the solution of the Bloch equations in the presence of collision broadening, but similar rate-equation limits can be established more generally in the case where Doppler broadening is also present[19]. Thus rate equations are valid in general when *either* (i) the bandwidth of the incident light exceeds the atomic transition linewidth *or* (ii) the combined collision and Doppler linewidth greatly exceeds the radiative linewidth of the transition. Note that the rate equation involves only the intensity of the incident light while both the phase and amplitude of the electric vector of the light enter the optical Bloch equations via $\mathscr{V}$ and $\mathscr{V}^*$.

References

1. See, for example, ANDERSON, E. E. (1971). *Modern physics and quantum mechanics*, p. 143. W. B. Saunders, Philadelphia.
2. See ref. 1, p. 150.
3. See, for example, DWIGHT, H. B. (1961). *Tables of integrals*, p. 221. Macmillan, New York.
4. BETHE, H. A. and SALPETER, E. E. (1957). *Quantum mechanics of one- and two-electron atoms*, p. 266. Springer-Verlag, Berlin.
5. ALLEN, L. and EBERLY, J. H. (1975). *Optical resonance and two-level atoms*. Wiley-Interscience, New York.
6. RABI, I. I. (1937). *Phys. Rev.* **51,** 652.
7. BREWER, R. G. (1977). *Nonlinear spectroscopy* (ed. N. Bloembergen), p. 87. North-Holland, Amsterdam.
8. MACGILLIVRAY, W. R., PEGG, D. T., and STANDAGE, M. C. (1978). *Optics Commun.* **25,** 355.
9. SMITH, R. A. (1978) *Proc. R. Soc.* **A362,** 1.
10. WEISSKOPF, V. (1933). *Phys. Z.* **34,** 1. This paper is reprinted, translated, and discussed by HINDMARSH, W. R. (1967). In *Atomic spectra*. Pergamon, Oxford; the book contains a useful account of spectral linewidth theory.
11. PEACH, G. (1975). *Contemp. Phys.* **16,** 17; (1981) *Advan. Phys.* **30,** 367.
12. For a review of radiative and collisional linewidth theory see VAN VLECK, J. H. and HUBER, D. L. (1977). *Rev. Mod. Phys.* **49,** 939.
13. CORNEY, A. (1977). *Atomic and laser spectroscopy*, Chapter 8. Clarendon Press, Oxford.
14. See, for example, LIFSHITZ, E. M. and PITAEVSKII, L. P. (1980). *Statistical physics*, Part 1, §39. Pergamon, Oxford.
15. See §29 of ref. 14.
16. BRIDGES, T. J., HAUS, H. A., and HOFF, P. W. (1968). *Appl. Phys. Lett.* **13,** 316.
17. ABRAMOWITZ, M. and STEGUN, I. A. (1965). *Handbook of mathematical functions*, Chapter 7. Dover, New York.
18. DAVIES, J. T. and VAUGHAN, J. M. (1963). *Astrophys. J.* **137,** 1302; ELSTE, G. (1953). *Z. Astrophys.* **33,** 157; HUMMER, D. G. (1965). *Mem. R. Ast. Soc.* **70,** part 1.
19. SMITH, R. A. (1978). *Proc. R. Soc.* **A362,** 13; ibid. (1979). **A368,** 163.

3. Fluctuation properties of chaotic light

THE various line-broadening mechanisms described in the previous chapter produce the same lineshapes in both the absorption and emission spectra associated with a given atomic transition. In the present chapter we consider the characteristics of the emitted light generated by radiative transitions of excited atoms. The characteristics can in principle be measured by two different kinds of experiment. Ordinary spectroscopy measures the frequency distribution of the light and thus provides, via the theory outlined in Chapter 2, information on the nature and strengths of the line-broadening processes in the source.

Our main concern in the present chapter is with the second kind of experiment, which measures the time dependence of the amplitude or intensity of the light beam. It is shown that the line-broadening processes in the source also cause the electric field and intensity of the beam to fluctuate around their mean values on a time-scale inversely proportional to the frequency breadth of the light. These temporal fluctuations and the frequency spread are manifestations of the same physical properties of the radiating atoms that constitute the light source, but both aspects are needed to interpret the complete range of optical experiments.

It is important to distinguish between two types of light source. The common spectroscopic source is the gas discharge lamp, where the different atoms are excited by an electrical discharge and emit their radiation independently of one another. The shape of an emission line is determined by the statistical spread in atomic velocities and the random occurrence of collisions. A conventional light source of this kind is called a chaotic source. The thermal cavity and the filament lamp are other examples of chaotic source. The light beams from any variety of chaotic source have a similar statistical description; only the parameters of the statistical distribution vary from one chaotic light beam to another.

The second type of light source is the laser, and this has quite different statistical properties. The properties of laser light are mentioned only briefly in the present chapter, a detailed discussion being deferred until Chapter 7.

The calculations that follow use a classical description of the light beam. The classical model is useful not only for a physical appreciation of the nature of the fluctuation effects, but also, as is shown in Chapter 6, the classical and quantum theories yield identical predictions for chaotic light. For other kinds of light, where the two theories may differ, the significance of the quantum predictions is more clearly discerned against the background of the corresponding classical theory.

3.1. Spectrum of a fluctuating light beam

Consider an experiment in which a beam of light passes a fixed observation point where the time dependence of its electric field is measured. Much of the present chapter is concerned with the way in which the properties of the light source determine the fluctuation properties of the beam electric field and intensity.

The frequency spectrum of the light at the observation point is determined by the Fourier components of the electric field, defined by

$$E(\omega) = (1/2\pi)\int_{-\infty}^{\infty} E(t)\exp(i\omega t)\,dt. \tag{3.1}$$

The cycle-averaged intensity of the light of frequency ω is proportional to

$$\begin{aligned}|E(\omega)|^2 &= (1/4\pi^2)\int_{-\infty}^{\infty}\int_{-\infty}^{\infty} E^*(t)E(t')\exp\{i\omega(t'-t)\}\,dt\,dt'\\ &= (1/4\pi^2)\int_{-\infty}^{\infty}\int_{-\infty}^{\infty} E^*(t)E(t+\tau)\exp(i\omega\tau)\,dt\,d\tau,\end{aligned} \tag{3.2}$$

where

$$\tau = t'-t. \tag{3.3}$$

It is shown in §3.4 that some kinds of optical interference experiment essentially perform the integral over t that appears on the right-hand side of eqn (3.2). The period covered by the integration in a practical experiment is of course never infinite, and we replace the range of the t integration by a large but finite time T. The first-order electric-field correlation function is then defined to be

$$\langle E^*(t)E(t+\tau)\rangle = \frac{1}{T}\int_T E^*(t)E(t+\tau)\,dt. \tag{3.4}$$

The correlation function describes the way in which the value of the electric field at time t affects the probabilities of its various possible values at a later time $t+\tau$.

The nature of the correlation function will become clear when examples are treated in later sections. Its form is determined by the kind of fluctuations produced by the light source. If the statistical properties of the source are *stationary*, that is the influences that govern the fluctuation statistics do not change with time, then the average in (3.4) does not depend on the particular starting time of the period T provided that T is long compared to the characteristic time scale of the fluctuations. The time averaging in eqn (3.4) can then sample all the electric-field values allowed by the statistical properties of the source with their appropriate relative probabilities, and the result is independent of the magnitude of T. Thus, although the experimental determination of the correlation function is made by a *time* averaging as on the right of eqn (3.4), the function is calculated by a *statistical* average over all values of the field at times t and $t+\tau$. The result does not of course depend on the time t, and the correlation is a function only of the time delay τ between the two field values. The averaging procedure accords with the ergodic theorem mentioned in §1.4.

The intensity (3.2) at frequency ω now becomes

$$|E(\omega)|^2 = (T/4\pi^2)\int_{-\infty}^{\infty}\langle E^*(t)E(t+\tau)\rangle\exp(i\omega\tau)\,d\tau. \tag{3.5}$$

This function provides the frequency-dependent spectrum of the light as measured by ordinary spectroscopy. It is convenient to express the spectrum in a normalized form as was done in Chapter 2. The integrated intensity given by eqn (3.5) is

$$\int_{-\infty}^{\infty}|E(\omega)|^2\,d\omega = (T/2\pi)\langle E^*(t)E(t)\rangle, \tag{3.6}$$

where eqn (2.64) has been used. The normalized spectral distribution function is defined to be

$$F(\omega) = |E(\omega)|^2\Big/\int_{-\infty}^{\infty}|E(\omega)|^2\,d\omega = (1/2\pi)\int_{-\infty}^{\infty}g^{(1)}(\tau)\exp(i\omega\tau)\,d\tau, \tag{3.7}$$

where we have introduced the normalized first-order correlation function

$$g^{(1)}(\tau) = \frac{\langle E^*(t)E(t+\tau)\rangle}{\langle E^*(t)E(t)\rangle}. \tag{3.8}$$

This quantity is called the *degree of first-order temporal coherence* of the light.

The connection (3.7) between the spectrum of the light and its first-order correlation function is a form of the Wiener-Khintchine theorem. It gives the formal relation between the results of spectroscopic experiments and the results of measurements of the time-dependent fluctuation properties of light. The relation can be cast into a form that involves only integration over positive τ and is sometimes more useful. Thus if τ is replaced by $-\tau$ in the integration over negative τ,

$$F(\omega) = (1/2\pi)\int_{0}^{\infty}g^{(1)}(\tau)\exp(i\omega\tau)\,d\tau + (1/2\pi)\int_{0}^{\infty}g^{(1)}(-\tau)\exp(-i\omega\tau)\,d\tau. \tag{3.9}$$

It is however clear from the definition (3.4) that the correlation function depends only on the relative times of the two field measurements, and hence

$$g^{(1)}(-\tau) = \frac{\langle E^*(t)E(t-\tau)\rangle}{\langle E^*(t)E(t)\rangle} = \frac{\langle E^*(t+\tau)E(t)\rangle}{\langle E^*(t)E(t)\rangle} = g^{(1)}(\tau)^*. \tag{3.10}$$

Thus eqn (3.9) becomes

$$F(\omega) = (1/\pi)\mathrm{Re}\int_{0}^{\infty}g^{(1)}(\tau)\exp(i\omega\tau)\,d\tau \tag{3.11}$$

and only the degree of first-order coherence at positive τ is needed to compute the spectrum. The degree of coherence at negative τ can in any case be found from the symmetry property (3.10).

3.2. Model of a collision-broadened light source

The general theory of fluctuations is easily applied to the light generated by a source in which collision broadening predominates. We ignore radiative and Doppler broadening, and we suppose that the collisions are of the elastic phase-interruption variety that does not change the atomic state.

Consider a particular excited atom radiating light of frequency ω_0. One can envisage a wave train of electromagnetic radiation steadily emanating from the atom until it suffers a collision. During a collision, the energy levels of the radiating atom are shifted by the forces of interaction between the two colliding atoms. Thus the radiated wave train is interrupted for the duration of the collision. When the wave of frequency ω_0 is resumed after the collision, its characteristics are identical to those that it had prior to the collision, except that the phase of the wave is unrelated to the phase before the collision.

If the duration of the collision is sufficiently brief, it is possible to ignore any radiation emitted during the collision while the frequency is shifted from ω_0. The collision-broadening effect can then be adequately represented by a model

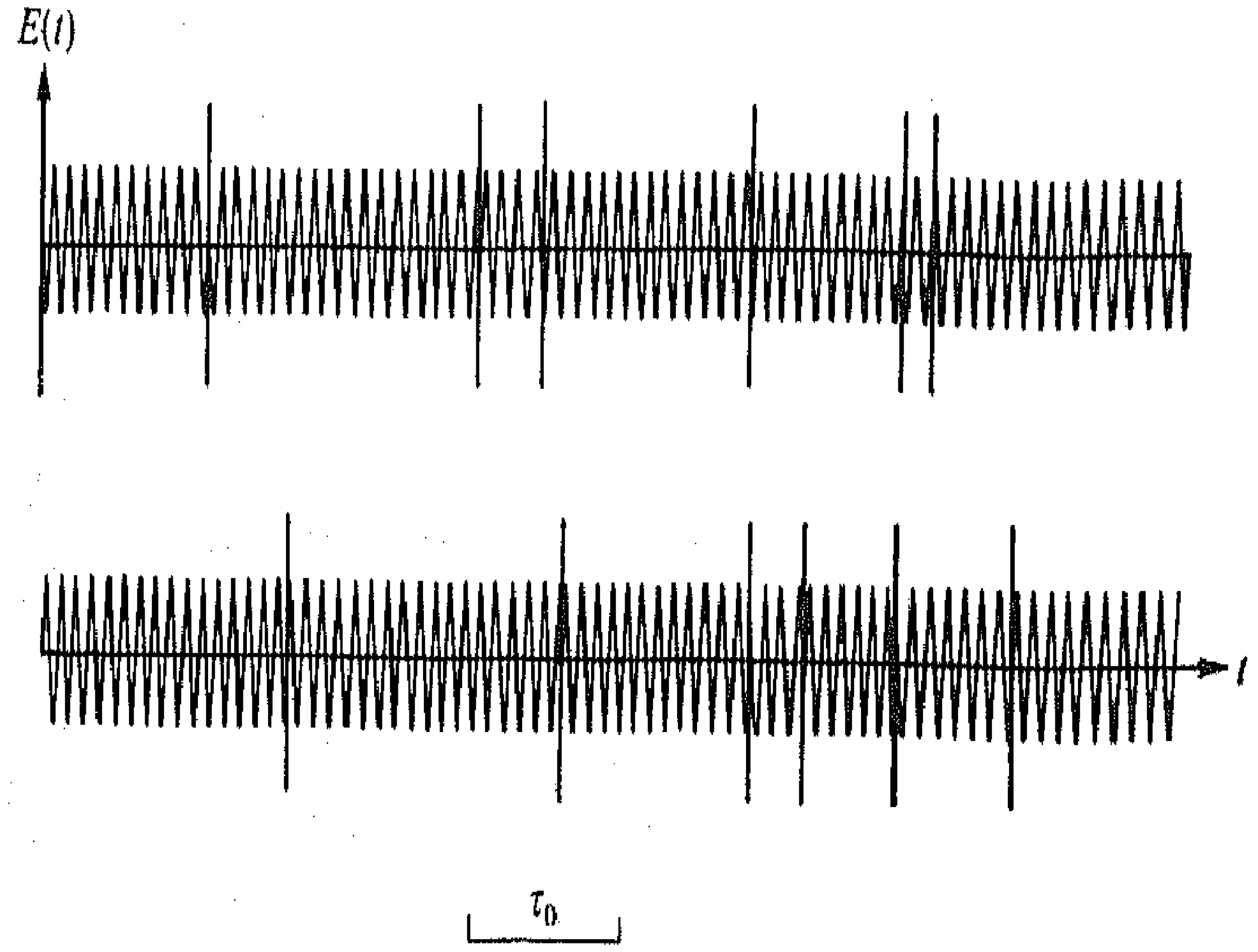

FIG. 3.1. The electric-field amplitude of the wave train radiated by a single atom. The vertical lines represent collisions, separated by periods of free flight with a mean τ_0 of the magnitude indicated. The quantity $\omega_0\tau_0$ is chosen unrealistically small in order to show the random phase changes caused by the collisions.

in which each excited atom always radiates at frequency ω_0, but with random changes in the phase of the radiated wave each time a collision occurs. The apparent spread in the emitted frequencies arises because the wave is chopped up into finite sections whose Fourier decompositions include frequencies other than ω_0.

The wave train radiated by a single atom is illustrated schematically in Fig. 3.1, which shows the variation of the electric field amplitude $E(t)$ at a fixed observation point as a function of time. The occurrence of a collision is represented by a vertical line accompanied by a random change in the phase of the wave. The periods of free flight in the figure are chosen in accordance with the probability distribution (2.131). The variation of the phase of the wave train with time is shown in Fig. 3.2. In order to make Fig. 3.1 easy to draw, the quantity $\omega_0\tau_0$ is given the small value of 60. With the typical value of the collision time given in eqn (2.141) and the visible light frequency given in eqn (1.65), we have

$$\omega_0\tau_0 \approx 9\times 10^4. \tag{3.12}$$

For these values, the wave train radiated by an atom undergoes on average about 15 000 periods of oscillation between successive collisions.

The field amplitude of the wave illustrated in Figs. 3.1 and 3.2 can be written in complex form as

$$E(t) = E_0\exp\{-\mathrm{i}\omega_0 t+\mathrm{i}\phi(t)\}. \tag{3.13}$$

As shown in Fig. 3.2, the phase $\phi(t)$ remains constant during periods of free flight but changes abruptly each time a collision occurs. The amplitude E_0 and frequency ω_0 are the same for any period. The total wave emitted by the collision-broadened source is represented by a sum of terms like eqn (3.13), one for each radiating atom. If there is a large number ν of such atoms, the total electric field amplitude is

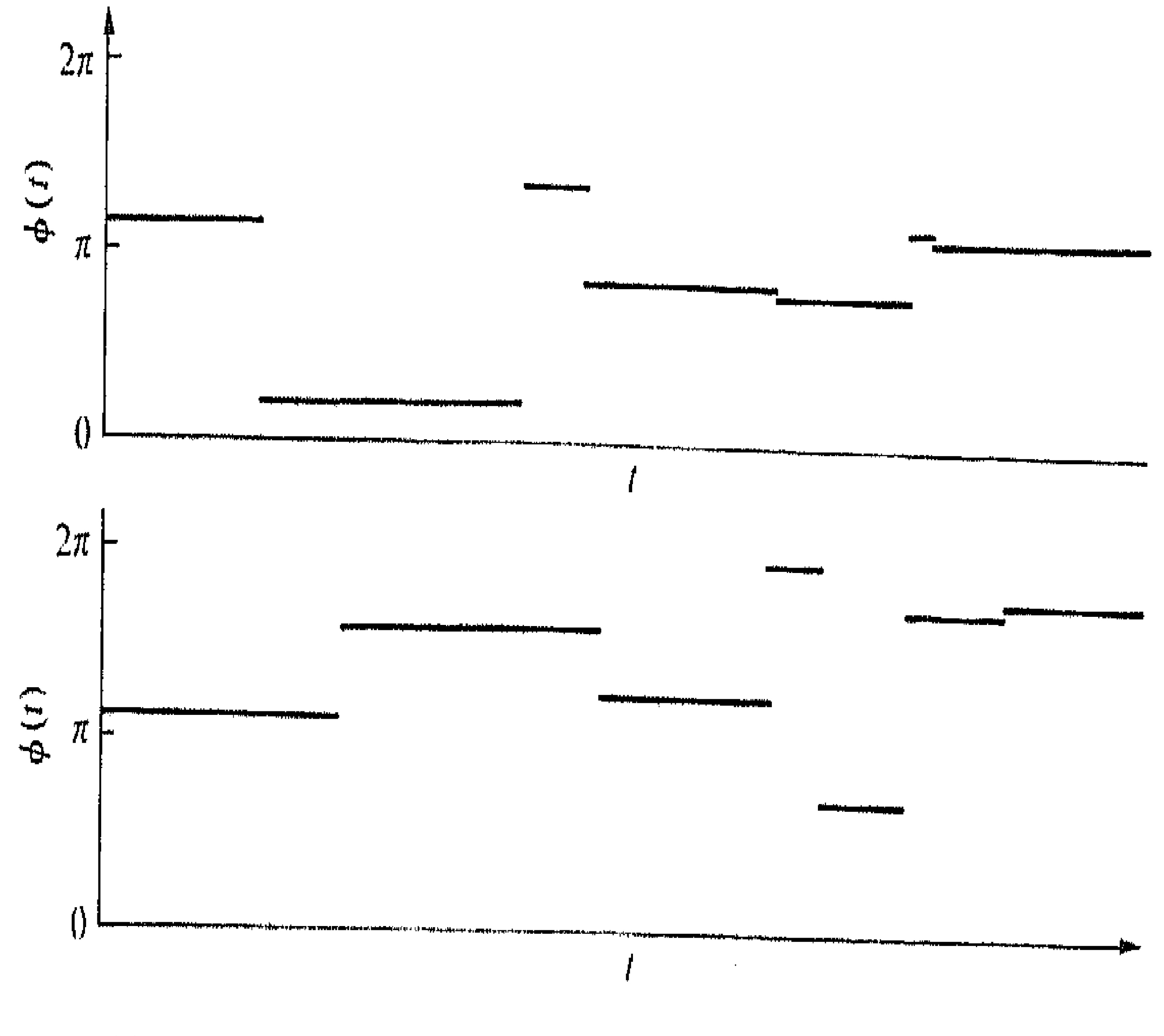

FIG. 3.2. Time dependence of the phase angle of the wave train illustrated in Fig. 3.1.

$$\begin{aligned} E(t) &= E_1(t)+E_2(t)+\ldots+E_\nu(t)\\ &= E_0\exp(-\mathrm{i}\omega_0 t)\{\exp(\mathrm{i}\phi_1(t))+\exp(\mathrm{i}\phi_2(t))+\ldots+\exp(\mathrm{i}\phi_\nu(t))\}\\ &= E_0\exp(-\mathrm{i}\omega_0 t)a(t)\exp(\mathrm{i}\varphi(t)), \end{aligned} \tag{3.14}$$

where every atom has been assigned the same amplitude E_0 and frequency ω_0, but the phases for the different atoms are completely unrelated. It is assumed for simplicity that the observed light has a fixed polarization so that the electric fields can be added algebraically.

The formal summation of the phase factors carried out in the final line of eqn (3.14) is illustrated in Fig. 3.3. Since the phase angles $\phi_1, \phi_2, \ldots, \phi_\nu$ each have different random variations similar to that shown in Fig. 3.2, the amplitude $a(t)$ and phase $\varphi(t)$ are different at different instants of time. The real electric field obtained from eqn (3.14) consists of a carrier wave of frequency ω_0 subjected to random amplitude and phase modulation. The Fourier decomposition of the modulated wave contains frequencies spread about ω_0 in a manner governed by the collision-broadened lineshape.

It is not possible in practice to resolve the oscillations in $E(t)$ that occur at the frequency of the carrier wave. A good experimental resolving time is of order 10^{-9} s, six orders of magnitude too long to detect oscillations at the

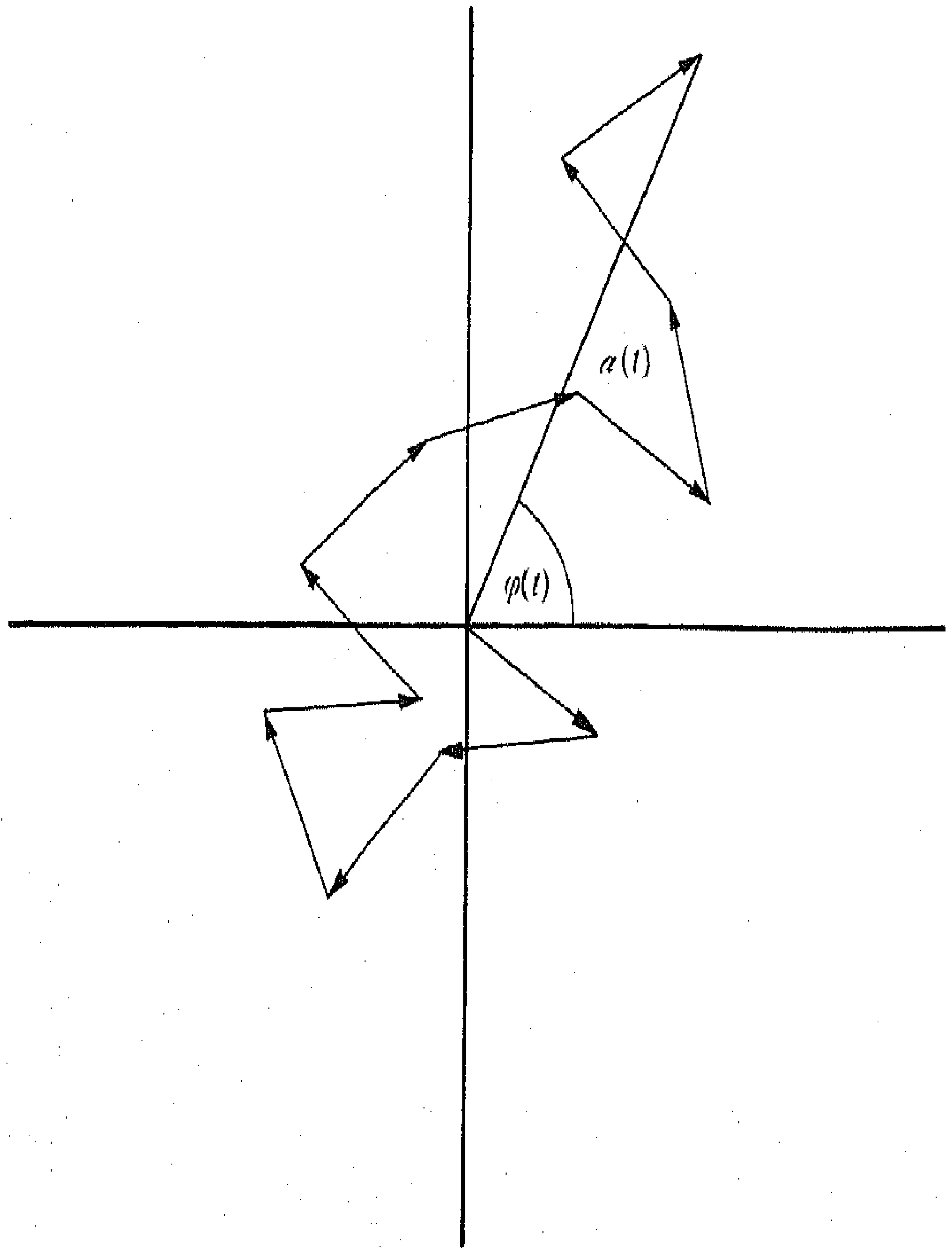

FIG. 3.3. Argand diagram to show the amplitude $a(t)$ and phase $\varphi(t)$ of the resultant vector formed by a large number of unit vectors, each of which has a randomly chosen phase angle.

frequency ω_0 given in eqn (1.65). It is therefore appropriate for comparison with experiment to average the theoretical results over a cycle of oscillation of the carrier wave. The real electric field from eqn (3.14) has a zero cycle-average. According to eqn (1.89), the cycle average of the beam intensity in free space is

$$\bar{I}(t) = \tfrac{1}{2}\epsilon_0 c|E(t)|^2 = \tfrac{1}{2}\epsilon_0 c E_0^2 a(t)^2. \qquad (3.15)$$

The intensity $\bar{I}(t)$ still contains the time dependence resulting from the random amplitude modulation $a(t)$.

Figs. 3.4 and 3.5 illustrate the types of fluctuation that occur in the beam intensity and phase. The figures have been constructed by a computer simulation of a collision-broadened light source in which the summation of phase factors in eqn (3.14) is carried out explicitly for a large number of atoms ν. The phase variation for each atom has the form shown in Fig. 3.2 with free-flight times distributed in accordance with the probability law of eqn (2.131). The horizontal time-scales for both $\bar{I}(t)$ and $\varphi(t)$ in Figs. 3.4 and 3.5 are determined solely by the magnitude of the mean time τ_0 of free flight indicated

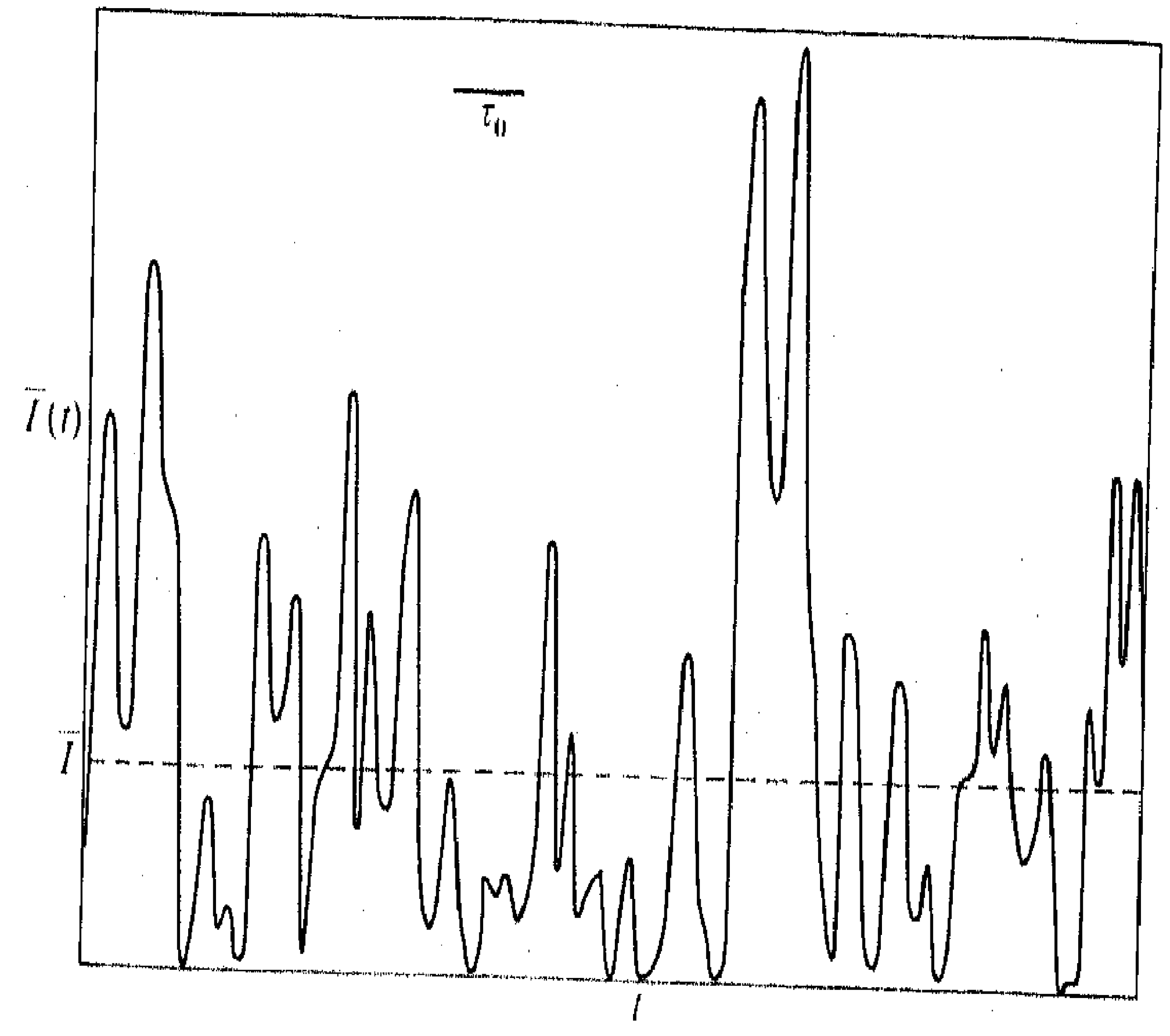

FIG. 3.4. Time dependence of the cycle-averaged intensity for a chaotic light beam, obtained from a computer simulation. The mean time τ_0 between collisions has the magnitude indicated. The dashed line shows the mean value of the intensity averaged over a time long compared to τ_0. (Computation carried out by Mrs S. Sussmann.)

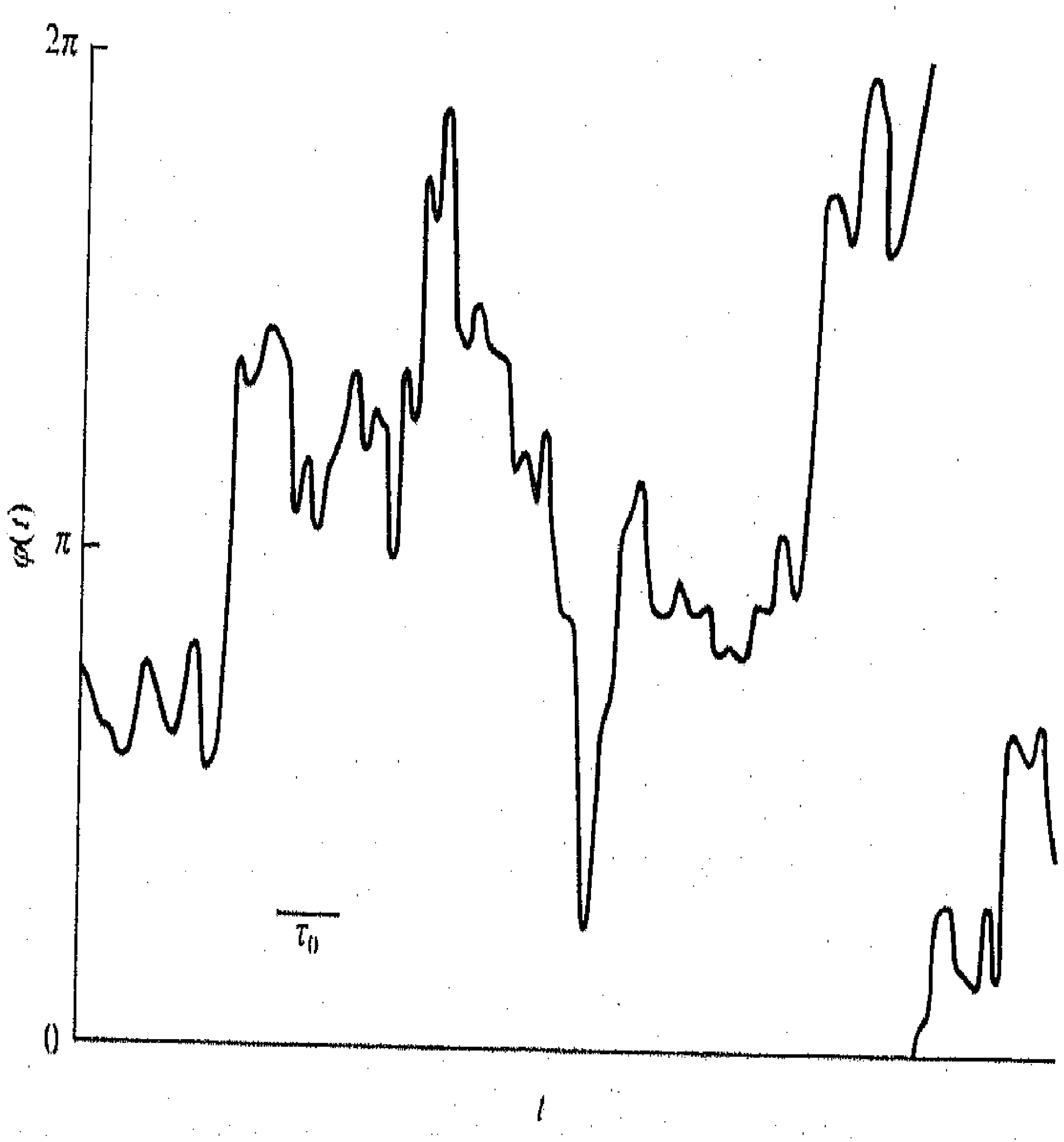

FIG. 3.5. Time dependence of the phase of the wave emitted by a collision-broadened source. The graph is a result of the same computation that produced Fig. 3.4.

on the graphs. It is seen that substantial changes in intensity and phase can occur over a time span τ_0, but that these quantities are reasonably constant over time intervals $\Delta t \ll \tau_0$.

The inclusion of radiative and Doppler broadening would modify the details of the above discussion but the fluctuations in intensity and phase remain similar to those illustrated in Figs. 3.4 and 3.5. For any combination of line-broadening mechanisms there exists some characteristic time, analogous to τ_0 in the collision-broadening case, which determines the time-scale of the random fluctuations. This characteristic time is called, in general, the *coherence time* τ_c of the light beam. Its magnitude is of the order of the inverse of the frequency spread of the beam. The relevance of τ_c to the usual definition of coherence is discussed later in the chapter.

In all the theory that follows, attention is restricted to light beams whose frequency spreads are small compared with the mean frequency, that is, where $\omega_0\tau_c$ is very much larger than unity. It is seen from Fig. 1.6 that the light generated by thermal excitation of a cavity (the black-body radiation) has a frequency spread nearly equal to the mean frequency and does not fall into this category.

The path length

$$\lambda_c = c\tau_c \tag{3.16}$$

associated with the coherence time is known as the *coherence length*. The graph of the cycle-averaged intensity as a function of time at a fixed point in the beam given in Fig. 3.4 could equally well be regarded as a graph of the intensity as a function of the distance z along the beam at a fixed instant of time. The horizontal axis would be relabelled z and the mean time τ_0 would be relabelled λ_c. At a given instant of time, the cycle-averaged intensity changes only slightly over distances that are small compared to λ_c, but large changes occur over distances that are comparable to or larger than λ_c. The temporal and spatial aspects of the beam fluctuations are related by the simple scaling factor c. The coherence length for the beams considered is always much larger than the wavelength of the light.

3.3. First-order coherence and frequency spectrum

The model of a collision-broadened light source described above can be used to calculate the first-order electric-field correlation function of the light, its degree of first-order coherence, and its frequency spectrum.

Consider first the correlation function of the fields at different times, defined by the time average in eqn (3.4). It is clear from the discussion of Figs. 3.4 and 3.5 that the electric field $E(t)$ changes little over periods much smaller than the coherence time, but that large changes occur over periods much longer than the coherence time. The fields at times separated by such long periods are essentially uncorrelated. The time average in eqn (3.4) depends only on the characteristics of the light and is independent of the sampling time T if the latter extends over many coherence times. In addition, it is assumed that the theory refers to an experiment that is capable of resolving the fluctuation properties; the detector resolving time must therefore be much smaller than τ_c, and its dimension parallel to the beam must be much smaller than λ_c.

These are the conditions for use of the ergodic theorem to evaluate the correlation function (3.4). The angle brackets are thus interpreted as a statistical average, and the required function is

$$\begin{aligned}\langle E^*(t)E(t+\tau)\rangle = E_0^2 \exp(-\mathrm{i}\omega_0\tau)\langle\{&\exp(-\mathrm{i}\phi_1(t))+\ldots+\exp(-\mathrm{i}\phi_\nu(t))\}\\ &\times\{\exp(\mathrm{i}\phi_1(t+\tau))+\ldots+\exp(\mathrm{i}\phi_\nu(t+\tau))\}\rangle,\end{aligned} \tag{3.17}$$

where eqn (3.14) has been used. In multiplying out the large brackets, the phase angles of the wave trains from different atoms have different random values and the cross-terms give a zero average contribution. The remaining terms give

$$\begin{aligned}\langle E^*(t)E(t+\tau)\rangle &= E_0^2\exp(-\mathrm{i}\omega_0\tau)\sum_{i=1}^{\nu}\langle\exp[\mathrm{i}(\phi_i(t+\tau)-\phi_i(t))]\rangle\\ &= \nu\langle E_i^*(t)E_i(t+\tau)\rangle\end{aligned} \tag{3.18}$$

since all the radiating atoms are equivalent.

The correlation function for the beam as a whole is thus determined by the single-atom contributions. Now the phase angle of each wave train jumps to a random value after its atom suffers a collision, subsequently producing a zero average contribution. Thus the single-atom correlation function in eqn (3.18) is proportional to the probability that the atom has a period of free flight longer than τ, and with use of the probability distribution (2.131) we can put

$$\begin{aligned}\langle E_i^*(t)E_i(t+\tau)\rangle &= E_0^2\exp(-\mathrm{i}\omega_0\tau)\langle\exp[\mathrm{i}(\phi_i(t+\tau)-\phi_i(t))]\rangle\\ &= E_0^2\exp(-\mathrm{i}\omega_0\tau)\int_\tau^\infty p(\tau)\,\mathrm{d}\tau\\ &= E_0^2\exp\{-\mathrm{i}\omega_0\tau-(\tau/\tau_0)\}.\end{aligned} \tag{3.19}$$

The correlation function (3.18) thus becomes

$$\langle E^*(t)E(t+\tau)\rangle = \nu E_0^2\exp\{-\mathrm{i}\omega_0\tau-(\tau/\tau_0)\} \tag{3.20}$$

and the normalized correlation or degree of first-order coherence (3.8) is

$$g^{(1)}(\tau) = \exp\{-\mathrm{i}\omega_0\tau-(\tau/\tau_0)\}. \tag{3.21}$$

The spectrum of the collision-broadened light is obtained by integration of the degree of first-order coherence as in eqn (3.11) to give

$$F(\omega) = \frac{1/\pi\tau_0}{(\omega_0-\omega)^2+(1/\tau_0)^2}. \tag{3.22}$$

This is a normalized Lorentzian lineshape similar to eqn (2.112). The linewidth $2/\tau_0$ agrees with that in eqn (2.140) when radiative broadening is ignored if

$$\gamma_{\text{coll}} = 1/\tau_0, \tag{3.23}$$

as assumed without proof in eqn (2.133). The degree of first-order coherence can thus be written

$$g^{(1)}(\tau) = \exp(-\mathrm{i}\omega_0\tau-\gamma_{\text{coll}}\tau). \tag{3.24}$$

The degree of first-order coherence and the spectrum in the presence of both collision and radiative broadening can be calculated by a generalization of the model of the light source[1]. It is found that the results are much the same as above except that γ_{coll} must be augmented by addition of the radiative damping parameter γ to form the total damping γ' defined in eqn (2.135). Thus the correlation function and degree of first-order coherence are generalized to

$$\langle E^*(t)E(t+\tau)\rangle = \nu E_0^2 \exp(-\mathrm{i}\omega_0\tau-\gamma'\tau) \tag{3.25}$$

and

$$g^{(1)}(\tau) = \exp(-\mathrm{i}\omega_0\tau-\gamma'\tau). \tag{3.26}$$

The spectrum is a Lorentzian with width (2.140), and the coherence time is

$$\tau_c = 1/\gamma'. \tag{3.27}$$

The effect of Doppler broadening on the coherence is considered in §3.5.

We note that the correlations in any kind of chaotic light must vanish for times τ much longer than τ_c, and since

$$\langle E(t)\rangle = 0, \tag{3.28}$$

it follows that the degree of first-order coherence must have a limiting value

$$g^{(1)}(\tau) \to 0 \qquad \text{for} \qquad \tau \gg \tau_c. \tag{3.29}$$

Apart from its usefulness in deriving the frequency spectrum of the light, the degree of first-order coherence plays a more direct role in determining the results of interference experiments. It is convenient to illustrate the role by consideration of a specific experiment.

3.4. Young's interference fringes

Young's fringes provide a simple example of an interference experiment, and their treatment illustrates some general principles that are common to the whole class of experiments. The experiment is here analysed in some detail to determine the conditions under which the field fluctuations, resulting from the chaotic nature of the light source, affect the visibility of the interference fringes. Fig. 3.6 shows a simplified version of Young's experiment. Chaotic light from a point source is rendered parallel by a lens and then falls on a screen that contains two slits, or pinholes as we shall assume for simplicity. Interference fringes are sought on a second screen placed to the right of the first screen. The model experiment ignores complications arising from the finite source diameter and consequent lack of perfect parallelism in the beam that illuminates the first screen. It is essential to take such effects into account in a rigorous treatment of the experiment but they are omitted here in order that attention can be focused on the effects of the random field fluctuations alone.

Let $E(\mathbf{r}t)$ be the total electric field of the radiation at the position $\mathbf{r}$ on the observation screen at time t. The field is a linear superposition of the electric fields at the two pinholes (positions $\mathbf{r}_1$ and $\mathbf{r}_2$) at earlier times t_1 and t_2 determined by the velocity of light c. Thus formally,

$$E(\mathbf{r}t) = u_1E(\mathbf{r}_1t_1)+u_2E(\mathbf{r}_2t_2), \tag{3.30}$$

where

$$t_1 = t-(s_1/c), \qquad t_2 = t-(s_2/c), \tag{3.31}$$

and the coefficients u_1, u_2 are inversely proportional to s_1, s_2, respectively, the distances defined in Fig. 3.6. The coefficients u_1 and u_2 depend on the geometry of the experiment, for example on the pinhole sizes, but their exact form is not important for the present calculation; they are purely imaginary, since the secondary waves radiated by the pinholes are $\pi/2$ out of phase with the primary light beam[2]. Diffraction effects at the individual pinholes are ignored.

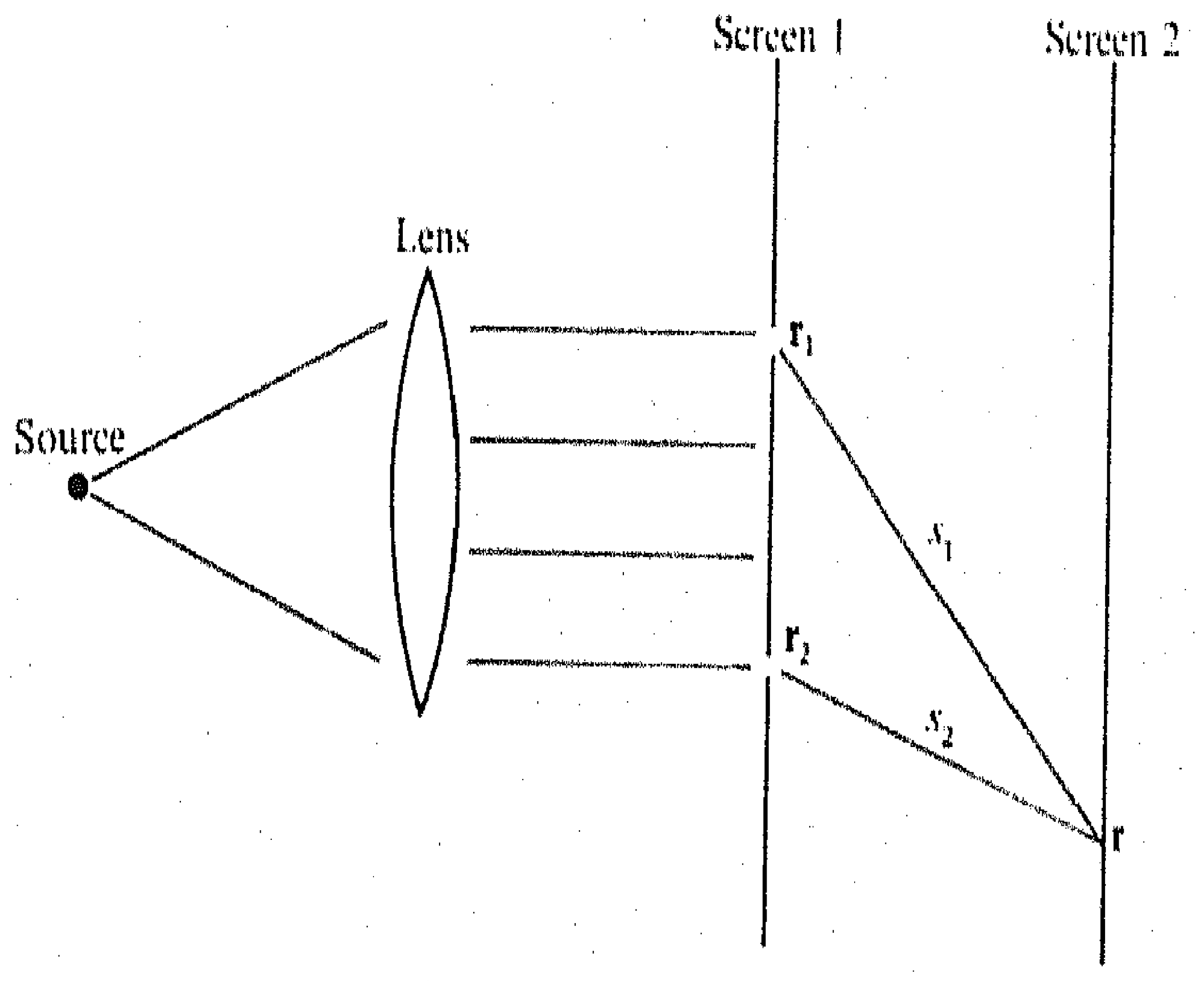

FIG. 3.6. Arrangement of components for an idealized Young's interference experiment.

The intensity of the light at position **r**, averaged over a cycle of oscillation, is

$$\begin{aligned}\bar{I}(\mathbf{r}t) &= \tfrac{1}{2}\epsilon_0 c|E(\mathbf{r}t)|^2\\ &= \tfrac{1}{2}\epsilon_0 c\{|u_1|^2|E(\mathbf{r}_1t_1)|^2+|u_2|^2|E(\mathbf{r}_2t_2)|^2\\ &\quad +2u_1^*u_2\,\mathrm{Re}(E^*(\mathbf{r}_1t_1)E(\mathbf{r}_2t_2))\},\end{aligned} \tag{3.32}$$

where the pure imaginary form of u_1 and u_2 has been used. The intensity $\bar{I}(\mathbf{r}t)$ is similar to that defined in eqn (3.15).

The fringes in Young's interference experiment are normally recorded by photographic plates or are observed with the naked eye. In either case, the recording time is long compared to τ_c, the coherence time of the chaotic light. To compare theory with experiment it is necessary to average $\bar{I}(\mathbf{r}t)$ over a period long compared with τ_c. This average of $\bar{I}(\mathbf{r}t)$ is denoted $\bar{I}(\mathbf{r})$, and the averaged form of eqn (3.32) is then

$$\begin{aligned}\bar{I}(\mathbf{r}) &= \langle\bar{I}(\mathbf{r}t)\rangle\\ &= \tfrac{1}{2}\epsilon_0 c\{|u_1|^2\langle|E(\mathbf{r}_1t_1)|^2\rangle+|u_2|^2\langle|E(\mathbf{r}_2t_2)|^2\rangle\\ &\quad +2u_1^*u_2\,\mathrm{Re}\langle E^*(\mathbf{r}_1t_1)E(\mathbf{r}_2t_2)\rangle\}.\end{aligned} \tag{3.33}$$

It is seen that the intensity on the second screen consists of three contributions. The first two terms represent the intensities caused by each of the pinholes in the absence of the other. These two terms do not give rise to any interference effects. The fringes arise from the term that involves the correlation function for the fields at the two pinholes.

The correlation function is a slight generalization of that defined in eqn (3.4) to take account of the different spatial positions of the two fields. The formal definition is

$$\langle E^*(\mathbf{r}_1t_1)E(\mathbf{r}_2t_2)\rangle = \frac{1}{T}\int_T E^*(\mathbf{r}_1t_1)E(\mathbf{r}_2\,t_1+t_{21})\,\mathrm{d}t_1, \tag{3.34}$$

where

$$t_{21} = t_2-t_1. \tag{3.35}$$

The required correlation function is in fact less general than this because the light beam that strikes the first screen in Young's experiment is assumed to be parallel and to have plane wave-fronts.

Let the direction of propagation of the beam be taken as the z-axis. The electric field of the light can be represented as in eqn (3.14) except that the position dependence must now be included. The light beam with its fluctuations travels along the z-axis at velocity c, and the position-dependent field is accordingly

$$E(zt) = E\left(t-\frac{z}{c}\right), \tag{3.36}$$

where the field on the right is the same as in eqn (3.14). The calculation of the correlation function now proceeds as in eqns (3.17)–(3.20) and the result is essentially the same as before except that now

$$\tau = t_2-\frac{z_2}{c}-t_1+\frac{z_1}{c}. \tag{3.37}$$

With this definition, the generalization of eqn (3.25) is

$$\langle E^*(z_1t_1)E(z_2t_2)\rangle = \nu E_0^2\exp(-\mathrm{i}\omega_0\tau-\gamma'\tau). \tag{3.38}$$

The fringe intensity in Young's experiment is determined by substitution of eqn (3.38) into eqn (3.33). The two pinholes have the same z coordinate, and the intensity reduces to

$$\bar{I}(\mathbf{r}) = \tfrac{1}{2}\epsilon_0 cE_0^2\nu\{|u_1|^2+|u_2|^2+2u_1^*u_2\exp(-\gamma'|\tau|)\cos\omega_0\tau\}, \tag{3.39}$$

where τ, determined from eqns (3.31) and (3.37), is

$$\tau = (s_1-s_2)/c. \tag{3.40}$$

This quantity can be either positive or negative and the use of $|\tau|$ in the exponential in eqn (3.39) accords with the symmetry property of eqn (3.10). The fringe visibility at position **r** on the second screen is conventionally defined to be

$$\frac{\bar{I}(\mathbf{r})_{\max}-\bar{I}(\mathbf{r})_{\min}}{\bar{I}(\mathbf{r})_{\max}+\bar{I}(\mathbf{r})_{\min}} = \frac{2u_1^*u_2\exp(-\gamma'|s_1-s_2|/c)}{|u_1|^2+|u_2|^2}. \tag{3.41}$$

The fringe visibility is unity at the centre of the second screen in Fig. 3.6, where $u_1 = u_2$ and $s_1 = s_2$, but is less than unity off the axis, where $u_1 \neq u_2$ and $s_1 \neq s_2$.

The chaotic nature of the light source influences the fringe visibility via the exponential term in eqn (3.41) which, in principle, causes the fringes to disappear altogether for s_1 sufficiently different from s_2. However, it is seen from eqn (3.39) that for a narrow emission line, where $\omega_0 \gg \gamma'$, very many fringes are generated by the cosine term before τ becomes sufficiently large for the exponential term to blur the fringes. For the coherence time and frequency assumed in eqns (2.141) and (1.65), there are about 10^4 sharp fringes on the second screen centred about the axis of the experiment. In a practical Young's interference experiment the chaotic nature of the light is not usually the most important cause of fringe blurring. The finite extent of the source perpendicular to the axis, neglected in the above treatment, is often the most important limiting factor, and there are, in fact, techniques for determining the angular diameters of distant light sources, for example stars, by observation of fringe blurring[3]. Source-size effects belong to the theory of spatial coherence considered briefly in §3.9.

The chaotic properties of the light source assumed in the interference fringe calculation thus have very little effect on the results of experiments that use suitably narrow emission lines. The exponential factors in eqns (3.39) and (3.41) would however be of great importance in attempts to observe fringes with light from a broad-band source, for example a thermal cavity where the frequency spread of the light is comparable to its mean frequency. At the opposite extreme, the above treatment of interference is inappropriate for an emission line so narrow that the time-dependent intensity fluctuations are observed directly. However, the longest coherence time ordinarily available for a chaotic source is of order 10^{-9} s, and the experimental resolving time in interference experiments is usually much longer than τ_c.

The important feature of the above treatment is the way in which the formation of fringes is governed by the first-order electric-field correlation function. The correlation function plays a similar role in other classical interference experiments, for example the Michelson interferometer.

3.5. Degree of first-order coherence

The properties of a light beam that are relevant to an interference experiment can be conveniently expressed in terms of the concept of optical coherence. Light at two points in space or time that is capable, in principle, of being superimposed to produce interference effects is said to be coherent. An example is the light at the two pinholes in Young's interference experiment. The potential magnitude of the interference effects in most of the classical interference experiments is governed by the first-order coherence of the light beam employed.

The degree of first-order temporal coherence is defined as the normalized electric-field correlation function, similar to eqn (3.8). However, we now generalize the previous definition to include the spatial dependence of the electric fields. The degree of first-order temporal coherence between the light fields at the space–time points $(\mathbf{r}_1, t_1)$ and $(\mathbf{r}_2, t_2)$ is defined to be

$$g^{(1)}(\mathbf{r}_1 t_1, \mathbf{r}_2 t_2) = \frac{\langle E^*(\mathbf{r}_1 t_1) E(\mathbf{r}_2 t_2)\rangle}{[\langle |E(\mathbf{r}_1 t_1)|^2\rangle \langle |E(\mathbf{r}_2 t_2)|^2\rangle]^{\frac{1}{2}}} \tag{3.42}$$

where the angle brackets again denote statistical averages. The light at the two points has the following designations that depend upon the value of the degree of first-order coherence.

$$\text{For}\quad |g^{(1)}(\mathbf{r}_1 t_1, \mathbf{r}_2 t_2)| \begin{cases} = 1 \\ = 0 \\ \neq 0 \text{ or } 1 \end{cases} \quad \text{the light is} \begin{cases} \text{first-order coherent} \\ \text{incoherent} \\ \text{partially coherent.} \end{cases} \tag{3.43}$$

The examples to be treated here all involve plane parallel light beams where only a single spatial coordinate, taken as the z-axis, is needed. Consider first the chaotic light source of Lorentzian frequency distribution assumed above for the theory of Young's experiment. The required correlation function given by eqn (3.38) contains the positions and times only in the combination τ defined in eqn (3.37). It is therefore convenient to introduce a shorthand for the degree of coherence, writing

$$g^{(1)}(z_1 t_1, z_2 t_2) \equiv g^{(1)}(\tau) = \exp(-\mathrm{i}\omega_0 \tau - \gamma' |\tau|). \tag{3.44}$$

The result is formally identical to eqn (3.26) except that the symmetry (3.10) is used to include both positive and negative τ. The dependence of $|g^{(1)}(\tau)|$ on τ is shown in Fig. 3.7. The light at the two points is first-order coherent if

$$|t_2 - t_1 - (z_2 - z_1)/c| \ll \tau_c, \tag{3.45}$$

where eqn (3.27) has been used. In Young's experiment, where $z_1 = z_2$, sharp fringes occur provided that the two sets of wavelets, which impinge at a point on the second screen, left the pinholes at times separated by an amount small compared to the coherence time, where τ_c is typically of order 3×10^{-11} s according to eqn (2.141). The corresponding coherence length is about 10^{-2} m. It is possible to form interference fringes in general from a parallel beam of light only by superposition of light from two points whose distances along the beam differ by less than the coherence length, and which leaves the two points at times that differ by less than the coherence time.

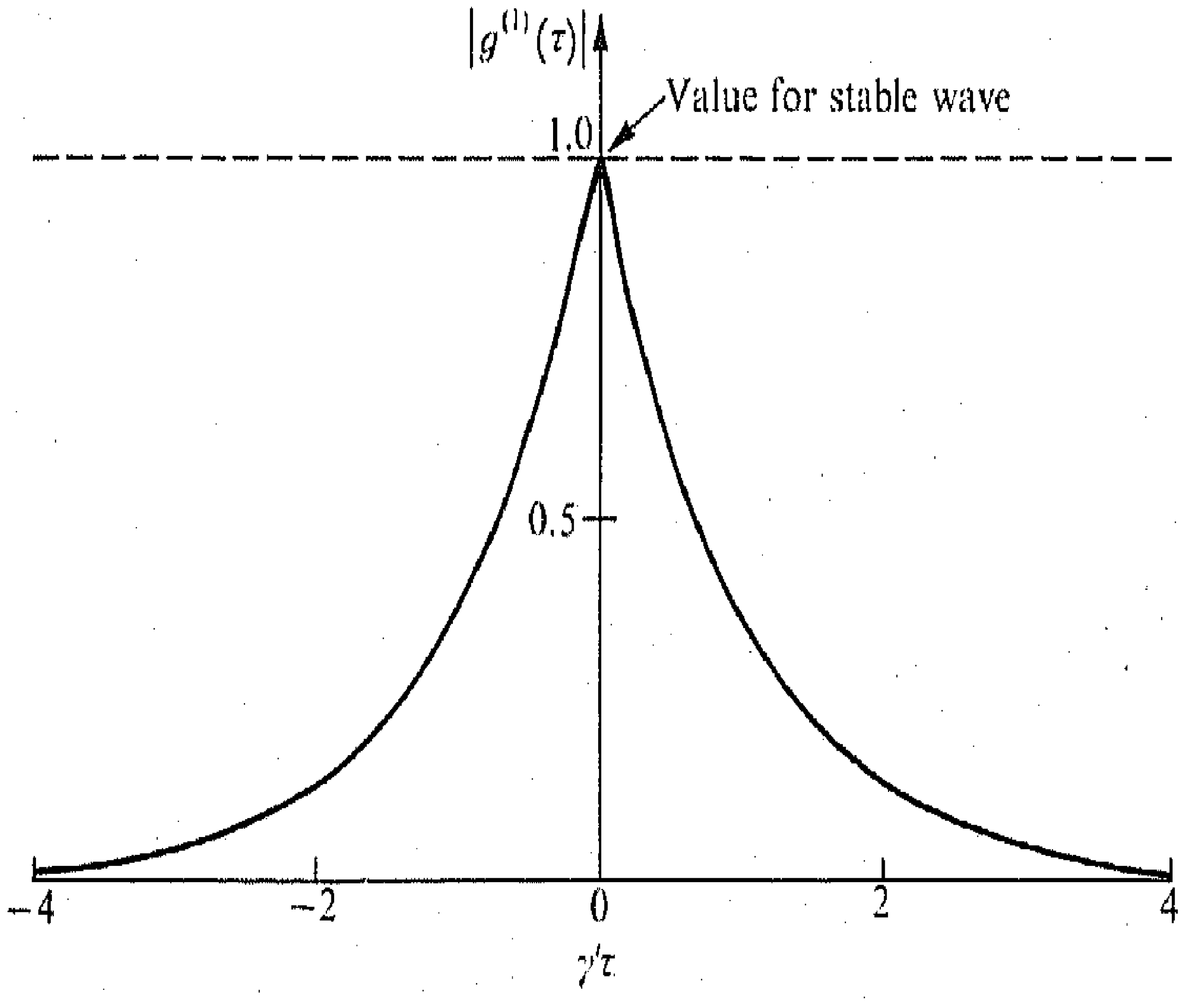

FIG. 3.7. The modulus of the degree of first-order coherence for chaotic light of linewidth parameter γ'. The constant unit value for a classical stable wave is indicated by the dashed line.

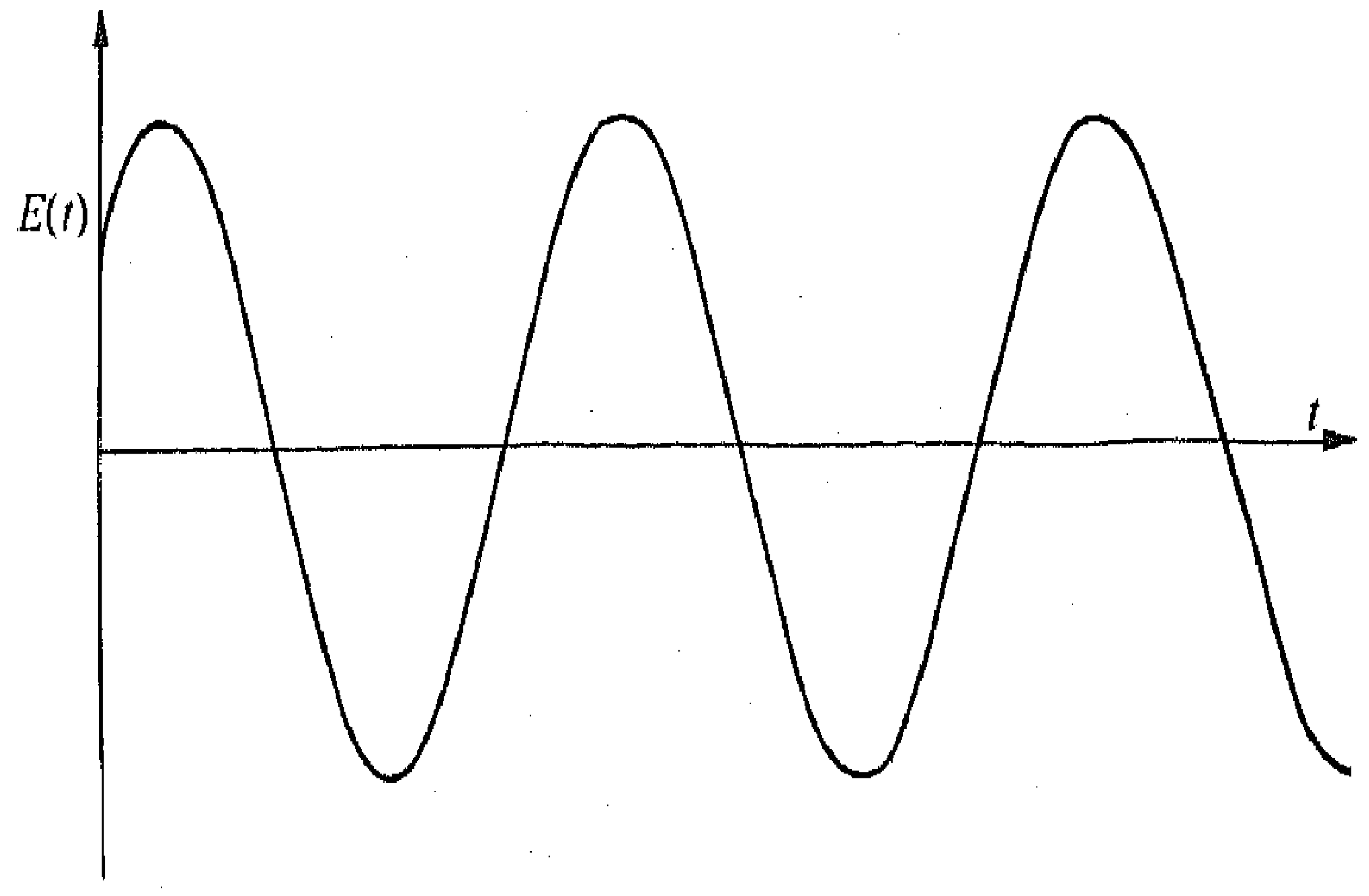

FIG. 3.8. Variation of electric field with time at a fixed observation point for a classical stable wave.

All of the above analysis is based on the assumption of a collision-broadened light source. It is not difficult to evaluate the degree of first-order coherence for other kinds of light. The simplest example of all is provided by the classical wave of stable amplitude and phase that is often assumed in the theoretical treatment of optical experiments. For such a wave, assumed to be propagated in the z-direction, the electric field can be written

$$E(zt) = E_0 \exp(ikz - i\omega_0 t + i\phi), \qquad (3.46)$$

where the amplitude and phase are fixed quantities, in contrast to the chaotic field of eqn (3.14), and the wavevector is $k = \omega_0/c$. Fig. 3.8 shows the variation of electric field with time at a fixed observation point. The first-order correlation function is determined without any ensemble averaging in this case, since the field has no statistical uncertainty, and

$$\langle E^*(z_1t_1)E(z_2t_2)\rangle = E_0^2 \exp(-i\omega_0\tau), \qquad (3.47)$$

with τ given by eqn (3.37). Thus, from eqn (3.42), the first-order coherence is

$$g^{(1)}(\tau) = \exp(-i\omega_0\tau). \qquad (3.48)$$

The beam is first-order coherent at all space–time points and it can be said to have perfect first-order coherence. The result (3.48) is the same as obtained by letting the linewidth parameter γ' tend to zero in the chaotic beam result (3.44) (or equivalently $\tau_c \to \infty$). The stable-wave result is also shown in Fig. 3.7. As is discussed in Chapter 7, the beam from a single-mode laser source can approximate a noiseless classical stable wave of the kind shown in Fig. 3.8.

Between the two extremes of the chaotic beam and the classical stable wave, there are other examples of light beam whose first-order coherence can be easily evaluated. These examples give insight into the conditions required to obtain coherent light.

Problem 3.1. Consider a one-dimensional cavity that contains a chaotic light beam, and suppose that all the cavity-mode contributions to the field except one are removed by means of a filter. The mode that remains has a large number of contributions similar to the stable wave of Fig. 3.8, all with the same frequency and wavevector but with a random distribution of phase angles. Prove that the beam is first-order coherent at any pair of space–time points in the cavity.

Problem 3.2. Consider the beam of light produced by excitation of two stable waves where the electric field is

$$E(zt) = E_1 \exp(ik_1z - i\omega_1 t) + E_2 \exp(ik_2z - i\omega_2 t). \qquad (3.49)$$

Prove that the beam of light is first-order coherent at all pairs of points.

These are examples of some general conditions under which light can have perfect first-order coherence. The conditions are satisfied if either (1) only a single cavity mode is excited, or (2) the field can be specified precisely, with no statistical features. If the beam involves excitation of more than one mode *and* exhibits statistical fluctuations, it is not possible for the light to be first-order coherent at all pairs of space–time points.

Problem 3.3. Consider a beam of light produced by excitation of two modes as in eqn (3.49), but where both modes exhibit random phase and amplitude fluctuations. If the average intensity is equally divided between the modes, prove that

$$|g^{(1)}(\tau)| = \cos\{\tfrac{1}{2}(\omega_1 - \omega_2)\tau\}. \qquad (3.50)$$

As a final topic in first-order coherence theory, we return to the case of a chaotic light source but now consider the degree of coherence that results when Doppler broadening is the main cause of the spread in emission frequencies. The emission lineshape is the same as that in absorption, given by eqn (2.153). If all other sources of line-broadening are ignored, the total electric field of the radiated light beam at a fixed observation point can be written

$$E(t) = E_0 \sum_{i=1}^{\nu} \exp(-i\omega_i t + i\phi_i), \qquad (3.51)$$

where E_0 and ϕ_i are the fixed amplitude and phase of the wave train radiated by the ith atom. Different atoms have different frequencies ω_i of radiation that are Doppler-shifted from ω_0 by an amount depending on the atomic velocity.

The first-order electric-field correlation function is written with the help of eqns (3.36) and (3.51) as

$$\langle E^*(z_1t_1)E(z_2t_2)\rangle = E_0^2\sum_{i,j=1}^{\nu}\left\langle \exp\left\{\mathrm{i}\omega_i\left(t_1-\frac{z_1}{c}\right)+\mathrm{i}\phi_i -\mathrm{i}\omega_j\left(t_2-\frac{z_2}{c}\right)-\mathrm{i}\phi_j\right\}\right\rangle. \qquad (3.52)$$

The phase angles have fixed values but are randomly distributed, and the contributions for $i \neq j$ average to zero, leaving

$$\langle E^*(z_1t_1)E(z_2t_2)\rangle = E_0^2\sum_{i=1}^{\nu}\exp(-\mathrm{i}\omega_i\tau), \qquad (3.53)$$

where τ is defined in eqn (3.37). The sum that remains is converted to an integration over the Gaussian distribution of Doppler-shifted frequencies given in eqn (2.153),

$$\begin{aligned}\langle E^*(z_1t_1)E(z_2t_2)\rangle &= \nu E_0^2(2\pi\delta^2)^{-\frac{1}{2}}\int_0^\infty \exp(-\mathrm{i}\omega_i\tau)\exp\{-(\omega_i-\omega_0)^2/2\delta^2\}\,\mathrm{d}\omega_i\\ &= \nu E_0^2\exp(-\mathrm{i}\omega_0\tau-\tfrac{1}{2}\delta^2\tau^2). \qquad (3.54)\end{aligned}$$

This result is the analogue for Doppler-broadened light of the correlation function (3.38) for collision- and radiatively-broadened light.

The corresponding degree of first-order coherence is

$$g^{(1)}(\tau) = \exp(-\mathrm{i}\omega_0\tau-\tfrac{1}{2}\delta^2\tau^2). \qquad (3.55)$$

The coherence time in this case is

$$\tau_c \approx 1/\delta \qquad (3.56)$$

and it has the same qualitative significance as the coherence time for light of Lorentzian frequency distribution. The modulus of the degree of first-order coherence (3.55) is illustrated in Fig. 3.9.

Problem 3.4. Consider light from a source that simultaneously has some Lorentzian broadening with parameter γ' and some Gaussian broadening with parameter δ. Prove that the degree of first-order coherence is

$$g^{(1)}(\tau) = \exp(-\mathrm{i}\omega_0\tau-\gamma'|\tau|-\tfrac{1}{2}\delta^2\tau^2). \qquad (3.57)$$

In the treatment of simultaneous collision and Doppler broadening it is assumed here, as in §2.13, that the two mechanisms are independent.

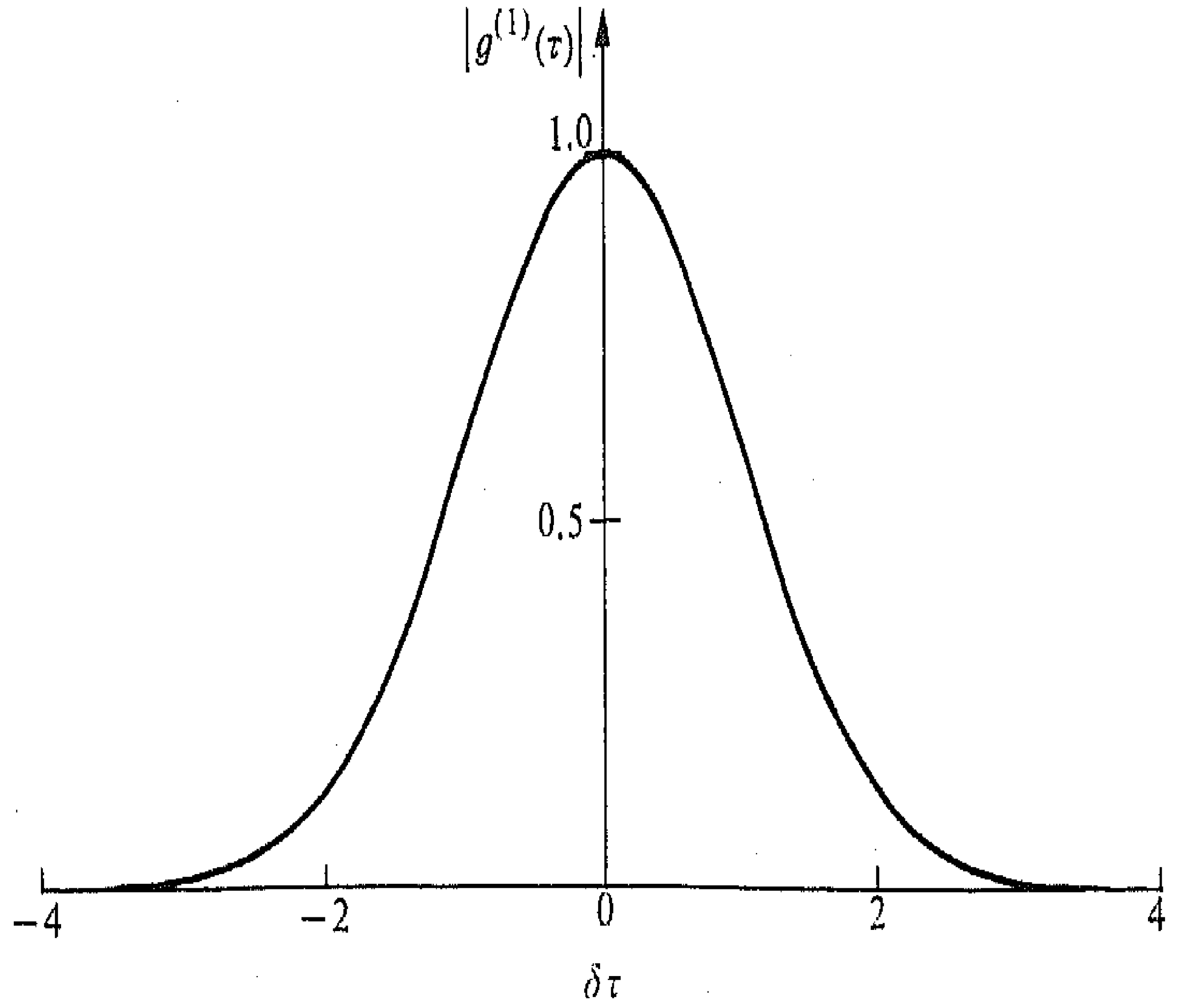

FIG. 3.9. The modulus of the degree of first-order coherence for chaotic light of Gaussian frequency distribution with root-mean-square width δ. Compare with Fig. 3.7 for the Lorentzian frequency distribution.

3.6. Intensity fluctuations of chaotic light

The present chapter has so far been concerned almost exclusively with the fluctuations in the electric field of a chaotic light beam. The main outcome of the theory is the first-order electric-field correlation function and its normalized version, the degree of first-order temporal coherence. We have seen how these functions determine the formation of fringes in the classical interference experiments.

The second main topic of the chapter concerns the direct measurement of intensity fluctuations of the kind shown in Fig. 3.4. We describe the measurement of higher-order interference effects that depend upon the correlations of two *intensities* at different times rather than the correlations of two *fields*. The results of such measurements are governed by the degree of second-order temporal coherence of the light.

As a preliminary to the discussion of intensity interference experiments, the present section considers the statistical properties of the intensity fluctuations in chaotic light. In many cases the fluctuations in the cycle-averaged intensity are too rapid for direct observation, and what is measured is some average of the fluctuations over the detector response time. We suppose initially however that there is available an ideal detector, with response time much shorter than the coherence time τ_c, that can take effectively instantaneous measurements of the intensity.

The average value of a large number of measurements of the cycle-averaged intensity $\bar{I}(t)$ taken over a period of time very much longer than τ_c is easy to calculate. With the long observation period and the assumption of instantaneous intensity measurements, the conditions for application of the ergodic theorem are satisfied, and its validity is assumed throughout the present section. The time average can thus be replaced by a statistical average over the distribution of phase angles, denoted by angle brackets. From eqns (3.14) and (3.15) the long-time average intensity is

$$\begin{aligned}\bar{I} \equiv \langle \bar{I}(t)\rangle &= \tfrac{1}{2}\epsilon_0 cE_0^2\langle|\exp(\mathrm{i}\phi_1(t))+\exp(\mathrm{i}\phi_2(t))+\ldots+\exp(\mathrm{i}\phi_\nu(t))|^2\rangle\\ &= \tfrac{1}{2}\epsilon_0 cE_0^2\nu, \end{aligned}\tag{3.58}$$

since the cross-terms between the phase factors for different radiating atoms give zero average contributions. The value of $\bar{I}$ for the fluctuating intensity illustrated in Fig. 3.4 is indicated by the dashed horizontal line. This average intensity is the quantity that is ordinarily used in theories of light transmission through absorbing media, as in Chapter 1.

The average values of higher powers of the cycle-averaged intensity can be calculated in a similar fashion. Thus the mean square intensity is

$$\langle \bar{I}(t)^2\rangle = \tfrac{1}{4}\epsilon_0^2c^2E_0^4\langle|\exp(\mathrm{i}\phi_1(t))+\exp(\mathrm{i}\phi_2(t))+\ldots+\exp(\mathrm{i}\phi_\nu(t))|^4\rangle. \tag{3.59}$$

In taking the average of the fourth power of the sum of phase factors, the only non-zero terms are those in which each factor is multiplied by its complex conjugate. These terms give

$$\begin{aligned}\langle \bar{I}(t)^2\rangle &= \tfrac{1}{4}\epsilon_0^2c^2E_0^4\left\{\sum_i\langle|\exp(\mathrm{i}\phi_i(t))|^4\rangle\right.\\ &\qquad\left.+\sum_{i\neq j}\langle|2\exp[\mathrm{i}(\phi_i(t)+\phi_j(t))]|^2\rangle\right\}\\ &= \tfrac{1}{4}\epsilon_0^2c^2E_0^4\{\nu+2\nu(\nu-1)\}.\end{aligned}\tag{3.60}$$

Thus in terms of the average intensity given by eqn (3.58), the mean-square intensity is

$$\langle \bar{I}(t)^2\rangle = \left(2-\frac{1}{\nu}\right)\bar{I}^2. \tag{3.61}$$

The number ν of radiating atoms is normally very large and eqn (3.61) can then be written

$$\langle \bar{I}(t)^2\rangle = 2\bar{I}^2 \qquad (\nu \gg 1) \tag{3.62}$$

to a very good approximation.

The root-mean-square deviation of the cycle-averaged intensity is

$$(\langle \bar{I}(t)^2\rangle-\langle \bar{I}(t)\rangle^2)^{\frac{1}{2}} = \bar{I}. \tag{3.63}$$

The size of fluctuation is thus equal to the average intensity, as is qualitatively evident in Fig. 3.4. A similar result was found in eqns (1.41) or (1.42) for the fluctuations in number of the thermally excited photons in a single cavity mode.

The averages of higher powers of $\bar{I}(t)$ than the second are quite complicated in general, but relatively simple results are obtained if the number of radiating atoms is assumed to be very large. Then as in the second moment calculation in eqn (3.60) the dominant contribution comes from terms that involve the square modulus of products of the phase factors of distinct atoms. The approximate average of the rth power of the intensity is

$$\begin{aligned}\langle \bar{I}(t)^r\rangle &= (\tfrac{1}{2}\epsilon_0 cE_0^2)^r\sum_{\substack{i,j,k,\ldots\\ (r\text{ different atoms})}}{}^{'}\langle|r!\exp[\mathrm{i}(\phi_i(t)+\phi_j(t)+\phi_k(t)+\ldots)]|^2\rangle\\ &= (\tfrac{1}{2}\epsilon_0 cE_0^2)^r\,{}^{\nu}C_r(r!)^2.\end{aligned}\tag{3.64}$$

Thus with ν assumed very much larger than r and the average intensity taken from eqn (3.58),

$$\langle \bar{I}(t)^r\rangle = r!\bar{I}^r \qquad (\nu \gg r). \tag{3.65}$$

This result for the rth moment of the intensity fluctuation distribution, although derived here for the collision-broadened source, is in fact valid for any kind of chaotic light. The occurrence of the $r!$ factor in eqn (3.65) is a distinctive feature of chaotic light. The similarity to the rth factorial moment (1.38) for the thermal photon distribution should be noted.

Provided that the number of radiating atoms is very large, it is possible to calculate not only the moments derived above but also the explicit form of the probability distribution for the cycle-averaged intensity. The first step is the determination of the statistical distribution of the values of $a(t)$.

It is seen from eqn (3.14) and Fig. 3.3 that at any instant of time t, $a(t)$ is the distance from the origin in an Argand diagram arrived at by taking ν steps of unit length and in random directions specified by the angles $\phi_1(t), \phi_2(t), \ldots, \phi_\nu(t)$. The calculation is an example of the 'random walk' problem, well known in the theory of stochastic processes[4]. Let $p[a(t)]$ be the probability that the end-point of a random walk of ν steps lies in unit area around the point specified by coordinates $a(t), \varphi(t)$ in Fig. 3.3. The result given by random-walk theory for the present problem is[5]

$$p[a(t)] = (1/\pi\nu)\exp(-a(t)^2/\nu), \tag{3.66}$$

being independent of $\varphi(t)$ as expected from the physical nature of the problem. The probability is normalized,

$$\int_0^\infty \mathrm{d}a(t)\int_0^{2\pi} a(t)p[a(t)]\,\mathrm{d}\varphi(t) = 1. \tag{3.67}$$

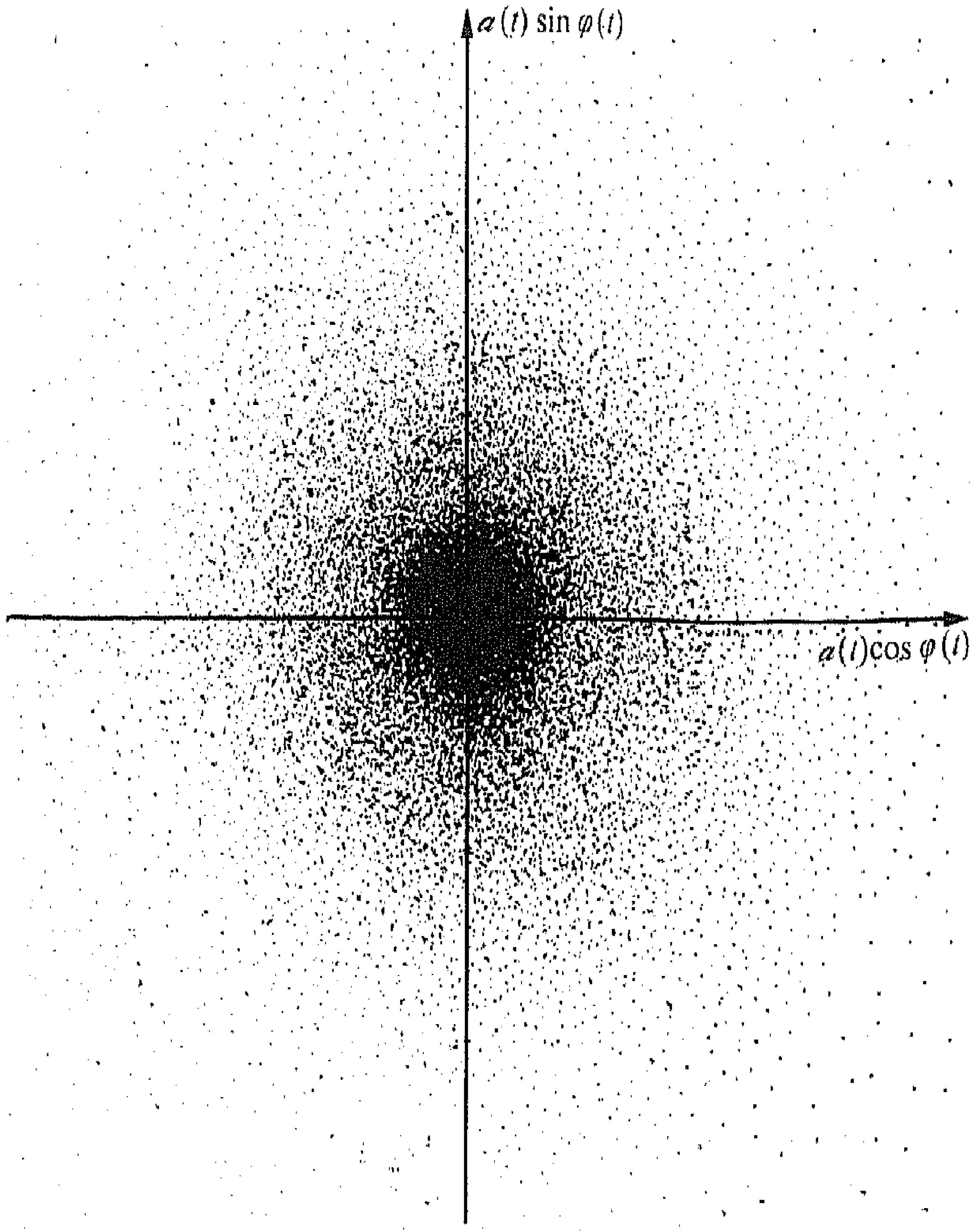

FIG. 3.10. Probability distribution for the amplitude and phase of the electric field of a chaotic light beam. The density of shading is proportional to the probability at the point in the plane corresponding to polar coordinates $a(t)$ and $\varphi(t)$. Note that the probability is greatest at the origin and is independent of $\varphi(t)$.

The probability distribution (eqn (3.66)) is a Gaussian function, whose form is shown in Fig. 3.10. A similar distribution arises for any chaotic light beam, and because of this the light from a chaotic source is sometimes called Gaussian light. It is important not to confuse the Gaussian distribution of $|E(t)|$ with the distribution of frequencies in the beam, which can be Lorentzian, Gaussian, or an intermediate function, and is indeed Lorentzian for the collision-broadening mechanism assumed here.

The probability distribution for $a(t)$ can be converted to a probability distribution for $\bar{I}(t)$ with the help of eqn (3.15).

Problem 3.5. Prove that the probability for an instantaneous measurement of the cycle-averaged intensity to yield a value between $\bar{I}(t)$ and $\bar{I}(t)+\mathrm{d}\bar{I}(t)$ is $p[\bar{I}(t)]\,\mathrm{d}\bar{I}(t)$, where

$$p[\bar{I}(t)] = (1/\bar{I})\exp(-\bar{I}(t)/\bar{I}), \qquad (3.68)$$

and $\bar{I}$ is given by eqn (3.58). Note that the most probable value of $\bar{I}(t)$ is always zero.

The random-walk probability distribution strictly refers to the results of a large number of walks that all begin at the origin. For the problem in hand, the end-point of each walk defines an amplitude a and a phase φ for a light beam. Random-walk theory assigns a certain probability to every possible a and φ. The collection of light beams with all possible amplitudes and phases forms a statistical ensemble of the type mentioned in §1.4. Each light beam in the ensemble has fixed a and φ, and the intensity distribution shown in eqn (3.68) is rigorously valid for such an ensemble of fixed-amplitude and fixed-phase beams. Its application to determine time averages of a long series of instantaneous intensity measurements on a single beam of chaotic light relies once more on the ergodic theorem. The moments of the distribution (3.68), given by

$$\langle \bar{I}(t)^r \rangle = (1/\bar{I})\int_0^\infty \bar{I}(t)^r \exp(-\bar{I}(t)/\bar{I})\,\mathrm{d}\bar{I}(t) = r!\,\bar{I}^r, \qquad (3.69)$$

agree with the result (3.65) obtained previously.

All of the above results refer to idealized experiments that measure the instantaneous intensity. The effects of a finite detector response time, particularly on the second moment of the intensity fluctuations, are discussed in §3.9. At the extreme limit of a very long coherence time, it is possible by somewhat artificial means to construct a light beam in which the intensity fluctuations are easily visible. Such a beam can be generated[6] by the scattering of laser light from small polystyrene balls suspended in water. Small Doppler shifts of the scattered frequency result from the Brownian motion of the balls. The suspension is a slowed-down analogue of a radiating gas, with the sharp laser frequency replacing the atomic transition frequency. The coherence time τ_c is of order 10^{-1} s, and the intensity fluctuations are apparent to the naked eye.

A contrast to the above results for chaotic light is provided by the classical stable wave of Fig. 3.8. There is no need to employ statistics in this case; the cycle-averaged intensity is constant and there are no intensity fluctuations. The result analogous to eqn (3.65) is

$$\langle \bar{I}(t)^r \rangle = \bar{I}^r, \qquad (3.70)$$

and the root-mean-square deviation is zero.

3.7. Degree of second-order coherence

The intensity-fluctuation properties of chaotic light described in the previous section refer to averages of intensity readings taken at single instants of time. We now consider two-time measurements in which a series of pairs of intensity readings are taken with a fixed time-delay τ. The average of the product of each pair of intensity readings is the intensity correlation function of the light, analogous to the electric-field correlation function defined in eqn (3.4). The measurement of intensity correlations is described in §3.9; we here consider the theory of the correlation function.

It is convenient to work with a normalized form of the correlation function called the *degree of second-order temporal coherence*,

$$g^{(2)}(\tau) = \frac{\langle \bar{I}(t)\bar{I}(t+\tau)\rangle}{\bar{I}^2} = \frac{\langle E^*(t)E^*(t+\tau)E(t+\tau)E(t)\rangle}{\langle E^*(t)E(t)\rangle^2}, \tag{3.71}$$

where $\bar{I}$ is the average intensity defined as in eqn (3.58), and the order of electric-field factors in the second-order electric-field correlation function follows a convention. It is clear from the symmetry of the definition that the property analogous to eqn (3.10) is

$$g^{(2)}(-\tau) = g^{(2)}(\tau), \tag{3.72}$$

and calculations need only be made for positive τ. It is assumed that the measurements are made at a fixed point in space and satisfy the conditions for equivalence of statistical and time averages as before.

We have seen that the degree of first-order coherence takes values in the range 0 to 1, and it might be expected at first sight that the degree of second-order coherence would have a similar range. This is not however correct. The allowed range of values of the degree of second-order coherence is controlled by two inequalities; both are based on Cauchy's inequality[7], according to which two measurements of the intensity at times t_1 and t_2 must satisfy

$$2\bar{I}(t_1)\bar{I}(t_2) \leqslant \bar{I}(t_1)^2 + \bar{I}(t_2)^2. \tag{3.73}$$

By applying this inequality to the cross-terms, it is easy to show that

$$\left\{\frac{\bar{I}(t_1)+\bar{I}(t_2)+\ldots+\bar{I}(t_N)}{N}\right\}^2 \leqslant \frac{\bar{I}(t_1)^2+\bar{I}(t_2)^2+\ldots+\bar{I}(t_N)^2}{N} \tag{3.74}$$

for the results of N measurements of the intensity. Thus in the correlation function notation,

$$\bar{I}^2 \equiv \langle \bar{I}(t)\rangle^2 \leqslant \langle \bar{I}(t)^2\rangle, \tag{3.75}$$

and the zero time-delay degree of second-order coherence from eqn (3.71) satisfies

$$g^{(2)}(0) \geqslant 1. \tag{3.76}$$

It is not possible to establish any upper limit, and the complete range is given by

$$\infty \geqslant g^{(2)}(0) \geqslant 1. \tag{3.77}$$

The above proof cannot be extended to finite time delays, and the only restriction then results from the essentially positive nature of the intensity, which gives

$$\infty \geqslant g^{(2)}(\tau) \geqslant 0 \qquad \tau \neq 0. \tag{3.78}$$

There is however another important property that follows from the inequality

$$[\bar{I}(t_1)\bar{I}(t_1+\tau)+\ldots+\bar{I}(t_N)\bar{I}(t_N+\tau)]^2 \leqslant [\bar{I}(t_1)^2+\ldots+\bar{I}(t_N)^2][\bar{I}(t_1+\tau)^2+\ldots+\bar{I}(t_N+\tau)^2], \tag{3.79}$$

which is also readily established with the help of eqn (3.73). The two summations on the right of eqn (3.79) are equal for a sufficiently long and numerous series of measurements, and the square root then produces the result

$$\langle \bar{I}(t)\bar{I}(t+\tau)\rangle \leqslant \langle \bar{I}(t)^2\rangle, \tag{3.80}$$

or

$$g^{(2)}(\tau) \leqslant g^{(2)}(0). \tag{3.81}$$

These general properties of the degree of second-order coherence are illustrated by the example shown in Fig. 3.11. Part (a) of the figure shows a train of rectangular classical pulses of duration τ_0. Suppose that the intensity I_0 within each pulse is constant and that the duration and separation of the pulses give a mean intensity that can be written

$$\bar{I} = fI_0 \qquad 0 < f \leqslant 1. \tag{3.82}$$

Here f is the number of pulses per unit time multiplied by τ_0. It is a trivial exercise to show from eqn (3.71) that

$$g^{(2)}(0) = 1/f, \tag{3.83}$$

and only a brief calculation is needed to verify the time dependence of the degree of second-order coherence shown in part (b) of Fig. 3.11. The degree of coherence correctly satisfies the inequalities (3.77) and (3.81), and indeed the zero time-delay value (3.83) covers the whole range allowed by eqn (3.77) for the different choices of f.

The special case of a beam of constant intensity I_0 is obtained for $f = 1$, when it is easily shown that

$$g^{(2)}(\tau) = 1, \tag{3.84}$$

independent of the time delay τ. This is the case of a classical stable wave, and for $\tau = 0$ eqn (3.84) agrees with the result obtained from eqn (3.70).

3.8. Second-order coherence of chaotic light

The statistical properties of chaotic light produce beam intensities that are uncorrelated after time separations long compared to the coherence time τ_c.

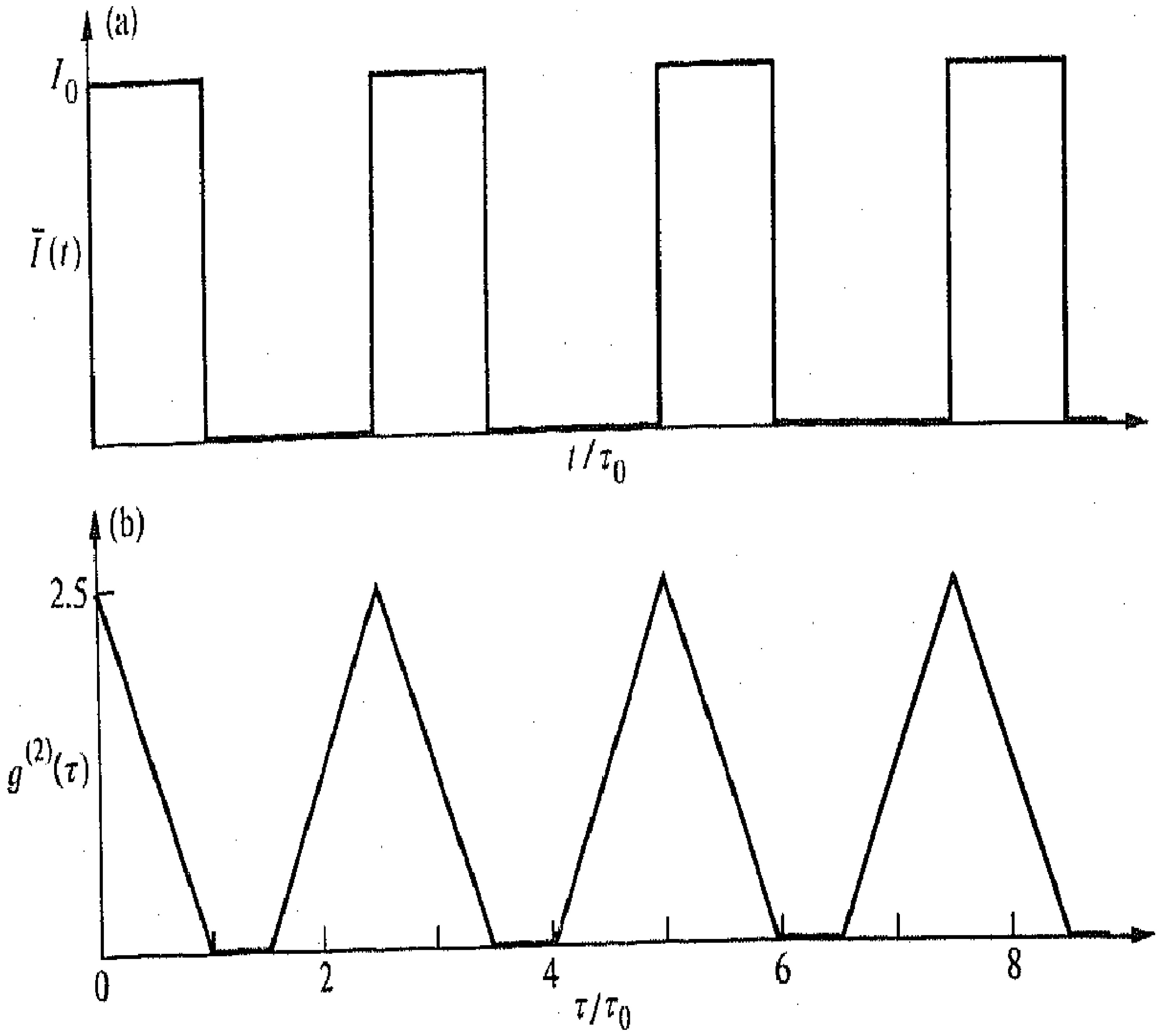

FIG. 3.11. (a) Intensity variation for a train of rectangular pulses of duration τ_0 and separation $1{\cdot}5\tau_0$, giving $f = 0{\cdot}4$. (b) The corresponding degree of second-order coherence.

The degree of second-order coherence (3.71) thus has a limiting value

$$g^{(2)}(\tau) \to 1 \qquad \text{for} \qquad \tau \gg \tau_c, \tag{3.85}$$

in contrast to the zero limiting value of the degree of first-order coherence given in eqn (3.29). The regular wave train of Fig. 3.11 has an infinitely long coherence time and the limit does not apply in this case.

In order to determine the degree of second-order coherence of chaotic light we suppose, as in the models used earlier in the present chapter for both collision and Doppler-broadened light, that the electric field of the light beam is made up of independent contributions from the different radiating atoms i,

$$E(t) = \sum_i E_i(t). \tag{3.86}$$

The second-order electric-field correlation function that appears in eqn (3.71) is thus

$$\begin{aligned}\langle E^*(t)E^*(t+\tau)E(t+\tau)E(t)\rangle = {} & \sum_{i=1}^{\nu} \langle E_i^*(t)E_i^*(t+\tau)E_i(t+\tau)E_i(t)\rangle \\ & + \sum_{i \neq j} \{\langle E_i^*(t)E_j^*(t+\tau)E_j(t+\tau)E_i(t)\rangle \\ & + \langle E_i^*(t)E_j^*(t+\tau)E_i(t+\tau)E_j(t)\rangle\},\end{aligned} \tag{3.87}$$

where only those terms are retained in which the field of each atom is multiplied by its complex conjugate. All other terms vanish because of the random relative phases of the waves from different atoms. Thus taking account of the equivalence of the contribution from each atom

$$\begin{aligned}\langle E^*(t)E^*(t+\tau)E(t+\tau)E(t)\rangle = {} & \nu\langle E_i^*(t)E_i^*(t+\tau)E_i(t+\tau)E_i(t)\rangle \\ & + \nu(\nu-1)\{\langle E_i^*(t)E_i(t)\rangle^2 + |\langle E_i^*(t)E_i(t+\tau)\rangle|^2\}.\end{aligned} \tag{3.88}$$

If the number ν of radiating atoms is now assumed to be very large, the contributions that involve pairs of atoms greatly exceed the single-atom contributions, and to a good approximation

$$\langle E^*(t)E^*(t+\tau)E(t+\tau)E(t)\rangle = \nu^2\{\langle E_i^*(t)E_i(t)\rangle^2 + |\langle E_i^*(t)E_i(t+\tau)\rangle|^2\}. \tag{3.89}$$

The corresponding result for the first-order electric-field correlation function is given in eqn (3.18). Thus with the definitions (3.8) and (3.71) of the degrees of first- and second-order coherence, eqns (3.18) and (3.89) give

$$g^{(2)}(\tau) = 1 + |g^{(1)}(\tau)|^2 \qquad (\nu \gg 1). \tag{3.90}$$

This important relation holds for all varieties of chaotic light.

The second-order electric-field correlation function in eqn (3.88) can be explicitly evaluated for the model of a collision-broadened light-source used to evaluate the first-order correlation function (3.25). The only additional result needed is

$$\langle E_i^*(t)E_i^*(t+\tau)E_i(t+\tau)E_i(t)\rangle = E_0^4, \tag{3.91}$$

and eqn (3.88) then gives

$$\langle E^*(t)E^*(t+\tau)E(t+\tau)E(t)\rangle = \nu E_0^4 + \nu(\nu-1)E_0^4\{1+\exp(-2\gamma'\tau)\}. \tag{3.92}$$

Thus with the help of eqn (3.25), the degree of second-order coherence (3.71) is

$$g^{(2)}(\tau) = \frac{1}{\nu} + \left(1 - \frac{1}{\nu}\right)\{1+\exp(-2\gamma'\tau)\}, \tag{3.93}$$

in agreement at $\tau = 0$ with the zero time-delay degree of second-order coherence obtained from eqn (3.61). The degree of coherence at negative τ is obtained from the symmetry property (3.72), and in the limit of a large number of radiating atoms, eqn (3.93) gives

$$g^{(2)}(\tau) = 1 + \exp(-2\gamma'|\tau|) \qquad (\nu \gg 1), \tag{3.94}$$

in agreement with the general result (3.90).

Fig. 3.12 shows the form of the degree of second-order coherence for the chaotic light of Lorentzian frequency distribution assumed in the derivation of

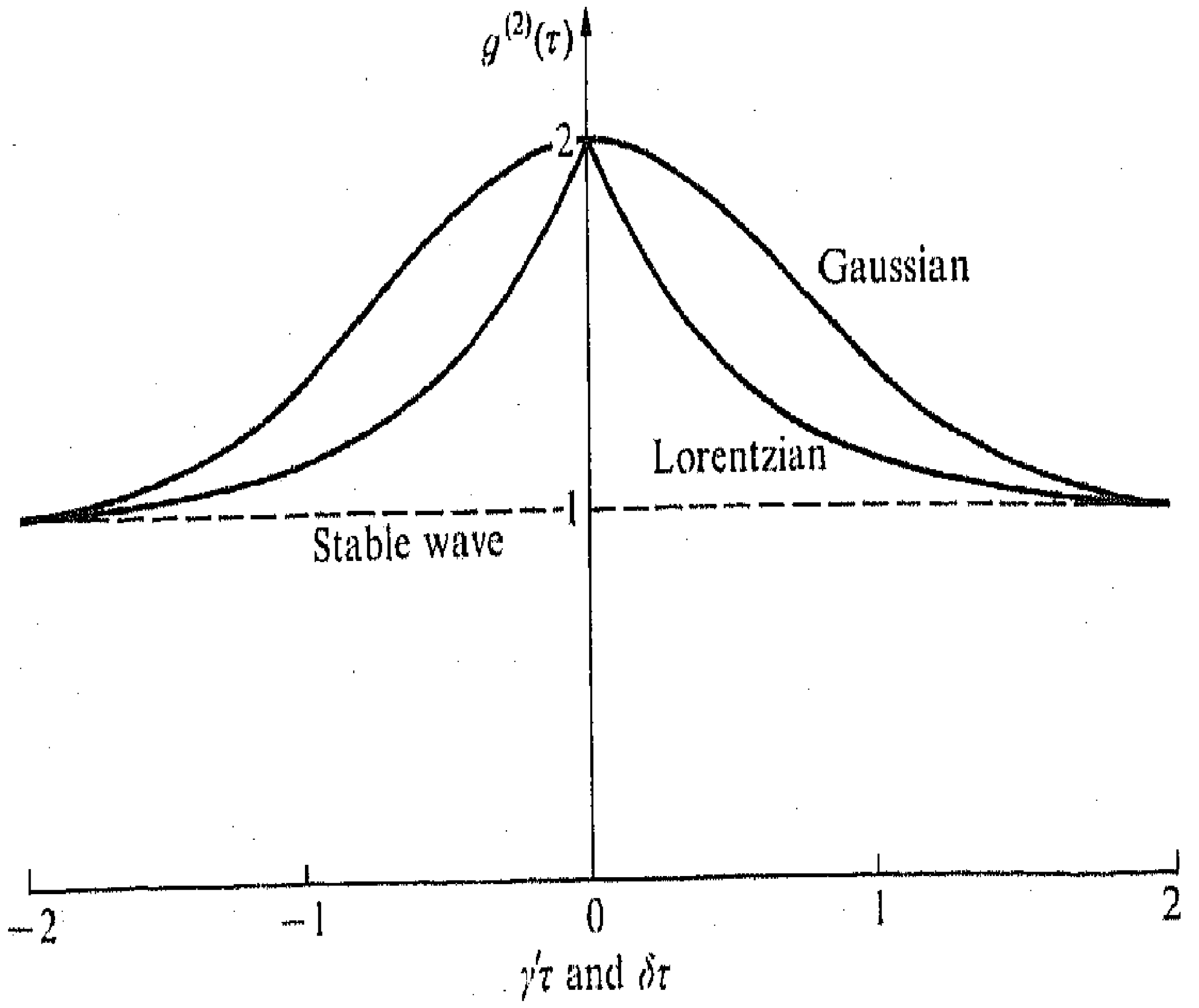

FIG. 3.12. The degrees of second-order coherence of chaotic light having Gaussian and Lorentzian frequency distributions with linewidth parameters δ and γ' respectively. The dashed line shows the constant unit second-order coherence of a classical stable wave.

eqn (3.94). The corresponding result for chaotic light of Gaussian frequency distribution,

$$g^{(2)}(\tau) = 1+\exp(-\delta^2\tau^2), \tag{3.95}$$

obtained from eqns (3.55) and (3.90) is also illustrated. The stable-wave result (3.84) is indicated by the horizontal dashed line. All three examples in the figure satisfy the general inequalities (3.77) and (3.81), and both kinds of chaotic light have the limiting value (3.85). It is evident from eqn (3.90) that

$$g^{(2)}(0) = 2 \tag{3.96}$$

for any kind of chaotic light since $g^{(1)}(0) = 1$ from its definition (3.8). This result is also evident from eqn (3.69).

The peak in the degree of second-order coherence of chaotic light for $\tau < \tau_c$ is a manifestation of the kind of intensity fluctuations shown in Fig. 3.4. For such small delay times, the two intensity measurements to be correlated in the degree of second-order coherence can fall within the same fluctuation peak to give an enhanced contribution. For longer delay-times, $\tau > \tau_c$, the two intensities tend to be uncorrelated and the degree of second-order coherence is close to unity.

The degrees of second-order coherence calculated above assume a polarized beam of light and a fixed observation point. The definition (3.71) can be generalized, analogous to eqn (3.42), to include the spatial dependence of the optical fields. The degree of second-order temporal coherence between the

light at space-time points $(\mathbf{r}_1, t_1)$ and $(\mathbf{r}_2, t_2)$ is defined to be

$$g^{(2)}(\mathbf{r}_1 t_1, \mathbf{r}_2 t_2; \mathbf{r}_2 t_2, \mathbf{r}_1 t_1) = \frac{\langle E^*(\mathbf{r}_1 t_1)E^*(\mathbf{r}_2 t_2)E(\mathbf{r}_2 t_2)E(\mathbf{r}_1 t_1)\rangle}{\langle |E(\mathbf{r}_1 t_1)|^2\rangle\langle |E(\mathbf{r}_2 t_2)|^2\rangle}, \tag{3.97}$$

where the angle brackets again denote ensemble averages. Note that this function is a special case of a more general second-order coherence in which the four fields in the correlation function are evaluated at four different space–time points, but we do not consider this further generalization. The light at points $(\mathbf{r}_1, t_1)$ and $(\mathbf{r}_2, t_2)$ is said to be second-order coherent if simultaneously

$$\left.\begin{aligned} |g^{(1)}(\mathbf{r}_1 t_1, \mathbf{r}_2 t_2)| &= 1 \\ g^{(2)}(\mathbf{r}_1 t_1, \mathbf{r}_2 t_2; \mathbf{r}_2 t_2, \mathbf{r}_1 t_1) &= 1. \end{aligned}\right\} \tag{3.98}$$

The inclusion of spatial dependence in the degree of second-order coherence is here restricted to plane-polarized parallel beams of light where only the single z-coordinate is needed. Then, as in the discussion of first-order coherence, the spatial dependence of the field is incorporated via eqn (3.36) and it is not difficult to verify that, analogous to eqn (3.44),

$$g^{(2)}(z_1 t_1, z_2 t_2; z_2 t_2, z_1 t_1) = g^{(2)}(\tau), \tag{3.99}$$

where τ is defined in eqn (3.37). With this interpretation of τ, the expressions already derived for the degree of second-order coherence apply to spatially separated points in the parallel beam.

As discussed in connection with eqn (3.44), chaotic light is always first-order coherent for space–time points sufficiently close together. This is illustrated by the approach of the first-order coherence of the chaotic light in Figs. 3.7 and 3.9 towards unity for small $\gamma'\tau$ or $\delta\tau$. However, the small τ limit produces a second-order coherence of 2 according to eqn (3.96), as illustrated in Fig. 3.12. It is not possible for chaotic light to be second-order coherent in accordance with the definition (3.98) for any choice of space–time points. By contrast, eqns (3.48) and (3.84) show that the classical stable wave is second-order coherent at all space–time points.

Problem 3.6. Consider the single-mode chaotic light beam, defined in problem 3.1 as a randomly-phased superposition of stable waves. Prove from first principles that

$$g^{(2)}(\tau) = 2. \tag{3.100}$$

The coherence time is infinite in this case and eqn (3.85) does not apply.

3.9. Experiment of Hanbury Brown and Twiss

The results of all the classical interference experiments, typified by Young's slits, are controlled by the correlation of two electric-field amplitudes, conveniently expressed in terms of the degree of first-order coherence of the light. The correlation of two optical intensities, conveniently expressed in terms of the degree of second-order coherence, was first measured by Hanbury Brown and Twiss[8,9], Their experiment typifies all subsequent measurements of degrees of second-order coherence. Such measurements have a particular significance in terms of the correspondence between the classical and quantum theories of light. We here consider the classical theory of the experiment, reserving the quantum discussion for Chapter 6, where the theory of optical coherence is reconsidered in terms of the quantized radiation field.

The experimental apparatus is shown schematically in Fig. 3.13. Light from a mercury arc is filtered to eliminate all but the 435·8-nm emission line of the mercury spectrum. The beam is split into two equal portions by a half-silvered mirror. The intensity of each portion is measured by a photomultiplier detector, the principles of which are outlined in §5.6, and the fluctuations in the outputs of the two detectors are multiplied together in the correlator. The integrated value of this product over a long period of observation provides a measurement of the magnitude of the intensity fluctuations.

One of the detectors is mounted on a slide so that its position can be varied laterally relative to the fixed detector. This enables the detector apertures as viewed from the pinhole to be superimposed or completely separated and provides a verification of the reality of the observed fluctuations, which must vanish for sufficient detector separation. Let us ignore this feature of the experiment and treat an idealized arrangement in which the two detectors are symmetrically placed with respect to the mirror. They then measure the intensities in the beams at equal linear distances z from the light source.

According to the classical theory, the half-silvered mirror divides the incident cycle-averaged intensity $\bar{I}(zt)$ into two identical beams in arms 1 and 2 of the experiment. In an obvious notation we can write

$$\bar{I}_1(zt) = \bar{I}_2(zt) = \tfrac{1}{2}\bar{I}(zt), \tag{3.101}$$

and the long-time average intensities in the two arms are

$$\bar{I}_1 = \bar{I}_2 = \tfrac{1}{2}\bar{I}. \tag{3.102}$$

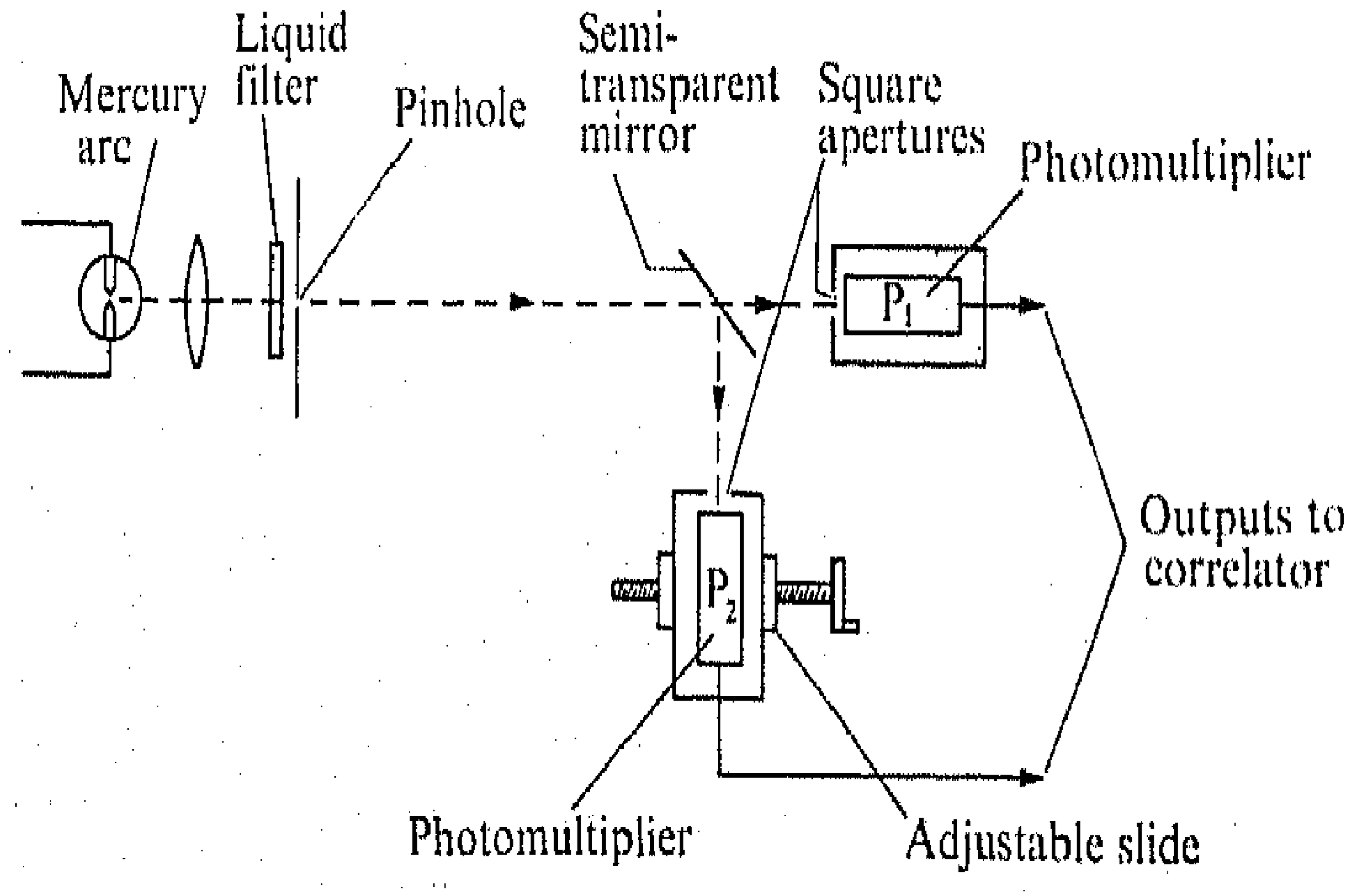

FIG. 3.13. Arrangement of the main components in an intensity interference experiment. (After R. Hanbury Brown and R. Q. Twiss, ref. 8.)

We ignore until later the complications introduced by the finite response times of the detectors, and assume that the experiment is capable of correlating the intensities at the two detectors measured instantaneously at different times t_1 and t_2. The correlator was designed to produce the average

$$\langle[\bar{I}_1(zt_1)-\bar{I}_1][\bar{I}_2(zt_2)-\bar{I}_2]\rangle = \tfrac{1}{4}\{\langle\bar{I}(zt_1)\bar{I}(zt_2)\rangle-\bar{I}^2\}. \tag{3.103}$$

The normalized version of the Hanbury Brown and Twiss correlation is readily expressed in terms of the degree of second-order coherence,

$$\frac{\langle[\bar{I}_1(zt_1)-\bar{I}_1][\bar{I}_2(zt_2)-\bar{I}_2]\rangle}{\bar{I}_1\bar{I}_2} = g^{(2)}(\tau)-1, \tag{3.104}$$

where in this case $\tau = t_2-t_1$.

It is seen therefore that apart from a normalization factor the experiment of Hanbury Brown and Twiss measures the deviation from unity of the degree of second-order coherence. The results of the experiment can be envisaged in terms of the examples shown in Fig. 3.12. Only chaotic light was available at the time of the original experiments; in this case the correlation (3.104) is unity for $\tau \ll \tau_c$ but falls to zero for $\tau \gg \tau_c$. Similar experiments have since been made on light that closely corresponds to the classical stable wave; in this case the Hanbury Brown and Twiss correlation is zero for all values of τ.

For chaotic light of Lorentzian frequency distribution, the correlation given by (3.94) and (3.104) is

$$g^{(2)}(\tau)-1 = \exp(-2\gamma'|t_2-t_1|). \tag{3.105}$$

This is however not a realistic prediction for the correlation expected in a practical experiment, where it is never possible to make instantaneous measurements of the beam intensity. There is always some minimum response time τ_r of the detection system such that the recorded intensity is a mean over the period τ_r. Consider a Hanbury Brown and Twiss experiment where the 'instantaneous' intensities are measured simultaneously by two detectors of equal response time τ_r. If the additional average over the detector response time is indicated by further angle brackets, the predicted result is

$$\begin{aligned}\langle g^{(2)}(\tau)\rangle_r-1 &= \frac{1}{\tau_r^2}\int_0^{\tau_r}\mathrm{d}t_1\int_0^{\tau_r}\exp(-2\gamma'|t_2-t_1|)\,\mathrm{d}t_2\\ &= (1/2\gamma'^2\tau_r^2)\{\exp(-2\gamma'\tau_r)-1+2\gamma'\tau_r\}.\end{aligned} \tag{3.106}$$

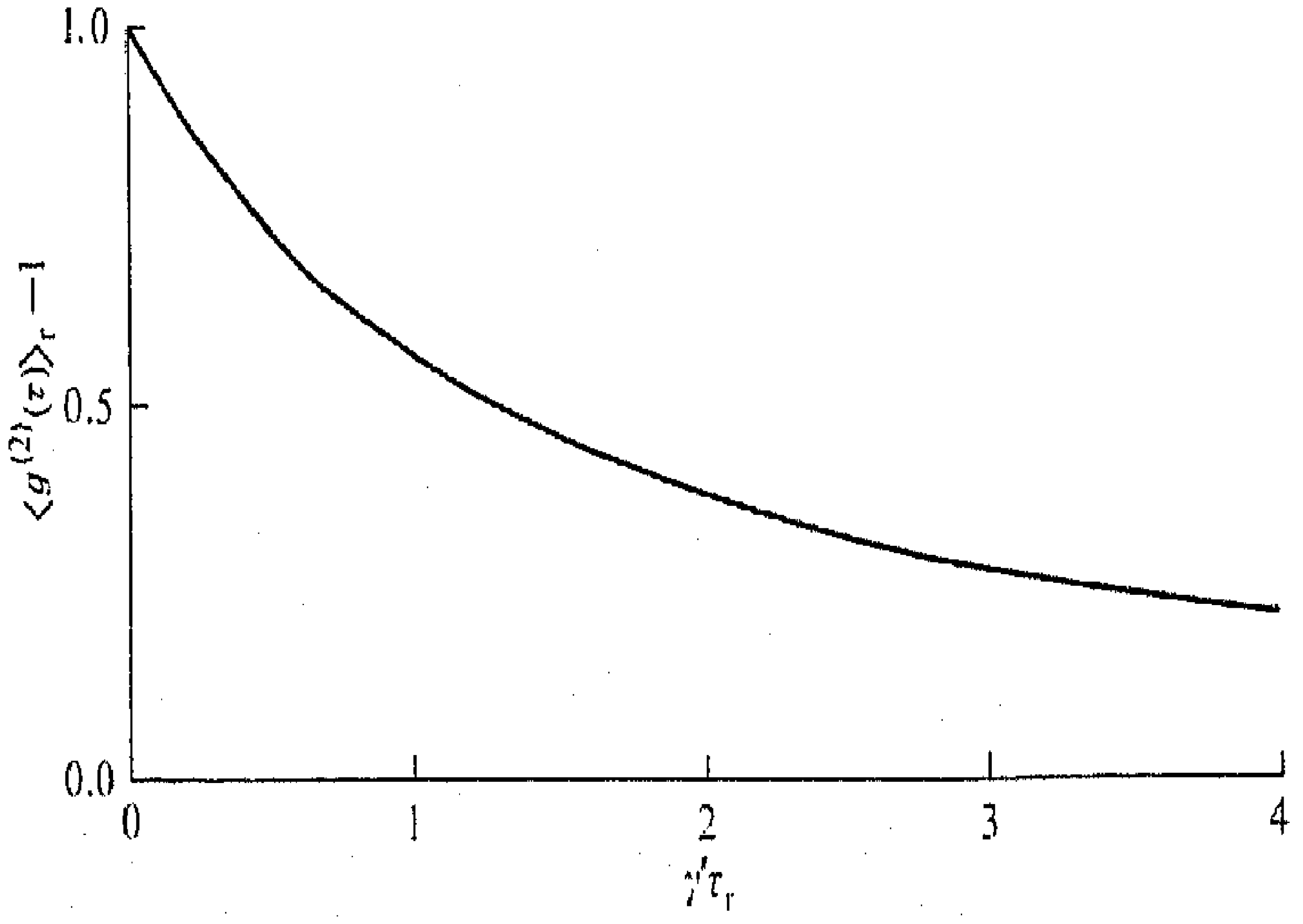

FIG. 3.14. Magnitude of the correlated intensity fluctuations of chaotic light having a Lorentzian frequency distribution with linewidth parameter γ'. Both detectors have response time τ_r.

This result is illustrated in Fig. 3.14.

For a very short detector response time where

$$\gamma'\tau_r \ll 1 \quad \text{or} \quad \tau_r \ll \tau_c, \tag{3.107}$$

the right-hand side of eqn (3.106) reduces to unity, in agreement with the result (3.105) in the case of simultaneous measurement of the instantaneous intensities. In the opposite limit of a long response time, where

$$\gamma'\tau_r \gg 1 \quad \text{or} \quad \tau_r \gg \tau_c, \tag{3.108}$$

eqn (3.106) gives

$$\langle g^{(2)}(\tau)\rangle_r - 1 = 1/\gamma'\tau_r = \tau_c/\tau_r; \tag{3.109}$$

the magnitude of the observed intensity fluctuations, inversely proportional to the response time, is seriously reduced in this case. Note that the final form of the reduction factor in eqn (3.109) applies whether or not the chaotic light has a Lorentzian frequency distribution. The original measurements[8] were carried out with a light source and detection equipment for which the reduction factor was as high as 10^5, and the success of the experiment depended upon the processing of the measured intensities to obtain the correlated intensity fluctuations (3.104) directly.

The intensity interference effects described above depend on the second-order *temporal coherence* of the light. However the practical observation of the intensity correlations is also affected by the *spatial coherence* of the light, associated with the finite dimensions of the source and the detectors. The corresponding effects of spatial coherence in first-order interference experiments have been mentioned in the discussion of Young's slits. The spatial coherence is not of great interest here since it is not so intrinsic a property of the light as the temporal coherence. However, it is of course of great importance in the design of interference experiments and we briefly consider it.

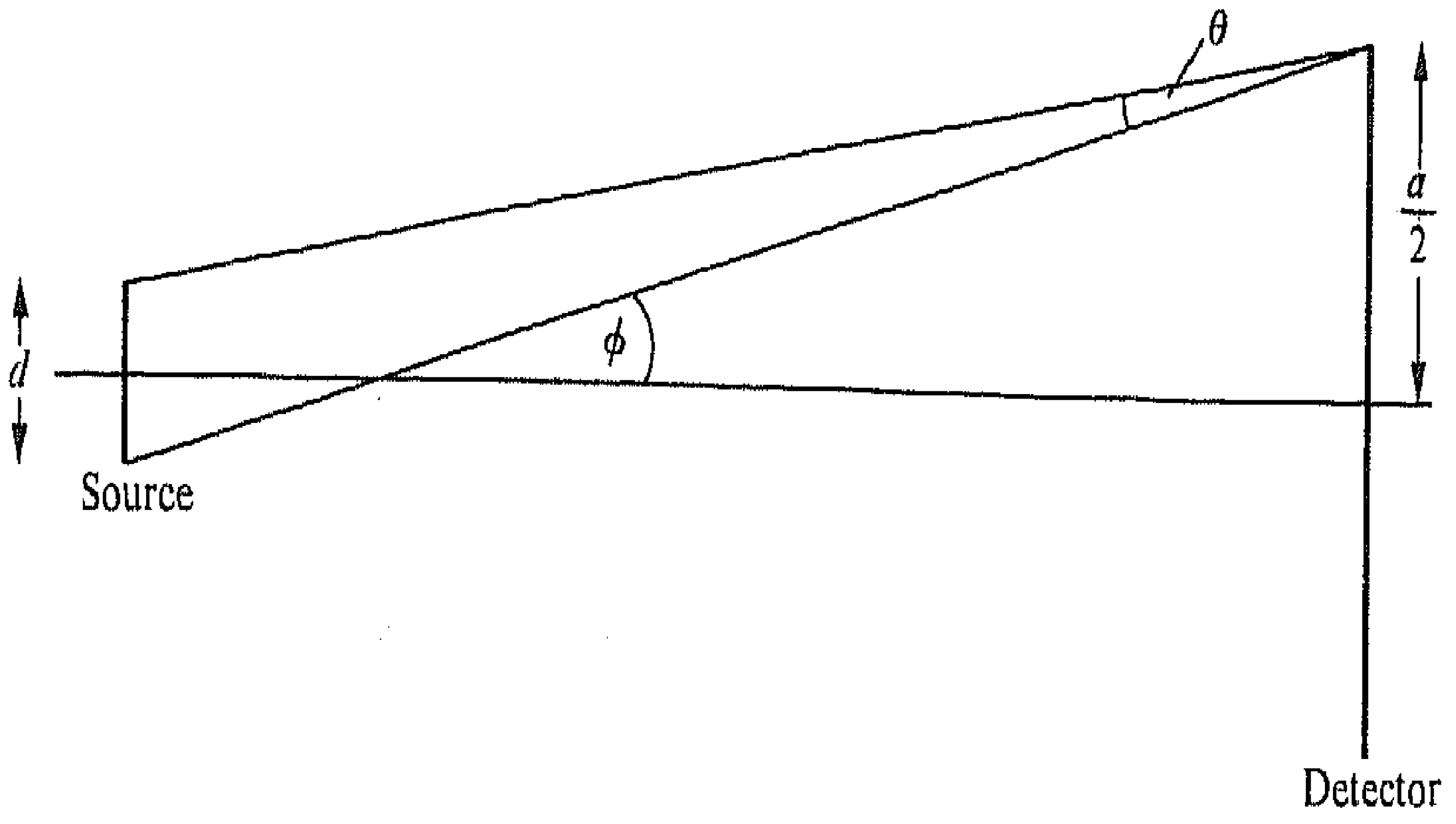

FIG. 3.15. Arrangement of source and detector for the consideration of spatial coherence.

Fig. 3.15 shows a light source of finite dimension d perpendicular to the axis of an optical experiment, in which the light is collected by a detector that also has finite dimensions perpendicular to the axis. The linear dimensions of source and detector are assumed to be very small compared to their separation. The phases of the light from different parts of the source have a varying relation across the detector. There is a 180° phase difference between light from the two ends of the source at a point in the detector distance $a/2$ off the axis if

$$\phi d = \tfrac{1}{2}\lambda, \tag{3.110}$$

where ϕ is the angle defined in Fig. 3.15 and λ is the wavelength of the light. Thus

$$a = 2\phi d/\theta = \lambda/\theta, \tag{3.111}$$

where θ is the angular diameter of the source viewed from the detector.

The dimension a gives a rough measure of the size of detector for which the desired field or intensity correlations begin to suffer diminutions as a result of cancellations between the contributions of different parts of the detector. The experiments of Hanbury Brown and Twiss used light with a wavelength of about 4×10^{-7} m and their light source had an angular diameter of about 8×10^{-5} rad viewed from the detectors. Their detector dimension of 5 mm thus satisfied the condition (3.111), and the spatial coherence effects caused only a modest reduction in the size of the observed intensity fluctuations. It is seen that the spatial coherence controls the phase variation of the light in a direction perpendicular to the beam and is determined by the closeness of the light beam to the ideal of plane parallelism. The temporal coherence controls the fluctuation and correlation properties of the fields and intensities of the light in a direction parallel to the beam, and is determined by the properties of the light-emitting atoms in the source[10].

Although the temporal coherence properties of light are of most interest for the present account, it must be emphasized that the main interest of Hanbury Brown and Twiss was in spatial coherence effects. Thus the purpose of the adjustable slide shown in Fig. 3.13 was to allow the spatial separation of the two detectors as viewed from the source by distances exceeding the spatial coherence length (3.111). The observed fall-off in the correlation between the intensities recorded in the two detectors allows an experimental determination of the angular diameter θ of the source. The laboratory experiment illustrated in Fig. 3.13 was a prototype for a large-scale optical intensity-interferometer that has been most successfully used in measuring the angular diameters of stars[9].

Returning now to the discussion of temporal coherence, it is clear from expressions given earlier in the present section that intensity-interference experiments can be used to determine the coherence time and hence the linewidth parameter of the light source. Because of the inverse relation between these quantities, a narrow emission line corresponds to a relatively long time scale for the intensity fluctuations. Thus determinations of linewidths by study of intensity fluctuations tend to be feasible for just those sources whose frequency spreads are so narrow that conventional frequency-domain spectroscopy is incapable of resolving them. Time-domain spectroscopy is considered further in Chapter 6, where the effects of quantization of the radiation field are also included.

3.10. Higher-order coherence and polarization effects

The degrees of first-and second-order coherence defined by eqns (3.42) and (3.97) are just the first two members of a hierarchy of coherence functions. It is possible to envisage a general interference experiment in which the measured result depends on the correlations of electric fields at an arbitrary number of space–time points. The result of any such measurement depends upon the hierarchy of coherence functions in some way. The degree of rth-order coherence can be defined as[11]

$$g^{(r)}(\mathbf{r}_1t_1,\ldots,\mathbf{r}_rt_r;\mathbf{r}_{r+1}t_{r+1},\ldots,\mathbf{r}_{2r}t_{2r})$$
$$=\frac{\langle E^*(\mathbf{r}_1t_1)\ldots E^*(\mathbf{r}_rt_r)E(\mathbf{r}_{r+1}t_{r+1})\ldots E(\mathbf{r}_{2r}t_{2r})\rangle}{(\langle|E(\mathbf{r}_1t_1)|^2\rangle\ldots\langle|E(\mathbf{r}_rt_r)|^2\rangle\langle|E(\mathbf{r}_{r+1}t_{r+1})|^2\rangle\ldots\langle|E(\mathbf{r}_{2r}t_{2r})|^2\rangle)^{\frac{1}{2}}}. \tag{3.112}$$

Clearly, eqns (3.42) and (3.97) are special cases of this general definition.

It is not intended to pursue the general rth-order coherence properties of light in any detail, since the first- and second-order coherence are usually of greatest experimental importance. However, it is worth noting two simple results. When the points $(\mathbf{r}_{r+1}t_{r+1}),\ldots,(\mathbf{r}_{2r}t_{2r})$ are the same as the points $(\mathbf{r}_rt_r),\ldots,(\mathbf{r}_1t_1)$, the correlation function in eqn (3.112) effectively contains the intensities at r different points. For the classical stable wave, the same arguments as are used for obtaining $g^{(2)}$ show that

$$g^{(r)}(\mathbf{r}_1t_1,\ldots,\mathbf{r}_rt_r;\mathbf{r}_rt_r,\ldots,\mathbf{r}_1t_1) = 1 \text{ for all } r. \tag{3.113}$$

By an obvious extension of the definition of second-order coherence in eqn (3.98), the classical stable wave can be said to be coherent in all orders.

There is no similarly simple result for a chaotic light beam, but the very special case where *all* the points in eqn (3.112) are the same space–time point $(\mathbf{r}_1t_1)$ can be quoted, since the correlation function is then the same as that evaluated in eqn (3.65), and

$$g^{(r)}(\mathbf{r}_1t_1,\ldots,\mathbf{r}_1t_1;\mathbf{r}_1t_1,\ldots,\mathbf{r}_1t_1) = r!. \tag{3.114}$$

Problem 3.7. Consider the rectangular pulse beam shown in Fig. 3.11. Prove that the rth-order coherence at a single space–time point $(\mathbf{r}_1t_1)$ is

$$g^{(r)}(\mathbf{r}_1t_1,\ldots,\mathbf{r}_1t_1;\mathbf{r}_1t_1,\ldots,\mathbf{r}_1t_1) = f^{-r+1}. \tag{3.115}$$

The result shows that $g^{(r)}$ can take any arbitrarily large value by choosing f sufficiently small, except for $r = 1$ where the degree of first-order coherence is unity, independent of f.

The entire chapter has been concerned with a beam of polarized light and the electric fields have been treated as scalar quantities. We conclude the discussion of intensity fluctuations of chaotic light with a brief consideration of the changes in some of the simpler results that occur when the beam is not plane polarized.[12]

Consider a beam of light propagated parallel to the z-axis that is made up of two independent beams, one of mean intensity $\bar{I}_x$ polarized parallel to the x-axis and one of mean intensity $\bar{I}_y$ polarized parallel to the y-axis. The total mean intensity is

$$\bar{I} = \bar{I}_x + \bar{I}_y \tag{3.116}$$

and the degree of polarization is defined to be

$$P = \frac{\bar{I}_x - \bar{I}_y}{\bar{I}_x + \bar{I}_y} \quad (\bar{I}_x \geqslant \bar{I}_y), \tag{3.117}$$

where the x-axis is chosen to be that with the larger mean intensity. Thus $P = 1$ corresponds to polarized light and $P = 0$ to unpolarized light, with intermediate values of P corresponding to partially polarized light.

For chaotic light, the two independent beams have cycle-averaged fluctuating intensities $\bar{I}_x(t)$ and $\bar{I}_y(t)$ that both obey the exponential probability distribution (3.68). The total intensity $\bar{I}(t)$, obtained by adding the two contributions, thus follows the probability distribution

$$p[\bar{I}(t)] = \int_0^{\bar{I}(t)} p_x[\bar{I}_x(t)]p_y[\bar{I}(t)-\bar{I}_x(t)]\,\mathrm{d}\bar{I}_x(t), \tag{3.118}$$

where

$$p_{x,y}[\bar{I}_{x,y}(t)] = (1/\bar{I}_{x,y})\exp(-\bar{I}_{x,y}(t)/\bar{I}_{x,y}). \tag{3.119}$$

The integration is readily carried out to give

$$p[\bar{I}(t)] = (1/P\bar{I})\{\exp[-2\bar{I}(t)/(1+P)\bar{I}]-\exp[-2\bar{I}(t)/(1-P)\bar{I}]\}. \tag{3.120}$$

Fig. 3.16 shows the form of the probability distribution for several degrees of polarization. The general expression (3.120) reduces to eqn (3.68) in the limit $P = 1$ of plane polarization. However, the probability is zero at $\bar{I}(t) = 0$ for all other degrees of polarization. The distributions corresponding to several values of P have been measured and the experimental results agree with the theoretical expressions.[13–15]

Problem 3.8. Derive the average value of the rth power of the cycle-averaged intensity for partially polarized chaotic light and show that it has the limiting values

$$\begin{aligned} \langle \bar{I}(t)^r \rangle &= r!\,\bar{I}^r && \text{for} \quad P = 1 \\ &= (r+1)!\,\bar{I}^r/2^r && \text{for} \quad P = 0. \end{aligned} \tag{3.121}$$

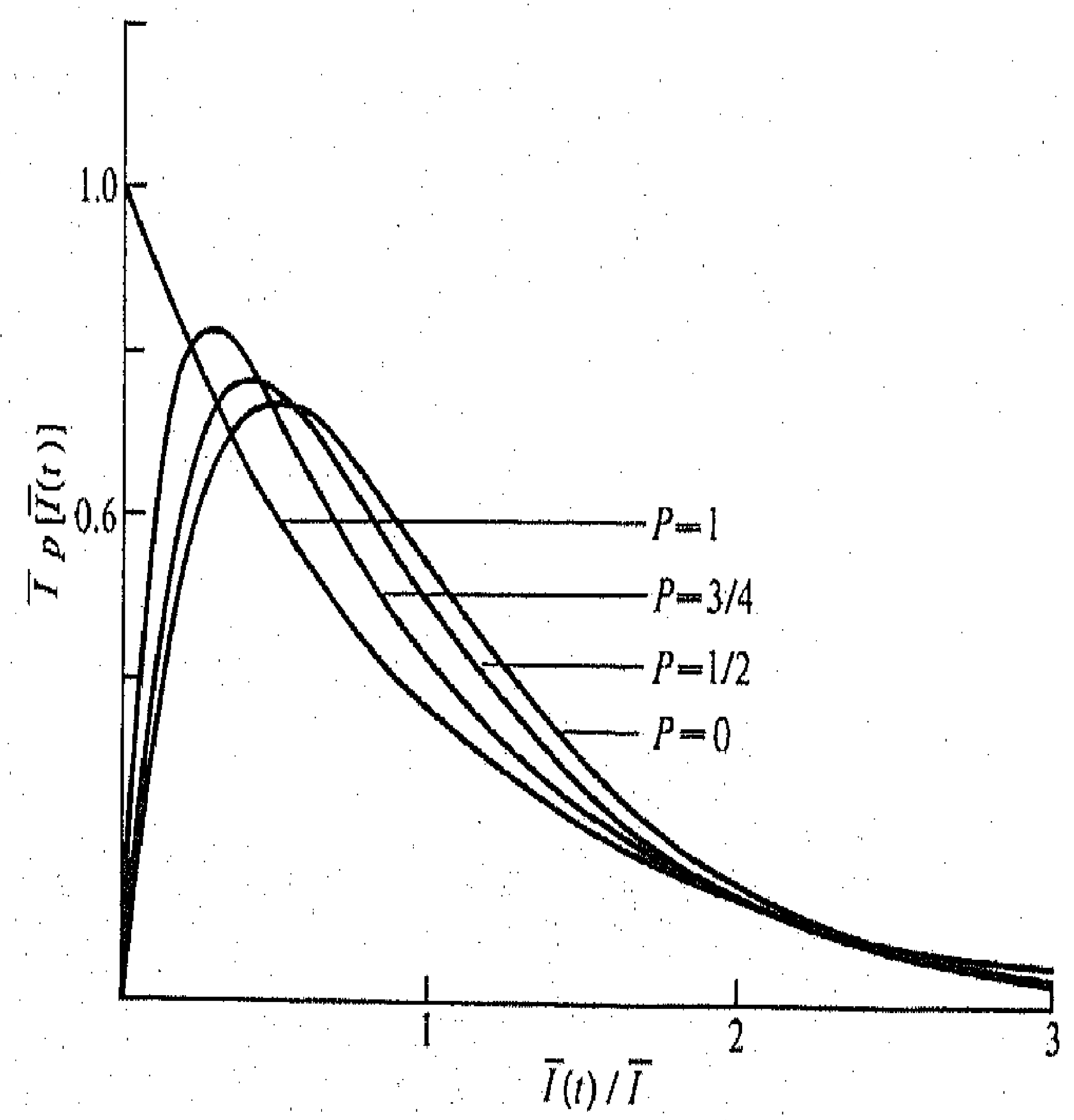

FIG. 3.16. Probability distributions for the cycle-averaged intensities of chaotic light with various degrees of polarization P. (After L. Mandel, ref. 12.)

Show that the zero time-delay degree of second-order coherence of the light is

$$g^{(2)}(0) = \tfrac{1}{2}(3+P^2). \tag{3.122}$$

This last result reduces to eqn (3.96) for polarized light but otherwise has a smaller value. Its form can be understood if it is rewritten as

$$g^{(2)}(0) = 1+\tfrac{1}{2}(1+P^2) = 1+(\bar{I}_x/\bar{I})^2+(\bar{I}_y/\bar{I})^2, \tag{3.123}$$

where eqns (3.116) and (3.117) have been used. Then with reference to Fig. 3.12, the unit term is the background contribution that occurs even in the absence of any fluctuations. The fluctuations cause the remaining terms, whose contribution is generally smaller than unity because there are no cross-correlations between the x- and y- polarized beams. With unpolarized light the fluctuation contribution to $g^{(2)}(0)$ is $\tfrac{1}{2}$; the theory of the Hanbury Brown and Twiss experiment given above remains valid if $\tfrac{1}{2}$ factors are substituted in appropriate places.

References

1. Simultaneous radiative and collision broadening is briefly considered by PARK, D. (1971). *Am. J. Phys.* **39,** 682.
2. See, for example, BORN, M. and WOLF, E. (1970). *Principles of optics*, p. 374. Pergamon, Oxford.
3. See p. 271 of ref. 2.
4. WAX, N. (Ed.) (1954). *Selected papers on noise and stochastic processes* Dover, New York.
5. CHANDRASEKHAR, S. (1943). *Rev. Mod. Phys.* **15,** 1. Reprinted in ref. 4.
6. PIKE, E. R. (1970). In *Quantum optics* (eds. S. M. Kay and A. Maitland), p. 127. Academic Press, New York.
7. HARDY, G. H., LITTLEWOOD, J. E., and PÓLYA, G. (1951). *Inequalities*. Cambridge University Press.
8. HANBURY BROWN, R. and TWISS, R. Q. (1956). *Nature* **177,** 27; (1957). *Proc. R. Soc.* **A242,** 300; (1958) *ibid.* **A243,** 291.
9. An interesting account of the original experiments and of their development for measurements of stellar diameters is given by HANBURY BROWN, R. (1974). *The intensity interferometer*. Taylor and Francis, London.
10. A most useful collection of original papers on all aspects of coherence theory is MANDEL, L. and WOLF, E. (Eds.) (1970). *Selected papers on coherence and fluctuations of light*, Vols. 1 and 2. Dover, New York.
11. GLAUBER, R. J. (1965). *Quantum optics and electronics* (eds. C. DeWitt, A. Blandin, and C. Cohen-Tannoudji), p. 63. Gordon and Breach, New York. (1970). *Quantum optics* (eds. S. M. Kay and A. Maitland), p. 53. Academic Press, New York.
12. MANDEL, L. (1963). *Proc. Phys. Soc.* **81,** 1104.
13. MARTIENSSEN, W. and SPILLER, E. (1966). *Phys. Rev. Lett.* **16,** 531.
14. WOLF, R. P. and CROOKER, P. P. (1982). *Am. J. Phys.* **50,** 406.
15. STEEGER, P. F. and FERCHER, A. F. (1982). *Optica Acta* **29,** 1395.

4. The quantized radiation field

THE calculations of the preceding chapters are based on a theory in which the radiation field strengths **E** and **B** are treated as classical variables, while the atoms are treated quantum-mechanically. Quantization conditions on the energy of the radiation field were used to derive Planck's law in Chapter 1, but the concept of photons has played a small role in the subsequent theory. This semiclassical theory provides the correct theoretical expressions for a wide range of quantities.

It is however generally accepted that quantum mechanics provides the best current picture of physical phenomena, and the most complete description of the radiation field must be sought in quantum-mechanical terms, where the field observables **E** and **B** are represented by operators. The present chapter is devoted to a description of the procedure by which quantum mechanics is applied to the electromagnetic field. We obtain expressions for the operators that represent the various field observables and we describe the various kinds of field state that can be envisaged in the quantum picture. It will be seen that quantization introduces characteristic quantum-mechanical effects into the properties of the radiation field. For example, it is not possible to have an electromagnetic wave whose amplitude and phase are both precisely defined; as is common in quantum mechanics, the accuracies of simultaneous measurements of pairs of observables are limited by uncertainty relations.

In view of the many successes of the semiclassical theory, it is of interest to consider the nature of the relation between the classical and quantum theories of the radiation field, and this is a recurrent topic in many of the subsequent chapters. Thus in Chapter 6 it is shown that, in terms of the coherence properties of light beams, there is a range of overlap between the two theories but the quantum field can have kinds of coherence not allowed by classical theory. Chaotic and coherent light have identical coherence properties in the two theories, but light with nonclassical coherence can also be generated, as described in Chapters 8 and 9.

The full quantum theory of the interaction between the radiation field and atoms is treated in Chapter 5. The assumptions of the phenomenological Einstein theory are justified and it is shown that the quantum theory produces the same transition rates for the absorption and emission processes as does the

semiclassical theory. The fully quantum-mechanical form of the optical Bloch equations is shown to be similar to their semiclassical form given in Chapter 2, at least in the case of a coherent driving light beam.

In other calculations, such as those of laser theory considered in Chapter 7 or nonlinear optics treated in Chapter 9, the semiclassical theory gives only partially correct solutions. We adopt the view in all subsequent calculations that quantum mechanics provides the best available predictions for measured quantities and that the results of semiclassical theory are reliable only when they reproduce the quantum results. It is nevertheless worthwhile to keep the semiclassical theory in mind since its methods are widely used and also because the similarities and differences between the classical and quantum fields sharpen one's appreciation of the quantum effects.

4.1. Potential theory for the classical electromagnetic field

The quantum theory of the radiation field has many similarities with the classical theory. The field vectors in quantum theory must be taken as operators instead of the algebraic quantities of classical theory, but both theories are based on Maxwell's equations. It is not, of course, possible to derive the quantum theory from the classical equations, but the transition to quantum mechanics can be accomplished most easily if the equations of classical electromagnetic theory are first put into a suitably suggestive form. As indicated in Chapter 1, the quantization is effected by the replacement of a classical harmonic-oscillator equation by the corresponding quantum-mechanical equation. The first task of the present chapter is to cast the classical equations in a form where the harmonic-oscillator dependence of the field variables is suitable for conversion to quantum mechanics.

Maxwell's equations for the electromagnetic fields in a nonmagnetic medium take the forms

$$\nabla\times\mathbf{E} = -\partial\mathbf{B}/\partial t, \tag{4.1}$$

$$\mu_0^{-1}\nabla\times\mathbf{B} = \epsilon_0(\partial\mathbf{E}/\partial t)+\mathbf{J}, \tag{4.2}$$

$$\epsilon_0\nabla.\mathbf{E} = \sigma, \tag{4.3}$$

$$\nabla.\mathbf{B} = 0, \tag{4.4}$$

where σ and $\mathbf{J}$ are the charge and current densities, respectively. The quantization procedure outlined in §4.5 is facilitated if the classical Maxwell equations are re-expressed in terms of the scalar and vector potentials, ϕ and $\mathbf{A}$ respectively. The fourth of these equations is satisfied identically if $\mathbf{B}$ is derived from a potential $\mathbf{A}$ according to

$$\mathbf{B} = \nabla\times\mathbf{A}. \tag{4.5}$$

Use of the identity

$$\nabla \times \nabla \phi \equiv 0, \tag{4.6}$$

where ϕ is a scalar function, then shows that the first Maxwell equation is satisfied identically if ϕ is defined by

$$\nabla \phi = -\mathbf{E} - (\partial \mathbf{A}/\partial t), \tag{4.7}$$

or equivalently

$$\mathbf{E} = -\nabla \phi - (\partial \mathbf{A}/\partial t). \tag{4.8}$$

If the potentials are known, eqns (4.5) and (4.8) enable **B** and **E** to be found.

The potentials can be determined, in principle, by equations that result from substitution of eqns (4.5) and (4.8) into the remaining Maxwell equations (4.2) and (4.3),

$$\nabla(\nabla . \mathbf{A}) - \nabla^2 \mathbf{A} + \frac{1}{c^2}\frac{\partial}{\partial t}\nabla\phi + \frac{1}{c^2}\frac{\partial^2 \mathbf{A}}{\partial t^2} = \mu_0 \mathbf{J} \tag{4.9}$$

and

$$-\epsilon_0 \nabla^2 \phi - \epsilon_0 \nabla . (\partial \mathbf{A}/\partial t) = \sigma, \tag{4.10}$$

where eqn (1.15) and the identity

$$\nabla \times \nabla \times \mathbf{A} \equiv \nabla(\nabla . \mathbf{A}) - \nabla^2 \mathbf{A} \tag{4.11}$$

have been used. These are the field equations; they determine the fields that result from a given distribution of charge σ and current **J**.

The field equations are quite complicated as they stand owing to the mixtures of terms involving **A** and ϕ that occur on their left-hand sides. It is possible to simplify the equations by the imposition of some additional condition on the potentials **A** and ϕ. It is important to realize that the definitions (4.5) and (4.7) of **A** and ϕ do not completely specify the forms of the potentials. The potentials can be varied, within certain limits, without any resulting change in the observable fields **E** and **B**. A transformation of **A** and ϕ that has this property is called a gauge transformation.

Suppose that $\mathbf{A}_0$ and ϕ_0 are solutions of the field equations for a given σ and **J**. The electric and magnetic fields **E** and **B** are determined by eqns (4.8) and (4.5). Consider a gauge transformation to a new pair of potentials **A** and ϕ defined by

$$\mathbf{A} = \mathbf{A}_0 - \nabla \Xi \tag{4.12}$$

and

$$\phi = \phi_0 + (\partial \Xi/\partial t), \tag{4.13}$$

where Ξ is an arbitrary function of the position **r** and the time t. It is evident from eqn (4.8) that **E** is unchanged by the gauge transformation; the corresponding invariance of **B** determined by eqn (4.5) is ensured by the identity (4.6), which also holds for Ξ.

A gauge for the electromagnetic field is specified by some condition on **A** and ϕ, which can be realized by a gauge transformation from an arbitrary pair of solutions of the field equations for the given σ and **J**. It should be emphasized that **E** and **B**, the physically measurable fields, do not depend in any way on the choice of gauge for **A** and ϕ. However, the freedom of choice provided by gauge invariance can often be used to obtain considerable simplifications in the calculations of **E** and **B**.

4.2. The Coulomb gauge

The electromagnetic field is said to be in the Coulomb gauge when the vector potential satisfies the condition

$$\nabla . \mathbf{A} = 0. \tag{4.14}$$

It will be seen later that the Coulomb gauge is convenient for quantization of the electromagnetic field. For a field specified originally by a pair of potentials $\mathbf{A}_0$ and ϕ_0, it is always possible to transform to the Coulomb gauge by a gauge transformation like eqns (4.12) and (4.13), where the function Ξ must be a solution of

$$\nabla^2 \Xi = \nabla . \mathbf{A}_0. \tag{4.15}$$

It should be noted that the potentials are still not completely specified even with the imposition of the Coulomb gauge condition (eqn (4.14)); further transformations are possible within the Coulomb gauge provided that Ξ satisfies

$$\nabla^2 \Xi = 0. \tag{4.16}$$

The choice of Coulomb gauge is made partly because of the resulting simplification in the field equations (4.9) and (4.10) which become

$$-\nabla^2 \mathbf{A} + \frac{1}{c^2}\frac{\partial^2 \mathbf{A}}{\partial t^2} + \frac{1}{c^2}\frac{\partial}{\partial t}\nabla\phi = \mu_0 \mathbf{J} \tag{4.17}$$

and

$$-\nabla^2 \phi = \sigma/\epsilon_0. \tag{4.18}$$

The scalar potential ϕ now satisfies Poisson's equation of electrostatics and the formal solution is[1,2]

$$\phi(\mathbf{r}) = \frac{1}{4\pi\epsilon_0}\int \frac{\sigma(\mathbf{r}')}{|\mathbf{r}-\mathbf{r}'|}\,\mathrm{d}^3 r', \tag{4.19}$$

where the spatial dependence of ϕ and σ is explicitly indicated. These quantities also depend in general on time, but t does not appear explicitly in Poisson's equation. The charge density to be used in the integral is that at the instant of time for which ϕ is required. The scalar potential in Coulomb gauge behaves as if it had an instantaneous knowledge of the charge density everywhere in space.

The field equation (4.17) that determines **A** is still complicated by a term in ϕ, but this can be removed by the following arguments. According to Helmholtz' theorem,[3] any vector field can be written as a sum of two components, one of which has zero divergence and the other of which has zero curl. For the case of the current density **J**, the sum can be written

$$\mathbf{J} = \mathbf{J}_T + \mathbf{J}_L, \tag{4.20}$$

where

$$\nabla . \mathbf{J}_T = 0 \tag{4.21}$$

$$\nabla \times \mathbf{J}_L = 0; \tag{4.22}$$

$\mathbf{J}_T$ is called the transverse or solenoidal component, while $\mathbf{J}_L$ is the longitudinal or irrotational component.

Consider first the equations satisfied by the longitudinal component. In view of eqn (4.21), the usual continuity equation obtained by elimination of the fields from eqns (4.2) and (4.3) can be written

$$\nabla . \mathbf{J}_L = -\partial\sigma/\partial t. \tag{4.23}$$

Because of the property (4.22), the vector field component $\mathbf{J}_L$ can be expressed in terms of a scalar potential ψ, say, and

$$\mathbf{J}_L = \nabla\psi. \tag{4.24}$$

Substitution in eqn (4.23) gives

$$\nabla^2\psi = -\partial\sigma/\partial t, \tag{4.25}$$

and comparison with eqn (4.18) shows that ψ and ϕ must be related by

$$\psi = \epsilon_0 \partial\phi/\partial t. \tag{4.26}$$

Hence from eqn (4.24)

$$\mathbf{J}_L = \epsilon_0 \nabla \partial\phi/\partial t. \tag{4.27}$$

This result can also be obtained more directly by taking the longitudinal part of eqn (4.17).

The field equation (4.17) can now be simplified, with the use of eqns (4.20) and (4.27), to become

$$-\nabla^2\mathbf{A} + \frac{1}{c^2}\frac{\partial^2\mathbf{A}}{\partial t^2} = \mu_0 \mathbf{J}_T. \tag{4.28}$$

The scalar potential has been eliminated, and it is shown in textbooks on electromagnetic theory[1,2] that the solution of eqn (4.28) is

$$\mathbf{A}(\mathbf{r}t) = \frac{\mu_0}{4\pi}\int \frac{\mathbf{J}_T(\mathbf{r}'t')}{|\mathbf{r}-\mathbf{r}'|}\,\mathrm{d}^3\mathbf{r}', \tag{4.29}$$

where

$$t' = t - |\mathbf{r}-\mathbf{r}'|/c. \tag{4.30}$$

The vector potential at position **r** and time t thus includes explicitly the effect of the finite velocity of light in delaying the arrival at **r** of the influence of the current at a distant point **r**′. An observer at **r** can have a knowledge of the current distribution at **r**′ only as it existed at the retarded time t' given by eqn (4.30).

The formal solutions to the problem of calculating the field generated by charge and current densities σ and **J** are provided by eqns (4.19) and (4.29) for ϕ and **A**. The particular form of these equations is a consequence of the assumed gauge condition (4.14), but the theory of gauge invariance outlined above shows that the derived fields **E** and **B** must be independent of the gauge.

One must beware of reading too much physical significance into the potentials ϕ and **A** themselves. For example, it appears from a superficial consideration of eqn (4.19) that a change in charge density at **r**′ leads to an immediate change in the scalar potential ϕ at **r**, contrary to the requirement of relativity theory that any information in the electromagnetic field can travel only with finite velocity c. It can be shown,[4] however, that the measurable fields **E** and **B** at **r** at time t are only affected by the charge and current densities at **r**′ as they existed at the retarded time t' given by eqn (4.30), and no violation of relativity principles occurs. The expression (4.19) for the scalar potential is allowed to be at variance with the known finiteness of the velocity of light because ϕ is not an observable quantity. Direct physical significance can be attached only to **E** and **B**.

The electric vector **E** can also be divided into transverse and longitudinal parts

$$\mathbf{E} = \mathbf{E}_T + \mathbf{E}_L, \tag{4.31}$$

where

$$\nabla . \mathbf{E}_T = \nabla \times \mathbf{E}_L = 0. \tag{4.32}$$

It is seen with the help of eqn (4.8) that the two parts of **E** can be explicitly expressed as

$$\mathbf{E}_T = -\partial\mathbf{A}/\partial t \tag{4.33}$$

and

$$\mathbf{E}_L = -\nabla\phi, \tag{4.34}$$

where the identity (4.6) and the Coulomb gauge condition (4.14) show that eqn (4.32) is satisfied by these components. The magnetic vector **B** is entirely transverse according to the Maxwell equation (4.4).

The great advantage of the Coulomb gauge, for the problem of the radiation field and its interaction with charges and currents, lies in the separation of the field equations and Maxwell's equations into two distinct parts. The longitudinal part is associated with the scalar potential ϕ as in eqn (4.34) and the relevant field equation is (4.18). Maxwell's equation (4.3) gives

$$\nabla.\mathbf{E}_\mathrm{L} = \sigma/\epsilon_0, \tag{4.35}$$

and the longitudinal current density obtained from eqns (4.27) and (4.34) is given by

$$\mathbf{J}_\mathrm{L} = -\epsilon_0\, \partial\mathbf{E}_\mathrm{L}/\partial t. \tag{4.36}$$

The longitudinal equations describe the fields arising from the charges, as determined by the equations of electrostatics.

The transverse part, on the other hand, is associated with the vector potential **A** as in eqn (4.33). The relevant field equation (4.28) has the form of a wave equation, and Maxwell's equations (4.1) to (4.4) give

$$\nabla\times\mathbf{E}_\mathrm{T} = -\partial\mathbf{B}/\partial t, \tag{4.37}$$

$$\mu_0^{-1}\nabla\times\mathbf{B} = \epsilon_0(\partial\mathbf{E}_\mathrm{T}/\partial t)+\mathbf{J}_\mathrm{T}, \tag{4.38}$$

$$\nabla.\mathbf{E}_\mathrm{T} = 0, \tag{4.39}$$

and

$$\nabla.\mathbf{B} = 0. \tag{4.40}$$

The transverse equations describe electromagnetic waves. In accordance with eqns (4.28) and (4.38), the electromagnetic waves are influenced only by the transverse part $\mathbf{J}_\mathrm{T}$ of the current density.

It should be stressed that the separation of the equations into a static part associated with the charge density and a dynamic part associated with the electromagnetic waves is a formal consequence of the Coulomb gauge condition. It is an example of the computational advantages that can be gained by the choice of an appropriate gauge.

4.3. The free classical field

For the remainder of the chapter we consider the electromagnetic waves in a region of space where

$$\mathbf{J}_\mathrm{T} = 0 \tag{4.41}$$

and, hence, from eqn (4.28)

$$-\nabla^2\mathbf{A}+\frac{1}{c^2}\frac{\partial^2\mathbf{A}}{\partial t^2} = 0. \tag{4.42}$$

The field in such a region of space is said to be free; the theory of the interaction of radiation with atoms requires solution of the more difficult problem where $\mathbf{J}_\mathrm{T}$ represents the transverse current due to the atomic electrons. The interaction of radiation with atoms is treated in Chapter 5.

The quantization of the electromagnetic field proceeds by the replacement of the classical vector potential **A** by a quantum-mechanical operator $\hat{\mathbf{A}}$. The final manipulation to be carried out on the classical field leads to a form of the classical equations in which the transition to quantum mechanics is straightforward.

Let us consider a cubic region of space of side L, similar to the cubic cavity illustrated in Fig. 1.1. However, we now regard the 'cavity' merely as a region of space, without any real boundaries. Instead of the standing-wave solutions for the field given in eqns (1.3) to (1.5), we take running waves and subject them to periodic boundary conditions. Also in contrast to the calculation of Chapter 1, we work with the vector potential instead of the electric field.

With these preliminaries, the vector potential in the cavity can be expanded in a Fourier series

$$\mathbf{A} = \sum_{\mathbf{k}}\{\mathbf{A}_\mathbf{k}(t)\exp(\mathrm{i}\mathbf{k}.\mathbf{r})+\mathbf{A}_\mathbf{k}^*(t)\exp(-\mathrm{i}\mathbf{k}.\mathbf{r})\}, \tag{4.43}$$

where the components of the wavevector **k** take the values

$$k_x = 2\pi\nu_x/L,\ k_y = 2\pi\nu_y/L,\ k_z = 2\pi\nu_z/L, \tag{4.44}$$

with

$$\nu_x,\ \nu_y,\ \nu_z = 0,\ \pm1,\ \pm2,\ \pm3,\ \ldots. \tag{4.45}$$

The density of modes defined in this way is the same as for the modes specified by eqns (1.3) to (1.5). The Coulomb gauge condition (4.14) is satisfied if

$$\mathbf{k}.\mathbf{A}_\mathbf{k}(t) = \mathbf{k}.\mathbf{A}_\mathbf{k}^*(t) = 0. \tag{4.46}$$

There are two independent directions of $\mathbf{A}_\mathbf{k}(t)$ for each **k**.

The different Fourier components of **A** are independent and must separately satisfy the field equation (4.42). Thus,

$$k^2\mathbf{A}_\mathbf{k}(t)+\frac{1}{c^2}\frac{\partial^2\mathbf{A}_\mathbf{k}(t)}{\partial t^2} = 0, \tag{4.47}$$

and $\mathbf{A}_\mathbf{k}^*(t)$ satisfies the same equation. The Fourier coefficients therefore satisfy the simple-harmonic equation

$$(\partial^2\mathbf{A}_\mathbf{k}(t)/\partial t^2)+\omega_\mathbf{k}^2\mathbf{A}_\mathbf{k}(t) = 0, \tag{4.48}$$

where

$$\omega_\mathbf{k} = ck. \tag{4.49}$$

The electromagnetic field is quantized by conversion of eqn (4.48) to a quantum-mechanical harmonic-oscillator equation. To see how the conversion should be made, it is helpful to express the classical oscillator in terms of an effective position and momentum associated with the cavity mode.

To this end, let us evaluate the classical energy of the cavity normal mode specified by wavevector **k**. The solution of eqn (4.48) can be taken as

$$\mathbf{A}_\mathbf{k}(t) = \mathbf{A}_\mathbf{k} \exp(-\mathrm{i}\omega_\mathbf{k}t), \tag{4.50}$$

and the complete vector potential (eqn (4.43)) becomes

$$\mathbf{A} = \sum_\mathbf{k} \{\mathbf{A}_\mathbf{k} \exp(-\mathrm{i}\omega_\mathbf{k}t + \mathrm{i}\mathbf{k}.\mathbf{r}) + \mathbf{A}_\mathbf{k}^* \exp(\mathrm{i}\omega_\mathbf{k}t - \mathrm{i}\mathbf{k}.\mathbf{r})\}. \tag{4.51}$$

The cycle-averaged energy content of a single mode **k** is

$$\bar{\mathscr{E}}_\mathbf{k} = \frac{1}{2} \int_{\text{cavity}} (\epsilon_0 \overline{\mathbf{E}_\mathbf{k}^2} + \mu_0^{-1} \overline{\mathbf{B}_\mathbf{k}^2}) \mathrm{d}V, \tag{4.52}$$

where the bars denote a cycle average, and $\mathbf{E}_\mathbf{k}$ and $\mathbf{B}_\mathbf{k}$ are the electric and magnetic fields associated with the mode. From eqns (4.5), (4.8), and (4.51)

$$\mathbf{E}_\mathbf{k} = \mathrm{i}\omega_\mathbf{k}\{\mathbf{A}_\mathbf{k} \exp(-\mathrm{i}\omega_\mathbf{k}t + \mathrm{i}\mathbf{k}.\mathbf{r}) - \mathbf{A}_\mathbf{k}^* \exp(\mathrm{i}\omega_\mathbf{k}t - \mathrm{i}\mathbf{k}.\mathbf{r})\}, \tag{4.53}$$

$$\mathbf{B}_\mathbf{k} = \mathrm{i}\mathbf{k} \times \{\mathbf{A}_\mathbf{k} \exp(-\mathrm{i}\omega_\mathbf{k}t + \mathrm{i}\mathbf{k}.\mathbf{r}) - \mathbf{A}_\mathbf{k}^* \exp(\mathrm{i}\omega_\mathbf{k}t - \mathrm{i}\mathbf{k}.\mathbf{r})\}. \tag{4.54}$$

It is evident from eqns (4.46) and (4.49) that the magnitudes of $\mathbf{E}_\mathbf{k}$ and $\mathbf{B}_\mathbf{k}$ are related by eqn (1.18) as expected for a free electromagnetic wave. Substitution into eqn (4.52) and evaluation of the time average gives

$$\bar{\mathscr{E}}_\mathbf{k} = 2\epsilon_0 V \omega_\mathbf{k}^2 \mathbf{A}_\mathbf{k}.\mathbf{A}_\mathbf{k}^*, \tag{4.55}$$

where $V = L^3$.

The mode variables $\mathbf{A}_\mathbf{k}$ and $\mathbf{A}_\mathbf{k}^*$ can be replaced by a generalized mode 'position' coordinate $Q_\mathbf{k}$ and a mode 'momentum' $P_\mathbf{k}$ in accordance with the transformations

$$\mathbf{A}_\mathbf{k} = (4\epsilon_0 V \omega_\mathbf{k}^2)^{-\frac{1}{2}} (\omega_\mathbf{k} Q_\mathbf{k} + \mathrm{i}P_\mathbf{k}) \boldsymbol{\varepsilon}_\mathbf{k}. \tag{4.56}$$

and

$$\mathbf{A}_\mathbf{k}^* = (4\epsilon_0 V \omega_\mathbf{k}^2)^{-\frac{1}{2}} (\omega_\mathbf{k} Q_\mathbf{k} - \mathrm{i}P_\mathbf{k}) \boldsymbol{\varepsilon}_\mathbf{k}. \tag{4.57}$$

The coordinates $Q_\mathbf{k}$ and $P_\mathbf{k}$ are scalar quantities, the directional properties of $\mathbf{A}_\mathbf{k}$ and $\mathbf{A}_\mathbf{k}^*$ having been separated by the introduction of a unit polarization vector $\boldsymbol{\varepsilon}_\mathbf{k}$ for the mode.

The single-mode energy (eqn (4.55)) is transformed by eqns (4.56) and (4.57) into

$$\bar{\mathscr{E}}_\mathbf{k} = \tfrac{1}{2}(P_\mathbf{k}^2 + \omega_\mathbf{k}^2 Q_\mathbf{k}^2). \tag{4.58}$$

This is precisely the usual form of the energy of a classical harmonic oscillator. The problem of the vector potential associated with a cavity mode has thus been made formally equivalent to a classical harmonic-oscillator problem. The complete classical Hamiltonian for the cavity is formed by taking a sum over **k**, and the two independent directions of $\boldsymbol{\varepsilon}_\mathbf{k}$, of the single-mode expression (4.58).

4.4. The quantum-mechanical harmonic oscillator

The electromagnetic field is now quantized by conversion of $Q_\mathbf{k}$ and $P_\mathbf{k}$ into quantum-mechanical position and momentum operators $\hat{q}_\mathbf{k}$ and $\hat{p}_\mathbf{k}$. As a preliminary to this conversion, it is convenient to develop the theory of the quantum-mechanical harmonic oscillator in the form most suitable for the field quantization.

The quantum-mechanical Hamiltonian for a one-dimensional harmonic oscillator of unit mass is

$$\hat{\mathscr{H}} = \tfrac{1}{2}(\hat{p}^2 + \omega^2\hat{q}^2), \tag{4.59}$$

where $\hat{p}$ and $\hat{q}$ obey the usual commutation relation

$$[\hat{q}, \hat{p}] = \mathrm{i}\hbar. \tag{4.60}$$

Define a pair of operators $\hat{a}$ and $\hat{a}^\dagger$ to replace $\hat{q}$ and $\hat{p}$,

$$\hat{a} = (2\hbar\omega)^{-\frac{1}{2}}(\omega\hat{q} + \mathrm{i}\hat{p}) \tag{4.61}$$

and

$$\hat{a}^\dagger = (2\hbar\omega)^{-\frac{1}{2}}(\omega\hat{q} - \mathrm{i}\hat{p}) \tag{4.62}$$

or, conversely

$$\hat{q} = (\hbar/2\omega)^{\frac{1}{2}}(\hat{a} + \hat{a}^\dagger) \tag{4.63}$$

$$\hat{p} = -\mathrm{i}(\hbar\omega/2)^{\frac{1}{2}}(\hat{a} - \hat{a}^\dagger). \tag{4.64}$$

The operators $\hat{a}$ and $\hat{a}^\dagger$ are called, respectively, the destruction and creation operators for the harmonic oscillator. As will become clear, they are extremely useful, on account of their simple properties. They do not, however, represent observables of the harmonic oscillator, as is shown below.

From eqns (4.61) and (4.62) we have

$$\begin{aligned} \hat{a}^\dagger\hat{a} &= (2\hbar\omega)^{-1}(\hat{p}^2 + \omega^2\hat{q}^2 + \mathrm{i}\omega\hat{q}\hat{p} - \mathrm{i}\omega\hat{p}\hat{q}) \\ &= (\hbar\omega)^{-1}(\hat{\mathscr{H}} - \tfrac{1}{2}\hbar\omega), \end{aligned} \tag{4.65}$$

where eqns (4.59) and (4.60) have been used. Similarly

$$\hat{a}\hat{a}^\dagger = (\hbar\omega)^{-1}(\hat{\mathscr{H}} + \tfrac{1}{2}\hbar\omega). \tag{4.66}$$

The commutator of the new operators is easily found from these results,

$$[\hat{a}, \hat{a}^\dagger] = \hat{a}\hat{a}^\dagger - \hat{a}^\dagger\hat{a} = 1. \tag{4.67}$$

From eqn (4.65), the Hamiltonian can be written

$$\hat{\mathscr{H}} = \hbar\omega(\hat{a}^\dagger\hat{a} + \tfrac{1}{2}). \tag{4.68}$$

The combination of operators $\hat{a}^\dagger\hat{a}$ occurs frequently; it is called the number operator of the oscillator, and we denote it

$$\hat{n} = \hat{a}^\dagger\hat{a}. \tag{4.69}$$

In the derivation of Planck's law in Chapter 1, we have already used the well-known result (eqn (1.20)) that the eigenvalues of $\hat{n}$ are zero and the positive integers. This result will now be rigorously derived as part of an investigation of the properties of the operators $\hat{a}$ and $\hat{a}^\dagger$.

Let $|n\rangle$ be an energy eigenstate of the harmonic oscillator with eigenvalue E_n. The eigenvalue equation is

$$\hat{\mathscr{H}}|n\rangle = \hbar\omega(\hat{a}^\dagger\hat{a}+\tfrac{1}{2})|n\rangle = E_n|n\rangle. \tag{4.70}$$

Multiply both sides from the left by $\hat{a}^\dagger$,

$$\hbar\omega(\hat{a}^\dagger\hat{a}^\dagger\hat{a}+\tfrac{1}{2}\hat{a}^\dagger)|n\rangle = E_n\hat{a}^\dagger|n\rangle. \tag{4.71}$$

Use of the commutator given by eqn (4.67) on the first term on the left yields

$$\hbar\omega(\hat{a}^\dagger\hat{a}\hat{a}^\dagger-\hat{a}^\dagger+\tfrac{1}{2}\hat{a}^\dagger)|n\rangle = E_n\hat{a}^\dagger|n\rangle, \tag{4.72}$$

which can be rearranged to give

$$\hbar\omega(\hat{a}^\dagger\hat{a}+\tfrac{1}{2})\hat{a}^\dagger|n\rangle = \hat{\mathscr{H}}\hat{a}^\dagger|n\rangle = (E_n+\hbar\omega)\hat{a}^\dagger|n\rangle. \tag{4.73}$$

This last equation again has the form of an energy eigenvalue equation. It shows that the state $\hat{a}^\dagger|n\rangle$ is an eigenstate of the harmonic oscillator with eigenvalue $E_n+\hbar\omega$. We define the new eigenstate and eigenvalue as

$$|n+1\rangle = \hat{a}^\dagger|n\rangle \tag{4.74}$$

and

$$E_{n+1} = E_n+\hbar\omega, \tag{4.75}$$

and equation (4.73) can then be written

$$\hat{\mathscr{H}}|n+1\rangle = E_{n+1}|n+1\rangle. \tag{4.76}$$

These results show that, given a harmonic-oscillator energy level E_n, there exists another level $\hbar\omega$ above the first. The energy levels thus form an equally-spaced ladder. As in classical mechanics there is no maximum energy restriction for the harmonic oscillator, and the ladder of levels extends upwards to infinity. The situation is illustrated in Fig. 4.1.

The lower end of the ladder can be investigated by multiplication of the energy eigenvalue equation (4.70) from the left by $\hat{a}$. Manipulations similar to those that led from eqn (4.71) to eqn (4.73) give

$$\hat{\mathscr{H}}\hat{a}|n\rangle = (E_n-\hbar\omega)\hat{a}|n\rangle. \tag{4.77}$$

The state $\hat{a}|n\rangle$ is thus an energy eigenstate with eigenvalue $E_n-\hbar\omega$. We define

$$|n-1\rangle = \hat{a}|n\rangle \tag{4.78}$$

and

$$E_{n-1} = E_n-\hbar\omega, \tag{4.79}$$

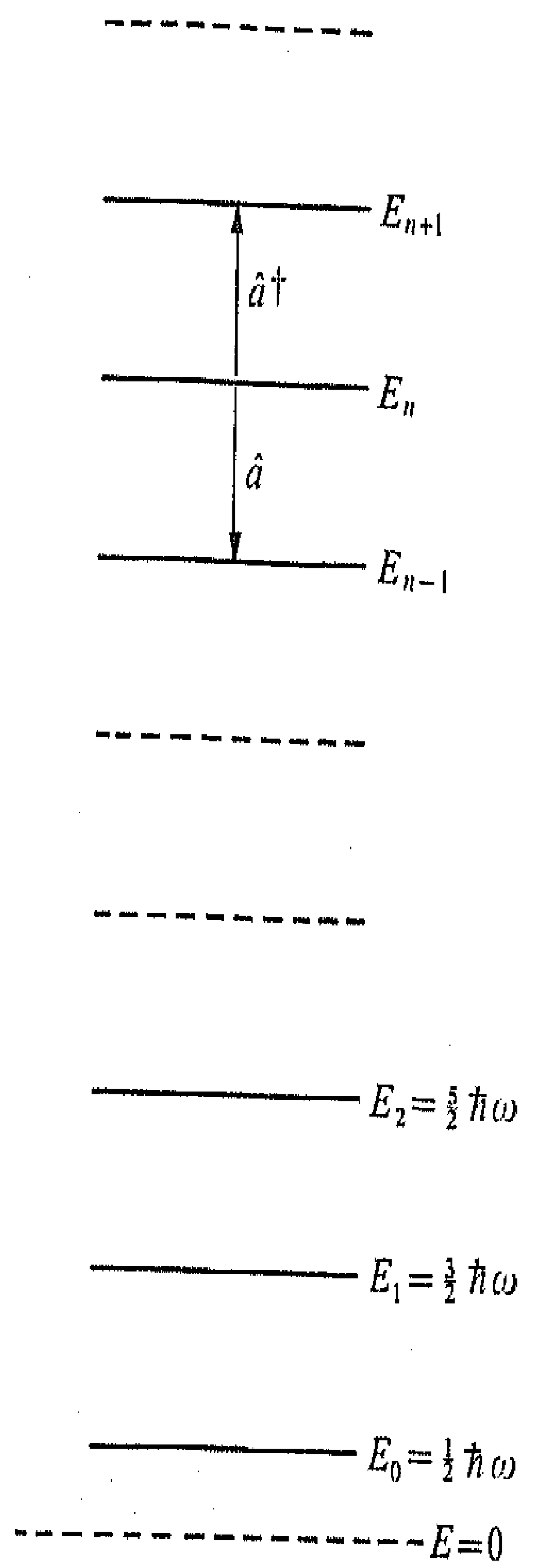

E_{n+1}
$\hat{a}^\dagger$
E_n
$\hat{a}$
E_{n-1}
$E_2=\frac{5}{2}\hbar\omega$
$E_1=\frac{3}{2}\hbar\omega$
$E_0=\frac{1}{2}\hbar\omega$
$E=0$

FIG. 4.1. Energy-level diagram for the quantum-mechanical harmonic oscillator, showing the roles of the creation operator $\hat{a}^\dagger$ and the destruction operator $\hat{a}$ in respectively adding and subtracting a quantum $\hbar\omega$ to or from the energy.

so that eqn (4.77) becomes

$$\hat{\mathscr{H}}|n-1\rangle = E_{n-1}|n-1\rangle. \tag{4.80}$$

The ladder of energy levels thus extends downwards with equal steps $\hbar\omega$. However, the ladder must have a lower end because the oscillator kinetic and potential energies are positive quantities, and the eigenvalues are not allowed to be negative. Let $|0\rangle$ be the ground state with energy E_0. Eqn (4.77) gives, for the ground state,

$$\hat{\mathscr{H}}\hat{a}|0\rangle = (E_0-\hbar\omega)\hat{a}|0\rangle. \tag{4.81}$$

Since by hypothesis there is no eigenstate of lower energy than the ground state, the only solution of eqn (4.81) consistent with this physical interpretation is

$$\hat{a}|0\rangle = 0. \tag{4.82}$$

This ground-state condition can be used to determine E_0, since the eigenvalue equation (4.70) for the ground state becomes

$$\hat{\mathscr{H}}|0\rangle = \tfrac{1}{2}\hbar\omega|0\rangle = E_0|0\rangle. \tag{4.83}$$

Thus,

$$E_0 = \tfrac{1}{2}\hbar\omega, \tag{4.84}$$

and it follows from eqn (4.75) that

$$E_n = (n+\tfrac{1}{2})\hbar\omega, \qquad n = 0, 1, 2, \ldots, \tag{4.85}$$

the usual result for the harmonic oscillator.

Fig. 4.1 shows the energy-level scheme and indicates the roles of $\hat{a}$ and $\hat{a}^\dagger$ in, respectively, destroying or creating a quantum $\hbar\omega$ in the oscillator's excitation energy, and thus producing a step down or up the ladder. The states $|n\rangle$ are simultaneous eigenstates of $\hat{\mathscr{H}}$ and $\hat{n}$,

$$\hat{n}|n\rangle = \hat{a}^\dagger\hat{a}|n\rangle = n|n\rangle. \tag{4.86}$$

The eigenvalue of $\hat{n}$ indicates the number of quanta $\hbar\omega$ excited above the oscillator ground state.

The above derivation has not paid any attention to normalization of the eigenstates $|n\rangle$. Additional factors appear in the equations that relate different eigenstates if the states are normalized. The normalization conditions are

$$\langle n-1|n-1\rangle = \langle n|n\rangle = \langle n+1|n+1\rangle = 1. \tag{4.87}$$

Consider the effect of these conditions on eqn (4.78). For $|n\rangle$ and $|n-1\rangle$ to be normalized it is necessary to insert a numerical factor $\mathscr{C}_n$ in eqn (4.78), which becomes

$$\mathscr{C}_n|n-1\rangle = \hat{a}|n\rangle. \tag{4.88}$$

Multiply both sides from the left by their Hermitian conjugates,

$$\langle n-1|\mathscr{C}_n^*\mathscr{C}_n|n-1\rangle = \langle n|\hat{a}^\dagger\hat{a}|n\rangle, \tag{4.89}$$

or with the help of eqns (4.86) and (4.87),

$$|\mathscr{C}_n|^2 = n. \tag{4.90}$$

We take the phase of the normalization constant to be zero, as usual, and eqn (4.88) becomes

$$\hat{a}|n\rangle = n^{\frac{1}{2}}|n-1\rangle. \tag{4.91}$$

A similar analysis for eqn (4.74) produces the result

$$\hat{a}^\dagger|n\rangle = (n+1)^{\frac{1}{2}}|n+1\rangle. \tag{4.92}$$

We shall always use eqns (4.91) and (4.92) in preference to eqns (4.74) and (4.78) since we wish to work with the normalized eigenstates. Note that the ground-state condition (4.82) is included in the general result (4.91) as a special case.

Different energy eigenstates of the harmonic oscillator are, of course, orthogonal and it follows from eqns (4.91) and (4.92) that the only non-vanishing matrix elements of $\hat{a}$ and $\hat{a}^\dagger$ are those of the types

$$\langle n-1|\hat{a}|n\rangle = n^{\frac{1}{2}} \tag{4.93}$$

$$\langle n+1|\hat{a}^\dagger|n\rangle = (n+1)^{\frac{1}{2}}. \tag{4.94}$$

Every Hermitian operator $\hat{O}$ has matrix elements that satisfy the condition[5]

$$\langle i|\hat{O}|j\rangle = \langle j|\hat{O}|i\rangle^*. \tag{4.95}$$

It is clear that $\hat{a}$ and $\hat{a}^\dagger$ are not Hermitian operators, and according to the general principles of quantum mechanics[5] they cannot represent observable quantities. Their property of destroying or creating a quantum of energy, when applied to an energy eigenstate of the oscillator, is, however, easily appreciated in a physical sense. The simple matrix-element properties (eqns (4.93) and (4.94)) of the destruction and creation operators make them more convenient to manipulate than the position and momentum, to which they are related by eqns (4.63) and (4.64).

Problem 4.1. Prove that the nth excited state of the oscillator can be expressed in terms of the ground state according to

$$|n\rangle = (n!)^{-\frac{1}{2}}(\hat{a}^\dagger)^n|0\rangle. \tag{4.96}$$

Problem 4.2. Prove by expressing $\hat{q}$ and $\hat{p}$ in terms of $\hat{a}$ and $\hat{a}^\dagger$ that

$$\langle n|\hat{q}^2|n\rangle = (\hbar/\omega)(n+\tfrac{1}{2}), \tag{4.97}$$

and

$$\langle n|\hat{p}^2|n\rangle = \hbar\omega(n+\tfrac{1}{2}). \tag{4.98}$$

Problem 4.3. Prove that

$$(n+3)(n+2)\langle n|(\hat{a}^\dagger)^3\hat{a}^4\hat{a}^\dagger|n\rangle = (n-1)(n-2)\langle n|\hat{a}^3(\hat{a}^\dagger)^4\hat{a}|n\rangle. \tag{4.99}$$

Problem 4.4. Prove the commutators

$$\begin{aligned} [\hat{a}, (\hat{a}^\dagger)^2] &= 2\hat{a}^\dagger, \\ [\hat{a}^2, \hat{a}^\dagger] &= 2\hat{a}, \end{aligned} \tag{4.100}$$

and, in general, where n is a positive integer,

$$\begin{aligned} [\hat{a}, (\hat{a}^\dagger)^n] &= n(\hat{a}^\dagger)^{n-1} \\ \text{and} \qquad & \\ [\hat{a}^n, \hat{a}^\dagger] &= n\hat{a}^{n-1}. \end{aligned} \tag{4.101}$$

Hence show that

$$[\hat{a}, \exp(\beta\hat{a}^\dagger)] = \beta\exp(\beta\hat{a}^\dagger). \tag{4.102}$$

4.5. Quantization of the field

The electromagnetic field is now quantized by the association of a quantum-mechanical harmonic oscillator with each mode **k** of the radiation field. The mode to which a quantum-mechanical operator refers is indicated by a subscript; thus $\hat{a}_{\mathbf{k}}^{\dagger}$ and $\hat{a}_{\mathbf{k}}$ are the operators that create and destroy a quantum of energy $\hbar\omega_{\mathbf{k}}$ in the cavity electromagnetic-field mode of wavevector **k**. These quanta are the photons of wavevector **k**; the number of photons **k** excited in the cavity is determined by the eigenvalue $n_{\mathbf{k}}$ of the appropriate number operator $\hat{n}_{\mathbf{k}} = \hat{a}_{\mathbf{k}}^{\dagger}\hat{a}_{\mathbf{k}}$, and has possible values 0, 1, 2, ... The excitation level of a cavity mode **k** is determined by its eigenstate $|n_{\mathbf{k}}\rangle$. The creation and destruction operators for mode **k** applied to $|n_{\mathbf{k}}\rangle$ obey the rules (4.91) and (4.92) derived above,

$$\hat{a}_{\mathbf{k}}|n_{\mathbf{k}}\rangle = n_{\mathbf{k}}^{\frac{1}{2}}|n_{\mathbf{k}}-1\rangle \tag{4.103}$$

and

$$\hat{a}_{\mathbf{k}}^{\dagger}|n_{\mathbf{k}}\rangle = (n_{\mathbf{k}}+1)^{\frac{1}{2}}|n_{\mathbf{k}}+1\rangle. \tag{4.104}$$

The states of the total radiation field in the cavity can be specified by the numbers of photons $n_{\mathbf{k}_1}, n_{\mathbf{k}_2}, n_{\mathbf{k}_3}, \ldots$ excited in the complete set of cavity modes $\mathbf{k}_1, \mathbf{k}_2, \mathbf{k}_3, \ldots$. In counting the normal modes, it must be remembered that for each wavevector **k** there are two independent directions of the mode polarization $\boldsymbol{\varepsilon}_{\mathbf{k}}$ (see the following section). It is usually convenient, however, not to display the mode polarization explicitly, since this would complicate much of the notation. We thus let the single symbol **k** stand for both the wavevector and polarization of a mode. With this convention, the phrase 'a particular normal mode **k**' implies that both the wavevector and polarization of the mode are specified.

A state of the total field can be written $|n_{\mathbf{k}_1}, n_{\mathbf{k}_2}, n_{\mathbf{k}_3}, \ldots\rangle$, and is specified by a string of numbers, with the convention that the cavity modes are arranged in some particular order as, for example, in Fig. 1.4. Since the different cavity modes are independent, the state of the total field can be written as a product of the states of the individual modes.

$$|n_{\mathbf{k}_1}, n_{\mathbf{k}_2}, n_{\mathbf{k}_3}, \ldots\rangle = |n_{\mathbf{k}_1}\rangle|n_{\mathbf{k}_2}\rangle|n_{\mathbf{k}_3}\rangle \ldots. \tag{4.105}$$

The states of the individual cavity modes will always be assumed normalized, and it follows that the total state (eqn (4.105)) of the field is also normalized. An operator that refers to a particular normal mode $\mathbf{k}_i$ affects only the photons in that particular mode, for example,

$$\hat{a}_{\mathbf{k}_i}^{\dagger}|n_{\mathbf{k}_1}, n_{\mathbf{k}_2}, n_{\mathbf{k}_3}, \ldots, n_{\mathbf{k}_i}, \ldots\rangle = (n_{\mathbf{k}_i}+1)^{\frac{1}{2}}|n_{\mathbf{k}_1}, n_{\mathbf{k}_2}, n_{\mathbf{k}_3}, \ldots, n_{\mathbf{k}_i}+1, \ldots\rangle, \tag{4.106}$$

which is merely an application of the rule (4.104) to the product state of eqn (4.105).

The notation (4.105) is rather cumbersome, and we shall sometimes denote the states of the total field by the short-hand

$$|\{n_{\mathbf{k}}\}\rangle = |n_{\mathbf{k}_1}\rangle|n_{\mathbf{k}_2}\rangle|n_{\mathbf{k}_3}\rangle \ldots. \tag{4.107}$$

The symbols $\{n_{\mathbf{k}}\}$ here denote the complete set of numbers that specify the excitation levels of all the harmonic oscillators associated with the cavity modes. There is always, of course, an infinite numbers of oscillators. The $|\{n_{\mathbf{k}}\}\rangle$ form a complete set of states for the electromagnetic field in the cavity when every member $n_{\mathbf{k}_i}$ of the set $\{n_{\mathbf{k}}\}$ is allowed to take on the values zero and all the positive integers.

So much for the basic states of the radiation field. The classical vector potentials $\mathbf{A}_{\mathbf{k}}$ and $\mathbf{A}_{\mathbf{k}}^{*}$ for cavity mode **k** expressed in terms of $P_{\mathbf{k}}$ and $Q_{\mathbf{k}}$ by eqns (4.56) and (4.57) are now converted into quantum-mechanical operators expressed in terms of $\hat{p}_{\mathbf{k}}$ and $\hat{q}_{\mathbf{k}}$ by means of the straightforward substitutions

$$\begin{aligned}\mathbf{A}_{\mathbf{k}} &= (4\epsilon_0 V\omega_{\mathbf{k}}^2)^{-\frac{1}{2}}(\omega_{\mathbf{k}}Q_{\mathbf{k}}+\mathrm{i}P_{\mathbf{k}})\boldsymbol{\varepsilon}_{\mathbf{k}} \rightarrow \\ &\qquad (4\epsilon_0 V\omega_{\mathbf{k}}^2)^{-\frac{1}{2}}(\omega_{\mathbf{k}}\hat{q}_{\mathbf{k}}+\mathrm{i}\hat{p}_{\mathbf{k}})\boldsymbol{\varepsilon}_{\mathbf{k}} = (\hbar/2\epsilon_0 V\omega_{\mathbf{k}})^{\frac{1}{2}}\hat{a}_{\mathbf{k}}\boldsymbol{\varepsilon}_{\mathbf{k}}, \qquad (4.108)\\ \mathbf{A}_{\mathbf{k}}^{*} &= (4\epsilon_0 V\omega_{\mathbf{k}}^2)^{-\frac{1}{2}}(\omega_{\mathbf{k}}Q_{\mathbf{k}}-\mathrm{i}P_{\mathbf{k}})\boldsymbol{\varepsilon}_{\mathbf{k}} \rightarrow \\ &\qquad (4\epsilon_0 V\omega_{\mathbf{k}}^2)^{-\frac{1}{2}}(\omega_{\mathbf{k}}\hat{q}_{\mathbf{k}}-\mathrm{i}\hat{p}_{\mathbf{k}})\boldsymbol{\varepsilon}_{\mathbf{k}} = (\hbar/2\epsilon_0 V\omega_{\mathbf{k}})^{\frac{1}{2}}\hat{a}_{\mathbf{k}}^{\dagger}\boldsymbol{\varepsilon}_{\mathbf{k}}. \qquad (4.109)\end{aligned}$$

The relations (4.61) and (4.62) have been used in the last steps of these equations.

The transition from classical to quantum mechanics thus consists of the replacement of the classical Fourier coefficients $\mathbf{A}_{\mathbf{k}}$ and $\mathbf{A}_{\mathbf{k}}^{*}$ by the destruction operator $\hat{a}_{\mathbf{k}}$ and the creation operator $\hat{a}_{\mathbf{k}}^{\dagger}$, multiplied by a numerical factor and a unit vector. The quantum-mechanical expression for the total vector potential is obtained by substitution of eqns (4.108) and (4.109) into eqn (4.51),

$$\hat{\mathbf{A}} = \sum_{\mathbf{k}}(\hbar/2\epsilon_0 V\omega_{\mathbf{k}})^{\frac{1}{2}}\boldsymbol{\varepsilon}_{\mathbf{k}}\{\hat{a}_{\mathbf{k}}\exp(-\mathrm{i}\omega_{\mathbf{k}}t+\mathrm{i}\mathbf{k}.\mathbf{r})+\hat{a}_{\mathbf{k}}^{\dagger}\exp(\mathrm{i}\omega_{\mathbf{k}}t-\mathrm{i}\mathbf{k}.\mathbf{r})\}. \tag{4.110}$$

Note that the vector potential is now an operator, and it must be manipulated in accordance with the operator properties of the $\hat{a}_{\mathbf{k}}$ and $\hat{a}_{\mathbf{k}}^{\dagger}$.

The corresponding results for the electric and magnetic field operators $\hat{\mathbf{E}}_{\mathbf{k}}$ and $\hat{\mathbf{B}}_{\mathbf{k}}$ associated with mode **k** are obtained by making similar substitutions in eqns (4.53) and (4.54),

$$\hat{\mathbf{E}}_{\mathbf{k}} = \mathrm{i}(\hbar\omega_{\mathbf{k}}/2\epsilon_0 V)^{\frac{1}{2}}\boldsymbol{\varepsilon}_{\mathbf{k}}\{\hat{a}_{\mathbf{k}}\exp(-\mathrm{i}\omega_{\mathbf{k}}t+\mathrm{i}\mathbf{k}.\mathbf{r})-\hat{a}_{\mathbf{k}}^{\dagger}\exp(\mathrm{i}\omega_{\mathbf{k}}t-\mathrm{i}\mathbf{k}.\mathbf{r})\}, \tag{4.111}$$

$$\hat{\mathbf{B}}_{\mathbf{k}} = \mathrm{i}(\hbar/2\epsilon_0 V\omega_{\mathbf{k}})^{\frac{1}{2}}\mathbf{k}\times\boldsymbol{\varepsilon}_{\mathbf{k}}\{(\hat{a}_{\mathbf{k}}\exp(-\mathrm{i}\omega_{\mathbf{k}}t+\mathrm{i}\mathbf{k}.\mathbf{r})-\hat{a}_{\mathbf{k}}^{\dagger}\exp(\mathrm{i}\omega_{\mathbf{k}}t-\mathrm{i}\mathbf{k}.\mathbf{r})\}. \tag{4.112}$$

The operators for the total transverse electric and magnetic fields are then

$$\hat{\mathbf{E}}_{\mathrm{T}} = \sum_{\mathbf{k}} \hat{\mathbf{E}}_{\mathbf{k}}, \tag{4.113}$$

$$\hat{\mathbf{B}} = \sum_{\mathbf{k}} \hat{\mathbf{B}}_{\mathbf{k}}. \tag{4.114}$$

As a first calculation that uses the field operators $\hat{\mathbf{E}}_{\mathbf{k}}$ and $\hat{\mathbf{B}}_{\mathbf{k}}$, we consider the electromagnetic energy content of mode **k** for the state where $n_{\mathbf{k}}$ photons are excited. The classical formula (4.52) for the field energy becomes

$$\bar{\mathscr{E}}_{\mathbf{k}} = \frac{1}{2}\int_{\text{cavity}} \overline{\langle n_{\mathbf{k}}|\epsilon_0 \hat{\mathbf{E}}_{\mathbf{k}}.\hat{\mathbf{E}}_{\mathbf{k}} + \mu_0^{-1}\hat{\mathbf{B}}_{\mathbf{k}}.\hat{\mathbf{B}}_{\mathbf{k}}|n_{\mathbf{k}}\rangle}\,\mathrm{d}V, \tag{4.115}$$

where the bar again denotes a cycle average, to be taken after evaluation of the matrix element.

Problem 4.5. Prove that

$$\epsilon_0\langle n_{\mathbf{k}}|\hat{\mathbf{E}}_{\mathbf{k}}.\hat{\mathbf{E}}_{\mathbf{k}}|n_{\mathbf{k}}\rangle = \mu_0^{-1}\langle n_{\mathbf{k}}|\hat{\mathbf{B}}_{\mathbf{k}}.\hat{\mathbf{B}}_{\mathbf{k}}|n_{\mathbf{k}}\rangle = (\hbar\omega_{\mathbf{k}}/V)(n_{\mathbf{k}}+\tfrac{1}{2}), \tag{4.116}$$

and hence that the mode energy is

$$\bar{\mathscr{E}}_{\mathbf{k}} = (n_{\mathbf{k}}+\tfrac{1}{2})\hbar\omega_{\mathbf{k}}. \tag{4.117}$$

Note that no cycle-averaging is in fact necessary since the matrix element is time-independent.

The result for the mode energy is, of course, the usual harmonic oscillator expression, as assumed in the derivation of Planck's law in Chapter 1. However, the energy expression is now a consequence of the quantization of the electromagnetic field at the more fundamental level embodied in the eqn (4.110) for the vector potential operator $\hat{\mathbf{A}}$. It should be noted that the quantization procedure is such as to guarantee the energy expression to be of the form shown in eqn (4.117); in other words, the choice of numerical factors in the transition to quantum-mechanical operators is governed by the requirement that the mode energy should have the harmonic-oscillator form, both in the classical and quantum-mechanical theories.

The Hamiltonian for the total electromagnetic field in the cavity consists of a sum of terms like eqn (4.68), which we denote by

$$\mathscr{H}_{\mathrm{R}} = \sum_{\mathbf{k}} \hbar\omega_{\mathbf{k}}(\hat{a}_{\mathbf{k}}^{\dagger}\hat{a}_{\mathbf{k}}+\tfrac{1}{2}). \tag{4.118}$$

The total energy of the radiation for cavity state $|\{n_{\mathbf{k}}\}\rangle$ is then

$$\bar{\mathscr{E}} = \sum_{\mathbf{k}} \bar{\mathscr{E}}_{\mathbf{k}} = \sum_{\mathbf{k}} (n_{\mathbf{k}}+\tfrac{1}{2})\hbar\omega_{\mathbf{k}}, \tag{4.119}$$

being a sum of the single-mode contributions of eqn (4.117).

Problem 4.6. Prove the commutation relation

$$[\mathscr{H}_{\mathrm{R}},\hat{\mathbf{A}}] = \mathrm{i}\hbar\hat{\mathbf{E}}_{\mathrm{T}}. \tag{4.120}$$

Problem 4.7. Prove that the form

$$\mathscr{H}_{\mathrm{R}} = \frac{1}{2}\int(\epsilon_0\hat{\mathbf{E}}_{\mathrm{T}}^2+\mu_0^{-1}\hat{\mathbf{B}}^2)\,\mathrm{d}V \tag{4.121}$$

for the Hamiltonian of the radiation field is equivalent to the expression (4.118) above.

4.6. Field commutation properties

The field operators do not all commute amongst themselves and it is necessary for later use to consider some of their commutation properties. With the aid of the basic commutator (4.67), it is simple to show that Cartesian components of the electric field operator (4.113) and the vector potential operator (4.110) have the commutator

$$[\hat{E}_{\mathrm{T}i}(\mathbf{r}),\hat{A}_j(\mathbf{r}')] = (\mathrm{i}\hbar/2\epsilon_0 V)\sum_{\mathbf{k}} \varepsilon_{\mathbf{k}i}\varepsilon_{\mathbf{k}j}\{\exp[\mathrm{i}\mathbf{k}.(\mathbf{r}-\mathbf{r}')]+\exp[-\mathrm{i}\mathbf{k}.(\mathbf{r}-\mathbf{r}')]\}, \tag{4.122}$$

where the operators are assumed to have a common time but the different spatial positions indicated.

In order to proceed further it is necessary to carry out the wavevector summation, which also includes a summation over the two independent mode polarizations. The polarizations have so far only appeared through the factor of 2 that they contribute to the density of modes in eqn (1.8). It is now necessary to consider their effect in greater detail. Let k, θ and ϕ be the polar coordinates of the wavevector **k**, so that its Cartesian components are

$$\mathbf{k} = k(\sin\theta\cos\phi, \sin\theta\sin\phi, \cos\theta). \tag{4.123}$$

Then possible choices for the transverse polarization vectors are

$$\varepsilon_{\mathbf{k}}(1) = (\sin\phi, -\cos\phi, 0) \tag{4.124}$$

and

$$\varepsilon_{\mathbf{k}}(2) = (\cos\theta\cos\phi, \cos\theta\sin\phi, -\sin\theta). \tag{4.125}$$

It is easily verified that

$$\varepsilon_{\mathbf{k}i}(1)\varepsilon_{\mathbf{k}j}(1)+\varepsilon_{\mathbf{k}i}(2)\varepsilon_{\mathbf{k}j}(2) = \delta_{ij}-(k_ik_j/k^2), \tag{4.126}$$

where

$$\delta_{ij} = \begin{cases} 1 & \text{for} \quad i = j \\ 0 & \text{for} \quad i \neq j. \end{cases} \tag{4.127}$$

The result (4.126) holds for any choice of orthogonal polarization vectors.

It is convenient to convert the summation over **k** in eqn (4.122) to an integration. The conversion is given by eqn (1.11) except that the function to be integrated is not isotropic in wavevector space, and the two polarizations are taken account of in eqn (4.126). The appropriate relation is

$$\sum_{\mathbf{k}} \rightarrow \{V/(2\pi)^3\}\int d\mathbf{k}, \tag{4.128}$$

where the integration runs over all of three-dimensional wavevector space. Note that eqn (4.128) reduces to eqn (1.11) for integration over an isotropic function, where the volume element becomes $4\pi k^2\,dk$, and when the effect of the two polarizations is a simple doubling of the result.

With these changes, and noting that the two terms in the large bracket of eqn (4.122) make the same contribution to the commutator, we find

$$[\hat{E}_{\mathrm{T}i}(\mathbf{r}),\, \hat{A}_j(\mathbf{r}')] = \frac{i\hbar}{\epsilon_0(2\pi)^3}\int d\mathbf{k}\left(\delta_{ij}-\frac{k_ik_j}{k^2}\right)\exp[i\mathbf{k}.(\mathbf{r}-\mathbf{r}')]. \tag{4.129}$$

The integration on the right-hand side produces a singular result and it can be written in terms of a Dirac delta-function.[6] It has the property of extracting the transverse part of any vector field, and we make a slight digression to establish this result, which is needed in Chapter 5.

Let **V**(**r**) be any vector field and let **V**(**k**) be its Fourier transform, related by

$$\mathbf{V}(\mathbf{r}) = \{1/(2\pi)^3\}\int d\mathbf{k}\mathbf{V}(\mathbf{k})\exp(i\mathbf{k}.\mathbf{r}). \tag{4.130}$$

By the ordinary expansion of a vector triple product, we can write

$$\mathbf{V}(\mathbf{k}) = \mathbf{V}_{\mathrm{T}}(\mathbf{k})+\mathbf{V}_{\mathrm{L}}(\mathbf{k}), \tag{4.131}$$

where

$$\mathbf{V}_{\mathrm{T}}(\mathbf{k}) = \{\mathbf{k}\times\mathbf{V}(\mathbf{k})\}\times\mathbf{k}/k^2 \tag{4.132}$$

$$\mathbf{V}_{\mathrm{L}}(\mathbf{k}) = \{\mathbf{k}.\mathbf{V}(\mathbf{k})\}\mathbf{k}/k^2. \tag{4.133}$$

The corresponding separation of **V**(**r**) obtained from eqn (4.130) is

$$\mathbf{V}(\mathbf{r}) = \mathbf{V}_{\mathrm{T}}(\mathbf{r})+\mathbf{V}_{\mathrm{L}}(\mathbf{r}), \tag{4.134}$$

where

$$\mathbf{V}_{\mathrm{T}}(\mathbf{r}) = \frac{1}{(2\pi)^3}\int d\mathbf{k}\,\frac{\{\mathbf{k}\times\mathbf{V}(\mathbf{k})\}\times\mathbf{k}}{k^2}\exp(i\mathbf{k}.\mathbf{r}) \tag{4.135}$$

$$\mathbf{V}_{\mathrm{L}}(\mathbf{r}) = \frac{1}{(2\pi)^3}\int d\mathbf{k}\,\frac{\{\mathbf{k}.\mathbf{V}(\mathbf{k})\}\mathbf{k}}{k^2}\exp(i\mathbf{k}.\mathbf{r}). \tag{4.136}$$

These clearly satisfy

$$\nabla.\mathbf{V}_{\mathrm{T}}(\mathbf{r}) = 0 \tag{4.137}$$

$$\nabla\times\mathbf{V}_{\mathrm{L}}(\mathbf{r}) = 0, \tag{4.138}$$

and they are the transverse and longitudinal parts of **V**(**r**) defined in accordance with eqns (4.21) and (4.22).

When the transverse part (4.135) is written in terms of Cartesian components, the wavevectors occur in the same form as on the right-hand side of eqn (4.129). It is possible to establish a simple result that will be useful in §5.2.

Problem 4.8. If **V**(**r**) is a vector field that commutes with $\hat{\mathbf{E}}_{\mathrm{T}}(\mathbf{r})$, prove that

$$\int d\mathbf{r}'[\hat{\mathbf{E}}_{\mathrm{T}}(\mathbf{r}),\hat{\mathbf{A}}(\mathbf{r}')\,.\,\mathbf{V}(\mathbf{r}')] = (i\hbar/\epsilon_0)\mathbf{V}_{\mathrm{T}}(\mathbf{r}). \tag{4.139}$$

The commutators of other combinations of field operators are found in a similar manner.

Problem 4.9. Prove the following commutation relations for operators taken at common times

$$\begin{aligned}[][\hat{E}_{\mathrm{T}i}(\mathbf{r}),\, \hat{E}_{\mathrm{T}j}(\mathbf{r}')] &= [\hat{B}_i(\mathbf{r}),\, \hat{B}_j(\mathbf{r}')]\\ &= [\hat{A}_i(\mathbf{r}),\, \hat{A}_j(\mathbf{r}')]\\ &= [\hat{B}_i(\mathbf{r}),\, \hat{A}_j(\mathbf{r}')]\\ &= 0.\end{aligned} \tag{4.140}$$

Problem 4.10. Prove that

$$[\hat{E}_{\mathrm{T}i}(\mathbf{r}),\, \hat{B}_j(\mathbf{r}')] = \{\hbar/(2\pi)^3\epsilon_0\}\int d\mathbf{k}k_h\,\exp[i\mathbf{k}.(\mathbf{r}-\mathbf{r}')] \tag{4.141}$$

if *ijh* are a cyclic permutation of *xyz*. The sign of the result is changed for a non-cyclic permutation and the commutator vanishes for $i = j$.

4.7. The zero-point energy

The state of the electromagnetic field in which no photons are excited in any of the field modes, i.e.

$$n_{\mathbf{k}_1} = n_{\mathbf{k}_2} = n_{\mathbf{k}_3} = \ldots = 0 \tag{4.142}$$

is called the vacuum state of the field. This state has the interesting property that although no excitations are present, the total energy does not vanish. According to eqn (4.119) the energy of the vacuum state is

$$\bar{\mathscr{E}}_0 = \sum_{\mathbf{k}}\tfrac{1}{2}\hbar\omega_{\mathbf{k}}. \tag{4.143}$$

The quantity $\bar{\mathscr{E}}_0$ is called the zero-point energy of the field; it is the sum of the energies of the ground states of the harmonic oscillators associated with all the field modes.

The summation in eqn (4.143) can be converted to an integration by use of eqn (1.11), and the zero-point energy becomes

$$\bar{\mathscr{E}}_0 = \int (V\hbar\omega_{\mathbf{k}}^3/2\pi^2c^3)\,\mathrm{d}\omega_{\mathbf{k}}. \qquad (4.144)$$

The allowed frequencies $\omega_{\mathbf{k}}$ have no upper bound, and the integral is thus highly divergent. The zero-point energy is accordingly infinite, an awkward feature of the quantized electromagnetic field, and one whose significance is difficult to explain in a satisfactory manner.

Fortunately for the quantized field theory, it turns out that, in extracting theoretical results for comparison with experiment, there is no great embarrassment in the existence of the infinite zero-point energy. No measurements have been devised in which an apparatus would register a response proportional to the zero-point energy. Practical experiments respond to some *change* in the total energy of the electromagnetic field. The infinite zero-point energy is a matter of conceptual difficulty in quantized radiation-field theory, but it does not lead to any infinite predictions for the results of the experiments considered in the present book.

In the vast majority of experiments, the measured response is proportional to the excitation energy of the field above its zero-point value. We denote this energy by a prime,

$$\bar{\mathscr{E}}' = \bar{\mathscr{E}} - \bar{\mathscr{E}}_0 = \sum_{\mathbf{k}} \bar{\mathscr{E}}'_{\mathbf{k}}, \qquad (4.145)$$

where

$$\bar{\mathscr{E}}'_{\mathbf{k}} = n_{\mathbf{k}}\hbar\omega_{\mathbf{k}}. \qquad (4.146)$$

For example, the determination of the intensity of a light beam is a measurement where the result is proportional to $\bar{\mathscr{E}}'$ rather than $\bar{\mathscr{E}}$. The theory of this type of experiment is fully discussed in §5.7.

A smaller class of experiments consists of measurements where some change in the zero-point energy itself is detected. Consider a closed cubic cavity with standing-wave solutions for the electromagnetic field, as given by eqns (1.3)–(1.5). The smallest frequency allowed in such a cavity is

$$\omega_{\mathbf{k}} = 2^{\frac{1}{2}}\pi c/L, \qquad (4.147)$$

as indicated in Fig. 1.4. This frequency must be the lower limit on the integration of eqn (4.144) which determines the zero-point energy in the closed cavity. The zero-point energy thus depends on the magnitude L of the cube edge, and the energy can be lowered by change in L. The cavity walls accordingly experience a force associated with the zero-point energy. Note that the cavity dimensions affect only the lower limit of the integral in eqn (4.144), and the change in the zero-point energy produced by variation in the size of cavity is a finite quantity.

Such zero-point effects are known as van der Waals forces. They act between all macroscopic bodies since the space between the bodies forms an effective optical cavity. They are however very weak and have a short range, with contributions proportional to the inverse third and fourth powers of the separation between the bodies[7]. The strength of the force depends upon the boundary conditions at the cavity walls and hence upon the dielectric properties of the materials involved. Recent accurate measurements[8] for an open-sided cavity formed by a pair of plates separated by distances in the range 0·1 to 1 μm have confirmed theoretical predictions for the size and variation of the van der Waals forces.

4.8. The mode phase operators

Because of the independence of the excitations in different modes of the cavity, it is permissible to examine the modes one at a time. For the next several sections we restrict attention to a particular mode **k** of the electromagnetic field, having specified polarization. With this understanding, the subscript **k** can be dropped from the variables that describe the mode under consideration, and the electric and magnetic fields can be written as scalars.

In the classical theory of light waves, it is convenient to write the complex electric field as a product of a real amplitude and a phase factor, as in eqn (3.46). If this procedure is followed for the classical electric field of eqn (4.53), the single-mode contribution can be written

$$E = \tfrac{1}{2}E_0\{\exp(-\mathrm{i}\omega t + \mathrm{i}\mathbf{k}.\mathbf{r} + \mathrm{i}\phi) + \exp(\mathrm{i}\omega t - \mathrm{i}\mathbf{k}.\mathbf{r} - \mathrm{i}\phi)\}. \qquad (4.148)$$

It is similarly convenient in quantum mechanics to make a separation into amplitude and phase factors. To do this, it is necessary to introduce the concept of phase into the quantum-mechanical description of the field.

The single-mode quantum-mechanical electric-field operator obtained from eqn (4.111) is

$$\hat{E} = \mathrm{i}(\hbar\omega/2\epsilon_0 V)^{\frac{1}{2}}\{\hat{a}\exp(-\mathrm{i}\omega t + \mathrm{i}\mathbf{k}.\mathbf{r}) - \hat{a}^\dagger\exp(\mathrm{i}\omega t - \mathrm{i}\mathbf{k}.\mathbf{r})\}, \qquad (4.149)$$

and it can be expressed in a form analogous to eqn (4.148) if $\hat{a}$ is separated into a product of amplitude and phase operators. There is in fact no unique prescription for the way in which the separation should be accomplished in quantum mechanics and there is a corresponding degree of arbitrariness in the definition of the quantum-mechanical phase operator. The main considerations are that the quantum-mechanical phase should have the same significance as the classical phase in the appropriate limit, and that the phase should be associated with Hermitian operators so that it is (at any rate in principle) an observable quantity.

Consider the phase operator $\mathrm{e\hat{x}p}(\mathrm{i}\phi)$ defined by the relation[9]

$$\hat{a} = (\hat{n}+1)^{\frac{1}{2}}\,\mathrm{e\hat{x}p}(\mathrm{i}\phi), \tag{4.150}$$

where $\hat{n}$ is the number operator defined in eqn (4.69). The Hermitian conjugate relation can be written

$$\hat{a}^{\dagger} = \mathrm{e\hat{x}p}(-\mathrm{i}\phi)(\hat{n}+1)^{\frac{1}{2}}. \tag{4.151}$$

The exponential operators defined by these two equations describe the quantum-mechanical phase of the electromagnetic field. We shall show that they generate the analogous classical phase factors in a suitable limit.

The basic properties of the phase operators can be calculated from the known properties of the creation, destruction, and number operators. According to eqns (4.150) and (4.151)

$$\mathrm{e\hat{x}p}(\mathrm{i}\phi) = (\hat{n}+1)^{-\frac{1}{2}}\hat{a} \tag{4.152}$$

and

$$\mathrm{e\hat{x}p}(-\mathrm{i}\phi) = \hat{a}^{\dagger}(\hat{n}+1)^{-\frac{1}{2}}. \tag{4.153}$$

From eqns (4.67) and (4.69)

$$\hat{a}\hat{a}^{\dagger} = \hat{n}+1 \tag{4.154}$$

and it therefore follows that

$$\mathrm{e\hat{x}p}(\mathrm{i}\phi)\mathrm{e\hat{x}p}(-\mathrm{i}\phi) = 1. \tag{4.155}$$

Note however that the reverse-order product of exponential operators is *not* equal to unity; the expressions should not be regarded as exponential functions of a phase operator and the operator symbol is accordingly attached to exp rather than to ϕ in the above expressions.

The results of applying the exponential operators to the states $|n\rangle$ can readily be calculated with the help of eqns (4.86), (4.91), and (4.92),

$$\begin{aligned} \mathrm{e\hat{x}p}(\mathrm{i}\phi)|n\rangle = (\hat{n}+1)^{-\frac{1}{2}}n^{\frac{1}{2}}|n-1\rangle &= |n-1\rangle \qquad \text{for} \quad n \neq 0 \\ &= 0 \qquad\qquad\;\; \text{for} \quad n = 0, \end{aligned} \tag{4.156}$$

$$\mathrm{e\hat{x}p}(-\mathrm{i}\phi)|n\rangle = \hat{a}^{\dagger}(n+1)^{-\frac{1}{2}}|n\rangle = |n+1\rangle. \tag{4.157}$$

The two exponential phase operators thus have non-vanishing matrix elements

$$\langle n-1|\mathrm{e\hat{x}p}(\mathrm{i}\phi)|n\rangle = 1 \tag{4.158}$$

and

$$\langle n+1|\mathrm{e\hat{x}p}(-\mathrm{i}\phi)|n\rangle = 1. \tag{4.159}$$

and all other types of matrix element are zero. These results are similar to the matrix elements of eqns (4.93) and (4.94) of the destruction and creation operators except that eqns (4.158) and (4.159) do not include the normalization factors of these latter matrix elements.

The above equations display the formal properties of the phase operators that arise in the decompositions of $\hat{a}$ and $\hat{a}^{\dagger}$ into amplitude and phase contributions. It is seen from eqns (4.158) and (4.159) that $\mathrm{e\hat{x}p}(\mathrm{i}\phi)$ and $\mathrm{e\hat{x}p}(-\mathrm{i}\phi)$ do not satisfy the relation (4.95); therefore they are not Hermitian operators, and they cannot represent observable properties of the electromagnetic field. They can, however, be combined to produce another pair of operators

$$\mathrm{c\hat{o}s}\,\phi = \tfrac{1}{2}\{\mathrm{e\hat{x}p}(\mathrm{i}\phi)+\mathrm{e\hat{x}p}(-\mathrm{i}\phi)\} \tag{4.160}$$

and

$$\mathrm{s\hat{i}n}\,\phi = \tfrac{1}{2\mathrm{i}}\{\mathrm{e\hat{x}p}(\mathrm{i}\phi)-\mathrm{e\hat{x}p}(-\mathrm{i}\phi)\}, \tag{4.161}$$

whose non-vanishing matrix elements are

$$\langle n-1|\mathrm{c\hat{o}s}\,\phi|n\rangle = \langle n|\mathrm{c\hat{o}s}\,\phi|n-1\rangle = \tfrac{1}{2} \tag{4.162}$$

and

$$\langle n-1|\mathrm{s\hat{i}n}\,\phi|n\rangle = -\langle n|\mathrm{s\hat{i}n}\,\phi|n-1\rangle = 1/2\mathrm{i}. \tag{4.163}$$

These matrix elements do satisfy eqn (4.95) and the operators $\mathrm{c\hat{o}s}\,\phi$ and $\mathrm{s\hat{i}n}\,\phi$ are Hermitian. We adopt them as the quantum-mechanical operators that represent the observable phase properties of the electromagnetic field.

Problem 4.11. Prove the commutation relation

$$[\mathrm{c\hat{o}s}\,\phi, \mathrm{s\hat{i}n}\,\phi] = \{\hat{a}^{\dagger}(\hat{n}+1)^{-1}\hat{a}-1\}/2\mathrm{i} \tag{4.164}$$

and hence show that all matrix elements of the commutator are zero except for the diagonal ground-state matrix element

$$\langle 0|[\mathrm{c\hat{o}s}\,\phi, \mathrm{s\hat{i}n}\,\phi]|0\rangle = -1/2\mathrm{i}. \tag{4.165}$$

Problem 4.12. Prove the commutation relations

$$[\hat{n}, \hat{a}] = -\hat{a} \tag{4.166}$$

and

$$[\hat{n}, \hat{a}^{\dagger}] = a^{\dagger} \tag{4.167}$$

and hence show that

$$[\hat{n}, \mathrm{e\hat{x}p}(\mathrm{i}\phi)] = -\mathrm{e\hat{x}p}(\mathrm{i}\phi) \tag{4.168}$$

and

$$[\hat{n}, \mathrm{e\hat{x}p}(-\mathrm{i}\phi)] = \mathrm{e\hat{x}p}(-\mathrm{i}\phi), \tag{4.169}$$

and that

$$[\hat{n}, \mathrm{c\hat{o}s}\,\phi] = -\mathrm{i}\,\mathrm{s\hat{i}n}\,\phi \tag{4.170}$$

and

$$[\hat{n}, \mathrm{s\hat{i}n}\,\phi] = \mathrm{i}\,\mathrm{c\hat{o}s}\,\phi. \tag{4.171}$$

The above commutation relations show that the number and phase operators do not commute and it is therefore not possible, in principle, to set up states of the radiation field that are simultaneous eigenstates of two of the operators. The amplitude of an electromagnetic wave, associated with $\hat{n}$, and the phase, associated with $\widehat{\cos}\,\phi$ or $\widehat{\sin}\,\phi$, cannot both be precisely specified. The results of measurements of the amplitude and phase are governed by uncertainty relations derived from eqns (4.170) and (4.171) in the usual way[10,11]

$$\Delta n\,\Delta\cos\phi \geqslant \tfrac{1}{2}|\langle\widehat{\sin}\,\phi\rangle| \tag{4.172}$$

$$\Delta n\,\Delta\sin\phi \geqslant \tfrac{1}{2}|\langle\widehat{\cos}\,\phi\rangle|. \tag{4.173}$$

Here Δ indicates the root-mean-square deviation of a series of measurements of the quantity that follows it, for a state of the field in which $\widehat{\cos}\,\phi$ and $\widehat{\sin}\,\phi$ have the respective expectation values $\langle\widehat{\cos}\,\phi\rangle$ and $\langle\widehat{\sin}\,\phi\rangle$. Some examples of the operation of these photon number-phase uncertainty relations are given later in the chapter.

We have therefore shown that the separations (eqns (4.150) and (4.151)) of the creation and destruction operators into amplitude and phase contributions lead to phase operators that do not commute with the amplitude operator. The resulting uncertainty relations are a characteristic feature of the quantized radiation field.

4.9. Physical properties of the single-mode number states

The single-mode number states $|n\rangle$, where exactly n photons are excited, are energy eigenstates of the harmonic oscillator associated with the electromagnetic field in the mode. The number states are a very convenient complete set of states for the mode and they have simple properties. They are not of direct significance in the interpretation of experiments since the electromagnetic waves generated by practical light sources do not have definite numbers of photons, but we briefly consider their main features.

The uncertainty in the photon number is clearly zero for the states $|n\rangle$,

$$\Delta n = 0. \tag{4.174}$$

For the phase operators, use of eqns (4.162) and (4.163) gives

$$\langle n|\widehat{\cos}\,\phi|n\rangle = \langle n|\widehat{\sin}\,\phi|n\rangle = 0 \tag{4.175}$$

and

$$\begin{aligned}\langle n|\widehat{\cos}^2\,\phi|n\rangle = \langle n|\widehat{\sin}^2\,\phi|n\rangle &= \tfrac{1}{2} \quad \text{for} \quad n \neq 0\\ &= \tfrac{1}{4} \quad \text{for} \quad n = 0.\end{aligned} \tag{4.176}$$

Thus, if the $n = 0$ state is excluded from consideration, the phase uncertainties are

$$\Delta\cos\phi = \Delta\sin\phi = 2^{-\frac{1}{2}}, \tag{4.177}$$

appropriate to a phase angle that is equally likely to have any value between 0 and 2π. Note that the results (4.174), (4.175), and (4.177) are consistent with the uncertainty relations (4.172) and (4.173).

The expectation values of the electric field and its square can be found with the use of the electric-field operator (4.149),

$$\langle n|\hat{E}|n\rangle = 0 \tag{4.178}$$

and

$$\langle n|\hat{E}^2|n\rangle = (\hbar\omega/\epsilon_0 V)(n+\tfrac{1}{2}), \tag{4.179}$$

in agreement with eqn (4.116). The root-mean-square deviation of the electric field is thus

$$\Delta E = (\hbar\omega/\epsilon_0 V)^{\frac{1}{2}}(n+\tfrac{1}{2})^{\frac{1}{2}}. \tag{4.180}$$

Fig. 4.2 shows a pictorial representation of the single-mode excitation for state $|n\rangle$. The vertical axis represents the electric field at some fixed point in the cavity as a function of time. The field oscillates like a sine wave of known frequency ω. The above analysis shows that the electromagnetic wave amplitude can be represented by a quantity

$$E_0 = (2\hbar\omega/\epsilon_0 V)^{\frac{1}{2}}(n+\tfrac{1}{2})^{\frac{1}{2}}. \tag{4.181}$$

However, the lateral position of the wave along the horizontal axis is completely undetermined owing to the complete uncertainty in the phase angle. This is indicated in the figure by the inclusion of several waves, all of the same amplitude and frequency, but with their nodes progressively displaced along the axis. In fact, the possible horizontal positions of the wave form a continuum, and the field at any time can take a continuous range of values between $-E_0$ and E_0.

Any pictorial representation of a quantum-mechanical state must be treated with caution. Fig. 4.2 reproduces the various uncertainties shown in eqns (4.177) and (4.180), and also ensures the vanishing of the expectation values given in eqns (4.175) and (4.178). However, it does not in general agree with the higher-order expectation values and can only be taken as an accurate representation in the limit $n \gg 1$.

Problem 4.13. Evaluate the expectation value $\langle n|\hat{E}^4|n\rangle$ and show that it exceeds the corresponding average for the sine waves of Fig. 4.2 by an amount

$$\frac{3}{2}\left(\frac{\hbar\omega}{2\epsilon_0 V}\right)^2.$$

Since this is independent of n, the importance of the discrepancy that it represents diminishes for large n.

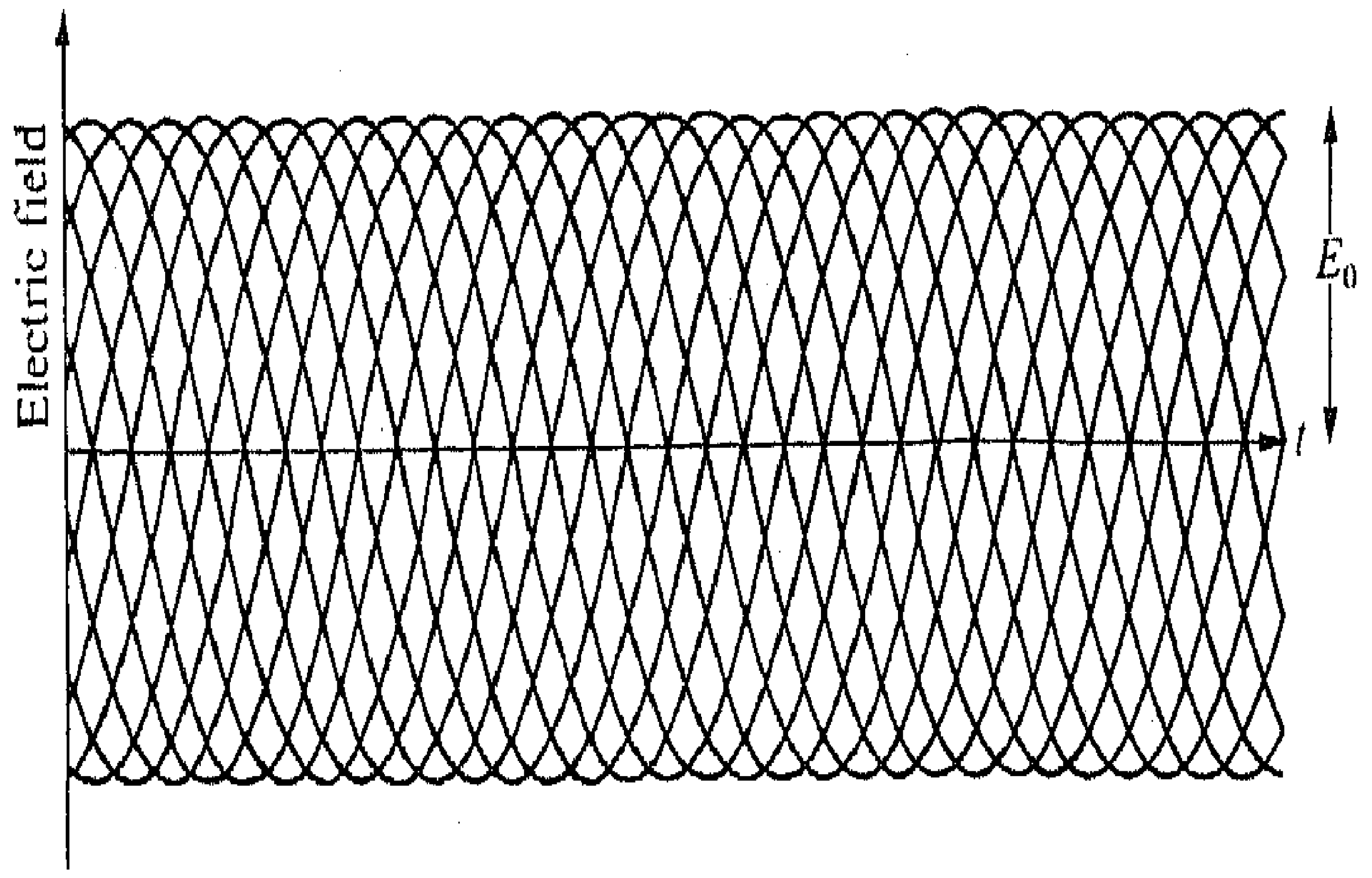

FIG. 4.2. Pictorial representation of the electric-field variation in a cavity mode excited to state $|n\rangle$. The sine waves should more accurately form a horizontal continuum. The amplitude E_0 is defined in the text.

4.10. The coherent photon states

The single-mode states of physical importance correspond not to the individual number states but to linear superpositions of the states $|n\rangle$. There is of course a wide variety of possible superposition states, but one kind, the coherent state, is of particular importance in the practical applications of the quantum theory of light. It should also be mentioned that another kind of superposition state can be constructed for which the uncertainties in the expectation values of the phase operators $\hat{\cos}\,\phi$ and $\hat{\sin}\,\phi$ are both equal to zero.[9,12] Such states have an infinite uncertainty Δn in the photon number n and are in some sense complementary to the number states $|n\rangle$; they cannot however be excited in any real experiment, and we do not consider them further.

The coherent states, so called for reasons that will be apparent from the treatment of the quantum theory of coherence in Chapter 6, are denoted by $|\alpha\rangle$. They have an electric-field variation that in the limit of high excitation approaches that of the classical wave of stable amplitude and fixed phase shown in Fig. 3.8. They are important not only because they are the closest quantum-mechanical approach to a classical electromagnetic wave, but also because a single-mode laser operated well above threshold generates a coherent state excitation, as discussed in Chapter 7.

Consider the properties of the state $|\alpha\rangle$ defined as the following linear superposition of the number states,[13]

$$|\alpha\rangle = \exp(-\tfrac{1}{2}|\alpha|^2)\sum_n \frac{\alpha^n}{(n!)^{\frac{1}{2}}}|n\rangle. \qquad (4.182)$$

In this expression α can be any complex number, and the coherent states so defined form a double continuum corresponding to the continuous ranges of values of the real and imaginary parts of α. It is easily verified that $|\alpha\rangle$ is normalized,

$$\langle\alpha|\alpha\rangle = \exp(-|\alpha|^2)\sum_n \frac{\alpha^{*n}\alpha^n}{n!} = 1. \qquad (4.183)$$

The states are not however orthogonal, since for two different complex numbers α and β,

$$\begin{aligned}\langle\alpha|\beta\rangle &= \exp(-\tfrac{1}{2}|\alpha|^2-\tfrac{1}{2}|\beta|^2)\sum_n \frac{\alpha^{*n}\beta^n}{n!}\\ &= \exp(-\tfrac{1}{2}|\alpha|^2-\tfrac{1}{2}|\beta|^2+\alpha^*\beta).\end{aligned} \qquad (4.184)$$

Thus

$$|\langle\alpha|\beta\rangle|^2 = \exp(-|\alpha-\beta|^2). \qquad (4.185)$$

It is apparent from the definition eqn (4.182) that there are many more coherent states $|\alpha\rangle$ than there are states $|n\rangle$. The $|\alpha\rangle$ form an overcomplete set of states for the harmonic oscillator, and their lack of orthogonality is a consequence of this. Note, however, from eqn (4.185) that the states $|\alpha\rangle$ and $|\beta\rangle$ become approximately orthogonal if $|\alpha-\beta|$ is much greater than unity.

The coherent states are eigenstates of the destruction operator, since

$$\hat{a}|\alpha\rangle = \exp(-\tfrac{1}{2}|\alpha|^2)\sum_n \frac{\alpha^n}{(n!)^{\frac{1}{2}}} n^{\frac{1}{2}}|n-1\rangle = \alpha|\alpha\rangle. \qquad (4.186)$$

The complex number α that labels the coherent state is thus the eigenvalue of the destruction operator. Note, however, that the state $|\alpha\rangle$ is not an eigenstate of the creation operator since the summation over n analogous to that in eqn (4.186) cannot be rearranged to reproduce the coherent state in the case of $\hat{a}^\dagger|\alpha\rangle$. An alternative approach to the coherent state is to take the eigenvalue eqn (4.186) as its definition; the expansion of eqn (4.182) can then be derived as one of the consequences.[13]

The relation (4.96) can be used to rewrite the definition (4.182) of the coherent state as

$$|\alpha\rangle = \exp(-\tfrac{1}{2}|\alpha|^2)\sum_n \frac{(\alpha\hat{a}^\dagger)^n}{n!}|0\rangle = \exp(\alpha\hat{a}^\dagger-\tfrac{1}{2}|\alpha|^2)|0\rangle. \qquad (4.187)$$

Problem 4.14. Prove that the creation operator $\hat{a}^\dagger$ has no normalizable eigenstates.

Problem 4.15. The result

$$\exp(\hat{c})\exp(\hat{d}) = \exp(\hat{c}+\hat{d}+\tfrac{1}{2}[\hat{c},\hat{d}]) \qquad (4.188)$$

can be proved[14] for any pair of operators $\hat{c}$ and $\hat{d}$ that commute with their commutator

$$[\hat{c},[\hat{c},\hat{d}]] = [\hat{d},[\hat{c},\hat{d}]] = 0. \tag{4.189}$$

With the help of this expression, cast eqn (4.187) into the compact form

$$|\alpha\rangle = \exp(\alpha\hat{a}^\dagger - \alpha^*\hat{a})|0\rangle. \tag{4.190}$$

The exponential operator in this equation is equivalent to a creation operator for the coherent state.

It is sometimes convenient to write α in terms of an amplitude and a phase. We take θ as a notation for the phase angle, $\arg\alpha$, and write

$$\alpha = |\alpha|e^{i\theta}. \tag{4.191}$$

4.11. Physical properties of the single-mode coherent states

The properties of a cavity mode excited to a coherent state $|\alpha\rangle$ can be determined by the method applied to the number states $|n\rangle$. The expectation values for the number operator are

$$\langle\alpha|\hat{n}|\alpha\rangle = \exp(-|\alpha|^2)\sum_n \frac{(\alpha^*\alpha)^n}{n!}\,n = |\alpha|^2, \tag{4.192}$$

$$\begin{aligned}\langle\alpha|\hat{n}^2|\alpha\rangle &= \exp(-|\alpha|^2)\sum_n \frac{(\alpha^*\alpha)^n}{n!}\,n^2 \\ &= \exp(-|\alpha|^2)\sum_n \frac{|\alpha|^{2n}}{n!}\{n(n-1)+n\} = |\alpha|^4+|\alpha|^2,\end{aligned} \tag{4.193}$$

and the root-mean-square deviation is therefore

$$\Delta n = |\alpha|. \tag{4.194}$$

The fractional uncertainty in the number of photons in the cavity mode is

$$\Delta n/\langle\alpha|\hat{n}|\alpha\rangle = |\alpha|^{-1}. \tag{4.195}$$

These results show that $|\alpha|^2$ is the mean number of photons in the cavity mode, and the uncertainty spread about the mean is equal to the square root of the mean number of photons. The fractional uncertainty in photon number given by eqn (4.195) is proportional to the inverse square root of the mean photon number, and decreases with increasing excitation of the cavity mode.

This result can be compared with the zero uncertainty in photon number for the state $|n\rangle$, shown in eqn (4.174).

The definition (4.182) shows that the probability of finding n photons in the mode is

$$|\langle n|\alpha\rangle|^2 = \exp(-|\alpha|^2)\frac{|\alpha|^{2n}}{n!}. \tag{4.196}$$

This is a Poisson probability distribution (see ref. 15 and Fig. 6.6) about a mean $|\alpha|^2$, and eqn (4.194) is the usual result for the spread of such a distribution.

The expectation values of the phase operators are given by somewhat complicated expressions for the coherent states.[16] We restrict attention to the cosine operator, and find

$$\begin{aligned}\langle\alpha|\hat{\cos}\,\phi|\alpha\rangle &= \frac{1}{2}\exp(-|\alpha|^2)\sum_n \frac{\alpha^{*n+1}\alpha^n+\alpha^{*n}\alpha^{n+1}}{\{(n+1)!\,n!\}^{\frac{1}{2}}} \\ &= |\alpha|\cos\theta\,\exp(-|\alpha|^2)\sum_n \frac{|\alpha|^{2n}}{n!\,(n+1)^{\frac{1}{2}}},\end{aligned} \tag{4.197}$$

where eqns (4.158), (4.159), (4.182), and (4,191) have been used. The expectation value of $\hat{\cos}\,\phi$ is thus proportional to the cosine of the phase of α. Similarly,

$$\begin{aligned}\langle\alpha|\hat{\cos}^2\phi|\alpha\rangle &= \tfrac{1}{2}-\tfrac{1}{4}\exp(-|\alpha|^2) \\ &\quad +|\alpha|^2(\cos^2\theta-\tfrac{1}{2})\exp(-|\alpha|^2)\sum_n \frac{|\alpha|^{2n}}{n!\,\{(n+1)(n+2)\}^{\frac{1}{2}}}.\end{aligned} \tag{4.198}$$

It is unfortunately not possible to evaluate the summations in eqns (4.197) and (4.198) analytically. There are, however, some simplifications in the limit where the mean number of photons in the mode is much larger than unity. The following asymptotic expansions[16], which we quote without proof, can then be used,

$$\sum_n \frac{|\alpha|^{2n}}{n!\,(n+1)^{\frac{1}{2}}} = \frac{\exp(|\alpha|^2)}{|\alpha|}\left(1-\frac{1}{8|\alpha|^2}+\ldots\right), \qquad |\alpha|^2 \gg 1, \tag{4.199}$$

$$\sum_n \frac{|\alpha|^{2n}}{n!\,\{(n+1)(n+2)\}^{\frac{1}{2}}} = \frac{\exp(|\alpha|^2)}{|\alpha|^2}\left(1-\frac{1}{2|\alpha|^2}-\ldots\right), \qquad |\alpha|^2 \gg 1. \tag{4.200}$$

Thus for large mean numbers of photons, the phase expectation values become

$$\langle\alpha|\hat{\cos}\,\phi|\alpha\rangle = \cos\theta\left(1-\frac{1}{8|\alpha|^2}+\cdots\right) \qquad |\alpha|^2 \gg 1, \tag{4.201}$$

$$\langle\alpha|\hat{\cos}^2\phi|\alpha\rangle = \cos^2\theta-\frac{\cos^2\theta-\frac{1}{2}}{2|\alpha|^2}-\cdots, \qquad |\alpha|^2 \gg 1, \tag{4.202}$$

and the phase uncertainty is therefore

$$\Delta \cos\phi = \sin\theta/2|\alpha|, \qquad |\alpha|^2 \gg 1. \tag{4.203}$$

From eqns (4.194) and (4.203), the product of uncertainties is

$$\Delta n\, \Delta \cos\phi = \tfrac{1}{2}\sin\theta, \qquad |\alpha|^2 \gg 1. \tag{4.204}$$

It is possible to derive a result analogous to eqn (4.201) which shows that the expectation value of $\widehat{\sin}\,\phi$ is equal to $\sin\theta$ for large $|\alpha|^2$. Thus for a large mean photon-number, the coherent state $|\alpha\rangle$ has the minimum uncertainty product allowed by the general relation (4.172). It is seen from eqns (4.195) and (4.203) that the fractional uncertainty in photon number and the phase uncertainty both vary like $|\alpha|^{-1}$; as the mean photon-number is increased, the wave becomes progressively better defined both in amplitude and in phase angle. The coherent states have some analogy in particle mechanics to the wave packet, which has uncertainty spreads in both its position and momentum, but is the quantum state that reproduces the classical behaviour in the large-mass limit. A more thorough treatment of the number-phase uncertainty relations[17] shows that the uncertainty properties of the coherent states are by no means unique, and that indeed there exist other states whose uncertainty products have the theoretical minimum value, which is achieved by the coherent states only in the $|\alpha|^2 \gg 1$ limit. It is the other properties of the coherent states, particularly eqn (4.186), that lead to their unique association with the classical stable electromagnetic wave.

The electric-field variation for the coherent state is obtained by evaluation of the expectation value of the electric-field operator (4.149),

$$\begin{aligned}\langle\alpha|\hat{E}|\alpha\rangle &= \mathrm{i}(\hbar\omega/2\epsilon_0 V)^{\frac{1}{2}}\{\alpha\exp(-\mathrm{i}\omega t+\mathrm{i}\mathbf{k}.\mathbf{r})-\alpha^*\exp(\mathrm{i}\omega t-\mathrm{i}\mathbf{k}.\mathbf{r})\}\\ &= -2(\hbar\omega/2\epsilon_0 V)^{\frac{1}{2}}|\alpha|\sin(\mathbf{k}.\mathbf{r}-\omega t+\theta),\end{aligned} \tag{4.205}$$

where we have used

$$\langle\alpha|\hat{a}^\dagger|\alpha\rangle = \alpha^*. \tag{4.206}$$

Similarly,

$$\langle\alpha|\hat{E}^2|\alpha\rangle = (\hbar\omega/2\epsilon_0 V)\{4|\alpha|^2\sin^2(\mathbf{k}.\mathbf{r}-\omega t+\theta)+1\}, \tag{4.207}$$

and the root-mean-square deviation in electric field is therefore

$$\Delta E = (\hbar\omega/2\epsilon_0 V)^{\frac{1}{2}}. \tag{4.208}$$

Note that the results of the present paragraph apply irrespective of the amplitude of the wave, unlike the previous two paragraphs where large amplitude approximations were made.

The time dependence of the electric field at a fixed point in the cavity is illustrated in Fig. 4.3 for coherent states $|\alpha\rangle$ all having the same phase angle, but three different values of the mean photon number. Since the uncertainty ΔE given by eqn (4.208) is independent of the wave amplitude, the definition of the waves improves with increasing $|\alpha|^2$. It is clear from the figure that the electric-field variation resembles that of a classical stable wave more and more closely as the mean number of photons in the coherent state is increased (compare Fig. 3.8). This is not a general property of the mode excitations and, for example, the number states $|n\rangle$ do not tend towards the classical form when the photon number is much larger than unity.

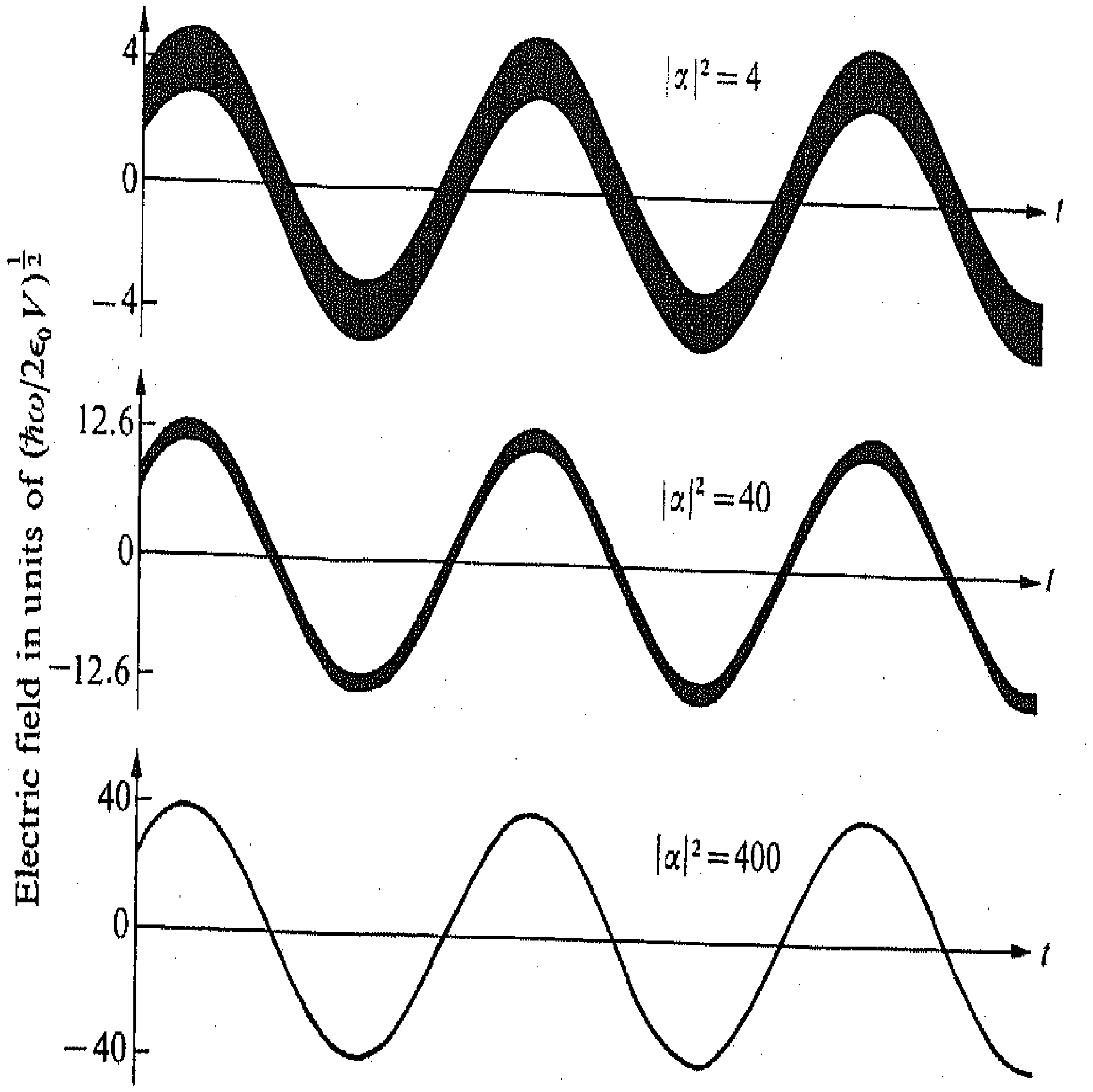

FIG. 4.3. Pictorial representation of the electric-field variation in a cavity mode excited to state $|\alpha\rangle$. Three different values of the mean photon number $|\alpha|^2$ are shown, the vertical scales being different for the three cases. The uncertainties in field values are indicated by the vertical widths $2\Delta E$ of the sine waves. These widths can also be regarded as combinations of the amplitude uncertainty associated with Δn and the phase uncertainty associated with $\Delta\cos\phi$.

It is seen by comparison of eqns (4.148) and (4.205) that in the classical limit the coherent state $|\alpha\rangle$ corresponds to a classical wave whose phase angle is determined by the phase θ of α, and whose electric-field amplitude is related to $|\alpha|$ by

$$E_0 = (2\hbar\omega/\epsilon_0 V)^{\frac{1}{2}}|\alpha|. \tag{4.209}$$

If the phase angle θ is chosen to be $-\pi/2$, then eqn (4.191) gives

$$\alpha = -\mathrm{i}|\alpha|. \tag{4.210}$$

and eqn (4.205) becomes

$$\langle\alpha|\hat{E}|\alpha\rangle = E_0\cos(\mathbf{k}.\mathbf{r}-\omega t), \tag{4.211}$$

identical at the origin $\mathbf{r} = 0$ to the electric-field variation (2.92) used in the semiclassical theory of the atom-radiation interaction.

4.12. The radiative density operator

The number and coherent state excitations are *pure states* of the radiation field, the former being a particular state $|n\rangle$ and the latter being expressible as a definite linear combination of the basic number states $|n\rangle$. No difficulty is presented by the generalization of the calculations given above to pure states of the complete radiation field in the cavity; the state of the total electromagnetic field is formed by a product of the states of the individual modes in the usual way, and any calculation for the multimode field reduces to a series of calculations for the single-mode fields taken one at a time.

There exist however mode excitations that are not expressible as definite linear superpositions of the complete set of basic states $|n\rangle$, and their treatment requires a more radical generalization of the theory. Some parallels can be drawn between the descriptions of light beams that occur in classical and quantum-mechanical theory. Thus, while the electric field of the classical stable wave illustrated in Fig. 3.8 is specified by a definite amplitude and phase, the electric field of the light beam from a chaotic source is shown in Chapter 3 to be specifiable only in terms of a probability for the field to have particular values of amplitude and phase. A similar situation occurs in quantum mechanics where the nature of a chaotic light source excludes the possibility of any definite prediction of the state of the emitted field, and only a probabilistic description is feasible. When all that can be specified is a set of probabilities that the radiation will be found in a range of states, each corresponding to a different linear combination of the basic number states, then the state of the field is called a *statistical mixture.*

Statistical distributions are introduced into quantum mechanics by means of the density operator. The matrix elements of the density operator for a two-level atom have already been used in the derivation of the optical Bloch equations in Chapter 2. It is however useful to review some general properties of the density operator and its matrix elements that are needed in applying quantum statistical theory to the radiation field. The pure state is a special case of the statistical mixture and both kinds of state are included within a common theoretical framework.

Let us consider a cavity electromagnetic field for which there is a known probability P_R that the field is in state $|R\rangle$. Here R is a label that runs over a set of pure states sufficient to describe the field. For a single cavity mode the states $|R\rangle$ could be the number states $|n\rangle$ or the coherent states $|\alpha\rangle$ or they could be some other type of pure state. For the complete cavity field, the states $|R\rangle$ would be all possible products of the single-mode states, with one state for each mode of the cavity included in each of the basic states $|R\rangle$. The states given by eqn (4.107) are a possible set $|R\rangle$, based on the single-mode number states. The state described by the probability P_R is a statistical mixture; the magnitudes of the P_R for a given set of pure states $|R\rangle$ contain all the available information about the state.

An example of a statistical mixture is provided by the thermal excitation of photons in a cavity mode, derived in Chapter 1 as a step on the way to Planck's law. The most detailed description that can be given in this case is the probability P_n in eqn (1.26) that n photons are excited at temperature T. The distribution P_n is an example of the general probability P_R introduced above.

The result of an experiment that can be carried out on a beam of light generally depends on an ensemble average of some observable quantity. For example, the fluctuation in photon number derived in eqn (1.41) requires a knowledge of the ensemble average of n^2, and the fringe intensity in eqn (3.33) requires the evaluation of an ensemble average of a product of electric fields. Consider some observable O that is represented by a quantum-mechanical operator $\hat{O}$. The average value of the observable for the pure state $|R\rangle$ is $\langle R|\hat{O}|R\rangle$, and hence the ensemble average of the observable for the statistical mixture specified by P_R is

$$\langle \hat{O}\rangle = \sum_R P_R \langle R|\hat{O}|R\rangle. \tag{4.212}$$

It will be assumed that P_R is a normalized probability distribution

$$\sum_R P_R = 1. \tag{4.213}$$

Eqn (4.212) is the basic expression that enables useful predictions to be made for known statistical mixtures of the radiation field. It is, however, convenient to cast eqn (4.212) into a different form, which is usually easier to work with and leads to more elegant expressions for the ensemble averages. Let $|S\rangle$ represent some complete set of states for the field considered, S being a label that can take a series of values. Then according to the closure theorem[18]

$$\sum_S |S\rangle\langle S| = 1. \tag{4.214}$$

Insertion of this unit quantity immediately after the operator $\hat{O}$ in eqn (4.212) gives

$$\begin{aligned}\langle \hat{O}\rangle &= \sum_R P_R \sum_S \langle R|\hat{O}|S\rangle\langle S|R\rangle \\ &= \sum_R\sum_S P_R \langle S|R\rangle\langle R|\hat{O}|S\rangle.\end{aligned} \tag{4.215}$$

The density operator $\hat{\rho}$ is defined to be[19]

$$\hat{\rho} = \sum_R P_R |R\rangle\langle R|, \tag{4.216}$$

and the average value of O from eqn (4.215) can be written

$$\langle\hat{O}\rangle = \sum_S \langle S|\hat{\rho}\hat{O}|S\rangle. \tag{4.217}$$

The density operator contains exactly the same information as the probability distribution P_R, and $\hat{\rho}$ is determined once the P_R are specified for a given set of pure states $|R\rangle$. The advantage of the density operator lies in the simplicity of the manipulations by which it produces average values of the various observables.

The general result (4.217) is independent of the particular complete set of states $|S\rangle$ chosen for the evaluation. This is apparent from the way in which the states $|S\rangle$ were introduced, but can also be proved directly. Let the $|T\rangle$ be some other complete set of states for the radiation field. Use of the closure theorem twice in eqn (4.217), both before and after the operator $\hat{\rho}\hat{O}$, gives

$$\langle\hat{O}\rangle = \sum_S\sum_T\sum_{T'} \langle S|T\rangle\langle T|\hat{\rho}\hat{O}|T'\rangle\langle T'|S\rangle, \tag{4.218}$$

where T and T' run over the same complete set of states. Rearrangement gives

$$\begin{aligned}\langle\hat{O}\rangle &= \sum_S\sum_T\sum_{T'} \langle T'|S\rangle\langle S|T\rangle\langle T|\hat{\rho}\hat{O}|T'\rangle \\ &= \sum_T \langle T|\hat{\rho}\hat{O}|T\rangle,\end{aligned} \tag{4.219}$$

where eqn (4.214) has been used and orthonormality of the $|T\rangle$ has been assumed.

Since $\langle\hat{O}\rangle$ is independent of the particular complete set of states used to evaluate the average, eqn (4.219) can be written

$$\langle\hat{O}\rangle = \mathrm{Trace}(\hat{\rho}\hat{O}), \tag{4.220}$$

where the trace of an operator (henceforth abbreviated to Tr) is the sum of its diagonal matrix elements for any complete set of states. This result is entirely equivalent to the basic expression (4.212).

The probability distribution P_R contains the physical information about the radiation field needed to evaluate the ensemble averages. It is important to choose carefully the particular complete set of pure states $|R\rangle$ to be used in defining the probability distribution. This choice must be made in such a way as to preserve all the available information about the state of the system, and the considerations involved are best appreciated by specific examples given later in the chapter.

It should be noted that the matrix elements of $\hat{\rho}$ itself have different properties for different complete sets of states. For the defining set $|R\rangle$ used in the construction of $\hat{\rho}$, only the diagonal matrix elements are non-zero,

$$\langle R'|\hat{\rho}|R''\rangle = \sum_R P_R\langle R'|R\rangle\langle R|R''\rangle = P_{R'}\,\delta_{R'R''}. \tag{4.221}$$

However, a typical matrix element for some other complete set of states is

$$\langle T|\hat{\rho}|T'\rangle = \sum_R P_R\langle T|R\rangle\langle R|T'\rangle, \tag{4.222}$$

and there are no general constraints on the $|T\rangle$ and $|T'\rangle$ for which the right-hand side is non-zero. The only general result is

$$\mathrm{Tr}(\hat{\rho}) = \sum_T \langle T|\hat{\rho}|T\rangle = \sum_R P_R = 1, \tag{4.223}$$

which can be regarded as a special case of eqn (4.220) with $\hat{O}$ a pure number. For any state of the radiation field, there is some complete set of states $|R\rangle$ for which the density operator has only diagonal matrix elements as in eqn (4.221). The result (2.73) is the analogue of eqn (4.223) for the atomic density operator of Chapter 2.

4.13. Density operators for pure states

A pure state can be regarded as a special case of a statistical mixture in which one of the probabilities P_R is equal to unity, and all the remaining P_R are zero. From eqn (4.216), the density operator is

$$\hat{\rho} = |R\rangle\langle R|. \tag{4.224}$$

The radiation field is definitely in a particular pure state $|R\rangle$ in this case, and the statistical description becomes somewhat redundant. However, the concept of the density operator remains valid for the pure state, and some of its simpler properties can be conveniently illustrated in this limit. One result that holds only for a pure-state density operator is

$$\hat{\rho}^2 = \hat{\rho}, \tag{4.225}$$

easily proved from eqn (4.224).

The density operators for the various types of single-mode pure state considered earlier in the chapter are easily constructed. For a field in one of the number states $|n\rangle$, where n photons are definitely present, the density operator is simply

$$\hat{\rho} = |n\rangle\langle n|. \tag{4.226}$$

The only non-vanishing matrix element for the number states is

$$\langle n|\hat{\rho}|n\rangle = 1, \tag{4.227}$$

and the average value of an observable represented by operator $\hat{O}$ according to eqn (4.220) is

$$\langle\hat{O}\rangle = \mathrm{Tr}(|n\rangle\langle n|\hat{O}) = \langle n|\hat{O}|n\rangle, \tag{4.228}$$

where the complete set of number states is used to evaluate the trace. The expression on the right of eqn (4.228) is the same as ordinarily used to compute an average value for state $|n\rangle$. The density-operator formalism leads to all the usual results for the special case of a pure state.

The density operator for one of the coherent states $|\alpha\rangle$ can be similarly constructed,

$$\hat{\rho} = |\alpha\rangle\langle\alpha|. \tag{4.229}$$

It is evident from the normalization of the coherent states as in eqn (4.183) that

$$\langle\alpha|\hat{\rho}|\alpha\rangle = 1, \tag{4.230}$$

analogous to the corresponding result (4.227) for the case of the number states. However, it follows that since different coherent states are not orthogonal, as shown by eqn (4.184), $\langle\alpha|\hat{\rho}|\alpha\rangle$ is not the only non-zero matrix element of $\hat{\rho}$ given by eqn (4.229). Indeed, every coherent-state matrix element of $\hat{\rho}$ is non-vanishing. This peculiar feature results from the over-completeness of the states $|\alpha\rangle$, mentioned earlier. Some of the normal theory of the density operator requires careful extension^{20} to cover the use of coherent states, and some of the associated theorems must be generalized. These extensions and generalizations are not required for the calculations to be given below, which mainly employ density operators expressed in terms of the number states $|n\rangle$.

Consider now a general matrix element of the pure coherent-state density operator of eqn (4.229) for the number states. We have

$$\langle n|\hat{\rho}|n'\rangle = \exp(-|\alpha|^2)\frac{\alpha^n\alpha^{*n'}}{(n!\,n'!)^{\frac{1}{2}}}, \tag{4.231}$$

where eqn (4.182) has been used. The density operator for the pure coherent state thus has non-vanishing off-diagonal matrix elements for the number states. This is an example of the importance of choosing the appropriate states $|R\rangle$ in which to express the density operator, so that no information about the state of the system is lost. It is not possible to describe the pure coherent state $|\alpha\rangle$ fully in terms of a diagonal density operator based on the number states $|n\rangle$; such a density operator would have zero off-diagonal matrix elements $\langle n|\hat{\rho}|n'\rangle$ and the information contained in eqn (4.231) for $n \neq n'$ could not be reproduced.

The off-diagonal matrix elements of the density operator are particularly important in the calculation of average values of operators $\hat{O}$ which themselves have non-zero off-diagonal matrix elements $\langle n|\hat{O}|n'\rangle$. Consider, for example, the single-mode electric-field operator given in eqn (4.149). The average electric field determined by eqn (4.220) with the trace evaluated in terms of the number states is

$$\begin{aligned}\langle\hat{E}\rangle &= \sum_n\langle n|\hat{\rho}\hat{E}|n\rangle\\ &= \mathrm{i}(\hbar\omega/2\epsilon_0V)^{\frac{1}{2}}\sum_n\{\langle n|\hat{\rho}|n-1\rangle n^{\frac{1}{2}}\exp(-\mathrm{i}\omega t+\mathrm{i}\mathbf{k}.\mathbf{r})\\ &\quad-\langle n|\hat{\rho}|n+1\rangle(n+1)^{\frac{1}{2}}\exp(\mathrm{i}\omega t-\mathrm{i}\mathbf{k}.\mathbf{r})\}.\end{aligned} \tag{4.232}$$

When n is replaced by $n+1$ in the first term of the large bracket, the average becomes

$$\langle\hat{E}\rangle = -2(\hbar\omega/2\epsilon_0V)^{\frac{1}{2}}\sum_n(n+1)^{\frac{1}{2}}\,\mathrm{Im}\{\langle n+1|\hat{\rho}|n\rangle\exp(-\mathrm{i}\omega t+\mathrm{i}\mathbf{k}.\mathbf{r})\}. \tag{4.233}$$

It is evident that a state of the radiation field can have a non-vanishing average electric vector only if the density operator has non-zero off-diagonal matrix elements of the type $\langle n+1|\hat{\rho}|n\rangle$. For the pure coherent state $|\alpha\rangle$, eqns (4.191) and (4.231) give

$$\langle n+1|\hat{\rho}|n\rangle = \exp(-|\alpha|^2+\mathrm{i}\theta)\frac{|\alpha|^{2n+1}}{n!\,(n+1)^{\frac{1}{2}}}, \tag{4.234}$$

and substitution into eqn (4.233) yields the same result as previously derived in eqn (4.205).

The diagonal number-state matrix element of the density operator, $\langle n|\hat{\rho}|n\rangle$, is the probability that n photons are excited in the state of the field described by $\hat{\rho}$. The diagonal matrix element for the pure coherent-state density operator obtained from eqn (4.231) reproduces the result (4.196) found earlier for the photon-number probability.

Pure states of the complete radiation field are treated in a similar manner. The state $|R\rangle$ in eqn (4.224) now represents all the modes of the cavity. If, for example, each cavity mode has a definite number of photons excited, the state $|R\rangle$ is one of the states $|\{n_{\mathbf{k}}\}\rangle$ defined in eqn (4.107) and the density operator is

$$\begin{aligned}\hat{\rho} &= |\{n_{\mathbf{k}}\}\rangle\langle\{n_{\mathbf{k}}\}|\\ &= |n_{\mathbf{k}_1}\rangle|n_{\mathbf{k}_2}\rangle|n_{\mathbf{k}_3}\rangle\ldots\langle n_{\mathbf{k}_3}|\langle n_{\mathbf{k}_2}|\langle n_{\mathbf{k}_1}|.\end{aligned} \tag{4.235}$$

Another example would be a state of the field in which each cavity mode is excited to a definite coherent state. The state of the total field in this case can be written

$$|\{\alpha_{\mathbf{k}}\}\rangle = |\alpha_{\mathbf{k}_1}\rangle|\alpha_{\mathbf{k}_2}\rangle|\alpha_{\mathbf{k}_3}\rangle\ldots, \tag{4.236}$$

and the corresponding density operator for the multimode coherent state is

$$\hat{\rho} = |\{\alpha_{\mathbf{k}}\}\rangle\langle\{\alpha_{\mathbf{k}}\}|. \tag{4.237}$$

Other pure states of the complete field are similarly treated. In each case, the matrix elements of $\hat{\rho}$ break up into products of matrix elements each of which refers to a single cavity mode, and no new physical principles are introduced by the generalization from one mode to many.

4.14. Statistical mixture states of the radiation field

The great utility of the density operator is made apparent in its application to the treatment of statistical-mixture states. As a first example, consider the thermal excitation of photons in a single mode of a cavity maintained at temperature T. This is the problem treated in Chapter 1 in the derivation of Planck's law, and the probability P_n that n photons are excited is given by eqns (1.23) and (1.26). Thus according to eqn (4.216) the density operator based on the number states is

$$\begin{aligned}\hat{\rho} &= \sum_n P_n|n\rangle\langle n| \\ &= \{1-\exp(-\hbar\omega/k_BT)\}\sum_n \exp(-n\hbar\omega/k_BT)|n\rangle\langle n|. \qquad (4.238)\end{aligned}$$

The number states $|n\rangle$ are the correct basis for the density operator in this case because the thermal probability distribution gives information only on the probabilities of finding a system in its various energy eigenstates; the number states are the energy eigenstates of the photon system.

The density operator for the thermal photon distribution has only diagonal number-state matrix elements and thus by eqn (4.233), which holds equally for pure states and statistical mixtures, the average electric field is always zero. The density operator can be written in an alternative form if the mean number $\bar{n}$ of thermally excited photons is introduced. According to eqn (4.220),

$$\bar{n} = \langle\hat{n}\rangle = \mathrm{Tr}(\hat{\rho}\hat{a}^{\dagger}\hat{a}). \qquad (4.239)$$

Problem 4.16. Use eqns (4.238) and (4.239) to evaluate the mean photon number $\bar{n}$ and show that the density operator can be re-expressed as

$$\hat{\rho} = \sum_n \frac{(\bar{n})^n}{(1+\bar{n})^{1+n}}|n\rangle\langle n|. \qquad (4.240)$$

Note that the calculation is algebraically similar to that of eqn (1.27).

Problem 4.17. Show that the density operator (4.238) for single-mode thermally excited light can be written in the equivalent form

$$\hat{\rho} = \{1-\exp(-\hbar\omega/k_BT)\}\exp(-\hbar\omega\hat{a}^{\dagger}\hat{a}/k_BT), \qquad (4.241)$$

where the exponential is defined by its usual power-series expansion.

Now consider the thermal excitation of all the cavity modes. The number states $|\{n_{\mathbf{k}}\}\rangle$ for the totality of modes are formed from products of number states for the individual cavity modes as in eqn (4.107). Since the different field modes are independent, the combined density operator is a product of the contributions of the different modes. Thus the density operator, expressed in general as

$$\hat{\rho} = \sum_{\{n_{\mathbf{k}}\}} P_{\{n_{\mathbf{k}}\}}|\{n_{\mathbf{k}}\}\rangle\langle\{n_{\mathbf{k}}\}|, \qquad (4.242)$$

is obtained for the thermal case by multiplying together the factors $(\bar{n}_{\mathbf{k}})^{n_{\mathbf{k}}}/(1+\bar{n}_{\mathbf{k}})^{1+n_{\mathbf{k}}}$ for all the modes, to obtain a grand probability

$$P_{\{n_{\mathbf{k}}\}} = \prod_{\mathbf{k}} \frac{(\bar{n}_{\mathbf{k}})^{n_{\mathbf{k}}}}{(1+\bar{n}_{\mathbf{k}})^{1+n_{\mathbf{k}}}}. \qquad (4.243)$$

In these expressions $\bar{n}_{\mathbf{k}}$ is the mean number of photons excited in mode $\mathbf{k}$, and the symbols $\{n_{\mathbf{k}}\}$ denote a set of numbers $n_{\mathbf{k}_1}, n_{\mathbf{k}_2}, n_{\mathbf{k}_3}, \ldots$, etc. of photons excited in every cavity mode. The summation in eqn (4.242) embraces every possible set of numbers $\{n_{\mathbf{k}}\}$.

The density operator for the radiation field in a thermal cavity obtained from eqns (4.242) and (4.243) is therefore

$$\hat{\rho} = \sum_{\{n_{\mathbf{k}}\}} |\{n_{\mathbf{k}}\}\rangle\langle\{n_{\mathbf{k}}\}| \prod_{\mathbf{k}} \frac{(\bar{n}_{\mathbf{k}})^{n_{\mathbf{k}}}}{(1+\bar{n}_{\mathbf{k}})^{1+n_{\mathbf{k}}}}. \qquad (4.244)$$

Problem 4.18. For the density operator given by eqn (4.244), prove the normalization requirement (4.223) explicitly,

$$\mathrm{Tr}(\hat{\rho}) = 1,$$

and show that the mean number of photons in the cavity is

$$\bar{n} = \sum_{\mathbf{k}} \bar{n}_{\mathbf{k}}. \qquad (4.245)$$

The mean photon numbers $\bar{n}_{\mathbf{k}}$ in eqn (4.244) are related to the mode frequency $\omega_{\mathbf{k}}$ and the temperature by eqn (1.28),

$$\bar{n}_{\mathbf{k}} = \{\exp(\hbar\omega_{\mathbf{k}}/k_BT)-1\}^{-1}. \qquad (4.246)$$

With this expression for the $\bar{n}_{\mathbf{k}}$, the density operator (4.244) contains essentially the same information as the results of the thermal probability calculation employed in the derivation of Planck's radiation law. However, eqn (4.244) applies not only to the thermal photon distribution but also to a wide range of excitations in which the statistical properties of the light generation are suitably random. For example, it is shown in §7.2 that the light generated by a source in which atoms are kept at an excitation level higher than that in thermal equilibrium has the same form of density operator as thermal radiation. This does not imply that the spectral distribution of the radiation is the same as that in thermal equilibrium and, of course, the mean photon numbers $\bar{n}_{\mathbf{k}}$ are not given by eqn (4.246) in this more general case, but are determined by the nature of the random field excitation.

The density operator (eqn (4.244)) applies in particular to the light beam emitted by a chaotic source and provides the tool by which the classical discussions of chaotic light given in Chapter 3 can be recast in quantum-mechanical form. For example, $\hat{\rho}$ in eqn (4.244) is the correct density operator for a beam of Lorentzian frequency distribution emitted by a chaotic source if the magnitude of $\bar{n}_{\mathbf{k}}\omega_{\mathbf{k}}$ is taken to have a Lorentzian dependence on $\omega_{\mathbf{k}}$.

It is clear from the above remarks that the density operator of eqn (4.244) for the complete radiation field has wide applicability for chaotic light. It is, of course, possible to set up density operators for total fields on the basis of other complete sets of states for the cavity modes, or on the basis of the overcomplete set $|\{\alpha_{\mathbf{k}}\}\rangle$ defined in eqn (4.236). However, the physical problems to be treated in subsequent chapters involve either multimode chaotic light, where eqn (4.244) is appropriate, or single-mode excitations, where the density operator simplifies, and we do not consider the other possible forms of density operator for the total field.

The single-mode density operator of eqn (4.240), for a random excitation of photons of the type associated with chaotic light, does not give any indication of the time-scale of the fluctuations in photon number. The quantum-mechanical averages, which can be obtained with the use of the density operator, are similar to the classical ensemble averages described in Chapter 3, and there are similar conditions on the type of measurement that must be carried out in order to make comparisons with the theoretical predictions. In general, the experimental averages must be computed from a series of measurements that extend over a time long compared to the fluctuation time, but each individual measurement must be completed in a time short compared to the period of the fluctuations.

Except in the case of a single-mode source, the frequency components in a light beam normally excite many cavity modes **k**. Thus, as mentioned above, the beam emitted by a Lorentzian chaotic source produces a degree of mode excitation determined by a Lorentzian dependence on the mode frequency. The mean photon numbers $\bar{n}_{\mathbf{k}}$ are therefore controlled by the linewidth parameter γ, and the multimode density operator (4.244) contains information on the coherence time τ_c $(= 1/\gamma)$ of the beam as a whole. In general, although the density operator for each individual mode of a cavity provides no information on the time dependence of the mode excitation, the multimode density operator for a beam whose frequency components spread across many modes does contain the magnitude of the coherence time of the beam.

Problem 4.19. Consider the quantum-mechanical analogues of the classical excitations of a pair of cavity modes envisaged in problems 3.2 and 3.3. If subscripts 1 and 2 denote the states of the modes, show that the quantum-mechanical excitation most closely analogous to that described classically by eqn (3.49) is a pure state with density operator

$$\hat{\rho} = |\alpha_1\rangle|\alpha_2\rangle\langle\alpha_2|\langle\alpha_1|. \tag{4.247}$$

Derive the relation between α_1, α_2 and the classical fields E_1 and E_2 such that the quantum field has eqn (3.49) as its classical limit.

For the random excitation of the modes described in problem 3.3 show that the quantum-mechanical density operator is

$$\hat{\rho} = \sum_{n_1=0}^{\infty}\sum_{n_2=0}^{\infty} |n_1\rangle|n_2\rangle\langle n_2|\langle n_1| \frac{(\bar{n})^{n_1+n_2}}{(1+\bar{n})^{2+n_1+n_2}}, \tag{4.248}$$

where $\bar{n}$ is the mean number of photons in each mode, and the validity of eqn (4.244) for any random excitation has been assumed.

References

1. JACKSON, J. D. (1975). *Classical electrodynamics*, Chapter 6. Wiley, New York.
2. REITZ, J. R., MILFORD, F. J., and CHRISTY, R. W. (1979). *Foundations of electromagnetic theory*, Chapter 16. Addison-Wesley, Reading, Massachusetts.
3. See, for example, MORSE, P. M. and FESHBACH, H. (1953). *Methods of theoretical physics*, p. 53. McGraw-Hill, New York.
4. BRILL, O. L. and GOODMAN, B. (1967). *Am. J. Phys.* **35**, 832.
5. See, for example, ANDERSON, E. E. (1971). *Modern physics and quantum mechanics*, Chapter 6. W. B. Saunders, Philadelphia.
6. POWER, E. A. (1964). *Introductory quantum electrodynamics*, Chapter 6. Longmans, London.
7. See, for example, LANDAU, L. D. and LIFSHITZ, E. M. (1960). *Electrodynamics of continuous media*, §90. Pergamon, Oxford; or Chapter 3 of ref. 6.
8. ARNOLD, W., HUNKLINGER, S., and DRANSFELD, K. (1979). *Phys. Rev.* **B19**, 6049.
9. SUSSKIND, L. and GLOGOWER, J. (1964). *Physics* **1**, 49.
10. See, for example, LANDAU, L. D. and LIFSHITZ, E. M. (1977). *Quantum mechanics*, p. 45. Pergamon, Oxford.
11. LOUISELL, W. H. (1963). *Phys. Lett.* **7**, 60.
12. CARRUTHERS, P. and NIETO, M. M. (1968). *Rev. Mod. Phys.* **40**, 411.
13. GLAUBER, R. J. (1963). *Phys. Rev.* **131**, 2766.
14. DAVYDOV, A. S. (1976). *Quantum mechanics*, p. 132. Pergamon, Oxford.
15. KITTEL, C. and KROEMER, H. (1980). *Thermal physics*, Appendix C, p. 453. W. H. Freeman, San Francisco.
16. CARRUTHERS, P. and NIETO, M. M. (1965). *Phys. Rev. Lett.* **14**, 387.
17. JACKIW, R. (1968). *J. Math. Phys.* **9**, 339.
18. See, for example, p. 223 of ref. 5; or p. 107 of ref. 14.
19. ZIMAN, J. M. (1969.) *Elements of advanced quantum theory*, p. 94. Cambridge University Press; LOUISELL, W. H. (1964). *Radiation and noise in quantum electronics*, Chapter 6. McGraw-Hill, New York.
20. See, for example, ref. 13; VINSON, J. F. (1969). *Cohérence optique, classique et quantique*, Part 2, Chapter 4. Dunod, Paris; and GLAUBER, R. J. (1970). In *Quantum optics* (eds. S. M. Kay and A. Maitland), p. 53. Academic Press, London.

5. Interaction of the quantized field with atoms

The discussion of the previous chapter is exclusively concerned with the properties of the free radiation field, that is, the field in a region of space where there is no matter to interact with the radiation. On the other hand, all experiments concerned with the generation and detection of light involve the interactions of electromagnetic waves with atoms. The semiclassical theory of Chapter 2 treats the coupling of quantum-mechanical atoms with the classical electromagnetic field. The purpose of the present chapter is the treatment of the coupling of atoms with the quantized radiation field.

All of the subsequent chapters in the book are concerned with aspects of the atom–radiation interaction, for example the calculation of the coherence properties of light emitted by different kinds of source, the measurement of coherence of light by excitation of atoms in the photoelectric effect, the scattering of light by atoms, and the study of higher-order processes in which two or more photons are simultaneously absorbed or emitted in a single nonlinear event. It is necessary to lay the groundwork for such calculations and much of the present chapter deals with the formal properties of the atom–radiation interaction and the basic techniques needed to treat the various processes. Some of the simpler effects are however considered here, and it is shown that the full quantum theory gives the same results as semiclassical theory for the rates of absorption and stimulated emission. It is also shown that the phenomenological Einstein theory of absorption and emission agrees with the full quantum theory.

The aim of much of the general theory given below is the provision of the most convenient expressions for the later applications to specific radiative processes. The quantum theory leads in most cases to remarkably simple and compact results for the physical quantities of interest.

5.1. Atomic multipole moments

It is convenient to approach the full quantum theory via a more complete discussion of the interaction of an atom with the classical electromagnetic field. Consider a neutral atom, as in Fig. 2.1, having a massive nucleus

essentially stationary at the origin of coordinates and electrons at positions $\mathbf{r}_j$. The charge and current densities of the atom are

$$\sigma(\mathbf{r}) = -\sum_j e\,\delta(\mathbf{r}-\mathbf{r}_j)+Ze\,\delta(\mathbf{r}) \tag{5.1}$$

and

$$\mathbf{J}(\mathbf{r}) = -\sum_j e\dot{\mathbf{r}}_j\,\delta(\mathbf{r}-\mathbf{r}_j). \tag{5.2}$$

The positions of the point charges are here specified by three-dimensional delta functions, that is, products of the three delta functions that specify the individual Cartesian coordinates of the charges. With the representation (2.64), we can write

$$\delta(\mathbf{r}-\mathbf{r}_j) = \frac{1}{(2\pi)^3}\int \exp\{i\mathbf{k}.(\mathbf{r}-\mathbf{r}_j)\}\,d\mathbf{k}, \tag{5.3}$$

where the integration runs over all of three-dimensional wavevector space.

If the Coulomb gauge, specified by eqn (4.14) is adopted, then the scalar potential is given by eqn (4.19) and on substitution of eqn (5.1), the integral can be performed to give

$$\phi(\mathbf{r}) = \frac{1}{4\pi\epsilon_0}\left\{-\sum_j\frac{e}{|\mathbf{r}-\mathbf{r}_j|}+\frac{Ze}{r}\right\}. \tag{5.4}$$

This is of course just the usual instantaneous Coulomb potential of the electrons and nucleus. The vector potential generated by the electron current could in principle be obtained by substitution of the transverse part of eqn (5.2) into the integral of eqn (4.29).

The interaction between the atom and the electromagnetic field is best treated in terms of the polarization $\mathbf{P}(\mathbf{r})$ and magnetization $\mathbf{M}(\mathbf{r})$ associated with the atomic charges. These quantities are determined by the charge and current densities via the usual relations[1]

$$\sigma(\mathbf{r}) = -\nabla.\mathbf{P}(\mathbf{r}) \tag{5.5}$$

$$\mathbf{J}(\mathbf{r}) = \dot{\mathbf{P}}(\mathbf{r})+\nabla\times\mathbf{M}(\mathbf{r}). \tag{5.6}$$

Note that there is some arbitrariness in the solutions for $\mathbf{P}(\mathbf{r})$ and $\mathbf{M}(\mathbf{r})$. Thus, since any vector field can be separated into transverse and longitudinal parts that satisfy eqns (4.21) and (4.22), it is clear that only the longitudinal part of $\mathbf{P}(\mathbf{r})$ is determined by eqn (5.5). By comparison with eqn (4.35)

$$\mathbf{P}_{\mathrm{L}}(\mathbf{r}) = -\epsilon_0\mathbf{E}_{\mathrm{L}}. \tag{5.7}$$

Furthermore, the longitudinal part of $\mathbf{M}(\mathbf{r})$ is not determined by eqn (5.6), and this equation is satisfied by a range of choices for the transverse parts of $\mathbf{P}(\mathbf{r})$ and $\mathbf{M}(\mathbf{r})$.

Problem 5.1. Prove that

$$\mathbf{P}(\mathbf{r}) = -e\sum_j \mathbf{r}_j \int_0^1 \delta(\mathbf{r}-\lambda\mathbf{r}_j)\,\mathrm{d}\lambda \tag{5.8}$$

and

$$\mathbf{M}(\mathbf{r}) = -e\sum_j \mathbf{r}_j\times\dot{\mathbf{r}}_j \int_0^1 \lambda\,\delta(\mathbf{r}-\lambda\mathbf{r}_j)\,\mathrm{d}\lambda \tag{5.9}$$

are solutions of eqns (5.5) and (5.6) for the charge and current densities (5.1) and (5.2).

The integral forms of solution[2] are convenient for the calculations that follow, and these choices lead to simple multipolar expansions of the interaction energy.

The potential energy of the atom in the transverse electric field $\mathbf{E}_\mathrm{T}(\mathbf{r})$ is simply

$$V_\mathrm{E} = -\int \mathbf{P}(\mathbf{r}).\mathbf{E}_\mathrm{T}(\mathbf{r})\,\mathrm{d}\mathbf{r} = e\sum_j \int_0^1 \mathbf{r}_j.\mathbf{E}_\mathrm{T}(\lambda\mathbf{r}_j)\,\mathrm{d}\lambda, \tag{5.10}$$

where eqn (5.8) has been used. As a consequence of a general theorem, only the transverse part of the polarization contributes to the integral.

Problem 5.2. If $\mathbf{V}(\mathbf{r})$ and $\mathbf{W}(\mathbf{r})$ are any vector fields, prove with the help of eqns (4.135) and (4.136) that

$$\int \mathbf{V}_\mathrm{T}(\mathbf{r}).\mathbf{W}_\mathrm{L}(\mathbf{r})\,\mathrm{d}\mathbf{r} = 0. \tag{5.11}$$

It is convenient in eqn (5.10) to insert the complete polarization vector even though its longitudinal part makes zero contribution. A Taylor expansion of the electric field vector gives

$$\begin{aligned} V_\mathrm{E} &= e\sum_j \int_0^1 \{1+\lambda\mathbf{r}_j.\nabla+(1/2!)(\lambda\mathbf{r}_j.\nabla)^2+\ldots\}\mathbf{r}_j.\mathbf{E}_\mathrm{T}(0)\,\mathrm{d}\lambda \\ &= e\sum_j \{1+(1/2!)\mathbf{r}_j.\nabla+(1/3!)(\mathbf{r}_j.\nabla)^2+\ldots\}\mathbf{r}_j.\mathbf{E}_\mathrm{T}(0). \end{aligned} \tag{5.12}$$

The gradient operator ∇ in these expressions acts only on the spatial coordinate of the transverse electric field, which is set equal to zero after the differentiations have been carried out.

The expansion (5.12) expresses the electrical potential energy in terms of the multipole moments of the atomic charge distribution. The first term is equivalent to the electric-dipole interaction assumed in eqn (2.18), with the atomic dipole moment

$$-e\mathbf{D} = -\sum_j e\mathbf{r}_j \tag{5.13}$$

as defined in eqn (2.17). The second term contains the product of the electric quadrupole moment

$$\mathbf{Q} = -\frac{1}{2}\sum_j e\mathbf{r}_j\mathbf{r}_j \tag{5.14}$$

with the electric field gradients. The subsequent terms are the contributions of the third- and higher-order multipoles.

The potential energy of the atom in the magnetic field $\mathbf{B}(\mathbf{r})$ is

$$V_\mathrm{M} = -\int \mathbf{M}(\mathbf{r}).\mathbf{B}(\mathbf{r})\,\mathrm{d}\mathbf{r} = e\sum_j \int_0^1 \lambda\mathbf{r}_j\times\dot{\mathbf{r}}_j.\mathbf{B}(\lambda\mathbf{r}_j)\,\mathrm{d}\lambda, \tag{5.15}$$

where eqn (5.9) has been used. The magnetic field is transverse, and only the transverse part of $\mathbf{M}(\mathbf{r})$ contributes in accordance with eqn (5.11). A Taylor expansion similar to that in eqn (5.12) gives

$$V_\mathrm{M} = \frac{e}{m}\sum_j \left\{\frac{1}{2!}+\frac{2}{3!}\mathbf{r}_j.\nabla+\frac{3}{4!}(\mathbf{r}_j.\nabla)^2+\ldots\right\}\mathbf{l}_j.\mathbf{B}(0), \tag{5.16}$$

where

$$\mathbf{l}_j = m\mathbf{r}_j\times\dot{\mathbf{r}}_j \tag{5.17}$$

is the angular momentum of electron j.

This expansion expresses the magnetic potential energy in terms of the magnetic multipole moments of the moving atomic charges. The first term is the energy of the magnetic dipole moment

$$-e\mathbf{D}_\mathrm{M} = -\frac{1}{2}\sum_j (e/m)\mathbf{l}_j \tag{5.18}$$

in the magnetic field $\mathbf{B}(0)$. The second term contains the product of the magnetic quadrupole moment

$$\mathbf{Q}_\mathrm{M} = -(2/3!)\sum_j (e/m)\mathbf{r}_j\mathbf{l}_j \tag{5.19}$$

with the magnetic field gradients. The subsequent terms represent the energies of the higher-order magnetic multipole moments.[3]

The above results refer to an atom whose nucleus lies at the origin of coordinates. For a nucleus located at a general position $\mathbf{R}$, the electron coordinates $\mathbf{r}_j$ are replaced by $\mathbf{r}_j-\mathbf{R}$ and the electric and magnetic fields are evaluated at position $\mathbf{R}$. Motion of the relatively massive nucleus produces a component $Ze\dot{\mathbf{R}}\,\delta(\mathbf{r}-\mathbf{R})$ in the current (5.2), but such contributions can be neglected for the phenomena to be treated here.

5.2. The multipolar interaction Hamiltonian

We now consider the interaction of the quantized radiation field with a quantum-mechanical atom. It might be expected that the quantum couplings of the atom to the electric and magnetic fields of the radiation could be cast in forms that parallel the classical interaction energies (5.10) and (5.15). This is indeed the case and we indicate in the present section how the quantum Hamiltonian is expressible in the multipolar form. The various forms of the interaction Hamiltonian have generated an interesting field of study.[2,4–6] Only an outline account is given here, and the interested reader can find more complete details in the references.

The quantum-mechanical Hamiltonian is obtained by the usual procedure[7] of quantizing the classical Hamiltonian, itself derived from the classical Lagrangian with the use of appropriate generalized coordinates and their conjugate momenta. It is well known[1] that the resulting Hamiltonian is similar to a sum of the uncoupled Hamiltonians of the atom and the fields except that the electron momentum must be replaced according to

$$\hat{\mathbf{p}}_j \rightarrow \hat{\mathbf{p}}_j + e\hat{\mathbf{A}}(\mathbf{r}_j). \tag{5.20}$$

The complete Hamiltonian in Coulomb gauge is thus

$$\hat{\mathscr{H}}' = (1/2m)\sum_j(\hat{\mathbf{p}}_j+e\hat{\mathbf{A}}(\mathbf{r}_j))^2+\frac{1}{2}\int\sigma(\mathbf{r})\phi(\mathbf{r})\,\mathrm{d}\mathbf{r}+\frac{1}{2}\int(\epsilon_0\hat{\mathbf{E}}_\mathrm{T}^2+\mu_0^{-1}\hat{\mathbf{B}}^2)\,\mathrm{d}\mathbf{r}. \tag{5.21}$$

The second term is the electrostatic energy of the various charges that constitute the atom, and it is verified by substitution of eqns (5.1) and (5.4) that it includes all the Coulomb interaction energies. It does indeed include the infinite self-energies of the Coulomb interactions of the charges with themselves, and these contributions must be removed from the Hamiltonian. The electrostatic energy can be written in a variety of forms,

$$\begin{aligned}\frac{1}{2}\int\sigma(\mathbf{r})\phi(\mathbf{r})\,\mathrm{d}\mathbf{r} &= -\frac{1}{2}\epsilon_0\int\phi\,\nabla^2\phi\,\mathrm{d}\mathbf{r} = \frac{1}{2}\epsilon_0\int(\boldsymbol{\nabla}\phi)^2\,\mathrm{d}\mathbf{r}\\ &= \frac{1}{2}\epsilon_0\int\mathbf{E}_\mathrm{L}^2\,\mathrm{d}\mathbf{r} = (1/2\epsilon_0)\int\mathbf{P}_\mathrm{L}^2\,\mathrm{d}\mathbf{r},\end{aligned} \tag{5.22}$$

where eqns (4.18), (4.34), and (5.7) have been used. This part of the Hamiltonian does not involve any quantum operators of the radiation field.

The form (5.21) is known as the minimal-coupling Hamiltonian. The interaction between the atom and the radiation is contained in the parts of the first term that involve the vector potential operator,

$$\hat{\mathscr{H}}'_\mathrm{I} = (e/m)\sum_j\hat{\mathbf{A}}(\mathbf{r}_j).\hat{\mathbf{p}}_j+(e^2/2m)\sum_j\hat{\mathbf{A}}(\mathbf{r}_j)^2. \tag{5.23}$$

This form is not convenient for calculations, since it is expressed in terms of the vector potential, which takes different values for different choices of gauge. Although exact calculations that use any correct form of the complete Hamiltonian should produce the same results, almost all practicable calculations are approximate and use of the minimal-coupling Hamiltonian can produce gauge-dependent results. Furthermore, the vector potential in eqn (5.23) is evaluated at the positions of all the electrons, and the expression does not take advantage of the smallness of the electromagnetic-field variations across the spatial extent of an atom, mentioned after eqn (2.16).

The Hamiltonian is converted to a more convenient form by a unitary transformation.[2,4,5] Define an operator

$$\hat{U} = \exp\left\{(i/\hbar)\int\mathbf{P}_\mathrm{T}(\mathbf{r}).\hat{\mathbf{A}}(\mathbf{r})\,\mathrm{d}\mathbf{r}\right\} \tag{5.24}$$

that is a function of the coordinates $\mathbf{r}_j$ of all the electrons and a functional of the vector potential. Since

$$\boldsymbol{\nabla}.\hat{\mathbf{A}}(\mathbf{r}) = 0, \tag{5.25}$$

and $\hat{\mathbf{A}}(\mathbf{r})$ is accordingly a transverse vector, the transverse part of the polarization in the integrand can be replaced by the complete expression (5.8) in view of eqn (5.11). Thus

$$\hat{U} = \exp\left\{-(ie/\hbar)\sum_j\int_0^1\mathbf{r}_j.\hat{\mathbf{A}}(\lambda\mathbf{r}_j)\,\mathrm{d}\lambda\right\}. \tag{5.26}$$

The transformed Hamiltonian is

$$\hat{\mathscr{H}} = \hat{U}^{-1}\hat{\mathscr{H}}'\hat{U}, \tag{5.27}$$

and the predictions that follow from the new Schrödinger equation are the same as from the original equation, the wavefunctions being transformed from ψ' to

$$\psi = \hat{U}^{-1}\psi'. \tag{5.28}$$

The transformation (5.27) is applied term-by-term to the Hamiltonian (5.21). The transformation of the first term is controlled by the commutation properties of $\hat{U}$ with the electron momentum operators, represented by $-i\hbar\boldsymbol{\nabla}_j$, where $\boldsymbol{\nabla}_j$ is the gradient operator in the coordinates of electron j. Thus with the use of eqn (5.26)

$$\hat{U}^{-1}(\hat{\mathbf{p}}_j+e\hat{\mathbf{A}}(\mathbf{r}_j))\hat{U} = \hat{\mathbf{p}}_j-e\,\nabla_j\int_0^1\mathbf{r}_j\cdot\hat{\mathbf{A}}(\lambda\mathbf{r}_j)\,\mathrm{d}\lambda+e\hat{\mathbf{A}}(\mathbf{r}_j). \tag{5.29}$$

It is not difficult to verify, by an expansion of the integrand similar to that in eqn (5.12), that

$$\hat{\mathbf{A}}(\mathbf{r}_j) = \int_0^1(1+\mathbf{r}_j\cdot\nabla_j)\hat{\mathbf{A}}(\lambda\mathbf{r}_j)\,\mathrm{d}\lambda \tag{5.30}$$

reproduces the standard Taylor expansion of the vector potential about the origin. Substitution of this expression into the final term converts the right-hand side of eqn (5.29) to

$$\hat{\mathbf{p}}_j-e\int_0^1\{\nabla_j(\mathbf{r}_j\cdot\hat{\mathbf{A}}(\lambda\mathbf{r}_j))-(1+\mathbf{r}_j\cdot\nabla_j)\hat{\mathbf{A}}(\lambda\mathbf{r}_j)\}\,\mathrm{d}\lambda. \tag{5.31}$$

The integrand is simplified by use of the magnetic-field relation

$$\nabla_j\times\hat{\mathbf{A}}(\lambda\mathbf{r}_j) = \lambda\hat{\mathbf{B}}(\lambda\mathbf{r}_j) \tag{5.32}$$

obtained from the operator form of eqn (4.5), and it is easily verified that eqn (5.31) can be written in the final form

$$\hat{U}^{-1}(\hat{\mathbf{p}}_j+e\hat{\mathbf{A}}(\mathbf{r}_j))\hat{U} = \hat{\mathbf{p}}_j-e\int_0^1\lambda\mathbf{r}_j\times\hat{\mathbf{B}}(\lambda\mathbf{r}_j)\,\mathrm{d}\lambda. \tag{5.33}$$

The vector potential has thus been removed in favour of the magnetic field operator.

The second term in the Hamiltonian (5.21), representing the Coulomb energies of the charges, is unaffected by the transformation (5.27). The transformation of the final term is controlled by the commutation properties of the electric and magnetic field operators with the vector potential that occurs in $\hat{U}$. The magnetic field commutes with the vector potential, as in eqn (4.140), and the magnetic contribution to the field energy is unchanged. The change in the electric contribution is obtained with the help of the commutation property (4.139).

Problem 5.3. Prove that

$$\hat{U}^{-1}\hat{\mathbf{E}}_{\mathrm{T}}(\mathbf{r})\hat{U} = \hat{\mathbf{E}}_{\mathrm{T}}(\mathbf{r})-(1/\epsilon_0)\mathbf{P}_{\mathrm{T}}(\mathbf{r}). \tag{5.34}$$

This quantity replaces the electric-field operator in the final term of eqn (5.21).

The complete transformed Hamiltonian (5.27) obtained from eqn (5.21) with the help of eqns. (5.10), (5.33) and (5.34) is

$$\begin{aligned}\mathscr{H} = {} & (1/2m)\sum_j\left\{\hat{\mathbf{p}}_j-e\int_0^1\lambda\mathbf{r}_j\times\hat{\mathbf{B}}(\lambda\mathbf{r}_j)\,\mathrm{d}\lambda\right\}^2\\ & +\frac{1}{2}\int\sigma(\mathbf{r})\phi(\mathbf{r})\,\mathrm{d}\mathbf{r}+\frac{1}{2}\int(\epsilon_0\hat{\mathbf{E}}_{\mathrm{T}}^2+\mu_0^{-1}\hat{\mathbf{B}}^2)\,\mathrm{d}\mathbf{r}\\ & +e\sum_j\int_0^1\mathbf{r}_j\cdot\hat{\mathbf{E}}_{\mathrm{T}}(\lambda\mathbf{r}_j)\,\mathrm{d}\lambda+(1/2\epsilon_0)\int\mathbf{P}_{\mathrm{T}}(\mathbf{r})^2\,\mathrm{d}\mathbf{r}.\end{aligned} \tag{5.35}$$

The removal of the vector potential from the minimal-coupling form of the Hamiltonian has thus been accomplished. The form (5.35) contains instead the electric and magnetic field operators, and when the λ integrals are expanded, as in eqns (5.12) and (5.16), these terms involve only the field operators and their gradients evaluated at the atomic nucleus. The quantum analogue of the electric multipolar energy (5.10) appears explicitly, and a quantum version of the magnetic multipolar energy (5.15) appears on multiplying out the square in the first term of eqn (5.35). The final term is a function only of the atomic variables; it produces changes in the atomic energy levels but does not contribute to the atom-field interactions.

The unitary transformation of eqns (5.24) and (5.27) is one of several methods for converting the minimal-coupling form of the Hamiltonian to the multipolar form. In addition there are several other forms of the same basic Hamiltonian that may be useful in specific applications.[6] Even if attention is restricted to the multipolar form (5.35), there are some subtleties in the physical significances of the field operators that appear. Thus it can be shown that $\hat{\mathbf{E}}_{\mathrm{T}}$, which started life as an electric field operator, now has more the significance of an electrical displacement operator. However, its representation (4.111) and (4.113) in terms of photon creation and destruction operators remains valid, and the third term in eqn (5.35), similar to eqn (4.121), continues to represent the field energy. We continue to refer to $\hat{\mathbf{E}}_{\mathrm{T}}$ as the electric field operator; a fuller account of its properties, and of the forms of the Hamiltonian in general, must be sought in the literature.[2,4-6]

5.3. The electric-dipole approximation

The electronic coordinates $\mathbf{r}_j$ have magnitudes of the order of the Bohr radius a_0. The gradient operator ∇ has a magnitude of the order of the radiation wavevector k when it operates on $\hat{\mathbf{E}}_{\mathrm{T}}$ or $\hat{\mathbf{B}}$. It is clear from eqn (2.16) that successive terms in the expansions of the λ integrals in the multipolar Hamiltonian diminish rapidly.

We retain only the first term, $-e\mathbf{r}_j \times \hat{\mathbf{B}}(0)$, in the expansion of the $\hat{\mathbf{B}}(\lambda\mathbf{r}_j)$ integral of eqn (5.35), but the first two terms in the expansion (5.12) of the $\hat{\mathbf{E}}_{\mathrm{T}}(\lambda\mathbf{r}_j)$ integral. We neglect the final term until §5.12, where its effect is briefly discussed. The Hamiltonian can then be written

$$\hat{\mathscr{H}} = \hat{\mathscr{H}}_{\mathrm{E}}+\hat{\mathscr{H}}_{\mathrm{R}}+\hat{\mathscr{H}}_{\mathrm{I}}, \tag{5.36}$$

where $\hat{\mathscr{H}}_{\mathrm{E}}$ is the Hamiltonian of the isolated atom in the same notation as used in Chapter 2,

$$\hat{\mathscr{H}}_{\mathrm{E}} = \sum_j(\hat{p}_j^2/2m)+\frac{1}{2}\int\sigma(\mathbf{r})\phi(\mathbf{r})\,\mathrm{d}\mathbf{r}, \tag{5.37}$$

and $\hat{\mathscr{H}}_{\mathrm{R}}$ is the radiation-field Hamiltonian,

$$\hat{\mathscr{H}}_{\mathrm{R}} = \frac{1}{2}\int(\epsilon_0\hat{\mathbf{E}}_{\mathrm{T}}^2+\mu_0^{-1}\hat{\mathbf{B}}^2)\,\mathrm{d}\mathbf{r}. \tag{5.38}$$

The Hamiltonian $\hat{\mathscr{H}}_{\mathrm{I}}$ for the interaction of the atom with the radiation field contains four contributions

$$\hat{\mathscr{H}}_{\mathrm{I}} = \hat{\mathscr{H}}_{\mathrm{ED}}+\hat{\mathscr{H}}_{\mathrm{EQ}}+\hat{\mathscr{H}}_{\mathrm{MD}}+\hat{\mathscr{H}}_{\mathrm{NL}}, \tag{5.39}$$

the terms on the right being the electric-dipole interaction

$$\hat{\mathscr{H}}_{\mathrm{ED}} = e\sum_j\mathbf{r}_j.\hat{\mathbf{E}}_{\mathrm{T}}(0) = e\mathbf{D}.\hat{\mathbf{E}}_{\mathrm{T}}(0), \tag{5.40}$$

the electric-quadrupole interaction

$$\hat{\mathscr{H}}_{\mathrm{EQ}} = \frac{1}{2}e\sum_j(\mathbf{r}_j.\nabla)(\mathbf{r}_j.\hat{\mathbf{E}}_{\mathrm{T}}(0)) = -\nabla.\mathbf{Q}.\hat{\mathbf{E}}_{\mathrm{T}}(0), \tag{5.41}$$

and the magnetic-dipole interaction

$$\hat{\mathscr{H}}_{\mathrm{MD}} = -(e/4m)\sum_j\{\hat{\mathbf{p}}_j.\mathbf{r}_j\times\hat{\mathbf{B}}(0)+\mathbf{r}_j\times\hat{\mathbf{B}}(0).\hat{\mathbf{p}}_j\}. \tag{5.42}$$

However, it is not difficult to prove that

$$\hat{\mathbf{p}}_j.\mathbf{r}_j\times\hat{\mathbf{B}}(0) = \mathbf{r}_j\times\hat{\mathbf{B}}(0).\hat{\mathbf{p}}_j, \tag{5.43}$$

and this term can be written

$$\hat{\mathscr{H}}_{\mathrm{MD}} = (e/2m)\hat{\mathbf{M}}.\hat{\mathbf{B}}(0), \tag{5.44}$$

where

$$\hat{\mathbf{M}} = \sum_j\hat{\mathbf{l}}_j = \sum_j\mathbf{r}_j\times\hat{\mathbf{p}}_j \tag{5.45}$$

is the sum of the electronic angular momentum operators, analogous to the angular momenta (5.17), except that $\hat{\mathbf{p}}_j$ now replaces $m\dot{\mathbf{r}}_j$.

The final term in the interaction Hamiltonian (5.39), sometimes called the diamagnetic term, is nonlinear since it includes the square of the magnetic vector,

$$\hat{\mathscr{H}}_{\mathrm{NL}} = (e^2/8m)\sum_j(\mathbf{r}_j\times\hat{\mathbf{B}}(0))^2. \tag{5.46}$$

We ignore this term for the present, but consider it further in §§8.6 and 9.1, where it is shown to be negligible even for those nonlinear radiative processes where its contribution does not vanish.

The orders of magnitude of the three linear interaction Hamiltonians can be compared by means of rough estimates of the quantities involved. We take $\mathbf{r}_j$ to be of the order of the Bohr radius a_0 given in eqn (2.15), $\hat{\mathbf{M}}$ to have magnitude $\hbar$, $\nabla\mathbf{E}_{\mathrm{T}}(0)$ to have magnitude $kE_{\mathrm{T}}(0)$ or equivalently $(\omega/c)E_{\mathrm{T}}(0)$, and we take ω to be of the order of the atomic transition frequency ω_0 given in eqn (2.28). Thus,

$$\hat{\mathscr{H}}_{\mathrm{ED}} \sim E_{\mathrm{T}}(0)4\pi\epsilon_0\hbar^2/me,$$

$$\hat{\mathscr{H}}_{\mathrm{EQ}} \sim E_{\mathrm{T}}(0)3e\hbar/16mc,$$

and

$$\hat{\mathscr{H}}_{\mathrm{MD}} \sim B(0)e\hbar/2m \sim E_{\mathrm{T}}(0)e\hbar/2mc. \tag{5.47}$$

It is seen that the electric-quadrupole and magnetic-dipole interactions have the same magnitude, but are smaller than the electric-dipole interaction by the order of a dimensionless factor

$$e^2/4\pi\epsilon_0\hbar c \approx 1/137, \tag{5.48}$$

known as the fine structure constant. Terms of higher order in $\mathbf{r}_j.\nabla$ in the expansion of the λ integrals in eqn (5.35), which have been neglected in eqn (5.39), are smaller than $\hat{\mathscr{H}}_{\mathrm{ED}}$ by a quantity of the second or some higher order in the fine structure constant.

As discussed in Chapter 2, and again in §5.5 below, the rate at which radiation is absorbed or emitted by an atomic transition between states ψ_1 and ψ_2 is proportional to the square of the matrix element $\langle\psi_1|\hat{\mathscr{H}}_{\mathrm{I}}|\psi_2\rangle$. The above discussion shows that if $\langle\psi_1|\hat{\mathscr{H}}_{\mathrm{ED}}|\psi_2\rangle$ is non-zero, the contributions of the remaining terms in the expansion of $\hat{\mathscr{H}}_{\mathrm{I}}$ in eqn (5.39) can certainly be neglected. The neglect of all terms except $\hat{\mathscr{H}}_{\mathrm{ED}}$ is equivalent to the assumption of a zero wavevector for the radiation, and is known as the electric-dipole approximation. The calculation of Chapter 2 made this approximation since the spatial variation of the electric vector of the radiation was there ignored.

Most of the strong absorption and emission lines of atoms in the visible region of the spectrum are associated with atomic transitions for which the electric-dipole interaction matrix element is non-vanishing. Such transitions are said to be electric-dipole allowed. The interactions $\hat{\mathscr{H}}_{\mathrm{EQ}}$ and $\hat{\mathscr{H}}_{\mathrm{MD}}$ may be important when $\langle\psi_1|\hat{\mathscr{H}}_{\mathrm{ED}}|\psi_2\rangle = 0$, and the transition is electric-dipole forbidden. The transition may still lead to observable absorption and emission if $\langle\psi_1|\hat{\mathscr{H}}_{\mathrm{EQ}}|\psi_2\rangle$ or $\langle\psi_1|\hat{\mathscr{H}}_{\mathrm{MD}}|\psi_2\rangle$ is non-zero, when the transition is said to be electric-quadrupole allowed or magnetic-dipole allowed, respectively.

The general rules that describe the conditions under which the various types of transition are allowed or forbidden are discussed in detail in books on atomic spectra.[8] We note here only the simplest type of selection rule which follows from parity considerations. The electron coordinates $\mathbf{r}_j$ have odd parity. Thus $\mathbf{D}$ and $\hat{\mathscr{H}}_{\mathrm{ED}}$ change sign when the inversion operation is applied to the $\mathbf{r}_j$. It follows that $\langle\psi_1|\hat{\mathscr{H}}_{\mathrm{ED}}|\psi_2\rangle$ can be non-zero only if ψ_1 and ψ_2 are wavefuctions of opposite parity, as mentioned in Chapter 2. On the other hand $\mathbf{Q}$ and $\mathbf{M}$ have even parity and the matrix elements of $\hat{\mathscr{H}}_{\mathrm{EQ}}$ and $\hat{\mathscr{H}}_{\mathrm{MD}}$ can be non-zero only for wavefunctions ψ_1 and ψ_2 that have the same parity.

We shall be concerned in all subsequent calculations with atomic transitions that are assumed to be electric-dipole allowed, although in most cases it would not be difficult to replace $\hat{\mathscr{H}}_{\mathrm{ED}}$ by $\hat{\mathscr{H}}_{\mathrm{EQ}}$ or $\hat{\mathscr{H}}_{\mathrm{MD}}$. In the electric-dipole approximation, the rigorous calculations of the present chapter show that the Hamiltonian for the interaction of the radiation field with an atom is the same as that derived in Chapter 2 on the basis of simple potential-energy considerations.

5.4. Second quantization of the atomic Hamiltonian

The radiative parts of the Hamiltonian of eqn (5.36) can be expressed in terms of the photon creation and destruction operators if the results of Chapter 4 are used to replace the field operators $\hat{\mathbf{E}}_{\mathrm{T}}(0)$ and $\hat{\mathbf{B}}(0)$. It is convenient to introduce creation and destruction operators for the atomic part of the Hamiltonian also. The entire Hamiltonian can then be expressed as products of algebraic magnitudes with creation and destruction operators. In this form it is particularly easy to apply the theory to complicated radiative processes where multiple interactions of light and atoms occur.

Consider the atomic Hamiltonian $\hat{\mathscr{H}}_{\mathrm{E}}$ of eqn (5.37), and let $|i\rangle$ be an energy eigenstate with eigenvalue $\hbar\omega_i$,

$$\hat{\mathscr{H}}_{\mathrm{E}}|i\rangle = \hbar\omega_i|i\rangle. \tag{5.49}$$

According to the closure theorem, similar to eqn (4.214),

$$\sum_i |i\rangle\langle i| = 1, \tag{5.50}$$

where the sum runs over all the eigenstates of $\hat{\mathscr{H}}_{\mathrm{E}}$, both bound and free. Use of the closure theorem twice establishes the identity.

$$\hat{\mathscr{H}}_{\mathrm{E}} = \sum_i |i\rangle\langle i|\hat{\mathscr{H}}_{\mathrm{E}}\sum_j |j\rangle\langle j|. \tag{5.51}$$

However, it follows from eqn (5.49) and the orthonormality of the energy eigenstates that

$$\langle i|\hat{\mathscr{H}}_{\mathrm{E}}|j\rangle = \hbar\omega_i\,\delta_{ij}, \tag{5.52}$$

and eqn (5.51) reduces to

$$\hat{\mathscr{H}}_{\mathrm{E}} = \sum_i \hbar\omega_i|i\rangle\langle i|. \tag{5.53}$$

The transformation to this form is known as second quantization of the Hamiltonian. In this terminology, the normal quantum-mechanical procedure for determining the energy eigenstates and eigenvalues is regarded as first quantization of the motion of the atomic electrons. In second quantization, the Hamiltonian is expressed in terms of the solutions of the energy eigenvalue problem, assumed to have been determined. The second-quantized Hamiltonian is a useful form for calculations where the atom interacts with some other physical system, such as the radiation field.

Now consider the effect of a general combination $|i\rangle\langle j|$ applied to some atomic eigenstate $|l\rangle$. Since the atomic eigenstates are orthonormal,

$$|i\rangle\langle j|\,l\rangle = |i\rangle\,\delta_{jl}. \tag{5.54}$$

Thus, $|i\rangle\langle j|$ applied to an atomic eigenstate $|l\rangle$ changes the state to $|i\rangle$ if the original state is $|j\rangle$, but gives zero otherwise. In other words, $|i\rangle\langle j|$ is an operator whose application to an atom in state $|j\rangle$ removes it from that state and puts it into state $|i\rangle$. We can say that $|i\rangle\langle j|$ destroys atomic state $|j\rangle$ and creates atomic state $|i\rangle$. Note that electrons cannot be created or destroyed in interactions that take place at photon energies in the visible region of the spectrum, but can only be shifted from one state to another. The atomic operators thus occur in creation–destruction pairs.

It remains to express the interaction Hamiltonian $\hat{\mathscr{H}}_{\mathrm{ED}}$ in terms of the electronic creation and destruction operators. According to eqn (5.40) the electronic coordinates enter $\hat{\mathscr{H}}_{\mathrm{ED}}$ only in the vector quantity $\mathbf{D}$, defined as the sum of the radius vectors of all the atomic electrons. Use of the closure theorem of eqn (5.50) twice establishes the identity

$$\begin{aligned}\mathbf{D} &= \sum_i |i\rangle\langle i|\mathbf{D}\sum_j |j\rangle\langle j| \\ &= \sum_{i,j} \mathbf{D}_{ij}|i\rangle\langle j|,\end{aligned} \tag{5.55}$$

where

$$\mathbf{D}_{ij} = \langle i|\mathbf{D}|j\rangle. \tag{5.56}$$

The result (5.53) for the second-quantized Hamiltonian is a special case of the more general expression (5.55) which occurs when the operator is not diagonal in the energy eigenstates.

The electric-dipole interaction of eqn (5.40) is now second-quantized by substitution of eqn (5.55) for $\mathbf{D}$ and insertion of $\hat{\mathbf{E}}_{\mathrm{T}}(0)$ from eqns (4.111) and

(4.113). However, for slightly greater generality we take the atomic nucleus to be placed at position **R** rather than at the origin of coordinates. The electric-dipole interaction is then

$$\hat{\mathscr{H}}_{\mathrm{ED}} = \mathrm{i}e\sum_{\mathbf{k}}\sum_{i,j}(\hbar\omega_{\mathbf{k}}/2\epsilon_0 V)^{\frac{1}{2}}\boldsymbol{\varepsilon}_{\mathbf{k}}.\mathbf{D}_{ij}$$
$$\times\{\hat{a}_{\mathbf{k}}\exp(-\mathrm{i}\omega_{\mathbf{k}}t+\mathrm{i}\mathbf{k}.\mathbf{R})-\hat{a}^{\dagger}_{\mathbf{k}}\exp(\mathrm{i}\omega_{\mathbf{k}}t-\mathrm{i}\mathbf{k}.\mathbf{R})\}|i\rangle\langle j|. \quad (5.57)$$

The electric-quadrupole and magnetic-dipole interactions can be second-quantized by a similar procedure, but we do not give any explicit results for these terms in the Hamiltonian, concerning ourselves only with electric-dipole allowed transitions.

The complete Hamiltonian for the atom–radiation system is now in second-quantized notation. All the operator properties of the Hamiltonian are contained in the creation and destruction operator factors, and the remaining factors are ordinary numbers, variables, or vector quantities.

It is often necessary to consider the part of the electric-dipole Hamiltonian that refers to a particular pair of atomic states, $|1\rangle$ and $|2\rangle$ say, with energies $\hbar\omega_1$ and $\hbar\omega_2$. It is assumed henceforth that the wavefunctions ψ_1 and ψ_2 are real so that $\mathbf{D}_{21}$ and $\mathbf{D}_{12}$ are equal real vectors. The relevant part of eqn (5.57), obtained from the terms with either i or j equal to 1 or 2, is then

$$\mathrm{i}\sum_{\mathbf{k}}\hbar g_{\mathbf{k}}\{\hat{a}_{\mathbf{k}}\exp(-\mathrm{i}\omega_{\mathbf{k}}t+\mathrm{i}\mathbf{k}.\mathbf{R})-\hat{a}^{\dagger}_{\mathbf{k}}\exp(\mathrm{i}\omega_{\mathbf{k}}t-\mathrm{i}\mathbf{k}.\mathbf{R})\}(|1\rangle\langle 2|+|2\rangle\langle 1|), \quad (5.58)$$

where

$$g_{\mathbf{k}} = e(\omega_{\mathbf{k}}/2\epsilon_0\hbar V)^{\frac{1}{2}}\boldsymbol{\varepsilon}_{\mathbf{k}}.\mathbf{D}_{12}. \quad (5.59)$$

The terms in eqn (5.57) with $i = j$ all vanish, as discussed in connection with eqn (2.19), because they involve diagonal matrix elements of the odd-parity operator **D**.

It is convenient to use a pictorial representation of the various kinds of interaction process included in $\hat{\mathscr{H}}_{\mathrm{ED}}$. When the brackets in eqn (5.58) are multiplied out, there are four distinct terms, each of which produces a definite final state of the atom-radiation system when applied to an appropriate initial state. These four types of term can be represented by the diagrams of Fig. 5.1. The initial state is represented on the right of each diagram, and the final state into which $\hat{\mathscr{H}}_{\mathrm{ED}}$ converts it is represented on the left.

Let us suppose that state $|2\rangle$ has higher energy than state $|1\rangle$, $\hbar\omega_2 > \hbar\omega_1$. In Fig. 5.1 the absorption of a photon **k** accompanied by excitation of the atom from state $|1\rangle$ to state $|2\rangle$ is represented by diagram (b), while the inverse process of photon emission corresponds to diagram (c). The events represented by the first and fourth diagrams do not correspond to allowed absorption and emission processes since it is not possible for the final state to have the same energy as the initial state. Neglect of these contributions corresponds to the same rotating-wave approximation as made in the treatment of absorption and emission processes in Chapter 2. It is shown in Chapters 8 and 9 that non-energy conserving terms in $\hat{\mathscr{H}}_{\mathrm{ED}}$ contribute to higher-order radiative processes where energy is conserved in the final state but not in some of the intermediate states.

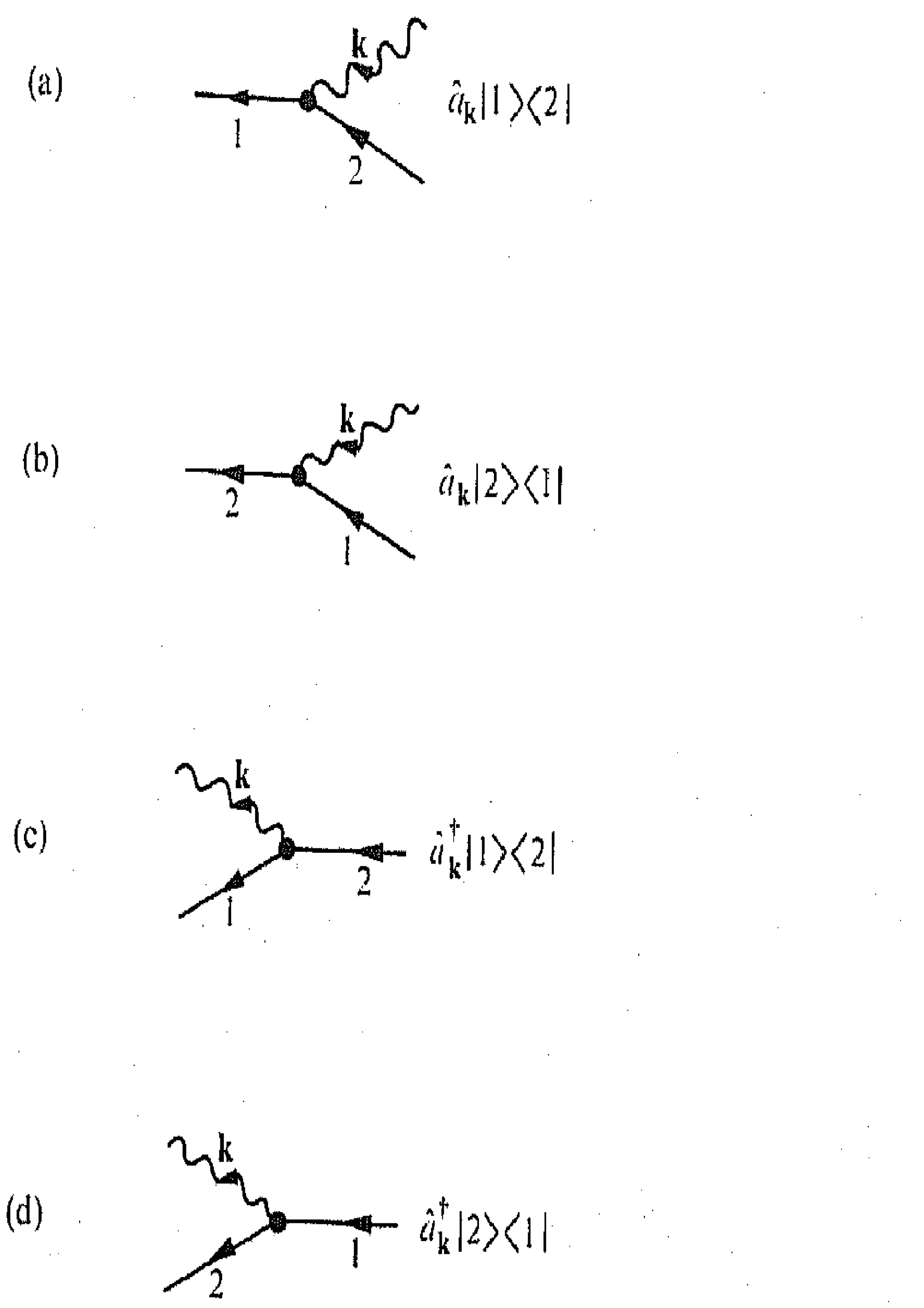
(a)
k
1
2
$\hat{a}_{\mathbf{k}}|1\rangle\langle 2|$
(b)
k
2
1
$\hat{a}_{\mathbf{k}}|2\rangle\langle 1|$
(c)
k
2
1
$\hat{a}^{\dagger}_{\mathbf{k}}|1\rangle\langle 2|$
(d)
k
1
2
$\hat{a}^{\dagger}_{\mathbf{k}}|2\rangle\langle 1|$

FIG. 5.1. Diagrammatic representations of the four kinds of term in the electric-dipole interaction. The wavy lines represent photons and the straight lines atomic states. A line whose arrow is directed towards (away from) the interaction point corresponds to a photon or atomic state that is destroyed (created) in the interaction.

5.5. Photon absorption and emission rates

As a first application of the second-quantized interaction Hamiltonian, we use it to calculate the rates of emission and absorption of photons by an atom that can make transitions between states $|1\rangle$ and $|2\rangle$. The problem is the same as that treated by semiclassical radiation theory in Chapter 2. However, the latter theory is incapable of treating spontaneous emission in a rigorous manner and the radiative lifetime of an atom was derived in eqn (2.56) via the relations between the Einstein A and B coefficients. The direct calculation carried out below includes spontaneous emission automatically and provides a rigorous justification of the phenomenological Einstein theory.

Let us denote by $|n_{\mathbf{k}}, 1\rangle$ a state of the combined atom–radiation system, where $n_{\mathbf{k}}$ photons are present in mode **k** and the atom is in state $|1\rangle$. A similar notation is used for the other combination states. It is a simple matter to write down the matrix elements of $\mathscr{H}_{\mathrm{ED}}$ for the photon absorption and emission processes of diagrams (b) and (c) in Fig. 5.1. The matrix element for photon absorption is

$$\langle n_{\mathbf{k}}-1, 2|\hat{\mathscr{H}}_{\mathrm{ED}}|n_{\mathbf{k}}, 1\rangle = i\hbar g_{\mathbf{k}} \exp(-i\omega_{\mathbf{k}}t+i\mathbf{k}.\mathbf{R})n_{\mathbf{k}}^{\frac{1}{2}}, \tag{5.60}$$

while for emission

$$\langle n_{\mathbf{k}}+1, 1|\hat{\mathscr{H}}_{\mathrm{ED}}|n_{\mathbf{k}}, 2\rangle = -i\hbar g_{\mathbf{k}} \exp(i\omega_{\mathbf{k}}t-i\mathbf{k}.\mathbf{R})(n_{\mathbf{k}}+1)^{\frac{1}{2}}, \tag{5.61}$$

where eqns (4.103), (4.104), and (5.54) have been used. In working with second-quantized interaction Hamiltonians it is essential for the initial state of the system to be on the right of all matrix elements, and the final state on the left.

The above matrix elements can be used to calculate the transition rates for absorption and emission of photons with the use of time-dependent perturbation theory. Consider the absorption process first. At time $t = 0$ we suppose the atom to be in its lower state $|1\rangle$ with a beam of photons of wavevector **k** incident. The probability that the atom has been excited into state $|2\rangle$ at a later time t is equal to $|C_2(t)|^2$ in the notation of Chapter 2. According to eqn (2.70)

$$|C_2(t)|^2 = (\pi|\mathscr{V}|^2t/2)\delta(\omega_0-\omega), \tag{5.62}$$

where

$$\omega_0 = \omega_2-\omega_1, \tag{5.63}$$

and the transition matrix element that leads to this result is

$$(\hbar\mathscr{V}/2)\exp(-i\omega t), \tag{5.64}$$

the $\exp(i\omega t)$ term in the $\cos\omega t$ dependence of the matrix element having been shown to produce a negligible effect in the discussion that follows eqn (2.40).

These results from Chapter 2 can be used to calculate the absorption rate in the quantized field formulation of the problem. The matrix element shown in eqn (5.60) has the same form of time dependence as the semiclassical matrix element of eqn (5.64), and the transition rate expression (5.62) is transcribed by replacement of $\frac{1}{2}\mathscr{V}$ by $ig_{\mathbf{k}}n_{\mathbf{k}}^{\frac{1}{2}}$, and ω by $\omega_{\mathbf{k}}$, to give

$$|C_2(t)|^2 = 2\pi g_{\mathbf{k}}^2 n_{\mathbf{k}} t\, \delta(\omega_0-\omega_{\mathbf{k}}). \tag{5.65}$$

The transition rate is proportional to the number of photons $n_{\mathbf{k}}$ in the beam or, equivalently, to the energy

$$\bar{\mathscr{E}}'_{\mathbf{k}} = n_{\mathbf{k}}\hbar\omega_{\mathbf{k}} \tag{5.66}$$

of the beam as defined in eqn (4.146), and eqn (5.65) can be written

$$|C_2(t)|^2/t = (2\pi g_{\mathbf{k}}^2\bar{\mathscr{E}}'_{\mathbf{k}}/\hbar\omega_{\mathbf{k}})\, \delta(\omega_0-\omega_{\mathbf{k}}). \tag{5.67}$$

These results apply for a beam of photons whose initial state is $|n_{\mathbf{k}}\rangle$ and whose number is therefore specified precisely. It is shown in §5.7 that for a photon beam in some general state, the transition-rate equations are generalized in that $n_{\mathbf{k}}$ is replaced by the mean number $\bar{n}_{\mathbf{k}}$ of photons, but the above results are otherwise unchanged.

An expression for the Einstein B coefficient is obtained from eqn (5.67) by procedures similar to those of Chapter 2. The above transition-rate theory is applicable only for broad-band illumination of the atom where there is a slowly-varying energy density $\bar{W}(\omega_{\mathbf{k}})$ of the radiation for frequencies $\omega_{\mathbf{k}}$ in the vicinity of ω_0. Thus analogous to eqn (2.39) we put

$$\bar{\mathscr{E}}'_{\mathbf{k}} = V\int \bar{W}(\omega_{\mathbf{k}})\, d\omega_{\mathbf{k}}. \tag{5.68}$$

The random orientations of $\mathbf{D}_{12}$ are averaged as in eqn (2.54), and the result for the B coefficient is

$$B_{12} = \pi e^2 D_{12}^2/3\epsilon_0\hbar^2, \tag{5.69}$$

in agreement with the expression (2.55) derived by semiclassical radiation theory.

The photon emission process can be treated in the same way. The atom is now assumed to be in its excited state $|2\rangle$ at time $t = 0$, and the probability that the atom is in state $|1\rangle$ at a later time t is calculated. The probability is equal to $|C_1(t)|^2$ in the notation of Chapter 2, and the calculation follows the same lines as that for the absorption process except that the emission matrix element of eqn (5.61) must be used instead of that of eqn (5.60). The result is

$$|C_1(t)|^2 = 2\pi g_{\mathbf{k}}^2(n_{\mathbf{k}}+1)t\, \delta(\omega_0-\omega_{\mathbf{k}}). \tag{5.70}$$

This quantity is the probability that the atom has decayed into state $|1\rangle$ with emission of a photon having a particular wavevector **k**.

The factor $n_{\mathbf{k}}+1$ in eqn (5.70) leads to two contributions to the photon emission rate. The part linear in $n_{\mathbf{k}}$ gives a rate proportional to the number of photons **k** already present, and corresponds to stimulated emission. This term of eqn (5.70) is identical to the right-hand side of eqn (5.65) and leads to a rate of emission equal to the rate of photon absorption. The equality of the two rates, proved here quantum-mechanically, is equivalent to the equality of the Einstein coefficients B_{12} and B_{21} for a pair of nondegenerate states, derived in eqn (1.50). Note how the stimulated emission process arises naturally with the use of the second-quantized interaction Hamiltonian. Furthermore, it is evident from the matrix element of eqn (5.61) that the photon emitted in the stimulated process has a wavevector **k** and polarization direction (this being included in the label **k** by the convention of Chapter 4) that are the same as those of the $n_{\mathbf{k}}$ photons already present. These properties of the stimulated emission were stated without proof in the discussion of Fig. 1.9.

The contribution in eqn (5.70) that is independent of $n_{\mathbf{k}}$ corresponds to spontaneous emission, since the transitions occur even in the complete absence of any radiation ($n_{\mathbf{k}} = 0$). Note that the factor $n_{\mathbf{k}}+1$, which governs the ratio of the stimulated and spontaneous emission rates for a particular photon **k** in eqn (5.70), is similar to the factor $\bar{n}+1$, which controls the ratio of the two rates in eqn (1.53) in the presence of a mean number $\bar{n}$ per cavity mode of thermally excited photons. In the quantum theory of light, the dependences of the absorption and emission rates on the number of photons arise solely from the basic properties (4.91) and (4.92) for the subtraction and addition of a quantum of energy in the energy-level ladder of a simple harmonic oscillator.[9] Spontaneous emission can in principle occur into all modes of the cavity, unlike the stimulated emission which must always match the mode of the stimulating photons.[10]

The total spontaneous decay rate is thus obtained by summation of the spontaneous part of eqn (5.70) over all cavity modes. The radiative lifetime τ_{R} is then given by

$$1/\tau_{\mathrm{R}} = |C_1(t)|^2/t = 2\pi \sum_{\mathbf{k}} g_{\mathbf{k}}^2\, \delta(\omega_0-\omega_{\mathbf{k}}). \tag{5.71}$$

This formula is a special case of a general result known as Fermi's golden rule, which gives the transition rate $1/\tau$ from an initial state $|i\rangle$ to a set of final states $|f\rangle$ arising from the interaction $\hat{\mathscr{H}}_{\mathrm{ED}}$ as

$$1/\tau = (2\pi/\hbar^2)\sum_{f} |\langle f|\hat{\mathscr{H}}_{\mathrm{ED}}|i\rangle|^2\, \delta(\omega_i-\omega_f), \tag{5.72}$$

where $\hbar\omega_i$ and $\hbar\omega_f$ are the energies of the system before and after the transition. For the problem in hand, the initial state is one in which the atom is in state $|2\rangle$ with no photons present, and the final states correspond to the various photons **k** that can be emitted as the atom decays to state $|1\rangle$. The golden-rule expression (eqn (5.72)), which is proved in general in §5.10, reduces to eqn (5.71) for the transition considered.

To complete the evaluation of τ_{R}, it is necessary to convert the sum over **k** in eqn (5.71) to an integral as in eqn (4.128), and to add the contributions of the two mode polarizations for each direction of **k**. We take polar coordinates with wavevector and polarizations given by eqns (4.123)–(4.125). The coordinates may be chosen such that $\mathbf{D}_{12}$ lies in the zx-plane with orientation α to the z-axis,

$$\mathbf{D}_{12} = D_{12}(\sin\alpha, 0, \cos\alpha). \tag{5.73}$$

Problem 5.4. With the convention that the sum over **k** includes summation over polarization directions, prove that

$$\sum_{\mathbf{k}} (\boldsymbol{\varepsilon}_{\mathbf{k}}.\mathbf{D}_{12})^2 = (VD_{12}^2/3\pi^2c^3)\int \omega_{\mathbf{k}}^2\, \mathrm{d}\omega_{\mathbf{k}}. \tag{5.74}$$

Insertion of this result into eqn (5.71) with the use of eqns (2.102) and (5.59) produces

$$A_{21} \equiv 2\gamma \equiv 1/\tau_R = e^2\omega_0^3 D_{12}^2/3\pi\epsilon_0\hbar c^3. \tag{5.75}$$

This is the same as the result (2.57) for the *A* coefficient obtained previously.

The above calculations show how the various processes envisaged in the Einstein theory of absorption and emission of radiation all appear automatically in calculations that use the quantized radiation field. The transition rates can all be calculated straightforwardly, without any use of the phenomenological considerations inherent in the semiclassical approach. The result (5.69) for the Einstein *B* coefficient corroborates the expression obtained from semiclassical theory. The semiclassical method does not provide any direct calculation of the *A* coefficient. However, the fully quantized theory reproduces the relation between the two coefficients obtained in the phenomenological Einstein theory.

5.6. The photoelectric effect

Almost all devices that measure the intensity of a light beam depend for their operation on the absorption of a portion of the beam, whose energy is converted to a detectable form. The photographic plate, the photomultiplier tube, and the bolometer all fall into this category. The present and following sections therefore consider the absorption of light in more detail in order to understand the nature of the intensity measurement process. We determine the form of quantum-mechanical operator that represents the observable intensity of a light beam.

It is convenient to base the discussion on a practical intensity-measuring device, and we select the photomultiplier tube or, more briefly, phototube. Similar considerations apply to the other methods of intensity measurement. The phototube depends for its operation on the photoelectric effect, in which absorption of a photon by an atom causes excitation of an electron from a bound state to a free state in which it can leave the atom altogether. The phototube is essentially an arrangement whereby the freed electron produces more free electrons in a cascade process until the electron current is sufficiently large to be detectable. With the aid of a carefully designed phototube, it is possible to register the atomic ionization processes caused by isolated photons. The phototube measures the intensity of a light beam by counting the rate at which atomic ionizations take place, which is in turn proportional to the rate of photon arrivals at the tube and hence to the beam intensity.

Let us consider the rate at which a particular atom in a phototube is ionized by a beam of photons. The theory of the photoelectric effect is similar to the calculation of the photon absorption rate given in the previous section, except that the final atomic state is one in which the electron has been detached from the atom. The simplest possible example is that in which a hydrogen atom initially in its 1S ground state is ionized by absorption of a photon of wavevector **k**, frequency $\omega_{\mathbf{k}}$, and polarization $\boldsymbol{\varepsilon}_{\mathbf{k}}$. The magnitude of the wavevector **q** of the freed electron is given by the energy conservation requirement

$$\hbar\omega_{\mathbf{k}} = \hbar\omega_{\mathrm{R}} + (\hbar^2 q^2/2m), \tag{5.76}$$

where $\hbar\omega_{\mathrm{R}}$ is the hydrogen ground-state binding energy defined in eqn (2.29),

$$\hbar\omega_{\mathrm{R}} = me^4/32\pi^2\epsilon_0^2\hbar^2 = \hbar^2/2ma_0^2, \tag{5.77}$$

and a_0 is the Bohr radius defined in eqn (2.15).

The wavefunction for the final state of the electron should strictly be taken as one of the free-state solutions of the hydrogen-atom Schrödinger equation. However, these solutions are mathematically complicated, and we use an approximate wavefunction that is valid when the photon energy is much larger than the initial binding energy of the electron,

$$\hbar\omega_{\mathbf{k}} \gg \hbar\omega_{\mathrm{R}}. \tag{5.78}$$

In this case, the free-electron kinetic energy is much larger than the Coulomb binding energy $\hbar\omega_{\mathrm{R}}$, and the effect of the Coulomb potential on the free-electron wavefunction can be ignored to a good approximation. The final-state wavefunction can thus be taken to be a plane wave,

$$\psi_{\mathbf{q}} = V^{-\frac{1}{2}}\exp(\mathrm{i}\mathbf{q}.\mathbf{r}). \tag{5.79}$$

Note that the inequality of eqn (5.78) in conjunction with eqns (5.76) and (5.77) implies

$$q \gg 1/a_0, \tag{5.80}$$

and the free electron has a wavelength that is much smaller than the Bohr radius.

It is however assumed that the incident photon wavelength is much larger than a_0. For example, if $\hbar\omega_{\mathbf{k}}$ is as large as $100\hbar\omega_{\mathrm{R}}$, then a simple estimate gives the photon wavelength to be

$$\lambda = 2\pi/k \approx 10^{-9}\ \mathrm{m}, \tag{5.81}$$

much larger than the Bohr radius of 5×10^{-11} m. The interaction between radiation and atom can therefore be taken in the electric-dipole approximation, with the electron coordinate in the electric-field operator replaced by the coordinate of the atomic nucleus. It is convenient to take the nucleus located at position **R** and the electric-dipole interaction of eqn (5.40) becomes

$$\hat{\mathscr{H}}_{\mathrm{ED}} = e\mathbf{r}.\hat{\mathbf{E}}_{\mathrm{T}}(\mathbf{R}), \tag{5.82}$$

where **r** is the coordinate of the single electron relative to the hydrogen nucleus. It is convenient to divide the electric-field operator given by eqns (4.111) and (4.113) into two parts, and we also show the time dependence explicitly, putting

$$\hat{\mathbf{E}}_{\mathrm{T}}(\mathbf{R}t) = \hat{\mathbf{E}}^{+}(\mathbf{R}t) + \hat{\mathbf{E}}^{-}(\mathbf{R}t), \tag{5.83}$$

where

$$\hat{\mathbf{E}}^{+}(\mathbf{R}t) = \mathrm{i}\sum_{\mathbf{k}}(\hbar\omega_{\mathbf{k}}/2\epsilon_0 V)^{\frac{1}{2}}\boldsymbol{\varepsilon}_{\mathbf{k}}\hat{a}_{\mathbf{k}}\exp(-\mathrm{i}\omega_{\mathbf{k}}t + \mathrm{i}\mathbf{k}.\mathbf{R}) \tag{5.84}$$

and

$$\hat{\mathbf{E}}^{-}(\mathbf{R}t) = -\mathrm{i}\sum_{\mathbf{k}}(\hbar\omega_{\mathbf{k}}/2\epsilon_0 V)^{\frac{1}{2}}\boldsymbol{\varepsilon}_{\mathbf{k}}\hat{a}_{\mathbf{k}}^{\dagger}\exp(\mathrm{i}\omega_{\mathbf{k}}t - \mathrm{i}\mathbf{k}.\mathbf{R}). \tag{5.85}$$

The process of photon absorption accompanied by excitation of a photoelectron at time t is represented by a diagram similar to that of part (b) of Fig. 5.1. The corresponding matrix element is similar to that of eqn (5.60), and assuming to begin with that the photons are initially in a state $|n_{\mathbf{k}}\rangle$ of well-defined photon number, we have

$$\langle f|\hat{\mathscr{H}}_{\mathrm{ED}}|i\rangle = \langle n_{\mathbf{k}} - 1, \mathbf{q}|e\mathbf{r}.[\hat{\mathbf{E}}^{+}(\mathbf{R}t) + \hat{\mathbf{E}}^{-}(\mathbf{R}t)]|n_{\mathbf{k}}, 1\mathrm{S}\rangle. \tag{5.86}$$

The final electronic state has a higher energy than the initial electronic state, and real transitions are possible only for a process in which energy is removed from the electromagnetic field. Thus only the photon-destruction component of the electric-field operator contributes, and the matrix element reduces after factorization to

$$\langle f|\hat{\mathscr{H}}_{\mathrm{ED}}|i\rangle = e\langle n_{\mathbf{k}} - 1|\hat{\mathbf{E}}^{+}(\mathbf{R}t)|n_{\mathbf{k}}\rangle.\langle\mathbf{q}|\mathbf{r}|1\mathrm{S}\rangle. \tag{5.87}$$

Consider first the atomic part of the matrix element. The required wavefunctions are given by eqns (5.79) and (2.25). Define a coordinate system where the incident photons have wavevectors parallel to the z-axis and polarizations parallel to the x-axis, as in Fig. 5.2. The wavevector direction of the emitted photoelectron has spherical polar angles θ and ϕ with the z-direction taken as the polar axis, and the azimuthal angle ϕ measured from the x-axis.

Problem 5.5. Prove that

$$\langle\mathbf{q}|\boldsymbol{\varepsilon}_{\mathbf{k}}.\mathbf{r}|1\mathrm{S}\rangle = -\mathrm{i}\frac{32\pi^{\frac{1}{2}}q}{V^{\frac{1}{2}}a_0^{\frac{5}{2}}}\frac{\sin\theta\cos\phi}{(q^2 + a_0^{-2})^3} \approx -\mathrm{i}\frac{32\pi^{\frac{1}{2}}\sin\theta\cos\phi}{V^{\frac{1}{2}}a_0^{\frac{5}{2}}q^5}, \tag{5.88}$$

where the inequality of eqn (5.80) has been used in the final step.

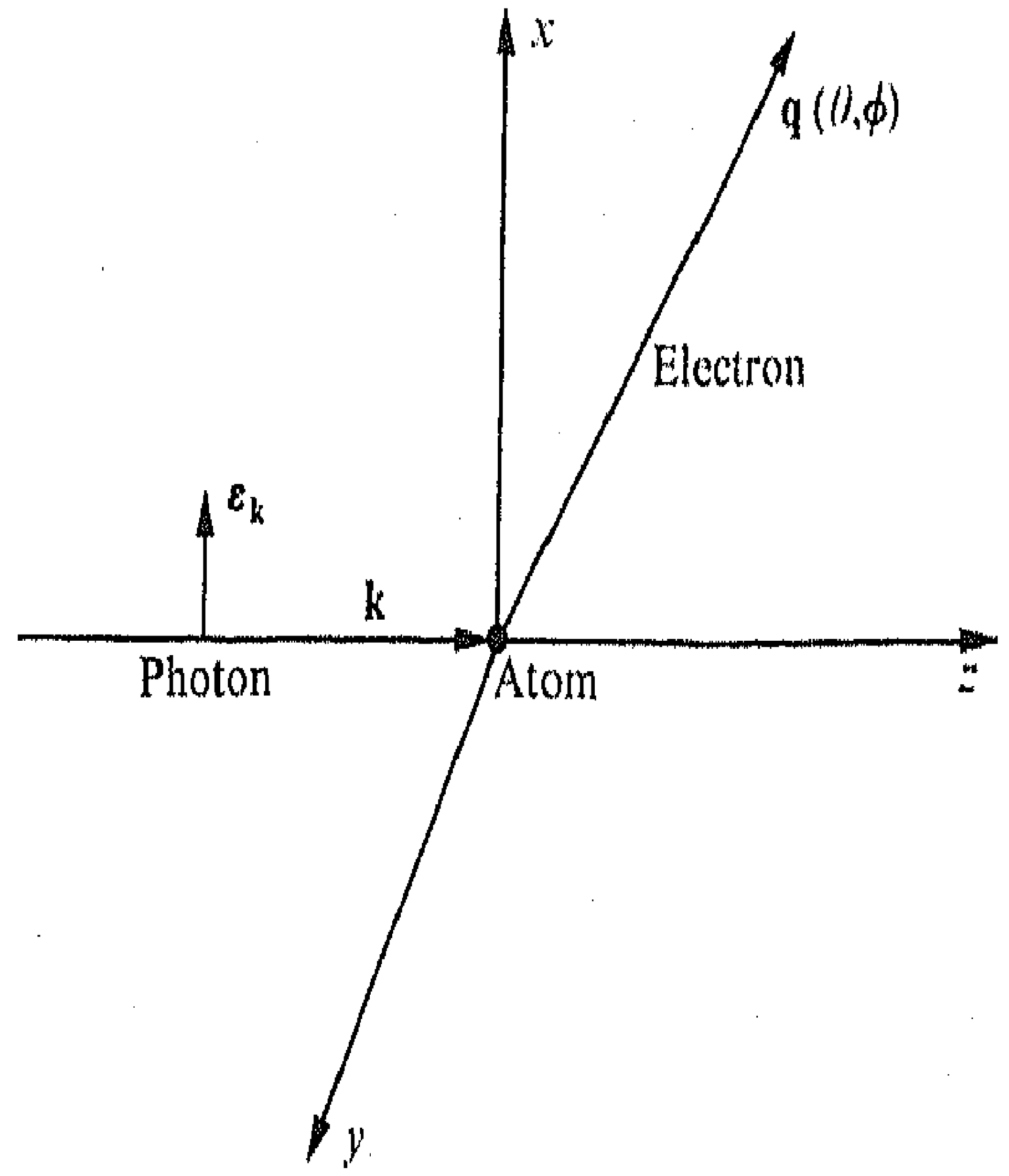

FIG. 5.2. Coordinate system for the calculation of the photoelectric emission rate.

The transition rate for the photoelectric effect can now be obtained by an application of the Fermi golden rule (eqn (5.72)). Let us calculate the total transition rate $1/\tau$ for all processes in which photons of frequency $\omega_{\mathbf{k}}$ are absorbed by the atom and cause emission of an electron. In accordance with eqn (5.72) we must sum over all the possible final-state electron wavevectors **q**, and with the help of eqns (5.87) and (5.88) we obtain

$$\frac{1}{\tau}=\frac{2\pi}{\hbar^2}\sum_{\mathbf{q}}|\langle n_{\mathbf{k}}-1|\hat{E}^{+}(\mathbf{R}t)|n_{\mathbf{k}}\rangle|^2\,\frac{2^{10}\pi e^2\sin^2\theta\cos^2\phi}{Va_0^5q^{10}}\,\delta\left(\omega_{\mathbf{k}}-\frac{\hbar}{2ma_0^2}-\frac{\hbar q^2}{2m}\right). \tag{5.89}$$

The way in which the photoelectric transition rate depends upon the properties of the radiation field is governed by the radiation-field matrix element in eqn (5.89). In the following section we discuss the properties of this matrix element for the photon number-state and more general kinds of incident light beam. The matrix element is easily evaluated for the number state with the help of eqns (5.84) and (4.103), and eqn (5.89) becomes

$$\frac{1}{\tau}=\sum_{\mathbf{q}}\frac{2^{10}\pi^2e^2\omega_{\mathbf{k}}n_{\mathbf{k}}\sin^2\theta\cos^2\phi}{\epsilon_0V^2\hbar a_0^5q^{10}}\,\delta\left(\omega_{\mathbf{k}}-\frac{\hbar q^2}{2m}\right), \tag{5.90}$$

where the term $\hbar/2ma_0^2$ has been dropped from the delta function in view of eqn (5.80). If $\mathrm{d}\Omega$ is an element of solid angle surrounding the vector **q**, the summation over **q** can be converted to an integration by

$$\sum_{\mathbf{q}}\rightarrow\{V/(2\pi)^3\}\iint q^2\,\mathrm{d}q\,\mathrm{d}\Omega, \tag{5.91}$$

similar to eqn (4.128). The integral over q is evaluated with the help of the delta-function property (2.68), and the transition rate becomes

$$\frac{1}{\tau}=\int\left(\frac{2m}{\hbar}\right)^{\frac{1}{2}}\frac{4e^2\hbar^3n_{\mathbf{k}}\sin^2\theta\cos^2\phi}{\pi\epsilon_0Vm^4a_0^5\omega_{\mathbf{k}}^{\frac{7}{2}}}\,\mathrm{d}\Omega. \tag{5.92}$$

It is customary to quote experimental and theoretical results for the strength of the photoelectric effect in terms of a cross-section σ, instead of a transition rate $1/\tau$. The cross-section has the dimensions of area, and is defined as the ratio of the rate $\hbar\omega_{\mathbf{k}}/\tau$ at which energy is removed from the photon beam by the photoelectric effect to the rate $c\hbar\omega_{\mathbf{k}}n_{\mathbf{k}}/V$ at which energy in the beam crosses a unit area perpendicular to its propagation direction. Thus

$$\sigma=V/\tau n_{\mathbf{k}}c, \tag{5.93}$$

and an expression for the cross-section is easily obtained from eqn (5.92).

The *differential* cross-section is defined in the same way as the cross-section except that it refers to the rate at which energy is removed from the photon beam by processes in which the photoelectron has a wavevector **q** whose direction falls within the element of solid angle $\mathrm{d}\Omega$. The differential cross-section is obtained by differentiation of σ with respect to Ω, and the result from eqns (5.92) and (5.93) is

$$\frac{\mathrm{d}\sigma}{\mathrm{d}\Omega}=\left(\frac{2m}{\hbar}\right)^{\frac{1}{2}}\frac{4e^2\hbar^3\sin^2\theta\cos^2\phi}{\pi\epsilon_0cm^4a_0^5\omega_{\mathbf{k}}^{\frac{7}{2}}}. \tag{5.94}$$

The main features of the differential cross-section are the fall-off with the inverse $\frac{7}{2}$ power of the photon frequency, and the predicted angular dependence. The most favourable direction for electron emission is parallel to the photon polarization, and the differential cross-section falls to zero when **q** is perpendicular to $\boldsymbol{\varepsilon}_{\mathbf{k}}$. At high frequencies, where the photoelectric cross-section is small, the photons are more likely to be scattered by the atom than absorbed in the photoelectric effect.

It should be emphasized that the theory which leads to eqn (5.94) is only approximate, the main approximation being the use of a plane wave (eqn (5.79)) for the wavefunction of the photoelectron. The correct Coulomb wavefunctions lead to somewhat different results,[11] particularly when $\hbar\omega_{\mathbf{k}}$ is only a little larger than the threshold value $\hbar\omega_R$ and the free-state wavefunctions are not at all plane-wave-like. The departure of the approximation shown in eqn (5.94) from the exact result at the smaller values of $\hbar\omega_{\mathbf{k}}$ is shown in Fig. 5.3. The approximate theory also fails at higher frequencies where $1/k$ becomes comparable to the Bohr radius, so that the electric-dipole approximation cannot be made, or $\hbar\omega_{\mathbf{k}}$ becomes comparable to mc^2, and relativistic wavefunctions must be used.

It was pointed out in the previous section that the semiclassical and fully quantized theories give identical predictions for the rate of absorption of

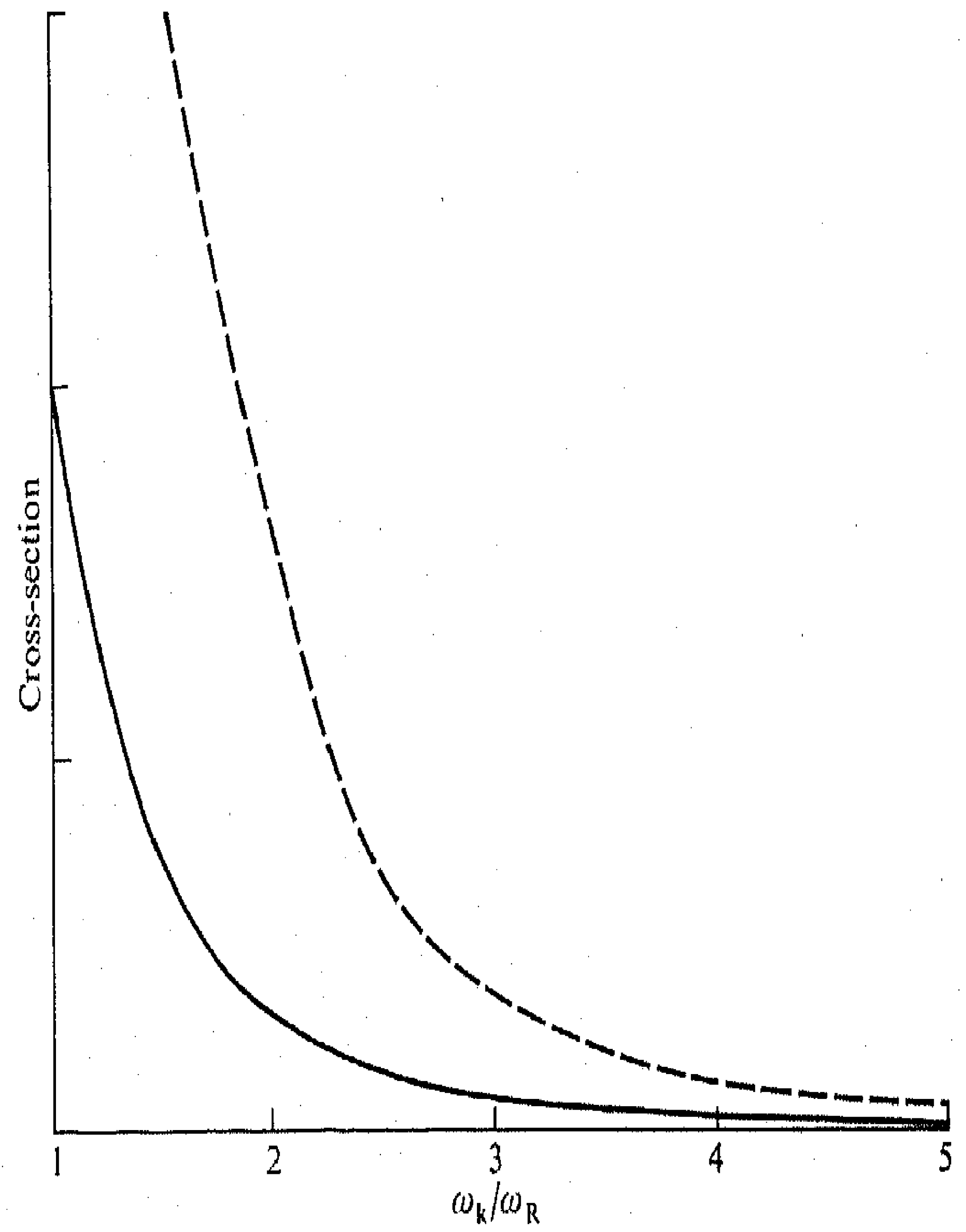

FIG. 5.3. The photoelectric cross-section in arbitrary units as a function of photon frequency in the region where this is *not* large compared to the Rydberg frequency. The solid curve shows the exact result from ref. 11, and the broken curve shows the approximation (5.94).

radiation by atoms. The statement remains correct when the atom is ionized in the final state of the transition, as in the calculations of the present section. Thus semiclassical theory accounts for all the main features of the photoelectric effect, and the latter's existence does not 'prove' the need for quantization of the radiation field, contrary to statements sometimes made.

5.7. The photon intensity operator

The electromagnetic field enters the photoelectric transition rate (5.89) via the factor

$$|\langle n_{\mathbf{k}}-1|\hat{E}^{+}(\mathbf{R}t)|n_{\mathbf{k}}\rangle|^{2} = \langle n_{\mathbf{k}}|\hat{E}^{-}(\mathbf{R}t)|n_{\mathbf{k}}-1\rangle\langle n_{\mathbf{k}}-1|\hat{E}^{+}(\mathbf{R}t)|n_{\mathbf{k}}\rangle$$
$$= \langle n_{\mathbf{k}}|\hat{E}^{-}(\mathbf{R}t)\hat{E}^{+}(\mathbf{R}t)|n_{\mathbf{k}}\rangle, \qquad (5.95)$$

where the final step is justified by the closure theorem for the states of the radiation field,

$$\sum_{n_{\mathbf{k}}}|n_{\mathbf{k}}\rangle\langle n_{\mathbf{k}}| = 1, \qquad (5.96)$$

since only the state $|n_{\mathbf{k}}-1\rangle$ makes a non-zero contribution as the final state in eqn (5.95).

The results are easily generalized to obtain the photoelectric transition rate for an incident beam that corresponds to a statistical mixture of the number states. Let the light beam in its initial state be specified by a probability $P_{n_{\mathbf{k}}}$ associated with the state $|n_{\mathbf{k}}\rangle$. The expression (5.89) for the transition rate remains valid, except that the electromagnetic field factor (5.95) is generalized to

$$\sum_{n_{\mathbf{k}}} P_{n_{\mathbf{k}}}\langle n_{\mathbf{k}}|\hat{E}^{-}(\mathbf{R}t)\hat{E}^{+}(\mathbf{R}t)|n_{\mathbf{k}}\rangle = \mathrm{Tr}\big(\hat{\rho}\hat{E}^{-}(\mathbf{R}t)\hat{E}^{+}(\mathbf{R}t)\big), \qquad (5.97)$$

where the electromagnetic field density operator $\hat{\rho}$ is used to obtain ensemble averages in accordance with the procedure of eqns (4.212) to (4.220). For the most general case of a multimode incident beam, the trace in eqn (5.97) is evaluated with the multimode density operator whose form is given in eqn (4.242).

The rate at which the radiation field causes an atom to emit a photoelectron is thus proportional to the expectation value of the operator $\hat{E}^{-}(\mathbf{R}t)\hat{E}^{+}(\mathbf{R}t)$. This quantity corresponds to the observable intensity of the light beam as measured by the current that the beam induces in the phototube. The approximate theory of the photoelectric effect is sufficiently realistic to produce the correct dependence on the characteristics of the incident light beam. Use of a better approximation to the electronic wavefunctions, or the assumption of some type of atom other than hydrogen, modifies the atomic part of the transition rate, but the conclusion that the radiation field enters the transition rate via the factor given in eqn (5.97) remains valid. Analysis of other types of intensity-measuring device leads to the same conclusion that their response is proportional to the expectation value (5.97).

The intensity of a light beam in classical electromagnetic theory is determined by the Poynting vector defined in eqn (1.88). The quantum-mechanical intensity operator can be defined by

$$\hat{\mathbf{I}}(\mathbf{R}t) = \{\hat{\mathbf{E}}^{-}(\mathbf{R}t)\times\hat{\mathbf{B}}^{+}(\mathbf{R}t)-\hat{\mathbf{B}}^{-}(\mathbf{R}t)\times\hat{\mathbf{E}}^{+}(\mathbf{R}t)\}/\mu_{0}, \qquad (5.98)$$

where the second term on the right, including the minus sign, is the Hermitian conjugate of the first term. The electric-field operators are defined by eqns (5.84) and (5.85), and the magnetic-field operators are obtained from the corresponding separation of $\hat{\mathbf{B}}$, given by eqns (4.112) and (4.114), into its destruction and creation operator parts.

The calculation of the photoelectric transition rate in the previous section assumed the geometrical arrangement of Fig. 5.2 with a unique direction for the wavevector of the incident light beam. We apply the definition of the intensity operator to this case alone, when eqn (5.98) can be written in a simpler form.

Problem 5.6. If the mode summations in the electromagnetic field operators are restricted to wavevectors that point in a common direction, prove that the intensity operator (5.98) is oriented in the common direction with a scalar magnitude that can be written

$$\hat{I}(\mathbf{R}t) = 2\epsilon_0 c\hat{\mathbf{E}}^-(\mathbf{R}t).\hat{\mathbf{E}}^+(\mathbf{R}t). \tag{5.99}$$

The expectation value of the intensity for a polarized beam of light is

$$\langle\hat{I}(\mathbf{R}t)\rangle = 2\epsilon_0 c\ \mathrm{Tr}(\hat{\rho}\hat{E}^-(\mathbf{R}t)\hat{E}^+(\mathbf{R}t)). \tag{5.100}$$

The definition of the intensity operator adopted in eqn (5.98) thus reproduces the form of observed intensity derived in eqn (5.97) by consideration of the photoelectric effect.

The intensity simplifies for incident light whose density operator has no off-diagonal number-state matrix elements, for example chaotic light described by eqn (4.244). The intensity obtained from eqn (5.100) with the help of eqns (5.84) and (5.85) is independent of position and time in this case, and we find

$$\langle\hat{I}\rangle = (c\hbar/V)\sum_{\mathbf{k}}\omega_{\mathbf{k}}\bar{n}_{\mathbf{k}}, \tag{5.101}$$

where

$$\bar{n}_{\mathbf{k}} = \mathrm{Tr}(\hat{\rho}\hat{a}^\dagger_{\mathbf{k}}\hat{a}_{\mathbf{k}}) \tag{5.102}$$

is the mean photon number for mode **k**. The photoelectric transition rate retains a simple form only for monochromatic incident light where $n_{\mathbf{k}}$ is replaced by $\bar{n}_{\mathbf{k}}$ in eqns (5.92) and (5.93). The final result (5.94) remains valid in this case.

Another simple case is that of multimode coherent incident light, where the state and density operator are defined in eqns (4.236) and (4.237). It follows from the definition (5.84) and the property (4.186) of the coherent states, that $|\{\alpha_{\mathbf{k}}\}\rangle$ is an eigenstate of $\hat{E}^+$,

$$\hat{E}^+(\mathbf{R}t)|\{\alpha_{\mathbf{k}}\}\rangle = \mathrm{i}\sum_{\mathbf{k}}(\hbar\omega_{\mathbf{k}}/2\epsilon_0 V)^{\frac{1}{2}}\alpha_{\mathbf{k}}\exp(-\mathrm{i}\omega_{\mathbf{k}}t+\mathrm{i}\mathbf{k}.\mathbf{R})|\{\alpha_{\mathbf{k}}\}\rangle. \tag{5.103}$$

The expectation value of the intensity is thus

$$\begin{aligned}\langle\hat{I}(\mathbf{R}t)\rangle &= 2\epsilon_0 c\langle\{\alpha_{\mathbf{k}}\}|\hat{E}^-(\mathbf{R}t)|\{\alpha_{\mathbf{k}}\}\rangle\langle\{\alpha_{\mathbf{k}}\}|\hat{E}^+(\mathbf{R}t)|\{\alpha_{\mathbf{k}}\}\rangle \\ &= (c\hbar/V)\left|\sum_{\mathbf{k}}\omega_{\mathbf{k}}^{\frac{1}{2}}\alpha_{\mathbf{k}}\exp(-\mathrm{i}\omega_{\mathbf{k}}t+\mathrm{i}\mathbf{k}.\mathbf{R})\right|^2.\end{aligned} \tag{5.104}$$

The quantum-mechanical intensity operator of eqn (5.99) has some similarity to the formula (3.15) for the classical cycle-averaged intensity, except for some different factors of 2 associated with the different definitions of electric fields in the two cases. Thus the intensity expectation value (5.104) for the pure coherent state contains components only at the differences of frequencies within the beam, and the result depends on **R** and t in exactly the same way as the classical cycle-averaged intensity for the analogous superposition of classical stable waves. The quantum result (5.101), which applies for example in the case of multimode chaotic light, includes the additional average over the probability distribution represented by $\hat{\rho}$ in eqn (5.100), and is analogous to the classical long-time average intensity of eqn (3.58).

The nature of the intensity-measuring process, which relies upon absorption of light, or destruction of photons, leads to the definition (5.98) or (5.100) of the intensity operator, in which the destruction operators lie to the right of the creation operators. An operator product that has this property is said to be *normally ordered.*[12] The expectation value of the operator product $\hat{E}^-\hat{E}^+$ is proportional, as in eqn (5.101) to the numbers of photons in the modes; from a physical viewpoint, light detectors give a reading only when there are photons at the detector position. The detector response is *not* proportional to the expectation value of $\hat{E}\hat{E}$, which was evaluated in eqn (4.116) and includes a zero-point contribution from every mode **k** of the radiation field, whether or not the beam contains photons in mode **k**. It can therefore be asserted that the zero-point energy makes no contribution to the observable radiative intensity, and the corresponding field energy is always given by $\mathscr{E}'$ of eqn (4.145) and not by $\mathscr{E}$ of eqn (4.119). The theory of measurements on light beams is further developed in the following chapter.

5.8. Transformation to the Schrödinger representation

The transition-probability calculations carried out earlier in the present chapter are based on the time-dependent perturbation theory developed in Chapter 2. The basic equation is the time-dependent wave equation (2.1), where the Hamiltonian $\mathscr{H}$ is expressed as a sum of the atomic Hamiltonian $\mathscr{H}_{\mathrm{E}}$ and an interaction Hamiltonian $\mathscr{H}_{\mathrm{I}}$ as in eqn (2.7). The interaction Hamiltonian depends on the time, and is regarded as inducing transitions between the eigenstates of $\mathscr{H}_{\mathrm{E}}$.

In the electric dipole approximation we may write the wave equation

$$(\mathscr{H}_{\mathrm{E}}+\mathscr{H}_{\mathrm{ED}}(t))\Psi(t) = \mathrm{i}\hbar\,\mathrm{d}\Psi(t)/\mathrm{d}t, \tag{5.105}$$

where we now indicate which functions depend on the time. The explicit forms of $\mathscr{H}_{\mathrm{E}}$ and $\mathscr{H}_{\mathrm{ED}}(t)$ are given in eqns (5.53) and (5.57). It can be seen that the time dependence of $\mathscr{H}_{\mathrm{ED}}(t)$ arises from the electric vector $\hat{\mathbf{E}}_{\mathrm{T}}$ of the radiation field. The treatment of the interacting atom and radiation field based on eqn (5.105) employs time-dependent operators for the radiative part of the coupled system, but time-independent operators for the atomic part.

It is shown in textbooks on quantum mechanics[13] that a given problem can be treated in several different types of *representation.* The representations differ in the way in which time dependence enters the quantum-mechanical equations. The extreme cases are the Schrödinger representation, where all the operator quantities are explicitly time-independent and the time dependence is all contained in the wavefunction, and the Heisenberg representation, where the wavefunctions are independent of time and the time dependence is carried by the operators.

The wave equation (5.105) is expressed in a mixed representation that is Schrödinger-like for the atomic part but Heisenberg-like for the radiative part. It is sometimes convenient to cast the whole system into a single representation, and subsequent calculations make various use of the Schrödinger and Heisenberg representations. We consider the Schrödinger representation in the present section and the Heisenberg representation in §5.11. An intermediate case, the interaction representation, is sometimes useful in radiative problems, and its properties are described in §5.14. It must be emphasized that all representations give the same predictions for measurable quantities, but for a given problem, the derivations may be much simpler and more transparent in a particular representation.

In order to transform eqn (5.105) to the Schrödinger representation we define a new wavefunction

$$\Phi_S(t) = \exp(-i\hat{\mathscr{H}}_R t/\hbar)\Psi(t), \tag{5.106}$$

where

$$\hat{\mathscr{H}}_R = \sum_{\mathbf{k}} \hbar\omega_{\mathbf{k}} \hat{a}_{\mathbf{k}}^{\dagger}\hat{a}_{\mathbf{k}} \tag{5.107}$$

is the radiative Hamiltonian from eqn (4.118), but with the zero-point energy dropped in accordance with the remarks of the previous section. Substitution of eqn (5.106) in eqn (5.105) gives

$$\begin{aligned}\{\hat{\mathscr{H}}_E+\hat{\mathscr{H}}_{ED}(t)\}\exp(i\hat{\mathscr{H}}_R t/\hbar)\Phi_S(t) = i\hbar \exp(i\hat{\mathscr{H}}_R t/\hbar)\{&(i\hat{\mathscr{H}}_R/\hbar)\Phi_S(t)\\ &+(d\Phi_S(t)/dt)\}.\end{aligned} \tag{5.108}$$

Multiplication of both sides from the left by $\exp(-i\hat{\mathscr{H}}_R t/\hbar)$ leads to

$$\{\hat{\mathscr{H}}_E+\hat{\mathscr{H}}_R+\exp(-i\hat{\mathscr{H}}_R t/\hbar)\hat{\mathscr{H}}_{ED}(t)\exp(i\hat{\mathscr{H}}_R t/\hbar)\}\Phi_S(t) = i\hbar\, d\Phi_S(t)/dt, \tag{5.109}$$

where the commutation of $\hat{\mathscr{H}}_E$ with $\hat{\mathscr{H}}_R$ has been used.

The time-dependent term in the Hamiltonian on the left-hand side of this equation can be greatly simplified.

Problem 5.7. Use the commutation relations (4.166) and (4.167) to prove that

$$\exp(-i\omega\hat{a}^{\dagger}\hat{a}t)\hat{a}\exp(i\omega\hat{a}^{\dagger}\hat{a}t) = \hat{a}\exp(i\omega t) \tag{5.110}$$

and

$$\exp(-i\omega\hat{a}^{\dagger}\hat{a}t)\hat{a}^{\dagger}\exp(i\omega\hat{a}^{\dagger}\hat{a}t) = \hat{a}^{\dagger}\exp(-i\omega t), \tag{5.111}$$

and hence show that

$$\exp(-i\hat{\mathscr{H}}_R t/\hbar)\hat{\mathscr{H}}_{ED}(t)\exp(i\hat{\mathscr{H}}_R t/\hbar) = \hat{\mathscr{H}}_{ED}(0). \tag{5.112}$$

The wave equation (5.109) thus reduces to

$$\hat{\mathscr{H}}\Phi_S(t) \equiv (\hat{\mathscr{H}}_E+\hat{\mathscr{H}}_R+\hat{\mathscr{H}}_{ED})\Phi_S(t) = i\hbar\, d\Phi_S(t)/dt, \tag{5.113}$$

where $\hat{\mathscr{H}}_{ED}$ is now the electric-dipole Hamiltonian from eqn (5.57) but with the time t set equal to zero,

$$\hat{\mathscr{H}}_{ED} = ie\sum_{\mathbf{k}}\sum_{i,j}(\hbar\omega_{\mathbf{k}}/2\epsilon_0 V)^{\frac{1}{2}}\boldsymbol{\varepsilon}_{\mathbf{k}}.\mathbf{D}_{ij}\{\hat{a}_{\mathbf{k}}\exp(i\mathbf{k}.\mathbf{R}) - \hat{a}_{\mathbf{k}}^{\dagger}\exp(-i\mathbf{k}.\mathbf{R})\}|i\rangle\langle j|. \tag{5.114}$$

The Hamiltonian in eqn (5.113) is entirely time-independent, the transformation shown in eqn (5.106) having transferred the time dependence of the radiation field to the wavefunction $\Phi_S(t)$. The problem is now completely in the Schrödinger representation. A similar transformation can be carried out for the total interaction Hamiltonian $\hat{\mathscr{H}}_I$ of eqn (5.39); the resulting wave equation is the same as eqn (5.113) but with $\hat{\mathscr{H}}_I$ at $t = 0$ replacing $\hat{\mathscr{H}}_{ED}$.

The physical predictions that follow from the new wave equation (5.113) are identical to those that result from the original equation (5.105). The transformed equation is symmetric in the atomic and electromagnetic field contributions to the total Hamiltonian, and is often more convenient for calculations in which both atom and radiation are treated quantum mechanically.

The operators that represent observables are all time-independent in the Schrödinger representation,

$$d\hat{O}/dt = 0. \tag{5.115}$$

The expectation value of an operator for a system in the pure state $\Phi_S(t)$,

$$\langle\hat{O}(t)\rangle = \langle\Phi_S(t)|\hat{O}|\Phi_S(t)\rangle, \tag{5.116}$$

has a time dependence entirely determined by the time variation of the state. The formal solution of eqn (5.113) is

$$\Phi_S(t) = \exp(-i\hat{\mathscr{H}}t/\hbar)\Phi_S(0). \tag{5.117}$$

The exponential quantity is known as the time-development operator.

For a statistical mixture in the Schrödinger representation with a probability P_S that the system is in state Φ_S at time $t = 0$, the density operator at a general time t is defined in accordance with eqn (4.216) to be

$$\begin{aligned}\hat{\rho}_S(t) &= \sum_S P_S|\Phi_S(t)\rangle\langle\Phi_S(t)|\\ &= \sum_S P_S\exp(-i\hat{\mathscr{H}}t/\hbar)|\Phi_S(0)\rangle\langle\Phi_S(0)|\exp(i\hat{\mathscr{H}}t/\hbar).\end{aligned} \tag{5.118}$$

The density operator *does* vary with time in the Schrödinger representation and it is easily shown by differentiation of eqn (5.118) that

$$i\hbar\, d\hat{\rho}_S(t)/dt = [\hat{\mathscr{H}}, \hat{\rho}_S(t)]. \tag{5.119}$$

The expectation value of an operator for a statistical mixture is

$$\langle \hat{O}(t)\rangle = \mathrm{Tr}\big(\hat{\rho}_{\mathrm{S}}(t)\hat{O}\big) \tag{5.120}$$

similar to eqn (4.220).

It is useful for later calculations to put the Schrödinger-representation Hamiltonian of an effectively two-level atom into its simplest possible form. We therefore consider once more an atom with ground state $|1\rangle$ and an excited state $|2\rangle$ at excitation energy $\hbar\omega_0$. The atomic parts of the Hamiltonian can be simplified by the introduction of *transition operators*

$$\hat{\pi}^\dagger = |2\rangle\langle 1| \tag{5.121}$$

$$\hat{\pi} = |1\rangle\langle 2|. \tag{5.122}$$

Thus $\hat{\pi}^\dagger$ shifts the atom from its ground state to its excited state, and $\hat{\pi}$ produces the reverse transition. The properties of the transition operators are easily obtained from their definitions. Thus if the atomic states are normalized and orthogonal,

$$\hat{\pi}^\dagger\hat{\pi} = |2\rangle\langle 1|1\rangle\langle 2| = |2\rangle\langle 2| \tag{5.123}$$

and similarly

$$\hat{\pi}\hat{\pi}^\dagger = |1\rangle\langle 1|. \tag{5.124}$$

The closure theorem for a two-level atom gives

$$|1\rangle\langle 1| + |2\rangle\langle 2| = \hat{\pi}^\dagger\hat{\pi} + \hat{\pi}\hat{\pi}^\dagger = 1. \tag{5.125}$$

Finally,

$$\hat{\pi}^\dagger\hat{\pi}^\dagger = |2\rangle\langle 1|2\rangle\langle 1| = 0 \tag{5.126}$$

and similarly

$$\hat{\pi}\hat{\pi} = 0. \tag{5.127}$$

If the energy zero is taken at the level of the lower state $|1\rangle$, the atomic Hamiltonian (5.53) reduces to

$$\hat{\mathscr{H}}_{\mathrm{E}} = \hbar\omega_0|2\rangle\langle 2| = \hbar\omega_0\hat{\pi}^\dagger\hat{\pi}. \tag{5.128}$$

The electric-dipole Hamiltonian can be similarly re-expressed. According to eqn (5.55), the second-quantized form of $\mathbf{D}$ reduces to

$$\mathbf{D} = \mathbf{D}_{12}(\hat{\pi}^\dagger + \hat{\pi}), \tag{5.129}$$

and the relevant part of the electric-dipole Hamiltonian (5.114) is

$$\hat{\mathscr{H}}_{\mathrm{ED}} = \mathrm{i}\sum_{\mathbf{k}}\hbar g_{\mathbf{k}}\{\hat{a}_{\mathbf{k}}\exp(\mathrm{i}\mathbf{k}.\mathbf{R}) - \hat{a}_{\mathbf{k}}^\dagger\exp(-\mathrm{i}\mathbf{k}.\mathbf{R})\}(\hat{\pi}^\dagger + \hat{\pi}), \tag{5.130}$$

where $g_{\mathbf{k}}$ is defined in eqn (5.59). The terms that result from multiplying out the brackets are represented by the four diagrams of Fig. 5.1. We make the rotating-wave approximation and retain only the energy-conserving terms represented by diagrams (b) and (c). The complete Schrödinger-representation Hamiltonian obtained from eqns (5.107), (5.128), and (5.130) is then

$$\begin{aligned}\hat{\mathscr{H}} &= \hat{\mathscr{H}}_{\mathrm{E}} + \hat{\mathscr{H}}_{\mathrm{R}} + \hat{\mathscr{H}}_{\mathrm{ED}}\\ &= \hbar\omega_0\hat{\pi}^\dagger\hat{\pi} + \sum_{\mathbf{k}}\hbar\omega_{\mathbf{k}}\hat{a}_{\mathbf{k}}^\dagger\hat{a}_{\mathbf{k}} + \mathrm{i}\sum_{\mathbf{k}}\hbar g_{\mathbf{k}}\{\hat{\pi}^\dagger\hat{a}_{\mathbf{k}}\exp(\mathrm{i}\mathbf{k}.\mathbf{R}) - \hat{a}_{\mathbf{k}}^\dagger\hat{\pi}\exp(-\mathrm{i}\mathbf{k}.\mathbf{R})\},\end{aligned} \tag{5.131}$$

where all the operator products are written in normal order, with destruction operators to the right of creation operators.

5.9. General expression for radiative transition rates

The transition rates determined earlier in the chapter are based on the result (2.70) derived for a two-level atom subjected to an oscillatory perturbation. The generalization of this result, Fermi's golden rule, quoted without proof in eqn (5.72), covers systems that have continuous distributions of energy levels, as in spontaneous emission, where the emitted photon has a distribution of possible states, or in the photoelectric effect, where the emitted electron has many available states. Fermi's golden rule applies only to first-order radiative processes, where a single interaction of the radiation with an atom occurs, as in the diagrams of Fig. 5.1.

In the present and following sections we derive general expressions for radiative transition rates using the Schrödinger representation. We give a proof of Fermi's golden rule and its generalization to higher-order radiative processes that involve two or more interactions of radiation with the atom. The theory is based on the Schrödinger wave equation (5.113) with a total Hamiltonian that can be written as the sum of two parts

$$\hat{\mathscr{H}} = \hat{\mathscr{H}}_0 + \hat{\mathscr{H}}_{\mathrm{I}}, \tag{5.132}$$

where $\hat{\mathscr{H}}_0$ is the Hamiltonian of the uncoupled electrons and radiation and $\hat{\mathscr{H}}_{\mathrm{I}}$ is the interaction between them, equal to $\hat{\mathscr{H}}_{\mathrm{ED}}$ in the electric-dipole approximation. The wavefunction at time t is related to that at an earlier time t_0 by

$$\Phi_{\mathrm{S}}(t) = \exp\{-\mathrm{i}\hat{\mathscr{H}}(t-t_0)/\hbar\}\Phi_{\mathrm{S}}(t_0), \tag{5.133}$$

where eqn (5.117) has been used.

Let ψ_f be an eigenstate of $\hat{\mathscr{H}}_0$ with energy $\hbar\omega_f$,

$$\hat{\mathscr{H}}_0\psi_f = \hbar\omega_f\psi_f. \tag{5.134}$$

The probability that the system is in state ψ_f at time t is given in the usual way by the square of the overlap integral of ψ_f and $\Phi_{\mathrm{S}}(t)$,

$$|\langle\psi_f|\Phi_{\mathrm{S}}(t)\rangle|^2 = |\langle\psi_f|\exp\{-\mathrm{i}\hat{\mathscr{H}}(t-t_0)/\hbar\}|\Phi_{\mathrm{S}}(t_0)\rangle|^2, \tag{5.135}$$

where eqn (5.133) has been used. The presence of $\hat{\mathscr{H}}_{\rm I}$ in the exponential causes $|\langle\psi_f|\Phi_{\rm S}(t)\rangle|^2$ to differ in general from $|\langle\psi_f|\Phi_{\rm S}(t_0)\rangle|^2$. The difference is physically described as being due to the occurrence of radiative transitions during the time interval between t_0 and t.

The state of the coupled system at time t_0 can be expressed as a linear superposition of the eigenstates of $\hat{\mathscr{H}}_0$. Let ψ_u be one of the eigenstates,

$$\hat{\mathscr{H}}_0\psi_u = \hbar\omega_u\psi_u. \tag{5.136}$$

The probability (eqn (5.135)) of the system being in state ψ_f at time t can be expressed in terms of the probabilities of observing the system to be in the various states ψ_u at time t_0. The proportionality factor by which the probability for state ψ_u at time t_0 must be multiplied to find the corresponding contribution to the probability for state ψ_f at time t is

$$|\langle\psi_f|\exp\{-{\rm i}\hat{\mathscr{H}}(t-t_0)/\hbar\}|\psi_u\rangle|^2. \tag{5.137}$$

The transition rate from state ψ_u to state ψ_f is equal to the time derivative of this proportionality factor. In the common experimental situation where transitions to a range of final states are observed simultaneously, the appropriate transition rate is

$$\frac{1}{\tau} = \frac{\rm d}{{\rm d}t}\sum_f|\langle f|\exp\{-{\rm i}\hat{\mathscr{H}}(t-t_0)/\hbar\}|u\rangle|^2, \tag{5.138}$$

where the notation for bras and kets has been simplified. Under steady-state conditions, the transition rate is expected to be independent of both t and t_0.

The expression (5.138) for the transition rate is not in a very useful form for calculations. It can be made more useful by an expansion in a series of powers of the matrix elements of $\hat{\mathscr{H}}_{\rm I}$. We have seen in Chapter 2 that the matrix elements of the atom–radiation interaction are small compared with the energies of the photons and atomic transitions in the visible region of the spectrum. Therefore the series expansion of the transition rate can be expected to converge rapidly. It is, in most cases, an excellent approximation to terminate the expansion at the first non-vanishing term for the type of transition considered. The expansion clearly separates the first, second, third, and so on, orders of radiative process.

The required series is obtained by expansion of $\exp\{-{\rm i}\hat{\mathscr{H}}(t-t_0)/\hbar\}$ in powers of $\hat{\mathscr{H}}_{\rm I}$. The expansion is not entirely straightforward because

$$\exp(-{\rm i}\hat{\mathscr{H}}t/\hbar) \neq \exp(-{\rm i}\hat{\mathscr{H}}_0t/\hbar)\exp(-{\rm i}\hat{\mathscr{H}}_{\rm I}t/\hbar) \tag{5.139}$$

owing to the fact that $\hat{\mathscr{H}}_0$ and $\hat{\mathscr{H}}_{\rm I}$ do not commute. Therefore it is not possible to use the ordinary expansion of the exponential. However, the difficulty can be overcome as follows. The identity

$$\exp({\rm i}\hat{\mathscr{H}}_0t/\hbar)\hat{\mathscr{H}}_{\rm I}\exp(-{\rm i}\hat{\mathscr{H}}t/\hbar) = {\rm i}\hbar\frac{\rm d}{{\rm d}t}\{\exp({\rm i}\hat{\mathscr{H}}_0t/\hbar)\exp(-{\rm i}\hat{\mathscr{H}}t/\hbar)\} \tag{5.140}$$

is easily proved by explicit differentiation on the right and with the use of eqn (5.132). Integration of both sides with respect to t gives

$$\int_{t_0}^{t}\exp({\rm i}\hat{\mathscr{H}}_0t_1/\hbar)\hat{\mathscr{H}}_{\rm I}\exp(-{\rm i}\hat{\mathscr{H}}t_1/\hbar)\,{\rm d}t_1$$
$$= {\rm i}\hbar\{\exp({\rm i}\hat{\mathscr{H}}_0t/\hbar)\exp(-{\rm i}\hat{\mathscr{H}}t/\hbar)-\exp({\rm i}\hat{\mathscr{H}}_0t_0/\hbar)\exp(-{\rm i}\hat{\mathscr{H}}t_0/\hbar)\}, \tag{5.141}$$

which can be rearranged as

$$\exp(-{\rm i}\hat{\mathscr{H}}t/\hbar) = \exp(-{\rm i}\hat{\mathscr{H}}_0t/\hbar)\Big\{\exp({\rm i}\hat{\mathscr{H}}_0t_0/\hbar)\exp(-{\rm i}\hat{\mathscr{H}}t_0/\hbar) - \frac{\rm i}{\hbar}\int_{t_0}^{t}\exp({\rm i}\hat{\mathscr{H}}_0t_1/\hbar)\hat{\mathscr{H}}_{\rm I}\exp(-{\rm i}\hat{\mathscr{H}}t_1/\hbar)\,{\rm d}t_1\Big\}. \tag{5.142}$$

In order to ensure that steady-state conditions have been achieved by the time t at which the transition rate is calculated, we assume that t_0 is a time in the infinitely remote past. Furthermore, we represent the interaction as having been gradually built up to its full strength from time $-\infty$, by insertion of a factor $\exp(\varepsilon t)$, where ε is a small quantity that is made to tend to zero in the final expressions for transition rates. The infinitely slow rate of build-up of $\hat{\mathscr{H}}_{\rm I}$ avoids any transient effects that might otherwise result from the apparent sudden application of the interaction $\hat{\mathscr{H}}_{\rm I}$ to the system that is represented as being in eigenstates of $\hat{\mathscr{H}}_0$ in the transition-rate expression (5.138).

With these modifications, and noting that $\hat{\mathscr{H}}_{\rm I}$ is now zero at time t_0 eqn (5.142) becomes

$$\exp(-{\rm i}\hat{\mathscr{H}}t/\hbar) = \exp(-{\rm i}\hat{\mathscr{H}}_0t/\hbar)$$
$$\times\Big\{1-\frac{\rm i}{\hbar}\int_{-\infty}^{t}\exp({\rm i}\hat{\mathscr{H}}_0t_1/\hbar)\hat{\mathscr{H}}_{\rm I}\exp(\varepsilon t_1)\exp(-{\rm i}\hat{\mathscr{H}}t_1/\hbar)\,{\rm d}t_1\Big\}. \tag{5.143}$$

The right-hand side can be developed as a power series in $\hat{\mathscr{H}}_{\rm I}$ by iteration. We consider the contributions of the terms in ascending orders of $\hat{\mathscr{H}}_{\rm I}$ to the transition rate $1/\tau$.

5.10. Time-dependent perturbation theory

(1) *Zero order.* The term of zero order in $\hat{\mathscr{H}}_{\rm I}$ contributes a matrix element

$$\langle f|\exp(-{\rm i}\hat{\mathscr{H}}_0t/\hbar)|u\rangle = \exp(-{\rm i}\omega_ut)\langle f\,|\,u\rangle. \tag{5.144}$$

The concept of a transition implies that ψ_u and ψ_f must be different states and the zero-order contribution is therefore zero.

(2) *First order.* The term of first order in $\hat{\mathscr{H}}_{\mathrm{I}}$ is obtained by setting $\hat{\mathscr{H}}$ equal to $\hat{\mathscr{H}}_0$ in the second term of eqn (5.143). The contribution of this term to the matrix element in eqn (5.138) is then

$$-\langle f|(\mathrm{i}/\hbar)\exp(-\mathrm{i}\hat{\mathscr{H}}_0 t/\hbar)\int_{-\infty}^{t}\exp(\mathrm{i}\hat{\mathscr{H}}_0 t_1/\hbar)\hat{\mathscr{H}}_{\mathrm{I}}\exp(\varepsilon t_1)\exp(-\mathrm{i}\hat{\mathscr{H}}_0 t_1/\hbar)\,\mathrm{d}t_1|u\rangle$$

$$= -(\mathrm{i}/\hbar)\exp(-\mathrm{i}\omega_f t)\langle f|\hat{\mathscr{H}}_{\mathrm{I}}|u\rangle\int_{-\infty}^{t}\exp(\mathrm{i}\omega_f t_1+\varepsilon t_1-\mathrm{i}\omega_u t_1)\,\mathrm{d}t_1$$

$$= \frac{\langle f|\hat{\mathscr{H}}_{\mathrm{I}}|u\rangle}{\hbar}\,\frac{\exp(\varepsilon t-\mathrm{i}\omega_u t)}{\omega_u-\omega_f+\mathrm{i}\varepsilon}. \qquad (5.145)$$

According to eqn (5.138) the transition rate is

$$\frac{1}{\tau}=\frac{\mathrm{d}}{\mathrm{d}t}\sum_f\frac{|\langle f|\hat{\mathscr{H}}_{\mathrm{I}}|u\rangle|^2}{\hbar^2}\,\frac{\exp(2\varepsilon t)}{(\omega_u-\omega_f)^2+\varepsilon^2}$$

$$=\frac{2}{\hbar^2}\sum_f|\langle f|\hat{\mathscr{H}}_{\mathrm{I}}|u\rangle|^2\,\frac{\varepsilon\exp(2\varepsilon t)}{(\omega_u-\omega_f)^2+\varepsilon^2}. \qquad (5.146)$$

We now take the limit of zero ε to produce the required slow introduction of the interaction $\hat{\mathscr{H}}_{\mathrm{I}}$. The exponential in eqn (5.146) tends to the value unity and the remaining term in ε has the form of the representation of the delta function given in eqn (2.66). Thus

$$\frac{1}{\tau}=\frac{2\pi}{\hbar^2}\sum_f|\langle f|\hat{\mathscr{H}}_{\mathrm{I}}|u\rangle|^2\,\delta(\omega_u-\omega_f). \qquad (5.147)$$

This is Fermi's golden rule quoted previously in eqn (5.72).

(3) *Second order.* The term of second order in $\hat{\mathscr{H}}_{\mathrm{I}}$ is obtained by a first iteration of eqn (5.143). That is, the term $\exp(-\mathrm{i}\hat{\mathscr{H}}t_1/\hbar)$ in the integrand is expressed in terms of $\hat{\mathscr{H}}_0$ and $\hat{\mathscr{H}}_{\mathrm{I}}$ by substituting for it the complete expression (5.143), with t replaced by t_1 and $\hat{\mathscr{H}}$ on the right replaced by $\hat{\mathscr{H}}_0$. The variable of integration in the substitution is changed to t_2 to avoid any confusion, and the matrix element of the resulting second-order contribution is

$$-\langle f|\hbar^{-2}\exp(-\mathrm{i}\hat{\mathscr{H}}_0 t/\hbar)\int_{-\infty}^{t}\mathrm{d}t_1\int_{-\infty}^{t_1}\mathrm{d}t_2\exp(\mathrm{i}\hat{\mathscr{H}}_0 t_1/\hbar)\hat{\mathscr{H}}_{\mathrm{I}}\exp(\varepsilon t_1)$$

$$\times\exp(-\mathrm{i}\hat{\mathscr{H}}_0(t_1-t_2)/\hbar)\hat{\mathscr{H}}_{\mathrm{I}}\exp(\varepsilon t_2)\exp(-\mathrm{i}\hat{\mathscr{H}}_0 t_2/\hbar)|u\rangle. \qquad (5.148)$$

The closure theorem of eqn (4.214) is now used to insert the unit quantity $\Sigma_l|l\rangle\langle l|$ somewhere between the two $\hat{\mathscr{H}}_{\mathrm{I}}$ operators in eqn (5.148). The l summation runs over the complete set of eigenstates of $\hat{\mathscr{H}}_0$. Its presence does not affect the value of the matrix element but it allows eqn (5.148) to be reduced to the more explicit form

$$-\hbar^{-2}\sum_l\exp(-\mathrm{i}\omega_f t)\langle f|\hat{\mathscr{H}}_{\mathrm{I}}|l\rangle\langle l|\hat{\mathscr{H}}_{\mathrm{I}}|u\rangle$$

$$\times\int_{-\infty}^{t}\mathrm{d}t_1\int_{-\infty}^{t_1}\exp(\mathrm{i}\omega_f t_1+\varepsilon t_1-\mathrm{i}\omega_l(t_1-t_2)+\varepsilon t_2-\mathrm{i}\omega_u t_2)\,\mathrm{d}t_2$$

$$=\sum_l\frac{\langle f|\hat{\mathscr{H}}_{\mathrm{I}}|l\rangle\langle l|\hat{\mathscr{H}}_{\mathrm{I}}|u\rangle}{\hbar^2}\,\frac{\exp(2\varepsilon t-\mathrm{i}\omega_u t)}{(\omega_u-\omega_l+\mathrm{i}\varepsilon)(\omega_u-\omega_f+2\mathrm{i}\varepsilon)}. \qquad (5.149)$$

Since ε is an arbitrary small quantity that will be made to tend to zero, it is permissible to replace 2ε by ε in eqn (5.149). The first and second-order matrix elements of eqns (5.145) and (5.149) can then be combined to give

$$\frac{1}{\hbar}\,\frac{\exp(\varepsilon t-\mathrm{i}\omega_u t)}{\omega_u-\omega_f+\mathrm{i}\varepsilon}\left(\langle f|\hat{\mathscr{H}}_{\mathrm{I}}|u\rangle+\frac{1}{\hbar}\sum_l\frac{\langle f|\hat{\mathscr{H}}_{\mathrm{I}}|l\rangle\langle l|\hat{\mathscr{H}}_{\mathrm{I}}|u\rangle}{\omega_u-\omega_l+\frac{1}{2}\mathrm{i}\varepsilon}\right). \qquad (5.150)$$

The expression for the transition rate that results from eqn (5.150) is the same as eqn (5.147) except that the first-order matrix element $\langle f|\hat{\mathscr{H}}_{\mathrm{I}}|u\rangle$ is replaced by the quantity in brackets in eqn (5.150). The $\varepsilon \to 0$ limit in the denominator of the second-order matrix element can usually be effected by merely setting ε equal to zero. For the majority of problems, the states $|l\rangle$ for which $\langle f|\hat{\mathscr{H}}_{\mathrm{I}}|l\rangle\langle l|\hat{\mathscr{H}}_{\mathrm{I}}|u\rangle$ is non-zero are such that ω_l is not equal to ω_u and no delta function arises from this term. The transition rate correct to second-order in $\hat{\mathscr{H}}_{\mathrm{I}}$ is thus

$$\frac{1}{\tau}=\frac{2\pi}{\hbar^2}\sum_f\left|\langle f|\hat{\mathscr{H}}_{\mathrm{I}}|u\rangle+\frac{1}{\hbar}\sum_l\frac{\langle f|\hat{\mathscr{H}}_{\mathrm{I}}|l\rangle\langle l|\hat{\mathscr{H}}_{\mathrm{I}}|u\rangle}{\omega_u-\omega_l}\right|^2\delta(\omega_u-\omega_f). \qquad (5.151)$$

It is necessary to examine the validity of removing ε from the denominator of the second-order matrix element for each problem to which eqn (5.151) is applied. Situations in which ω_l can equal ω_u will be encountered in §§8.7 and 8.8.

(4) *n*th *order.* The term of nth order in $\hat{\mathscr{H}}_{\mathrm{I}}$ in eqn (5.143) is obtained by iteration of the right-hand side $n-1$ times. The calculation is similar to that for second order, except that there are n integrations to perform, and the closure theorem is used $n-1$ times. The resulting transition rate with the nth-

order term included is

$$\frac{1}{\tau} = \frac{2\pi}{\hbar^2}\sum_f \left| \langle f|\hat{\mathscr{H}}_\mathrm{I}|u\rangle + \frac{1}{\hbar}\sum_l \frac{\langle f|\hat{\mathscr{H}}_\mathrm{I}|l\rangle\langle l|\hat{\mathscr{H}}_\mathrm{I}|u\rangle}{\omega_u-\omega_l} + \ldots \right.$$
$$\left. + \frac{1}{\hbar^{n-1}}\sum_{l_1}\sum_{l_2}\ldots\sum_{l_{n-1}} \frac{\langle f|\hat{\mathscr{H}}_\mathrm{I}|l_1\rangle\langle l_1|\hat{\mathscr{H}}_\mathrm{I}|l_2\rangle \ldots \langle l_{n-1}|\hat{\mathscr{H}}_\mathrm{I}|u\rangle}{(\omega_u-\omega_{l_1})(\omega_u-\omega_{l_2})\ldots(\omega_u-\omega_{l_{n-1}})} \right|^2 \delta(\omega_u-\omega_f). \tag{5.152}$$

The states $|l_1\rangle, |l_2\rangle$, etc. that occur in the higher-order terms of the transition probability are virtual intermediate states for the transition. The first-order term represents the rate of direct transitions from state $|u\rangle$ to state $|f\rangle$, while the higher-order terms represent transitions where the system changes indirectly from state $|u\rangle$ to state $|f\rangle$ via one or more intermediate states. The only energy-conservation requirement built into the transition-rate formula is that ω_u must equal ω_f. The intermediate states do not in general have the same energy as the initial state, although for each intermediate state there is an energy denominator $\hbar(\omega_u-\omega_l)$, which reduces the contribution to the matrix element for states whose energy $\hbar\omega_l$ differs from $\hbar\omega_u$ by a large amount. The system passes through the intermediate states $|l\rangle$ in a virtual sense. There is no need for energy to be conserved in the intermediate states since no real transitions are made into them.

The series of terms in eqn (5.152) normally diminishes sufficiently rapidly that only the lowest-order contributing term for a given radiative process need be retained. The required term can usually be determined by counting the number of photon states that are changed in the transition from $|u\rangle$ to $|f\rangle$. For simple absorption or emission of a photon, only one photon state is changed, and the first-order term suffices, as in the calculations of Chapter 2 and the earlier sections of the present chapter. For scattering of light, where one photon is absorbed and one emitted, the second-order term is required. In nonlinear optics, considered in Chapter 9, the two-photon absorption process requires the second-order term. For third-harmonic generation, where three photons are destroyed and one photon is created, the fourth-order term in eqn (5.152) is required.

It is clear from the symmetry of eqn (5.147) that the rates of transition from state $|u\rangle$ to state $|f\rangle$ and from state $|f\rangle$ to state $|u\rangle$ are equal in first order. A similar symmetry between the rate of a transition and its inverse is apparent in the second-order expression (5.151). However, it transpires on closer inspection that the symmetry is removed in cases where the wavefunctions are complex and there are virtual intermediate states in which ω_l is equal to ω_u. The pole in the second-order part of eqn (5.150) can then produce different contributions to the two transition rates. A similar phenomenon occurs in the higher-order terms. Thus if terms of the second or higher orders are included, the rates of a transition and its inverse are in general equal only for states with real wavefunctions. For states with complex wavefunctions, it can be shown[14] that a more complicated equality holds between the rates of a transition and the inverse transition that connects states with complex conjugate wavefunctions.

5.11. The Heisenberg representation

The time-dependent properties of quantum-mechanical quantities in the Heisenberg representation are the inverse of those in the Schrödinger representation, since the operators become time dependent but the Heisenberg wavefunctions are time-independent. The Heisenberg representation is convenient for understanding the time variations of the operators that describe the electromagnetic field. The analogies between classical and quantum theories are particularly clear in the Heisenberg representation. The field operators (4.110) to (4.114) obtained by analogy with the classical theory are indeed in the Heisenberg representation if the atom–radiation coupling is ignored. We now obtain the equations of the complete atom–radiation system in the Heisenberg representation.

The Heisenberg wavefunctions are related to the Schrödinger wavefunctions by

$$\Phi_\mathrm{H} = \exp(\mathrm{i}\hat{\mathscr{H}}t/\hbar)\Phi_\mathrm{S}(t) = \Phi_\mathrm{S}(0), \tag{5.153}$$

where $\hat{\mathscr{H}}$ is the time-independent Hamiltonian, and clearly

$$\mathrm{d}\Phi_\mathrm{H}/\mathrm{d}t = 0. \tag{5.154}$$

The time-dependent Heisenberg operators are defined in terms of the time-independent Schrödinger operators by

$$\hat{O}_\mathrm{H}(t) = \exp(\mathrm{i}\hat{\mathscr{H}}t/\hbar)\hat{O}\exp(-\mathrm{i}\hat{\mathscr{H}}t/\hbar). \tag{5.155}$$

The equation of motion of the operators is found by simple differentiation of eqn (5.155) to be

$$\mathrm{i}\hbar\,\mathrm{d}\hat{O}_\mathrm{H}(t)/\mathrm{d}t = [\hat{O}_\mathrm{H}(t), \hat{\mathscr{H}}], \tag{5.156}$$

and we note that, unlike most other operators, the total Hamiltonian remains independent of time in the Heisenberg representation,

$$\hat{\mathscr{H}}(t) = \hat{\mathscr{H}}. \tag{5.157}$$

The commutation properties of operators are unchanged by the transformation (5.155), even though the operators themselves vary with time.

Calculated results for measurable quantities are the same in all representations. Thus the Heisenberg expectation value

$$\langle\hat{O}(t)\rangle = \langle\Phi_\mathrm{H}|\hat{O}_\mathrm{H}(t)|\Phi_\mathrm{H}\rangle \tag{5.158}$$

is seen with the help of eqns (5.153) and (5.155) to be identical to eqn (5.116) for the Schrödinger expectation value. For statistical mixtures, the Heisenberg density operator obtained by analogy with eqn (5.155) is

$$\hat{\rho}_{\mathrm{H}} = \exp(\mathrm{i}\hat{\mathscr{H}}t/\hbar)\hat{\rho}_{\mathrm{S}}(t)\exp(-\mathrm{i}\hat{\mathscr{H}}t/\hbar). \tag{5.159}$$

It is seen from eqn (5.118) that this is another exception to the usual time dependence of operators in the Heisenberg representation, and

$$\mathrm{d}\hat{\rho}_{\mathrm{H}}/\mathrm{d}t = 0. \tag{5.160}$$

The Heisenberg expectation value for a statistical mixture, given by

$$\langle\hat{O}(t)\rangle = \mathrm{Tr}(\hat{\rho}_{\mathrm{H}}\hat{O}_{\mathrm{H}}(t)), \tag{5.161}$$

is seen with the help of eqns (5.155) and (5.159) to be identical to the Schrödinger value (5.120), since the trace of a product of operators is unchanged by cyclic permutation.

The rotating-wave-approximation Schrödinger Hamiltonian (5.131) for a two-level atom coupled to the radiation field becomes

$$\begin{aligned}\hat{\mathscr{H}} &= \hbar\omega_0\hat{\pi}^\dagger(t)\hat{\pi}(t)+\sum_{\mathbf{k}}\hbar\omega_{\mathbf{k}}\hat{a}_{\mathbf{k}}^\dagger(t)\hat{a}_{\mathbf{k}}(t)\\ &\quad+\mathrm{i}\sum_{\mathbf{k}}\hbar g_{\mathbf{k}}\{\hat{\pi}^\dagger(t)\hat{a}_{\mathbf{k}}(t)\exp(\mathrm{i}\mathbf{k}.\mathbf{R})-\hat{a}_{\mathbf{k}}^\dagger(t)\hat{\pi}(t)\exp(-\mathrm{i}\mathbf{k}.\mathbf{R})\}\end{aligned} \tag{5.162}$$

in the Heisenberg representation. It should be emphasized that although the complete Hamiltonian is time-independent in accordance with eqn (5.157), corresponding terms in eqns (5.131) and (5.162) are *not* equal except at $t = 0$.

The equations of motion of the various operators that appear in the Hamiltonian are obtained from eqn (5.156) with the use of their commutation properties, still given at time t by eqns (4.67) and (5.125)–(5.127). Thus

$$\mathrm{i}\hbar\,\mathrm{d}\hat{\pi}(t)/\mathrm{d}t = \hbar\omega_0\hat{\pi}(t)-\mathrm{i}\sum_{\mathbf{k}}\hbar g_{\mathbf{k}}[2\hat{\pi}^\dagger(t)\hat{\pi}(t)-1]\hat{a}_{\mathbf{k}}(t)\exp(\mathrm{i}\mathbf{k}.\mathbf{R}), \tag{5.163}$$

and the equation is formally integrated to give

$$\hat{\pi}(t) = \exp(-\mathrm{i}\omega_0 t)\left\{\hat{\pi}(0)-\sum_{\mathbf{k}}g_{\mathbf{k}}\int_0^t[2\hat{\pi}^\dagger(t')\hat{\pi}(t')-1]\hat{a}_{\mathbf{k}}(t')\exp(\mathrm{i}\mathbf{k}.\mathbf{R}+\mathrm{i}\omega_0 t')\,\mathrm{d}t'\right\}. \tag{5.164}$$

Similarly

$$\begin{aligned}\hat{\pi}^\dagger(t) &= \exp(\mathrm{i}\omega_0 t)\left\{\hat{\pi}^\dagger(0)\right.\\ &\quad\left.-\sum_{\mathbf{k}}g_{\mathbf{k}}\int_0^t\hat{a}_{\mathbf{k}}^\dagger(t')[2\hat{\pi}^\dagger(t')\hat{\pi}(t')-1]\exp(-\mathrm{i}\mathbf{k}.\mathbf{R}-\mathrm{i}\omega_0 t')\,\mathrm{d}t'\right\}.\end{aligned} \tag{5.165}$$

The analogous solutions for the radiative operators are

$$\hat{a}_{\mathbf{k}}(t) = \exp(-\mathrm{i}\omega_{\mathbf{k}}t)\left\{\hat{a}_{\mathbf{k}}(0)-g_{\mathbf{k}}\int_0^t\hat{\pi}(t')\exp(-\mathrm{i}\mathbf{k}.\mathbf{R}+\mathrm{i}\omega_{\mathbf{k}}t')\,\mathrm{d}t'\right\} \tag{5.166}$$

and

$$\hat{a}_{\mathbf{k}}^\dagger(t) = \exp(\mathrm{i}\omega_{\mathbf{k}}t)\left\{\hat{a}_{\mathbf{k}}^\dagger(0)-g_{\mathbf{k}}\int_0^t\hat{\pi}^\dagger(t')\exp(\mathrm{i}\mathbf{k}.\mathbf{R}-\mathrm{i}\omega_{\mathbf{k}}t')\,\mathrm{d}t'\right\}. \tag{5.167}$$

In each of these four last equations, the first term on the right-hand side gives the simple time dependence of the Heisenberg operator in the absence of coupling between the atom and the radiation field. The effect of the coupling, contained in the second term on the right-hand side, is to produce a complicated time dependence, together with a mixing of the field and atomic operators. There are no simple explicit solutions for the time-dependent operators of the coupled system.

The Heisenberg equations of motion and their implicit solutions given above can however be used to obtain quite simple iterative expressions for the time-dependent operators in ascending powers of the atom–radiation coupling $g_{\mathbf{k}}$. It is sufficient to obtain solutions to order $g_{\mathbf{k}}^2$ for many properties of interest, and the main results are derived in the following section. The commutation properties of the time-dependent operators can also be verified from the above solutions.

Problem 5.8. Assume that the atomic and radiative operators have their usual commutation properties at time $t = 0$, and hence prove that the creation and destruction operators given by eqns (5.166) and (5.167) satisfy

$$[\hat{a}_{\mathbf{k}}(t),\hat{a}_{\mathbf{k}}^\dagger(t)] = 1 \tag{5.168}$$

to order $g_{\mathbf{k}}^2$.

5.12. Time dependence of the atom–radiation system

As a first example of the iterative solution of the equations of motion, we consider the spontaneous emission by an excited atom. The level of excitation of an atom is given by the expectation value of the operator $\hat{\pi}^\dagger\hat{\pi}$. The equation of motion of this operator obtained from eqns (5.156) and (5.162) is

$$\mathrm{d}\hat{\pi}^\dagger(t)\hat{\pi}(t)/\mathrm{d}t = \sum_{\mathbf{k}}g_{\mathbf{k}}\{\hat{\pi}^\dagger(t)\hat{a}_{\mathbf{k}}(t)\exp(\mathrm{i}\mathbf{k}.\mathbf{R})+\hat{a}_{\mathbf{k}}^\dagger(t)\hat{\pi}(t)\exp(-\mathrm{i}\mathbf{k}.\mathbf{R})\}. \tag{5.169}$$

A solution correct to order $g_{\mathbf{k}}^2$ is obtained with the use of expressions for the radiative operators correct to order $g_{\mathbf{k}}$. Thus from eqn (5.166) we take the approximate expression

$$\hat{a}_{\mathbf{k}}(t) = \exp(-\mathrm{i}\omega_{\mathbf{k}}t)\left\{\hat{a}_{\mathbf{k}}(0) - g_{\mathbf{k}}\hat{\pi}(t)\exp(-\mathrm{i}\mathbf{k}.\mathbf{R}+\mathrm{i}\omega_0 t) \times \int_0^t \exp[\mathrm{i}(\omega_{\mathbf{k}}-\omega_0)t']\,\mathrm{d}t'\right\}, \qquad (5.170)$$

where in the integral of eqn (5.166) it is sufficient for the vacuum expectation value taken below, to use the zero-order result

$$\hat{\pi}(t') = \hat{\pi}(t)\exp[\mathrm{i}\omega_0(t-t')]. \qquad (5.171)$$

The creation operator is given by the Hermitian conjugate of eqn (5.170). Thus eqn (5.169) becomes

$$\mathrm{d}\hat{\pi}^\dagger(t)\hat{\pi}(t)/\mathrm{d}t = \sum_{\mathbf{k}} g_{\mathbf{k}}\hat{\pi}^\dagger(t)\left\{\hat{a}_{\mathbf{k}}(0)\exp(\mathrm{i}\mathbf{k}.\mathbf{R}-\mathrm{i}\omega_{\mathbf{k}}t) - g_{\mathbf{k}}\hat{\pi}(t)\int_0^t \exp[\mathrm{i}(\omega_{\mathbf{k}}-\omega_0)(t'-t)]\,\mathrm{d}t'\right\} \qquad (5.172)$$

$$+\text{hermitian conjugate.}$$

Suppose that the radiation field is in its vacuum state $|0\rangle$ at time $t = 0$ with

$$\langle 0|\hat{a}_{\mathbf{k}}(0)|0\rangle = \langle 0|\hat{a}^\dagger_{\mathbf{k}}(0)|0\rangle = 0. \qquad (5.173)$$

The expectation value of eqn (5.172) with respect to the vacuum state therefore gives

$$\mathrm{d}\langle 0|\hat{\pi}^\dagger(t)\hat{\pi}(t)|0\rangle/\mathrm{d}t$$

$$= -\langle 0|\hat{\pi}^\dagger(t)\hat{\pi}(t)|0\rangle\sum_{\mathbf{k}} g^2_{\mathbf{k}}\int_0^t \exp[\mathrm{i}(\omega_{\mathbf{k}}-\omega_0)(t'-t)]\,\mathrm{d}t'$$

$$+\text{complex conjugate}$$

$$= -\langle 0|\hat{\pi}^\dagger(t)\hat{\pi}(t)|0\rangle\sum_{\mathbf{k}} 2g^2_{\mathbf{k}}\sin[(\omega_{\mathbf{k}}-\omega_0)t]/(\omega_{\mathbf{k}}-\omega_0). \qquad (5.174)$$

For sufficiently large t the final factors in this expression form a representation of the delta function as in eqn (2.65). The summation in eqn (5.174) is then identical to eqn (5.71), and with the notation of eqn (5.75),

$$\mathrm{d}\langle 0|\hat{\pi}^\dagger(t)\hat{\pi}(t)|0\rangle/\mathrm{d}t = -2\gamma\langle 0|\hat{\pi}^\dagger(t)\hat{\pi}(t)|0\rangle. \qquad (5.175)$$

The level of excitation of the atom thus decays at a rate 2γ, and eqn (5.175) is the Heisenberg-representation description of the spontaneous emission process, equivalent to the phenomenological result (1.76).

It is straightforward to make a similar approximation to the equation of motion (5.163) of the atomic de-excitation operator, and the result obtained with the use of eqn (5.170) is

$$\mathrm{d}\langle 0|\hat{\pi}(t)|0\rangle/\mathrm{d}t = -\langle 0|\hat{\pi}(t)|0\rangle\left\{\mathrm{i}\omega_0 + \sum_{\mathbf{k}} g^2_{\mathbf{k}}\int_0^t \exp[\mathrm{i}(\omega_{\mathbf{k}}-\omega_0)(t'-t)]\,\mathrm{d}t'\right\}. \qquad (5.176)$$

This expression is somewhat more difficult to evaluate than the analogous result (5.174) and it is necessary to consider the nature of the integral in a little detail.

By standard integration we find

$$\int_0^t \exp[\mathrm{i}(\omega_{\mathbf{k}}-\omega_0)(t'-t)]\,\mathrm{d}t' = \frac{1-\cos(\omega_{\mathbf{k}}-\omega_0)t}{\mathrm{i}(\omega_{\mathbf{k}}-\omega_0)} + \frac{\sin(\omega_{\mathbf{k}}-\omega_0)t}{\omega_{\mathbf{k}}-\omega_0}. \qquad (5.177)$$

The real part on the right-hand side is equivalent to a delta function for large t, and only this part contributed to eqn (5.174). However eqn (5.176) also includes an imaginary part from the first term on the right of eqn (5.177). The principal value of $1/(\omega_{\mathbf{k}}-\omega_0)$ can be defined as[15]

$$\frac{P}{\omega_{\mathbf{k}}-\omega_0} = \mathop{\mathrm{Lt}}_{t\to\infty}\frac{1-\cos(\omega_{\mathbf{k}}-\omega_0)t}{\omega_{\mathbf{k}}-\omega_0}. \qquad (5.178)$$

When this function occurs in an integration over $\omega_{\mathbf{k}}$, the rapidly-oscillating cosine makes no contribution, except at the value $\omega_{\mathbf{k}} = \omega_0$, where it cancels with the 1 in the numerator to give a zero. The principal value thus behaves everywhere like $1/(\omega_{\mathbf{k}}-\omega_0)$ except for the removal of a small range of integration symmetrically placed around $\omega_{\mathbf{k}} = \omega_0$. We now write eqn (5.177) in the form

$$\int_0^t \exp[\mathrm{i}(\omega_{\mathbf{k}}-\omega_0)(t'-t)]\,\mathrm{d}t' = -\mathrm{i}[P/(\omega_{\mathbf{k}}-\omega_0)] + \pi\,\delta(\omega_{\mathbf{k}}-\omega_0). \qquad (5.179)$$

The equation of motion (5.176) is converted by substitution of eqn (5.179) to

$$\frac{\mathrm{d}\langle 0|\hat{\pi}(t)|0\rangle}{\mathrm{d}t} = -\langle 0|\hat{\pi}(t)|0\rangle\left\{\mathrm{i}\omega_0 - \mathrm{i}\frac{V}{(2\pi)^3}P\int\frac{g^2_{\mathbf{k}}\,\mathrm{d}\mathbf{k}}{\omega_{\mathbf{k}}-\omega_0} + \gamma\right\}, \qquad (5.180)$$

where the summation over **k** is converted to an integration by eqn (4.128) and the radiative decay rate is obtained from the delta-function part as in eqn (5.175). According to eqn (5.129), eqn (5.180) and the Hermitian conjugate equation determine the time dependence of the dipole moment of the radiating atom. The first two terms in the large bracket of eqn (5.180) give the frequency of oscillation of the dipole while the third term gives the rate of exponential decay of the dipole moment. The second term is a correction to the oscillation frequency ω_0 brought about by the coupling of the atom to the radiation field.

The calculation of radiative corrections to the energy-level separations of atoms forms an extensive field of study. The integral given in eqn (5.180) is not in fact an adequate starting point since there is a further contribution of the same order from the final term in the complete Hamiltonian (5.35) of the atom–radiation system. This term produces no change in ω_0 for a two-level atom, but real atoms have of course many levels, and the term then makes an important contribution. The resulting expression for the total shift needs careful treatment since it contains an integration over wavevector that diverges at its upper limit, similar to though not so serious as the divergence in the integral in eqn (5.180). The frequency shift was first successfully evaluated by Bethe[16] in 1947 using a technique known as mass renormalization. We do not consider the details of the calculation, and the interested reader can find good accounts in other texts.[17,18]

Calculations for the hydrogen atom show that the shift vanishes unless one of the states in the transition is an S state. The shift is always very small, and for example its value for the $2^2S_{\frac{1}{2}}$ state of hydrogen is about 10^9 Hz, roughly six orders of magnitude smaller than the $n = 2$ state excitation energy. The existence of level shifts was first demonstrated by Lamb and Retherford in experiments on radiative transitions between the $2^2S_{\frac{1}{2}}$ state of hydrogen and the unshifted $2^2P_{\frac{1}{2}}$ state. The splitting between these two states is known as the Lamb shift. In future calculations we ignore these small corrections, assuming them to have been included in the basic transition frequencies ω_0 between pairs of energy levels.

5.13. The source-field expression

As a third and final example of the solution of the Heisenberg equations of motion, we consider the time dependence of the electric-field operator at a point **r** some distance from a radiating atom at position **R**. The electric field is divided into two parts as in eqn (5.83) with

$$\hat{\mathbf{E}}^{+}(\mathbf{r}t) = \mathrm{i}\sum_{\mathbf{k}}(\hbar\omega_{\mathbf{k}}/2\epsilon_0 V)^{\frac{1}{2}}\boldsymbol{\varepsilon}_{\mathbf{k}}\hat{a}_{\mathbf{k}}(t)\exp(\mathrm{i}\mathbf{k}.\mathbf{r}), \tag{5.181}$$

and the conjugate expression for $\hat{\mathbf{E}}^{-}(\mathbf{r}t)$. The time-dependent destruction operator given by eqn (5.166) has two parts, an initial-value or freely propagating part that is independent of the atom, and a part that represents the field radiated by the atomic light source. The initial-value part makes no contribution to expectation values of normally-ordered operators for states of the field in which no photons are excited at time $t = 0$. Thus with the assumption that the field operators will be used only in such expectation-value calculations, the initial-value part can be dropped, and substitution of the source-field part of eqn (5.166) into eqn (5.181) gives

$$\hat{\mathbf{E}}^{+}(\mathbf{r}t) = -(\mathrm{i}e/16\pi^3\epsilon_0)\int \mathrm{d}\mathbf{k}\,\omega_{\mathbf{k}}\boldsymbol{\varepsilon}_{\mathbf{k}}(\boldsymbol{\varepsilon}_{\mathbf{k}}.\mathbf{D}_{12})\exp\{\mathrm{i}\mathbf{k}.(\mathbf{r}-\mathbf{R})-\mathrm{i}\omega_{\mathbf{k}}t\}$$
$$\times\int_0^t \hat{\pi}(t')\exp(\mathrm{i}\omega_{\mathbf{k}}t')\,\mathrm{d}t', \tag{5.182}$$

with $g_{\mathbf{k}}$ substituted from eqn (5.59) and the sum converted to an integral by eqn (4.128).

Fig. 5.4 shows the orientations of the various vector quantities that enter eqn (5.182). The line joining the atom to the observation point is taken as the *z*-axis of Cartesian and polar coordinates, with the atom as origin. The wavevector and the two independent polarizations of a radiated mode have polar coordinates given in eqns (4.123)–(4.125), and the orientation of the

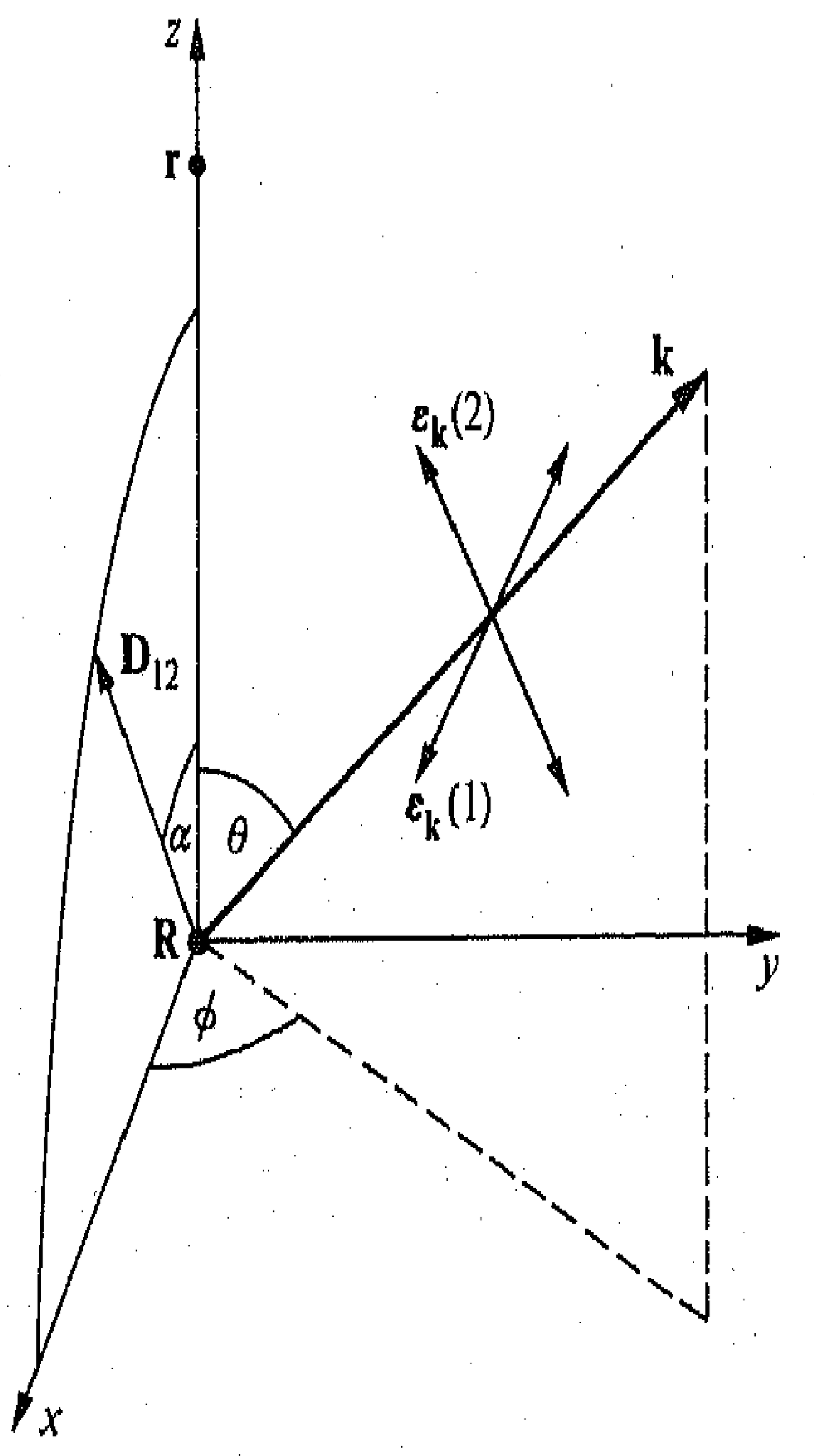
z
r
k
$\boldsymbol{\varepsilon}_{\mathbf{k}}(2)$
$\mathbf{D}_{12}$
$\boldsymbol{\varepsilon}_{\mathbf{k}}(1)$
α
θ
R
y
ϕ
x

FIG. 5.4. Orientations of the vectors used in the evaluation of the electric field at **r** produced by radiation from an atom at **R**.

atomic dipole moment is as given in eqn (5.73). It is clear from the symmetry of the figure that the radiated field has zero y-component. The x- and z-components are found by evaluation of the integrals in eqn (5.182). Just as in the corresponding classical theory of radiation by a dipole,[1] the field at $\mathbf{r}$ has nonzero x- and z-components close to the dipole but at distances such that

$$k|\mathbf{r}-\mathbf{R}| \gg 1 \qquad (5.183)$$

the field consists of transverse waves polarized parallel to the x-direction. We consider only the far field of the dipole and assume that the inequality (5.183) is valid for the wavevectors that contribute most strongly to the emission.

The angular part of the wavevector integration in eqn (5.182) is

$$\int_0^{\pi} \mathrm{d}\theta \int_0^{2\pi} \mathrm{d}\phi\, \boldsymbol{\varepsilon}_{\mathbf{k}}(\boldsymbol{\varepsilon}_{\mathbf{k}}.\mathbf{D}_{12}) \exp\{\mathrm{i}k|\mathbf{r}-\mathbf{R}|\cos\theta\}$$

$$= -\frac{2\pi \mathrm{i} D_{12}\sin\alpha}{k|\mathbf{r}-\mathbf{R}|}\{\exp(\mathrm{i}k|\mathbf{r}-\mathbf{R}|)-\exp(-\mathrm{i}k|\mathbf{r}-\mathbf{R}|)\}\mathbf{i}, \qquad (5.184)$$

where $\mathbf{i}$ is a unit vector parallel to the x-axis and the neglected terms have the denominator raised to higher powers. Substitution in eqn (5.182) gives two contributions to the electric-field operator corresponding to the two terms in the large bracket of eqn (5.184). Retaining for the moment only the first of these, we find

$$\hat{\mathbf{E}}^{+}(\mathbf{r}t) = -\frac{eD_{12}\sin\alpha}{8\pi^2\epsilon_0 c^2|\mathbf{r}-\mathbf{R}|}\mathbf{i}\int \mathrm{d}\omega_{\mathbf{k}}\,\omega_{\mathbf{k}}^2$$

$$\times \exp\left[-\mathrm{i}\omega_{\mathbf{k}}\left(t-\frac{|\mathbf{r}-\mathbf{R}|}{c}\right)\right]\int_0^t \mathrm{d}t'\hat{\pi}(t')\exp(\mathrm{i}\omega_{\mathbf{k}}t'). \qquad (5.185)$$

The field operator to lowest order in the atom-radiation coupling is obtained by taking the zero-order time dependence of eqn (5.171) for the atomic transition operator. A result that involves $\omega_{\mathbf{k}}$ only in the combination $\omega_{\mathbf{k}}-\omega_0$ is obtained by setting

$$\hat{\pi}(t') = \hat{\pi}\left(t-\frac{|\mathbf{r}-\mathbf{R}|}{c}\right)\exp\left[\mathrm{i}\omega_0\left(t-\frac{|\mathbf{r}-\mathbf{R}|}{c}-t'\right)\right]. \qquad (5.186)$$

The time integral in eqn (5.185) and the exponential factor that precedes it then give

$$\frac{\exp\left[\mathrm{i}(\omega_{\mathbf{k}}-\omega_0)\dfrac{|\mathbf{r}-\mathbf{R}|}{c}\right]-\exp\left[-\mathrm{i}(\omega_{\mathbf{k}}-\omega_0)\left(t-\dfrac{|\mathbf{r}-\mathbf{R}|}{c}\right)\right]}{\mathrm{i}(\omega_{\mathbf{k}}-\omega_0)}\hat{\pi}\left(t-\frac{|\mathbf{r}-\mathbf{R}|}{c}\right). \qquad (5.187)$$

We assume equivalent to the inequality (5.183) that

$$\omega_0|\mathbf{r}-\mathbf{R}|/c \gg 1, \qquad (5.188)$$

and we also assume that t is sufficiently large that

$$\omega_0\left(t-\frac{|\mathbf{r}-\mathbf{R}|}{c}\right) \gg 1. \qquad (5.189)$$

The prefactor of $\hat{\pi}$ in the expression (5.187) then generates a delta function by the representation (2.64), and the expression reduces to

$$2\pi\,\delta(\omega_{\mathbf{k}}-\omega_0)\hat{\pi}\left(t-\frac{|\mathbf{r}-\mathbf{R}|}{c}\right). \qquad (5.190)$$

The contribution of the second term in the large bracket of eqn (5.184) can be treated similarly but it gives a zero result since the signs of both exponents in the expression analogous to (5.187) are the same.

Thus inserting the expression (5.190) into eqn (5.185) and carrying out the frequency integral we find

$$\hat{\mathbf{E}}^{+}(\mathbf{r}t) = -\frac{e\omega_0^2 D_{12}\sin\alpha}{4\pi\epsilon_0 c^2|\mathbf{r}-\mathbf{R}|}\mathbf{i}\hat{\pi}\left(t-\frac{|\mathbf{r}-\mathbf{R}|}{c}\right). \qquad (5.191)$$

The other component $\hat{\mathbf{E}}^{-}$ of the field operator is given by the conjugate expression, and the two together express the field at point $\mathbf{r}$ in terms of the dipole operator of the radiating source atom. The expression is identical in form to that which relates the classical field radiated by a dipole to the classical dipole moment.[1] Note that the field operator at time t is determined by the dipole operator at a retarded time, similar to that in eqn (4.30), thus making proper allowance for the travel time of the electromagnetic waves from $\mathbf{R}$ or $\mathbf{r}$. An advanced component, which would have resulted from the second term in eqn (5.184), is removed in the subsequent integrations over $\omega_{\mathbf{k}}$ and t', as mentioned above.

The source-field expression (5.191) has been widely applied since its introduction[19,20,21] and we use it in Chapters 7 and 8 to obtain information on the coherence properties of the radiation fields emitted by atoms whose dipole moments have known time dependences. It should be emphasized that the relation is valid only for the evaluation of expectation values of normally-ordered operators when the distance and time satisfy the inequalities (5.188) and (5.189).

Problem 5.9. If a radiating atom is placed at the origin of coordinates, show that the radiated intensity defined in eqn (5.100) integrated over the surface of a large sphere of radius r centred on the origin is

$$r^2\int\langle\hat{I}(\mathbf{r}t)\rangle\,\mathrm{d}\Omega = 2\gamma\hbar\omega_0\left\langle\hat{\pi}^\dagger\left(t-\frac{r}{c}\right)\hat{\pi}\left(t-\frac{r}{c}\right)\right\rangle, \qquad (5.192)$$

where $\mathrm{d}\Omega$ is an element of solid angle and the integration runs over the complete 4π solid angle.

The right-hand side of eqn (5.192) is the same as the rate of spontaneous emission of energy per excited atom $(N_2/N)A\hbar\omega_0$ used in the Einstein theory of Chapter 1.

5.14. The interaction representation

This third and final representation to be considered is intermediate between the Schrödinger and Heisenberg representations, having both wavefunctions and operators that vary with the time. Let the Hamiltonian be written as in eqn (5.132), with $\hat{\mathscr{H}}_0$ the contribution of the uncoupled electrons and radiation and $\hat{\mathscr{H}}_\mathrm{I}$ the interaction between them. The interaction-representation wavefunction is related to the Schrödinger wavefunction by

$$\Phi_\mathrm{I}(t) = \exp(\mathrm{i}\hat{\mathscr{H}}_0t/\hbar)\Phi_\mathrm{S}(t) = \exp(\mathrm{i}\hat{\mathscr{H}}_0t/\hbar)\exp\{-\mathrm{i}(\hat{\mathscr{H}}_0+\hat{\mathscr{H}}_\mathrm{I})t/\hbar\}\Phi_\mathrm{S}(0), \qquad (5.193)$$

where the exponentials on the right cannot be combined since the two parts of the Hamiltonian do not commute. The equation of motion obtained by differentiation of eqn (5.193) is

$$\mathrm{i}\hbar\,\mathrm{d}\Phi_\mathrm{I}(t)/\mathrm{d}t = \hat{\mathscr{H}}_\mathrm{I}(t)\Phi_\mathrm{I}(t), \qquad (5.194)$$

where interaction-representation time-dependent operators like $\hat{\mathscr{H}}_\mathrm{I}(t)$ are defined by

$$\hat{O}_\mathrm{I}(t) = \exp(\mathrm{i}\hat{\mathscr{H}}_0t/\hbar)\hat{O}\exp(-\mathrm{i}\hat{\mathscr{H}}_0t/\hbar). \qquad (5.195)$$

The operator equation of motion obtained by differentiation of eqn (5.195) is

$$\mathrm{i}\hbar\,\mathrm{d}\hat{O}_\mathrm{I}(t)/\mathrm{d}t = [\hat{O}_\mathrm{I}(t),\hat{\mathscr{H}}_0]. \qquad (5.196)$$

Note that the uncoupled part of the Hamiltonian is time independent,

$$\hat{\mathscr{H}}_0(t) = \hat{\mathscr{H}}_0, \qquad (5.197)$$

but the interaction part of the Hamiltonian varies with time.

The nature of the interaction representation is characterized by eqns (5.194) and (5.196), which show that the motion of the wavefunctions is Schrödinger-like but only the interaction part of the Hamiltonian contributes to the time dependence, while the motion of the operators is Heisenberg-like but only the uncoupled part of the Hamiltonian contributes to the time dependence. The main time dependence in the theory is carried by the operators in cases where the coupling $\hat{\mathscr{H}}_\mathrm{I}$ between the two parts of the system is weak. The interaction representation becomes identical to the Heisenberg representation if the interaction part of the Hamiltonian is set equal to zero.

All calculated results for measurable quantities are again the same in the interaction representation as in the other representations. Thus the interaction expectation value

$$\langle\hat{O}(t)\rangle = \langle\Phi_\mathrm{I}(t)|\hat{O}_\mathrm{I}(t)|\Phi_\mathrm{I}(t)\rangle \qquad (5.198)$$

gives identical results to eqns (5.116) and (5.158). The interaction density-operator defined by analogy with eqn (5.195) is

$$\hat{\rho}_\mathrm{I}(t) = \exp(\mathrm{i}\hat{\mathscr{H}}_0t/\hbar)\hat{\rho}_\mathrm{S}(t)\exp(-\mathrm{i}\hat{\mathscr{H}}_0t/\hbar) \qquad (5.199)$$

and its equation of motion obtained with the help of eqn (5.119) is

$$\mathrm{i}\hbar\,\mathrm{d}\hat{\rho}_\mathrm{I}(t)/\mathrm{d}t = [\hat{\mathscr{H}}_\mathrm{I}(t),\hat{\rho}_\mathrm{I}(t)]. \qquad (5.200)$$

It is easily verified that the expectation value for a statistical mixture,

$$\langle\hat{O}(t)\rangle = \mathrm{Tr}\big(\hat{\rho}_\mathrm{I}(t)\hat{O}_\mathrm{I}(t)\big), \qquad (5.201)$$

is identical to the Schrödinger value (5.120) and the Heisenberg value (5.161).

The two parts of the Schrödinger Hamiltonian (5.131) for a two-level atom in the rotating-wave approximation are

$$\hat{\mathscr{H}}_0 = \hbar\omega_0\hat{\pi}^\dagger\hat{\pi}+\sum_\mathbf{k}\hbar\omega_\mathbf{k}\hat{a}_\mathbf{k}^\dagger\hat{a}_\mathbf{k} \qquad (5.202)$$

$$\hat{\mathscr{H}}_\mathrm{I} = \mathrm{i}\sum_\mathbf{k}\hbar g_\mathbf{k}\{\hat{\pi}^\dagger\hat{a}_\mathbf{k}\exp(\mathrm{i}\mathbf{k}.\mathbf{R})-\hat{a}_\mathbf{k}^\dagger\hat{\pi}\exp(-\mathrm{i}\mathbf{k}.\mathbf{R})\}. \qquad (5.203)$$

The time dependences of the atomic and radiative operators given by eqn (5.196) are simply

$$\hat{\pi}(t) = \hat{\pi}\exp(-\mathrm{i}\omega_0t),\ \hat{\pi}^\dagger(t) = \hat{\pi}^\dagger\exp(\mathrm{i}\omega_0t) \qquad (5.204)$$

and

$$\hat{a}_\mathbf{k}(t) = \hat{a}_\mathbf{k}\exp(-\mathrm{i}\omega_\mathbf{k}t),\ \hat{a}_\mathbf{k}^\dagger(t) = \hat{a}_\mathbf{k}^\dagger\exp(\mathrm{i}\omega_\mathbf{k}t). \qquad (5.205)$$

Thus the field operators (4.111) and (4.112) always have the correct time dependences for the interaction representation, whereas these forms are correct in the Heisenberg representation only for a radiation field not coupled to atoms; more generally, the radiative operators have the complicated time dependences (5.166) and (5.167) in the Heisenberg representation. Substitution of eqns (5.204) and (5.205) into $\hat{\mathscr{H}}_0(t)$ obtained from eqn (5.202) verifies the property (5.197); substitution into $\hat{\mathscr{H}}_{\mathrm{I}}(t)$ obtained from eqn (5.203) gives

$$\begin{aligned}\hat{\mathscr{H}}_{\mathrm{I}}(t) = \mathrm{i}\sum_{\mathbf{k}}\hbar \mathscr{g}_{\mathbf{k}}\{&\hat{\pi}^{\dagger}\hat{a}_{\mathbf{k}}\exp[\mathrm{i}(\omega_0-\omega_{\mathbf{k}})t+\mathrm{i}\mathbf{k}.\mathbf{R}]\\ &-\hat{a}^{\dagger}_{\mathbf{k}}\hat{\pi}\exp[-\mathrm{i}(\omega_0-\omega_{\mathbf{k}})t-\mathrm{i}\mathbf{k}.\mathbf{R}]\}.\end{aligned} \tag{5.206}$$

The simple time dependences of the basic operators make the interaction representation very convenient for the solution of a range of problems involving the atom-radiation interaction. Consider the expectation values of the transition operators for a two-level atom. With the definitions (5.121)-(5.123), we find with the use of eqns (5.201) and (5.204) that

$$\langle\hat{\pi}(t)\rangle = \mathrm{Tr}\big(\hat{\rho}_{\mathrm{I}}(t)\hat{\pi}\big)\exp(-\mathrm{i}\omega_0 t) = \rho_{21}(t)\exp(-\mathrm{i}\omega_0 t), \tag{5.207}$$

$$\langle\hat{\pi}^{\dagger}(t)\rangle = \rho_{12}(t)\exp(\mathrm{i}\omega_0 t), \tag{5.208}$$

and

$$\langle\hat{\pi}^{\dagger}(t)\hat{\pi}(t)\rangle = \rho_{22}(t), \tag{5.209}$$

where $\rho_{ij}(t)$ is the atomic density matrix in the interaction representation.

The time dependences of the density matrix elements are determined by eqn (5.200) with the interaction Hamiltonian (5.206). The equation of motion for an atom placed at the origin ($\mathbf{R} = 0$) is

$$\begin{aligned}\mathrm{i}\hbar\,\mathrm{d}\rho_{ij}(t)/\mathrm{d}t = \mathrm{i}\sum_{\mathbf{k}}\hbar \mathscr{g}_{\mathbf{k}}\{&\langle i|\hat{\pi}^{\dagger}\hat{a}_{\mathbf{k}}\hat{\rho}-\hat{\rho}\hat{\pi}^{\dagger}\hat{a}_{\mathbf{k}}|j\rangle\exp[\mathrm{i}(\omega_0-\omega_{\mathbf{k}})t]\\ &-\langle i|\hat{a}^{\dagger}_{\mathbf{k}}\hat{\pi}\hat{\rho}-\hat{\rho}\hat{a}^{\dagger}_{\mathbf{k}}\hat{\pi}|j\rangle\exp[-\mathrm{i}(\omega_0-\omega_{\mathbf{k}})t]\}.\end{aligned} \tag{5.210}$$

The equation takes a particularly simple form when the radiation is in the multimode coherent state defined in eqn (4.236). Then as a result of the property (4.186), the operators $\hat{a}_{\mathbf{k}}$ and $\hat{a}^{\dagger}_{\mathbf{k}}$ are replaced by $\alpha_{\mathbf{k}}$ and $\alpha^{*}_{\mathbf{k}}$ respectively when the expectation value of eqn (5.210) is taken with respect to the coherent state, and

$$\mathrm{d}\rho_{22}/\mathrm{d}t = \sum_{\mathbf{k}}\mathscr{g}_{\mathbf{k}}\{\alpha_{\mathbf{k}}\exp[\mathrm{i}(\omega_0-\omega_{\mathbf{k}})t]\rho_{12}+\alpha^{*}_{\mathbf{k}}\exp[-\mathrm{i}(\omega_0-\omega_{\mathbf{k}})t]\rho_{21}\} \tag{5.211}$$

$$\mathrm{d}\rho_{12}/\mathrm{d}t = \sum_{\mathbf{k}}\mathscr{g}_{\mathbf{k}}\alpha^{*}_{\mathbf{k}}\exp[-\mathrm{i}(\omega_0-\omega_{\mathbf{k}})t](\rho_{11}-\rho_{22}). \tag{5.212}$$

It is seen by comparison with eqns (2.78) and (2.79) that these are the same as the optical Bloch equations derived by semiclassical theory, apart from the additional summation over modes in the above equations. The correspondence in the case of a single-mode excitation is

$$\tfrac{1}{2}\mathrm{i}\mathscr{V} \leftrightarrow \mathscr{g}_{\mathbf{k}}\alpha^{*}_{\mathbf{k}}, \tag{5.213}$$

or

$$\tfrac{1}{2}\mathscr{V} \leftrightarrow \mathscr{g}_{\mathbf{k}}|\alpha_{\mathbf{k}}| \tag{5.214}$$

for the choice of phase in (4.210). Thus

$$\tfrac{1}{4}\mathscr{V}^{2} \leftrightarrow \mathscr{g}^{2}_{\mathbf{k}}\bar{n}_{\mathbf{k}}, \tag{5.215}$$

where the mean number of photons $\bar{n}_{\mathbf{k}}$ is determined as in eqn (4.192).

We note that the theory of Chapter 2 is presented in a kind of semiclassical interaction representation, with time dependences for the atomic and radiative parts of the problem similar to those in eqns (5.204) and (5.205). The quantum equations take the forms (5.211) and (5.212) only for interaction of atoms with a coherent state of the radiation field, another property of the coherent states that illustrates their correspondence to the classical stable electromagnetic wave. A treatment of the effects of radiative damping, similar to that which leads in the Heisenberg representation to eqns (5.175) and (5.180), shows that the interaction representation Bloch equations (5.211) and (5.212) are modified by the same additional terms in γ as appear in the semiclassical equations (2.114) and (2.115). The various solutions considered in Chapter 2 therefore apply also in the quantum case, always provided that the radiation field is in a coherent state.

References

1. JACKSON, J. D. (1975). *Classical electrodynamics*. Wiley, New York.
2. WOOLLEY, R. G. (1971). *Proc. R. Soc.* **A321**, 557; BABIKER, M., POWER, E. A., and THIRUNAMACHANDRAN, T. (1973). *Proc. R. Soc.* **A332**, 187.
3. CASTELLANOS, A., PANIZO, M., and RIVAS, J. (1978). *Am. J. Phys.* **46**, 1116.
4. POWER, E. A. and ZIENAU, S. (1959). *Phil. Trans. R. Soc.* **251**, 427; POWER, E. A. (1964). *Introductory quantum electrodynamics*. Longmans, London; POWER, E.A. and THIRUNAMACHANDRAN, T. (1978). *Am. J. Phys.* **46**, 370.
5. ATKINS, P. W. and WOOLLEY, R. G. (1970). *Proc. R. Soc.* **A319**, 549; WOOLLEY, R. G. (1975). *Adv. chem. Phys.* **33**, 153.
6. RZAZEWSKI, K. and WODKIEWICZ, K. (1980). *Ann. Phys.* (*NY*) **130**, 1.
7. MESSIAH, A. (1961). *Quantum mechanics*. North-Holland, Amsterdam.
8. See, for example, CORNEY, A. (1977). *Atomic and laser spectroscopy*. Clarendon Press, Oxford.
9. For a discussion of the $(n+1)/n$ ratio, with historical remarks, see VAN VLECK, J. H. and HUBER, D. L. (1977). *Rev. mod. Phys.* **49**, 939.
10. The observational significance of emission into the same mode as the stimulating light is discussed by DURRANT, A. V. (1981). *Optica Acta* **28**, 627.
11. For a more complete discussion of the photoelectric effect in hydrogen-like atoms, see BETHE, H. A. and SALPETER, E. E. (1957) *Quantum mechanics of one- and two-electron atoms*, Chapter 4, Part b. Springer-Verlag, Berlin.
12. See, for example, ZIMAN, J. M. (1969). *Elements of advanced quantum theory*, p. 70. Cambridge University Press.
13. See Chapter 8 of ref. 7, or Chapter 3 of ref. 12.
14. LANDAU, L. D. and LIFSHITZ, E. M. (1977). *Quantum mechanics*, p. 602. Pergamon, Oxford.
15. HEITLER, W. (1954). *The quantum theory of radiation*, p. 69. Clarendon Press, Oxford.

16. BETHE, H. A. (1947). *Phys. Rev.* **72**, 339. Reprinted (1958) in *Quantum electrodynamics* (Ed. J. Schwinger), p. 139. Dover, New York.
17. See, for example, SAKURAI, J. J. (1967). *Advanced quantum mechanics*, §§2–8 and 4–7. Addison-Wesley, Reading, Massachusetts. The treatments in this and the previous reference use the **A.p** form of interaction between the electron and the radiation field, as in eqn (5.23).
18. MILONNI, P. W. (1976). *Phys. Reps.* **25**, 1. This treatment uses the **E.r** form of interaction first employed in the calculation of frequency shifts by POWER and ZIENAU, ref. 4.
19. MOLLOW, B. R. (1969). *Phys. Rev.* **188**, 1969.
20. LEHMBERG, R. H. (1970). *Phys. Rev.* **A2**, 883.
21. For a more recent discussion, see DURRANT, A. V. (1977). *Am. J. Phys.* **45**, 752.

6. Photon optics

THE previous two chapters have developed the techniques needed to apply the quantum theory of light to a range of optical experiments. The main purpose of the present chapter is a reconsideration of the fluctuation properties of light in terms of the quantum theory. Much of the material given below is essentially a photon version of the phenomena treated classically in Chapter 3. It is convenient to treat the same interference experiments and to express their results in terms of quantum degrees of coherence that have a similar physical significance to the previously-defined classical degrees of coherence.

A remarkable feature of the theory of light is the large measure of agreement between the predictions of classical and quantum theory, despite the fundamental differences between the two approaches. Thus, it turns out that classical and quantum theories predict identical interference effects and associated degrees of coherence for experiments that use coherent or chaotic light, or light with coherence properties intermediate between the two. In these cases, the quantum theory provides different conceptual descriptions of the experiments, but the electromagnetic field quantization has little impact on the observable phenomena.

Exclusively quantum effects occur however in experiments made on other kinds of light that cannot be envisaged in classical electromagnetic theory. In the present and later chapters we consider the regions of overlap of the classical and quantum theories, and pay particular attention to experiments that generate light with nonclassical fluctuation and coherence properties. The main tool in the quantum description of a beam of light is its photon probability distribution, or more generally, its density operator. Photon-counting experiments provide a fairly direct measurement of the photon probability distribution for all kinds of light embraced by the quantum theory. Such experiments form the observational basis of *quantum optics* and play a leading role in the study of quantum phenomena in light beams.

6.1. Quantum theory of Young's interference experiment

Consider Young's interference experiment pictured in Fig. 3.6, with the incident light regarded as a stream of photons and the intensity at the second screen measured in accordance with the form of the photon intensity operator (5.99). The quantum theory of the experiment parallels the classical theory outlined in §3.4. We consider the superposition of the radiation fields from the two pinholes at a phototube or other light detector on the second screen. The Heisenberg electric-field operator at position **r** on the screen is given by eqn (5.83) with

$$\hat{E}^{+}(\mathbf{r}t) = u_1\hat{E}^{+}(\mathbf{r}_1t_1)+u_2\hat{E}^{+}(\mathbf{r}_2t_2), \tag{6.1}$$

analogous to eqn (3.30), where we assume for simplicity a single polarization direction for the light.

The superposition theory proceeds in much the same way as the classical treatment, except that the classical intensity, proportional to an ensemble average of E^*E, must be replaced by the quantum-mechanical detector response, proportional to an average of the intensity operator $\hat{E}^{-}\hat{E}^{+}$. The replacement for the classical intensity distribution (3.33) is

$$\begin{aligned}\langle\hat{I}(\mathbf{r}t)\rangle = 2\epsilon_0 c\{&|u_1|^2\langle\hat{E}^{-}(\mathbf{r}_1t_1)\hat{E}^{+}(\mathbf{r}_1t_1)\rangle+|u_2|^2\langle\hat{E}^{-}(\mathbf{r}_2t_2)\hat{E}^{+}(\mathbf{r}_2t_2)\rangle\\ &+u_1^*u_2\langle\hat{E}^{-}(\mathbf{r}_1t_1)\hat{E}^{+}(\mathbf{r}_2t_2)\rangle+u_1u_2^*\langle\hat{E}^{-}(\mathbf{r}_2t_2)\hat{E}^{+}(\mathbf{r}_1t_1)\rangle\},\end{aligned} \tag{6.2}$$

where the angle-bracket expressions are evaluated in accordance with eqn (5.100), for example

$$\langle\hat{E}^{-}(\mathbf{r}_1t_1)\hat{E}^{+}(\mathbf{r}_2t_2)\rangle = \mathrm{Tr}\big(\hat{\rho}\hat{E}^{-}(\mathbf{r}_1t_1)\hat{E}^{+}(\mathbf{r}_2t_2)\big). \tag{6.3}$$

The two final expectation values in eqn (6.2) are complex conjugates, and bearing in mind the purely imaginary character of u_1 and u_2, the intensity reduces to

$$\begin{aligned}\langle\hat{I}(\mathbf{r}t)\rangle = 2\epsilon_0 c\{&|u_1|^2\langle\hat{E}^{-}(\mathbf{r}_1t_1)\hat{E}^{+}(\mathbf{r}_1t_1)\rangle+|u_2|^2\langle\hat{E}^{-}(\mathbf{r}_2t_2)\hat{E}^{+}(\mathbf{r}_2t_2)\rangle\\ &+2u_1^*u_2\ \mathrm{Re}\langle\hat{E}^{-}(\mathbf{r}_1t_1)\hat{E}^{+}(\mathbf{r}_2t_2)\rangle\}.\end{aligned} \tag{6.4}$$

The electric-field operators that occur in eqn (6.4) are related to photon creation and destruction operators by eqns (5.84) and (5.85). It is not difficult to evaluate the averages for incident light whose density operator is known. As in the analogous classical theory, the first two terms in eqn (6.4) give the intensities on the second screen that result from each pinhole in the absence of the other. The interference fringes result from the third term, whose normalized form determines the quantum degree of first-order coherence of the light. The electric-field correlation functions and degrees of coherence for various kinds of incident light are calculated in the following section.

It is however useful to look first at the finer details of the quantum picture of the interference experiment[1], and in particular at the way in which photons, endowed with particle-like properties, pass through the pinholes to produce the fringe pattern. To make the discussion as simple as possible, we assume that only a single mode of the cavity is excited, with photon creation and destruction operators $\hat{a}^\dagger$ and $\hat{a}$.

Consider a preliminary experiment in which phototubes are set up to the right of each pinhole, to determine the route each photon takes through the first screen. Clearly a single photon can only be registered by one of the phototubes, either that behind pinhole 1 or that behind pinhole 2. Let the spatial distribution of light corresponding to the emergence of a photon from pinhole 1 be designated mode 1, with creation and destruction operators $\hat{a}_1^\dagger$ and $\hat{a}_1$. Mode 2 is defined similarly for the emergence of a photon from pinhole 2. Fig. 6.1 illustrates the two modes. The two phototubes of the preliminary experiment measure directly the photon excitations in modes 1 and 2 respectively.

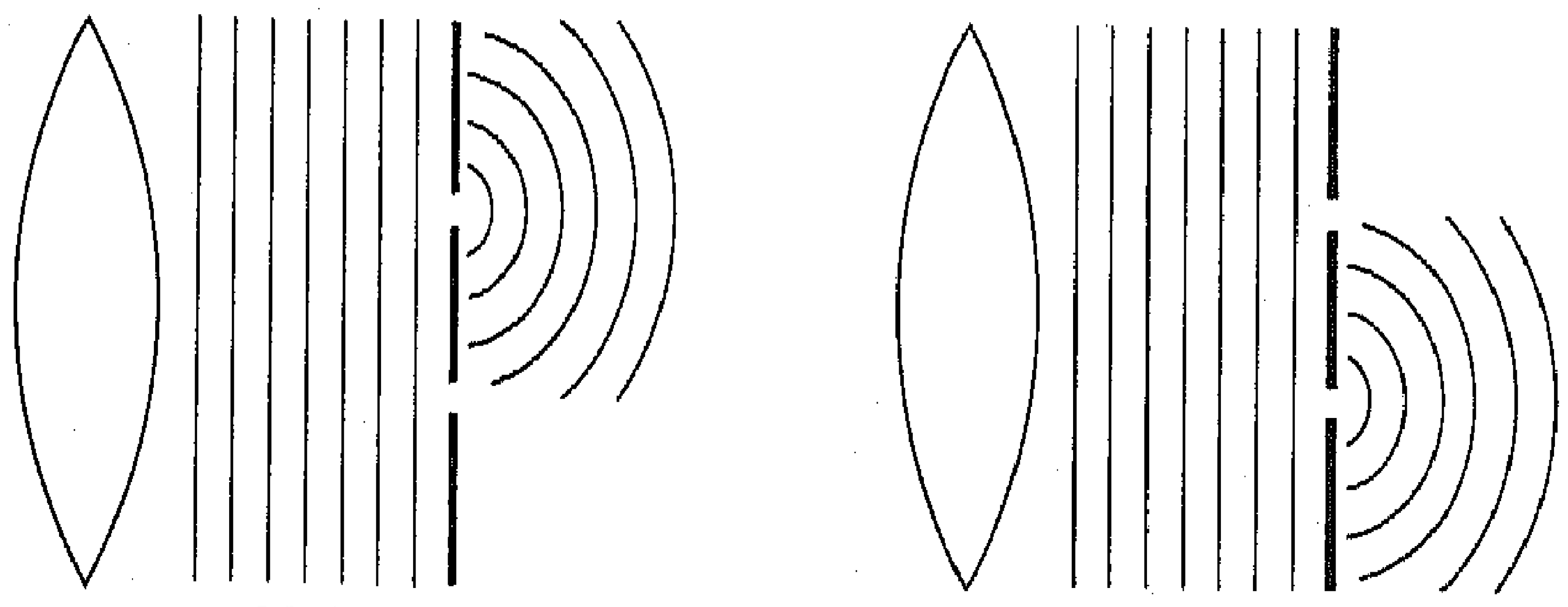

FIG. 6.1. Modes for the transmission of light through the two pinholes in Young's interference experiment.

Suppose that the two pinholes provide the only means of escape for photons in the cavity formed by the lens and the first screen. For pinholes of equal size, the incident photons are equally likely to be registered in mode 1 or mode 2, and we can write

$$\begin{aligned}\hat{a}^\dagger &= (\hat{a}_1^\dagger+\hat{a}_2^\dagger)/2^{\frac{1}{2}}\\ \hat{a} &= (\hat{a}_1+\hat{a}_2)/2^{\frac{1}{2}},\end{aligned} \tag{6.5}$$

where the $2^{\frac{1}{2}}$ factors ensure that all like pairs of creation and destruction operators have the same commutation rule (4.67). The operators for mode 1 all commute with those for mode 2 since the two modes are orthogonal.

The numbers $\bar{n}_1$ and $\bar{n}_2$ of photons registered at the two phototubes are given by the expectation values of $\hat{a}_1^\dagger\hat{a}_1$ and $\hat{a}_2^\dagger\hat{a}_2$ respectively, similar to eqn (5.102). Let $|0\rangle$ be the vacuum state for all kinds of mode. The state with n incident photons can be written

$$|n\rangle = (n!)^{-\frac{1}{2}}(\hat{a}^\dagger)^n|0\rangle \tag{6.6}$$

as in eqn (4.96). The average number registered behind pinhole 1 is

$$\bar{n}_1 = \langle n|\hat{a}_1^\dagger \hat{a}_1|n\rangle = \langle 0|(\hat{a})^n \hat{a}_1^\dagger \hat{a}_1 (\hat{a}^\dagger)^n|0\rangle/n!. \tag{6.7}$$

This expression is readily evaluated by substitution of eqn (6.5) and use of the usual creation- and destruction-operator properties, to give

$$\bar{n}_1 = \tfrac{1}{2}n, \tag{6.8}$$

and similarly

$$\bar{n}_2 = \langle n|\hat{a}_2^\dagger \hat{a}_2|n\rangle = \tfrac{1}{2}n. \tag{6.9}$$

These are of course just the expected results for *n* photons incident on a pair of identical pinholes.

Now consider the original arrangement of Young's experiment, with the phototubes immediately behind the pinholes removed. The electric-field operator (6.1) is essentially a linear superposition of the contributions of the modes 1 and 2 transmitted through the first screen. With the continuing assumptions of single-mode incident light, pinholes at a common coordinate parallel to the incident beam, and times given by eqn (3.31), eqn (6.1) can be written[1]

$$\hat{E}^+(\mathbf{r}t) \propto u_1\hat{a}_1 \exp(iks_1) + u_2\hat{a}_2 \exp(iks_2). \tag{6.10}$$

Thus for an *n*-photon incident beam as before, the intensity of the interference pattern given by eqn (6.4) is

$$\begin{aligned}\langle \hat{I}(\mathbf{r}t)\rangle \propto\ & |u_1|^2\langle n|\hat{a}_1^\dagger \hat{a}_1|n\rangle + |u_2|^2\langle n|\hat{a}_2^\dagger \hat{a}_2|n\rangle \\ & + 2u_1^* u_2 \cos\{k(s_1 - s_2)\}\langle n|\hat{a}_1^\dagger \hat{a}_2|n\rangle. \end{aligned} \tag{6.11}$$

The first two terms again give the contributions of each pinhole individually, now expressed in terms of the mean numbers of transmitted photons evaluated in eqns (6.7)–(6.9).

The fringe-producing term in the intensity expression is again the final contribution, proportional to

$$\begin{aligned}\langle n|\hat{a}_1^\dagger \hat{a}_2|n\rangle &= \langle 0|(\hat{a}_1 + \hat{a}_2)^n \hat{a}_1^\dagger \hat{a}_2 (\hat{a}_1^\dagger + \hat{a}_2^\dagger)^n|0\rangle/2^n n! \\ &= \tfrac{1}{2}n, \end{aligned} \tag{6.12}$$

where eqns (6.5) and (6.6) have been used and the final result includes all nonzero contributions from the expansions of the *n*th powers. It follows that the entire intensity expression (6.11) is directly proportional to the number of incident photons. Thus the same intensity distribution as observed in an interference experiment with *n* incident photons can be built up by a series of *n* identical experiments each sending a single photon through the interferometer. Classical interference and diffraction experiments have in fact been carried out[2] with light sources so feeble that only one photon at a time passes through the apparatus. It is found that after a recording time sufficiently long to overcome the feebleness of the source, the interference or diffraction pattern under one-photon conditions is exactly the same as for a normally strong light source. The interference is a one-photon effect, and does not depend in any way on the interaction of photons with each other.

For Young's experiment each photon must be capable of interfering with itself in such a way that its probability of striking the second screen at a particular point is proportional to the calculated intensity at that point. This can be achieved only if each photon passes partly through both pinholes, so that it can have a knowledge of the entire pinhole geometry as it strikes the screen. There is indeed no way in which one can simultaneously assign a photon to a particular pinhole *and* record the interference pattern. If a phototube is placed behind one of the pinholes to detect photons passing through, then it is not possible to avoid obscuring that pinhole, with consequent destruction of the interference pattern.

These remarks are in agreement with the principles of quantum mechanics. Photons do not interact with each other, and interference effects must be sought in the process by which each single photon passes from the source to the second screen. Quantum-mechanically, the interference occurs between the probability amplitudes for passage from source to screen via the two different paths corresponding to the two pinholes. The intensity on the second screen is proportional to the square modulus of the sum of the two probability amplitudes.

The same general ideas apply to a variation of Young's experiment in which the two light beams are obtained not by placing a pair of pinholes in front of a single source, but by the use of two completely independent light sources. Interference effects have been observed[3] in the field formed by superposition of light from two independent single-mode lasers. The conceptual situation is similar to that for Young's experiment. The interference occurs between the probability amplitudes that a photon which arrives at the detector has been emitted by one source or the other, and the field operator at the detector is similar to eqn (6.10). The modes of the complete system of two sources and optical cavity used in the experiment are created and destroyed by operators similar to those defined in eqn (6.5) if the sources have equal strength. Thus the modes are excited equally by the two sources, but as in Young's experiment there is no method by which a photon can simultaneously contribute to the interference effects *and* be assigned to a particular one of the two sources.

Problem 6.1. Consider a Young's experimental arrangement in which two photodetectors are placed immediately behind the pinholes. If *n* photons are transmitted through screen 1, show with the help of eqns (6.5) and (6.6) that the probability for n_1 photons to be registered behind pinhole 1 and n_2 behind pinhole 2 (with $n_1 + n_2 = n$) is

$$P_{n_1,n_2} \equiv |\langle n_1, n_2|n\rangle|^2 = n!/n_1!n_2!2^n. \tag{6.13}$$

6.2. Quantum degree of first-order coherence

The quantum-mechanical expression (6.4) for the fringe intensity in Young's experiment strongly resembles the corresponding classical expression (3.33). The theories can be continued along parallel lines, and the next step is the introduction of an appropriately-defined quantum-mechanical degree of first-order coherence.[4] By analogy with the classical expression (3.42) we define the quantum degree of first-order coherence to be

$$g^{(1)}(\mathbf{r}_1t_1,\mathbf{r}_2t_2) = \frac{\langle \hat{E}^-(\mathbf{r}_1t_1)\hat{E}^+(\mathbf{r}_2t_2)\rangle}{[\langle \hat{E}^-(\mathbf{r}_1t_1)\hat{E}^+(\mathbf{r}_1t_1)\rangle\langle \hat{E}^-(\mathbf{r}_2t_2)\hat{E}^+(\mathbf{r}_2t_2)\rangle]^{\frac{1}{2}}}. \quad (6.14)$$

We use here the same notation for the degree of first-order coherence as in the classical case, and this quantity retains its physical significance in terms of the ability of the light at the space-time points $(\mathbf{r}_1t_1)$ and $(\mathbf{r}_2t_2)$ to form interference fringes when superposed. The angle brackets on the right are ensemble averages evaluated in accordance with eqn (6.3). The terminology associated with the first-order coherence of light is the same as in the classical definitions of eqn (3.43).

The general properties of the quantum-mechanical first-order coherence are illustrated by consideration of some simple special cases.

Problem 6.2. Prove that a light beam in which a single mode of the radiation field is excited to the number state $|n\rangle$ or the coherent state $|\alpha\rangle$ is first-order coherent, that is, $|g^{(1)}(\tau)| = 1$ for all pairs of space-time points.

Show that any arbitrary pure-state excitation of a single mode is first-order coherent. This result can be established by writing the pure state as an expansion in the complete set of number states $|n\rangle$.

Problem 6.3. Prove that any statistical-mixture state, in which a single mode of the radiation field is excited, is first-order coherent. This result can be proved by evaluation of $g^{(1)}(\tau)$ with an arbitrary single-mode density operator $\hat{\rho}$ and $\hat{E}^-$ and $\hat{E}^+$ reduced to the single terms appropriate to the selected mode.

These results show that any single-mode excitation has first-order coherence, a property that is common to the quantum-mechanical and classical definitions of the degree of first-order coherence.

The quantum-mechanical coherence properties of light beams that involve the excitation of several modes are more varied.

Problem 6.4. Consider an excitation of the total field of the type $|\{\alpha_\mathbf{k}\}\rangle$ defined in eqn (4.236), where each mode is in a coherent state. With the use of the fundamental property of the coherent states shown in eqn (5.103) prove that the state $|\{\alpha_\mathbf{k}\}\rangle$ is first-order coherent.

Problem 6.5. Consider the pure state formed from a linear superposition of states each of which has a single photon excited in an arbitrary mode and no photons in the remaining modes. Prove that this generalized single-photon pure state is first-order coherent.

These two examples of multimode pure states have perfect first-order coherence but this is not a general property of pure states in which more than one mode and more than one photon are excited.

Problem 6.6. Consider a pure state in which two photons are excited, one in each of two modes, whose wavevectors $\mathbf{k}_1$ and $\mathbf{k}_2$ are parallel to the z-axis, the corresponding frequencies being ω_1 and ω_2. Prove that the degree of first-order coherence is

$$g^{(1)}(\tau) = \{\omega_1 \exp(-\mathrm{i}\omega_1\tau)+\omega_2 \exp(-\mathrm{i}\omega_2\tau)\}/(\omega_1+\omega_2), \quad (6.15)$$

where

$$\tau = t_2-(z_2/c)-t_1+(z_1/c) \quad (6.16)$$

as in eqn (3.37). The light is first-order coherent at an arbitrary pair of space–time points (z_1,t_1) and (z_2,t_2) only if the two photons are in the same mode.

The classical result, that light is first-order coherent if the field can be specified precisely with no statistical features, translates into quantum mechanics as the statement that any pure state of the type $|\{\alpha_\mathbf{k}\}\rangle$ is first-order coherent. There is no general property of quantum-mechanical first-order coherence for multimode pure states that contain more than one photon.

The degree of first-order coherence of a multimode statistical mixture can be readily determined from eqn (6.14) if the density operator is known. A case of particular interest is that of chaotic light where the density operator is given in eqn (4.244). The classical first-order coherence of chaotic light has been evaluated in eqn (3.44).

Problem 6.7. Consider a beam of chaotic light whose density operator is given by eqn (4.244) with the $\mathbf{k}$ summations restricted to wavevectors parallel to the z-axis. Prove that the degree of first-order coherence is

$$g^{(1)}(\tau) = \frac{\sum_k \bar{n}_k\omega_k \exp(-\mathrm{i}\omega_k\tau)}{\sum_k \bar{n}_k\omega_k}. \quad (6.17)$$

If the beam has a Lorentzian frequency distribution (2.112) with a collision-broadening linewidth parameter γ' given by eqn (2.135), then according to (5.101) the quantity $\bar{n}_k\omega_k$ is proportional to the beam intensity at frequency ω_k, and we can write

$$\bar{n}_k\omega_k \propto \frac{\gamma'/\pi}{(\omega_0-\omega_k)^2+\gamma'^2}. \tag{6.18}$$

The summations over k in eqn (6.17) are converted to integrations by the one-dimensional analogue of eqn (1.11),

$$\sum_k \to \int_0^\infty (L/\pi)\,\mathrm{d}k \to \int_0^\infty (L/\pi c)\,\mathrm{d}\omega_k, \tag{6.19}$$

where L is the length of optical cavity in the z-direction. The degree of first-order coherence (6.17) thus becomes

$$g^{(1)}(\tau) = \int_0^\infty \frac{(\gamma'/\pi)\exp(-\mathrm{i}\omega_k\tau)}{(\omega_0-\omega_k)^2+\gamma'^2}\,\mathrm{d}\omega_k. \tag{6.20}$$

For a beam of narrow frequency spread, the lower limit on the integral can be replaced by $-\infty$ without significant change in its value. The integral can then be evaluated by a simple contour integration, and the result is

$$g^{(1)}(\tau) = \exp(-\mathrm{i}\omega_0\tau-\gamma'|\tau|). \tag{6.21}$$

This expression is identical to the classical result (3.44).

The quantum calculation can also be extended without difficulty to include the effects of Doppler broadening, and the results obtained in the presence of Doppler broadening alone or in combination with collision broadening agree with the classical expressions (3.55) and (3.57). The classical and quantum-mechanical derivations of the degree of first-order coherence produce the same results for beams of chaotic light, and the same intensity distributions are predicted for Young's fringes and for the other kinds of classical interference experiment. Indeed, it can be shown[5] that the light emitted by a single excited atom has the same $g^{(1)}(\tau)$ as eqn (6.21) with γ' reduced to its radiative decay part γ. The single photon emitted by the atom thus independently makes its appropriate contribution to first-order interference effects, in the manner described in the previous section.

In summary, the above results support the predictions of classical theory for experiments that depend upon first-order coherence in the cases of chaotic light and the coherent light represented by the states $|\{\alpha_{\mathbf{k}}\}\rangle$. The states $|\{\alpha_{\mathbf{k}}\}\rangle$ have the same first-order coherence properties as a multimode excitation of classical stable waves. However, as exemplified by problem 6.6, the interference properties of other kinds of quantum-mechanical pure state must be determined by the quantum theory of first-order coherence. The coherent states form a special class, and other types of quantum-mechanical pure state do not always have classical analogues.

6.3. Quantum degree of second-order coherence

Despite the possibility of quantum states of light beams, whose degrees of first-order coherence need to be evaluated by the quantum theory, the differences between classical and quantum predictions for first-order interference experiments tend to be difficult to detect. Thus, both the classical and quantum degrees of first-order coherence have numerical values in the same range,

$$1 \geqslant |g^{(1)}(\tau)| \geqslant 0, \tag{6.22}$$

so that the same varieties of interference pattern occur in the two theories. More striking differences occur in measurements that depend upon the degree of second-order coherence, and all the existing experiments that distinguish classical from quantum coherence properties belong to this category.

The quantum degree of second-order coherence is defined analogous to the classical form (3.97) in terms of the correlation of light intensities at two space–time points. The procedure is similar to that used for first-order coherence in the earlier part of the present chapter. With the intensities measured by phototubes, the correlation is proportional to the transition rate for a joint absorption of photons at the two points. A simple extension of the photoelectric theory of Chapter 5 shows that the transition amplitude is proportional to a matrix element of $\hat{E}^+(\mathbf{r}_2t_2)\hat{E}^+(\mathbf{r}_1t_1)$, and the transition rate involves the square of the matrix element, analogous to eqn (5.95). These considerations lead to the definition of the quantum-mechanical degree of second-order coherence as[4,6]

$$g^{(2)}(\mathbf{r}_1t_1,\mathbf{r}_2t_2;\mathbf{r}_2t_2,\mathbf{r}_1t_1) = \frac{\langle \hat{E}^-(\mathbf{r}_1t_1)\hat{E}^-(\mathbf{r}_2t_2)\hat{E}^+(\mathbf{r}_2t_2)\hat{E}^+(\mathbf{r}_1t_1)\rangle}{\langle \hat{E}^-(\mathbf{r}_1t_1)\hat{E}^+(\mathbf{r}_1t_1)\rangle\langle \hat{E}^-(\mathbf{r}_2t_2)\hat{E}^+(\mathbf{r}_2t_2)\rangle}, \tag{6.23}$$

where the angle-bracket ensemble averages are evaluated with the use of the density operator as in eqn (6.3). A more explicit derivation of the numerator in eqn (6.23) is presented in the theory of the rate of nonlinear two-photon absorption in §9.1.

The general significance of the quantum coherence is again the same as its classical counterpart, and in particular the second-order coherence condition at the two space–time points is the same as eqn (3.98). Only parallel light beams are to be considered in detail here, and the space–time coordinates then enter the coherence in the combination τ defined in eqn (6.16). All of the factors in eqn (6.23) are expectation values of products of operators with their Hermitian conjugates. These must be positive,[6] and it follows that

$$\infty \geqslant g^{(2)}(\tau) \geqslant 0, \tag{6.24}$$

similar to the classical range (3.78).

It is *not* however possible to prove that the quantum degree of second-order coherence (6.23) satisfies either of the classical inequalities (3.77) and (3.81).

This situation leads to significant differences between the two theories, and in the remainder of the book there are various examples of light beams whose degrees of second-order coherence violate the classical inequalities. The distinction between the theories is emphasized by noting that even for zero time delay τ between the intensity measurements, only the inequality (6.24) can be proved in the quantum case,

$$\infty \geqslant g^{(2)}(0) \geqslant 0. \tag{6.25}$$

By comparison with eqn (3.77) there is an exclusively quantum range of values,

$$\text{exclusive quantum range:} \qquad 1 > g^{(2)}(0) \geqslant 0. \tag{6.26}$$

We now consider some examples of light beams to illustrate the quantum theory. A considerable simplification in the degree of second-order coherence occurs when the light beam excites only a single mode of the optical system. Most factors then cancel when eqns (5.84) and (5.85) are inserted into eqn (6.23), leaving

$$g^{(2)}(\tau) = \frac{\langle \hat{a}^{\dagger}\hat{a}^{\dagger}\hat{a}\hat{a}\rangle}{\langle \hat{a}^{\dagger}\hat{a}\rangle^{2}}. \tag{6.27}$$

With the usual properties (4.91) and (4.92) of the destruction and creation operators, the degree of coherence can be expressed in terms of the mean and mean-square photon numbers as

$$g^{(2)}(\tau) = \frac{\langle \hat{n}(\hat{n}-1)\rangle}{\langle \hat{n}\rangle^{2}} = \frac{\overline{n^{2}}-\bar{n}}{\bar{n}^{2}}. \tag{6.28}$$

There is no time dependence in the single-mode case.

The quantity to be averaged on the right of eqn (6.28) exemplifies the quantum principle that the act of measurement can interfere with the measured system; a measurement of the number n of photons itself reduces the photon number by 1, so that the second measurement finds only $n-1$ photons. This effect lies at the root of the differences between the degrees of second-order coherence in classical and quantum theories.

The simplest example of nonclassical light is provided by a beam that contains exactly n photons, corresponding to an eigenstate $|n\rangle$ of the photon number operator, when eqn (6.28) gives

$$\begin{aligned} g^{(2)}(\tau) &= (n-1)/n \qquad \text{for} \qquad n \geqslant 2 \\ &= 0 \qquad\qquad\quad\;\; \text{for} \qquad n = 0 \text{ or } 1. \end{aligned} \tag{6.29}$$

This quantity is always less than unity, and therefore lies in the quantum range (6.26). Another simple example, with coherence in the classical range, is provided by single-mode coherent light where use of the basic property (4.186) in eqn (6.27) produces

$$g^{(2)}(\tau) = 1. \tag{6.30}$$

The state $|\alpha\rangle$ is therefore second-order coherent according to the prescription of eqn (3.98), similar to the classical stable wave considered in eqn (3.84). It is seen that the degree of second-order coherence takes different values for the different single-mode excitations, unlike the first-order coherence, which is always unity for single-mode states.

The degree of second-order coherence for a single-mode statistical mixture is readily calculated from eqn (6.28).

Problem 6.8. Consider a chaotic light beam in an optical cavity and suppose that all the normal-mode contributions except one are removed by a filter, as in problems 3.1 and 3.6. The density operator for the single mode that remains is given by eqn (4.240). Prove that

$$g^{(2)}(\tau) = 2, \tag{6.31}$$

similar to eqn (3.100). The degree of second-order coherence for an *unfiltered* chaotic beam is considered in problem 6.10.

For multimode excitations, it is necessary to use the more general definition (6.23) and the evaluation of the degree of coherence is more tedious. We consider only the two cases of multimode coherent light and parallel-beam multimode chaotic light.

Problem 6.9. Consider a multimode excitation of the type $|\{\alpha_{\mathbf{k}}\}\rangle$ defined in eqn (4.236), where each mode is in a coherent state. Use the density operator given in eqn (4.237) to prove that

$$g^{(2)}(\tau) = 1. \tag{6.32}$$

This result in conjuction with the result of problem 6.4 shows that the state $|\{\alpha_{\mathbf{k}}\}\rangle$ is second-order coherent.

Problem 6.10. Consider a multimode chaotic light beam whose density operator is given in eqn (4.244). Prove that the degree of second-order coherence is

$$\begin{aligned} g^{(2)}(\tau) &= \frac{\left|\sum_{k} \bar{n}_{k}\omega_{k}\exp(-i\omega_{k}\tau)\right|^{2}}{\left(\sum_{k} \bar{n}_{k}\omega_{k}\right)^{2}} + 1 \\ &= |g^{(1)}(\tau)|^{2} + 1 \end{aligned} \tag{6.33}$$

where eqn (6.17) has been used. The quantum-mechanical second-order coherence of a chaotic light beam is the same as the classical expression (3.90).

The calculations of the present section thus show that the important practical examples of coherent and chaotic light beams give identical degrees of second-order coherence in the classical and quantum theories. However, the photon number-state has a degree of coherence that lies outside the classical range. We consider this phenomenon in greater detail in the two following sections.

Problem 6.11. Use the condition that the mean-square deviation of any photon-number probability distribution cannot be negative to prove that the degree of second-order coherence of an arbitrary single-mode excitation must satisfy

$$g^{(2)}(\tau) \geqslant 1-(1/\bar{n}). \qquad (6.34)$$

The result (6.29) for the photon number-state $|n\rangle$ has the minimum value allowed by this inequality.

6.4. Hanbury Brown and Twiss experiment with photons

The reason for the differences between classical and quantum theories can be seen more clearly from an examination of the workings of the Hanbury Brown and Twiss experiment from the quantum viewpoint. In these terms, each photon that strikes the semitransparent mirror in Fig. 3.13 is *either* reflected *or* transmitted, and can only be registered in one of the phototubes. The two beams that arrive at the detectors are not therefore identical, contrary to the assumption (3.101) made in the classical theory of the experiment. We consider how the two sets of photon counts determine the degree of second-order coherence of the unsplit beam to the left of the mirror, analogous to the classical result (3.104).

The quantum theory of the Hanbury Brown and Twiss experiment is readily analysed by the method used earlier in the chapter to treat Young's interference experiment. Fig. 6.2(a) shows the bare details of the apparatus, and Fig. 6.2(b) shows the two modes of the optical system that correspond respectively to transmission and reflection at the mirror. The incident photons have equal probabilities of transmission or reflection and their creation and destruction operators can be written in the form (6.5), where the operators on the right-hand sides create and destroy photons in modes 1 and 2. A state with n incident photons has the form (6.6) and the probability P_{n_1,n_2} that n_1 photons are transmitted through the mirror to detector 1 while n_2 are reflected to detector 2 is given by eqn (6.13).

The probability distribution can be used to obtain average properties of the photon counts in the two arms of the apparatus. The mean numbers of counts

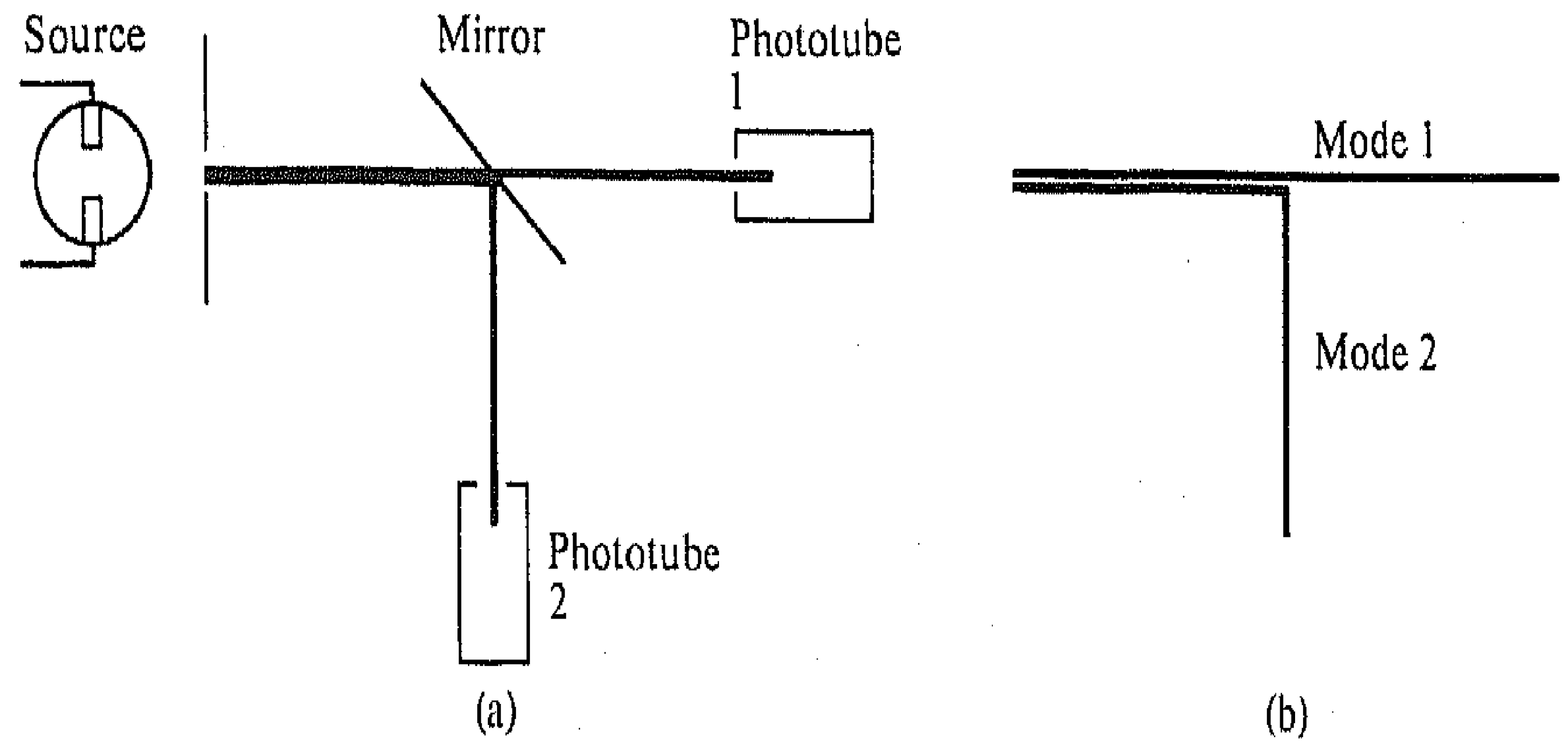

(a) (b)

FIG. 6.2. Experiment of Hanbury Brown and Twiss showing (a) the arrangement of the main components, and (b) the transmission and reflection modes.

$\bar{n}_1$ and $\bar{n}_2$ are both equal to $\frac{1}{2}n$ as in eqns (6.8) and (6.9), and the correlation is

$$\langle \hat{a}_1^\dagger \hat{a}_2^\dagger \hat{a}_2 \hat{a}_1 \rangle \equiv \langle n_1 n_2 \rangle = \tfrac{1}{4}n(n-1). \qquad (6.35)$$

The notation $\langle n_1 n_2 \rangle$ is a shorthand for the expectation value of the normally-ordered product of creation and destruction operators on the left-hand side of eqn (6.35), and it also indicates the experimental significance of this quantity as an average of the product of the photon counts at the two phototubes. Thus eqn (6.35) shows that the degree of second-order coherence computed from

$$g^{(2)}(\tau) = \langle n_1 n_2 \rangle / \bar{n}_1 \bar{n}_2 \qquad (6.36)$$

reproduces the quantum result (6.29) for a photon number-state incident beam. Table 6.1 shows the photon-count distributions and the degrees of second-order coherence for small numbers n of incident photons.

The Hanbury Brown and Twiss experiment was designed to produce the average

$$\langle (n_1-\bar{n}_1)(n_2-\bar{n}_2) \rangle = \langle n_1 n_2 \rangle - \bar{n}_1 \bar{n}_2, \qquad (6.37)$$

analogous to its classical counterpart (3.103). The normalized correlation gives

$$\frac{\langle (n_1-\bar{n}_1)(n_2-\bar{n}_2) \rangle}{\bar{n}_1 \bar{n}_2} = g^{(2)}(\tau)-1, \qquad (6.38)$$

and for a photon number-state incident beam, substitution of eqns (6.8), (6.9) and (6.35) gives a negative correlation

$$\frac{\langle (n_1-\bar{n}_1)(n_2-\bar{n}_2) \rangle}{\bar{n}_1 \bar{n}_2} = -\frac{1}{n}, \qquad (6.39)$$

equal to the minimum value allowed by the inequality (6.34).

It is seen from the above analysis that nonclassical light with a degree of second-order coherence smaller than unity occurs in the Hanbury Brown and

TABLE 6.1

Photon distribution in a Hanbury Brown and Twiss experiment showing respectively the number of incident photons, the possible numbers detected by the two phototubes, their mean, their correlation, and the degree of second-order coherence

n	n_1	n_2	$\bar{n}_1 = \bar{n}_2$	$\langle n_1 n_2 \rangle$	$g^{(2)}(\tau)$
1	1 0	0 1	1/2	0	0
2	2 1 1 0	0 1 1 2	1	1/2	1/2
3	—	—	3/2	3/2	2/3
4	—	—	2	3	3/4

Twiss experiment because the photons must make a choice between reflection and transmission at the mirror. This is of course an essential quantum requirement. A semiclassical-type of analysis in which each photon is represented by a constant-intensity pulse that is half-transmitted and half-reflected produces a degree of second-order coherence equal to unity for any given number of incident photons.

The quantum analysis of the Hanbury Brown and Twiss experiment is readily extended to incident beams that have some superposition or statistical mixture of the number states of a single mode. The degree of second-order coherence obtained from eqn (6.36) then reproduces the general single-mode result (6.28). In accordance with eqns (6.30) and (6.31), the examples of single-mode coherent and chaotic light give Hanbury Brown and Twiss correlations (6.38) equal respectively to zero and unity. These single-mode results are all independent of the time τ.

A further extension of the theory is required for multimode incident light. Each incident mode **k** has its creation and destruction operators expressed in terms of transmitted (mode 1) and reflected (mode 2) operators, similar to eqn (6.5). Provided that the frequencies in the light beam have a small spread about their mean value, it is not difficult to show with the use of eqns (5.84) and (5.85) that the degree of second-order coherence (6.23) is related to the photon-number correlation according to

$$g^{(2)}(\tau) = \langle n_1(\tau) n_2(0) \rangle / \bar{n}_1 \bar{n}_2. \tag{6.40}$$

The angle-bracket average has a significance similar to that in eqn (6.36), the correlation between the detector readings being made with a fixed time delay τ and the statistical properties of the light beam being assumed stationary. The correlation now generally depends on the time τ, with the exception of multimode coherent light where the degree of second-order coherence is constant as in eqn (6.32). Thus for multimode chaotic light with a Lorentzian frequency distribution eqn (6.40) gives

$$g^{(2)}(\tau) = \langle n_1(\tau) n_2(0) \rangle / \bar{n}_1 \bar{n}_2 = \exp(-2\gamma' |\tau|) + 1, \tag{6.41}$$

where eqns (6.21) and (6.33) have been used.

The first experiment[7,8] to measure photon-number correlations was made with apparatus similar to that shown in Figs. 3.13 and 6.2(a). If the phototubes are placed at equal linear distances from the source, the Hanbury Brown and Twiss correlation (6.38) obtained from eqn (6.41) is

$$g^{(2)}(\tau) - 1 = \exp(-2\gamma' |t_2 - t_1|), \tag{6.42}$$

where the times t_1 and t_2 of the readings are separated by an amount τ. As in the classical theory of the analogous intensity correlation experiment described in §3.9, it is necessary to allow for the finite response time τ_r of the detectors. The experiment registered as correlations, photons that arrived at detector 2 within a time interval τ_r of a photon arrival at detector 1. The additional average over the correlation period, indicated by further angle brackets, gives

$$\begin{aligned} \langle g^{(2)}(\tau) \rangle_r - 1 &= \frac{1}{2\tau_r} \int_{t_1 - \tau_r}^{t_1 + \tau_r} \exp(-2\gamma' |t_2 - t_1|)\, dt_2 \\ &= (1/2\gamma'\tau_r)\{1 - \exp(-2\gamma'\tau_r)\}. \end{aligned} \tag{6.43}$$

It should be noted that this is somewhat different from the analogous average (3.106) in the classical version of the experiment.

For a long response time eqn (6.43) reduces approximately to

$$\langle g^{(2)}(\tau) \rangle_r - 1 = 1/2\gamma'\tau_r = \tau_c / 2\tau_r \qquad \text{for} \qquad \tau_r \gg \tau_c = 1/\gamma', \tag{6.44}$$

where τ_c is the coherence time of the light defined as in eqn (3.27). This long response-time approximation holds for all forms of chaotic light, whether or not the frequency distribution is Lorentzian. The original experiment used a mercury isotope lamp with $\tau_c \approx 7 \times 10^{-10}$ s and τ_r/τ_c approximately equal to 5. An additional $\frac{1}{2}$ factor appeared in eqn (6.44) since the light was unpolarized, unlike the linearly polarized light assumed for all the above calculations, and there are further correction factors needed to take account of spatial coherence effects and small losses of correlation in the equipment. With all these factors included, there was satisfactory agreement between the theory and the experimental results.[7,8]

Problem 6.12. Prove that for single-mode incident light, the average mean-square difference between the numbers of photons transmitted and reflected at the Hanbury Brown and Twiss mirror is

$$\langle (n_1 - n_2)^2 \rangle = \bar{n}. \tag{6.45}$$

Note that the corresponding average in classical theory is equal to zero in accordance with (3.101).

6.5. Photon bunching and antibunching

The use of the half-silvered mirror in the Hanbury Brown and Twiss experiment allows two phototubes to be employed in the measurement of photon-number correlations. This facilitates the gathering of the required data, particularly for detection equipment whose response time is longer than the coherence time of the light. It is however clear from the analysis of the previous section that the information obtained from the experiment refers to the properties of the incident unsplit beam to the left of the mirror.

The same information can in principle be obtained from a simpler experiment in which the light is arranged to fall on a single phototube. One then measures the numbers $n(\tau)$ and $n(0)$ of photons counted in two equal time intervals separated by a time τ. If the time intervals are short compared to τ and the coherence time τ_c, then the correlation determines the degree of second-order coherence by

$$g^{(2)}(\tau) = \langle n(\tau) n(0) \rangle / \bar{n}^2, \tag{6.46}$$

where $\bar{n}$ is the mean number of counts in the brief time interval. With a detector response sufficiently rapid that no further time average need be taken, the measured photon-number correlation leads directly to the degree of second-order coherence of the incident light. For chaotic light, where classical and quantum theories give the same results, the degrees of second-order coherence (3.94) and (3.95) for Lorentzian and Gaussian frequency distributions illustrated in Fig. 3.12 show the expected forms of photon-number correlation.

The results of photon-number correlation measurements[9] for a laser and for chaotic light of Gaussian frequency distribution are shown in Fig. 6.3. The chaotic light was produced by passing laser light through a rotating ground-glass disc, which imposed a Gaussian randomness on the monochromatic frequency spectrum of the laser light. The fit of the experimental results to the theoretical expression (3.95) is seen to be good.

The excess positive correlation shown in Figs. 3.12 and 6.3 for photon counts on chaotic light over time spans shorter than the coherence time τ_c is described as the *photon-bunching effect.* This is just the translation into

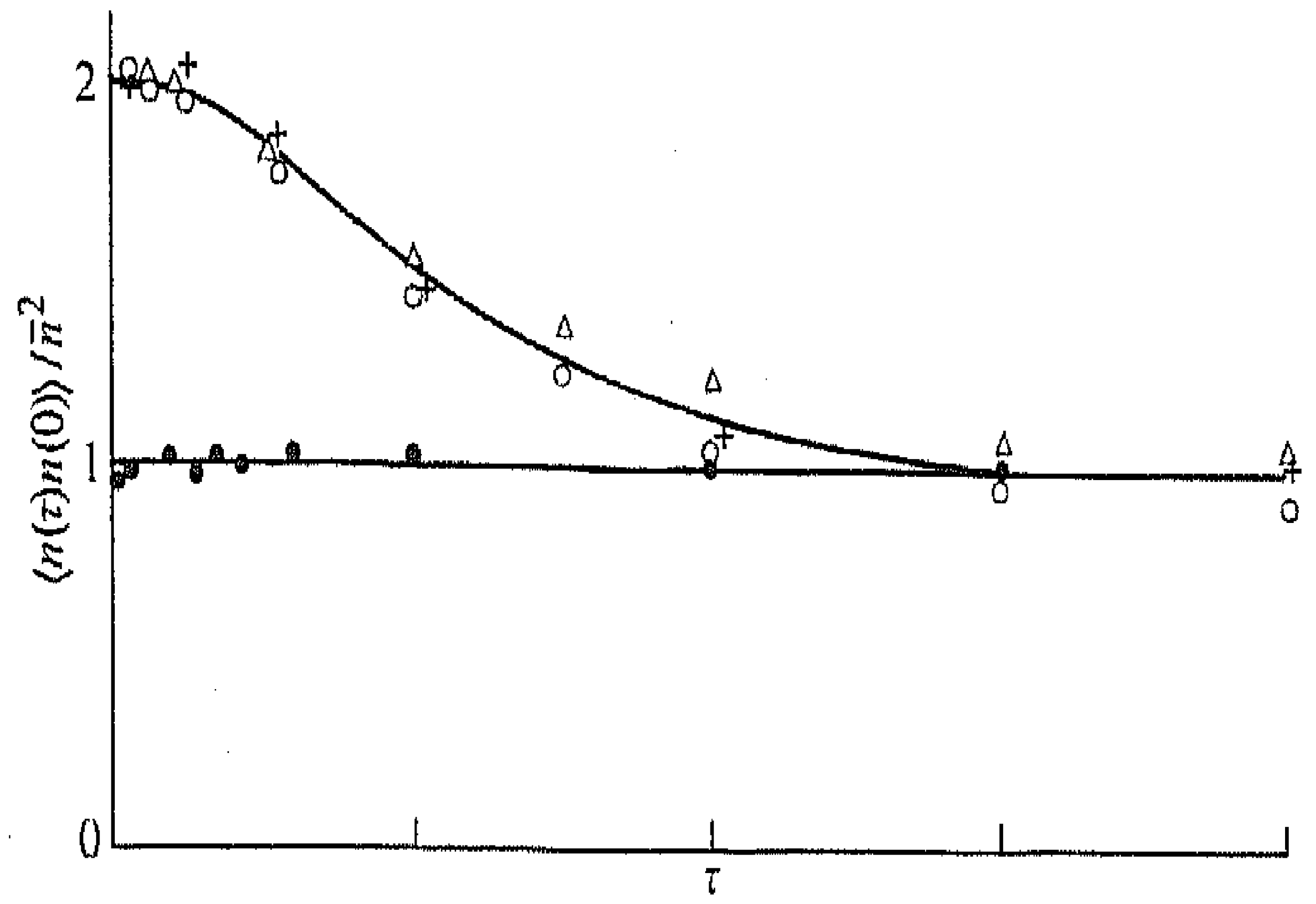

FIG. 6.3. Measured correlations between pairs of photon counts as functions of their time separation τ for laser light (filled circles) and chaotic light of Gaussian frequency distribution (all other points). The theoretical curves are the same as in Fig. 3.12. (After F. T. Arecchi *et al.*, ref. 9).

quantum language of the kind of intensity fluctuations that occur in the classical description of chaotic light, shown in Fig. 3.4. The arrival of a high-intensity fluctuation at the phototube generates closely spaced photon counts, while the arrival of an intensity trough produces very few photon counts. Fig. 6.4(a) shows a schematic representation of the occurrence of photon counts as a function of the time for chaotic light. The clusters of counts, or photon bunches, are clearly visible. Although the extent in time of the bunching is of the order of the coherence time τ_c, we describe light in general as

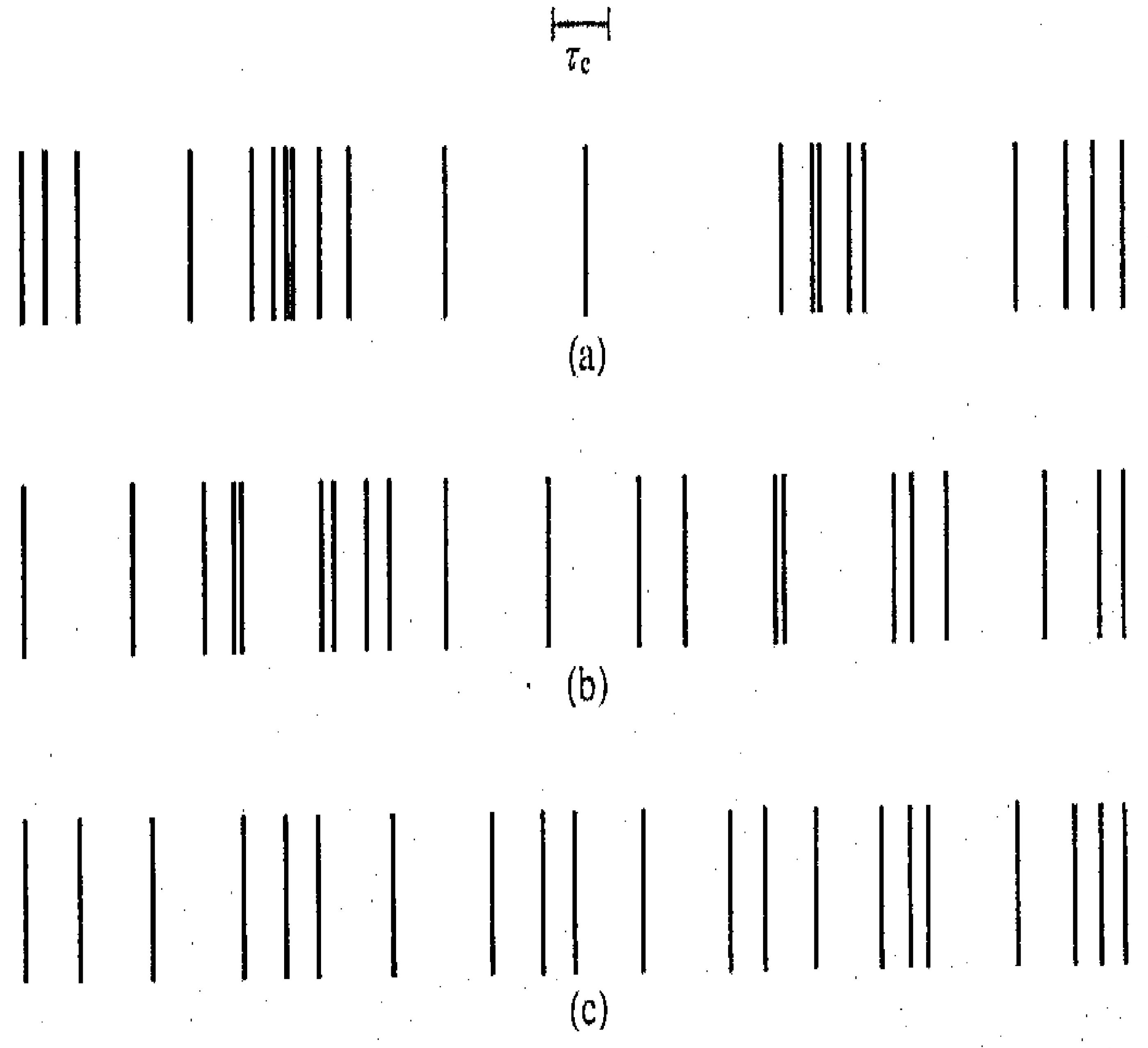

FIG. 6.4. Schematic representations of photon counts as functions of the time for light beams that are (a) bunched with $g^{(2)}(0) > 1$, (b) random with $g^{(2)}(0) = 1$, and (c) antibunched with $g^{(2)}(0) < 1$.

being photon-bunched if it satisfies the criterion

$$g^{(2)}(0) > 1. \tag{6.47}$$

Chaotic light, with $g^{(2)}(0) = 2$, is just one example of light that satisfies the photon-bunching condition.

Measurements of photon-bunching correlations are useful in practice for the determination of coherence times of chaotic light. One of the first experiments of this kind determined the coherence time of an emission line of a mercury vapour lamp.[10] The theoretical correlation given by eqn (6.41) was fitted to the experimental readings for several different delay times τ, and the coherence time was found to be $1{\cdot}7 \times 10^{-9}$ s. The experiment is a quantum version of the intensity-fluctuation spectroscopy mentioned in Chapter 3. Such time-domain spectroscopy has developed into a precise technique for the measurement of coherence times of chaotic light,[11,12] particularly for light with frequency widths (*not* angular frequency) in the range 1 to 10^8 Hz. It nicely complements frequency-domain spectroscopy, where Fabry–Perot interferometers can resolve spectral lines with widths in the range 10^6 to 10^{12} Hz, and grating spectrometers can resolve lines of width 10^{10} Hz or more.

Photon bunching is not of course a general property of light, and we now consider examples where the criterion (6.47) is not satisfied. Coherent light has no intensity fluctuations in the classical picture and it is seen from eqns (6.32) and (6.46) that the light has no photon bunches in the quantum picture. Indeed, these equations show that the photon counts have randomly-distributed time intervals, as illustrated in Fig. 6.4(b).

Light whose degree of second-order coherence lies in the range

$$1 > g^{(2)}(0) \geqslant 0 \tag{6.48}$$

is said to be *photon-antibunched*. It is seen by comparison with eqn (6.26) that antibunched light is synonymous with nonclassical light. The pattern of photon counts in this case is illustrated in Fig. 6.4(c), where it is assumed that

$$g^{(2)}(\tau) \to 1 \quad \text{for} \quad \tau \to \infty; \tag{6.49}$$

indeed all parts of Fig. 6.4 are drawn with this assumption, equivalent to a random distribution of separations between photon counts for sufficiently long time delays τ. The depression of the counting correlation below the random value for small and zero τ corresponds in the figure to the tendency of photon counts to be spaced out in time. The separation of counts in this case is reminiscent of the spacings between particles that ordinarily occur in beams of electrons.[13]

Antibunched light is of great importance for the quantum theory of light since it corresponds to the region of second-order coherence that distinguishes quantum and classical theories. A naïve example of nonclassical light that satisfies the antibunching condition (6.48) is provided by the beam with a definite number of photons, whose degree of second-order coherence is given in eqn (6.29). However, photon number-state beams have not been generated in practice, and the observation of antibunched light involves more complicated states of the radiation field. Schemes for the experimental production of nonclassical light are discussed in Chapters 8 and 9.

6.6. Photon counting

The most complete quantum-mechanical description of a light beam is contained in its density operator, whose properties are outlined in Chapter 4. Measurements of the quantum degrees of coherence by the interference experiments described above provide some information on the matrix elements of the density operator. Further information is obtained by the technique of *photon counting*, where the basic experimental procedure is as follows.

A beam of light under investigation is arranged to fall on a phototube, connected by suitable electronics to a count meter which registers the number of photons producing photoelectric emission in the phototube. A shutter in front of the phototube controls the length of time for which light falls on the detector. With the count meter set at zero, the shutter is opened for a length of time T. The shutter is then closed and the number m of counted photons is recorded. After a time delay long compared to the coherence time of the light, the shutter is again opened, the original experiment is repeated, and a second number of counted photons is recorded. The experiment is repeated a third time, and so on until a large number of readings have been accumulated, all referring to the number of photons counted during equal time durations T. The total number of readings in a complete experimental run might for example be of order 10^4. The results can be expressed as a probability distribution $P_m(T)$ for the counting of m photons during an observation time T.

It is assumed throughout that all the measured light beams are stationary. The measured statistical distribution $P_m(T)$ contains information about the statistical properties of the light source. We consider what this information is, and how it can be extracted from the results of a photon-counting experiment.

The photoelectric emission rate is proportional to the beam intensity, determined by the mean value of the operator product $\hat{E}^-\hat{E}^+$ as in eqn (5.100). It has been mentioned that the quantum-mechanical observable intensity operator (5.99) is analogous to the cycle-averaged classical intensity $\bar{I}(t)$ defined in eqn (3.15). It is convenient to begin with a calculation of the photon-count distribution that uses the classical beam intensity. The corresponding quantum-mechanical result is considered later in the chapter. Let $p(t)$ be the probability that the light beam causes an atom in the phototube to emit an electron and register a single count on the meter during the time interval between t and $t+\mathrm{d}t$. Then, according to eqns (5.89) or (5.92), we may write

$$p(t)\,\mathrm{d}t = \zeta\bar{I}(t)\,\mathrm{d}t, \tag{6.50}$$

where $\mathrm{d}t$ is assumed sufficiently large for transition probability theory to be valid (see the discussion that precedes eqn (2.49)), but sufficiently small for the probability of emission of electrons by more than one atom during the period to be negligible. The constant of proportionality ζ represents the efficiency of the phototube. It includes the matrix elements for the photoelectric process discussed in Chapter 5 and factors that depend on the density and positions of the ionizable atoms in the phototube:

Consider a particular period of counting that extends from t to $t+T$ and let $P_m(t, T)$ be the probability that m photons are counted in this time interval. The required distribution $P_m(T)$ is determined by a subsequent average over a large number of different starting times t.

Let $t+t'$ be a time that lies within the interval between t and $t+T$ as shown in Fig. 6.5, and let $\mathrm{d}t'$ be a short period of time similar to that used in eqn (6.50). The probability that m photons are counted between t and $t+t'+\mathrm{d}t'$ is by definition

$$P_m(t, t'+\mathrm{d}t'). \tag{6.51}$$

There are, however, two distinct ways in which m photons can be counted during the given time interval. Either

(1) m photons are counted between t and $t+t'$ and none in the interval $\mathrm{d}t'$, with total probability

$$P_m(t, t')(1-p(t')\,\mathrm{d}t'), \tag{6.52}$$

or (2) $m-1$ photons are counted between t and $t+t'$ and one photon is counted in the interval $\mathrm{d}t'$, with total probability

$$P_{m-1}(t, t')p(t')\,\mathrm{d}t'. \tag{6.53}$$

The probability of more than one photon being counted during the time interval $\mathrm{d}t'$ is negligible by hypothesis.

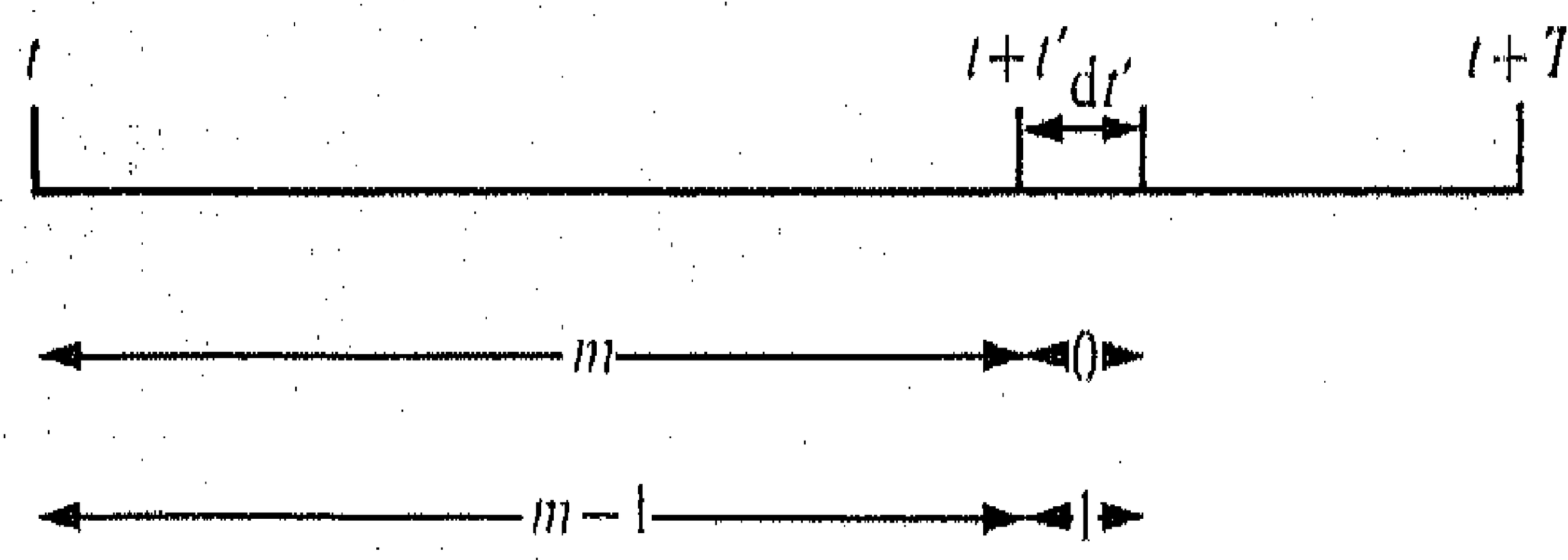

FIG. 6.5. Time intervals used in the calculation of $P_m(t, T)$ showing the two ways in which m photons can be counted in the period between t and $t+t'+\mathrm{d}t'$.

The two ways of computing the probability that m photons are counted between t and $t+t'+\mathrm{d}t'$ must be equivalent, so from eqns (6.51), (6.52), and (6.53),

$$P_m(t, t'+\mathrm{d}t') = P_m(t, t')(1-p(t')\,\mathrm{d}t')+P_{m-1}(t, t')p(t')\,\mathrm{d}t'. \tag{6.54}$$

With the use of eqn (6.50) and the definition of differentiation, this can be rearranged to give

$$\mathrm{d}P_m(t, t')/\mathrm{d}t' = \zeta\bar{I}(t')(P_{m-1}(t, t')-P_m(t, t')). \tag{6.55}$$

The probabilities $P_m(t, t')$ for the different values of m are thus related by a chain of differential equations. The first equation in the chain, for $m = 0$, differs from the general result in that the term in P_{m-1} is, of course, absent and

$$\mathrm{d}P_0(t, t')/\mathrm{d}t' = -\zeta\bar{I}(t')P_0(t, t'). \tag{6.56}$$

The chain of equations for $P_m(t, t')$ can be solved by recursion, beginning with $m = 0$. The probability $P_0(t, t')$ is subjected to the boundary condition that certainly no photons are counted in a time interval of zero,

$$P_0(t, 0) = 1. \tag{6.57}$$

With this boundary condition, eqn (6.56) can be integrated to give

$$P_0(t, T) = \exp\left(-\zeta\int_t^{t+T}\bar{I}(t')\,\mathrm{d}t'\right). \tag{6.58}$$

It is convenient to define $\bar{I}(t, T)$ as the mean intensity at the phototube during the counting period,

$$\bar{I}(t, T) = (1/T)\int_t^{t+T}\bar{I}(t')\,\mathrm{d}t', \tag{6.59}$$

in terms of which eqn (6.58) becomes

$$P_0(t, T) = \exp(-\zeta\bar{I}(t, T)T). \tag{6.60}$$

The remaining $P_m(t, T)$ can be determined from eqn (6.55), beginning with $m = 1$ and proceeding to the higher values of m. The boundary condition complementary to eqn (6.57) is

$$P_m(t, 0) = 0 \qquad \text{for} \qquad m \neq 0. \tag{6.61}$$

Problem 6.13. Prove that the general solution of eqn (6.55) subject to eqn (6.61) is

$$P_m(t, T) = \frac{\{\zeta\bar{I}(t, T)T\}^m}{m!}\exp(-\zeta\bar{I}(t, T)T). \tag{6.62}$$

The probability $P_m(t, T)$ represents the distribution of readings of the photon count obtained in a series of experiments all of which begin at the same time t. It is normally possible in practice to conduct only one counting measurement at a time, and successive counting periods run consecutively rather than simultaneously. The intensity $\bar{I}(t, T)$ in general fluctuates between one period and the next, as discussed in Chapter 3 for chaotic light, and the measured photon-count distribution $P_m(T)$ is an average of $P_m(t, T)$ over a large number of different starting times t. We can write[14]

$$P_m(T) = \langle P_m(t, T)\rangle = \left\langle \frac{\{\zeta\bar{I}(t, T)T\}^m}{m!} \exp(-\zeta\bar{I}(t, T)T) \right\rangle, \tag{6.63}$$

where, consistent with the notation of Chapter 3, the angle brackets denote an average over t.

6.7. Photon-count distributions for coherent and chaotic light

The distribution shown in eqn (6.63) for $P_m(T)$, which applies generally to any variety of stationary light source, contains a time average that can be explicitly evaluated for some special cases. Consider first the simplest case in which $\bar{I}(t)$ is independent of t. It follows from eqn (6.59) that $\bar{I}(t, T)$ is then independent of both t and T and we can put

$$\bar{I}(t, T) = \bar{I}. \tag{6.64}$$

The quantity to be averaged in eqn (6.63) is thus independent of the averaging parameter t, and the angle brackets can be ignored, to give

$$P_m(T) = \frac{\bar{m}^m}{m!} \exp(-\bar{m}), \tag{6.65}$$

where we have introduced the quantity

$$\bar{m} = \zeta\bar{I}T. \tag{6.66}$$

The photon distribution $P_m(T)$ for the constant-intensity case is thus a Poisson distribution similar to eqn (4.196), with a mean number $\bar{m}$ of counted photons given by eqn (6.66). The counting statistics are the same as those found for the arrival of raindrops in a 'steady' downpour, or for the arrival of particles emitted during radioactive decay of a long-lived isotope.

The form of the Poisson distribution is illustrated in Fig. 6.6 for three values of the mean number of counts $\bar{m}$. The size of the fluctuations in the photon count about the mean is determined by the root-mean-square deviation Δm of the distribution. The calculation of Δm is algebraically the same as that given in eqns (4.192)–(4.194) but with $|\alpha|^2$ replaced by $\bar{m}$, and the result is

$$(\Delta m)^2 = \bar{m}. \tag{6.67}$$

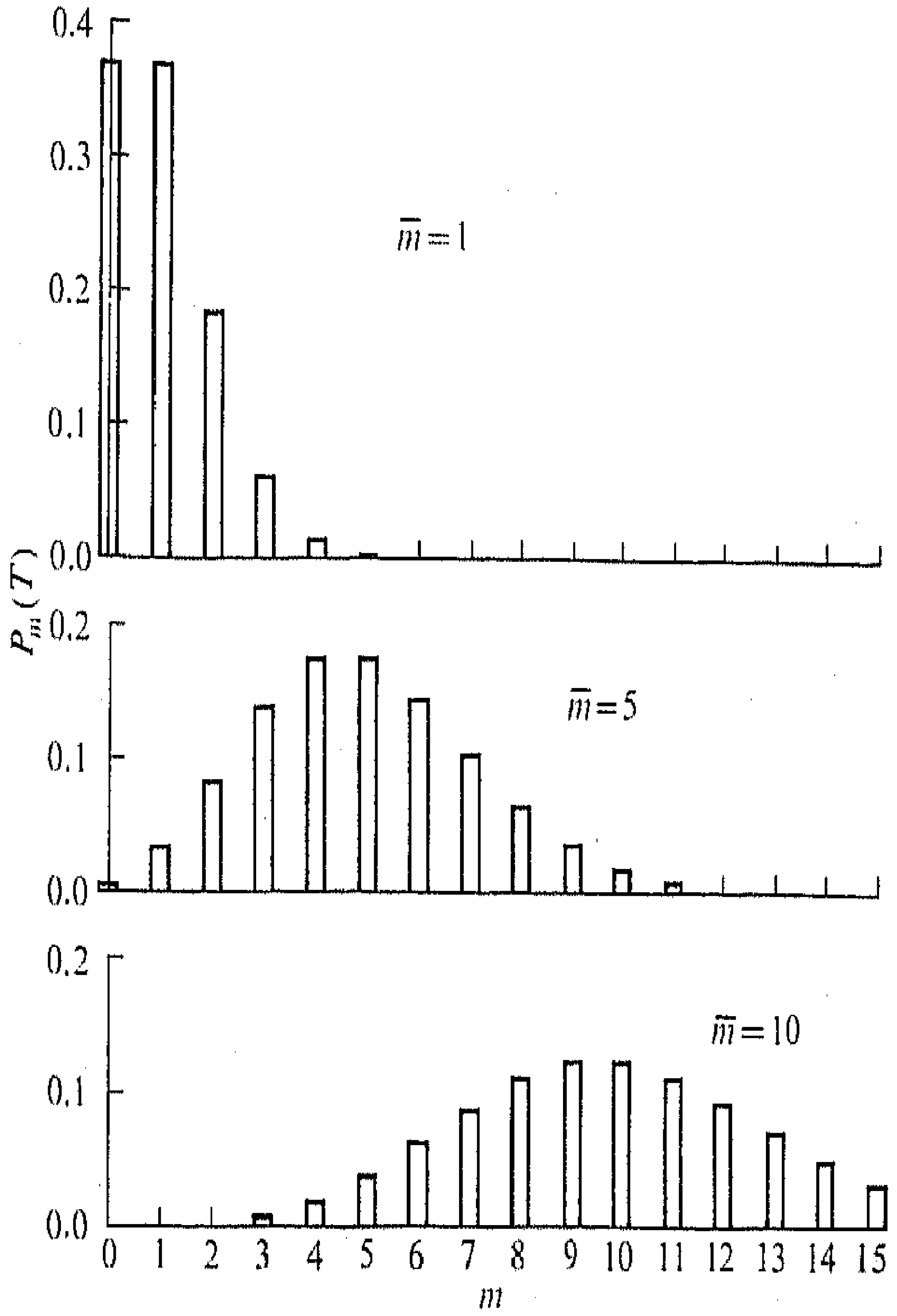

FIG. 6.6. The Poisson form of the photon-count distribution for light beams of constant intensity. The values of $\bar{m}$ are the mean numbers of photons counted during the period T.

The fluctuations that occur for a beam of constant intensity are called *particle fluctuations*. They are due to the discrete, random nature of the photoelectric process, in which energy can be removed from the light only in whole photons. It is seen from eqns (6.66) and (6.67) that the particle fluctuation Δm is proportional to the square root of the beam intensity.

The above results for a beam of constant intensity are clearly appropriate for the classical stable wave of eqn (3.46) and Fig. 3.8, and it is shown in §6.8 that the same distribution is valid for the quantum-mechanical coherent state.

The other important case for which the distribution shown in eqn (6.65) holds follows from the fact that $\bar{I}(t, T)$ can be a constant even if $\bar{I}(t)$ is a fluctuating intensity. Thus, for a chaotic light beam with coherence time τ_c, it is seen from eqn (6.59) that $\bar{I}(t, T)$ is independent of t if T is very large compared to τ_c, so that all the fluctuations are averaged out during the long counting period T. The equality shown in eqn (6.64) is therefore valid for chaotic light when $T \gg \tau_c$, and the Poisson distribution holds in this limit.

The photon-count distribution can also be simply derived for chaotic light in the opposite extreme of a counting time T which is short compared to the coherence time, that is $T \ll \tau_c$. For this limit the instantaneous intensity $\bar{I}(t)$ is essentially a constant during a single counting period, and eqn (6.59) becomes

$$\bar{I}(t,T) = \bar{I}(t) \qquad (T \ll \tau_c). \tag{6.68}$$

The probability distribution $p[\bar{I}(t)]$ for the instantaneous intensity of chaotic light is given by eqn (3.68). With the usual ergodic hypothesis, assumed valid for a stationary light source, the time average in eqn (6.63) can be converted to an ensemble average over the distribution $p[\bar{I}(t)]$, leading to

$$\begin{aligned} P_m(T) &= \frac{1}{\bar{I}}\int \exp(-\bar{I}(t)/\bar{I})\,\frac{(\zeta\bar{I}(t)T)^m}{m!}\exp(-\zeta\bar{I}(t)T)\,\mathrm{d}\bar{I}(t) \\ &= \frac{\bar{m}^m}{(1+\bar{m})^{1+m}}, \end{aligned} \tag{6.69}$$

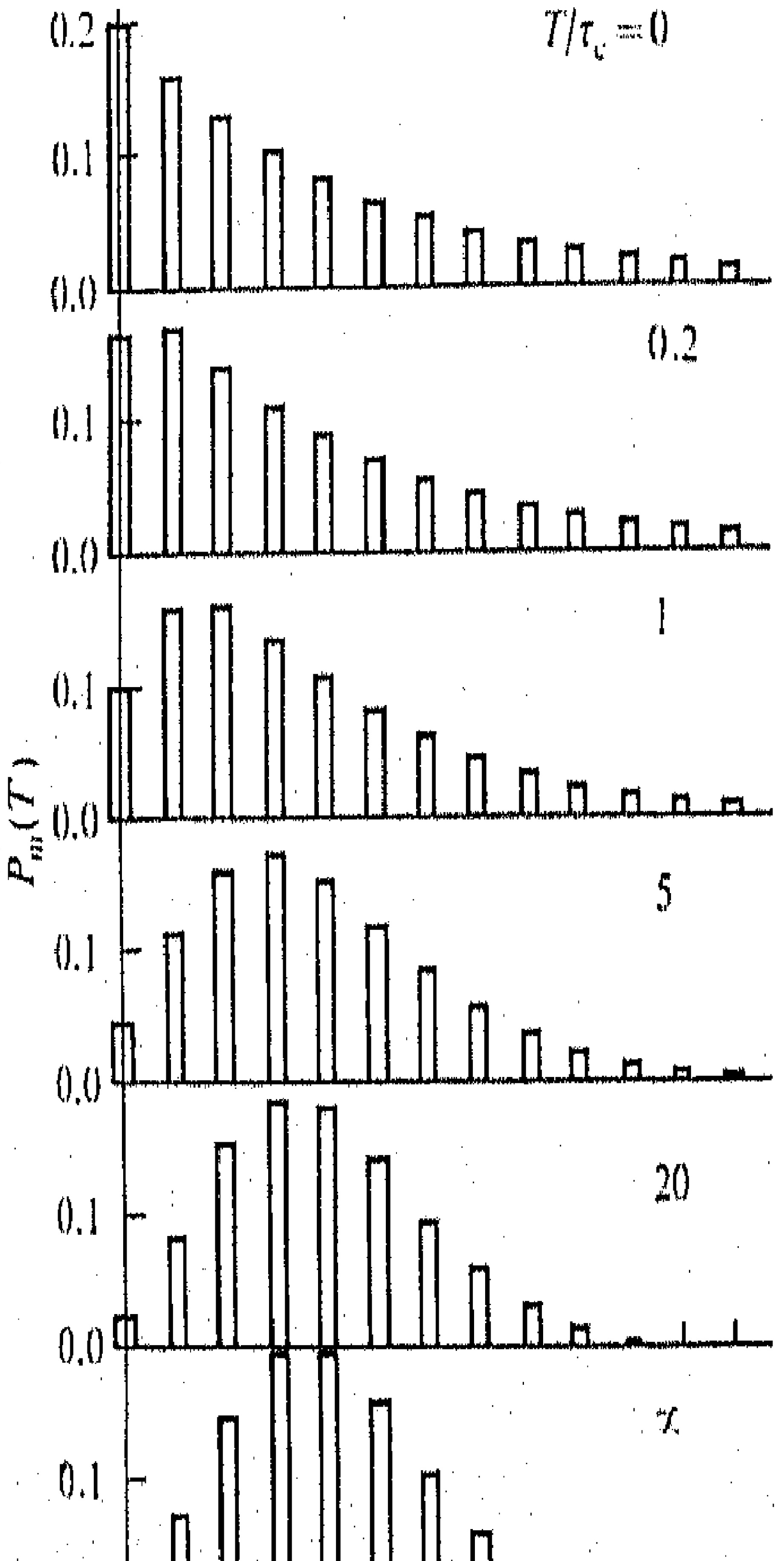

FIG. 6.7. The photon-count distributions for chaotic light with $\bar{m} = 4$ and the indicated values of T/τ_c. The graphs for T/τ_c equal to 0 and ∞ are plotted from eqns (6.69) and (6.65). The data for intermediate values of T/τ_c are taken from E. Jakeman and E. R. Pike (ref. 15.)

where $\bar{m}$ is defined by eqn (6.66). Thus for short counting times, the photon-count distribution for chaotic light is similar to that of the photon distribution in a single mode of a thermal source given by eqn (1.36) and illustrated in Fig. 1.7. However, the result (6.69) for the photon-count distribution is not restricted to excitation of a single mode but applies generally to any chaotic light.

The form of the photon-count distribution is much more difficult to evaluate for counting times T that are neither long nor short compared to the coherence time τ_c of chaotic light. We do not give the details of such calculations here but show in Fig. 6.7 some computed[15] photon-count distributions for a fixed mean number of counted photons $\bar{m} = 4$. The graphs show how the probability distribution changes continuously from the form (6.69) for $T \ll \tau_c$ to the form (6.65) for $T \gg \tau_c$.

It is clear from Fig. 6.7 that the photon-count distribution is sensitive to the coherence time τ_c for counting times T that are comparable to τ_c. Thus a measurement of $P_m(T)$ for chaotic light can be used to determine the coherence time by fitting the experimental distribution to the theoretical curves. Fig. 6.8 shows an example of a measured photon-count distribution[16]. The experiment was carried out on a beam of laser light after scattering by a suspension of spherical particles in water at room temperature. The theory of Brownian motion shows that such scattered light has a Lorentzian frequency

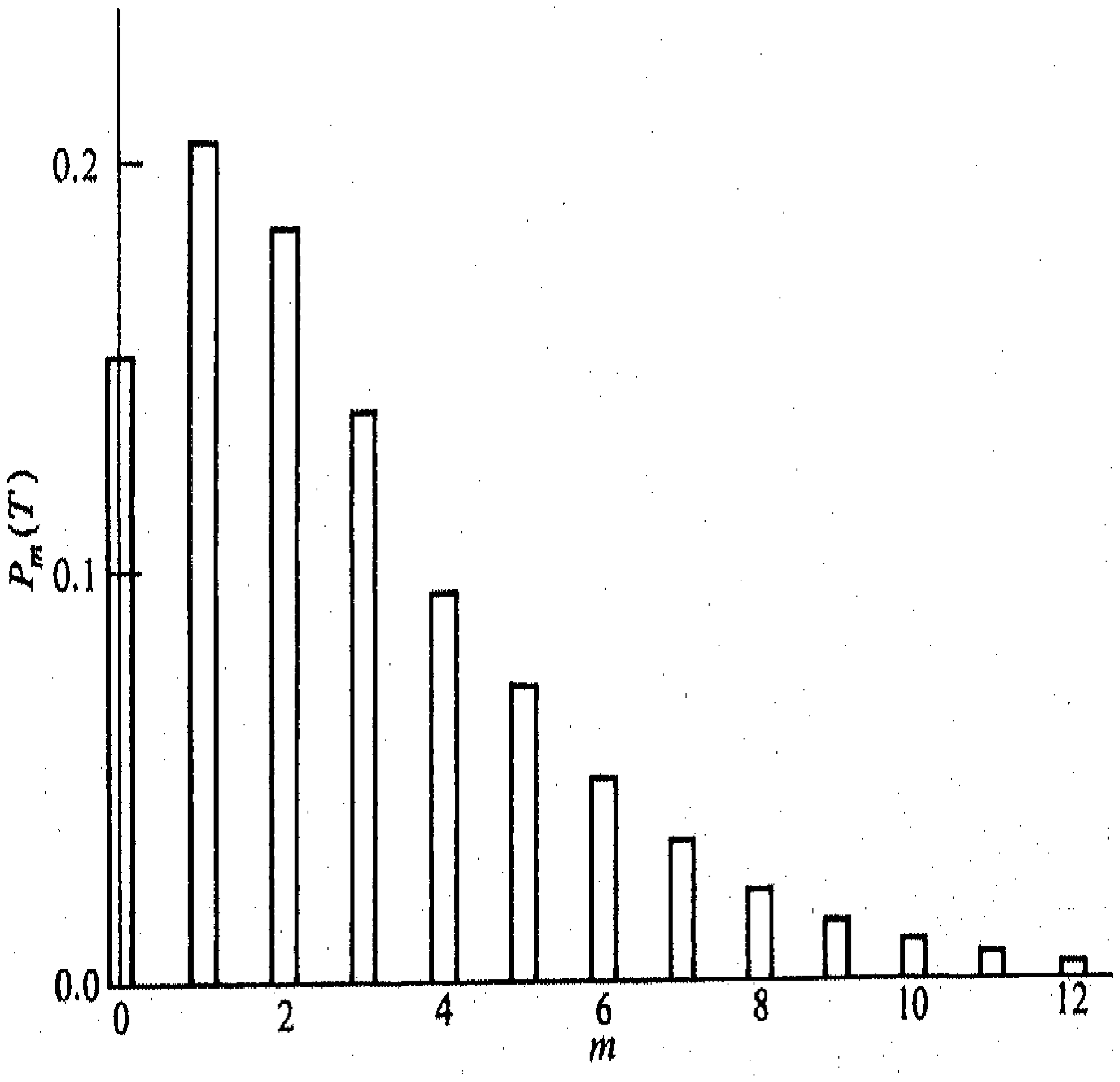

FIG. 6.8. Experimental photon-count distribution for laser light after scattering by a suspension of spherical particles in water. The counting time T is 10^{-1} s and the mean count $\bar{m}$ is equal to 3. (After E. Jakeman *et al.*, ref. 16.)

distribution[17]. The random motion imposes on the scattered laser light temporal properties characteristic of a chaotic source and the experimental distribution of Fig. 6.8 is similar to those of Fig. 6.7. The complete experiment involved a series of counting times ranging from 10^{-2} to 2×10^{-1} s, and the coherence time τ_c obtained from a comparison of theory and experiment is 10^{-1} s. The corresponding angular-frequency linewidth of 20 s^{-1} could not, of course, be measured by conventional frequency spectroscopy.

Although the complete distribution function requires a lengthy calculation for general values of T, it is not difficult to evaluate the size of the fluctuations in the number of counted photons for chaotic light. From eqn (6.63) the mean number of counted photons is

$$\bar{m} = \sum_{m=0}^{\infty} mP_m(T) = \langle \zeta \bar{I}(t,T)T \rangle = \zeta \bar{I} T, \tag{6.70}$$

where the definition of $\bar{I}$ as the long-time-averaged intensity has been used, together with the normalization of the probability distribution,

$$\sum_{m=0}^{\infty} P_m(T) = 1. \tag{6.71}$$

The mean count agrees with eqn (6.66), derived under more restrictive conditions.

In a similar way, the second moment of the distribution is

$$\overline{m^2} = \sum_{m=0}^{\infty} m^2 P_m(T) = \langle \zeta \bar{I}(t,T)T \rangle + \langle (\zeta \bar{I}(t,T)T)^2 \rangle$$
$$= \bar{m} + \langle (\zeta \bar{I}(t,T)T)^2 \rangle. \tag{6.72}$$

The mean-square deviation, or variance, of the distribution can be written

$$(\Delta m)^2 = \overline{m^2} - \bar{m}^2 = \bar{m} + \zeta^2 T^2 (\langle \bar{I}(t,T)^2 \rangle - \bar{I}^2). \tag{6.73}$$

The first term represents the same particle fluctuations as the result (6.67) for a beam of constant intensity. The additional fluctuations represented by the second term in eqn (6.73) arise from the random variations in the instantaneous intensity and are known as *wave fluctuations*. The wave fluctuations clearly depend upon the properties of the light beam under investigation, unlike the constant particle-fluctuation component. The more general result (6.73) reduces to eqn (6.67) for the constant-intensity case.

The wave-fluctuation contribution in eqn (6.73) involves the same kind of average over squared intensities as the Hanbury Brown and Twiss correlation in eqn (3.103). Conversely the measured response in the Hanbury Brown and Twiss experiment is entirely controlled by the size of the wave fluctuations. The rejected particle-fluctuation contribution contains no information on the light under investigation, and its presence would otherwise tend to obscure the more informative wave fluctuations.

The wave fluctuation in eqn (6.73) can be evaluated for a chaotic beam of Lorentzian frequency profile with linewidth parameter γ' related to the coherence time by

$$\gamma' = 1/\tau_c, \tag{6.74}$$

as in eqn (3.27). The integral required to evaluate the average in eqn (6.73) has already been performed in eqn (3.106), except that τ_r must be replaced by T. The variance is

$$(\Delta m)^2 = \bar{m} + (\bar{m}^2/2\gamma'^2 T^2)\{\exp(-2\gamma' T) - 1 + 2\gamma' T\}. \tag{6.75}$$

Fig. 6.9 shows how the mean-square deviation varies with the counting time T. The constant-intensity particle fluctuation from eqn (6.67) is included for comparison.

For a counting time T short compared to the coherence time τ_c, eqn (6.75) reduces to

$$(\Delta m)^2 = \bar{m} + \bar{m}^2 \qquad (\gamma' T \ll 1). \tag{6.76}$$

In this limit all chaotic sources produce the same counting statistics given by eqn (6.69), and the variance is the same as that found in eqn (1.41) for single-mode thermally-excited photons. We have noted that the average to be evaluated in eqn (6.73) is similar to that which controls the Hanbury Brown and Twiss correlations. The variance depends upon second-order coherence properties of the light and consequently the result for chaotic light in the limit of infinite coherence time differs from the coherent-light result, as shown in Fig. 6.9, and by eqns (6.67) and (6.76).

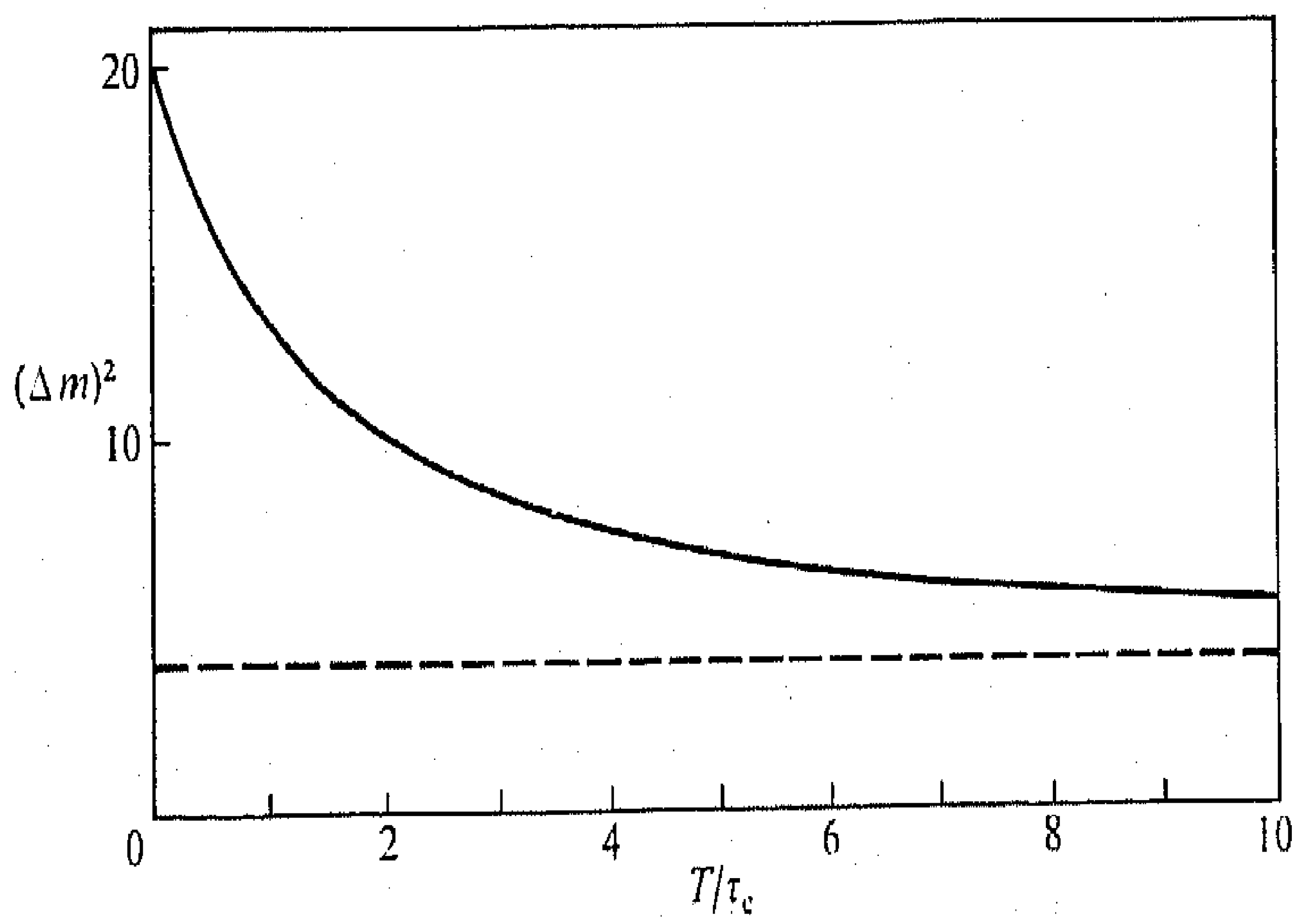

FIG. 6.9. Variance of the number of counted photons for chaotic light of coherence time τ_c. The mean count is maintained at $\bar{m} = 4$ independent of the counting time T. The horizontal line shows the constant level of particle fluctuations.

For a counting time T that is long compared to τ_c, the general result (6.75) becomes

$$(\Delta m)^2 = \bar{m} + (\bar{m}^2/\gamma' T) \qquad (\gamma' T \gg 1), \tag{6.77}$$

and reduces to eqn (6.67) for very long counting times, where the photon-count distribution has the Poisson form (eqn (6.65)), as discussed above.

6.8. Quantum-mechanical photon-count distribution

The photon-count distributions derived above are based on the semiclassical expression (6.63). A more general theory of the photon-count distribution is provided by a fully quantum-mechanical formulation of the problem. The more general theory can handle field excitations that are not describable in classical terms, and it provides the definitive results for all types of excitation.

The quantum-mechanical theory of the photon-count distribution proceeds, like the semiclassical theory, by considering the sequence of photoelectric processes that are involved in the detection of a series of photons by a phototube. The calculations are similar to those described above for the derivation of the quantum-mechanical degrees of coherence except that the photon-count distribution is more complicated owing to the appearance of all powers of the intensity in the probability of a count of m, as in the semiclassical result (6.63).

The quantum-mechanical photon-count distribution was first derived by Kelley and Kleiner,[18] and their paper can be consulted for details of the somewhat lengthy derivation. For the case in which the dimensions of the phototube cathode are small compared with the coherence length of the radiation, their result can be written

$$P_m(T) = \mathrm{Tr}\left\{\hat{\rho}\mathscr{N}\,\frac{(\zeta\hat{I}(T)T)^m}{m!}\exp(-\zeta\hat{I}(T)T)\right\}. \tag{6.78}$$

The intensity operator that appears in this expression is an average of the usual operator (5.99) over the counting time,

$$\hat{I}(T) = (1/T)\int_0^T \hat{I}(\mathbf{r}t)\,\mathrm{d}t \equiv (1/T)\int_0^T 2\epsilon_0 c\hat{E}^-(\mathbf{r}t)\hat{E}^+(\mathbf{r}t)\,\mathrm{d}t, \tag{6.79}$$

where $\mathbf{r}$ is the detector position, and the light beam is assumed plane polarized and parallel.

The quantum-mechanical distribution bears a clear resemblance to the semiclassical result (6.63), but care must be taken with the order of operators in the quantum-mechanical formula. The operator $\mathscr{N}$ imposes normal ordering on the electric-field operators that follow it. That is, if the exponential in eqn (6.78) is expanded in a power series, then for each term in the series, the electric-field operators must be ordered with all the $\hat{E}^+$ operators to the right of the $\hat{E}^-$ operators. The normal ordering of field operators ensures a correct representation of the detection process in terms of photon destruction. Use of the normal-ordering operator $\mathscr{N}$ allows the distribution to be written in the compact form shown in eqn (6.78), but the $\hat{E}^-$ and $\hat{E}^+$ factors of $\hat{I}(T)$ become separated when the exponential is expanded.

The quantum-mechanical form of the photon-count distribution can be evaluated for the same cases as considered above in the discussion of the semiclassical expression (6.63). It is quite simple to evaluate the distribution for a pure coherent-state excitation $|\{\alpha_k\}\rangle$. The coherent state is an eigenstate of $\hat{E}^+(\mathbf{r}t)$ with eigenvalue given in eqn (5.103). Thus in eqn (6.78) each $\hat{E}^+$ operator can be replaced by the eigenvalue and each $\hat{E}^-$ operator by the complex conjugate. The distribution therefore simplifies to a Poisson distribution similar to eqn (6.65). The quantum-mechanical results also substantiate the semiclassical calculations for chaotic light.[18]

The physical significance of the quantum-mechanical distribution is however most transparent for photon-counting experiments on light beams whose photons are restricted to a single mode, and we consider only this case in detail. The product of field operators in eqn (6.79) then reduces to a simple form, with the use of eqns (5.84) and (5.85), and the photon-count distribution can be written

$$P_m(T) = \mathrm{Tr}\left\{\hat{\rho}\mathscr{N}\,\frac{(\xi\hat{a}^\dagger\hat{a})^m}{m!}\exp(-\xi\hat{a}^\dagger\hat{a})\right\}, \tag{6.80}$$

where $\mathscr{N}$ now orders the single-mode photon creation operators $\hat{a}^\dagger$ to the left of the corresponding destruction operators $\hat{a}$, and

$$\xi = \zeta c\hbar\omega T/V \tag{6.81}$$

is known as the *quantum efficiency* of the detector. Note that the product of field operators in eqn (6.79) is independent of the time in the single-mode case, as in the analogous products that occur in the quantum degrees of coherence.

The operator whose ensemble average is to be evaluated in eqn (6.80) has only diagonal matrix elements for the number states $|n\rangle$. Let the density operator for the photon excitation have diagonal matrix elements P_n,

$$P_n = \langle n|\hat{\rho}|n\rangle. \tag{6.82}$$

Thus P_n specifies (completely or partially depending on whether $\hat{\rho}$ is or is not diagonal for the states $|n\rangle$) the probability distribution of the single-mode excitation amongst the various number states $|n\rangle$; we seek the connection between P_n and the photon-count distribution to which the excitation gives rise.

If the exponential is expanded in eqn (6.80) and the number states are used to evaluate the trace, we have

$$P_m(T) = \sum_n P_n(\xi^m/m!)\langle n|\sum_{l=0}^{\infty}(-1)^l(\xi^l/l!)(\hat{a}^\dagger)^{m+l}(\hat{a})^{m+l}|n\rangle. \qquad (6.83)$$

The matrix element is evaluated by the normal rules (4.91) and (4.92) to give

$$P_m(T) = \sum_{n=m}^{\infty} P_n \frac{\xi^m}{m!}\sum_{l=0}^{n-m}(-1)^l\frac{\xi^l}{l!}\frac{n!}{(n-m-l)!}. \qquad (6.84)$$

The l-summation is equivalent to a binomial expansion and can be expressed in closed form to yield

$$P_m(T) = \sum_{n=m}^{\infty} P_n \binom{n}{m}\xi^m(1-\xi)^{n-m}, \qquad (6.85)$$

where

$$\binom{n}{m} \equiv {}^nC_m = \frac{n!}{m!(n-m)!}. \qquad (6.86)$$

This form[19,20] of the photon-count distribution is equivalent to eqn (6.78) for a single-mode excitation. It is known as a Bernoulli distribution, and has a simple physical interpretation as the probability that m photons are counted and $n-m$ photons escape detection, the probability of an individual photon being detected during the counting period being ξ. The factor (6.86) takes care of our lack of interest in which m photons are counted, and the sum over n allows for the possible numbers of photons excited in the single mode. The mean number of counted photons for the distribution (6.85) is

$$\bar{m} = \xi\bar{n}. \qquad (6.87)$$

It is seen from the definition of ξ in eqn (6.81) that $\bar{m}$ increases linearly with the counting time T. This behaviour is expected for experiments in which a steady beam of photons travels from a source to the detector. It cannot however be correct for detection in a closed cavity, where the number of counts cannot exceed the initial number of photons. In addition, the probability (6.85) takes negative values for sufficiently long counting times T. The difficulties arise from the neglect of the quantum effects of the measurement process on the measured system. The photon detections attenuate the light beam, and more accurate treatments[19-22] show that the photon-count distribution (6.85) must be modified by making the replacement

$$\xi \rightarrow 1-\exp(-\xi) \qquad (6.88)$$

to give

$$P_m(T) = \sum_{n=m}^{\infty} P_n \binom{n}{m}\{1-\exp(-\xi)\}^m\exp\{-(n-m)\xi\}, \qquad (6.89)$$

with a mean count of

$$\bar{m} = \{1-\exp(-\xi)\}\bar{n}. \qquad (6.90)$$

The distribution (6.85) and the mean count (6.87) are recovered in the limit $\xi \ll 1$, but the new results are well behaved for long counting times when ξ may be much larger than unity.

It is clear from eqn (6.89) that the photon-count distribution is the same as the photon distribution P_n only in the case of very large ξ, when

$$P_m(T) = P_n\,\delta_{nm} \qquad (\xi \rightarrow \infty). \qquad (6.91)$$

For smaller quantum efficiencies, the distributions $P_m(T)$ and P_n are different, and an experimental photon-count distribution yields only indirect information on the photon excitation. Practical quantum efficiencies are usually much smaller than unity and it is not necessary to make the replacement (6.88) in such cases.

We assume for simplicity that ξ is indeed much smaller than unity, and there are two important photon distributions P_n for which the summation in eqn (6.85) can be carried out.

Problem 6.14. Consider single-mode coherent light where eqns (4.192) and (4.231) give

$$P_n = \frac{\bar{n}^n}{n!}\exp(-\bar{n}). \qquad (6.92)$$

Use eqn (6.85) to prove that

$$P_m(T) = \frac{(\xi\bar{n})^m}{m!}\exp(-\xi\bar{n}). \qquad (6.93)$$

Problem 6.15. Consider filtered single-mode chaotic light as in problem 6.8, where eqn (4.240) gives

$$P_n = \frac{\bar{n}^n}{(1+\bar{n})^{1+n}}. \qquad (6.94)$$

Prove that

$$P_m(T) = \frac{(\xi\bar{n})^m}{(1+\xi\bar{n})^{1+m}}. \qquad (6.95)$$

These results agree with eqns (6.65) and (6.69) calculated by the semiclassical method. In both examples, the mean number $\bar{m}$ of counted photons is given by eqn (6.87), and the distributions P_n and $P_m(T)$ have the same mathematical form. This is, however, not a general property of the photon-count distribution, which can differ in form from the photon distribution P_n. A simple case in which the two distributions are different is provided by a photon number-state light beam where the photon-count distribution is nonzero for all m less than or equal to the number of photons in the beam. The normalized second factorial moments of the two distributions are however the same in all cases.

Problem 6.16. Prove from eqn (6.85) or (6.89) that for all forms of photon distribution in a single mode

$$\sum_m m(m-1)P_m(T)/\bar{m}^2 = \sum_n n(n-1)P_n/\bar{n}^2 \equiv g^{(2)}(\tau). \qquad (6.96)$$

The degree of second-order coherence of the light is therefore directly obtainable from the photon-count distribution, without any dependence on the quantum efficiency of the detector. For multimode light beams, there exists[23] a more complicated relation between the degree of second-order coherence and the second factorial moment of the general photon-count distribution. It follows from eqn (6.96) and the properties of $g^{(2)}(\tau)$ discussed in §6.3 that the variance of the quantum-mechanical photon-count distribution can take any non-negative value, unlike the semiclassical variance of eqn (6.73) which can never be smaller than $\bar{m}$.

All of the detailed derivations in the present section refer to light beams that interact *only* with the detection equipment. More general photon-count distributions can be derived[22] for light beams whose photon numbers fluctuate during the detection period T because of absorption and emission by atoms, as for example in a laser cavity or other light source. The more general distributions reduce to the results discussed above when T is much shorter than the characteristic fluctuation times of the photon numbers.

6.9. Photon counting in the Michelson interferometer

Interference experiments provide examples of the application of the quantum-mechanical photon-count distribution. We consider the Michelson interferometer and determine how the photon-count statistics of the output light are related to the photon probability distribution P_n of the input light.

The Michelson interferometer is represented schematically in Fig. 6.10. The input light beam is split in the usual way by a semitransparent mirror inclined at 45° to the axes. The mirrors in arms 1 and 2 of the interferometer, inclined at 90° to each other, return the split beams to the semitransparent mirror, and thence to the phototube detector. The beam splittings are assumed to be perfectly symmetrical and the incident light is assumed to be in a plane parallel beam. With these conditions, the field of view of the detector is uniformly illuminated. For given choices $\frac{1}{2}z_1$, and $\frac{1}{2}z_2$ of the arm lengths, there are no spatial variations of intensity at the detector to complicate the theory of photon counting. This feature makes the Michelson interferometer more convenient than Young's interference experiment for the application of photon-counting theory.

The properties of the light at the phototube are however described by a theory very similar to that presented for Young's experiment in §6.1. Thus the photon creation and destruction operators $\hat{a}^\dagger$ and $\hat{a}$ for the input light are

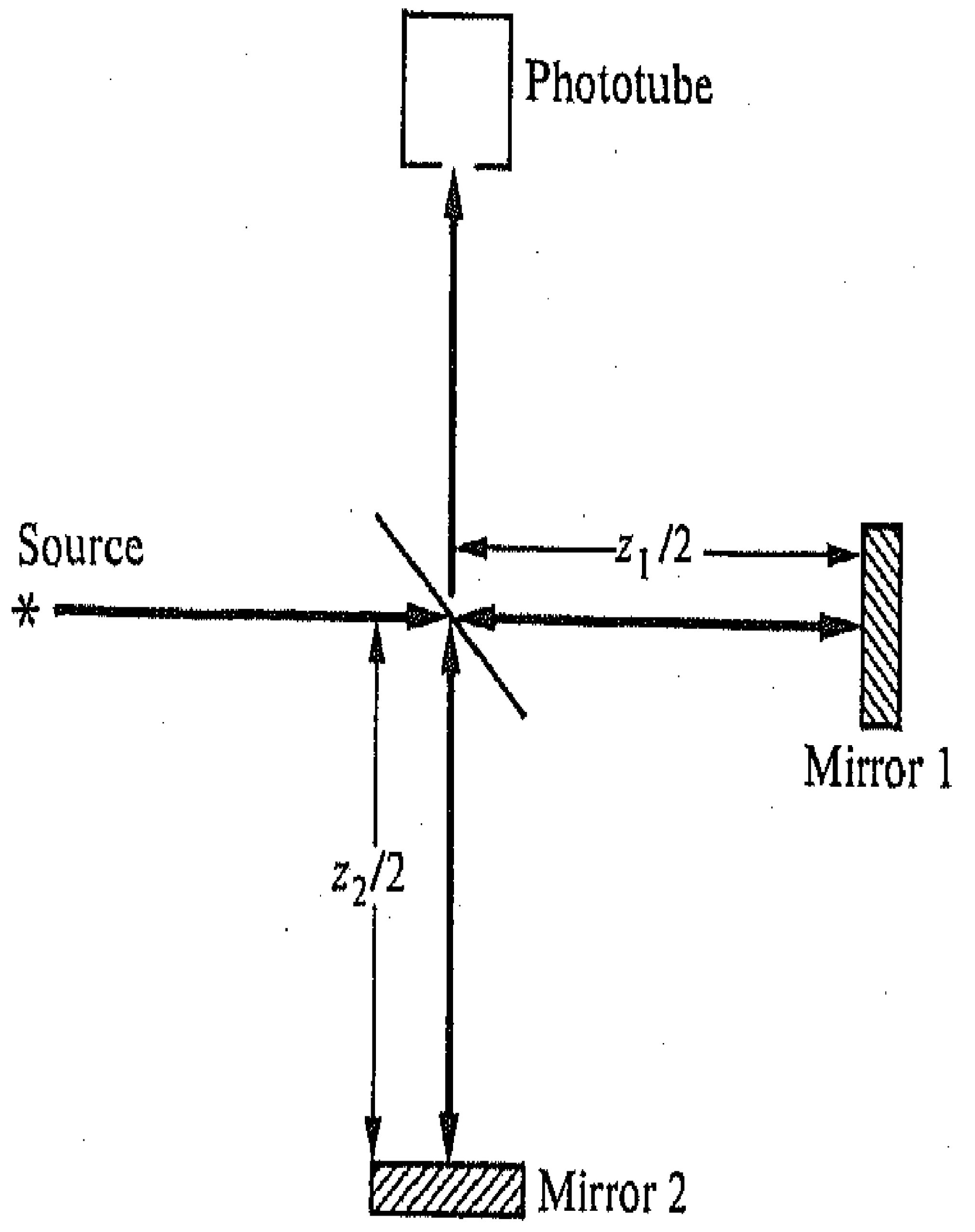

FIG. 6.10. Schematic Michelson interferometer.

related by eqn (6.5) to the operators $\hat{a}_i^\dagger$ and $\hat{a}_i$ for photons in the modes corresponding to arms $i = 1$ and 2 of the interferometer. It is assumed that the two arms are excited with the same phase, and with only one mode of wavevector k in each.

The light that falls on the phototube consists of a superposition of contributions from arms 1 and 2, and the electric field operator has a form similar to eqn (6.10). With only a single mode excited, it is simpler to use the corresponding photon creation and destruction operators defined by

$$\hat{d}^\dagger = \{\hat{a}_1^\dagger \exp(-ikz_1) + \hat{a}_2^\dagger \exp(-ikz_2)\}/2^{\frac{1}{2}}$$
$$\hat{d} = \{\hat{a}_1 \exp(ikz_1) + \hat{a}_2 \exp(ikz_2)\}/2^{\frac{1}{2}} \qquad (6.97)$$

for the detector arm of the interferometer. In these expressions, the phase factors included are those for which there is a difference between arms 1 and 2, remembering that the optical paths are twice the arm lengths; the additional phase factors that result from the common stretches of the optical paths make no contributions to the final results and they are set equal to unity in eqn (6.97). The effects of phase changes caused by the mirrors are assumed to be included in the optical path lengths z_1 and z_2. With the same commutation relations,

$$[\hat{a}_1, \hat{a}_1^\dagger] = [\hat{a}_2, \hat{a}_2^\dagger] = 1 \qquad (6.98)$$

and

$$[\hat{a}_1, \hat{a}_2^\dagger] = [\hat{a}_2, \hat{a}_1^\dagger] = 0 \qquad (6.99)$$

as used in §6.1, it is easily shown that

$$[\hat{d}, \hat{d}^\dagger] = 1. \qquad (6.100)$$

The photon-count distribution at the detector obtained from eqn (6.80) is

$$P_m(T) = \mathrm{Tr}\left\{\hat{\rho}\mathcal{N}\,\frac{(\xi\hat{d}^\dagger\hat{d})^m}{m!}\exp(-\xi\hat{d}^\dagger\hat{d})\right\}. \tag{6.101}$$

The main goal of the present section is the connection between this photon-count distribution and the photon-number distribution P_n of the light incident from the source. Thus we need to evaluate the trace in eqn (6.101) for input light of given statistical properties specified by $\hat{\rho}$, and we therefore need the relations between the input operators $\hat{a}^\dagger$ and $\hat{a}$ of eqn (6.5) and the output operators $\hat{d}^\dagger$ and $\hat{d}$ of eqn (6.97).

Define another creation–destruction pair of operators

$$\begin{aligned}\hat{b}^\dagger &= (\hat{a}_1^\dagger - \hat{a}_2^\dagger)/2^{\frac{1}{2}}\\ \hat{b} &= (\hat{a}_1 - \hat{a}_2)/2^{\frac{1}{2}}.\end{aligned} \tag{6.102}$$

It is verified with the use of eqns (6.98) and (6.99) that

$$[\hat{a},\hat{a}^\dagger] = [\hat{b},\hat{b}^\dagger] = 1 \tag{6.103}$$

and

$$[\hat{a},\hat{b}^\dagger] = [\hat{b},\hat{a}^\dagger] = 0. \tag{6.104}$$

The operators for arms 1 and 2 are expressible as

$$\begin{aligned}\hat{a}_1^\dagger &= (\hat{a}^\dagger + \hat{b}^\dagger)/2^{\frac{1}{2}} &\quad \hat{a}_2^\dagger &= (\hat{a}^\dagger - \hat{b}^\dagger)/2^{\frac{1}{2}}\\ \hat{a}_1 &= (\hat{a} + \hat{b})/2^{\frac{1}{2}} &\quad \hat{a}_2 &= (\hat{a} - \hat{b})/2^{\frac{1}{2}},\end{aligned} \tag{6.105}$$

and hence the output operators of eqn (6.97) are related to input operators by

$$\begin{aligned}\hat{d}^\dagger &= \tfrac{1}{2}\{\hat{a}^\dagger[\exp(-ikz_1)+\exp(-ikz_2)]+\hat{b}^\dagger[\exp(-ikz_1)-\exp(-ikz_2)]\}\\ \hat{d} &= \tfrac{1}{2}\{\hat{a}[\exp(ikz_1)+\exp(ikz_2)]+\hat{b}[\exp(ikz_1)-\exp(ikz_2)]\}.\end{aligned} \tag{6.106}$$

The density operator $\hat{\rho}$ for the input light is based on the number states $|n\rangle$, related to the vacuum state $|0\rangle$ by eqn (6.6). Since $\hat{b}$ commutes with $\hat{a}^\dagger$ as in eqn (6.104), it follows from the ground-state condition of the $\hat{b}$ operator that

$$\hat{b}|n\rangle = 0. \tag{6.107}$$

Thus when eqn (6.106) is inserted into eqn (6.101) and the normal ordering is carried out, it follows that the parts of $\hat{d}^\dagger$ and $\hat{d}$ that involve $\hat{b}^\dagger$ and $\hat{b}$ make zero contributions to the trace. The relations (6.101) can therefore be reduced to

$$\begin{aligned}\hat{d}^\dagger &= \tfrac{1}{2}\hat{a}^\dagger[\exp(-ikz_1)+\exp(-ikz_2)]\\ \hat{d} &= \tfrac{1}{2}\hat{a}[\exp(ikz_1)+\exp(ikz_2)],\end{aligned} \tag{6.108}$$

provided that their use is restricted to the evaluation of $|n\rangle$ matrix elements of normally-ordered products. The $\hat{b}^\dagger$ and $\hat{b}$ operators are thus removed from the calculation, and eqn (6.108) provides the required relation between input and output operators.

With these substitutions, the photon-count distribution (6.101) can be developed straightforwardly into a Bernoulli form analogous to eqn (6.85),

$$P_m(T) = \sum_{n=m}^{\infty} P_n\binom{n}{m}\{\xi\cos^2[\tfrac{1}{2}k(z_1-z_2)]\}^m\{1-\xi\cos^2[\tfrac{1}{2}k(z_1-z_2)]\}^{n-m}, \tag{6.109}$$

with a mean number of counted photons

$$\bar{m} = \xi\bar{n}\cos^2[\tfrac{1}{2}k(z_1-z_2)]. \tag{6.110}$$

This result reproduces the usual variation in output with the difference between the optical path lengths in the two arms of the Michelson interferometer.

The spread of the photon counts about the mean is determined by the variance, which can be written

$$(\Delta m)^2 = \overline{m(m-1)} + \bar{m} - \bar{m}^2. \tag{6.111}$$

The equality (6.96) between the second factorial moments of $P_m(T)$ and P_n remains valid, and the variance can be expressed in the forms

$$\begin{aligned}(\Delta m)^2 &= \bar{m}^2[g^{(2)}(\tau)-1]+\bar{m}\\ &= \frac{\bar{m}^2}{\bar{n}^2}(\Delta n)^2+\bar{m}\left(1-\frac{\bar{m}}{\bar{n}}\right),\end{aligned} \tag{6.112}$$

where $g^{(2)}(\tau)$ is the degree of second-order coherence (6.28) of the input light and $(\Delta n)^2$ is its photon-number variance. The photon count thus inherits the scaled photon-number fluctuations of the input light, but in addition acquires fluctuations generated by the random division of photons between the two arms of the interferometer in accordance with the probability distribution (6.13).

The expressions (6.109) and (6.110) for the photon-count distribution and its mean can be corrected for high detection efficiency by the replacement (6.88). We assume in what follows that all of the output photons are detected, equivalent to setting ξ equal to unity in eqns (6.109) and (6.110). Fig. 6.11 shows some calculated variations of photon count with optical path difference in the vicinity of equal path lengths. The heavy curve in each part of the figure is the mean count from eqn (6.110). The shading shows the variation of the deviations $\pm\Delta m$ from the mean value, obtained from eqn (6.112) for the different kinds of input light as

$$\Delta m = \begin{cases}\bar{m}^{\frac{1}{2}}[1-(\bar{m}/\bar{n})]^{\frac{1}{2}} & \text{(number state)}\\ \bar{m}^{\frac{1}{2}} & \text{(coherent)}\\ m^{\frac{1}{2}}(\bar{m}+1)^{\frac{1}{2}} & \text{(chaotic).}\end{cases} \tag{6.113}$$

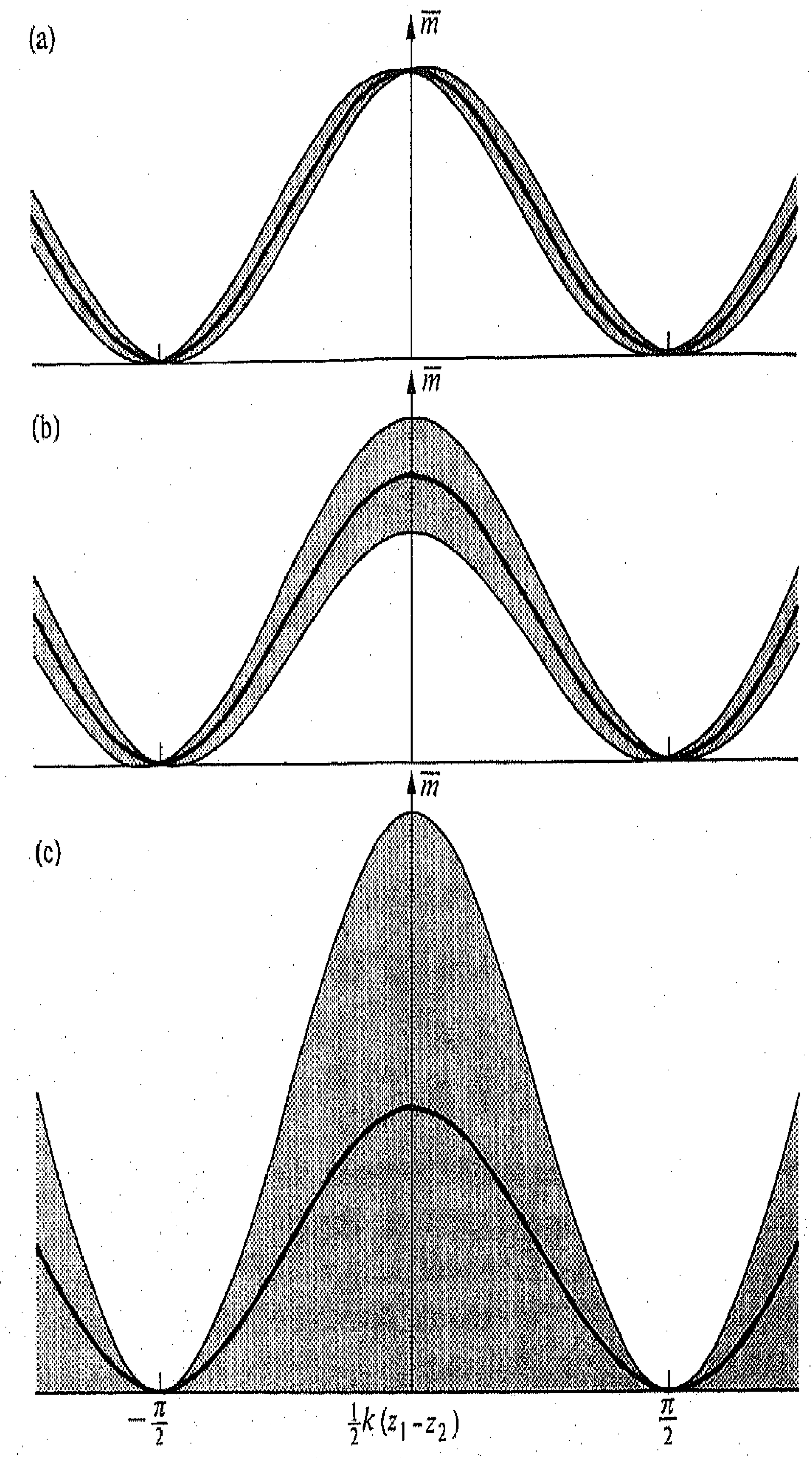

FIG. 6.11. Variations of photon count with optical path difference in a Michelson interferometer for perfect detection. The shading shows the root-mean-square uncertainties in the count. The nature of the single-mode input light is (a) number state, (b) coherent, and (c) chaotic.

The above derivation is restricted to single-mode input light. The treatment of multimode light requires a generalization in which the various kinds of creation and destruction operator are summed over all the excited modes k. The principles of the calculation are unchanged but the equations are algebraically more complicated. In the case of chaotic input light with Lorentzian line broadening, the oscillations in mean photon count given by eqn (6.110) are damped out for large path differences $|z_1 - z_2|$, similar to the off-axis fringe blurring in Young's interference experiment. For small path differences, where eqn (6.110) remains valid, and for counting times T much longer than the difference in transit times via arms 1 and 2, the variance in photon count is identical to eqn (6.75). The photon-count pattern is similar to the single-mode chaotic result of Fig. 6.11(c) when T is much smaller than the coherence time τ_c, but is similar to the single-mode coherent result of Fig. 6.11(b) when T is much larger than τ_c.

These results apply for the photon-count distributions of individual, well-separated detection periods. More general expressions[24] apply for the predicted variance in series of measurements where the separation between adjacent counting periods may be comparable to or smaller than the coherence time. In the usual way, the uncertainty in a determination of the mean count $\bar{m}$ becomes inversely proportional to $N^{\frac{1}{2}}$ when the measurements from a large number N of counting periods are combined. Interest in the use of Michelson interferometers with photon-counting detection has been stimulated by their potential use in the detection of gravitational waves[25], where the small changes in relative path length $z_1 - z_2$ caused by gravitational displacements of the mirrors may be detectable by the resulting changes in mean photon count.

The Michelson interferometer becomes similar to the apparatus of Hanbury Brown and Twiss when the mirrors are replaced by phototubes, and the analysis of the two experiments makes some use of the same properties of the input light. Note however that the mean photon count in the Michelson experiment depends only on the mean photon number in the input, whereas the average correlation measured by Hanbury Brown and Twiss is governed by the degree of second-order coherence of the input light. Second-order properties such as the coherence or variance of the input light enter the theory of the Michelson interferometer only in the evaluation of the scatter of data about the mean count. An analogous treatment of the scatter of measurements of the Hanbury Brown and Twiss correlation about its average value would show a dependence on the degree of fourth-order coherence of the incident light.

6.10. Higher-order coherence and polarization effects

The quantum-mechanical version of the classical degree of rth-order coherence defined in eqn (3.112) is

$$g^{(r)}(\mathbf{r}_1t_1,\ldots,\mathbf{r}_rt_r;\ \mathbf{r}_{r+1}t_{r+1},\ldots,\mathbf{r}_{2r}t_{2r})$$
$$= \frac{\langle \hat{\mathbf{E}}^-(\mathbf{r}_1t_1)\ldots\hat{E}^-(\mathbf{r}_rt_r)\hat{E}^+(\mathbf{r}_{r+1}t_{r+1})\ldots\hat{E}^+(\mathbf{r}_{2r}t_{2r})\rangle}{(\langle\hat{E}^-(\mathbf{r}_1t_1)\hat{E}^+(\mathbf{r}_1t_1)\rangle\ldots\langle\hat{E}^-(\mathbf{r}_{2r}t_{2r})\hat{E}^+(\mathbf{r}_{2r}t_{2r})\rangle)^{\frac{1}{2}}}. \quad (6.114)$$

The first and second-order degrees of coherence given in eqns (6.14) and (6.23) are special cases of this more general definition.

The degree of rth-order coherence determines the measured response in experiments where r photons are simultaneously detected in some way. An example is to be found in §9.5, where it is shown that the rate of simultaneous absorption of three photons from a light beam, accompanied by emission of a single third-harmonic photon, is proportional to $g^{(3)}$.

There are two simple properties of the rth-order coherence, analogous to the classical results (3.113) and (3.114). We consider first a multimode coherent state $|\{\alpha_k\}\rangle$, this being an eigenstate of $\hat{E}^+$ as in eqn (5.103). Thus, for the pure state $|\{\alpha_k\}\rangle$ the numerator and denominator of the expression (6.114) for $g^{(r)}$ both involve products of factors similar to the eigenvalue in eqn (5.103) and its complex conjugate. A closer inspection shows that the numerator and denominator are in fact identical when pairs of space–time points are the same, and we have the result

$$g^{(r)}(\mathbf{r}_1 t_1, \ldots, \mathbf{r}_r t_r; \mathbf{r}_r t_r, \ldots, \mathbf{r}_1 t_1) = 1 \qquad \text{for all } r. \tag{6.115}$$

The quantum-mechanical coherent state therefore has exactly the same coherence properties as the classical stable wave and is coherent in all orders. In any interference experiment, however complicated, the quantum mechanical coherent state produces the same interference fringes and field correlations as would be calculated for the classical stable wave. It is this property of the basic states $|\alpha\rangle$ that causes them to be called the coherent states.

For the opposite extreme of a multimode chaotic state, with density operator given by eqn (4.244), it is not difficult to evaluate $g^{(r)}$ for the special case where all the space–time points in eqn (6.114) are the same. The result is a degree of rth-order coherence equal to $r!$, as in the classical result (3.114). Indeed, all the quantum-mechanical properties of chaotic light are identical to those derived in classical coherence theory. The theories of interference experiments that use chaotic light can be treated equally well by the two theories.

It is not difficult to generalize the relation (6.96) between the degree of second-order coherence and the second factorial moment of the photon-count distribution of single-mode light, and it can be shown that the degree of rth-order coherence is equal to the normalized rth factorial moment of the photon-count distribution. Photon-counting experiments thus provide a means of measuring the degrees of coherence of arbitrary orders.

The light beams treated in the present chapter have so far been assumed plane polarized. Some of the results can be generalized without difficulty to apply to partially-polarized beams. Consider a light beam propagated parallel to the z-axis made up of two independent beams, one with mean photon number $\bar{n}_x$ polarized parallel to the x-axis, and one of mean photon number $\bar{n}_y$ polarized parallel to the y-axis. The total mean photon number is

$$\bar{n} = \bar{n}_x + \bar{n}_y \tag{6.116}$$

and the degree of polarization is

$$P = \frac{\bar{n}_x - \bar{n}_y}{\bar{n}_x + \bar{n}_y} \qquad (\bar{n}_x \geqslant \bar{n}_y) \tag{6.117}$$

where the x-axis is chosen to be that with the larger mean photon number. Thus

$$\bar{n}_x = \tfrac{1}{2}(1+P)\bar{n} \tag{6.118}$$

and

$$\bar{n}_y = \tfrac{1}{2}(1-P)\bar{n}. \tag{6.119}$$

For chaotic light, the two independent beams have photon distributions given by the same function as in eqn (6.94). The photon distribution for the combined beams[26] is then found by a procedure analogous to that used for the classical calculation of eqns (3.118)–(3.120).

Problem 6.17. Prove that the photon distribution for chaotic light with mean photon number $\bar{n}$ and degree of polarization P is

$$P_n = \frac{1}{\bar{n}P}\left\{\left(\frac{\bar{n}_x}{1+\bar{n}_x}\right)^{1+n} - \left(\frac{\bar{n}_y}{1+\bar{n}_y}\right)^{1+n}\right\}, \tag{6.120}$$

where $\bar{n}_x$ and $\bar{n}_y$ are given by eqns (6.118) and (6.119).

This expression is the quantum analogue of the classical result (3.120). It reduces to eqn (6.94) in the limit of a plane polarized beam ($P = 1$).

Problem 6.18. Prove that in the limit $P \to 0$ of an unpolarized beam eqn (6.120) gives

$$P_n = \frac{(1+n)(\tfrac{1}{2}\bar{n})^n}{(1+\tfrac{1}{2}\bar{n})^{2+n}}. \tag{6.121}$$

Problem 6.19. Prove that the zero time-delay degree of second-order coherence of the light with photon distribution (6.120) is

$$g^{(2)}(0) = \tfrac{1}{2}(3+P^2), \tag{6.122}$$

identical to the classical result (3.122).

References

1. Walls, D. F. (1977). *Am. J. Phys.* **45**, 952.
2. For an early example of this kind of experiment see Taylor, G. I. (1909). *Proc. Camb. Phil. Soc.* **15**, 114. The following reference describes a more recent experiment.
3. Pfleegor, R. L. and Mandel, L. (1967). *Phys. Rev.* **159**, 1084; (1968). *J. Opt. Soc. Am.* **58**, 946.

4. The quantum theory of optical coherence was mainly originated by R. J. Glauber. Detailed accounts are to be found in his articles in (1965). *Quantum optics and electronics* (eds. C. DeWitt, A. Blandin, and C. Cohen-Tannoudji), p. 63. Gordon and Breach, New York and in (1970). *Quantum optics* (eds. S. M. Kay and A. Maitland), p. 53. Academic Press, London.
5. Knight, P. L. and Allen, L. (1973). *Optics Commun.* **7**, 44.
6. Glauber, R. J. (1963). *Phys. Rev.* **130**, 2529.
7. Twiss, R. Q., Little, A. G., and Hanbury Brown, R. (1957). *Nature* **180**, 324; Twiss, R. Q. and Little, A. G. (1959). Aust. J. Phys. **12**, 77.
8. See also Hanbury Brown, R. (1974). *The intensity interferometer.* Taylor and Francis, London.
9. Arecchi, F. T., Gatti, E., and Sona, A. (1966). *Phys. Lett.* **20**, 27.
10. Morgan, B. L. and Mandel, L. (1966). *Phys. Rev. Lett.* **16**, 1012.
11. Pike, E. R. and Jakeman, E. (1973). *Adv. Quant. Elec.* **2**, 1.
12. See the reviews in (1974). *Photon correlation and light beating spectroscopy* (eds. H. Z. Cummins and E. R. Pike). Plenum Press, New York.
13. Every, I. M. (1973). *J. Phys.* **A6**, 1375; *ibid.* (1975). **A8**, 133.
14. The result for $P_m(T)$ was first derived by Mandel, L. (1958). *Proc. Phys. Soc.* **72**, 1037; (1959). *ibid.* **74**, 233.
15. Jakeman, E. and Pike, E. R. (1968). *J. Phys.* **A1**, 128.
16. Jakeman, E., Oliver, C. J., and Pike, E. R. (1968). *J. Phys.* **A1**, 406.
17. Pecora, R. (1964). *J. Chem. Phys.* **40**, 1604.
18. Kelley, P. L. and Kleiner, W. H. (1964). *Phys. Rev.* **A136**, 316.
19. Mollow, B. R. (1968). *Phys. Rev.* **168**, 1896.
20. Scully, M. O. and Lamb, W. E. (1969). *Phys. Rev.* **179**, 368.
21. Rousseau, M. (1977). *J. Phys.* **A10**, 1043.
22. Shepherd, T. J. (1981). *Optica Acta* **28**, 567.
23. Freed, C. and Haus, H. A. (1966). *Phys. Rev.* **141**, 287.
24. See the article by E. Jakeman in ref. 12, p. 75.
25. Thorne, K. S. (1980). *Rev. Mod. Phys.* **52**, 285.
26. Mandel, L. (1963). *Proc. Phys. Soc.* **81**, 1104.

7. Generation and amplification of light

The present chapter considers the properties of the light emitted by various kinds of source. The simplest property is of course the intensity or mean-photon number of the light but it is often necessary to calculate more detailed properties such as the degree of second-order coherence or the complete photon probability distribution.

The earlier sections of the chapter are devoted to sources in which the light excites only a single mode of an optical cavity. We begin with an account of the statistical and coherence properties of the light emitted by two-level atoms. The equations employed in the analysis can also be used to deduce the changes from the initial properties of a light beam subjected to interaction with a gas of two-level atoms; the cases of attenuation and amplification of the incident light are both treated.

The theory is subsequently generalized to apply to a single-mode three-level laser system. In contrast to the semiclassical laser theory of §1.12, which strictly applies only to the amplification of radiation supplied externally, the fully-quantized theory of the present chapter includes spontaneous emission and thus describes the self-initiating operation of the normal laser light source. The steady-state fluctuation and coherence properties of single-mode laser light are discussed in some detail.

The single-mode restriction is dropped in the final section of the chapter, which describes the emission of radiation in all spatial directions, and hence into all modes, by a single driven two-level atom. This system is important in connection with the basic theory since the light has nonclassical coherence properties of the kind described in Chapter 6.

The light-emitting atoms covered by the present chapter are restricted to those with time-dependent level populations that can be adequately described by rate equations. The discussion of emission by driven atoms is continued in Chapter 8, where the optical Bloch equations for the atomic density matrix are used to obtain the characteristics of the fluorescent light for more general experimental conditions.

7.1. Single-mode photon rate equations

Suppose that a large number N of identical two-level atoms with transition frequency ω_0 is contained in a volume V. We treat the interaction of the atoms with radiation in a single mode **k** of an optical cavity, and omit the **k** subscripts from the radiation field variables. The atomic transition is assumed to be collision broadened, with a linewidth parameter γ' whose collisional part γ_{coll} greatly exceeds the radiative part γ. The interaction of light with the atoms is then well described by rate equations, as discussed in §2.14.

The photon absorption rate obtained from eqn (2.169) is converted to quantum-mechanical notation as in eqn (5.215) to give

$$2g^2\gamma' n/[(\omega_0-\omega)^2+\gamma'^2], \tag{7.1}$$

where

$$g^2 = (e^2\omega/2\epsilon_0\hbar V)\overline{(\boldsymbol{\varepsilon}.\mathbf{D}_{12})^2} = e^2\omega D_{12}^2/6\epsilon_0\hbar V, \tag{7.2}$$

with the usual angular average to allow for random atomic orientations. Thus the absorption rate is

$$\frac{e^2\omega D_{12}^2}{3\epsilon_0\hbar V}\,\frac{\gamma'}{(\omega_0-\omega)^2+\gamma'^2}\,n. \tag{7.3}$$

The same expression for the probability per unit time of photon absorption is obtained from eqn (5.65) if the delta function is replaced by a normalized collision-broadened lineshape. Note that, with the Einstein B coefficient taken from eqns (2.55) or (5.69), the absorption rate can be expressed as

$$B\,\frac{\hbar\omega n}{V}\,\frac{\gamma'/\pi}{(\omega_0-\omega)^2+\gamma'^2}, \tag{7.4}$$

namely a product of B coefficient, photon energy density, and normalized lineshape function.

Suppose that the frequency ω of the chosen cavity mode coincides with the peak of the atomic absorption line at ω_0 and define

$$\mathscr{G} = \frac{e^2\omega_0 D_{12}^2}{3\epsilon_0\hbar V\gamma'} = \frac{2\pi c^3}{V\omega_0^2}\,\frac{\gamma}{\gamma'}, \tag{7.5}$$

where eqn (5.75) has been used. The absorption probability becomes simply

$$\mathscr{G}n. \tag{7.6}$$

Note that this quantity is proportional to the photon spatial density n/V.

The probability of emission of a photon of frequency $\omega = \omega_0$ by an excited atom is obtained by replacing n by $n+1$ in eqn (7.6) (compare eqns (5.65) and (5.70)) to give

$$\mathscr{G}(n+1). \tag{7.7}$$

The two terms n and 1 correspond to stimulated and spontaneous emission; $\mathscr{G}$ is the rate of spontaneous emission into the particular cavity mode considered, whereas the Einstein A coefficient or $1/\tau_{\text{R}}$ given by eqn (5.75) is the total rate of spontaneous emission into all modes.

The state of the radiation field in the single cavity mode is determined by the photon density operator $\hat{\rho}$ discussed in Chapter 4. We characterize the photon state by the values of the diagonal number-state matrix elements P_n of $\hat{\rho}$ defined in eqn (6.82). According to eqns (6.92) and (6.94)

$$P_n = \frac{\bar{n}^n}{n!}\exp(-\bar{n}) \tag{7.8}$$

for a single-mode coherent photon excitation, and

$$P_n = \frac{\bar{n}^n}{(1+\bar{n})^{1+n}} \tag{7.9}$$

for single-mode chaotic light. The P_n are sufficient to describe the main statistical features of the radiation but it must be remembered that the description is incomplete for photon states whose off-diagonal matrix elements $\langle n|\hat{\rho}|n'\rangle$ are not all zero. The corresponding degrees of second-order coherence are

$$g^{(2)}(\tau) = 1 \qquad \text{(coherent)} \tag{7.10}$$

and

$$g^{(2)}(\tau) = 2 \qquad \text{(chaotic)}, \tag{7.11}$$

taken from eqns (6.30) and (6.31).

The effect of photon absorption and emission by the two-level atoms is to cause changes in the photon distribution P_n. The time-dependent changes in the P_n can be described by rate equations. Rate equations have been used for the occupation probabilities of the atomic states in Chapter 1. The rate equations for the photon probabilities can be derived analogously.

Fig. 7.1 shows the energy-level diagram for the cavity mode, and is similar to Fig. 1.3. The quantity P_n is the probability that the photon field is in its nth excited state. We suppose that the mean numbers of atoms in the ground and excited states are N_1 and N_2. The radiative transitions clearly tend to change both the P_n and the atomic excitation probability. We shall however assume that some external influence maintains N_1 and N_2 at fixed values. Thus only the photon distribution P_n is subject to change with time, and the fluctuations in N_1 and N_2 are excluded from consideration.

There are four types of transition that contribute to the rate of change of P_n. If n photons are indeed present in the mode, the N_1 atoms in their ground states each absorb photons at the rate shown in eqn (7.6), and the N_2 excited atoms each emit photons at the rate given in eqn (7.7). Both processes decrease P_n, at a combined rate of

$$-N_1\mathscr{G}nP_n - N_2\mathscr{G}(n+1)P_n. \tag{7.12}$$

There are also two positive contributions to $\mathrm{d}P_n/\mathrm{d}t$. If $n-1$ photons are excited, the probability of this excitation being P_{n-1}, the N_2 excited atoms can emit a photon to excite the field into its nth state. The rate of this process is

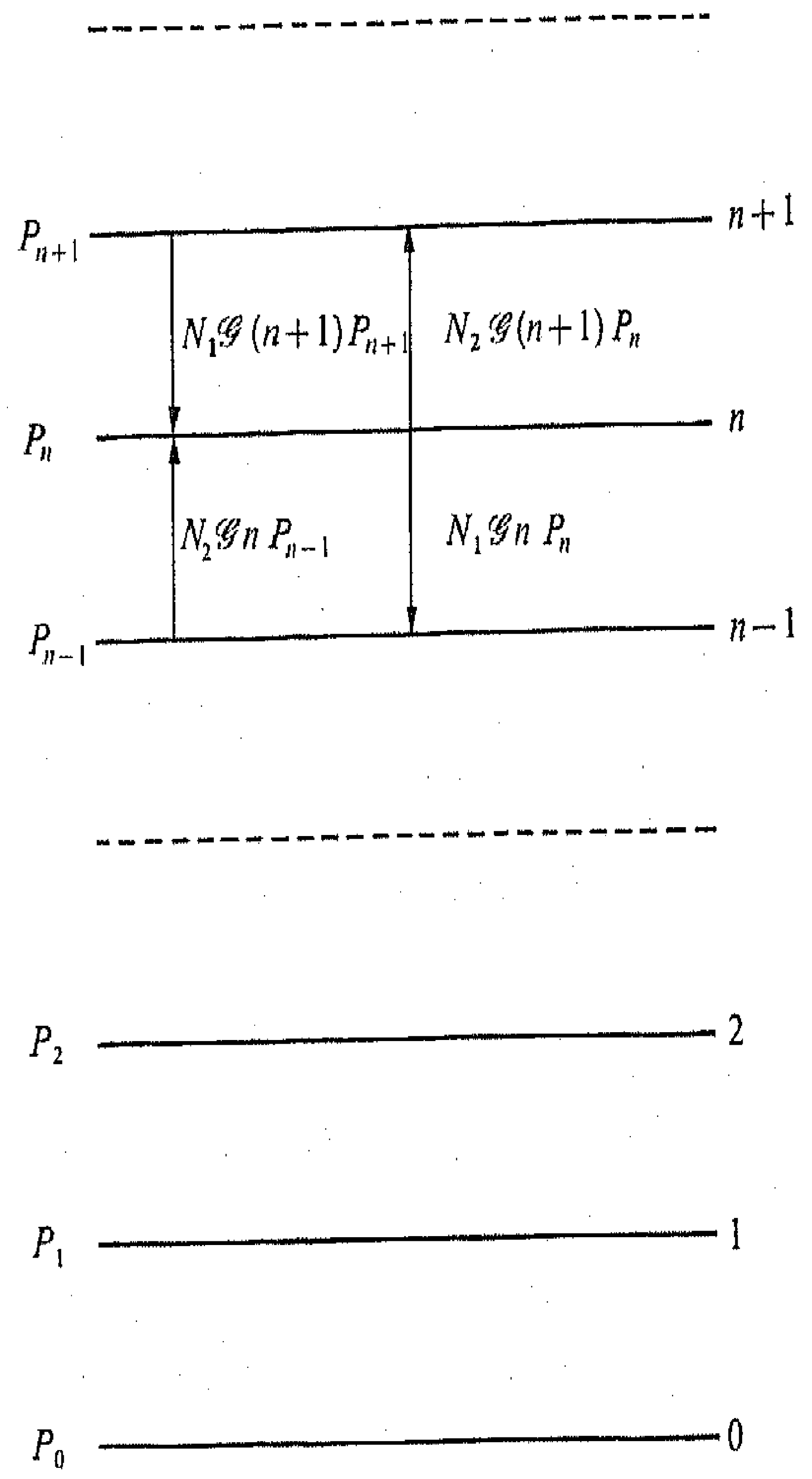

FIG. 7.1. Energy-level diagram for photons in the selected mode. The transition rates indicated are the contributions to $\mathrm{d}P_n/\mathrm{d}t$. The energy interval is $\hbar\omega_0$.

obtained from eqn (7.7) with n replaced by $n-1$ to give

$$N_2\mathscr{G}nP_{n-1}. \tag{7.13}$$

Similarly, if $n+1$ photons are present, with probability P_{n+1}, the N_1 ground-state atoms can absorb a photon to drop the field into its nth excited state and thus increase P_n. The rate is obtained from eqn (7.6) with n replaced by $n+1$ to give

$$N_1\mathscr{G}(n+1)P_{n+1}. \tag{7.14}$$

The contributions of eqns (7.12), (7.13), and (7.14) combine to give a total rate

$$\mathrm{d}P_n/\mathrm{d}t = -N_2\mathscr{G}(n+1)P_n + N_1\mathscr{G}(n+1)P_{n+1} - N_1\mathscr{G}nP_n + N_2\mathscr{G}nP_{n-1}. \tag{7.15}$$

The four transitions that contribute to $\mathrm{d}P_n/\mathrm{d}t$ are illustrated in Fig. 7.1. Note that for $n = 0$, where only two types of transition contribute to $\mathrm{d}P_0/\mathrm{d}t$, eqn (7.15) becomes

$$\mathrm{d}P_0/\mathrm{d}t = -N_2\mathscr{G}P_0 + N_1\mathscr{G}P_1. \tag{7.16}$$

7.2. Steady-state solutions

Consider first the steady-state solution for the photon distribution, where the right-hand sides of eqns (7.15) and (7.16) must be set equal to zero. The resulting chain of equations for the different values of n is solved by starting with the steady-state solution of eqn (7.16). This is then used to simplify eqn (7.15) for the $n = 1$ case, which can in turn be used to simplify eqn (7.15) for $n = 2$, and so on. The general condition for a steady state is

$$N_2\mathscr{G}nP_{n-1} - N_1\mathscr{G}nP_n = 0. \tag{7.17}$$

This result is an example of the principle of detailed balance in steady-state conditions. It can be shown in general[1] that states connected by weak non-vanishing transition probabilities must have the same probabilities of occupation in the steady state. The occupation probabilities are N_2P_{n-1} and N_1P_n in the present problem.

The solution of the chain of equations (7.17) is

$$P_n = (N_2/N_1)P_{n-1} = (N_2/N_1)^n P_0. \tag{7.18}$$

The remaining unknown P_0 is determined by the normalization condition

$$\sum_n P_n = 1, \tag{7.19}$$

and the final result is

$$P_n = (N_2/N_1)^n\{1-(N_2/N_1)\}. \tag{7.20}$$

The photon distribution is the same as eqn (7.9) with

$$\bar{n} = N_2/(N_1-N_2). \tag{7.21}$$

The steady-state photon distribution is therefore that of chaotic light. It is the same as that determined in eqn (1.60) as the photon distribution for light in interaction with atoms in thermal equilibrium. The more general proof given here shows that the light generated by a source in which the atoms are maintained at some excitation level different from that in thermal equilibrium has the same chaotic nature as thermal light.

It is also possible[2,3] to calculate the degree of second-order coherence in the steady state. According to the form given in eqn (6.46),

$$\frac{\mathrm{d}g^{(2)}(\tau)}{\mathrm{d}\tau} = \frac{1}{\bar{n}^2}\left\langle \frac{\mathrm{d}n(\tau)}{\mathrm{d}\tau}\, n(0)\right\rangle, \tag{7.22}$$

and a differential equation for $g^{(2)}(\tau)$ is obtained if the right-hand side can be related to $\langle n(\tau)n(0)\rangle$. This is accomplished with the help of the equation of motion (7.15) evaluated at time τ. It is seen by reference to Fig. 7.1 that if n photons are present at time τ, then the only elements of the photon probability distribution that change linearly over a short time $\mathrm{d}\tau$ are $P_{n-1}(\tau)$, $P_n(\tau)$, and $P_{n+1}(\tau)$. The rates of change are attached to the two arrows on the right of

Fig. 7.1, and they lead to

$$\frac{\mathrm{d}g^{(2)}(\tau)}{\mathrm{d}\tau} = \frac{1}{\bar{n}^2}\left\{N_1\mathcal{G}\langle n(\tau)(n(\tau)-1)n(0)\rangle \right.$$
$$-\mathcal{G}\langle[N_1 n(\tau)+N_2(n(\tau)+1)]n(\tau)n(0)\rangle$$
$$\left. +N_2\mathcal{G}\langle(n(\tau)+1)^2 n(0)\rangle\right\}, \qquad (7.23)$$

which reduces after cancellations and rearrangement to

$$\mathrm{d}g^{(2)}(\tau)/\mathrm{d}\tau = \{-N_1\mathcal{G}\langle n(\tau)n(0)\rangle + N_2\mathcal{G}\langle(n(\tau)+1)n(0)\rangle\}/\bar{n}^2$$
$$= -(N_1-N_2)\mathcal{G}\{g^{(2)}(\tau)-1\}, \qquad (7.24)$$

where $\langle n(0)\rangle$ is set equal to the steady-state mean photon number $\bar{n}$ given by eqn (7.21).

The zero time-delay degree of second-order coherence of chaotic light is always equal to 2, and with this boundary condition the solution of eqn (7.24) can be written

$$g^{(2)}(\tau) = 1+\exp(-\tau/\tau_{\mathrm{P}}), \qquad (7.25)$$

where

$$1/\tau_{\mathrm{P}} = (N_1-N_2)\mathcal{G} = N_2\mathcal{G}/\bar{n}. \qquad (7.26)$$

The rate at which the degree of second-order coherence decays from its $\tau = 0$ value is thus equal to the rate of spontaneous emission into the mode by the N_2 excited atoms divided by the mean number of photons in the mode. The spontaneous emissions produce random phase changes in the light, similar to the effect of collisions in the model that leads to the degrees of coherence (3.26) and (3.94).

The steady-state degree of second-order coherence (7.25) tends to unity for long time delays τ, and clearly differs from the time-independent result (7.11) expected for single-mode chaotic light. The apparent discrepancy arises because the photons in the single mode postulated here take part in absorption and emission processes that limit their undisturbed existence. The light thus acquires a finite coherence time of order $2\tau_{\mathrm{P}}$, and its degree of first-order coherence has the standard chaotic form of eqn (3.26) with γ' replaced by $1/2\tau_{\mathrm{P}}$. The spectrum of the light is Lorentzian with a very modest width of order $1/\tau_{\mathrm{P}}$, and the frequencies in the light are therefore no longer strictly confined to a single mode. With this interpretation, eqn (7.25) has the form expected from the general degree of second-order coherence (3.94) for Lorentzian chaotic light. An analogous line broadening occurs in the theory of the 'single-mode' laser given in §7.9. The degree of second-order coherence of the light emitted by an atom radiating into all modes, calculated in §§7.10, 8.3, and 8.4, has a decay rate quite different from eqn (7.26).

7.3. Photon statistics of attenuated light

The photon rate equations (7.15) can also be used to determine the effect of the atomic absorption and emission processes on the statistical properties of an incident beam of arbitrary photon distribution. The beam is attenuated if $N_1 > N_2$ and amplified if $N_1 < N_2$. We treat the attenuator and amplifier in the present and following sections respectively.

A particularly simple case is that in which all N atoms in the cavity are in their ground states. Then only absorption processes occur and eqn (7.15) reduces to

$$\mathrm{d}P_n/\mathrm{d}t = N\mathcal{G}(n+1)P_{n+1} - N\mathcal{G}nP_n. \qquad (7.27)$$

The physical situation is very similar to the quantum-mechanical photon-counting experiment considered in §6.8. The probability that an individual photon present in the cavity at time 0 still remains at time t is $\exp(-N\mathcal{G}t)$. Thus if l photons are present at time 0, there remain n at time t if $l-n$ photons are absorbed and n photons are not absorbed. We therefore expect[4] the solution of eqn (7.27) to be a Bernoulli distribution similar to eqn (6.89),

$$P_n(t) = \sum_{l=n}^{\infty} P_l(0)\binom{l}{n}\exp(-nN\mathcal{G}t)\{1-\exp(-N\mathcal{G}t)\}^{l-n}. \qquad (7.28)$$

Note that with ξ given by eqn (6.81), eqns (6.89) and (7.28) have almost identical forms except that the photon-counting problem requires the distribution of absorbed photons whereas our present concern is the statistical distribution of nonabsorbed photons.

Problem 7.1. Prove that eqn (7.28) is indeed the solution of eqn (7.27).

The effect of the absorption on the statistical properties of an incident beam is determined by insertion of the initial photon distribution into eqn (7.28). For initially coherent or chaotic light, with photon distributions (7.8) and (7.9), the calculations are essentially the same as in problems 6.14 and 6.15. The light remains respectively coherent and chaotic in these cases with a diminishing mean photon number

$$\bar{n} = \bar{n}_0\exp(-N\mathcal{G}t). \qquad (7.29)$$

This expression is valid for all kinds of incident light, but the preservation of the initial statistical properties does not occur in general. A simple example of incident light whose photon distribution changes its form as a result of the absorption is again provided by the photon number state.

The solution of the rate equations (7.15) in the more general case where some of the atoms are in their excited states is more complicated,[2] and we do not consider the complete photon distribution. However, much can be learnt about the time development of the photon distribution by study of its first and second moments, defined as

$$\bar{n} = \sum_n nP_n \tag{7.30}$$

and

$$\overline{n^2} = \sum_n n^2 P_n. \tag{7.31}$$

Simple differential equations for $\bar{n}$ and $\overline{n^2}$ can be obtained by multiplication of both sides of eqn (7.15) by n or n^2 and summation over n. For $\bar{n}$ we obtain,

$$\begin{aligned} \mathrm{d}\bar{n}/\mathrm{d}t &= \sum_n \mathscr{G}\{-N_2 n(n+1)P_n + N_1 n(n+1)P_{n+1} - N_1 n^2 P_n + N_2 n^2 P_{n-1}\} \\ &= \sum_n \mathscr{G}\{-N_2 n(n+1) + N_1(n-1)n - N_1 n^2 + N_2(n+1)^2\}P_n \\ &= (N_2 - N_1)\mathscr{G}\bar{n} + N_2\mathscr{G}, \end{aligned} \tag{7.32}$$

where eqns (7.19) and (7.30) have been used. The solution is

$$\bar{n} = \frac{\{\bar{n}_0(N_1-N_2) - N_2\}\exp\{-(N_1-N_2)\mathscr{G}t\} + N_2}{N_1 - N_2}, \tag{7.33}$$

where $\bar{n}_0$ is the initial value of the mean photon number $\bar{n}$ at time $t = 0$.

The differential equation for the mean-square photon number is

$$\mathrm{d}\overline{n^2}/\mathrm{d}t = 2(N_2-N_1)\mathscr{G}\overline{n^2} + (3N_2+N_1)\mathscr{G}\bar{n} + N_2\mathscr{G}. \tag{7.34}$$

The equation can be solved straightforwardly with substitution of the expression (7.33) for $\bar{n}$, but the solution is somewhat lengthy. The result can be written in a more compact form in terms of the zero time-delay degree of second-order coherence defined as in eqn (6.28),

$$\bar{n}^2\{g^{(2)}(0) - 2\} = \bar{n}_0^2\{g_0^{(2)}(0) - 2\}\exp\{-2(N_1-N_2)\mathscr{G}t\}. \tag{7.35}$$

Note that unlike the previous calculations of the degree of second-order coherence, which referred to steady-state situations, the quantity is here time-dependent, $g_0^{(2)}(0)$ being the initial value and $g^{(2)}(0)$ the value at time t.

Eqns (7.33) and (7.35) determine the time development of the statistical properties of the light produced by its interaction with the atoms.[5] Fig. 7.2 shows the time dependences of the mean photon numbers given by eqn (7.33) for various initial numbers of photons. Note that the mean number of photons at long times always tends to $N_2/(N_1-N_2)$ in agreement with eqn (7.21).

The properties of the degree of second-order coherence are best appreciated by consideration of some simple cases. The simplest cases of all are those where either there are no photons initially present in the cavity ($\bar{n}_0 = 0$) or the initial photon distribution is chaotic ($g_0^{(2)}(0) = 2$). For both these initial states, eqn (7.35) gives

$$g^{(2)}(0) = 2, \tag{7.36}$$

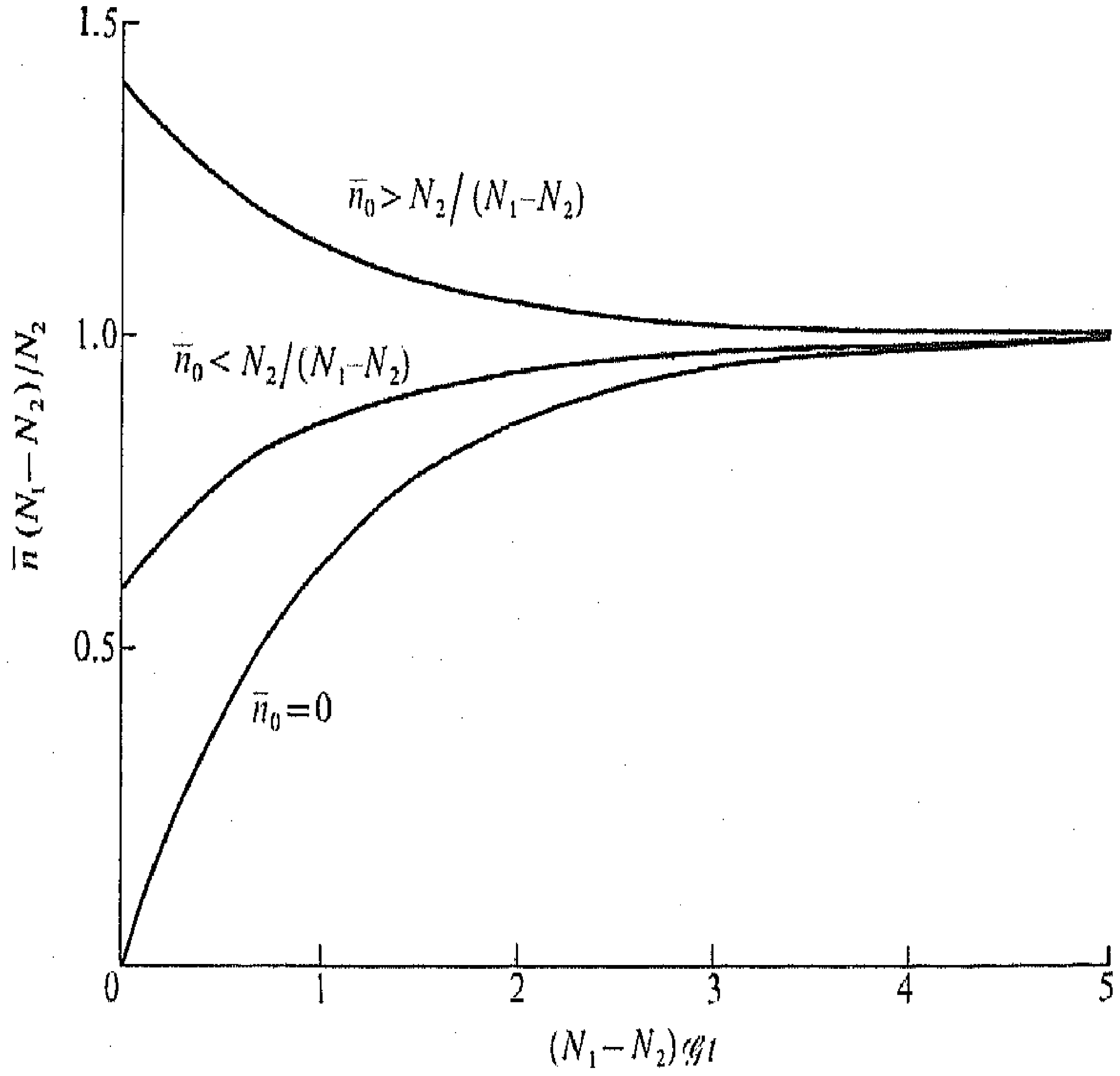

FIG. 7.2. Time dependence of the mean photon number in a cavity mode interacting with atoms, most of which are in their ground states ($N_1 > N_2$). The three curves correspond to the initial values $\bar{n}_0$ of the mean photon number indicated.

and the degree of second-order coherence has the chaotic value at all times t. The same value is obtained more generally in the long time limit of eqn (7.35), irrespective of the nature of the initial photon distribution.

Now suppose that the initial photon distribution is coherent with $g_0^{(2)}(0) = 1$. It is convenient to separate $\bar{n}$ into two contributions and rewrite eqn (7.33) as

$$\bar{n} = \bar{n}_c + \bar{n}_i, \tag{7.37}$$

where

$$\bar{n}_c = \bar{n}_0\exp\{-(N_1-N_2)\mathscr{G}t\} \tag{7.38}$$

and

$$\bar{n}_i = \{N_2/(N_1-N_2)\}[1 - \exp\{-(N_1-N_2)\mathscr{G}t\}]. \tag{7.39}$$

With these definitions eqn (7.35) can be written

$$\bar{n}^2\{g^{(2)}(0) - 2\} = -\bar{n}_c^2 \tag{7.40}$$

or

$$g^{(2)}(0) = \frac{2\bar{n}_i^2 + 4\bar{n}_i\bar{n}_c + \bar{n}_c^2}{(\bar{n}_i + \bar{n}_c)^2}. \tag{7.41}$$

The two contributions to the photons present in the cavity mode at time t are interpreted as follows. The part $\bar{n}_i$ is that which remains in the absence of any initial photon excitation ($\bar{n}_0 = 0$). We have seen that the light in this case has chaotic properties at all times, and eqn (7.41) reproduces the chaotic result (7.36) when $\bar{n}_c$ is set equal to zero. More generally $\bar{n}_i$ represents a chaotic (or incoherent) contribution to the total photon number, irrespective of the initial conditions.

The contribution $\bar{n}_c$ on the other hand represents coherent light. Thus, the degree of second-order coherence (7.41) takes the coherent value of unity if $\bar{n}_i$ is set equal to zero, and indeed it can be proved[6] that this is the correct expression for an arbitrary superposition of coherent light of mean photon number $\bar{n}_c$ and chaotic light of mean photon number $\bar{n}_i$. The coherent light present initially thus provides a coherent component at later times, which is attenuated in accordance with eqn (7.38). This component is completely removed at large times when only the chaotic component remains. Fig. 7.3 shows the time development of the two mean photon numbers and of the degree of second-order coherence for an initial average excitation of 10 coherent photons and a steady-state average excitation of one chaotic photon. It should be emphasized that at intermediate times t the photons cannot be individually characterized as either chaotic or coherent; the numbers $\bar{n}_i$ and $\bar{n}_c$ merely specify the weights of the two contributions to the superposition.

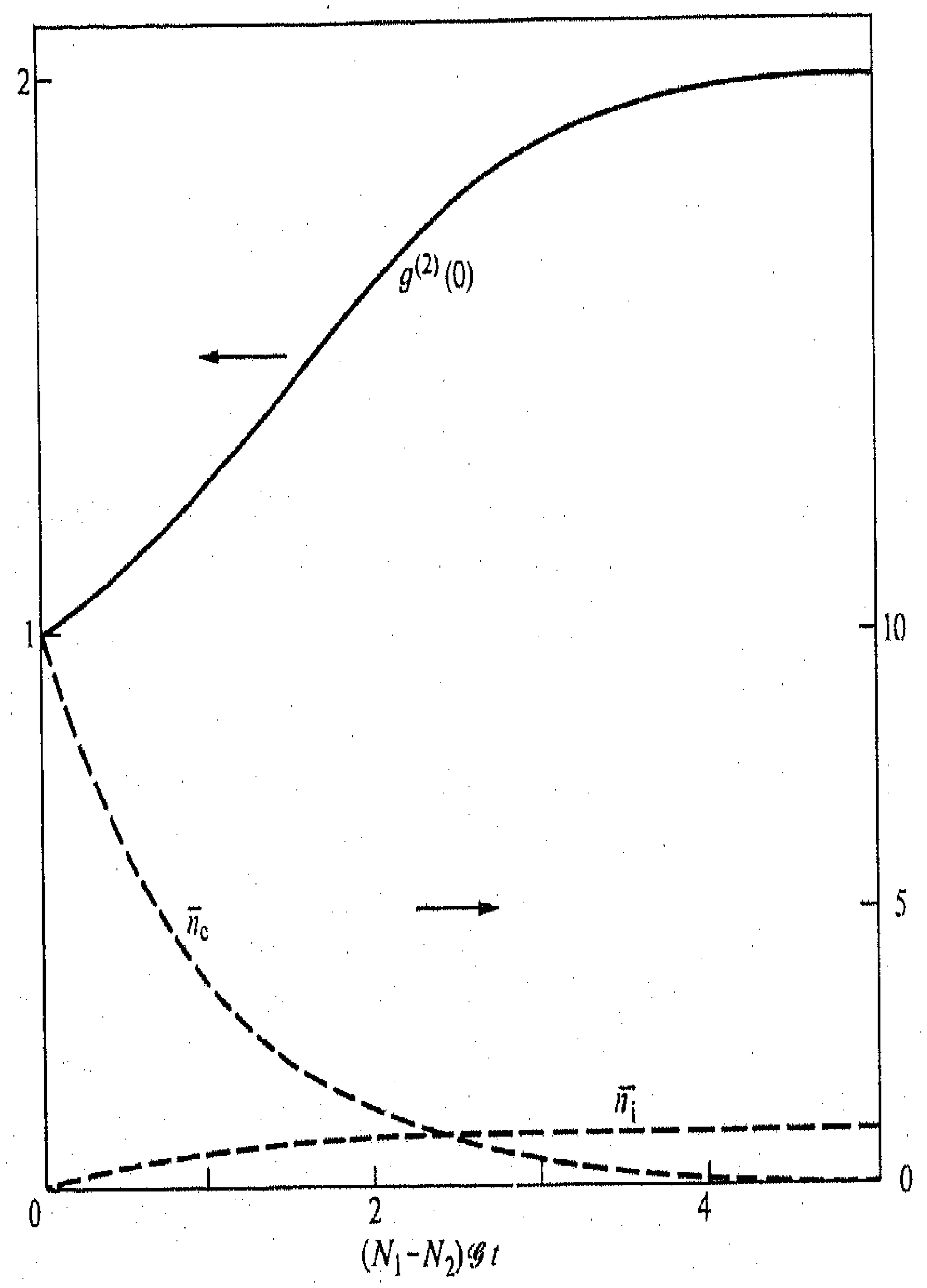

FIG. 7.3. Time development of an initial excitation of coherent light showing the mean photon numbers of the chaotic and coherent components and the degree of second-order coherence of the superposition.

The above calculation of the statistical properties is incomplete since only the first and second moments of the photon distribution are evaluated. This procedure should be treated with caution since different distributions can have the same low-order moments. For example, in the absorption-only case treated at the beginning of the section, an initial photon number-state has its distribution changed while its degree of second-order coherence remains constant (compare problem 6.16). However, in the case considered here, evaluation[2] of the complete time-dependent photon distribution $P_n(t)$ shows that the light is indeed a superposition of chaotic and coherent components at all times t.

7.4. Photon statistics of amplified light

Many of the results of the previous section remain valid for the case of atomic population inversion, where $N_1 < N_2$. Thus the mean photon number and degree of second-order coherence are given by eqns (7.33) and (7.35), with the exponents in these equations now positive, giving exponentials that increase with time.

The simplest examples are again those where there is either no light at all, or purely chaotic light present initially, when eqn (7.36) holds at all subsequent times. The light is always chaotic and the mean photon number $\bar{n}$ now grows without limit. Atomic population inversion is one ingredient of a laser system, but a realistic theory of the laser requires some additional features described later in the chapter. The more realistic theory predicts quite different statistical properties for the light generated by the inverted atomic population.

Now suppose that the initial photon distribution is coherent with $g_0^{(2)}(0)=1$. The solutions (7.37)–(7.41) continue to hold for the case of atomic population inversion, but eqns (7.38) and (7.39) can be rewritten to emphasize the exponential growth that now occurs for both $\bar{n}_c$ and $\bar{n}_i$,

$$\bar{n}_c = \bar{n}_0 \exp\{(N_2-N_1)\mathcal{G}t\} \tag{7.42}$$

and

$$\bar{n}_i = \{N_2/(N_2-N_1)\}[\exp\{(N_2-N_1)\mathcal{G}t\}-1]. \tag{7.43}$$

The strength of the chaotic contribution $\bar{n}_i$ remains independent of the initial strength of the coherent component. The time dependence of the chaotic component is illustrated by the curve labelled $\bar{n}_i$ in Fig. 7.4.

The statistical properties of the light at large times depend on the relative magnitudes of $\bar{n}_0$ and $N_2/(N_2-N_1)$. For a feeble initial excitation of coherent light, where

$$\bar{n}_0 \ll N_2/(N_2-N_1), \tag{7.44}$$

that is,

$$\bar{n}_0(N_2-N_1) \ll N_2, \tag{7.45}$$

the spontaneous emission of photons, at a rate proportional to N_2, dominates the net result of the absorption and stimulated emission, at a combined rate proportional to $\bar{n}_0(N_2-N_1)$. The result at large times is a predominance of chaotic light.

On the other hand, for a strong initial excitation of coherent light, where

$$\bar{n}_0(N_2-N_1) \gg N_2, \tag{7.46}$$

the stimulated emission dominates, and leads to predominantly coherent light at large times. Fig. 7.4 includes representative curves for the two cases of $\bar{n}_0$ greater of smaller than $N_2/(N_2-N_1)$. For large times, the ratio of coherent to chaotic photon numbers is

$$\frac{\bar{n}_c}{\bar{n}_i} = \frac{\bar{n}_0(N_2-N_1)}{N_2}, \qquad (N_2-N_1)\mathcal{G}t \gg 1, \tag{7.47}$$

where eqns (7.42) and (7.43) have been used.

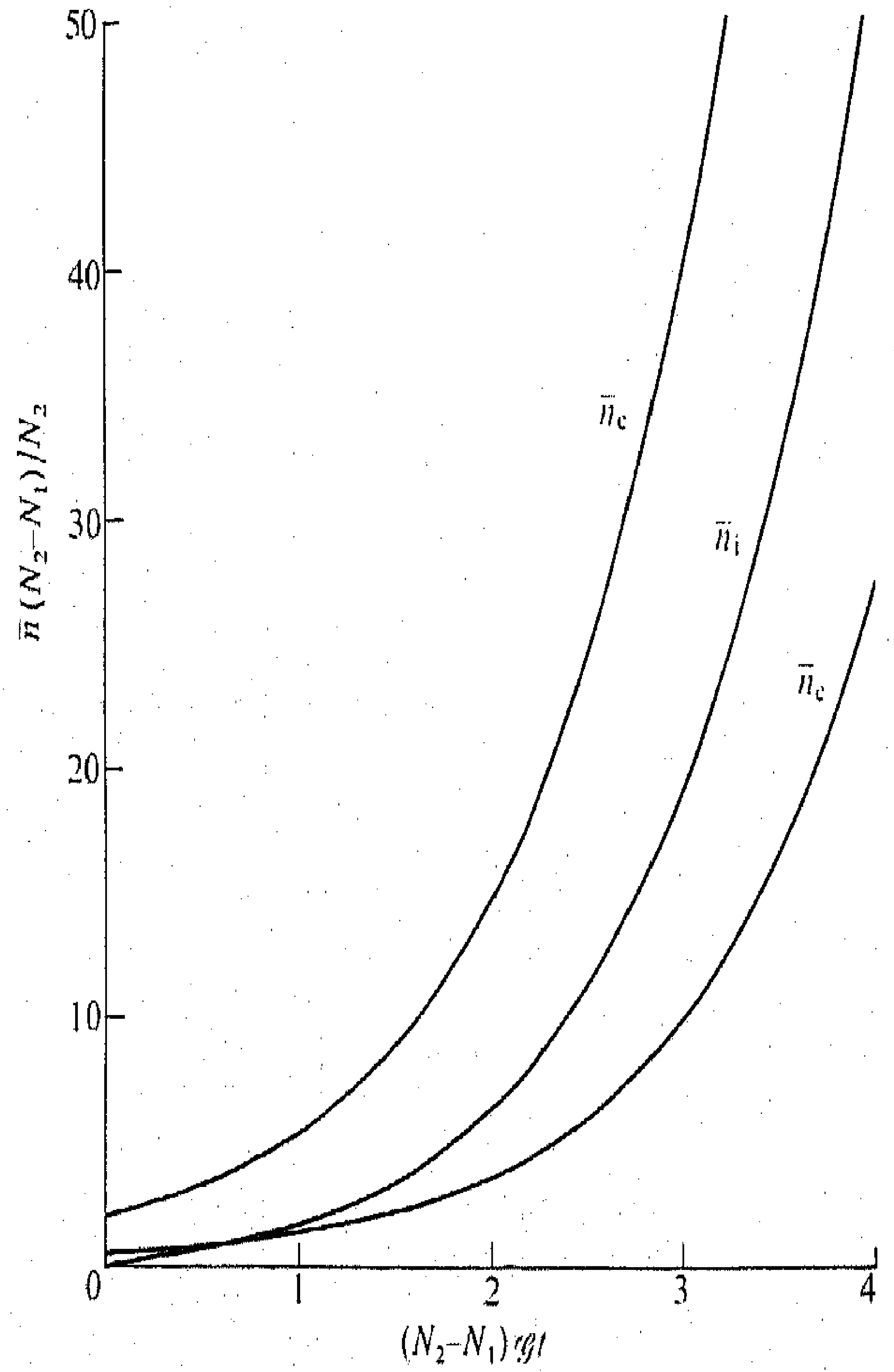

FIG. 7.4. Growth in the mean photon number for atomic population inversion where $N_2 > N_1$. The curve labelled $\bar{n}_i$ shows the time dependence of the chaotic component. The other curves show the time dependence of the coherent component $\bar{n}_c$ for values of the initial number $\bar{n}_0$ of coherent photons greater than (upper curve) or less than (lower curve) $N_2/(N_2-N_1)$.

These results show that stimulated emission by a collection of atoms tends to conserve the coherence properties of the stimulating light. Thus the exponential terms in eqns (7.42) and (7.43) correspond, respectively, to the production of more coherent light by the stimulating coherent light, and more chaotic light by the stimulating chaotic light. Spontaneous emission on the other hand generates chaotic light. The random phase of the spontaneous emission is the cause of the decay rate (7.26) and of the analogous linewidth of the single-mode laser described in §7.9. These properties of stimulated and spontaneous emission[7] were mentioned in §1.8. They must be used with caution because the two kinds of emission always occur together in the quantum theory and their separate characterization requires a careful discussion.[8] The above statements do not apply to emission by a single atom.

Problem 7.2. Show that, to a good approximation, the degree of second-order coherence of incident light of arbitrary statistical properties is unchanged by interaction with two-level atoms provided that either

$$N_2 \ll N_1$$

or

$$N_2 > N_1 \quad \text{and} \quad \bar{n}_0(N_2-N_1) \gg N_2.$$

The first case, that of absorption processes alone, was mentioned in the previous section.

7.5. Laser threshold condition

The next few sections present a calculation of the properties of single-mode laser light. Laser physics is an extensive field of study[9] and the discussion given here is restricted to a simple idealized model of a gas laser. We treat mainly the statistical and fluctuation properties of the light.

The preceding theory requires some extensions before it can be used to describe the operation of a laser in a realistic way. It has been pointed out that it is not normally possible to achieve population inversion by the excitation of transitions restricted to only two levels of an atom. The simplest laser model employs three levels, similar to the scheme envisaged in the elementary laser theory of §1.12. We study the statistical properties of a beam of light in interaction with a gas of similar atoms in which three levels are significantly populated.

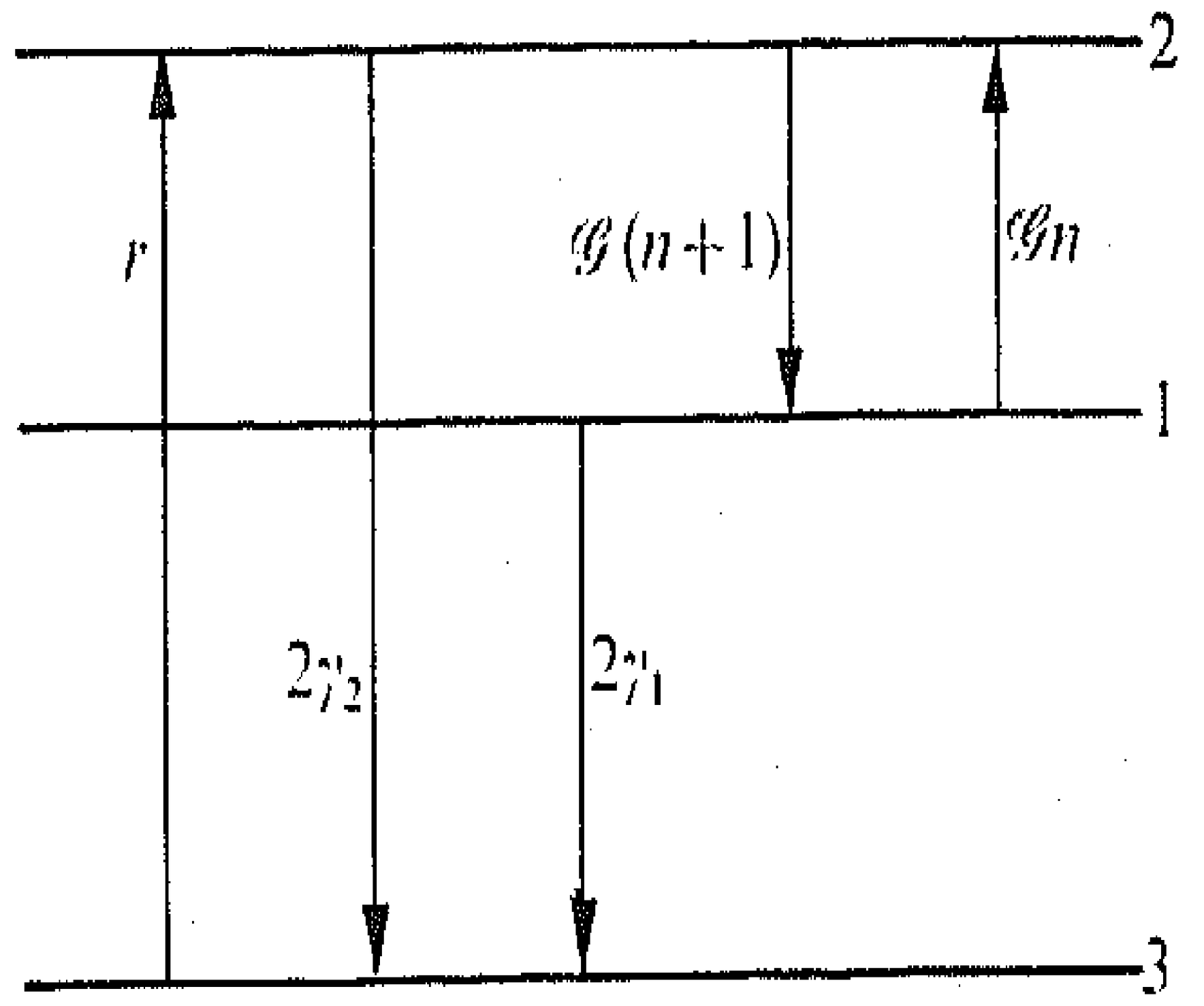

FIG. 7.5. Atomic energy-level scheme of a three-level laser showing the important transition rates.

The atomic energy-level scheme is shown in Fig. 7.5 and it is the same as that of Fig. 1.14. The three levels are assumed to be non-degenerate and the relevant transition rates are marked on the figure. The types of transition that must be considered are the same as those of Fig. 1.14, but the notations for the transition rates have been changed. The laser action is initiated by an external light beam which pumps atoms from the ground state $|3\rangle$ to the upper excited state $|2\rangle$ at a steady rate Nr, where r is defined in eqn (1.110). The total spontaneous decay rates for the two upper levels are denoted $2\gamma_1$ and $2\gamma_2$.

We consider specifically the interaction between the atoms and the photons in a single mode of an optical cavity. As in the two-level case, we assume that the cavity-mode frequency resonates with the peak of the emission or absorption line for the atomic transition between states $|1\rangle$ and $|2\rangle$. The interaction between the atom and the selected cavity mode is expressed in terms of the quantity $\mathscr{G}$ as in the two-level calculation. However, since level $|1\rangle$ is no longer the atomic ground state but has a finite lifetime, γ' in eqn (7.5) must be replaced by the total linewidth parameter $\gamma_1+\gamma_2$ for the transition, and the modified $\mathscr{G}$ for the three-level atom is

$$\mathscr{G} = \frac{e^2\omega_0 D_{12}^2}{3\epsilon_0\hbar V(\gamma_1+\gamma_2)} = \frac{2\pi c^3}{V\omega_0^2}\cdot\frac{\gamma}{\gamma_1+\gamma_2}, \tag{7.48}$$

where γ is again the spontaneous decay rate from level 2 to level 1.

The condition (1.113) for laser action becomes

$$\gamma < \gamma_1, \tag{7.49}$$

and we assume this to be satisfied. Rate equations can be used when γ is much smaller than the total linewidth $\gamma_1+\gamma_2$ of the transition. The photon absorption and emission rates in the presence of n photons in the mode are then as given in eqns (7.6) and (7.7) with $\mathscr{G}$ taken from eqn (7.48). Note that only spontaneous emission into the chosen cavity mode is considered explicitly, the line-broadening effects of emission into the other modes being included in the parameter γ_2.

In a practical laser, the number of photons in the cavity is affected not only by interaction with the atoms but also by several loss mechanisms associated with the cavity itself. The steady extraction of photons from the cavity to form the usable output beam of the laser is one of the sources of loss. The loss of photons is represented in the theory by the introduction of a probability C per unit time that a photon is removed from the cavity mode. Consider a one-dimensional laser cavity of length L whose ends are made of highly-reflecting mirrors. The interval between successive reflections of the light in the cavity is L/c, and at each reflection a fraction $1-\mathscr{R}$ of the beam intensity escapes from the cavity, where $\mathscr{R}$ is the reflection coefficient of the mirrors. The corresponding loss rate is

$$C = c(1-\mathscr{R})/L, \tag{7.50}$$

and the average power output of the laser is $\bar{n}\hbar\omega_0 C$, where $\bar{n}$ is the mean number of photons in the mode. The minimum decay rate (7.50) of the photons in the cavity is augmented by the rates of any other loss processes, excepting those associated with coupling to the atomic transitions between levels 1 and 2.

In order for a substantial number of photons to build up in the cavity mode, it is necessary for the atoms to emit photons at a sufficiently high rate to overcome the cavity loss. When the pumping rate r is just sufficient for the rate of photon production to balance the loss rate C, the laser is said to be at *threshold*. We determine the laser threshold condition that expresses this minimum pumping rate for the build-up of photons in the cavity mode.

Consider a laser below threshold where the number n of photons in the cavity mode is small. The main decay of level 2 is by spontaneous emission at a rate $2\gamma_2$. The mean number of atoms N_2 in state $|2\rangle$ is determined by the interplay of the excitation rate r and the decay rate $2\gamma_2$, and hence

$$N_2 = Nr/2\gamma_2 \qquad \text{(below threshold).} \tag{7.51}$$

This relation is in fact valid even when a fairly large number of photons is excited (see eqn (7.74)). Note that the same result follows from eqn (1.115) if $\bar{W}$ is neglected below threshold and a suitable change of notation is made. The rate at which photons are emitted into the chosen cavity mode is thus

$$N_2\mathscr{G} = Nr\mathscr{G}/2\gamma_2 \qquad \text{(below threshold),} \tag{7.52}$$

where stimulated emission is neglected.

The quantity on the right of eqn (7.52) occurs frequently in the equations of laser theory and it is convenient to define

$$\alpha \equiv Nr\mathscr{G}/2\gamma_2. \tag{7.53}$$

For a given type of atom, all the quantities in the definition of α are fixed except for the pumping rate r and the atomic density. In the theory that follows, we examine the behaviour of the laser as a function of r or, equivalently, α.

Laser oscillation occurs when the spontaneous emission rate (eqn (7.52)) exceeds the photon loss rate, or when α is greater than C, and the laser threshold condition is

$$\alpha = C \qquad \text{(threshold)}. \tag{7.54}$$

The laser is above or below threshold when α is greater or smaller than C, respectively.

The numerical orders of magnitude of the laser parameters are important in suggesting methods of approximation in laser theory. We make no attempt in the remainder of the chapter to produce a theory that is applicable to all types of laser, but instead we assume some particular numerical magnitudes that enable the statistical properties of the laser light to be calculated in a simple approximation.

The numerical values are appropriate to certain types of gas laser that operate in the visible region of the spectrum[10], for example the helium–neon laser. The linewidth parameters are equal to Einstein A coefficients, whose values for hydrogen are shown in Fig. 2.4. We assume the representative values

$$2\gamma_1 \approx 2\gamma_2 \approx 3\times10^{7}\ \mathrm{s}^{-1}. \tag{7.55}$$

The total number of atoms is taken to be

$$N \approx 2\times10^{20} \tag{7.56}$$

in an active volume V of $2\times10^{-5}\ \mathrm{m}^3$. The quantity $\mathscr{G}$ defined in eqn (7.48) is then approximately

$$\mathscr{G} \approx 0{\cdot}5\ \mathrm{s}^{-1}, \tag{7.57}$$

where a visible frequency (eqn (1.65)) has been assumed and the inequality (7.49) has been taken into account.

We assume a cavity length of order 1 m and a mirror reflectivity of 99·5 per cent, leading to a minimum cavity loss rate (7.50) of order

$$C \approx 10^{6}\ \mathrm{s}^{-1}, \tag{7.58}$$

which corresponds to a cavity quality factor ω_0/C of order 3×10^{9}. At threshold, eqns (7.53) and (7.54) show that

$$Nr = 2\gamma_2 C/\mathscr{G} \approx 6\times10^{13}\,\mathrm{s}^{-1} \qquad \text{(threshold)}, \tag{7.59}$$

where eqns (7.55), (7.57), and (7.58) have been used. With the use of eqn (7.56), the threshold pumping rate is

$$r \approx 3\times10^{-7}\ \mathrm{s}^{-1} \qquad \text{(threshold)}. \tag{7.60}$$

Thus for the numerical values assumed here, threshold is achieved by the excitation to the upper state in one second of only about one part in a million of the total number of atoms in the cavity.

7.6. Rate equations for the atoms

The external influence that drives the laser in the model described above is the pumping of atoms into the upper excited state. In a practical laser system the pumping can be achieved by an external light beam or by an electrical discharge. The magnitude of r, or equivalently α, can, in practice, be varied to examine the dependence of the laser characteristics on pumping rate. The two-level atom calculations presented earlier in the chapter assumed that the level populations N_1 and N_2 could be fixed by some external influence. Such an assumption makes the calculations much simpler to carry out, but does not provide a realistic model of a laser, where it is not in practice possible to fix N_1 and N_2.

The theoretical problem presented by the laser is quite complicated, even when the treatment is restricted to the steady state. The probability distribution P_n of the photons in the cavity mode is determined by the equilibrium achieved between their generation by the atomic transitions and their loss from the cavity, described by the damping rate C. The steady-state values of the atomic level populations are themselves determined by the given pumping rate r and by the photon probability distribution. The laser system thus involves the coupled motions of the atoms and photons. The equations of motion are in general very difficult to solve.

The problem is made tractable, however, by the relative magnitudes of the laser parameters assumed above. It is seen from eqns (7.55) and (7.58) that the atomic radiative transition rates are one or two orders of magnitude faster than the rate of loss of photons from the cavity mode. These two rates control the speed of movement of the atomic and photon parts of the laser system, and all the rates that govern the number of photons in the cavity mode are about 10 or 100 times slower than the atomic transition rates.

This feature enables an adiabatic decoupling of the atomic and photon systems to be made. As the photon distribution develops in time, the more rapid atomic system adjusts its level populations to attain equilibrium with the instantaneous photon distribution. It is therefore appropriate to carry out the calculation in two stages. In the first stage we set up rate equations for the atomic populations in the presence of a stationary photon distribution P_n. The steady-state solution of these equations determines the atomic populations for a given P_n. In the second stage we treat the much slower time development of the photon distribution itself, as determined by interaction with the atoms and by the cavity loss rate.

The approximation depends on the relative magnitudes of γ_1, γ_2, and C, and would not be valid if C were comparable to or greater than the γs. It is very similar to the adiabatic approximation in the theory of crystal lattice dynamics.[11] The electrons in a crystal move much more rapidly than the nuclei, and one first solves for the electronic motion, assuming the nuclei to be fixed. The nuclear motion is determined in the second stage of the calculation, where the electronic wavefunctions play a role in determining the effective potential in which the nuclei move.

The rate-equation method used here is a simple technique for determining the laser photon distribution P_n. It is not so general or so rigorous as other techniques[9,12,13] that have been used to find P_n. It is, however, equivalent to some of the more sophisticated calculations for the particular results that it yields, including the detailed form of the photon distribution.[14]

To carry out the first stage of the calculation, we must determine the atomic populations in the presence of a given photon distribution. We work only with the mean numbers of atoms in states 1 and 2 and do not investigate fluctuations in the atomic populations. Let us define R_n^1 to be the probability of simultaneously finding n photons in the cavity mode *and* finding an arbitrary atom in state 1. That is, NR_n^1/P_n is the mean number of atoms in state 1 in the presence of n photons. Since the probability of finding an atom to be in state 1, irrespective of the number of photons present, is N_1/N we have

$$\sum_n R_n^1 = N_1/N. \tag{7.61}$$

If R_n^2 is defined analogously for state 2, we have

$$\sum_n R_n^2 = N_2/N. \tag{7.62}$$

The photon distribution is effectively frozen for the first stage of the calculation and only the atomic parts of the joint probability functions vary with time. It is not possible to factorize the R_n^1 and R_n^2, for example,

$$R_n^1 \neq (N_1/N)P_n \tag{7.63}$$

because the atomic probabilities depend on the number of photons excited and are not fixed as in the two-level atom calculations earlier in the chapter.

Consider the rates of change of R_n^2 and R_{n+1}^1. Fig. 7.6 shows the combined energy levels of the atom–photon system with the transition rates that affect R_n^2 and R_{n+1}^1 indicated. Since the pump generates atoms in state 2 at a rate independent of the number of atoms already in that state and of the photon distribution, its contribution to R_n^2 is a rate of increase rP_n. The remaining rates are all proportional to R_n^2 or R_{n+1}^1, and by inspection of Fig. 7.6 the rate equations are

$$\mathrm{d}R_n^2/\mathrm{d}t = rP_n + R_{n+1}^1\mathscr{G}(n+1) - R_n^2\mathscr{G}(n+1) - 2\gamma_2 R_n^2, \tag{7.64}$$

$$\mathrm{d}R_{n+1}^1/\mathrm{d}t = -R_{n+1}^1\mathscr{G}(n+1) + R_n^2\mathscr{G}(n+1) - 2\gamma_1 R_{n+1}^1. \tag{7.65}$$

These equations are a more detailed version of the rate equations (1.107) and (1.108), which represent the radiation only by a mean energy density $\bar{W}$ and take no account of the photon distribution.

In time spans that are long compared with the atomic decay times of order 10^{-7} to 10^{-8} s, but short compared with the cavity-mode decay time of order 10^{-6} s, the atomic system reaches equilibrium with the comparatively static photon distribution. In this steady state R_n^2 and R_{n+1}^1 are time-independent, and the rates given in eqns (7.64) and (7.65) can be set equal to zero,

$$rP_n + R_{n+1}^1\mathscr{G}(n+1) - R_n^2\mathscr{G}(n+1) - 2\gamma_2 R_n^2 = 0 \tag{7.66}$$

and

$$-R_{n+1}^1\mathscr{G}(n+1) + R_n^2\mathscr{G}(n+1) - 2\gamma_1 R_{n+1}^1 = 0. \tag{7.67}$$

Addition of eqns (7.66) and (7.67) gives

$$rP_n = 2\gamma_2 R_n^2 + 2\gamma_1 R_{n+1}^1. \tag{7.68}$$

With the use of eqns (7.19), (7.61), and (7.62), summation of both sides over n gives

$$rN = 2\gamma_2 N_2 + 2\gamma_1 N_1, \tag{7.69}$$

where we note that R_0^1 is zero for the transition scheme of Fig. 7.6. The result (7.69) expresses the equality of the transition rates into and out of the ground state 3, and is equivalent to eqn (1.112).

The atom-photon probability functions are obtained straightforwardly by solution of eqns (7.66) and (7.67),

$$R_n^2 = \frac{rP_n\{\mathscr{G}(n+1)+2\gamma_1\}}{4\gamma_1\gamma_2 + 2(\gamma_1+\gamma_2)\mathscr{G}(n+1)} \tag{7.70}$$

and

$$R_{n+1}^1 = \frac{rP_n\mathscr{G}(n+1)}{4\gamma_1\gamma_2 + 2(\gamma_1+\gamma_2)\mathscr{G}(n+1)}. \tag{7.71}$$

These are the main results of the first stage of the calculation. Note that the expressions (7.70) and (7.71) have a similar structure to eqns (1.115) and (1.114).

The relative magnitudes of the various terms in eqns (7.70) and (7.71) can be estimated from the parameter values given earlier. Consider the two terms in the denominators. It is convenient to define a new quantity

$$\beta = \frac{2\gamma_1\gamma_2}{(\gamma_1+\gamma_2)\mathscr{G}}. \tag{7.72}$$

From eqns (7.55) and (7.57)

$$\beta \approx 3\times 10^7. \tag{7.73}$$

It is seen from eqns (7.70) and (7.71) that for photon number n much smaller than β, the first term in the denominators is much larger than the second and the second term in the numerator is much larger than the first, giving

$$R_n^2 \approx rP_n/2\gamma_2 \tag{7.74}$$

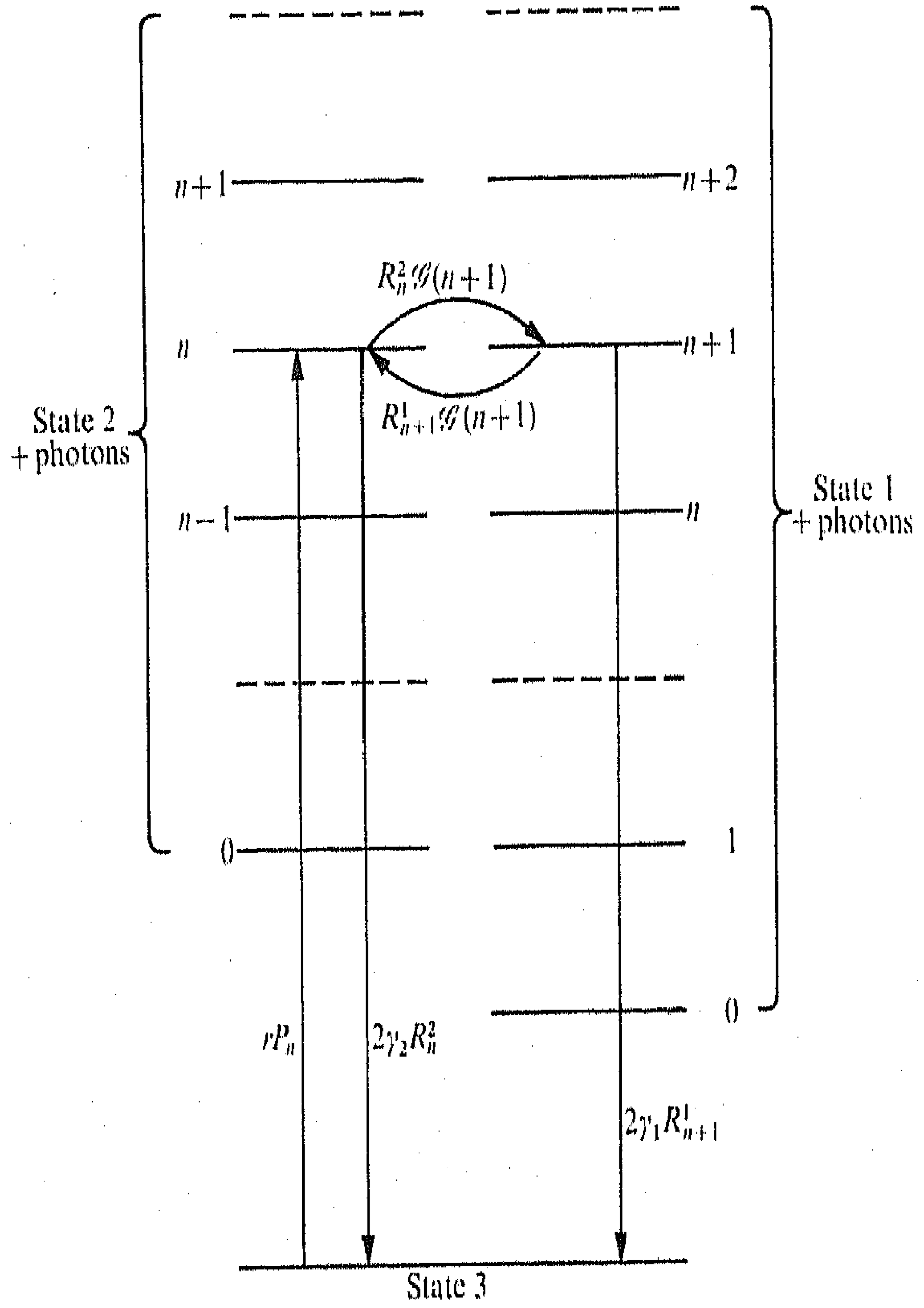

FIG. 7.6. Combined energy levels of a three-level atom and the photons, showing the kinds of transition that influence the probabilities R^2_n and R^1_{n+1}. The corresponding rates of change of the probabilities are shown against the arrows.

and

$$R^1_{n+1} \approx rP_n\mathcal{G}(n+1)/4\gamma_1\gamma_2 \approx R^2_n\mathcal{G}(n+1)/2\gamma_1 \qquad (n \ll \beta). \qquad (7.75)$$

The atomic population in state 2 is much larger than in state 1. Summation of both sides of eqn (7.74) over n shows that N_2 is approximately equal to $Nr/2\gamma_2$, the expression derived in eqn (7.51) by more qualitative arguments.

On the other hand, for a photon number n much larger than β, the terms $\mathcal{G}(n+1)$ dominate in eqns (7.70) and (7.71), to give

$$R^2_n \approx R^1_{n+1} \approx rP_n/2(\gamma_1+\gamma_2) \qquad (n \gg \beta). \qquad (7.76)$$

The atomic populations in the two excited states are now almost identical and equal to $Nr/2(\gamma_1+\gamma_2)$. This is the saturation effect described in Chapter 1, which will be shown to be important in determining the statistical properties of the laser photons.

7.7. Rate equations for the laser photons

In the second stage of the laser calculation, we now treat the influence of the atomic transitions on the state of the photons in the cavity mode. Consider the effect on the photon number of the transitions shown in Fig. 7.6. Only the two horizontal transitions directly affect P_n, to produce a rate of increase $R^1_{n+1}\mathcal{G}(n+1)$ and a rate of decrease $R^2_n\mathcal{G}(n+1)$ for each of the N atoms in the cavity. Since according to eqns (7.70) and (7.71)

$$R^2_n > R^1_{n+1}, \qquad (7.77)$$

the net effect of the two types of transition is a negative contribution

$$(\mathrm{d}P_n/\mathrm{d}t)_{n,n+1} = N(R^1_{n+1}-R^2_n)\mathcal{G}(n+1). \qquad (7.78)$$

The photon probability P_n is also influenced by the horizontal transitions between the next lower pair of levels in Fig. 7.6. By analogy with the above

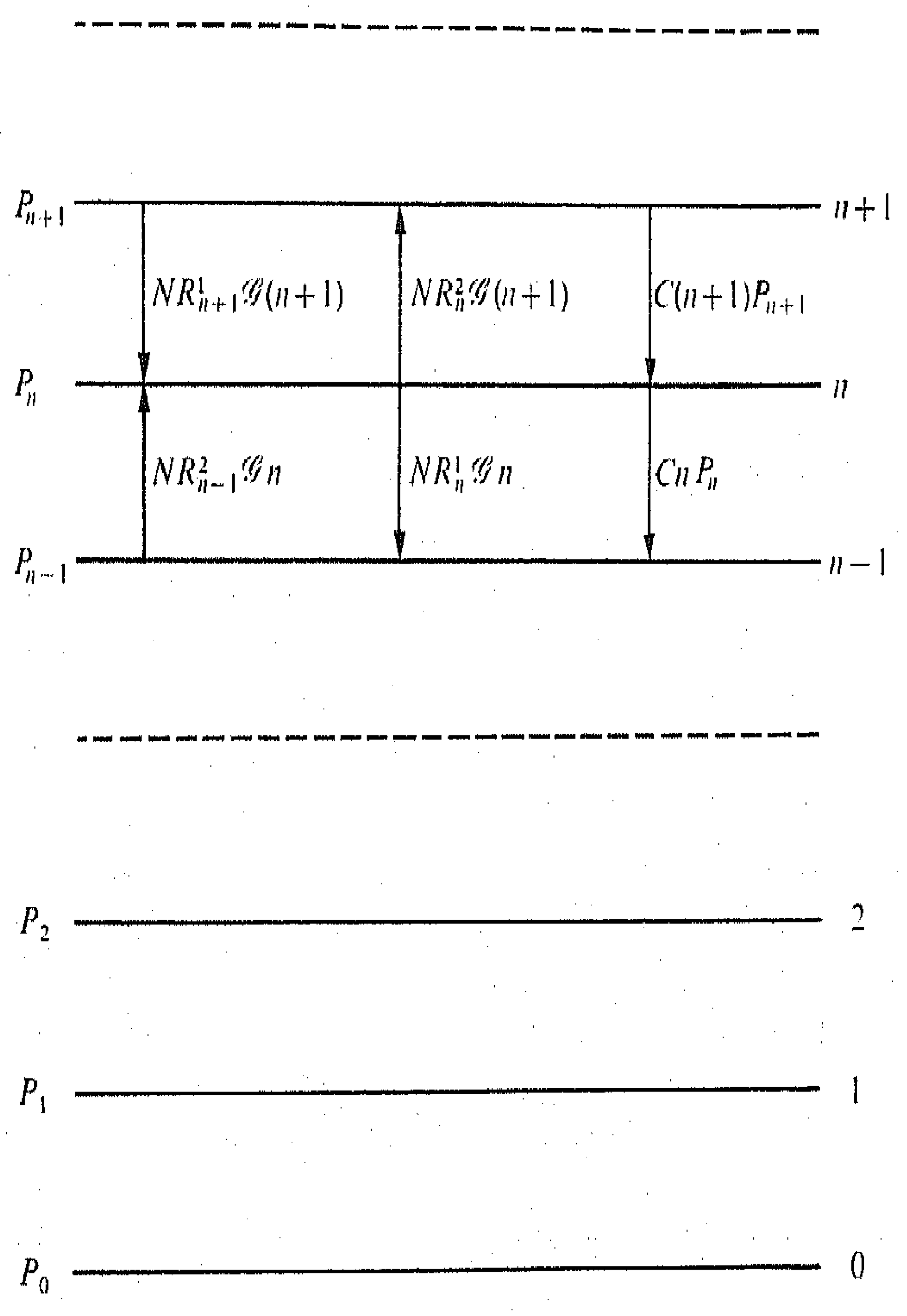

FIG. 7.7. Photon energy-level diagram showing the rates of growth and decay of P_n produced by the atomic transitions and the cavity loss process.

result, such transitions produce a positive contribution

$$(\mathrm{d}P_n/\mathrm{d}t)_{n,n-1} = N(R^2_{n-1} - R^1_n)\mathscr{G}n. \tag{7.79}$$

The four types of atomic transition that influence P_n have their contributions entered on the photon energy-level diagram in Fig. 7.7. The diagram is similar to Fig. 7.1, but the transition rates are now given by the more general expressions that allow for the role played by the photon distribution in determining the atomic excitation levels.

The generation of photons by the atomic transitions is opposed by the loss rate C. The loss of photons produces descending transitions only in Fig. 7.7, and two such transitions affect the nth photon energy level, to give a rate of change

$$(\mathrm{d}P_n/\mathrm{d}t)_{\text{loss}} = -CnP_n + C(n+1)P_{n+1}. \tag{7.80}$$

The total rate of change of P_n is given by the sum of eqns (7.78), (7.79), and (7.80). With the joint probabilities taken from eqns (7.70) and (7.71), and use of the quantities α and β defined in eqns (7.53) and (7.72), the result is

$$\frac{\mathrm{d}P_n}{\mathrm{d}t} = -\frac{\alpha\beta P_n(n+1)}{\beta+n+1} + \frac{\alpha\beta P_{n-1}n}{\beta+n} - CnP_n + C(n+1)P_{n+1}. \tag{7.81}$$

It is seen that the dynamical properties of the photon distribution are governed by the three parameters α, β, and C. The same equation (7.81) for the photon distribution is obtained by more rigorous calculations[15] that use density-operator techniques.

The set of coupled equations for the P_n is difficult to solve. Even the moments of the photon distribution are difficult to evaluate as functions of time, unlike the corresponding calculation based on the somewhat similar eqn (7.15) for the two-level atom. The occurrence of n in the denominators of the first two terms on the right of eqn (7.81) prevents the formation of simple equations of motion for the moments. The time development of the laser photon distribution has been investigated[16] by numerical computer integration of eqn (7.81) but we do not consider such calculations here.

It is, however, easily possible to obtain the steady-state photon distribution, for which the rate of change shown in eqn (7.81) is set equal to zero. As in the steady-state solution of eqn (7.15), the net rate of transition between any pair of photon energy levels must be zero, and for the levels n and $n-1$ in Fig. 7.7 we have

$$NR^2_{n-1}\mathscr{G}n - NR^1_n\mathscr{G}n - CnP_n = 0. \tag{7.82}$$

With the use of eqns (7.53), (7.70), (7.71), and (7.72), this can be written

$$P_n = \frac{\alpha\beta/C}{\beta+n}P_{n-1}. \tag{7.83}$$

The value of P_n is expressed in terms of P_0 by iteration

$$\begin{aligned} P_n &= \frac{(\alpha\beta/C)^n P_0}{(\beta+n)(\beta+n-1)\dots(\beta+2)(\beta+1)} \\ &= \frac{(\alpha\beta/C)^n \beta!\, P_0}{(\beta+n)!}. \end{aligned} \tag{7.84}$$

The photon distribution P_n is therefore determined apart from P_0, the probability of finding no photons in the cavity mode. The remaining unknown is determined by the normalization condition (7.19),

$$\sum_n P_n = P_0\sum_n \frac{(\alpha\beta/C)^n\beta!}{(\beta+n)!} = 1. \tag{7.85}$$

The n summation can be expressed in terms of a standard confluent hypergeometric function, defined by the usual power-series expansion[17]

$${}_1F_1(a,b;\,x) = \sum_n \frac{(a+n-1)!(b-1)!}{(b+n-1)!(a-1)!}\frac{x^n}{n!}. \tag{7.86}$$

Comparison of eqns (7.85) and (7.86) shows that the former equation can be written

$${}_1F_1(1, 1+\beta;\,\alpha\beta/C)P_0 = 1. \tag{7.87}$$

The complete solution for the photon distribution[18] from eqn (7.84) is thus

$$P_n = \frac{(\alpha\beta/C)^n\beta!}{(\beta+n)!\,{}_1F_1(1,1+\beta;\,\alpha\beta/C)}. \tag{7.88}$$

7.8. The laser photon distribution

The most important characteristic of the laser to be obtained from the above theory is the mean number of photons generated for a given pumping rate. The pumping rate is proportional to α, and it is seen from eqn (7.88) that P_n depends on α only in the combination α/C. The photon distribution can thus be investigated as a function of α/C for given β. With the help of eqn (7.84), the mean photon number is

$$\begin{aligned} \bar{n} = \sum_n nP_n &= \sum_{n=0}^{\infty} \frac{n(\alpha\beta/C)^n\beta!\,P_0}{(\beta+n)!} \\ &= \sum_{n=1}^{\infty}(\beta+n-\beta)\frac{(\alpha\beta/C)^n\beta!\,P_0}{(\beta+n)!} \\ &= (\alpha\beta/C) - \beta(1-P_0), \end{aligned} \tag{7.89}$$

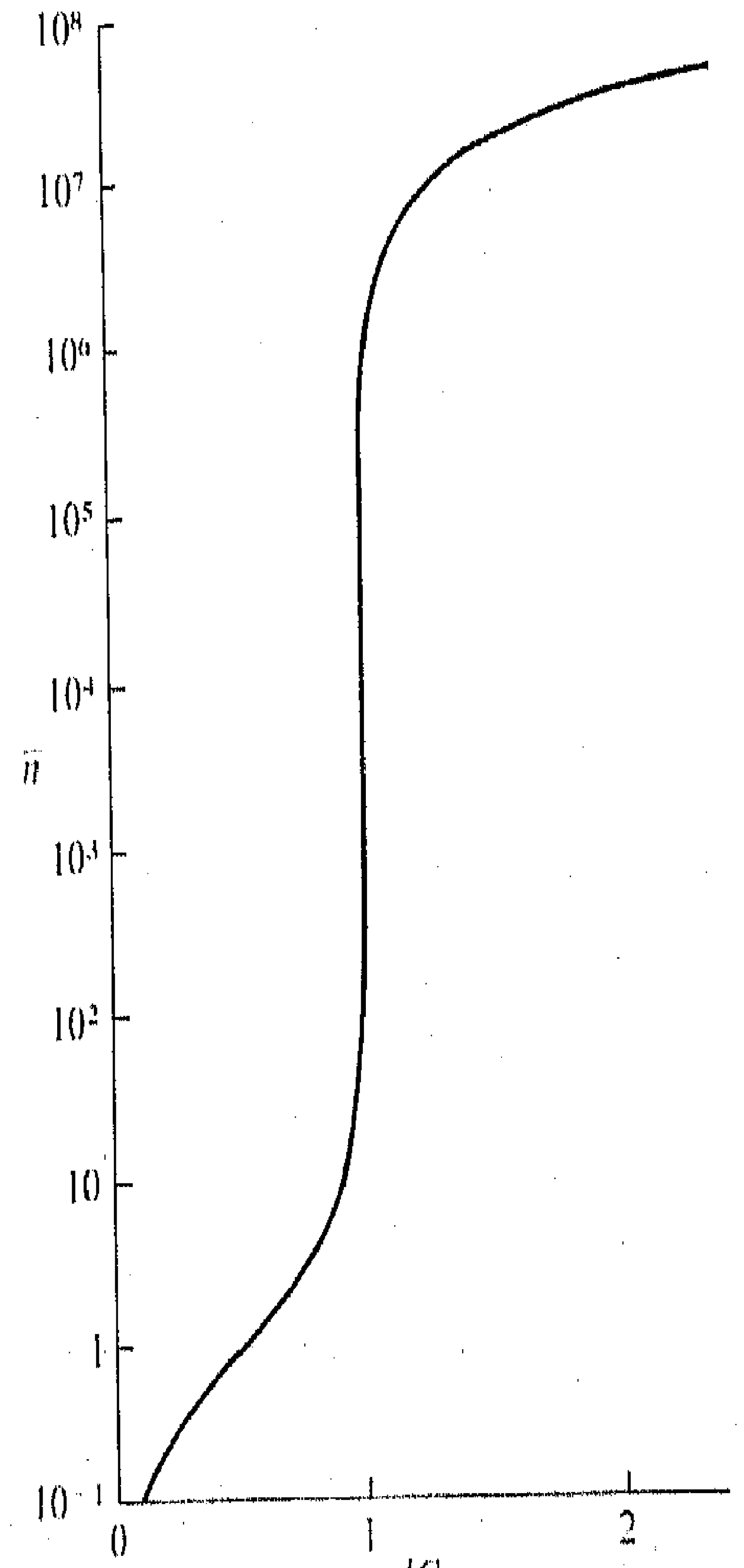

FIG. 7.8. Mean number $\bar{n}$ of photons in a single-mode laser as a function of the pumping rate, proportional to α/C, for $\beta = 3\times10^7$.

where the normalization condition has been used, and P_0 is determined by eqn (7.87). These results are not very explicit because of the presence of P_0 expressed as a confluent hypergeometric function. However, it is possible to cast this function into simpler forms, and we consider in turn the regions below and above threshold.

The analysis that follows is anticipated in Fig. 7.8 which shows the mean photon number $\bar{n}$ as a function of α/C for the value of β given in eqn (7.73). Note the extremely sharp rise in $\bar{n}$ at the laser threshold $\alpha/C = 1$, followed by a slower increase for higher rates of pumping.

(1) *Laser below threshold*, $\alpha/C < 1$. The simplifications that can be made in the expression for the laser photon distribution depend on approximations to the confluent hypergeometric function which are valid for the different ranges of α/C. The parameter β is a very large number and it is appropriate to expand the confluent hypergeometric function in inverse powers of β. The expansions are standard[17] and we do not give any details of their mathematical justification.

Below threshold, the second argument of ${}_1F_1$ is larger than the third, and the appropriate expansion is

$${}_1F_1(1,1+\beta;\,\alpha\beta/C) = \frac{1}{1-(\alpha/C)}\left[1-\frac{\alpha/C}{\beta\{1-(\alpha/C)\}^2}+O(\beta^{-2})\right]. \qquad (7.90)$$

If terms of order β^{-2} are ignored, substitution in eqn (7.87) gives

$$P_0 = \left(1-\frac{\alpha}{C}\right)+\frac{\alpha/C}{\beta\{1-(\alpha/C)\}}, \qquad (7.91)$$

and the mean number of photons from eqn (7.89) is

$$\bar{n} = \frac{\alpha/C}{1-(\alpha/C)} \qquad (\alpha/C < 1). \qquad (7.92)$$

Except when α/C is very close to unity, the number of photons in the cavity mode is always small compared to β, and we make the approximation

$$(\beta+n)! = \beta!\,\beta^n \qquad (\beta \gg n). \qquad (7.93)$$

With this result and with P_0 approximated by the first term in eqn (7.91), the photon distribution of eqn (7.84) becomes

$$P_n = \left(\frac{\alpha}{C}\right)^n\left(1-\frac{\alpha}{C}\right) = \frac{\bar{n}^n}{(1+\bar{n})^{1+n}} \qquad (\alpha/C < 1), \qquad (7.94)$$

where $\bar{n}$ is given by eqn (7.92). The photon distribution is identical to eqn (7.9), and the light is therefore chaotic below threshold. Fig. 7.9(a) shows a plot of eqn (7.94) for the case $\alpha/C = \frac{1}{2}$.

(2) *Laser above threshold*, $\alpha/C > 1$. The third argument in the confluent hypergeometric function is now larger than the second, and the appropriate expansion in powers of β^{-1} is[17]

$${}_1F_1(1,1+\beta;\,\alpha\beta/C) = \beta!\,\exp(\alpha\beta/C)(\alpha\beta/C)^{-\beta}\{1+O(C/\alpha\beta)\}. \qquad (7.95)$$

This number is much larger than unity, and P_0 is accordingly negligible. The mean number of photons from eqn (7.89) is therefore

$$\bar{n} = \beta\{(\alpha/C)-1\} \qquad (\alpha/C > 1). \qquad (7.96)$$

This result does not hold very close to threshold.

If only the leading term in eqn (7.95) is retained, the photon distribution shown in eqn (7.88) becomes

$$\begin{aligned} P_n &= \frac{(\alpha\beta/C)^{\beta+n}\exp(-\alpha\beta/C)}{(\beta+n)!} \\ &= \frac{(\beta+\bar{n})^{\beta+n}\exp(-\beta-\bar{n})}{(\beta+n)!} \qquad (\alpha/C > 1), \qquad (7.97) \end{aligned}$$

where eqn (7.96) has been used.

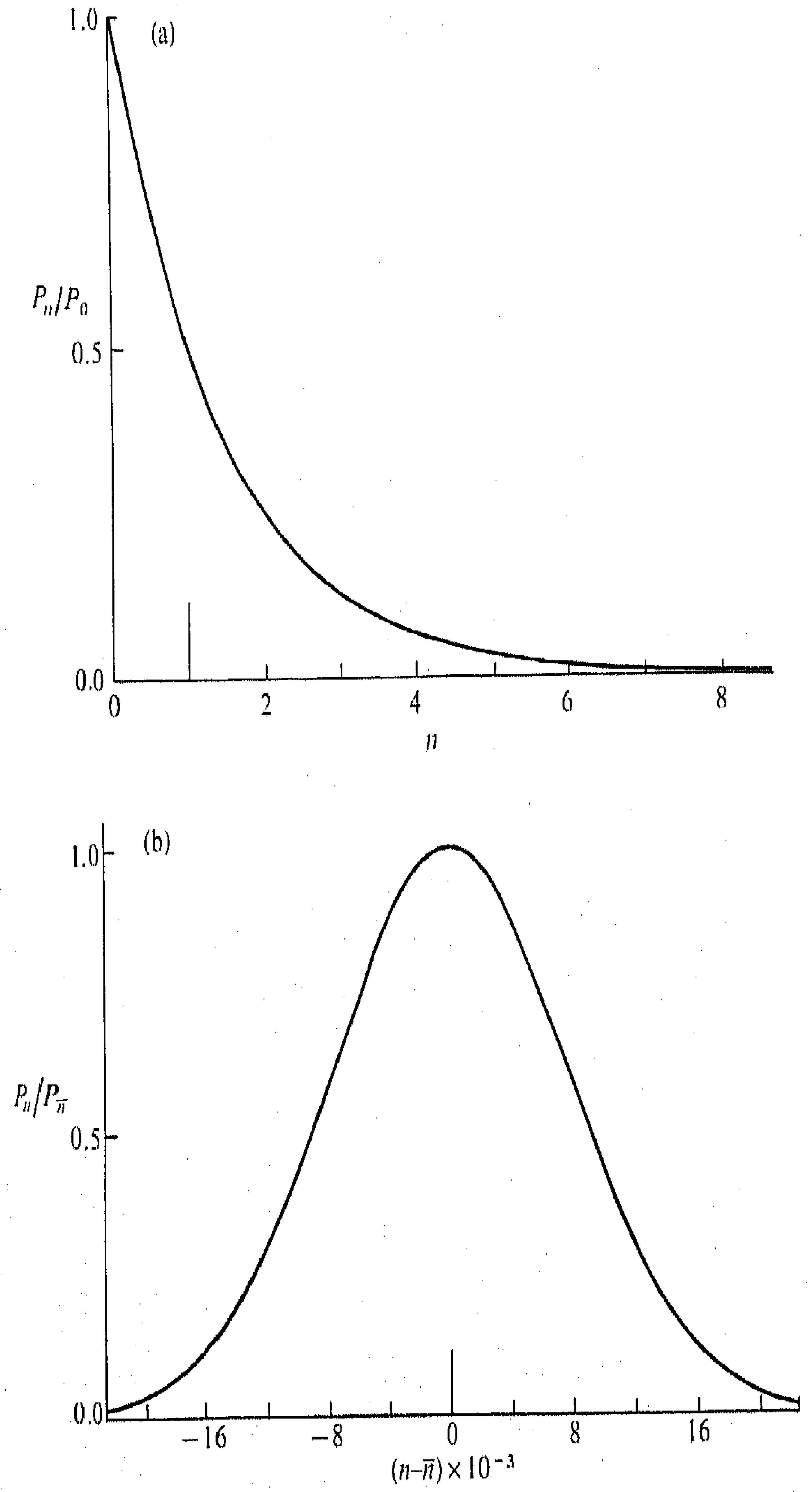

FIG. 7.9. The photon distributions P_n for a laser respectively below and above threshold. The distributions are drawn as continuous curves although P_n is strictly defined only for integer n. The vertical markers indicate the mean photon numbers $\bar{n}$. With $\beta = 3\times 10^7$, the numerical data are

(a) $\alpha/C = \frac{1}{2}, \bar{n} = 1, P_0 = 0{\cdot}5$

(b) $\alpha/C = 2, \bar{n} = 3\times 10^7, P_{\bar{n}} = 5{\cdot}3\times 10^{-5}$.

The properties of the photon distribution above threshold depend on the relative magnitudes of β and $\bar{n}$. We note from eqn (7.96) that

$$\bar{n} = \beta \quad \text{for} \quad \alpha/C = 2. \tag{7.98}$$

Values of $\bar{n}$ greater than β correspond to pumping rates where the active atomic excited states approach saturation, as mentioned in the discussion of eqn (7.76). For $\bar{n}$ very much larger than β, P_n reduces approximately to

$$P_n = \frac{\bar{n}^n \exp(-\bar{n})}{n!} \qquad (\alpha/C \gg 2). \tag{7.99}$$

This is the same as the photon distribution (eqn (7.8)) for coherent light. It is seen that the laser must be operated at a pumping rate well above twice the threshold value before the output becomes coherent. The form of the photon distribution for $\alpha/C = 2$ is illustrated in Fig. 7.9(b).

There is clearly a range of values of α/C close to unity in which the approximations given in (1) and (2) above are invalid. However, it can be shown that this threshold region extends only over values of α/C that differ from unity by a few times $\beta^{-\frac{1}{2}}$. The threshold region is therefore so small as to be invisible on the scale of Fig. 7.8 and we do not consider the nature of the photon distribution there.

The graph of $\bar{n}$ as a function of α/C in Fig. 7.8 is constructed by using the approximations given in eqns (7.92) and (7.96) below and above threshold. The rapid increase in photon number by about five orders of magnitude in the threshold region is the most striking feature of the figure.

The coherent photon distribution in a laser operating well above threshold arises in the theory because of the presence, in the first two terms of eqn (7.81), of denominators that vary linearly with the photon number n. If the factors n and $n+1$ are neglected in the two denominators, the chaotic photon distribution (eqn (7.94)) is obtained for all values of α/C. The denominators in eqn (7.81) result in turn from the denominators in the atomic probability functions R_n^2 and R_{n+1}^1 given by eqns (7.70) and (7.71). It has been pointed out above that the role of these denominators is to allow for saturation of the two atomic level populations at the value $Nr/2(\gamma_1+\gamma_2)$. The presence of atomic saturation is thus an essential factor in determining the laser photon distribution, and particularly in producing the approach to a coherent beam of light at high pumping rates.

The photon distributions derived above are investigated most directly by means of photon-counting experiments of the kind described in Chapter 6. As has been pointed out, the photon-count distribution differs from the photon distribution even for single-mode light, and the former is obtained for laser light by substitution of eqn (7.88) into eqn (6.85) or eqn (6.89). The results of photon-counting experiments[19–21] are in very good agreement with the theory. The transition between the two kinds of distribution shown in Fig. 7.9 at the laser threshold has been particularly carefully studied.

Problem 7.3. Prove that the degree of second-order coherence of the laser beam described above is

$$g^{(2)}(0) = 2 \tag{7.100}$$

below threshold, and

$$g^{(2)}(0) = 1+(\beta/\bar{n}^2) \tag{7.101}$$

above threshold. These results are again invalid in the very narrow threshold region. The second term on the right of eqn (7.101) represents fluctuations additional to those of coherent light, but their importance diminishes rapidly above threshold.

Problem 7.4. Prove that the laser photon-count distribution is related to the photon distribution by[22]

$$P_m(T) = P_m\{1-\exp(-\xi)\}^m {}_1F_1(m+1, m+1+\beta; \alpha\beta \exp(-\xi)/C), \tag{7.102}$$

where P_m is given by eqn (7.88) and ξ by eqn (6.81).

7.9. Fluctuations in laser light

The light emitted by a laser operated below threshold has the chaotic character discussed in detail in earlier parts of the book. The probability distribution for the electric field amplitude of the light beam in the classical picture is illustrated in Fig. 3.10. The most probable amplitude is zero, and the probability has a Gaussian dependence on the amplitude. The corresponding exponential probability distribution for the beam intensity is given in eqn (3.68). In photon terms, the equivalent behaviour is the exponential fall-off of P_n as a function of the photon number n shown in Fig. 7.9(a). The coherence properties of the light are the same as derived earlier in the present chapter for the steady state of a cavity mode in interaction with two-level atoms.

Now consider a laser operated above threshold, where the photon probability distribution is given by eqn (7.97). For the parameters chosen in Fig. 7.9(b), the distribution is peaked at a large mean photon number $\bar{n}$, and the width of the distribution is about three orders of magnitude smaller than $\bar{n}$. The mean photon number is thus quite sharply defined, with only small fluctuations about the mean. These features of the photon distribution can be represented in a qualitative picture of the probability distribution for the electric field in the laser beam, similar to the analogous distribution for chaotic light in Fig. 3.10. For a beam that contains $\bar{n}$ photons of frequency ω_0, the electric field amplitude obtained from eqns (5.84) and (5.85) is

$$E = \langle \hat{E}^- \hat{E}^+ \rangle^{\frac{1}{2}} = (\hbar\omega_0/2\epsilon_0 V)^{\frac{1}{2}} \bar{n}^{\frac{1}{2}}. \tag{7.103}$$

The root-mean-square spread in photon number given by eqn (7.101) with the use of eqn (6.28) is

$$\Delta n = (\overline{n^2} - \bar{n}^2)^{\frac{1}{2}} = (\bar{n}+\beta)^{\frac{1}{2}}. \tag{7.104}$$

The spread in total field amplitude well above threshold ($\bar{n} \gg \beta$) is of order

$$\Delta E \approx (\hbar\omega_0/2\epsilon_0 V)^{\frac{1}{2}}, \tag{7.105}$$

in agreement with eqn (4.208). All values of the phase ϕ of the electric field are equally probable, as in the field distribution for chaotic light. The field distribution for a laser above threshold thus has the qualitative form shown in Fig. 7.10.

The basic differences between the field distributions for chaotic and laser light, Figs. 3.10 and 7.10, arise from the predominance of coherence-conserving stimulated-emission processes in the generation of laser light. It has been shown in §7.4 that coherent light has its coherence maintained by photons that are produced by stimulated emission, but not by photons produced by spontaneous emission. The same state of affairs applies to a good approximation for laser light, with some slight differences due to the departure of the laser photon distribution shown in eqn (7.97) from the perfectly coherent form. Thus, at any instant of time, the photons that contribute to the laser field are mainly coherent in their phase. The common phase is maintained by the new stimulated photons, which dominate the new spontaneous photons in the ratio $\bar{n}$:1. The mean number of photons of course remains constant at $\bar{n}$ due to the steady loss of photons from the laser cavity.

The effect of spontaneous emission on the field can be represented graphically on the Argand diagram in Fig. 7.10. Suppose that the electric field at some instant is as indicated by the large arrow. If a spontaneous photon is now produced, its addition to the field is represented by a small vector of length $(\hbar\omega_0/2\epsilon_0 V)^{\frac{1}{2}}$ oriented in a random direction. The repeated emission of spontaneous photons causes the point of the large arrow in Fig. 7.10 to move across the shaded area in accordance with the calculated probability distribution.

The spontaneous emission fluctuations can be resolved into two components, (a) amplitude fluctuations, which change the length of the field vector but not the angle ϕ, and (b) phase fluctuations, which change the phase angle ϕ but leave the length of the field vector unchanged. The amplitude fluctuations alone cause a relatively small random modulation of the field amplitude about its mean value E. The phase fluctuations produce a more drastic effect on the field vector, causing the phase angle ϕ to sample all values between 0 and 2π. The ensemble average of the real electric field amplitude $E\cos\phi$ is therefore equal to zero, and with the usual ergodic assumption, the time-averaged field for a single laser is also zero.

The theory of the laser photon distribution given in the previous section determines only the diagonal matrix elements P_n of the photon density operator, whereas the quantum-mechanical electric-field expectation value (4.233) is proportional to the off-diagonal matrix elements. However, the above argument leads one to expect that the off-diagonal elements vanish, and

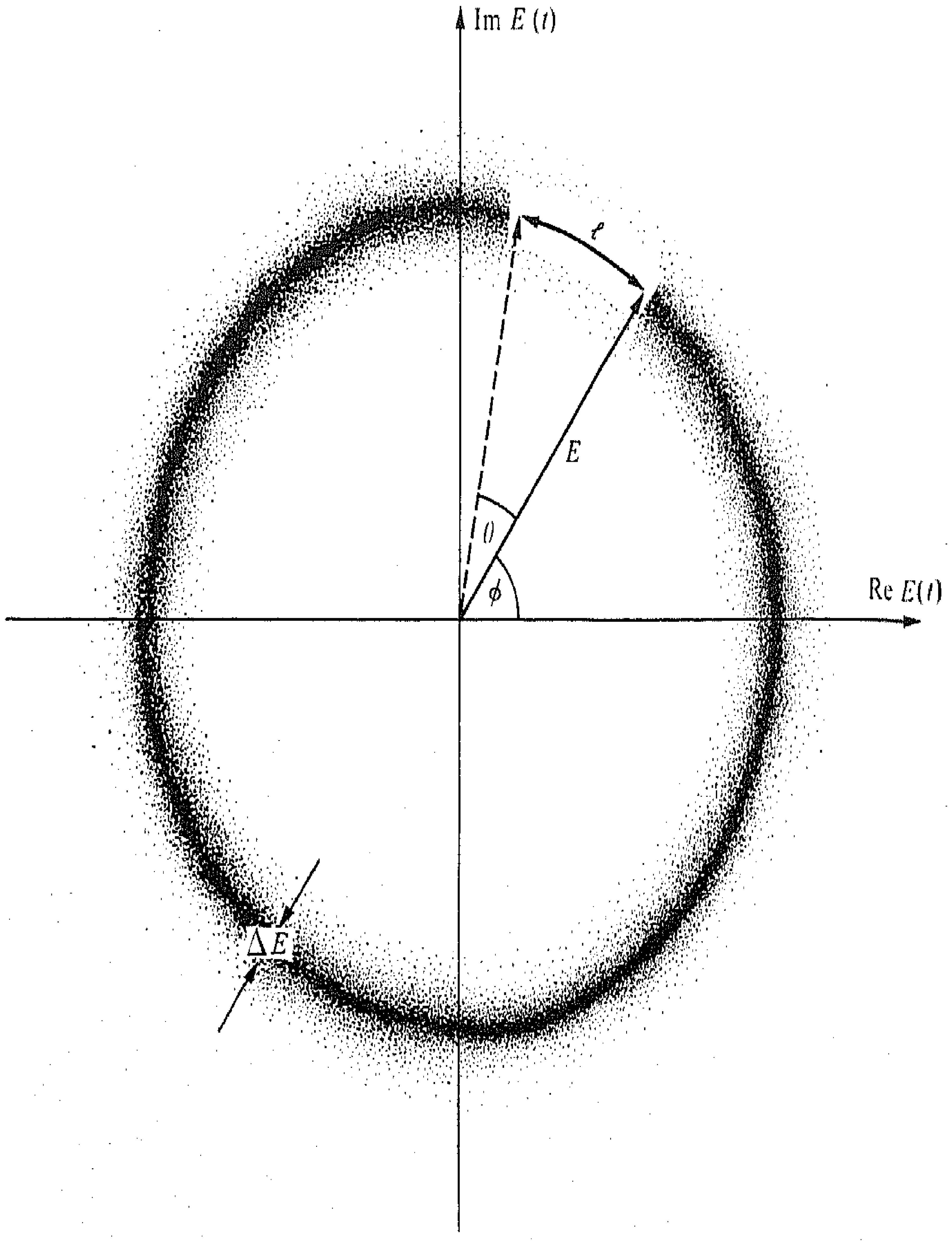

FIG. 7.10. Probability distribution for the amplitude and phase of the electric field in the light beam of a laser operating above threshold. The magnitude of the probability is proportional to the density of shading. The amplitude E and spread ΔE of the distribution are defined by eqns (7.103) and (7.105). The relative spread $\Delta E/E$, of order $\bar{n}^{-\frac{1}{2}}$, is greatly exaggerated for ease of drawing.

this is substantiated by more rigorous calculations.[9] By contrast, the coherent-state density operator has non-zero off-diagonal matrix elements given by eqn (4.234). The laser photon distribution P_n approaches that of coherent light at high pumping rates, but the off-diagonal matrix elements of the density operator are quite different.

Despite these basic differences between laser light and coherent light, the properties of the two types of light beam are often almost indistinguishable. What makes the output beam of the laser very similar to a coherent photon state is the very slow rate at which the phase of the electric field of the laser beam drifts away from its value at some instant of time. We show below that

the characteristic decay time for the phase is of order 100 s or longer. Thus for quite long periods of time, the laser beam has a steady phase and its electric-field variation is similar to that of coherent light.

The rate of change of the phase angle ϕ of the electric field owing to spontaneous emission can be determined by a simple calculation based on the pictorial representation of Fig. 7.10. The rate at which photons escape from the cavity is $\bar{n}C$, and in the steady state this must equal the rate of production of photons by the atoms. Since the ratio of stimulated to spontaneous emission must be $\bar{n}:1$, the rate of photon production can be divided into its spontaneous and stimulated contributions as

$$\bar{n}C = \left(\frac{1}{1+\bar{n}}+\frac{\bar{n}}{1+\bar{n}}\right)\bar{n}C. \tag{7.106}$$

The rate of spontaneous emission of photons is therefore

$$\frac{\bar{n}C}{1+\bar{n}} \approx C \qquad \text{for} \qquad \bar{n} \gg 1. \tag{7.107}$$

The spontaneous contribution is independent of $\bar{n}$ and its relative importance diminishes with increasing $\bar{n}$.

Consider the effect on the field vector E in Fig. 7.10 of the spontaneous emission. The change θ in the phase angle ϕ that occurs after a time duration τ can be related to the distance ℓ through which the point of the field vector is moved,

$$E\theta = \ell, \tag{7.108}$$

where E is given by eqn (7.103). Since the contribution of each spontaneous photon is a small vector of length $(\hbar\omega_0/2\epsilon_0 V)^{\frac{1}{2}}$ oriented in random direction, the mean-square contribution to the distance ℓ is

$$\overline{\ell^2} = \tfrac{1}{2}(\hbar\omega_0/2\epsilon_0 V). \tag{7.109}$$

The mean change in phase angle owing to a single spontaneous photon can be obtained from eqns (7.108) and (7.109); the change in ϕ has equal probability of being positive or negative.

We require the change in phase angle produced by the $C\tau$ spontaneous emissions that occur in a time τ. The calculation is equivalent to that of a random walk by the point of the field vector around a circle of radius E. According to standard one-dimensional random-walk theory,[23] the normalized probability that a distance ℓ is travelled after $C\tau$ steps of mean-square length $\overline{\ell^2}$ is

$$p(\ell) = (2\pi\overline{\ell^2}C\tau)^{-\frac{1}{2}}\exp(-\ell^2/2\overline{\ell^2}C\tau). \tag{7.110}$$

By means of eqns (7.103), (7.108), and (7.109), this probability distribution for ℓ

can be transformed into an equivalent distribution for the change θ in phase angle after a time τ,

$$p(\theta) = (\bar{n}/\pi C\tau)^{\frac{1}{2}} \exp(-\theta^2\bar{n}/C\tau). \tag{7.111}$$

The probability distribution for the phase angle satisfies a one-dimensional diffusion equation

$$\partial p/\partial\tau = \mathscr{D}(\partial^2 p/\partial\theta^2), \tag{7.112}$$

where the diffusion constant $\mathscr{D}$ must be

$$\mathscr{D} = C/4\bar{n} \tag{7.113}$$

in order for $p(\theta)$ in eqn (7.111) to be a solution. The phase angle thus diffuses away from its initial value at a rate inversely proportional to the mean number of laser photons.

The effect of phase diffusion on the electric field can best be displayed by evaluation of the average projection of the field at time τ on to the field at time zero,

$$\langle\hat{E}^-(0)\hat{E}^+(\tau)\rangle = E^2 \exp(-\mathrm{i}\omega_0\tau)\langle\cos\theta\rangle, \tag{7.114}$$

where the angle brackets denote averages over the phase distribution. The theory given here represents the electric fields by classical variables, but the quantum-mechanical notation is used on the left of eqn (7.114) because the same results are obtained by a more rigorous calculation[9] that solves the equation of motion for the photon density operator. With the use of a standard integral,[24] we find

$$\langle\cos\theta\rangle = \int_{-\infty}^{\infty} p(\theta)\cos\theta\, \mathrm{d}\theta = \exp(-C\tau/4\bar{n}). \tag{7.115}$$

If the phase diffusion time τ_p is defined by

$$1/\tau_\mathrm{p} = C/2\bar{n}, \tag{7.116}$$

then eqn (7.114) can be written

$$\langle\hat{E}^-(0)\hat{E}^+(\tau)\rangle = E^2 \exp\{-\mathrm{i}\omega_0\tau-(\tau/2\tau_\mathrm{p})\}. \tag{7.117}$$

Note the similarity of the phase-diffusion rate (7.116) to the phase decay rate (7.26) for light interacting with two-level atoms whose populations are not inverted; both are equal to a spontaneous emission rate divided by a mean photon number.

The most striking feature of τ_p is its large magnitude; with C taken from eqn (7.58) and a mean photon number $\bar{n}$ equal to β given by eqn (7.73), the phase diffusion time is 60 s. Times larger than this are readily accessible at higher $\bar{n}$, corresponding to faster pumping rates. The phase diffusion rate is therefore about seven orders of magnitude slower than the cavity loss rate C, which in turn is slow compared to the atomic radiative transition rates. The phase of the laser beam is almost constant over times shorter than τ_p, and for such periods the beam has an electric-field variation similar to that of a classical stable wave. Experimentally, the period of stability of the laser beam is several orders of magnitude shorter than τ_p owing to effects not considered here, for example, mechanical vibrations of the cavity. However, the theoretical limitation on the beam stability is determined by the phase diffusion time.

The correlation function (7.117) is very similar to that obtained for collision-broadened chaotic light, given by eqn (3.20). The frequency distribution of the light, obtained by Fourier transformation in the usual way, has a Lorentzian lineshape centred on ω_0, similar to eqns (2.112) or (3.22). The linewidth, equal to $1/\tau_\mathrm{p}$ given by eqn (7.116), is exceedingly small for a laser operating well above threshold, but in practice the mechanical stability of the system limits the order of obtainable linewidths to 10^5 Hz or more. The minimum linewidth (7.116) is essentially set by the uncertainty principle.[25] This expression for the width is one way of writing a more general result known as the Schawlow–Townes formula;[26] its most important feature is the inverse dependence on the laser power output.

The similarity of the first-order correlation function of the phase-diffusing laser beam above threshold to that of chaotic light does not extend to higher-order correlations. Thus for example, the overall phase of the beam cancels when the fields are squared to form intensity correlation functions, and the phase fluctuations make no additional contribution to the degree of second-order coherence given by eqn (7.101). This contrasts with the situation below threshold where the theory of §7.2 applies, and the degree of second-order coherence (7.25) has the usual chaotic relationship of eqn (3.90) to the degree of first-order coherence.

The laser threshold has close analogies with a second-order phase transition, for example the ferromagnetic phase transition in a magnetic crystal.[9] In the latter case, the magnetic moments of paramagnetic ions in the crystal align parallel to each other as the temperature is lowered through the Curie temperature. For an isotropic Heisenberg ferromagnet, the direction in which the magnetic moments align is not determined by the Hamiltonian of the system, and all directions are equally likely. However, despite the equivalences of different directions, the state of the crystal in which the total magnetization points a certain way diffuses only very slowly into a state in which the magnetization points in a different direction. Indeed, in a real ferromagnetic crystal there is always some surface or volume inhomogeneity which pins the magnetization in a direction that is effectively fixed.

The electric field in the laser beam has a property similar to the magnetization in a ferromagnet, of diffusing only very slowly from a given phase angle, even though all phases are equally likely in principle. In the phase-transition analogy, the laser pumping rate plays the role of temperature, and the threshold pumping rate is the analogue of the transition temperature.

7.10. Multimode emission by a driven atom

All of the analysis carried out so far in the present chapter applies to single-mode light interacting with large numbers of two- or three-level atoms. It is of course common practice to construct single-mode laser systems and such light sources are used in experiments where it is advantageous to employ light of the highest coherence and spectral purity. However, the excited atoms in light sources often radiate freely into all modes of some optical cavity. We conclude the chapter by considering the multimode emission by a single driven atom in a fairly general way. The topic is continued in the following chapter, which treats the specific problem of resonance fluorescence, that is, reradiation by atoms excited by light whose frequency ω lies close to the atomic transition frequency ω_0.

The electric field operators obtained by integration over all modes of the radiation from a two-level atom at position $\mathbf{R}$ are given by eqn (5.191) and the conjugate expression. We consider only field measurements for polarization in the x-direction so that the field operators can be treated as scalars. The degrees of first and second-order coherence defined in eqns (6.14) and (6.23) can then be expressed in the forms

$$g^{(1)}(\tau) = \frac{\langle \hat{E}^-(\mathbf{r}t)\hat{E}^+(\mathbf{r}t+\tau)\rangle}{\langle \hat{E}^-(\mathbf{r}t)\hat{E}^+(\mathbf{r}t)\rangle} = \frac{\langle \hat{\pi}^\dagger(t)\hat{\pi}(t+\tau)\rangle}{\langle \hat{\pi}^\dagger(t)\hat{\pi}(t)\rangle} \tag{7.118}$$

and

$$g^{(2)}(\tau) = \frac{\langle \hat{E}^-(\mathbf{r}t)\hat{E}^-(\mathbf{r}t+\tau)\hat{E}^+(\mathbf{r}t+\tau)\hat{E}^+(\mathbf{r}t)\rangle}{\langle \hat{E}^-(\mathbf{r}t)\hat{E}^+(\mathbf{r}t)\rangle^2}$$

$$= \frac{\langle \hat{\pi}^\dagger(t)\hat{\pi}^\dagger(t+\tau)\hat{\pi}(t+\tau)\hat{\pi}(t)\rangle}{\langle \hat{\pi}^\dagger(t)\hat{\pi}(t)\rangle^2}, \tag{7.119}$$

where the time delay τ is assumed to be a positive quantity. Note that the normal-ordering requirement for the validity of eqn (5.191) is satisfied by the expectation values in the degrees of coherence. The time t in the above relations is assumed sufficiently long for the atoms and the field to have arrived at steady states. The degrees of coherence are then independent of t and in addition the fixed retardation time difference $|\mathbf{r}-\mathbf{R}|/c$ between the field and atomic operators in eqn (5.191) can be ignored. The prefactors of the atomic operators in eqn (5.191) and its conjugate conveniently cancel in the degrees of coherence.

The calculation of the field coherence properties of the emitted light is thus converted to a problem of determining steady-state expectation values of products of atomic transition operators. The zero time-delay degrees of coherence are simply obtained. From eqn (7.118) it is obvious that

$$g^{(1)}(0) = 1. \tag{7.120}$$

For the degree of second-order coherence, we use the properties (5.126) and (5.127), which apply for any products of like transition operators evaluated at common times,

$$\hat{\pi}^\dagger(t)\hat{\pi}^\dagger(t) = \hat{\pi}(t)\hat{\pi}(t) = 0. \tag{7.121}$$

Thus from eqn (7.119)

$$g^{(2)}(0) = 0, \tag{7.122}$$

and the light emitted by a single driven atom is always antibunched in accordance with the criterion (6.48).

The atomic expectation values needed for the complete time dependences of the degrees of coherence are most conveniently calculated in the interaction representation. It follows from eqns (5.207)–(5.209) that

$$\langle \hat{\pi}(t)\rangle = \rho_{21}(t)\exp(-\mathrm{i}\omega_0 t) = \tilde{\rho}_{21}(t)\exp(-\mathrm{i}\omega t) \tag{7.123}$$

$$\langle \hat{\pi}^\dagger(t)\rangle = \rho_{12}(t)\exp(\mathrm{i}\omega_0 t) = \tilde{\rho}_{12}(t)\exp(\mathrm{i}\omega t) \tag{7.124}$$

and

$$\langle \hat{\pi}^\dagger(t)\hat{\pi}(t)\rangle = \rho_{22}(t), \tag{7.125}$$

where

$$\tilde{\rho}_{12}(t) = \rho_{12}(t)\exp\{\mathrm{i}(\omega_0-\omega)t\} \quad \text{and} \quad \tilde{\rho}_{21}(t) = \rho_{21}(t)\exp\{-\mathrm{i}(\omega_0-\omega)t\} \tag{7.126}$$

are the modified off-diagonal density matrix elements defined in eqn (2.160). The time dependences of the density matrix elements can in principle be calculated, using where appropriate rate equations or the interaction-representation Bloch equations. However, the above expectation values involve only a single time t, whereas the degrees of coherence involve expectation values of products of operators evaluated at different times t and $t+\tau$. It is necessary to generalize the results of the present paragraph.

Consider first the relation between density matrix elements at different times. Since all three independent elements are coupled by the equations of motion, the elements at time $t+\tau$ can be expressed in the general forms

$$\tilde{\rho}_{21}(t+\tau) = \alpha_1(\tau)+\alpha_2(\tau)\tilde{\rho}_{21}(t)+\alpha_3(\tau)\tilde{\rho}_{12}(t)+\alpha_4(\tau)\rho_{22}(t), \tag{7.127}$$

with the complex conjugate expression for $\tilde{\rho}_{12}(t+\tau)$, and

$$\rho_{22}(t+\tau) = \beta_1(\tau)+\beta_2(\tau)\tilde{\rho}_{21}(t)+\beta_3(\tau)\tilde{\rho}_{12}(t)+\beta_4(\tau)\rho_{22}(t), \tag{7.128}$$

where the coefficients $\alpha_i(\tau)$ and $\beta_i(\tau)$ are to be obtained by solution of the equations of motion. They must clearly satisfy the initial conditions

$$\alpha_2(0) = \beta_4(0) = 1$$

$$\alpha_1(0) = \alpha_3(0) = \alpha_4(0) = \beta_1(0) = \beta_2(0) = \beta_3(0) = 0. \qquad (7.129)$$

In addition, it can be assumed that the density matrix elements after a very long time delay τ are independent of their values at time t, so that

$$\alpha_2(\infty) = \alpha_3(\infty) = \alpha_4(\infty) = \beta_2(\infty) = \beta_3(\infty) = \beta_4(\infty) = 0. \qquad (7.130)$$

The forms of solution (7.127) and (7.128) for the density matrix elements can be re-expressed in terms of atomic-operator expectation values with the use of eqns (7.123)–(7.125),

$$\begin{aligned}\langle\hat{\pi}(t+\tau)\rangle\exp\{\mathrm{i}\omega(t+\tau)\} &= \alpha_1(\tau)+\alpha_2(\tau)\langle\hat{\pi}(t)\rangle\exp(\mathrm{i}\omega t)\\ &\quad+\alpha_3(\tau)\langle\hat{\pi}^\dagger(t)\rangle\exp(-\mathrm{i}\omega t)\\ &\quad+\alpha_4(\tau)\langle\hat{\pi}^\dagger(t)\hat{\pi}(t)\rangle \qquad (7.131)\end{aligned}$$

$$\begin{aligned}\langle\hat{\pi}^\dagger(t+\tau)\hat{\pi}(t+\tau)\rangle &= \beta_1(\tau)+\beta_2(\tau)\langle\hat{\pi}(t)\rangle\exp(\mathrm{i}\omega t)\\ &\quad+\beta_3(\tau)\langle\hat{\pi}^\dagger(t)\rangle\exp(-\mathrm{i}\omega t)\\ &\quad+\beta_4(\tau)\langle\hat{\pi}^\dagger(t)\hat{\pi}(t)\rangle. \qquad (7.132)\end{aligned}$$

In view of eqn (7.130), the steady-state expectation values can be written

$$\underset{t\to\infty}{\mathrm{Lt}}\ \langle\hat{\pi}(t)\rangle\exp(\mathrm{i}\omega t) = \alpha_1(\infty) \qquad (7.133)$$

and

$$\langle\hat{\pi}^\dagger(\infty)\hat{\pi}(\infty)\rangle = \beta_1(\infty). \qquad (7.134)$$

The results (7.131) and (7.132) are used to obtain the expectation values required for the degrees of coherence with the help of the *quantum regression theorem*,[27,28] which is stated as follows. Suppose that the expectation value of any operator $\hat{A}$ at time $t+\tau$ is related to the expectation values of a set of operators $\hat{A}_i$ at an earlier time t according to

$$\langle\hat{A}(t+\tau)\rangle = \sum_i \alpha_i(\tau)\langle\hat{A}_i(t)\rangle. \qquad (7.135)$$

Then the regression theorem proves that

$$\langle\hat{B}(t)\hat{A}(t+\tau)\hat{C}(t)\rangle = \sum_i \alpha_i(\tau)\langle\hat{B}(t)\hat{A}_i(t)\hat{C}(t)\rangle, \qquad (7.136)$$

where the capital letters denote any operators. The theorem thus expresses double-time expectation values in terms of single-time expectation values in a manner that can be applied immediately to the present problem. It follows from eqns (7.131) and (7.132) with the use of eqn (7.121) that

$$\begin{aligned}\langle\hat{\pi}^\dagger(t)\hat{\pi}(t+\tau)\rangle &= \exp\{-\mathrm{i}\omega(t+\tau)\}\{\alpha_1(\tau)\langle\hat{\pi}^\dagger(t)\rangle\\ &\quad+\alpha_2(\tau)\langle\hat{\pi}^\dagger(t)\hat{\pi}(t)\rangle\exp(\mathrm{i}\omega t)\} \qquad (7.137)\end{aligned}$$

and

$$\langle\hat{\pi}^\dagger(t)\hat{\pi}^\dagger(t+\tau)\hat{\pi}(t+\tau)\hat{\pi}(t)\rangle = \beta_1(\tau)\langle\hat{\pi}^\dagger(t)\hat{\pi}(t)\rangle, \qquad (7.138)$$

where the first terms on the right-hand sides of eqns (7.131) and (7.132) correspond in eqn (7.135) to contributions in which the operator $\hat{A}_i$ is simply a numerical quantity.

The degrees of coherence are now obtained by substitution in eqns (7.118) and (7.119). Since t is assumed sufficiently large for steady-state conditions to be established, the expressions (7.133) (and its conjugate) and (7.134) should be used for the single-time expectation values. Thus

$$g^{(1)}(\tau) = \exp(-\mathrm{i}\omega\tau)\left\{\frac{\alpha_1(\tau)\alpha_1^*(\infty)}{\beta_1(\infty)}+\alpha_2(\tau)\right\} \qquad (7.139)$$

and

$$g^{(2)}(\tau) = \beta_1(\tau)/\beta_1(\infty). \qquad (7.140)$$

The infinite time-delay degrees of coherence obtained with the help of eqn (7.130) are

$$|g^{(1)}(\infty)| = |\alpha_1(\infty)|^2/\beta_1(\infty) \qquad (7.141)$$

and

$$g^{(2)}(\infty) = 1. \qquad (7.142)$$

For the complete time dependence of the degrees of coherence it is necessary to calculate $\alpha_1(\tau)$, $\alpha_2(\tau)$, and $\beta_1(\tau)$. The remaining coefficients in eqns (7.127) and (7.128) are not needed. Thus $\tilde{\rho}_{21}$ must be calculated for an arbitrary value of $\tilde{\rho}_{21}(t)$, but $\rho_{22}(t)$ can be set equal to zero, while ρ_{22} need only be calculated for the condition

$$\tilde{\rho}_{21}(t) = \tilde{\rho}_{12}(t) = \rho_{22}(t) = 0. \qquad (7.143)$$

A simple example of the methods of calculation described above is provided by physical situations where the atomic motion can be adequately described by a rate equation of the kind shown in eqn (2.170),

$$\mathrm{d}\rho_{22}/\mathrm{d}t = r-2\gamma\rho_{22}. \qquad (7.144)$$

As explained in §2.14, such a simple equation of motion is valid for broad-band incident light and for large collision- or Doppler-broadening. It may also be appropriate for methods of atomic excitation other than illumination, such as electron bombardment. Only the diagonal density matrix element appears in the rate equation and we consider only the degree of second-order coherence of the emitted light. The general solution of eqn (7.144) in the form of eqn (7.128) is

$$\rho_{22}(t+\tau) = (r/2\gamma)[1-\exp(-2\gamma\tau)]+\rho_{22}(t)\exp(-2\gamma\tau). \qquad (7.145)$$

Thus

$$\beta_1(\tau) = (r/2\gamma)[1-\exp(-2\gamma\tau)], \qquad (7.146)$$

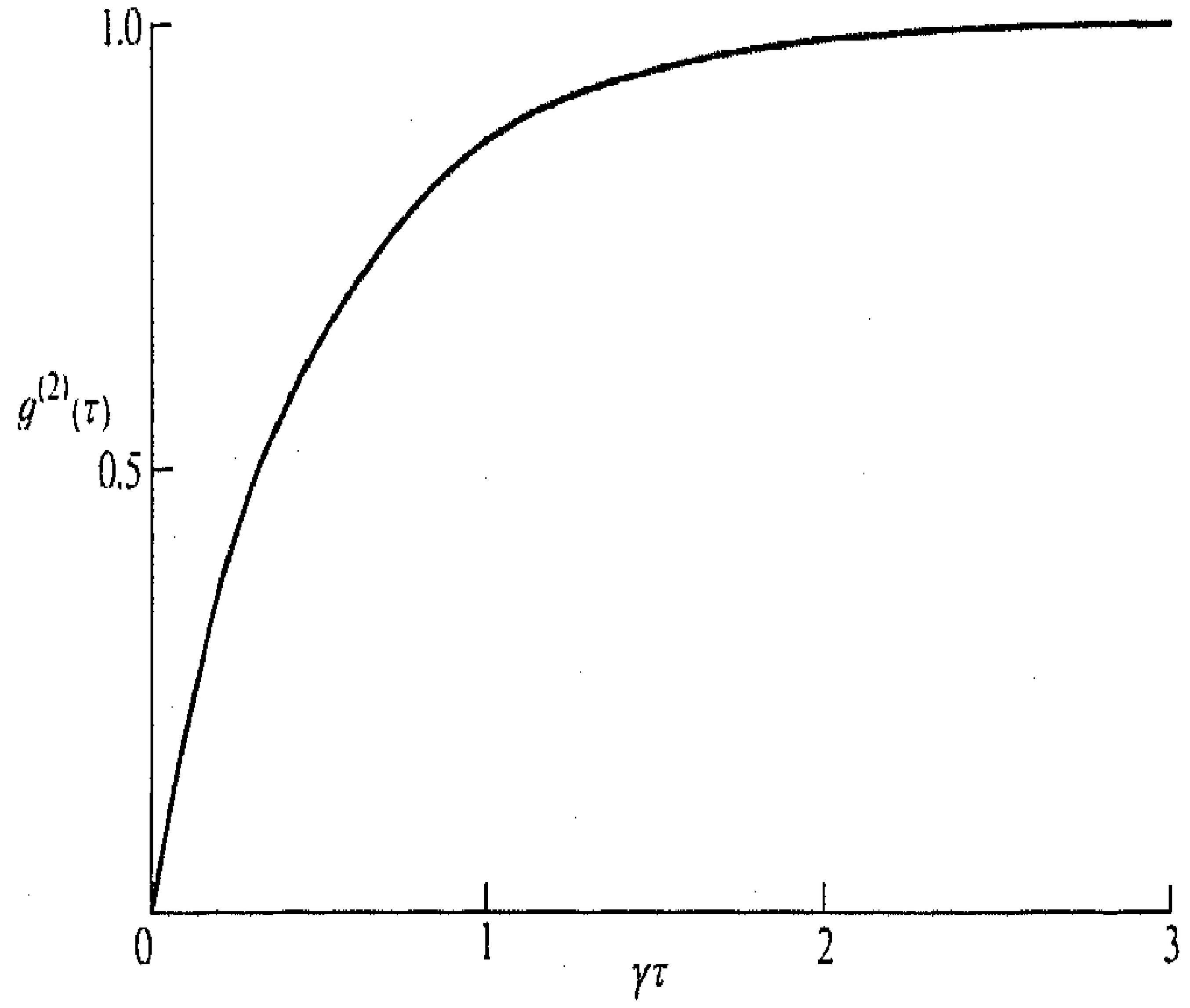

FIG. 7.11. Dependence on the time delay τ of the degree of second-order coherence of the light emitted by a single two-level atom.

and the degree of second-order coherence given by eqn (7.140) is

$$g^{(2)}(\tau) = 1-\exp(-2\gamma\tau). \tag{7.147}$$

This function is plotted in Fig. 7.11; it clearly violates the classical inequalities (3.76) and (3.81) and the emitted light is antibunched with a photon distribution similar to Fig. 6.4(c).

The zero value of the degree of second-order coherence at zero time delay, established in general in eqn (7.122), shows that the light emitted by a single driven atom is always antibunched, irrespective of the method of atomic excitation. In qualitative terms the phenomenon reflects the inability of a single two-level atom to emit a pair of photons simultaneously.[29,30] Successive photon emissions are separated by the time required for the atom arriving in its ground state after photon emission to be re-excited and emit a second photon. The emitted photons are thus 'spaced out' in the manner of Fig. 6.4(c).

The most favourable conditions for experimental observation of antibunched light occur for illumination of atoms by narrow-band light where the rate-equation example treated above does not apply. It is also necessary to consider the effects of interference between the radiation from all illuminated atoms in an experimental sample. These topics form the subject matter of the account of resonance fluorescence given in the following chapter.

References

1. See, for example, Kittel, C. and Kroemer, H. (1980). *Thermal physics*, p. 407. W. H. Freeman, San Francisco.

2. Schell, A. and Barakat, R. (1973). *J. Phys.* **A6,** 826.
3. Hildred, G. P. and Hall, A. G. (1978). *J. Phys.* **A11,** L135.
4. Voigt, H., Bandilla, A., and Ritze, H. H. (1980). *Z. Physik* **B36,** 215.
5. Results equivalent to these were first derived by Shimoda, K., Takahasi, H., and Townes, C. H. (1957). *J. Phys. Soc. Jpn* **12,** 686.
6. Lachs, G. (1965). *Phys. Rev.* **B138,** 1012; Jakeman, E. and Pike, E. R. (1969). *J. Phys.* **A2,** 115.
7. Carusotto, S. (1975). *Phys. Rev.* **A11,** 1629 establishes the same properties more rigorously by deriving the time dependences of all moments of the photon distribution.
8. Rockower, E. B., Abraham, N. B., and Smith, S. R. (1978). *Phys. Rev.* **A17,** 1100.
9. Sargent, M., Scully, M. O., and Lamb, W. E. (1974). *Laser physics*. Addison-Wesley, Reading Massachusetts.
10. See, for example, Garrett, C. G. B. (1967). *Gas lasers*. McGraw-Hill, New York.
11. See, for example, Ziman, J. M. (1972). *Principles in the theory of solids*. Cambridge University Press.
12. Haken, H. (1970). In *Handbuch der Physik* (ed. S. Flügge), Vol. XXV/2c *Light and matter* lc. Springer-Verlag, Berlin.
13. Louisell, W. H. (1973). *Quantum statistical properties of radiation*. Wiley, New York.
14. Rate equations were first used to determine the intensity fluctuations in a laser beam by McCumber, D. E. (1966). *Phys. Rev.* **141,** 306. For a similar calculation see Fleck, J. A. (1966). *Phys. Rev.* **149,** 309 and 322.
15. Compare eqn (7.81) with eqn (17) in Chapter 17 of ref. 9.
16. Sargent, M., Scully, M. O., and Lamb, W. E. (1970). *Appl. Opt.* **9,** 2423.
17. Slater, L. J. (1960). *Confluent hypergeometric functions*. Cambridge University Press.
18. This form of the distribution was first derived by Scully, M. O. and Lamb, W. E. (1967). *Phys. Rev.* **159,** 208.
19. Arecchi, F. T. (1969). In *Quantum optics* (ed. R. J. Glauber), p. 57. Academic Press, New York.
20. Meltzer, D., Davis, W., and Mandel, L. (1970). *Appl. Phys. Lett*, **17,** 242.
21. Jakeman, E., Oliver, C. J., Pike, E. R., Lax, M., and Zwanziger, M. (1970). *J. Phys.* **A3,** L52; Lax, M. and Zwanziger, M. (1973). *Phys. Rev.* **A7,** 750.
22. This result was first given by Scully, M. O. and Lamb, W. E. (1969). *Phys. Rev.* **179,** 368.
23. Chandrasekhar, S. (1943). *Rev. mod. Phys.* **15,** 1. Reprinted (1954) in *Selected papers on noise and stochastic processes* (ed. N. Wax). Dover, New York.
24. See, for example, Dwight, H. B. (1961). *Tables of integrals*, p. 236. Macmillan, New York.
25. Weichel, H. (1976). *Am. J. Phys.* **44,** 839.
26. Schawlow, A. L. and Townes, C. H. (1958). *Phys. Rev.* **112,** 1940.
27. Lax, M. (1968). *Phys. Rev.* **172,** 350.
28. Mollow, B. R. (1969). *Phys. Rev.* **188,** 1969.
29. Mollow, B. R. (1975). *Phys. Rev.* **A12,** 1919.
30. Carmichael, H. J. and Walls, D. F. (1976). *J. Phys.* **B9,** L43.

8. Resonance fluorescence and light scattering

THE basic components of a light-scattering experiment include a scattering region with the atoms of interest illuminated by a parallel beam of light, and a detector that measures the scattered intensity at some finite angle to the direction of the incident beam. The scattering at small angles is usually difficult to resolve from the transmitted incident beam itself, and it is convenient in many experiments to measure the light scattered at right angles. In high-resolution studies, the atoms may be supplied to the scattering region in the form of a beam directed in the third mutually perpendicular direction, to minimize Doppler broadening of the scattered light.

In terms of the quantum theory of light, the scattering involves the destruction of a photon of energy $\hbar\omega$ from the incident beam and the creation of a photon of energy $\hbar\omega_s$ in the scattered beam. The light scattering is thus a second-order process since two interactions of the radiation field and the atomic electrons take place. Scattering occurs for all values of the incident frequency relative to the transition frequencies of the scattering atoms. The intensity of the scattering is however particularly strong in resonance conditions where the incident frequency lies close to an atomic transition frequency.

Fig. 8.1 shows some atomic energy levels with the magnitude of the incident frequency ω represented by the arrow on the left. The remaining arrows represent the kinds of component that occur in the scattered frequencies ω_s. The spectrum of the scattered light generally contains an *elastic* contribution, where the scattered frequency ω_s equals the incident frequency ω, together with several *inelastic* components, where ω_s differs from ω. The elastic component is known as Rayleigh scattering. The inelastic components are subdivided according to whether or not the atom makes a transition to a final state that differs from its initial state before the scattering process. We consider only atoms that are initially in their ground states.

Suppose first that the atom is again in its ground state after the scattering event. Energy conservation suggests that the scattered photon must have $\omega_s = \omega$ and must therefore contribute to the elastic or Rayleigh component. However, when ω is close to resonance with an atomic excitation frequency ω_i that suffers collision broadening, the scattered light has an additional inelastic component with the same central frequency and linewidth as the atomic transition concerned. This is a fluorescent contribution in which the atom reradiates by ordinary emission after excitation by the incident light; the energy difference between $\hbar\omega$ and $\hbar\omega_s$ is taken up within the energy uncertainty associated with the line-broadening process. These Rayleigh and fluorescent components are represented by the two arrows on the left of the energy-level diagram in Fig. 8.1.

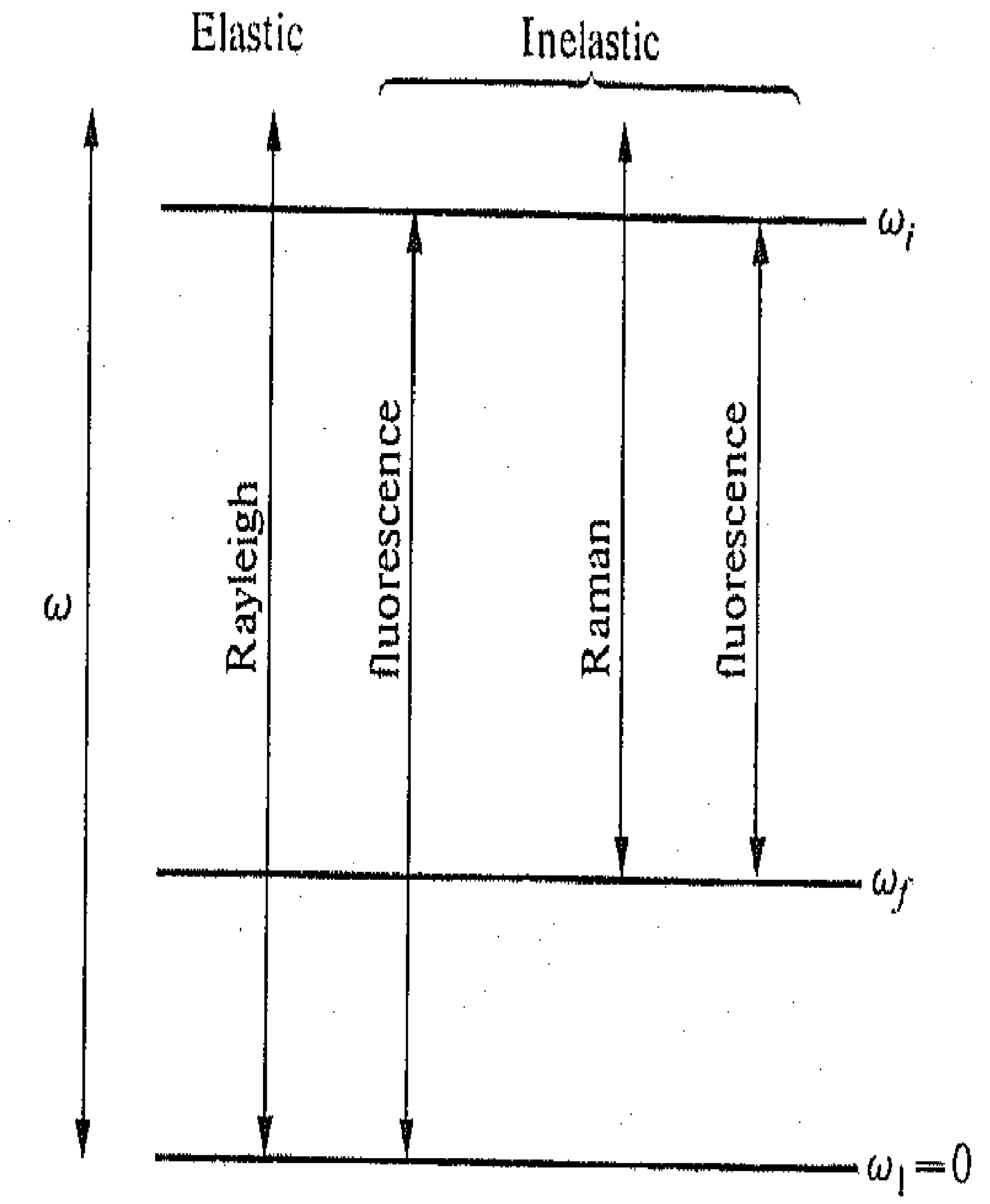

FIG. 8.1. Schematic energy-level diagram showing the incident frequency ω close to resonance with an atomic transition ω_i and the four kinds of contribution to the scattered frequencies ω_s.

Now suppose that the atom is left in an excited state of energy $\hbar\omega_f$ after the scattering. The scattering is entirely inelastic, and the component whose frequency ω_s satisfies the energy-conservation equality with $\omega-\omega_f$ is known as Raman scattering. There is in addition a further resonance fluorescence component associated with the radiative decay to the final-state energy level $\hbar\omega_f$ when the incident frequency lies close to an atomic excitation frequency ω_i. These Raman and excited-state fluorescent components are represented by the two arrows on the right of Fig. 8.1. There are similar pairs of contributions for each atomic energy level whose excitation frequency ω_f lies below the incident frequency ω.

The calculations presented below fall into two main parts. We first consider the scattering by a two-level atom where the atomic state after the scattering can only be the same as the initial ground state; it is possible to give a detailed theory of the spectral and coherence properties of the light generated in resonance fluorescence. The second main calculation refers to the light scattering by a multilevel atom; the resonance fluorescence is not included, but it is possible in this case to obtain the intensities of the Rayleigh and Raman components in the scattered spectrum.

8.1. The scattering cross-section

It is convenient to preface the more specific calculations by some general remarks concerning light scattering that apply irrespective of the distribution of scattered frequencies ω_s. Classical electromagnetic theory is used in the present section, but the definitions and main results apply to the quantum calculations of the remainder of the chapter.

Consider first the geometrical arrangement of a scattering experiment. The coordinate system to be used here is shown in Fig. 8.2. The scattering atom is placed at the origin of coordinates in a parallel beam of incident light having its electric vector **E** parallel to the x-axis and its propagation direction parallel to the z-axis. The cycle-averaged Poynting vector of the incident light beam is

$$\bar{I} = \tfrac{1}{2}\epsilon_0 c|E|^2, \tag{8.1}$$

where E is the magnitude of the complex field vector.

The scattered light is normally distributed over all directions in space. We consider the scattered light with electric vector $\mathbf{E}_s$ at position **r**. Its cycle-averaged Poynting vector is

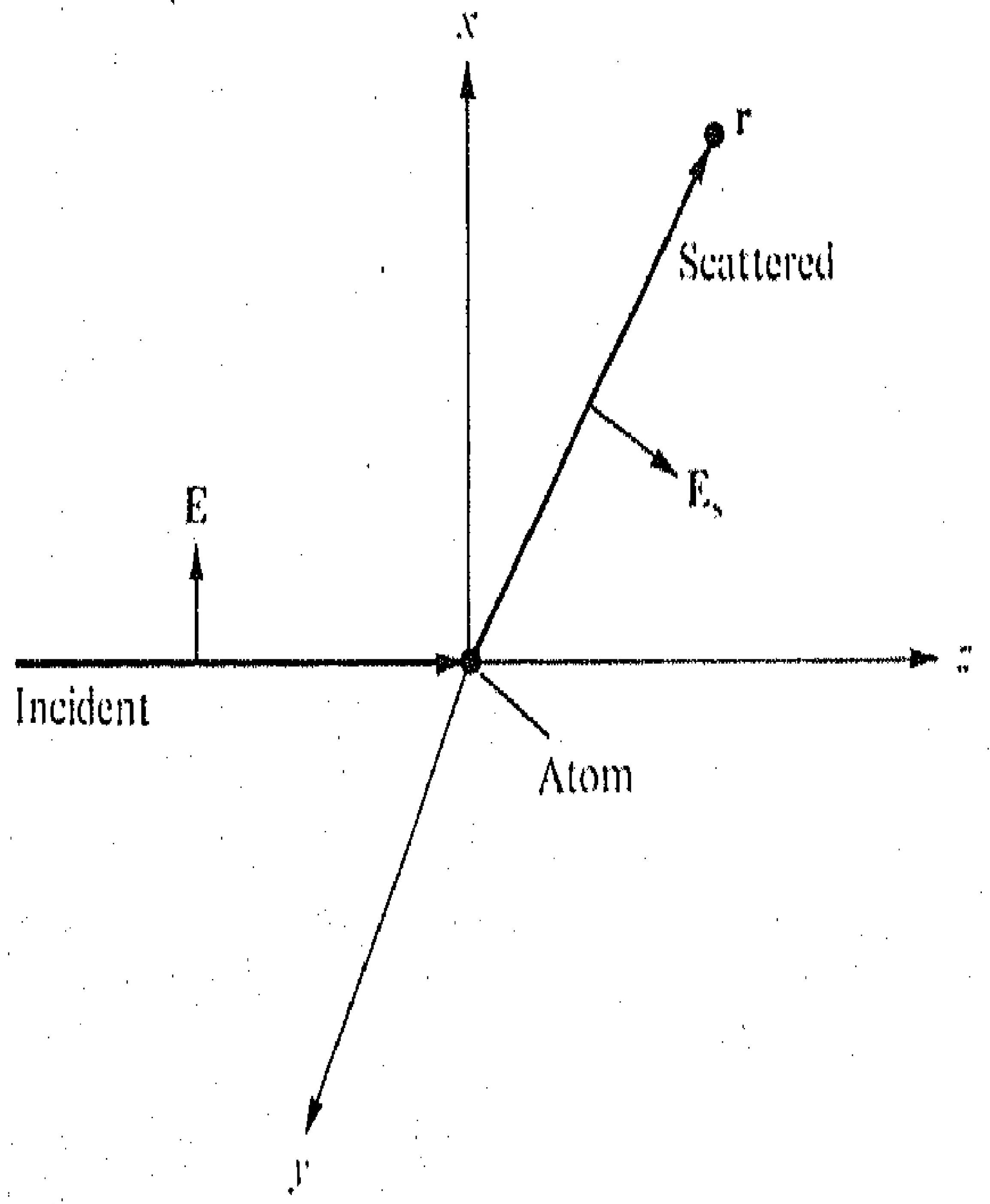

FIG. 8.2. Geometrical arrangement of a light-scattering experiment. The scattered photon has two independent polarization directions.

$$\bar{I}_s = \tfrac{1}{2}\epsilon_0 c|E_s|^2. \tag{8.2}$$

The total rate at which scattered electromagnetic energy is produced by the atom is determined by an integration of $\bar{I}_s$ over a sphere surrounding the origin. The result can be written

$$\int \bar{I}_s r^2\, \mathrm{d}\Omega, \tag{8.3}$$

where $\mathrm{d}\Omega$ is an elementary solid angle, and the integration runs over the complete 4π solid angle. The total scattered energy must include the contributions of the two independent polarizations of the scattered light at each position **r**.

The strength of the scattering is conveniently expressed in terms of the scattering cross-section σ, defined in a similar way to the photoelectric cross-section of eqn (5.93), as the rate at which energy is removed from the incident beam by the scattering, divided by the rate at which energy in the incident photon beam crosses a unit area perpendicular to its propagation direction. For elastic scattering the rate of removal of energy from the incident beam is equal to the rate of production of scattered energy given by eqn (8.3). This is not the case for inelastic scattering, where some of the energy removed from the incident beam is given to the atom, and only a fraction ω_s/ω of the energy appears in the form of scattered photons at frequency ω_s. Thus, in general, the cross-section is

$$\sigma = (\omega/\omega_s \bar{I}) \int \bar{I}_s r^2\, \mathrm{d}\Omega. \tag{8.4}$$

The cross-section clearly has the dimensions of area and it is independent of r since $\bar{I}_s$ falls off with the inverse square of the distance from the atom.

The differential cross-section is defined analogously to eqn (5.94) and refers to that part of the scattered light within the elementary solid angle $\mathrm{d}\Omega$. It is obtained by differentiation of both sides of eqn (8.4) with respect to Ω,

$$\mathrm{d}\sigma/\mathrm{d}\Omega = \omega \bar{I}_s r^2/\omega_s \bar{I}. \tag{8.5}$$

It should be noted that, in comparison with the photoelectric cross-section, the light-scattering cross-section involves the additional step of summing the contributions of the two independent photon polarizations for each direction of scattering.

The cross-section σ defined above refers to light scattering by a single atom. Some experiments on atomic beams do observe the scattering by very small numbers of atoms, but many light-scattering experiments use an atomic gas where the scattered beam is produced by a large number N of atoms, and one must consider how to add the contributions of the individual atoms. For the scattering of visible light by a gas of atoms, the mean separation between atoms is very small compared with the wavelength of the radiation, provided that the gas pressure at room temperature is greater than about 100 Pa. The total electric vector of the scattered light at position **r** is given by a linear superposition of the contributions of the N atoms.

Consider first the scattering by a homogeneous distribution of atoms. We assume the incident light to be a classical electromagnetic wave of well defined amplitude and phase. The components of the scattered field that arise from the atoms contained within a half-wavelength of the incident radiation are in phase with each other, but are out of phase with the fields arising from the atoms that lie within adjacent half-wavelengths. For a uniform distribution of scattering atoms, the contributions to the scattered field from the groups of atoms in the different half-wavelengths exactly cancel, except for the forward direction, $\theta = 0$, and no scattering occurs. There is, for example, no scattering of light by a perfect crystal in which the atoms are rigidly fixed on regularly spaced lattice sites.

Scattering of light can occur only as a result of inhomogeneities in the distribution of the scattering atoms. For the case of a crystal, light scattering can occur if the atoms are allowed to vibrate around the regularly spaced lattice sites. For the case of a gas, to which the subsequent discussion is restricted, the light scattering is a result of the fluctuations in the gas density owing to atomic motions. It is not difficult to evaluate the total scattered intensity that is caused by the density fluctuations.

Problem 8.1. Consider a gas of N atoms confined to a volume V. The total volume can be divided into smaller volumes υ such that all the atoms in volume υ produce a scattered field of the same phase, but adjacent volumes produce scattered fields of alternating sign. Prove that if the scattered intensity arising from a single atom is given by the right-hand side of eqn (8.2), then the total scattered intensity arising from all the atoms in the gas is

$$\bar{I}_s = \tfrac{1}{2}\epsilon_0 c|E_s|^2(V/\upsilon)(\Delta\nu)^2, \tag{8.6}$$

where $(\Delta\nu)^2$ is the mean-square deviation in the number of atoms in a volume υ.

The distribution of the N atoms between the different volumes υ is governed by random atomic motions. The probability of finding ν atoms in a given volume is related to the mean number $\bar{\nu}$ in a volume υ by a Poisson distribution similar to eqn (6.65). Thus by analogy with eqn (6.67)

$$(\Delta\nu)^2 = \bar{\nu} = N\upsilon/V, \tag{8.7}$$

and eqn (8.6) can be written

$$\bar{I}_s = \tfrac{1}{2}\epsilon_0 c|E_s|^2 N. \tag{8.8}$$

The scattering cross-section for the N atoms is thus equal to the cross-section for a single atom multiplied by N. It is assumed that the refractive indices of the gas at frequencies ω and ω_s are close to unity and need not appear in the Poynting vectors. The result (8.8) is analogous to eqn (3.18), which shows that the average intensity of the light radiated by ν atoms is equal to ν times the average intensity from a single atom. The coherence properties of the light scattered by arbitrary numbers of atoms are considered in §8.5.

It is emphasized in §1.8 that the absorption and scattering of light are different aspects of the same process; the light removed from a beam by absorption reappears as the scattered radiation. From the point of view of absorption, the rate of removal of energy from the incident beam in a volume V is given by eqns (1.90) and (1.96) to be

$$-V\partial\bar{W}/\partial t = -V\partial\bar{I}/\partial z = VK\bar{I}, \tag{8.9}$$

where K is the absorption coefficient for a light beam sufficiently weak to avoid saturation. From the point of view of scattering, the cross-section σ is defined by eqn (8.4) in such a way that the rate of removal of energy from the beam by scattering from a single atom is $\sigma\bar{I}$. Thus the rate of energy removal by N atoms is

$$N\sigma\bar{I}. \tag{8.10}$$

The expressions (8.9) and (8.10) describe the same physical quantity, so

$$\sigma = (V/N)K = (2V\omega/Nc)\kappa, \tag{8.11}$$

where eqn (1.91) has been used. Of course, the cross-section, absorption coefficient, and extinction coefficient must all be evaluated at the same frequency ω.

This result is known as the *optical theorem*. It is derived on the basis of general considerations of energy conservation, and it is valid for both quantum-mechanical and classical treatments of light scattering. Similar optical theorems hold for a wide variety of scattering problems.[1] The application of the theorem (8.11) is discussed in §§8.7 and 8.8.

8.2. Single-atom resonance fluorescence

The simplest scattering system is a two-level atom illuminated by single-mode coherent incident light. The two-level theory developed below[2,3] also applies to the Rayleigh and ground-state fluorescent scattering by real multilevel atoms when the exciting frequency ω lies close to only a single atomic transition frequency. However, multilevel atoms show the additional excited-state scattering represented on the right of Fig. 8.1. It is possible to treat the two-level scattering with a greater degree of detail than can easily be achieved for scattering by multilevel atoms. We use the methods outlined in

§§5.13 and 7.10 to relate the properties of the emitted light to the time development of the atomic states.

The behaviour of two-level atoms subjected to coherent incident light is described by the interaction-representation optical Bloch equations, identical to the semiclassical equations (2.161) and (2.162),

$$\mathrm{d}\rho_{22}/\mathrm{d}t = -\tfrac{1}{2}\mathrm{i}\mathcal{V}\tilde{\rho}_{12}+\tfrac{1}{2}\mathrm{i}\mathcal{V}\tilde{\rho}_{21}-2\gamma\rho_{22} \tag{8.12}$$

$$\mathrm{d}\tilde{\rho}_{12}/\mathrm{d}t = \tfrac{1}{2}\mathrm{i}\mathcal{V}(\rho_{11}-\rho_{22})+[\mathrm{i}(\omega_0-\omega)-\gamma']\tilde{\rho}_{12}, \tag{8.13}$$

where $\mathcal{V}$, taken to be real throughout, is the Rabi frequency. The remaining density matrix elements are determined as usual from

$$\rho_{11}+\rho_{22} = 1, \qquad \tilde{\rho}_{21} = \tilde{\rho}^*_{12}. \tag{8.14}$$

If the time dependence of the density matrix elements is known, then the motion of the expectation values of the atomic transition operators can be obtained from eqns (5.207)–(5.209), and the expectation values of the radiated-field operators are determined by eqn (5.191). The required connections between field expectation values and atomic density matrix elements are thus

$$\langle\hat{E}^+_{\mathrm{s}}(\mathbf{r}t)\rangle = -\frac{e\omega_0^2\boldsymbol{\varepsilon}_{\mathrm{s}}.\mathbf{D}_{12}}{4\pi\epsilon_0c^2r}\tilde{\rho}_{21}\left(t-\frac{r}{c}\right)\exp\left\{-\mathrm{i}\omega\left(t-\frac{r}{c}\right)\right\}, \tag{8.15}$$

with the conjugate relation for $\hat{E}^-_{\mathrm{s}}$, and

$$\langle\hat{E}^-_{\mathrm{s}}(\mathbf{r}t)\hat{E}^+_{\mathrm{s}}(\mathbf{r}t)\rangle = \left\{\frac{e\omega_0^2\boldsymbol{\varepsilon}_{\mathrm{s}}.\mathbf{D}_{12}}{4\pi\epsilon_0c^2r}\right\}^2\rho_{22}\left(t-\frac{r}{c}\right) \tag{8.16}$$

where the atom is placed at the origin, s subscripts distinguish scattered-field quantities, and $\boldsymbol{\varepsilon}_{\mathrm{s}}$ is the polarization vector of the scattered light (parallel to the x-axis in Fig. 5.4). These relations are used to determine the intensity, spectral properties and coherence of the scattered field. We consider only steady-state properties where t is taken infinite and the retardation time r/c can be neglected.

The steady-state scattered intensity obtained from eqn (8.16) is

$$\bar{I}_{\mathrm{s}} = \{e^2\omega_0^4(\boldsymbol{\varepsilon}_{\mathrm{s}}.\mathbf{D}_{12})^2/8\pi^2\epsilon_0c^3r^2\}\rho_{22}(\infty). \tag{8.17}$$

This is essentially the same as the quantity integrated over solid angle in eqn (5.192). The steady-state degree of atomic excitation given by eqn (2.136) is

$$\rho_{22}(\infty) = \frac{\tfrac{1}{4}(\gamma'/\gamma)\mathcal{V}^2}{(\omega_0-\omega)^2+\gamma'^2+\tfrac{1}{2}(\gamma'/\gamma)\mathcal{V}^2}. \tag{8.18}$$

The mean intensity of the single-mode coherent incident light obtained from eqn (5.104) is

$$\bar{I} = c\hbar\omega|\alpha|^2/V. \tag{8.19}$$

The differential cross-section (8.5) is thus

$$\frac{\mathrm{d}\sigma}{\mathrm{d}\Omega} = \frac{e^4\omega_0^4}{16\pi^2\epsilon_0^2\hbar^2c^4}\frac{(\boldsymbol{\varepsilon}_{\mathrm{s}}.\mathbf{D}_{12})^2(\boldsymbol{\varepsilon}.\mathbf{D}_{12})^2\gamma'/\gamma}{(\omega_0-\omega)^2+\gamma'^2+\tfrac{1}{2}(\gamma'/\gamma)\mathcal{V}^2}, \tag{8.20}$$

where eqns (5.59) and (5.214) have been used to express the Rabi frequency $\mathcal{V}$ in the numerator of eqn (8.18) in terms of the transition matrix element $\mathbf{D}_{12}$, and $\boldsymbol{\varepsilon}$ is the polarization vector of the incident light.

It is seen that the cross-section has a Lorentzian dependence on the incident frequency ω, centred on the atomic transition frequency ω_0 and with a width that combines the effects of radiative-, power-, and collision-broadening in the same manner as eqn (2.139). The cross-section is essentially independent of intensity for low incident intensities where the Rabi frequency is small. However, the cross-section falls off inversely with the intensity for high incident intensities, where the term in $\mathcal{V}^2$ dominates the denominator of eqn (8.20). This is the scattering analogue of the saturation effect on the absorption coefficient discussed in §1.11.

Some information on the coherence properties of the scattered light is obtained from the expectation values of $\hat{E}^+_{\mathrm{s}}$ and $\hat{E}^-_{\mathrm{s}}$, given by eqn (8.15) and its conjugate. The sum of these expectation values has a sinusoidal variation with position and time, similar to the electric field (4.205) associated with a coherent single-mode excitation. The ratio of the part of the scattered intensity that has this coherent behaviour to the total scattered intensity is expressed by[2,4]

$$\frac{\bar{I}^{\,\mathrm{coherent}}_{\mathrm{s}}}{\bar{I}_{\mathrm{s}}} = \frac{\langle\hat{E}^-_{\mathrm{s}}(\mathbf{r}t)\rangle\langle\hat{E}^+_{\mathrm{s}}(\mathbf{r}t)\rangle}{\langle\hat{E}^-_{\mathrm{s}}(\mathbf{r}t)\hat{E}^+_{\mathrm{s}}(\mathbf{r}t)\rangle}. \tag{8.21}$$

It is easy to show that the ratio is equal to unity for a purely coherent excitation of the scattered field, but the ratio is zero for chaotic light. For the expectation values given in eqns (8.15) and (8.16) the steady-state ratio is

$$\bar{I}^{\,\mathrm{coherent}}_{\mathrm{s}}/\bar{I}_{\mathrm{s}} = |\tilde{\rho}_{21}(\infty)|^2/\rho_{22}(\infty). \tag{8.22}$$

Problem 8.2. Prove by considering the most general form of density operator for a two-level atom that

$$\rho_{11}\rho_{22} \geqslant |\rho_{21}|^2, \tag{8.23}$$

and hence that the ratio in eqn (8.22) is less than or equal to unity.

The coherent fraction (8.22) can be expressed in various forms. With the use of eqns (7.127) and (7.128) and the properties (7.130), we find

$$\bar{I}^{\,\mathrm{coherent}}_{\mathrm{s}}/\bar{I}_{\mathrm{s}} = |\alpha_1(\infty)|^2/\beta_1(\infty) = |g^{(1)}(\infty)|, \tag{8.24}$$

where the infinite time-delay degree of first-order coherence is taken from eqn (7.141). Alternatively, with the steady-state solutions of the optical Bloch equations from eqns (2.136) and (2.137), eqn (8.22) becomes

$$\frac{\bar{I}_{\mathrm{s}}^{\text{coherent}}}{\bar{I}_{\mathrm{s}}} = \frac{[(\omega_0-\omega)^2+\gamma'^2]\gamma/\gamma'}{(\omega_0-\omega)^2+\gamma'^2+\frac{1}{2}(\gamma'/\gamma)\mathscr{V}^2}. \tag{8.25}$$

The scattered light is therefore almost entirely coherent when the collision broadening is small ($\gamma' \approx \gamma$) and the incident beam is weak ($\mathscr{V} \ll \gamma$). In the opposite limits of large collision broadening ($\gamma' \gg \gamma$) or an intense incident beam ($\mathscr{V} \gg \gamma$), the coherent part of the scattered light falls to a very small fraction.

More complete information on the nature of the light produced in resonance scattering conditions is obtained from the degrees of first and second-order coherence. These are determined from the solutions of the optical Bloch equations by the procedure described in §7.10. The complete time dependences of the degrees of coherence have useful explicit forms only when the Bloch equations have reasonably simple solutions; the cases of a weak incident beam and of zero detuning are treated in §§8.3 and 8.4 respectively. Only the limiting values

$$g^{(1)}(0) = 1 \tag{8.26}$$

and

$$g^{(2)}(0) = 0, \qquad g^{(2)}(\infty) = 1 \tag{8.27}$$

derived in §7.10 apply quite generally.

The spectrum of the scattered light is obtained from the degree of first-order coherence by eqn (3.7) or eqn (3.11),

$$F(\omega_{\mathrm{s}}) = \frac{1}{2\pi}\int_{-\infty}^{\infty} g^{(1)}(\tau)\exp(\mathrm{i}\omega_{\mathrm{s}}\tau)\,\mathrm{d}\tau = \frac{1}{\pi}\,\mathrm{Re}\int_{0}^{\infty} g^{(1)}(\tau)\exp(\mathrm{i}\omega_{\mathrm{s}}\tau)\,\mathrm{d}\tau. \tag{8.28}$$

The spectrum calculated in this way is automatically normalized since use of eqn (8.26) with the delta-function representation (2.64) gives

$$\int_{-\infty}^{\infty} F(\omega_{\mathrm{s}})\,\mathrm{d}\omega_{\mathrm{s}} = g^{(1)}(0) = 1. \tag{8.29}$$

The spectrum contains two distinct kinds of contribution corresponding to the parts of $g^{(1)}(\tau)$ that decay to zero as τ tends to infinity and to the constant-amplitude part

$$\exp(-\mathrm{i}\omega\tau)|g^{(1)}(\infty)| \tag{8.30}$$

that remains at infinite time delay. In the expression (7.139) for the degree of first-order coherence, the part $\alpha_1(\infty)$ of $\alpha_1(\tau)$ gives the constant contribution, while $\alpha_2(\tau)$ and the remainder of $\alpha_1(\tau)$ give the exponentially decaying contributions.

The Fourier transform of the decaying parts of the degree of first-order coherence produces a spectrum at frequencies ω_{s} that differ from the frequency ω of the incident light; this is the inelastic or fluorescent part of the scattered light. On the other hand, substitution of the constant-amplitude part (8.30) of the degree of first-order coherence into eqn (8.28) gives the elastic or Rayleigh part of the scattered spectrum,

$$F(\omega_{\mathrm{s}})_{\text{elastic}} = |g^{(1)}(\infty)|\;\delta(\omega_{\mathrm{s}}-\omega). \tag{8.31}$$

It is seen by comparison with eqn (8.24) that the strength of the elastic part of the spectrum is equal to the coherent fraction of the scattered light, and the elastic and inelastic contributions are sometimes called the coherent and incoherent parts, respectively. The explicit expression given in eqn (8.25) shows that the elastic contribution is significant only when the incident beam is weak and the collision broadening is small.

8.3. Weak incident beam

The incident beam is assumed in the present section to be so weak that the Rabi frequency is much smaller than the radiative decay rate,

$$\mathscr{V} \ll \gamma. \tag{8.32}$$

Then eqns (8.24) and (8.25) give

$$\bar{I}_{\mathrm{s}}^{\text{coherent}}/\bar{I}_{\mathrm{s}} = |g^{(1)}(\infty)| = \gamma/\gamma'; \tag{8.33}$$

the scattered light is entirely coherent and elastic in the absence of any collision broadening. The complete cross-section, including the elastic and inelastic contributions, is given by eqn (8.20) with the final term in the denominator neglected.

The solutions of the optical Bloch equations (8.12) and (8.13) in the limit of a weak incident beam are given by eqns (2.164) and (2.165). Then following the method of §7.10 for determining the degrees of coherence of the emitted light, we identify the required coefficients in the off-diagonal matrix element of eqn (7.127) as

$$\alpha_1(\tau) = \frac{\frac{1}{2}\mathrm{i}\mathscr{V}}{\mathrm{i}(\omega_0-\omega)+\gamma'}\left(\exp\{-[\mathrm{i}(\omega_0-\omega)+\gamma']\tau\}-1\right) \tag{8.34}$$

and

$$\alpha_2(\tau) = \exp\{-[\mathrm{i}(\omega_0-\omega)+\gamma']\tau\}, \tag{8.35}$$

while the coefficient $\beta_1(\tau)$ in the diagonal element (7.128) is given by the entire expression (2.164).

The degree of first-order coherence obtained from eqn (7.139) is

$$g^{(1)}(\tau) = \frac{\gamma'-\gamma}{\gamma'}\exp(-\mathrm{i}\omega_0\tau-\gamma'\tau)+\frac{\gamma}{\gamma'}\exp(-\mathrm{i}\omega\tau). \tag{8.36}$$

The exponential in the first term is identical to the normal degree of first-order coherence for collision-broadened chaotic light centred on the atomic transition frequency ω_0. The second exponential is the same as the degree of first-order coherence for coherent light of frequency ω.

The spectrum derived from the degree of first-order coherence by means of eqn (8.28) is[5,6]

$$F(\omega_s) = \frac{\gamma'-\gamma}{\gamma'}\frac{\gamma'/\pi}{(\omega_0-\omega_s)^2+\gamma'^2}+\frac{\gamma}{\gamma'}\,\delta(\omega_s-\omega). \tag{8.37}$$

This simple form of scattered spectrum is illustrated in Fig. 8.3. It includes an inelastic part whose strength is directly proportional to the collision-broadening decay rate γ_{coll} defined in eqn (2.133). This part of the spectrum has the same lineshape as the absorption spectrum of the atom, and the scattering can be regarded as caused by absorption of incident light followed by fluorescent emission. The difference between the energies of the incident and scattered photons lies within the energy uncertainty of the excited state that results from the collisions, as described by eqn (2.159); the effect is sometimes called collisional redistribution of energy. The remainder of the scattered intensity lies in the Rayleigh elastic part represented by the delta-function term in eqn (8.37). Both contributions to the spectrum are observed, for example, in the light scattering by strontium vapour.[7]

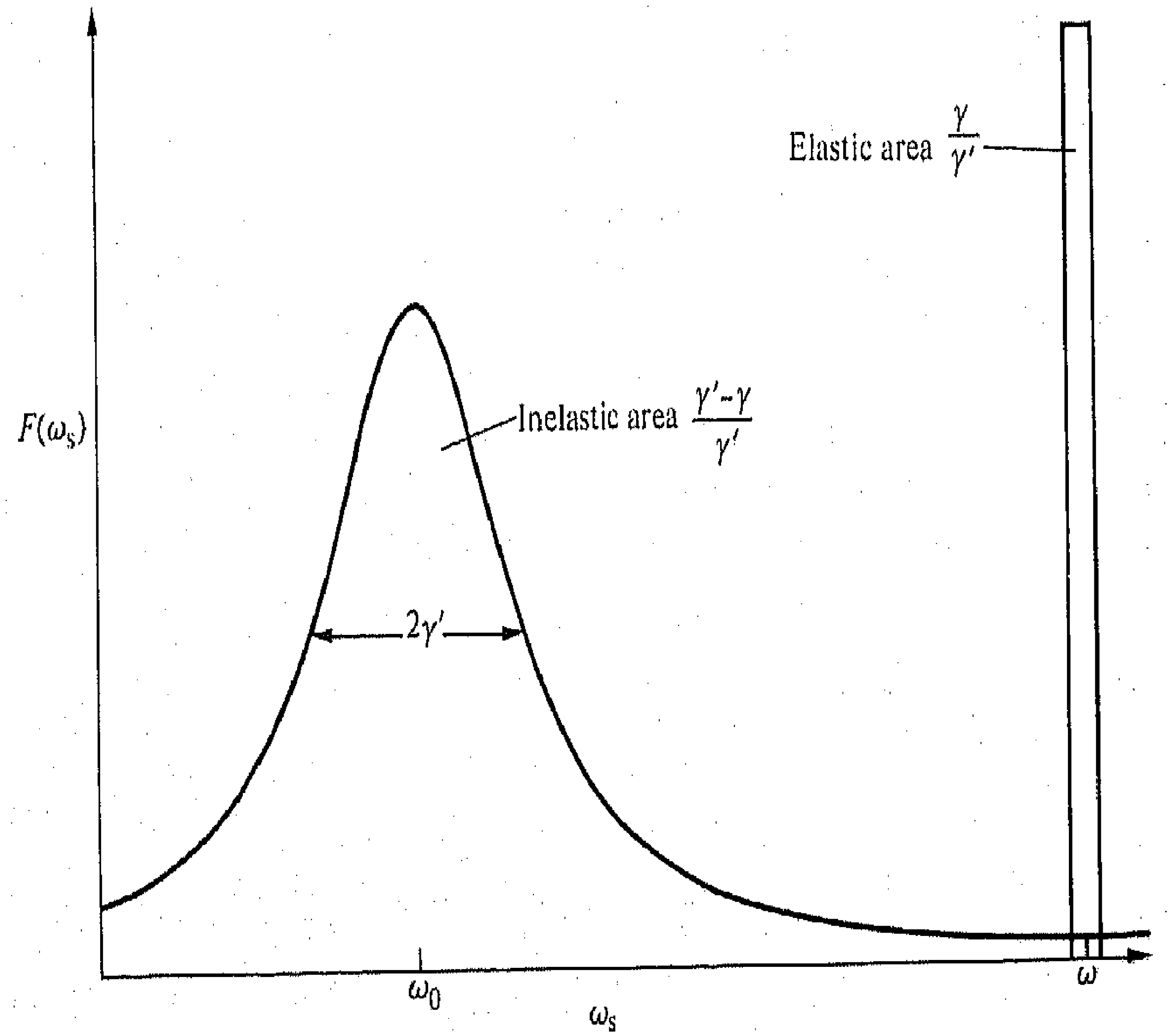

FIG. 8.3. Light scattering spectrum of a two-level atom drawn for the case $\omega > \omega_0$. The Rayleigh delta-function component at frequency ω and the fluorescent Lorentzian centred on the atomic transition frequency ω_0 correspond to the two arrows on the left of the energy-level diagram in Fig. 8.1.

The above results suggest that the scattered light can be represented as a sum of ordinary chaotic and coherent components. This picture is however based on a consideration only of the first-order coherence properties, and the simple model does not embrace the second-order coherence of the scattered light. The degree of second-order coherence obtained from eqns (2.164) and (7.140) is

$$g^{(2)}(\tau) = 1+\frac{(2\gamma-\gamma')[(\omega_0-\omega)^2+\gamma'^2]/\gamma'}{(\omega_0-\omega)^2+(2\gamma-\gamma')^2}\exp(-2\gamma\tau)$$
$$-\frac{2\gamma[(\omega_0-\omega)^2+\gamma'(2\gamma-\gamma')]\cos[(\omega_0-\omega)\tau]+4\gamma(\omega_0-\omega)(\gamma'-\gamma)\sin[(\omega_0-\omega)\tau]}{\gamma'[(\omega_0-\omega)^2+(2\gamma-\gamma')^2]}$$
$$\times\exp(-\gamma'\tau). \tag{8.38}$$

This rather complicated result is best appreciated by considering a couple of limiting cases.

Suppose first that there is no collision broadening, when the spectrum contains only the elastic Rayleigh component and eqn (8.38) reduces to

$$g^{(2)}(\tau) = 1+\exp(-2\gamma\tau)-2\cos[(\omega_0-\omega)\tau]\exp(-\gamma\tau) \qquad (\gamma' = \gamma). \tag{8.39}$$

The simplest possible case is that of zero detuning where[8]

$$g^{(2)}(\tau) = [1-\exp(-\gamma\tau)]^2 \qquad (\gamma' = \gamma, \omega = \omega_0). \tag{8.40}$$

The variations of the degree of second-order coherence for different values of the detuning are shown by the full curves of Fig. 8.4. For comparison, the appropriate limit of eqn (8.36) gives,

$$g^{(1)}(\tau) = \exp(-i\omega\tau) \qquad (\gamma' = \gamma), \tag{8.41}$$

the ordinary result for coherent light. The degree of second-order coherence of coherent light is ordinarily equal to unity for all τ, unlike the expression (8.39) obtained for the light scattered in resonance fluorescence. As is clear from Fig. 8.4 the fluorescent light has a degree of second-order coherence that violates the classical inequalities (3.76) and (3.81). The scattered light is antibunched for the qualitative reasons discussed after eqn (7.147).

The second simple limit is that of very large collision broadening when the spectrum contains only the inelastic fluorescent component. The second exponential in eqn (8.38) now decays to zero at much shorter time delays τ than does the first exponential. Thus for τ sufficiently large that the final term can be neglected, eqn (8.38) reduces to

$$g^{(2)}(\tau) = 1-\exp(-2\gamma\tau) \qquad (\gamma' \gg \gamma, \gamma'\tau \gg 1). \tag{8.42}$$

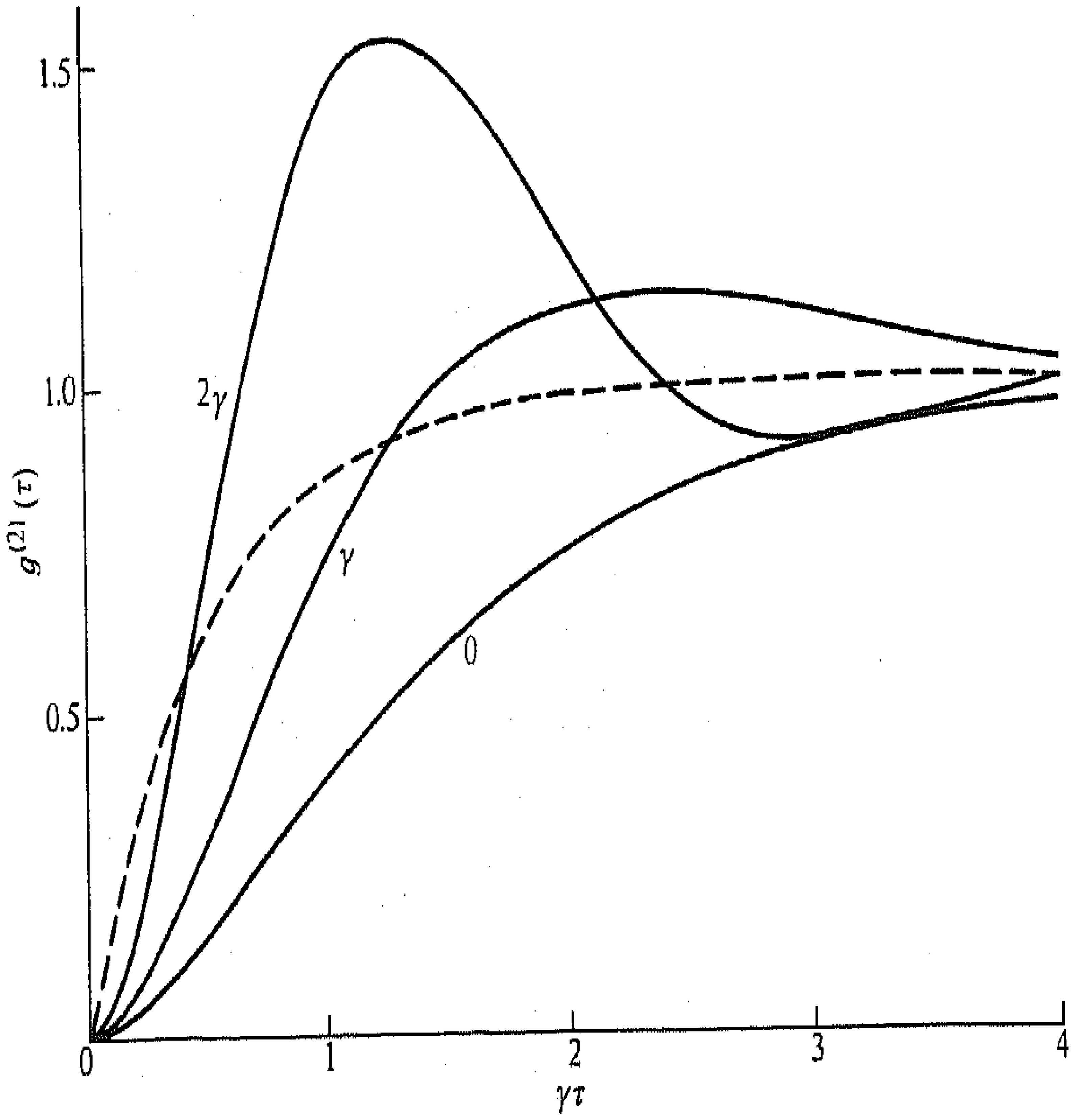

FIG. 8.4. Dependence of the degree of second-order coherence on the time delay τ. Full curves: the weak-beam, zero collision broadening case for values of the detuning $|\omega_0-\omega|$ indicated against the curves. Broken curve: the case of large collision broadening.

The conditions assumed here are those in which the diagonal elements of the atomic density matrix have a time dependence described by rate equations, as discussed in §2.14. The result (8.42), illustrated by the broken curve in Fig. 8.4, is the same as that derived in eqn (7.147) and illustrated in Fig. 7.11. The corresponding degree of first-order coherence obtained from eqn (8.36) is

$$g^{(1)}(\tau) = \exp(-i\omega_0\tau-\gamma'\tau) \qquad (\gamma' \gg \gamma), \tag{8.43}$$

the ordinary result for chaotic light. However, the degree of first-order coherence reduces to zero for the time-scale assumed in eqn (8.42).

The special cases treated in the two previous paragraphs illustrate the general antibunched characteristics of the light emitted by a single atom. They show that the time delay τ needed for the degree of second-order coherence to increase significantly from its zero initial value is of the order of the radiative lifetime of the atomic transition concerned. The experimental observation of antibunched light is discussed in §8.5.

As is explained above, the inelastic conversion of some of the incident photons of frequency ω into scattered photons of different frequencies ω_s depends upon the collisional uncertainty in the atomic excited state energy. Doppler broadening results from the thermal distribution of atomic velocities, and it causes no additional uncertainty in the energy of a particular atom with a given velocity. The Doppler effect changes the spectral distribution of the inelastically-scattered light but it does not affect its total strength. We ignore the effect of Doppler broadening on the inelastic lineshape.

8.4. Exactly-resonant incident beam

It is assumed throughout the present section that the frequency ω of the incident beam equals the atomic transition frequency ω_0. The optical Bloch equations can be solved analytically in this zero-detuning case. However, a great simplification in the solutions occurs if the collision broadening is ignored, so we also set $\gamma' = \gamma$ throughout the section. Then eqns (8.24) and (8.25) give

$$\frac{\bar{I}_s^{\text{coherent}}}{\bar{I}_s} = |g^{(1)}(\infty)| = \frac{2\gamma^2}{2\gamma^2+\mathscr{V}^2}. \tag{8.44}$$

The coherent fraction of the scattered light depends solely on the strength of the incident light. The calculations that follow are concerned with the ways in which the scattered spectrum and the detailed coherence properties vary with incident beam strength.

The optical Bloch equations (8.12) and (8.13) in the limit of zero collision broadening and zero detuning are partially solved in eqn (2.126). It is not difficult to obtain the corresponding solution for the off-diagonal density matrix elements.

Problem 8.3. Show that solution of the optical Bloch equations for the case $\gamma' = \gamma$ and $\omega=\omega_0$ gives an off-diagonal element of the form shown in eqn (7.127) with

$$\begin{aligned}\alpha_1(\tau) = \frac{i\mathscr{V}}{2\gamma^2+\mathscr{V}^2}\Big\{\gamma-\frac{\exp(-3\gamma\tau/2)}{16i\lambda}\\ \times[(4(\gamma+i\lambda)^2-\gamma^2)\exp(i\lambda\tau)\\ -(4(\gamma-i\lambda)^2-\gamma^2)\exp(-i\lambda\tau)]\Big\}\end{aligned} \tag{8.45}$$

and

$$\alpha_2(\tau) = \tfrac{1}{2}\exp(-\gamma\tau) \tag{8.46}$$

$$+\frac{\exp(-3\gamma\tau/2)}{8i\lambda}\{(\gamma+2i\lambda)\exp(i\lambda\tau)-(\gamma-2i\lambda)\exp(-i\lambda\tau)\}$$

where

$$\lambda = (\mathscr{V}^2-\tfrac{1}{4}\gamma^2)^{\frac{1}{2}}. \tag{8.47}$$

The coefficient $\beta_1(\tau)$ in the diagonal element (7.128) is given by the entire expression (2.126).

The degree of first-order coherence given by eqn (7.139) is[8]

$$g^{(1)}(\tau) = \exp(-\mathrm{i}\omega\tau)\left\{\frac{2\gamma^2}{2\gamma^2+\mathscr{V}^2}+\frac{1}{2}\exp(-\gamma\tau)\right.$$
$$\left.+\frac{(\gamma-2\mathrm{i}\lambda)^2\exp[-\mathrm{i}\lambda\tau-(3\gamma\tau/2)]}{8\mathrm{i}\lambda(3\gamma+2\mathrm{i}\lambda)}+(\lambda\to-\lambda)\right\}, \qquad (8.48)$$

where the fourth term in the large bracket is the same as the third term with the sign of λ reversed. The spectrum given by eqn (8.28) is then[2]

$$F(\omega_s) = \frac{2\gamma^2}{2\gamma^2+\mathscr{V}^2}\,\delta(\omega_s-\omega)+\frac{\gamma/2\pi}{(\omega-\omega_s)^2+\gamma^2}$$
$$+\frac{3\gamma\lambda(\mathscr{V}^2-2\gamma^2)+\gamma(5\mathscr{V}^2-2\gamma^2)(\omega+\lambda-\omega_s)}{8\pi\lambda(2\gamma^2+\mathscr{V}^2)[(\omega+\lambda-\omega_s)^2+(3\gamma/2)^2]}$$
$$+(\lambda\to-\lambda) \qquad \text{for} \qquad \mathscr{V} > \tfrac{1}{2}\gamma. \qquad (8.49)$$

We do not write down the detailed expression for the spectrum for weaker incident beams where $\mathscr{V} < \frac{1}{2}\gamma$ and λ is purely imaginary. However, it is seen from the form of eqn (8.48) that in this case the spectrum consists of the usual elastic contribution together with three inelastic Lorentzian components all centred on the frequency ω. For very weak incident beams, $\mathscr{V} \ll \frac{1}{2}\gamma$, the results of the previous section apply, and with the zero collision broadening assumed here, there remains only the elastic delta-function contribution in eqn (8.37).

The main interest in the results for an exactly-resonant beam lies in the region of strong beams, where the spectrum (8.49) applies. The four contributions consist of an elastic delta-function peak at $\omega_s = \omega$ and three inelastic Lorentzian-type contributions centred on the frequencies $\omega_s = \omega$, $\omega+\lambda$, and $\omega-\lambda$ respectively. The degree of first-order coherence (8.48) correspondingly consists of the sum of a contribution with the usual coherent time dependence and three contributions with chaotic-light time dependences. Fig. 8.5 shows how the central frequencies of the Lorentzians vary with the Rabi frequency $\mathscr{V}$, proportional to the electric field of the incident beam. For $\mathscr{V} > \gamma$, the separations between the three frequencies are very close to $\mathscr{V}$. The integrated strengths of the four contributions in eqn (8.49) are respectively

$$\frac{2\gamma^2}{2\gamma^2+\mathscr{V}^2},\ \frac{1}{2},\ \frac{\mathscr{V}^2-2\gamma^2}{4(2\gamma^2+\mathscr{V}^2)},\ \frac{\mathscr{V}^2-2\gamma^2}{4(2\gamma^2+\mathscr{V}^2)}; \qquad (8.50)$$

these quantities add to give unity in accordance with eqn (8.29).

The spectral contributions in eqn (8.49) overlap to give a complicated dependence on frequency ω_s when $\mathscr{V}$ is only a little larger than $\frac{1}{2}\gamma$. The spectrum takes on a much simpler form for very large $\mathscr{V}$ when the elastic Rayleigh contribution is negligible and the inelastic contributions reduce to

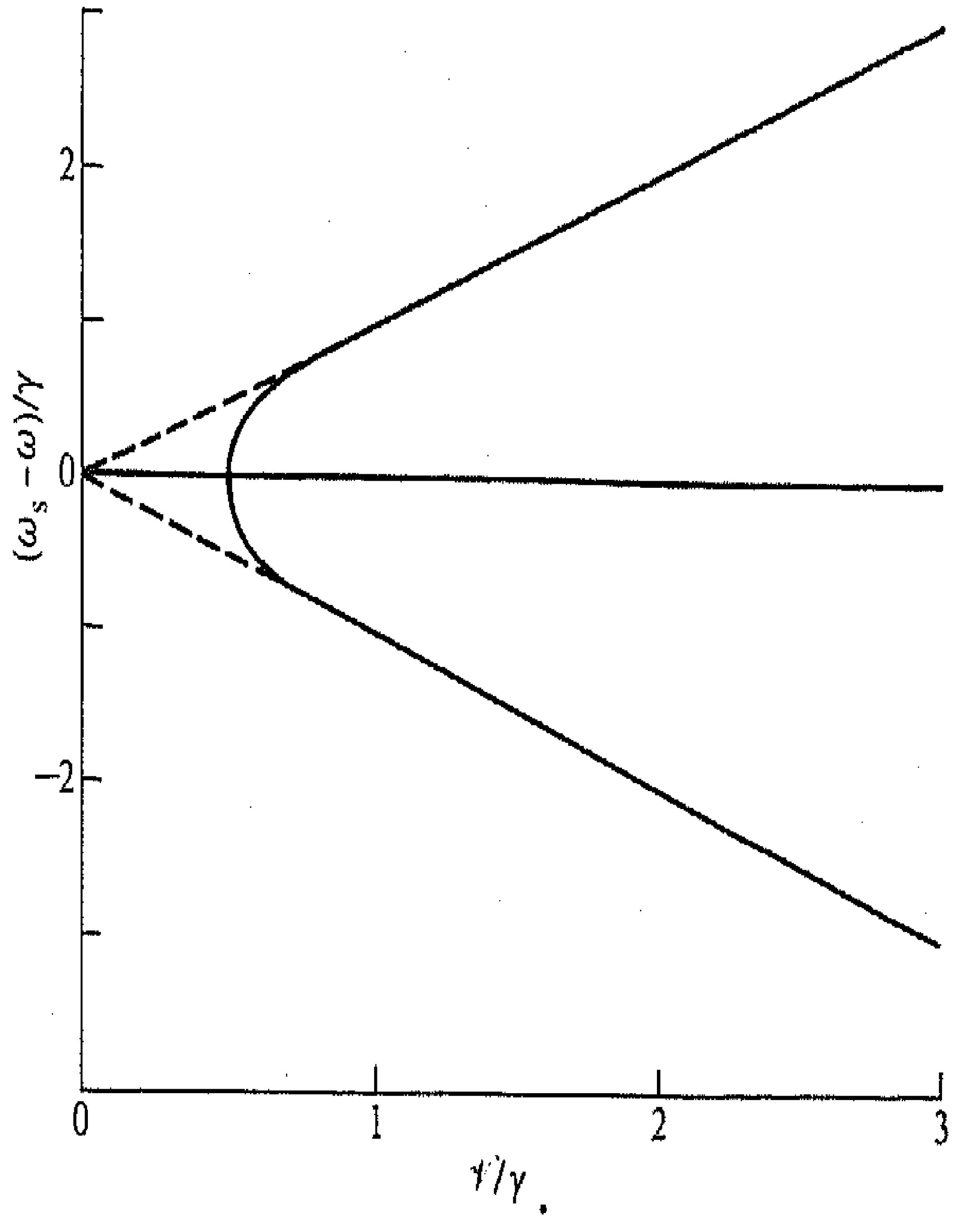

FIG. 8.5. Variation with Rabi frequency $\mathscr{V}$ of the central frequencies of the inelastic spectral lines.

$$F(\omega_s) = \frac{3\gamma/8\pi}{(\omega-\mathscr{V}-\omega_s)^2+(3\gamma/2)^2}+\frac{\gamma/2\pi}{(\omega-\omega_s)^2+\gamma^2}+\frac{3\gamma/8\pi}{(\omega+\mathscr{V}-\omega_s)^2+(3\gamma/2)^2}, \qquad (8.51)$$

now written in order of ascending central frequency. The three peaks have integrated strengths of $\frac{1}{4}$, $\frac{1}{2}$, and $\frac{1}{4}$, and radiative linewidths of 3γ, 2γ, and 3γ respectively. Fig. 8.6(a) shows the spectrum of scattered light predicted by eqn (8.51) for the case $\mathscr{V} = 15{\cdot}6\gamma$ and Fig. 8.6(b) shows a measured spectrum[9] for the appropriate strength of incident light beam. The experiment utilized sodium-atom energy levels from the $3^2S_{\frac{1}{2}}$ ground state and $3^2P_{\frac{3}{2}}$ excited state in such a way that two-level theory is valid for interpretation of the results.

The occurrence of triple-peaked spectra in the light scattered by a two-level atom at high incident intensities can be understood qualitatively[8,10] in terms of the dynamic Stark splitting mentioned in §2.7. Consider a state of the coupled atom and incident radiation field in which $n+1$ quanta are excited. There are two possible states of this kind; either the atom is in its ground state and $n+1$ photons are present, or the atom is in its excited state and n photons are present. The coupled system oscillates between the two states in the manner shown in Fig. 2.5. In terms of stationary states, the effect of the

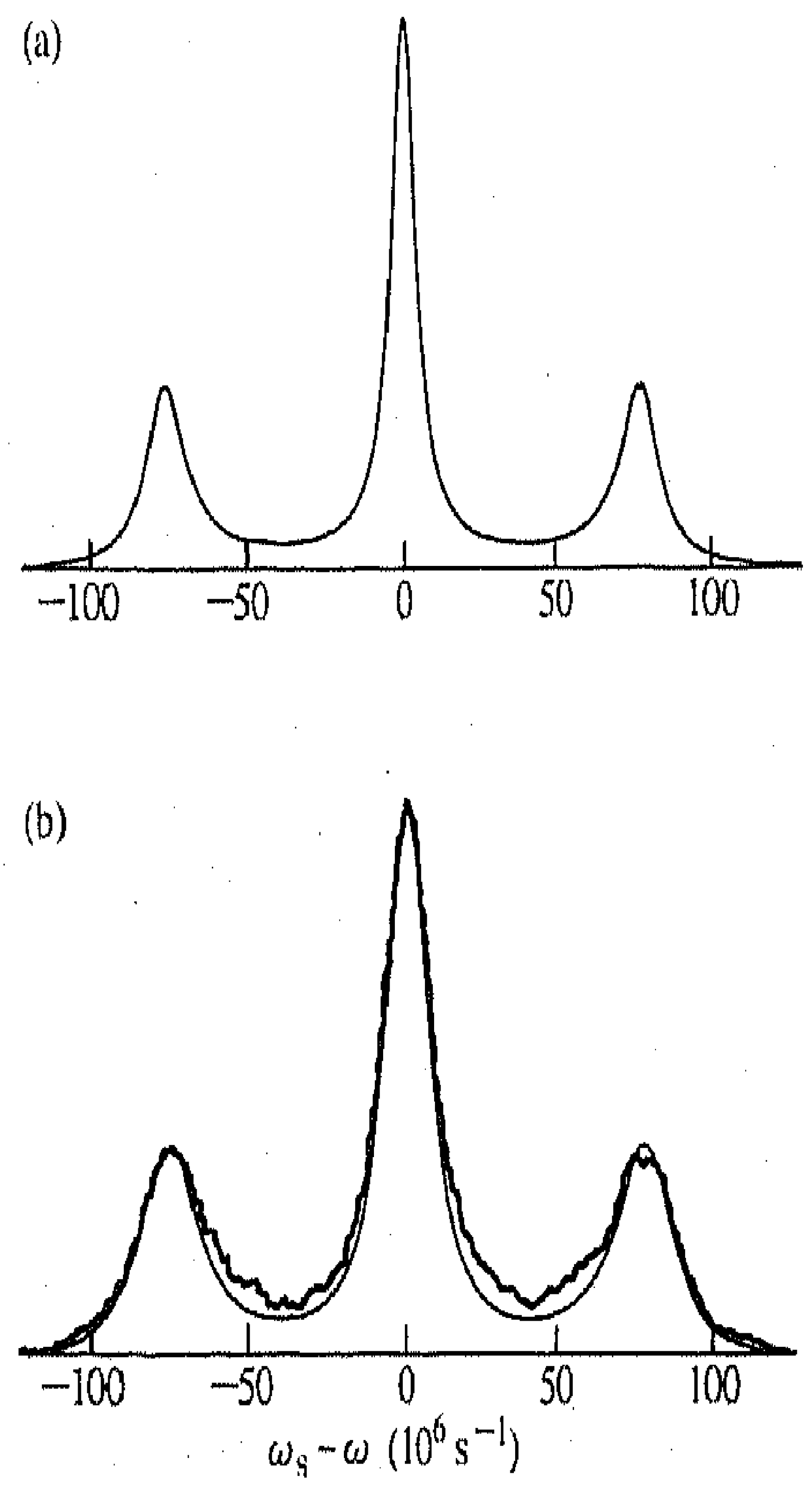

FIG. 8.6. Resonance fluorescence spectrum of Na for the transition between the levels $3^2S_{\frac{1}{2}}$ (F = 2, m_F = 2) and $3^2P_{\frac{3}{2}}$(F = 3, m_F = 3) with $\mathscr{V} = 7.8\times10^7\,\mathrm{s}^{-1}$ and $\gamma = 5\times10^6\,\mathrm{s}^{-1}$ showing (a) theory and (b) the experiment compared to a convolution of the instrumental response with the theoretical lineshape. (After R. E. Grove *et al.*, ref. 9.)

coupling is to split the two $n+1$ quantum states by an energy $\hbar\mathscr{V}$, as shown in Fig. 8.7. The n-quantum states are also split in a similar fashion. When the $n+1$-quantum states decay into n-quantum states by fluorescent emission of a photon into the scattered beam, the four downward transitions indicated in the figure occur. There are clearly three distinct transition frequencies separated by the Rabi frequency $\mathscr{V}$, and the intensity of the central peak acquires contributions from two kinds of transition, thus gaining twice the strength of the outer peaks.

The degree of second-order coherence of the scattered light obtained from eqns (2.126) and (7.140) is[8]

$$g^{(2)}(\tau) = 1-[\cos\lambda\tau+(3\gamma/2\lambda)\sin\lambda\tau]\exp(-3\gamma\tau/2). \qquad (8.52)$$

This expression reduces to eqn (8.40) in the limit of a weak incident beam, where the degree of second-order coherence shows a monotonic increase from 0 to 1 as τ increases from 0 to ∞. For $\mathscr{V}$ greater than $\frac{1}{2}\gamma$, where λ is real, the degree of second-order coherence shows an oscillatory dependence on τ. Fig. 8.8 shows the dependence of the degree of second-order coherence on time delay for $\mathscr{V} = 5\gamma$ and for $\mathscr{V}$ very much smaller than γ, where the curve repeats

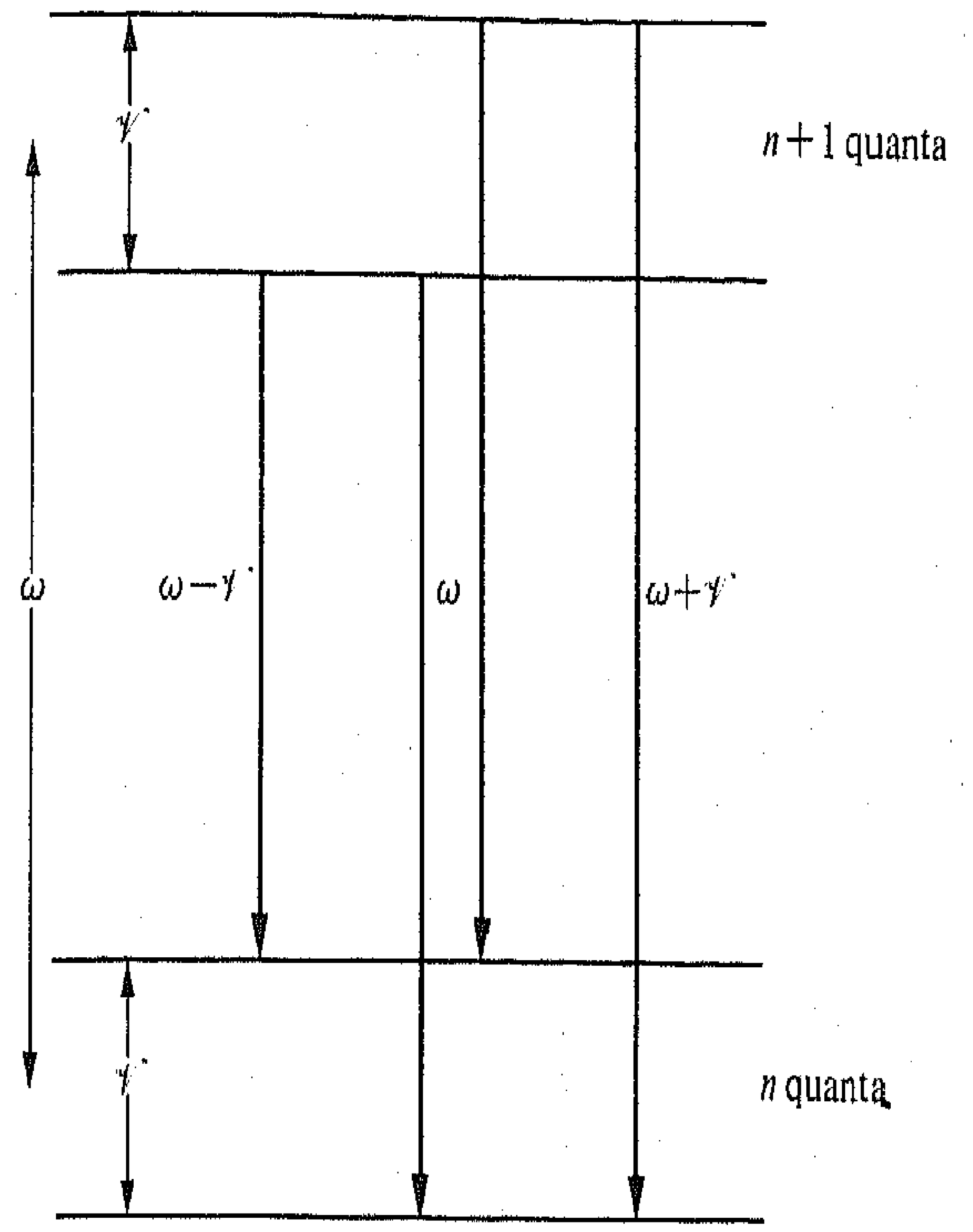

FIG. 8.7. Illustration of the formation of a three-peaked emission spectrum by radiative decay between atomic levels split by the dynamic Stark effect.

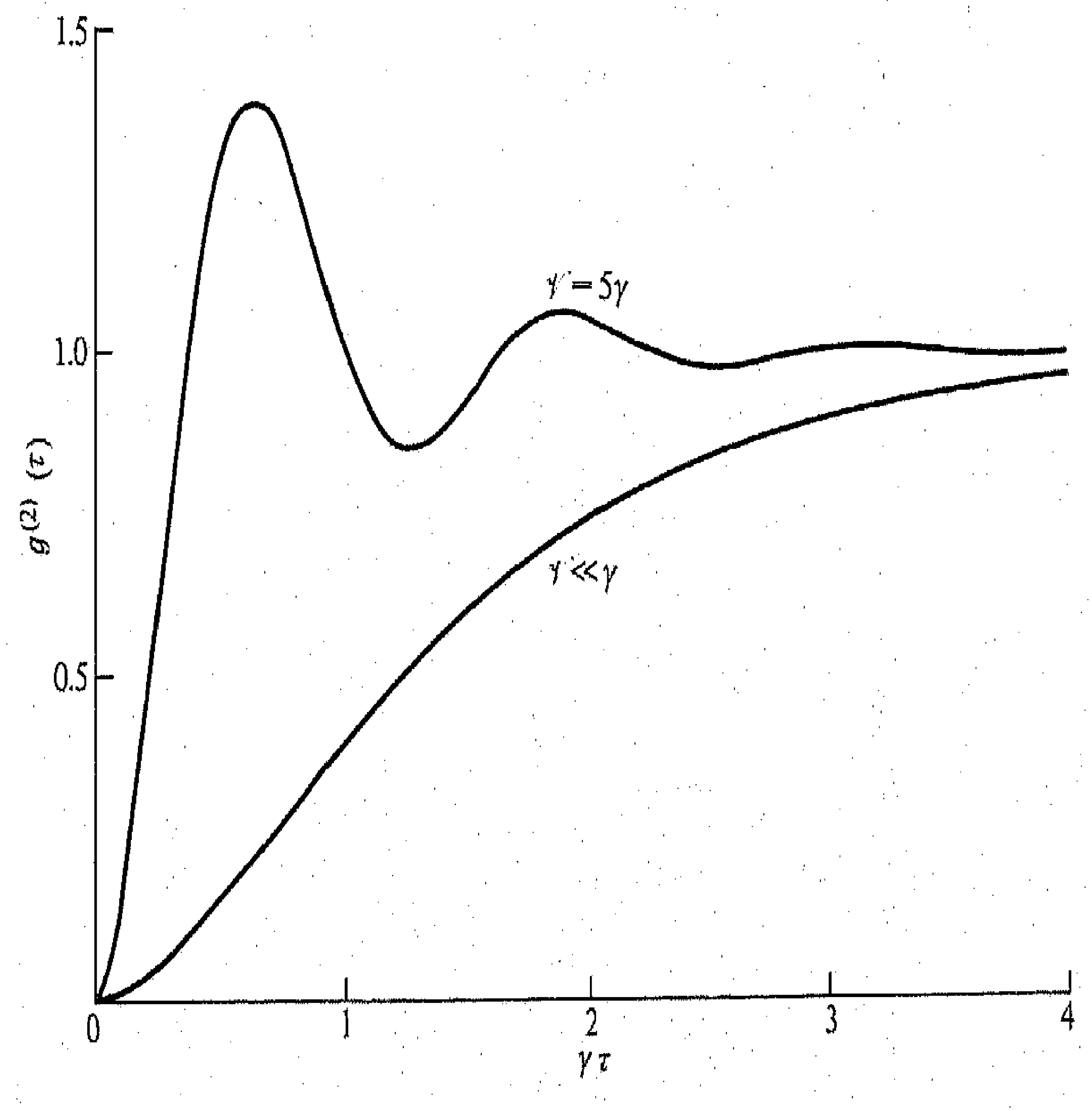

FIG. 8.8. Dependence of the degree of second-order coherence on the time delay τ for zero detuning, zero collision broadening, and the values of Rabi frequency indicated.

the zero-detuning trace in Fig. 8.4. The degree of second-order coherence again violates the classical inequalities, and the scattered light is antibunched. There exist measurements of the degree of second-order coherence for light emitted in resonance fluorescence but before comparing experiment with theory it is necessary to consider the effects of combining the emissions from several atoms.

8.5. Multiatom resonance fluorescence

The preceding sections give a detailed account of the properties of the light scattered by a single atom in conditions of resonance between the frequency of the incident light and an atomic transition. It is not usually feasible to make observations of resonance fluorescence by a single atom. A common experimental arrangement uses an atomic beam sent at right angles through the beam of incident light, and the scattered light is collected in the third mutually perpendicular direction. The number of atoms simultaneously in the observation region depends upon the strength of the atomic beam, and the number fluctuates because of nonuniformities in the atomic density.

Suppose first that scattered light is collected from a fixed number ν of atoms. The effect on the degrees of coherence of the superposition of light from several different atoms is considered in Chapter 3 and a very similar discussion applies here. The relative phases of the light waves from different atoms are randomly distributed and in all electric-field correlation functions, only those terms contribute where pairs of field operators $\hat{E}_i^-$ and $\hat{E}_i^+$ for the same atom i appear multiplied together. Thus analogous to eqns (3.18) and (3.88) we have

$$\langle \hat{E}^-(t)\hat{E}^+(t+\tau)\rangle = \nu\langle \hat{E}_i^-(t)\hat{E}_i^+(t+\tau)\rangle \tag{8.53}$$

and

$$\begin{aligned}\langle \hat{E}^-(t)\hat{E}^-(t+\tau)\hat{E}^+(t+\tau)\hat{E}^+(t)\rangle &= \nu\langle \hat{E}_i^-(t)\hat{E}_i^-(t+\tau)\hat{E}_i^+(t+\tau)\hat{E}_i^+(t)\rangle \\ &\quad + \nu(\nu-1)\{\langle \hat{E}_i^-(t)\hat{E}_i^+(t)\rangle^2 + |\langle \hat{E}_i^-(t)\hat{E}_i^+(t+\tau)\rangle|^2\}. \end{aligned}\tag{8.54}$$

The degrees of coherence of the combined emission from the ν atoms are defined as in eqns (7.118) and (7.119), where the field correlation functions are now the quantities on the left-hand sides of the above pair of equations. If the small letter g is retained for the single-atom degrees of coherence but the capital letter G is used for the ν-atom degrees of coherence, the connections obtained from eqns (8.53) and (8.54) are[11,12]

$$G^{(1)}(\tau) = g^{(1)}(\tau) \tag{8.55}$$

$$G^{(2)}(\tau) = \{g^{(2)}(\tau) + (\nu-1)(1+|g^{(1)}(\tau)|^2)\}/\nu. \tag{8.56}$$

The degree of first-order coherence, and hence also the spectral properties of the scattered light, are unchanged by the superposition and the results of the preceding sections remain valid. It is however necessary to consider the modifications of the degree of second-order coherence described by eqn (8.56).

Some limiting values of the ν-atom degree of second-order coherence are easily found. Thus eqns (8.26) and (8.27) give

$$G^{(2)}(0) = 2(\nu-1)/\nu; \tag{8.57}$$

the classical inequality (3.76) is no longer violated when the fluorescence of two or more atoms is observed simultaneously, and the antibunched property of the single-atom fluorescent light is removed. In the limit of a long time delay eqn (8.27) gives

$$G^{(2)}(\infty) = 1 + [(\nu-1)/\nu]|g^{(1)}(\infty)|^2. \tag{8.58}$$

If the collision broadening and the incident beam intensity are sufficiently small to make $|g^{(1)}(\infty)|$ given by eqns (8.24) and (8.25) close to its maximum value of unity, then for a small number of atoms $G^{(2)}(\infty)$ is larger than $G^{(2)}(0)$ in violation of the inequality (3.81).

In the limit of a large number of atoms, $\nu \gg 1$, eqn (8.56) reduces with the use of eqn (8.55) to

$$G^{(2)}(\tau) = 1 + |G^{(1)}(\tau)|^2 \qquad (\nu \gg 1). \tag{8.59}$$

This is similar to the relation (3.90) between the degrees of first and second-order coherence of chaotic light, but eqn (8.59) applies in the present calculation irrespective of the nature of the scattered light. It gives

$$G^{(2)}(0) = 2 \qquad (\nu \gg 1) \tag{8.60}$$

for all values of the parameters. Its time dependence is illustrated by the example of a weak incident beam, where the degree of first-order coherence is given by eqn (8.36). If there is no collision broadening, then eqn (8.41) applies and

$$G^{(2)}(\tau) = 2 \qquad (\nu \gg 1, \mathscr{V} \ll \gamma, \gamma' = \gamma). \tag{8.61}$$

The scattered light in this case resembles a superposition, with random phases, of the coherent elastic Rayleigh contributions of the individual atoms, similar to the light considered in problems 3.1 and 3.6. If the collision broadening is large, then eqn (8.43) applies and

$$G^{(2)}(\tau) = 1 + \exp(-2\gamma'\tau) \qquad (\nu \gg 1, \mathscr{V} \ll \gamma, \gamma' \gg \gamma). \tag{8.62}$$

This is the normal result (3.94) for chaotic light, and it is totally different from the single-atom degree of second-order coherence given by eqn (8.42).

For an atomic beam experiment where the number of observed atoms fluctuates randomly about some mean number $\bar{\nu}$, it is necessary to average the field correlation functions (8.53) and (8.54) over a Poisson distribution in ν.[11,12] Rearrangement of eqn (8.7) shows that the second factorial moment of the distribution, required for eqn (8.54), is

$$\overline{\nu(\nu-1)} = \bar{\nu}^2. \tag{8.63}$$

Thus eqn (8.56) is replaced by an averaged degree of second-order coherence

$$\bar{G}^{(2)}(\tau) = \left(g^{(2)}(\tau)/\bar{\nu}\right) + 1 + |g^{(1)}(\tau)|^2, \tag{8.64}$$

with limiting values

$$\bar{G}^{(2)}(0) = 2 \tag{8.65}$$

and

$$\bar{G}^{(2)}(\infty) = (1/\bar{\nu}) + 1 + |g^{(1)}(\infty)|^2. \tag{8.66}$$

In view of eqn (8.65) there is no possibility of obtaining antibunched light from scattering by a fluctuating number of atoms. It is however possible to have $\bar{G}^{(2)}(\infty)$ larger than 2 for a sufficiently small mean number of atoms, thus violating the classical inequality (3.81).

The complete time dependence of the degree of second-order coherence in an atomic beam experiment is obtained by substituting the appropriate single-atom degrees of coherence, for example the weak-beam expressions (8.36) and (8.38) or the zero-detuning results (8.48) and (8.52), into eqn (8.64). The resulting expressions are complicated and we do not write them down. In addition, the comparison of theory with experiment requires further development of the theory, to include for example spatial coherence effects, and the effects of the finite transit time of the atoms in the beam across the observation region.[12] With all these aspects taken into account, it is possible to extract $g^{(2)}(\tau)$ from experimental data by fitting the more sophisticated version of eqn (8.64) to the measured degree of second-order coherence. Fig. 8.9 shows some single-atom degrees of second-order coherence determined in this way.[12-14] The experiment used the same pair of sodium energy levels as the spectral measurements shown in Fig. 8.6. The measured data in Fig. 8.9 refer to zero detuning and the theoretical curves are plotted from eqn (8.52). There is excellent agreement between theory and experiment; the single-atom degree of second-order coherence has all the properties predicted by the quantum theory of light, including the photon antibunching inherent in its zero value at zero time delay. The experiments also studied the resonance fluorescence for nonzero values of the detuning where there is a similarly good agreement with theoretical expressions[15] more general than those derived in the present treatment.

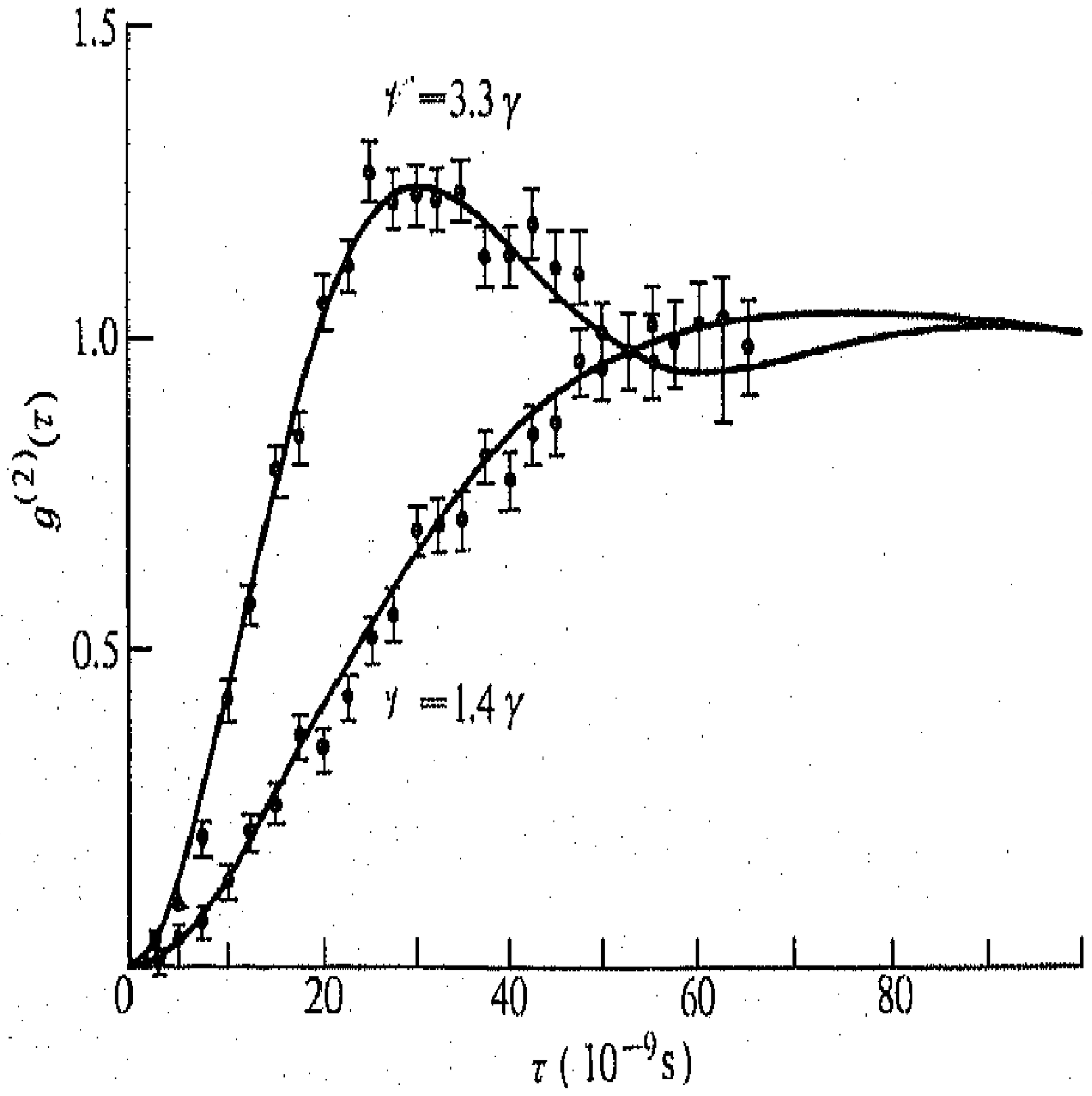

FIG. 8.9. Measured and theoretical time dependences of the degree of second-order coherence of the light scattered by a single sodium atom for zero detuning and two strengths of incident beam. (After M. Dagenais and L. Mandel, ref. 14.)

8.6. The Kramers–Heisenberg formula

The differential cross-section for light scattering into all modes by a single two-level atom is given by eqn (8.20). The spectral and coherence properties of the scattered light are discussed in some detail in the intervening sections. We now consider a more realistic model of the scattering atoms in which the theory allows for an unlimited number of atomic energy levels. It is however necessary to simplify other aspects of the model in order to keep the treatment reasonably compact. The incident beam is therefore assumed to be weak, with $\mathscr{V} \ll \gamma$, and the collision broadening is henceforth ignored. The two-level atom scattering derived above is extremely simple in this case, with all of the scattered intensity emitted in the elastic Rayleigh component with its frequency ω_s equal to the incident frequency ω. The treatment given below derives the total strengths of the various components in the scattered light but does not obtain their detailed spectral distributions or coherence properties. The required information is provided by transition rate theory and it is not necessary here to generalize the Bloch-equation method to multilevel atoms.

The scattering cross-section for a multilevel atom is therefore calculated by time-dependent perturbation theory. We need the transition rate for a process in which an incident photon is destroyed and a scattered photon is created. The leading terms in the multipole expansion of the atom–radiation interaction $\mathscr{H}_I$ are given by eqn (5.39) and the subsequent equations. We make the electric-dipole approximation and neglect $\mathscr{H}_{EQ}$, $\mathscr{H}_{MD}$ and terms of higher order in a_0k. The electric-dipole interaction $\mathscr{H}_{ED}$ is given by eqn (5.40) and it causes the scattering of light in second order. The nonlinear interaction $\mathscr{H}_{NL}$ given by eqn (5.46) is of second order in the photon creation and destruction operators. It therefore produces scattering of light in the first order of time-dependent perturbation theory and we retain it for the moment, although we shall show that its contribution is negligible. The interaction Hamiltonian for light scattering is thus

$$\mathscr{H}_I = \mathscr{H}_{ED} + \mathscr{H}_{NL} = e\mathbf{D}.\hat{\mathbf{E}}_T(0) + (e^2/8m)\sum_j(\mathbf{r}_j \times \hat{\mathbf{B}}(0))^2, \tag{8.67}$$

where $\mathbf{D}$ is the sum of the electron coordinates defined in eqn (5.13).

The geometry of the scattering process is shown in Fig. 8.2. The initial quantum-mechanical state consists of photons of fixed frequency ω and wavevector **k** incident on the atom. The scattering can convert the initial state into a range of possible final states in which an incident photon has been replaced by a scattered photon of frequency ω_s and wavevector $\mathbf{k}_s$. The initial photon state is thus converted to the final state by a product of the photon operators $\hat{a}_{\mathbf{k}}$ and $\hat{a}^{\dagger}_{\mathbf{k}_s}$ or, in a briefer notation, $\hat{a}$ and $\hat{a}^{\dagger}_s$. Scattering experiments generally use a laser source for the incident light beam, which can thus be represented by a single-mode excitation. The frequencies ω_s present in the scattered light emerge from the quantum-mechanical calculation, which includes both elastic and inelastic scattering.

The atom is assumed to be in its ground state $|1\rangle$ at the beginning of the scattering event and is left in some state $|f\rangle$ at the end of the scattering. The atomic ground-state is taken as the zero of energy and the final-state energy of the atom is denoted $\hbar\omega_f$. It is convenient to assume that a given number n of photons ω are present before the scattering event. Any practical beam of light contains a statistical distribution of photon numbers, which could be represented by a density-matrix description of the incident beam. However the characteristics of the cross-section derived below are independent of the photon distribution. The effects of the coherence properties of the incident light on stimulated Raman scattering and other nonlinear optical processes are discussed in Chapter 9.

The transition rate for the scattering is obtained by an adaptation of eqn (5.151) to the present problem where different parts of $\mathscr{H}_I$ contribute to the first-and second-order terms,

$$\frac{1}{\tau}=\frac{2\pi}{\hbar^2}\sum_f\sum_{\mathbf{k}_s}\left|\langle n-1,1,f|\hat{\mathscr{H}}_{\mathrm{NL}}|n,0,1\rangle\right.$$
$$\left.+\frac{1}{\hbar}\sum_l\frac{\langle n-1,1,f|\hat{\mathscr{H}}_{\mathrm{ED}}|l\rangle\langle l|\hat{\mathscr{H}}_{\mathrm{ED}}|n,0,1\rangle}{n\omega-\omega_l}\right|^2\delta(\omega-\omega_s-\omega_f). \quad (8.68)$$

The first, second, and third entries in the bras and kets for the initial and final states refer to the photons **k**, the photons $\mathbf{k}_s$, and the atomic state, respectively. The l summation runs over all states of the combined atom and radiation systems. The sum over final states in front of the square modulus now takes separate account of the possible atomic states f and scattered photons $\mathbf{k}_s$.

The contributions to the scattering matrix element are shown diagrammatically in Fig. 8.10. The conventions of the diagrams are the same as in Fig. 5.1. Diagram (a) shows the contribution of the first term in the square modulus of eqn (8.68). The single interaction $\hat{\mathscr{H}}_{\mathrm{NL}}$ destroys a photon **k** and creates a photon $\mathbf{k}_s$, in accordance with its second-order character.

The second term in the square modulus of eqn (8.68) generates two contributions, which differ in the type of intermediate state $|l\rangle$. The photon operators $\hat{a}$ and $\hat{a}^{\dagger}_s$ must be chosen one each from the two appearances of $\hat{\mathscr{H}}_{\mathrm{ED}}$ in this term, the explicit form of $\hat{\mathscr{H}}_{\mathrm{ED}}$ being given in eqn (5.114). There are clearly two possibilities; one of them produces the operators in the order $\hat{a}^{\dagger}_s\hat{a}$ and is represented by diagram (b) in Fig. 8.10; the other choice produces the operators in the order $\hat{a}\hat{a}^{\dagger}_s$ and is represented by diagram (c) in the figure. The intermediate atomic state is denoted $|i\rangle$; its energy is $\hbar\omega_i$. Diagram (c) of Fig. 8.10 is a combination of diagrams (a) and (d) of Fig. 5.1; these diagrams separately cannot represent energy-conserving processes, but it is possible for their combination to conserve energy. The second term in the square modulus of eqn (8.68) is written more explicitly as

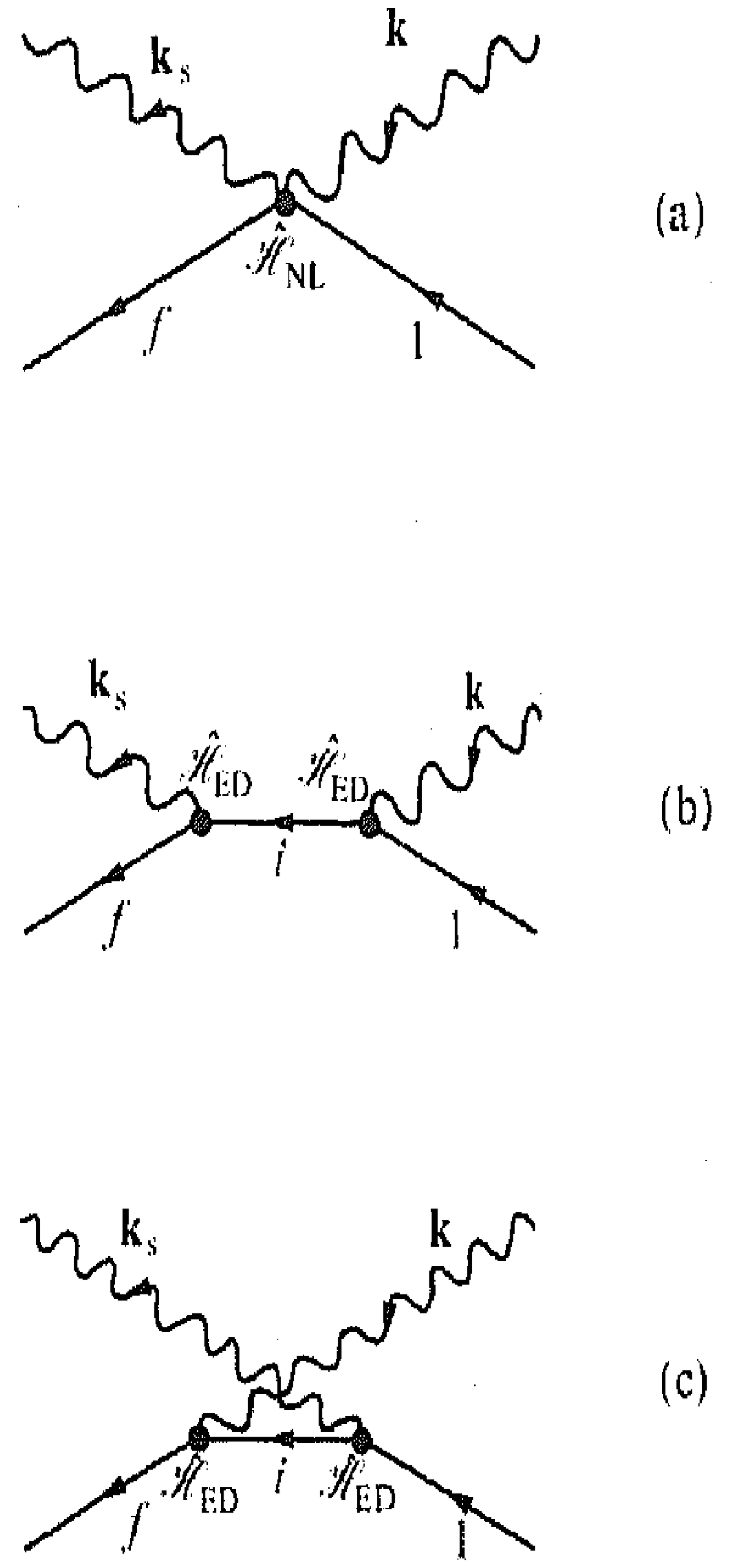
$\mathbf{k}_s$
$\mathbf{k}$
$\hat{\mathscr{H}}_{\mathrm{NL}}$
f
1
(a)
$\mathbf{k}_s$
$\mathbf{k}$
$\hat{\mathscr{H}}_{\mathrm{ED}}$
$\hat{\mathscr{H}}_{\mathrm{ED}}$
i
f
1
(b)
$\mathbf{k}_s$
$\mathbf{k}$
$\hat{\mathscr{H}}_{\mathrm{ED}}$
i
$\hat{\mathscr{H}}_{\mathrm{ED}}$
f
1
(c)

FIG. 8.10. Diagrammatic representations of the three kinds of interaction that contribute to light scattering. It is shown in the text that the contribution of the nonlinear interaction in diagram (a) is negligible.

$$\frac{1}{\hbar}\sum_i\left\{\frac{\langle n-1,1,f|\hat{\mathscr{H}}_{\mathrm{ED}}|n-1,0,i\rangle\langle n-1,0,i|\hat{\mathscr{H}}_{\mathrm{ED}}|n,0,1\rangle}{\omega-\omega_i}\right.$$
$$\left.+\frac{\langle n-1,1,f|\hat{\mathscr{H}}_{\mathrm{ED}}|n,1,i\rangle\langle n,1,i|\hat{\mathscr{H}}_{\mathrm{ED}}|n,0,1\rangle}{-\omega_s-\omega_i}\right\}. \quad (8.69)$$

The relative magnitudes of the contributions of the three diagrams can now be evaluated. Since the expectation value of $\hat{B}^2$ is the same as that of $\hat{E}^2_{\mathrm{T}}/c^2$ in free space, and all the contributions contain e^2 and matrix elements of

$\mathbf{r}_j$ squared, the main differences arise from the energy denominators, respectively, $8mc^2$, $\hbar\omega-\hbar\omega_i$, and $-\hbar\omega_s-\hbar\omega_i$. Now $8mc^2$ is of order 6×10^{-13} J, whereas the atomic and photon energies for scattering of light are typically in the range 10^{-18}–10^{-19} J. The contribution of the first term in the square modulus of eqn (8.68) is, therefore, entirely negligible. The remaining two energy denominators differ considerably when ω and ω_i are close in value, but they have the same order of magnitude in general, and both the terms in eqn (8.69) must be retained.

The transition rate (eqn (8.68)) can be simplified by omission of the nonlinear term, insertion of eqn (8.69) for the second-order contribution, and use of eqn (5.114) to evaluate the matrix elements of $\hat{\mathscr{H}}_{\mathrm{ED}}$,

$$\frac{1}{\tau} = \sum_f\sum_{\mathbf{k}_s}\frac{\pi e^4\omega\omega_s n}{2\epsilon_0^2\hbar^2V^2}\left|\sum_i\left(\frac{\boldsymbol{\varepsilon}_s.\mathbf{D}_{fi}\boldsymbol{\varepsilon}.\mathbf{D}_{i1}}{\omega_i-\omega}+\frac{\boldsymbol{\varepsilon}.\mathbf{D}_{fi}\boldsymbol{\varepsilon}_s.\mathbf{D}_{i1}}{\omega_i+\omega_s}\right)\right|^2\delta(\omega-\omega_s-\omega_f). \quad (8.70)$$

Here $\boldsymbol{\varepsilon}$ and $\boldsymbol{\varepsilon}_s$ are again the unit polarization vectors of the incident and scattered photons.

The transition rate is converted to a cross-section by the procedure used in eqn (5.93) for the photoelectric emission. In addition, the summation over $\mathbf{k}_s$ can be converted to an integration,

$$\sum_{\mathbf{k}_s}\to(V/(2\pi)^3)\iint k_s^2\,\mathrm{d}k_s\,\mathrm{d}\Omega = (V/(2\pi)^3)\iint(\omega_s^2/c^3)\,\mathrm{d}\omega_s\,\mathrm{d}\Omega, \quad (8.71)$$

similar to eqn (5.91). Note that the transition rate (eqn (8.70)) refers to a scattered photon of given polarization $\boldsymbol{\varepsilon}_s$ and that eqn (8.71) accordingly takes account of a single polarization.

The resulting differential cross-section is

$$\frac{\mathrm{d}\sigma}{\mathrm{d}\Omega} = \sum_f^{\omega_f<\omega}\frac{e^4\omega(\omega-\omega_f)^3}{16\pi^2\epsilon_0^2\hbar^2c^4}\left|\sum_i\left(\frac{\boldsymbol{\varepsilon}_s.\mathbf{D}_{fi}\boldsymbol{\varepsilon}.\mathbf{D}_{i1}}{\omega_i-\omega}+\frac{\boldsymbol{\varepsilon}.\mathbf{D}_{fi}\boldsymbol{\varepsilon}_s.\mathbf{D}_{i1}}{\omega_i-\omega_f+\omega}\right)\right|^2. \quad (8.72)$$

The summation over f is restricted because the delta function in eqn (8.70) can be satisfied only for atomic final states whose excitation energy is smaller than $\hbar\omega$. The complete differential cross-section is obtained by adding the contributions of the two independent photon polarizations.

Eqn (8.72) is the Kramers–Heisenberg formula for the differential cross-section. It is the basic expression of quantum-mechanical scattering theory. The cross-section includes both elastic Rayleigh scattering, corresponding to the case $f = 1$, $\omega_f = 0$, and inelastic Raman scattering, corresponding to all the remaining contributions in the summation over f.

8.7. Elastic Rayleigh Scattering

Consider first the elastic-scattering component, where the atom returns to its ground state $|1\rangle$ at the conclusion of the scattering event. If only this contribution is retained, the differential cross-section shown in eqn (8.72) reduces to

$$\frac{\mathrm{d}\sigma}{\mathrm{d}\Omega} = \frac{e^4\omega^4}{16\pi^2\epsilon_0^2\hbar^2c^4}\left|\sum_i\left(\frac{\boldsymbol{\varepsilon}_s.\mathbf{D}_{1i}\boldsymbol{\varepsilon}.\mathbf{D}_{i1}}{\omega_i-\omega}+\frac{\boldsymbol{\varepsilon}.\mathbf{D}_{1i}\boldsymbol{\varepsilon}_s.\mathbf{D}_{i1}}{\omega_i+\omega}\right)\right|^2. \quad (8.73)$$

It is instructive to obtain the limiting forms of the cross-section for ω very much larger or very much smaller than the atomic excitation frequencies ω_i.

Suppose first that ω is very much larger than all the ω_i. The frequency denominators in eqn (8.73) can be expanded,

$$\frac{1}{\omega_i-\omega} = -\frac{1}{\omega}\left(1+\frac{\omega_i}{\omega}+\ldots\right), \quad (8.74)$$

$$\frac{1}{\omega_i+\omega} = \frac{1}{\omega}\left(1-\frac{\omega_i}{\omega}+\ldots\right). \quad (8.75)$$

The first terms in eqns (8.74) and (8.75) produce a zero contribution when inserted in eqn (8.73), leaving

$$\frac{\mathrm{d}\sigma}{\mathrm{d}\Omega} = \frac{e^4}{16\pi^2\epsilon_0^2\hbar^2c^4}\left|\sum_i\omega_i(\boldsymbol{\varepsilon}_s.\mathbf{D}_{1i}\boldsymbol{\varepsilon}.\mathbf{D}_{i1}+\boldsymbol{\varepsilon}.\mathbf{D}_{1i}\boldsymbol{\varepsilon}_s.\mathbf{D}_{i1})\right|^2 \quad (\omega\gg\omega_i). \quad (8.76)$$

The summation over i corresponds to one of the standard sum rules that can be proved for the energy levels and wavefunctions of any atom.[16] The result is

$$\sum_i\omega_i\boldsymbol{\varepsilon}_s.\mathbf{D}_{1i}\boldsymbol{\varepsilon}.\mathbf{D}_{i1} = (Z\hbar/2m)\boldsymbol{\varepsilon}.\boldsymbol{\varepsilon}_s, \quad (8.77)$$

where Z is the number of electrons bound in the atom, and it converts eqn (8.76) to

$$\mathrm{d}\sigma/\mathrm{d}\Omega = Z^2r_e^2(\boldsymbol{\varepsilon}.\boldsymbol{\varepsilon}_s)^2 \quad (\omega\gg\omega_i), \quad (8.78)$$

where

$$r_e = e^2/4\pi\epsilon_0mc^2. \quad (8.79)$$

This quantity is called the classical electron radius and its magnitude is $2{\cdot}8\times10^{-15}$ m.

The elastic scattering of high-frequency incident light, with differential cross-section given by eqn (8.78), is known as Thomson scattering. The cross-section does not depend upon the atomic wavefunctions or energy levels, and indeed the same result is obtained for scattering by free electrons. Note the proportionality of the cross-section to the *square* of the number of electrons, which contrasts with the *linear* dependence of scattered intensity on the number of scatterers proved in eqn (8.8). It is assumed in using the electric-dipole approximation in the present calculation that the wavelength of the incident light is much larger than the atomic dimensions. The Z electrons on the same atom then radiate with the same phase in the kind of classical calculation made in §8.1 to give a cross-section that is Z^2 times that for a single-electron atom. The theory given here breaks down at incident frequencies so high that the electric-dipole approximation is invalid, and a more comprehensive breakdown occurs when $\hbar\omega$ is comparable to the relativistic rest-mass energy mc^2 of the electrons. A significant amount of energy is then transferred to the electron, and the scattering process becomes inelastic, with a scattered quantum $\hbar\omega_s$ smaller than $\hbar\omega$. Such inelastic scattering of light by free electrons, not considered here, is known as the Compton effect.[17]

Consider now the opposite limit where ω is much smaller than all the atomic excitation frequencies ω_i, and the elastic differential cross-section (eqn (8.73)) becomes

$$\frac{\mathrm{d}\sigma}{\mathrm{d}\Omega} = \frac{e^4\omega^4}{16\pi^2\epsilon_0^2\hbar^2c^4}\left|\sum_i \frac{1}{\omega_i}(\boldsymbol{\varepsilon}_s.\mathbf{D}_{1i}\boldsymbol{\varepsilon}.\mathbf{D}_{i1}+\boldsymbol{\varepsilon}.\mathbf{D}_{1i}\boldsymbol{\varepsilon}_s.\mathbf{D}_{i1})\right|^2 \qquad (\omega \ll \omega_i). \tag{8.80}$$

The cross-section is proportional to the fourth power of the frequency; the Rayleigh scattering of visible light by atoms whose main absorption frequencies are in the ultraviolet is thus greatest at the violet end of the spectrum and accounts for the blue colour of the sky and the red of the sunset.

The summation in eqn (8.80) can be explicitly evaluated for a hydrogen atom. The P excited states of hydrogen are the only states that contribute in the sum over i, and for each P state only one Cartesian component of $\mathbf{D}_{1i}$ is non-zero. For each trio of P states, the matrix elements X_{1i}, Y_{1i}, and Z_{1i} are all equal, and eqn (8.80) can be written

$$\frac{\mathrm{d}\sigma}{\mathrm{d}\Omega} = \frac{e^4\omega^4}{4\pi^2\epsilon_0^2\hbar^2c^4}\left|\sum_i \frac{X_{1i}^2}{\omega_i}\right|^2(\boldsymbol{\varepsilon}.\boldsymbol{\varepsilon}_s)^2 \qquad (\omega \ll \omega_i). \tag{8.81}$$

The value of the summation is[16]

$$\sum_i \frac{X_{1i}^2}{\omega_i} = \frac{9\hbar}{16m\omega_R^2}, \tag{8.82}$$

where $\hbar\omega_R$ is the hydrogen ground-state binding energy from eqn (2.29),

$$\hbar\omega_R = me^4/32\pi^2\epsilon_0^2\hbar^2. \tag{8.83}$$

Thus eqn (8.81) becomes

$$\frac{\mathrm{d}\sigma}{\mathrm{d}\Omega} = \frac{81r_e^2}{64}\left(\frac{\omega}{\omega_R}\right)^4(\boldsymbol{\varepsilon}\cdot\boldsymbol{\varepsilon}_s)^2 \qquad (\omega \ll \omega_i). \tag{8.84}$$

The general expression for the cross-section also takes on a simpler form when ω is very close to one of the atomic excitation frequencies ω_i, and a resonance peak occurs. It is clear that the first term in the large bracket of eqn (8.73) dominates the second term in the vicinity of a resonance and that it is a good approximation to neglect all contributions in the first term except the one that corresponds to the resonating level.

The cross-section becomes infinite exactly on resonance, $\omega = \omega_i$. Of course, no scattering process can have an infinite cross-section, and the divergence is a result of having neglected radiative damping in the derivation of eqn (8.72). A more rigorous calculation shows that inclusion of damping results in the addition of an imaginary part to ω in the denominators of eqn (8.73), similar to the imaginary parts in the susceptibility expression (2.108). For a multilevel atom, spontaneous emission from a particular excited state can occur in transitions to all levels of lower energy, the transition rates being equal to the Einstein coefficients A_{ij}. The coefficients are determined by a slight generalization of eqn (5.75),

$$A_{ij} \equiv 2\gamma_{ij} = e^2(\omega_i-\omega_j)^3D_{ij}^2/3\pi\epsilon_0\hbar c^3. \tag{8.85}$$

The total linewidth or damping parameter for level i is thus made up of a sum of the partial contributions γ_{ij},

$$\gamma_i = \sum_j^{\omega_j<\omega_i} \gamma_{ij}. \tag{8.86}$$

A word of caution is needed over the use of this expression to calculate the damping parameters for highly-excited atomic energy levels. It has been assumed throughout the book that all the transitions considered lie at sufficiently high frequencies for there to be no significant thermal excitation of radiation or atoms. While this assumption remains valid for the incident radiation and its resonant atomic state $|i\rangle$, some of the neighbouring states $|j\rangle$ that contribute to the damping γ_i in eqn (8.86) may be sufficiently close that $\hbar(\omega_i-\omega_j)$ is comparable to k_BT. This is particularly likely for highly-excited states where the levels tend to be closer together. There are then contributions to γ_i from the absorption and stimulated emission associated with thermal radiation. For example, the room-temperature damping parameters of some highly-excited sodium states show a threefold increase over their values contributed by spontaneous emission alone.[18] Such effects are ignored here, but their possible importance should be kept in mind.

With insertion of the damping, the resonant cross-section for level $|i\rangle$ given by eqn (8.73) is

$$\frac{\mathrm{d}\sigma}{\mathrm{d}\Omega} = \frac{e^4\omega_i^4}{16\pi^2\epsilon_0^2\hbar^2c^4}\frac{(\boldsymbol{\varepsilon}_s.\mathbf{D}_{1i})^2(\boldsymbol{\varepsilon}.\mathbf{D}_{i1})^2}{(\omega_i-\omega)^2+\gamma_i^2}. \tag{8.87}$$

This agrees with the two-level cross-section (8.20) for the conditions of a weak incident beam and zero collision broadening assumed in the present analysis.

The total resonant cross-section is obtained from the differential cross-section by integration over the wavevector directions of the scattered photon and summation of the contributions of its two independent polarizations. The calculation is similar to the angular part of eqn (5.74) and the result is

$$\sum_{\text{polarization}}\int(\boldsymbol{\varepsilon}_s.\mathbf{D}_{1i})^2\,\mathrm{d}\Omega = (8\pi/3)D_{1i}^2. \tag{8.88}$$

The calculation so far has envisaged scattering by a single atom, but in most experiments there are many scattering atoms and their orientations are randomly distributed. It is convenient for comparisons with experiment to work with a theoretical cross-section that has been subjected to a further average over atomic orientations. The scattering by a large number N of atoms is then obtained by multiplying the derived cross-section by N. The orientation average is the same as that in eqn (2.53), and gives

$$\overline{(\boldsymbol{\varepsilon}.\mathbf{D}_{i1})^2} = \tfrac{1}{3}D_{i1}^2. \tag{8.89}$$

The total averaged cross-section is thus

$$\sigma = \frac{e^4\omega_i^4}{18\pi\epsilon_0^2\hbar^2c^4}\,\frac{D_{1i}^4}{(\omega_i-\omega)^2+\gamma_i^2}. \tag{8.90}$$

Consider the special case where $|i\rangle$ is the first atomic excited state, which we denote $|2\rangle$. The summation in eqn (8.86) reduces to a single term, and the damping constant γ_2 is the same as the quantity γ defined in eqn (5.75). Thus eqn (8.90) can be written in the form

$$\sigma = \frac{e^2\omega_0D_{12}^2}{3\epsilon_0\hbar c}\,\frac{\gamma}{(\omega_0-\omega)^2+\gamma^2}, \tag{8.91}$$

where ω_0 is the transition frequency of the first excited state. It is seen by comparison of the absorption coefficient (2.111) with the cross-section (8.91) that these expressions correctly satisfy the optical theorem (8.11).

For exact resonance, $\omega = \omega_0$, the cross-section reduces, with a further application of eqn (5.75) or eqn (8.85) to

$$\sigma = 2\pi c^2/\omega^2 = \lambda^2/2\pi, \tag{8.92}$$

where λ is the wavelength of the incident light. This strikingly simple result shows that the cross-section for resonance with the first excited state of an atom depends only on the transition frequency and is independent of all other properties of the atom. For a resonance in the visible region of the spectrum, σ given by eqn (8.92) is of order 6×10^{-14} m^2. Away from resonance, on the other hand, the earlier discussion shows that the cross-section is typically of order r_e^2 or 8×10^{-30} m^2. The resonant enhancement of the cross-section is thus of enormous proportions.

Problem 8.4. If $|i\rangle$ is not the first excited state of an atom, prove that the resonant cross-section is given by a generalization of eqn (8.92),

$$\sigma = \frac{\lambda^2}{2\pi}\left(\frac{\gamma_{i1}}{\gamma_i}\right)^2, \tag{8.93}$$

where γ_{i1} is a partial contribution to the linewidth, defined in eqn (8.85). The resonant cross-section thus becomes smaller for the more highly excited states.

If the incident frequency ω is neither very high, nor very low, nor close to one of the atomic excitation frequencies, it is not possible to approximate the cross-section and the complete expression (8.73) must be used. Numerical results are available for scattering by hydrogen[19] and these are shown in Figs. 8.11 and 8.12. The argument preceding eqn (8.81), which shows that the scattering matrix element is proportional to $\boldsymbol{\varepsilon}.\boldsymbol{\varepsilon}_s$, holds good for all frequencies ω, and the differential cross-section of eqn (8.73) can be written

$$\mathrm{d}\sigma/\mathrm{d}\Omega = r_e^2|\mathscr{M}_1|^2(\boldsymbol{\varepsilon}.\boldsymbol{\varepsilon}_s)^2, \tag{8.94}$$

where

$$\mathscr{M}_1 = \frac{m\omega^2}{\hbar}\sum_i\frac{2\omega_i|X_{1i}|^2}{\omega_i^2-\omega^2}. \tag{8.95}$$

The frequency dependence of $\mathscr{M}_1$ for frequencies ω smaller than ω_R is shown in Fig. 8.11. The vertical dashed lines indicate the positions of the excitation frequencies ω_i where $\mathscr{M}_1$ diverges. When ω is close to ω_R, the excitation frequencies crowd together, and the numerical results continue only

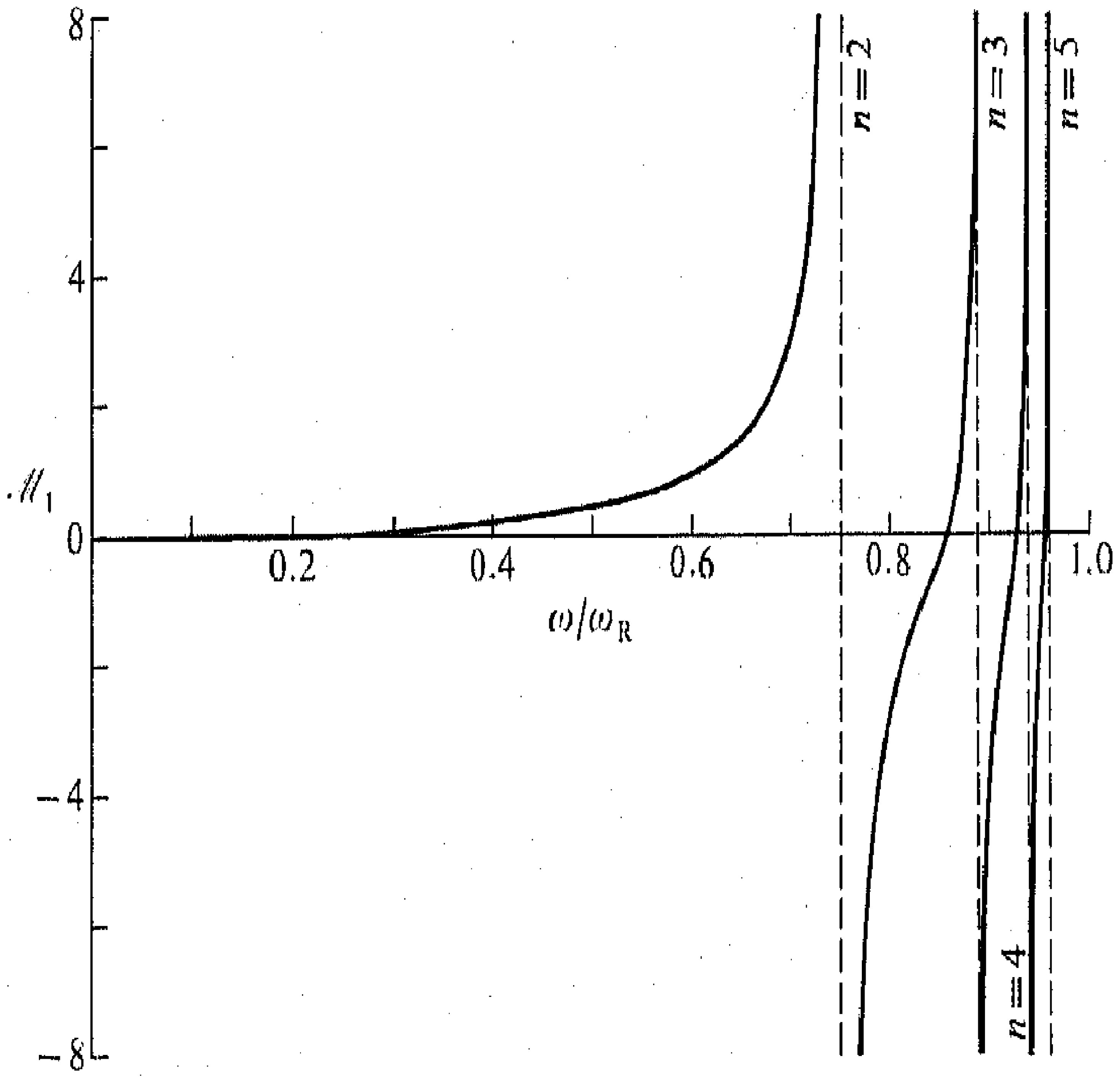

FIG. 8.11. Frequency dependence of the dimensionless matrix element $\mathscr{M}_1$ for elastic scattering of light by hydrogen for frequencies smaller than $24\omega_R/25$. The vertical dashed lines show the positions of the resonances with the n = 2, 3, 4, and 5 excited states. The graph is based on the numerical results of M. Gavrila (ref. 19.)

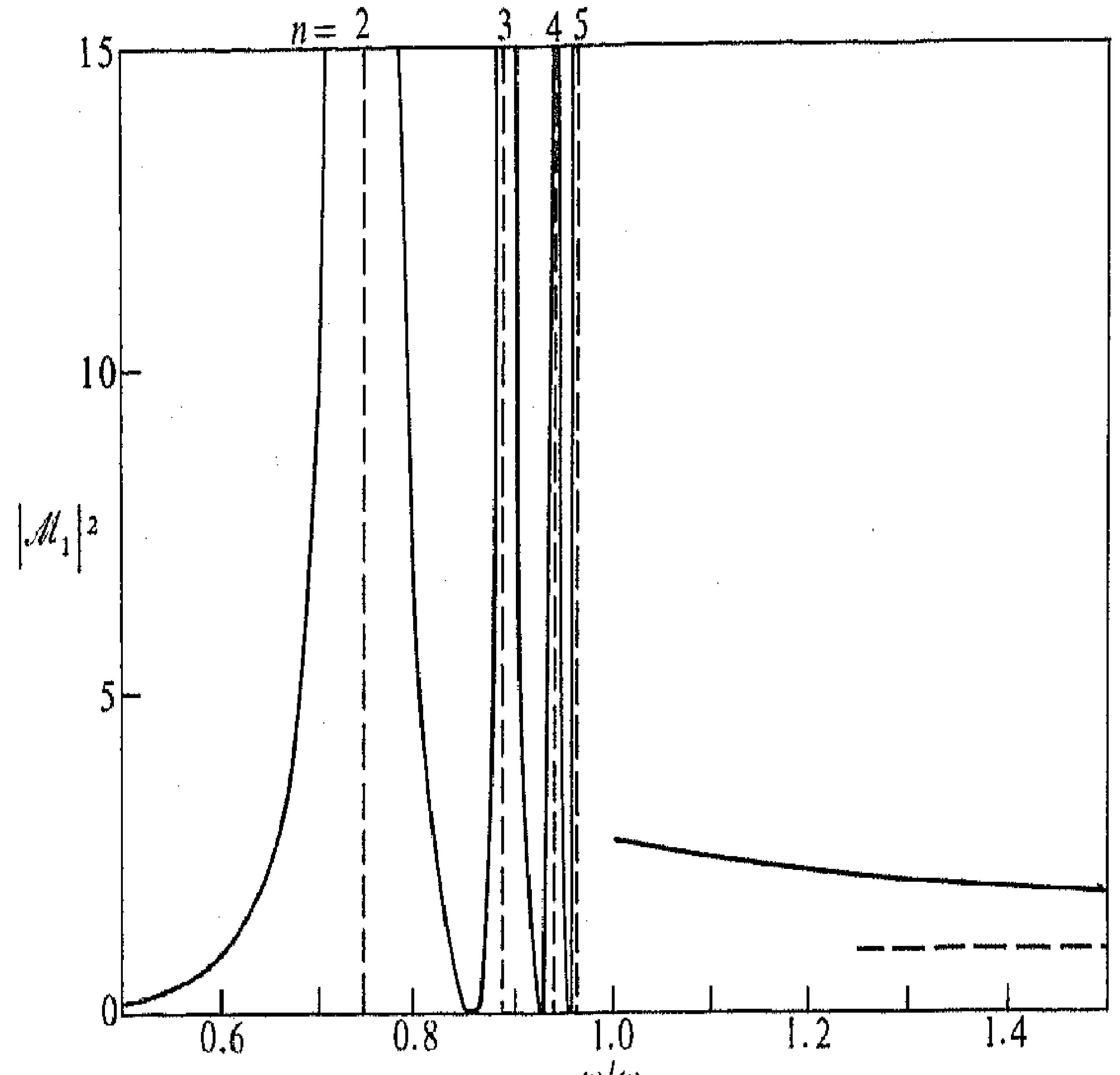

FIG. 8.12. Frequency dependence of $|\mathcal{M}_1|^2$ for hydrogen. The vertical dashed lines show the positions of the resonances and the horizontal line shows the limiting value of $|\mathcal{M}_1|^2$ in the Thomson scattering region. The graph is based on the work of M. Gavrila (ref. 19.)

up to the $n = 5$ excited state. Fig. 8.12 shows the frequency dependence of $|\mathcal{M}_1|^2$ for values of ω below and above ω_R. The region just below ω_R is again omitted. Note the strong resonant peaks and the zeros in the differential cross-section that occur between adjacent peaks. At high frequencies, $\omega \gg \omega_R$, $|\mathcal{M}_1|^2$ approaches the value unity, and the differential cross-section has the usual magnitude for Thomson scattering.

As discussed above, the insertion of radiative damping removes the infinities from the cross-section, and it also removes the zeros from between the infinities. However, on the scale of Figs. 8.11 and 8.12, the damping leads to imperceptible changes.

Problem 8.5. Prove that, with inclusion of damping, the value of $|\mathcal{M}_1|^2$ at the peak of the $n = 2$ resonance in hydrogen is of order 10^{14}.

8.8. Inelastic Raman scattering

If the incident frequency ω is higher than the lowest atomic excitation frequency, then scattering processes occur in which the final atomic state is not the ground state. To treat such processes we must return to the general expression (8.72) for the differential cross-section. The elastic scattering discussed above corresponds to the term for $f = 1$. The remaining terms correspond to inelastic Raman scattering, since the scattered frequency, governed by the delta function in eqn (8.70), is

$$\omega_s = \omega - \omega_f. \tag{8.96}$$

The scattered radiation generally has as many frequency components ω_s as there are distinct energy levels with frequency ω_f smaller than ω. The situation is illustrated in Fig. 8.13. Since the initial and final states are connected in eqn (8.72) by a pair of electric-dipole matrix elements, the selection rules that govern such matrix elements (discussed in §5.3) restrict the possible final states for the scattering process.[20] For example, since $\mathbf{D}_{fi}$ and $\mathbf{D}_{i1}$ can be non-zero only if $|f\rangle$ and $|i\rangle$ (and similarly $|i\rangle$ and $|1\rangle$) have opposite parity, it follows that the differential cross-section is non-vanishing only for atomic final states $|f\rangle$ that have the same parity as the ground state.

The most striking feature of the inelastic cross-section is again the occurrence of resonances when ω is close to one of the transition frequencies ω_i. The resonances arise from the first term in the large bracket of eqn (8.72). Let us consider the resonance arising from a particular atomic frequency, and

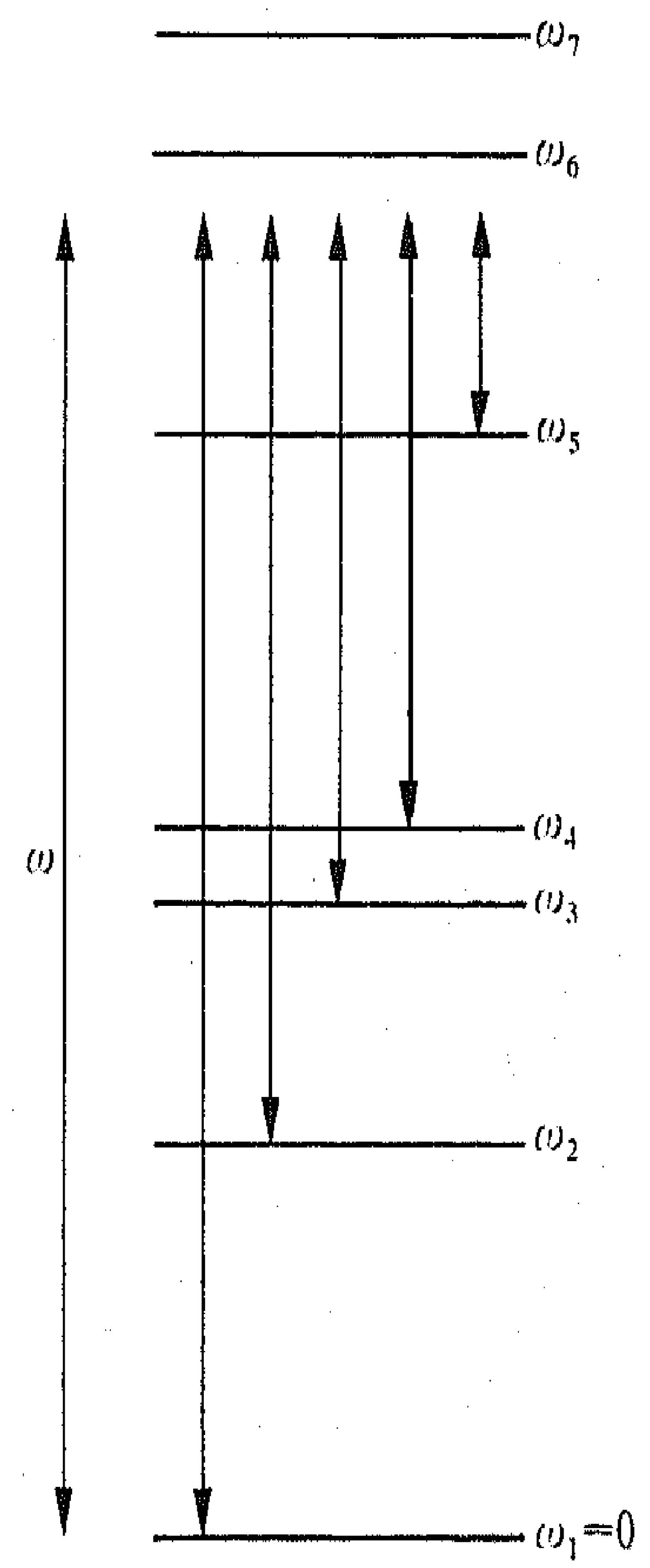

FIG. 8.13. Possible scattered frequencies ω_s for a multilevel atom with the incident frequency ω shown on the left. The left-hand scattered frequency is the Rayleigh component and the four remaining frequencies are Raman components.

retain only the corresponding resonant term. The total resonant cross-section is obtained in exactly the same way as the purely elastic contribution, by the introduction of the linewidth γ_i defined in eqn (8.86). The integration as in eqn (8.88) and the orientation average as in eqn (8.89) then produce a generalization of eqn (8.90) that includes inelastic scattering,

$$\sigma = \sum_{f}^{\omega_f<\omega_i} \frac{e^4\omega_i(\omega_i-\omega_f)^3}{18\pi\epsilon_0^2\hbar^2c^4}\frac{D_{fi}^2D_{i1}^2}{(\omega_i-\omega)^2+\gamma_i^2}. \qquad (8.97)$$

The elastic cross-section (eqn (8.90)) is the $f = 1$ term in this result. It is seen that enhancement of the cross-section for all scattered frequencies ω_s occurs when ω resonates with an atomic excitation frequency.

The total resonant cross-section can be written as a sum of contributions,

$$\sigma = \sum_f \sigma_f, \qquad (8.98)$$

where σ_f is the cross-section for scattering in which light of frequency $\omega-\omega_f$ is emitted, corresponding to a particular atomic final state. According to eqn (8.97), and with the use of eqn (8.85), we find

$$\sigma_f = \frac{2\pi c^2}{\omega_i^2}\frac{\gamma_{i1}\gamma_{if}}{(\omega_i-\omega)^2+\gamma_i^2}. \qquad (8.99)$$

Thus, when the incident light is in resonance with state $|i\rangle$, the intensity of scattered light of frequency $\omega-\omega_f$ is proportional to the radiative decay rate from state $|i\rangle$ to state $|f\rangle$. For exact resonance, $\omega = \omega_i$,

$$\sigma_f = \frac{\lambda^2}{2\pi}\frac{\gamma_{i1}\gamma_{if}}{\gamma_i^2}; \qquad (8.100)$$

the ratio of damping parameters is less than unity in view of eqn (8.86), except when $|i\rangle$ is the first excited state. The resonance cross-section (8.100) is therefore in general smaller than the value given in eqn (8.92), but it is still usually greatly increased by comparison with the nonresonant cross-section.

Summation of the cross-section (8.99) over f to form the total cross-section of eqn (8.98) gives

$$\sigma = \frac{2\pi c^2}{\omega_i^2}\frac{\gamma_{i1}\gamma_i}{(\omega_i-\omega)^2+\gamma_i^2}, \qquad (8.101)$$

where eqn (8.86) has been used. For exact resonance, $\omega = \omega_i$,

$$\sigma = \frac{\lambda^2}{2\pi}\frac{\gamma_{i1}}{\gamma_i}, \qquad (8.102)$$

which again has its maximum value of $\lambda^2/2\pi$ when $|i\rangle$ is the first excited state.

The above discussion of the inelastic cross-section is all concerned with the simplifications that occur in resonant conditions. The extremes of high and low incident frequencies also give simple results.

Problem 8.6. Consider the analogue of the Thomson-scattering region for the case of inelastic scattering. Prove that the inelastic contributions to the cross-section all tend to zero in the limit of high incident frequencies, $\omega \gg \omega_i$, unlike the elastic contribution which tends to the finite high-frequency limit (eqn (8.78)).

For the opposite extreme of low frequencies, $\omega \ll \omega_i$, the cross-section is, of course, also zero because the incident frequency has to be greater than the smallest atomic excitation frequency for any inelastic scattering to occur (cf. Fig. 8.13). The cross-section at the onset of inelastic scattering for the special case of hydrogen is given below.

Apart from the special cases where the cross-section expression can be simplified, it is generally the case that several states $|i\rangle$ in the intermediate-state summation of eqn (8.72) make comparable contributions to the cross-section. The frequency dependence of the cross-section can then only be determined by a detailed calculation in terms of known atomic wavefunctions and eigenvalues.

Numerical results for an atomic inelastic scattering cross-section are available for hydrogen. The contribution to the differential cross-section has been calculated for scattering in which the atom initially in its ground state is excited finally to its 2S state.[21] The differential cross-section (eqn (8.72)) for this process can be written

$$\frac{d\sigma}{d\Omega} = r_e^2\frac{\omega-\omega_f}{\omega}|\mathscr{M}_2|^2(\varepsilon.\varepsilon_s)^2, \qquad (8.103)$$

where

$$\mathscr{M}_2 = \frac{m\omega(\omega-\omega_f)}{\hbar}\sum_i X_{fi}X_{i1}\left(\frac{1}{\omega_i-\omega}+\frac{1}{\omega_i-\omega_f+\omega}\right), \qquad (8.104)$$

and $|f\rangle$ is the 2S state. Note that $\mathscr{M}_2$ reduces to $\mathscr{M}_1$ given by eqn (8.95) in the case of elastic scattering.

The frequency dependence of $\mathscr{M}_2$ for frequencies smaller than ω_R is shown in Fig. 8.14. Note that $\mathscr{M}_2$ is finite at the onset of scattering when $\omega = \omega_f$.

Problem 8.7. Prove that the value of $\mathscr{M}_2$, when the incident frequency ω is equal to the frequency ω_f of the final 2S state, is

$$\mathscr{M}_2 = 16\times 2^{\frac{1}{2}}/27 \qquad (\omega = \omega_f = \omega_{2S}). \qquad (8.105)$$

Hint: The intermediate 2P state gives the only non-zero contribution to the matrix element. The hydrogen 1S and $2P_x$

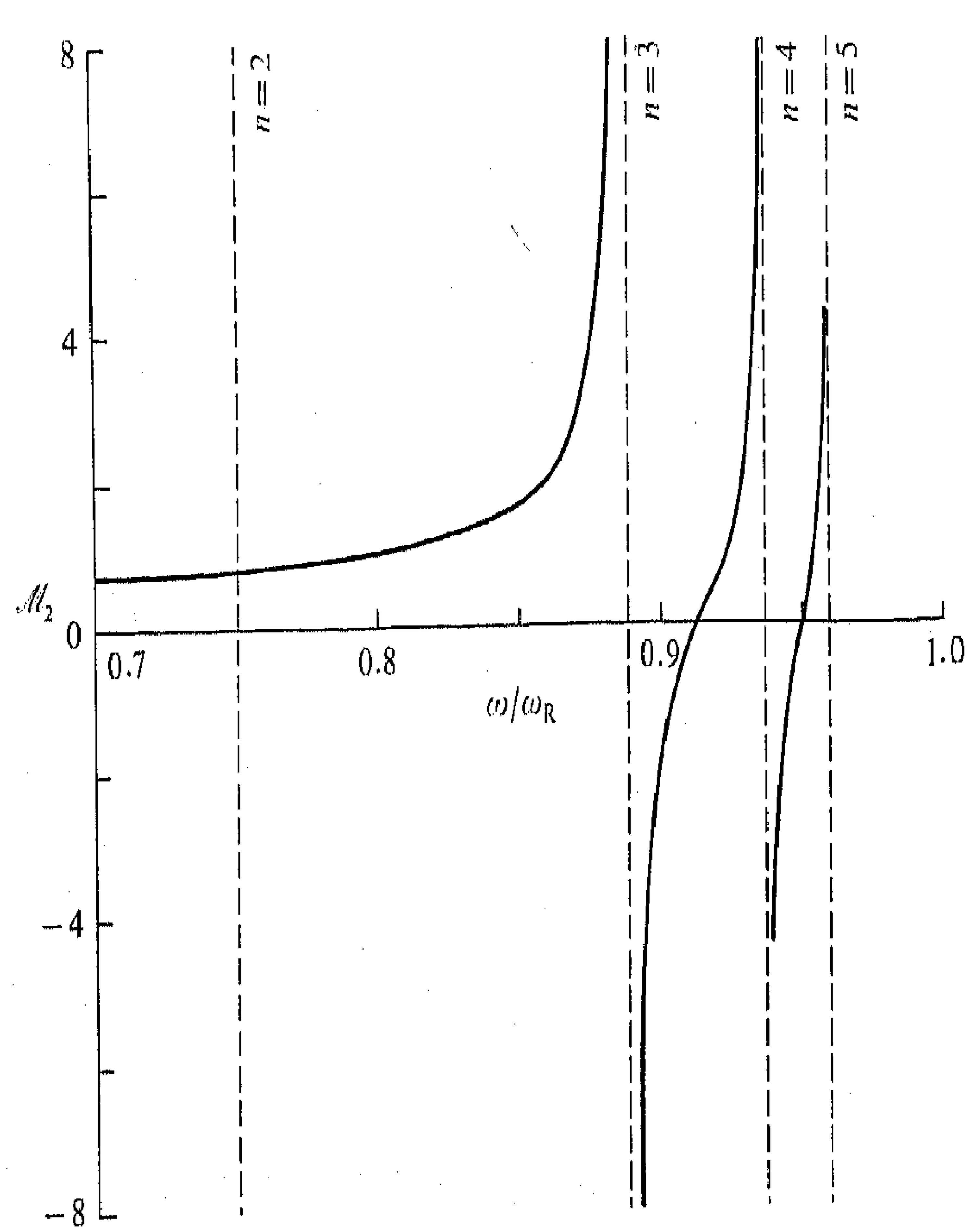

FIG. 8.14. Frequency dependence of the matrix element $\mathscr{M}_2$ for inelastic light scattering by hydrogen, when the final atomic state is 2S. The vertical lines show the positions of the resonances. Real inelastic scattering from the $n = 2$ state occurs only when ω is greater than $\frac{3}{4}\omega_R$, but $\mathscr{M}_2$ shows no particular feature at this frequency. (After W. M. Saslow and D. L. Mills, ref. 21.)

wavefunctions are given in eqns (2.25) and (2.26), and the 2S wavefunction is

$$\psi_{2S} = 2^{-\frac{3}{2}}\pi^{-\frac{1}{2}}a_0^{-\frac{3}{2}}\{1-(r/2a_0)\}\exp(-r/2a_0). \quad (8.106)$$

Fig. 8.15 shows the frequency dependence of the differential cross-section for values of ω, both below and above ω_R. Note the resonant peaks and zeros, similar to those of $|\mathscr{M}_1|^2$ shown in Fig. 8.12. At high frequencies the cross-section approaches zero in accordance with the theorem of problem 8.6. It is seen that the differential cross-section is zero at and below $\omega = \omega_{2S}$, and increases linearly with $\omega - \omega_{2S}$ in the frequency region just above the onset of inelastic scattering.

The insertion of radiative damping removes the infinities and zeros from the cross-section but produces negligible changes on the scales of Figs 8.14 and 8.15. The relative and absolute heights of the various resonant peaks in elastic and inelastic scattering by hydrogen can be obtained by the use of eqn (8.100) together with the data given in Fig. 2.4. For example, when the incident frequency resonates with the $n = 3$ level of hydrogen, it is seen that the peak

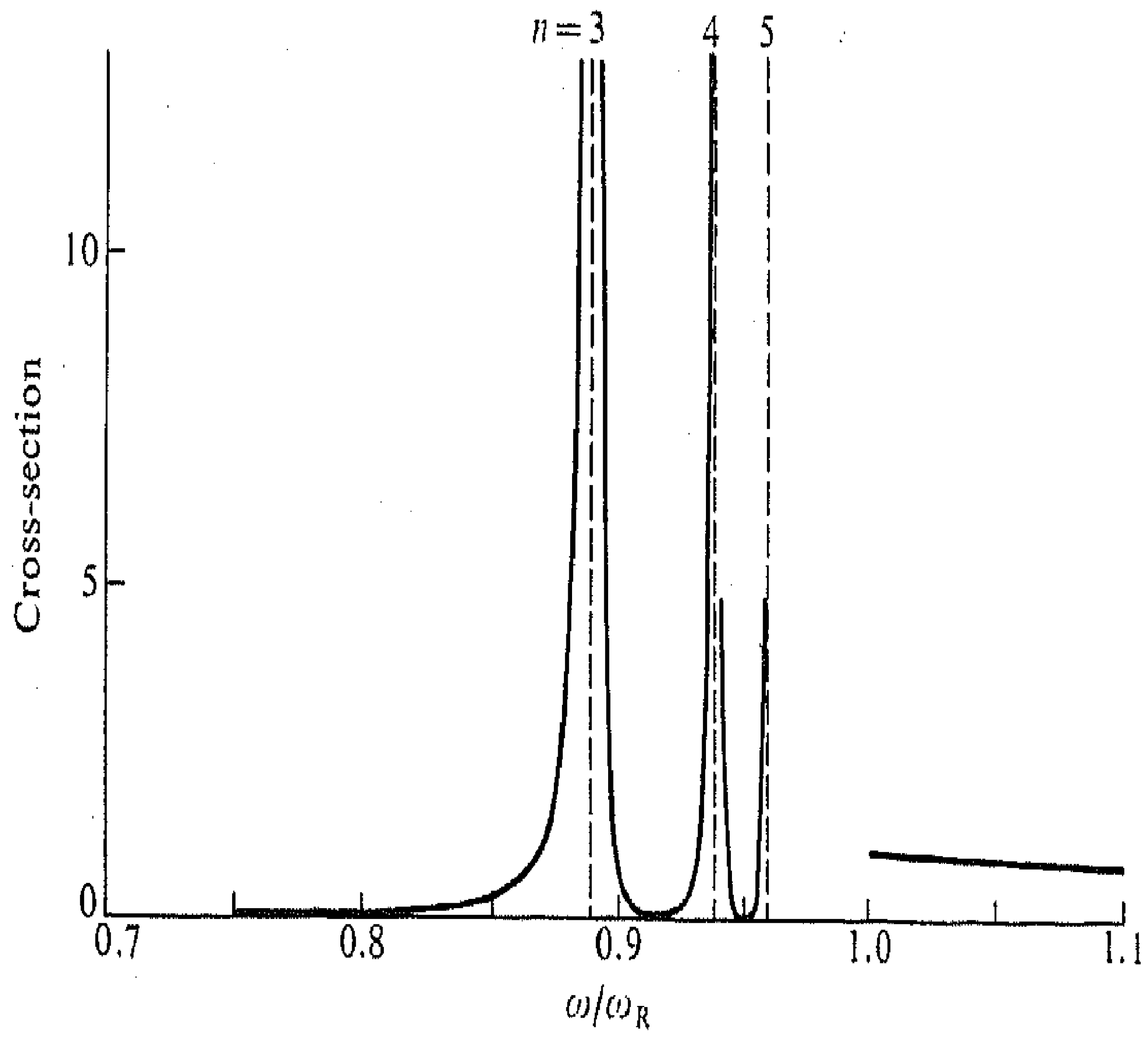

FIG. 8.15. Frequency dependence of the differential cross-section for inelastic scattering by hydrogen with 2S as the final atomic state. The quantity plotted is $(\omega - \omega_{2S})|\mathscr{M}_2|^2/\omega$, except for $\omega < \omega_{2S}$ where the cross-section is zero. (After W. M. Saslow and D. L. Mills, ref. 21.)

cross-section for elastic scattering is a factor 160/22 greater than the peak cross-section for inelastic scattering.

The optical theorem (8.11) applies generally to the absorption and scattering by a multilevel atom, where both the elastic and inelastic contributions to the cross-section must be included. It is not possible to demonstrate the theorem completely with results derived here because we do not have available a sufficiently general expression for the absorption coefficient that includes resonant, nonresonant, and cross-terms analogous to those in the square modulus contained in the cross-section (8.72). Absorption coefficients are usually only measurable close to resonance between the frequencies of the incident light and an atomic transition, the attenuation of a transmitted beam far from resonance conditions being too small for detection. On the other hand, it is often possible to detect scattering of nonresonant light (as in a visual inspection of the blue sky!) since the effect produces light in directions where none would otherwise be present. Thus even an elementary theory of the scattering cross-section needs to include the resonant and nonresonant contributions from the various excited states of a multilevel atom, as in eqn (8.72), whereas a useful expression for the absorption lineshape often needs to include only the two states involved in a resonant transition, as in eqn (2.111).

The calculations of the present section do not provide any detailed information on the spectral distribution of the scattered light. We conclude the discussion with a qualitative account of the spectral properties for resonance scattering of a weak incident beam of coherent light by atoms subjected to radiative and collision broadening. Fig. 8.1 represents the kinds of component that occur when ω is close to ω_i. An atom that returns to its ground state $|1\rangle$ at the end of the scattering process produces the two components represented on the left of the figure. The detailed form of the spectrum is expressed by eqn (8.37) and is illustrated in Fig. 8.3. There is an elastic Rayleigh line of zero width and an inelastic fluorescent line with the same Lorentzian frequency distribution of width $2\gamma_i'$ as ordinary absorption by the transition from $|1\rangle$ to $|i\rangle$. The strength of the inelastic component is proportional to the collision-broadening parameter of state $|i\rangle$.

Qualitatively similar components, represented on the right of Fig. 8.1, occur for an atom that is left in an excited state $|f\rangle$ at the end of the scattering event.[22] The Raman component has a frequency given by eqn (8.96); however, because the final atomic state is now an excited one, with some damping parameter γ_f', the Raman scattered light has a Lorentzian distribution around $\omega-\omega_f$ with a linewidth $2\gamma_f'$. There is also a fluorescent component whose strength is proportional to the collision-broadening parameter of state $|i\rangle$ and whose linewidth $2\gamma_i'+2\gamma_f'$ includes contributions from both states involved in the transition. The combined spectrum of these two contributions is therefore similar to that shown in Fig. 8.3 except that the frequencies are reduced by ω_f and both components gain an additional width $2\gamma_f'$. The cross-sections calculated in the present section refer to sums of the two contributions.

8.9. Two-photon cascade emission

All of the discussion so far in the present chapter is concerned with processes in which a single scattered photon is created by excitation or virtual excitation of an atom by an incident light beam. It is not difficult to extend the discussion to more complicated processes in which an excited atom emits two photons in succession as it decays back to its initial state via an intermediate energy level. The process is called cascade emission and it can in principle occur by any number of steps. The treatment here is limited to two-photon cascade emission, which is an important process in distinguishing the predictions of the classical and quantum theories of light.

Fig. 8.16 shows the energy-level scheme for two-photon emission. Atoms are excited into state $|3\rangle$, whence they decay to state $|2\rangle$ with emission of a photon of frequency ω_2 at a spontaneous rate $2\gamma_{32}$, and they subsequently decay to state $|1\rangle$ with emission of a second photon of frequency ω_1 at a spontaneous rate $2\gamma_{21}$. A gas of similar atoms emits detectable amounts of light at two distinct frequencies ω_1 and ω_2, and it is possible to investigate the intensity correlations or degrees of second-order coherence within and between the two beams.

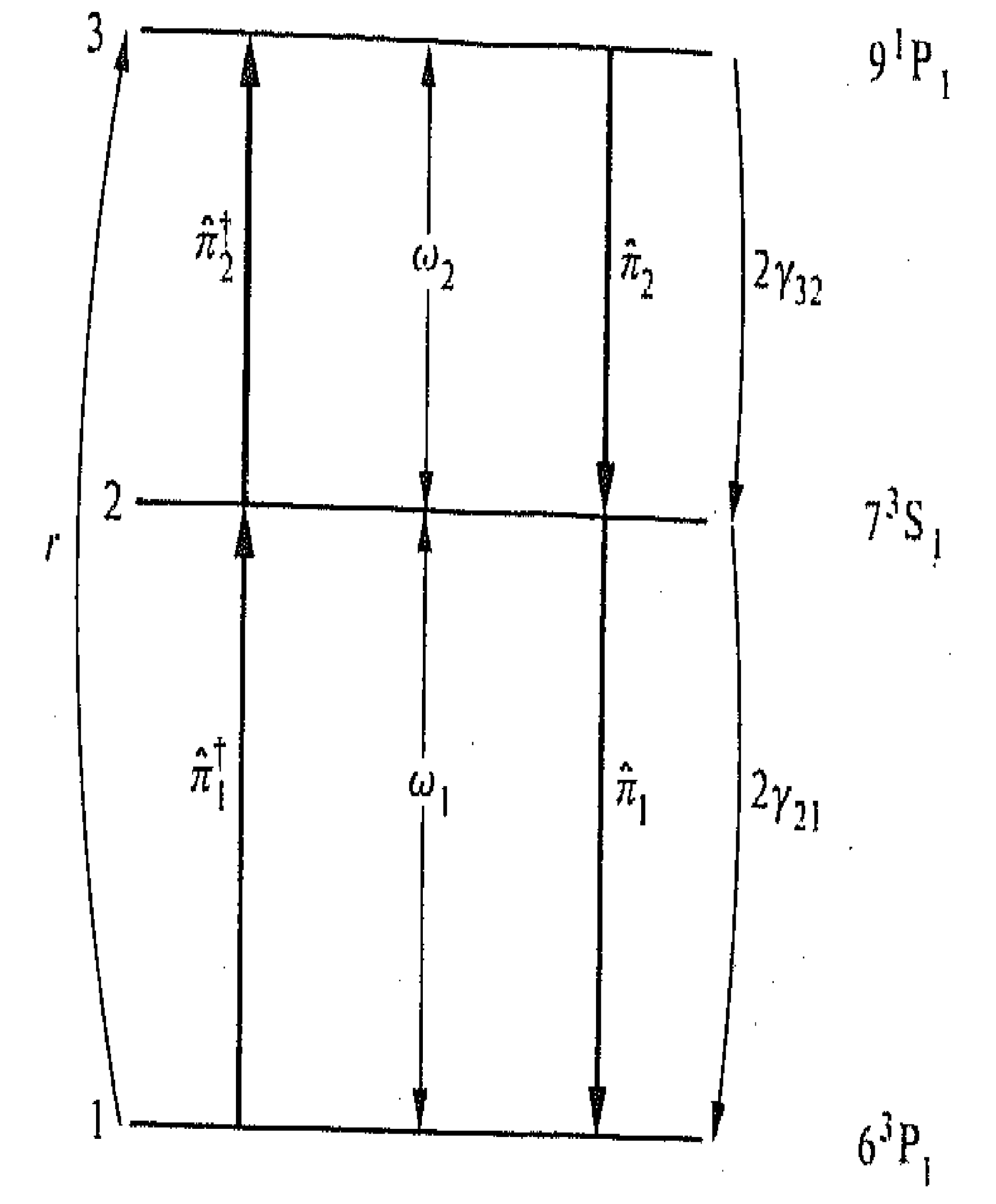

FIG. 8.16. Atomic energy levels used in two-photon cascade emission showing transition frequencies, transition operators, and rates used in the analysis. The mercury-level designations refer to the experiment of ref. 23.

The general theory of interactions of light beams with a three-level atom is complicated and we consider here only a special case, which not only leads to a simple calculation but also corresponds to the conditions of one of the main experiments[23] on two-photon emission. The experimental arrangement, shown in Fig. 8.17, consists of the two-photon light source surrounded by two distinct sets of detectors. The detectors are preceded by filters that remove one or other of the frequencies ω_1 and ω_2. The detection system for each frequency consists of a half-silvered mirror and double phototube arrangement similar to that of Hanbury Brown and Twiss shown in Fig. 3.13. It is possible in the experiment to record correlations between the readings of any pair of the four phototubes in the complete detection system. Experimental results are available for cascade emission by mercury using the levels indicated on the right of Fig. 8.16. The atoms were excited by electron bombardment and the light of frequencies ω_1 and ω_2 was collected from large solid angles.

The conditions in the light source, with large collision- and Doppler-broadening and the electron-bombardment excitation, are such that the time development of the matrix elements ρ_{ij} of the atomic density operator is adequately described by rate equations, similar to eqn (2.170) or eqn (7.144). If the excitation takes atoms from state $|1\rangle$ to state $|3\rangle$ at a rate r, then an obvious generalization of the two-level rate equation gives

$$d\rho_{33}/dt = r-2\gamma_{32}\rho_{33} \tag{8.107}$$

$$d\rho_{22}/dt = 2\gamma_{32}\rho_{33}-2\gamma_{21}\rho_{22} \tag{8.108}$$

$$d\rho_{11}/dt = 2\gamma_{21}\rho_{22}-r. \tag{8.109}$$

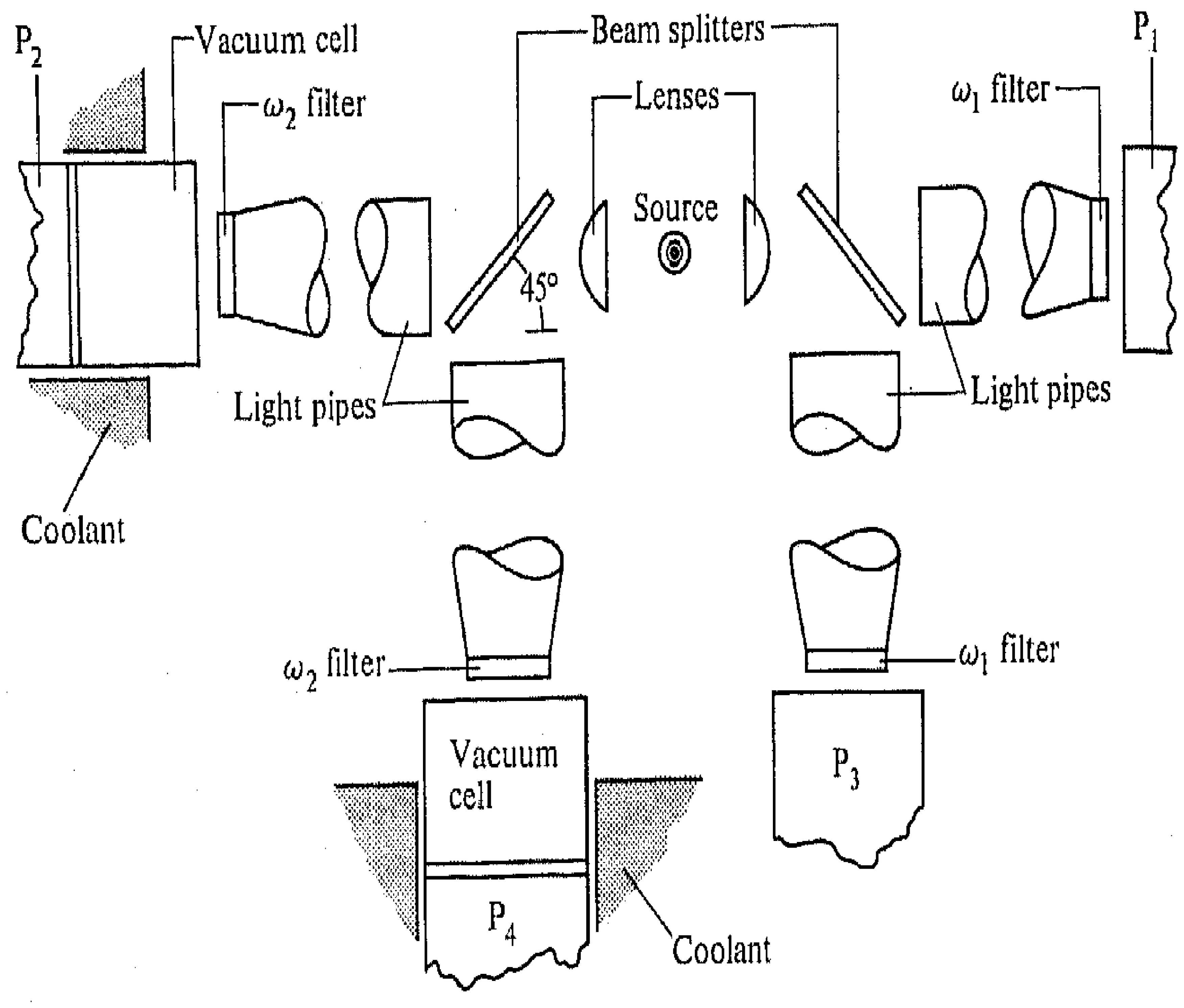

FIG. 8.17. Experiment for measuring the beam correlations in two-photon cascade emission. Phototubes P_1 and P_3 detect the beam of frequency ω_1, while phototubes P_2 and P_4 detect the beam of frequency ω_2. (After J. F. Clauser, ref. 23.)

State $|1\rangle$ is not the atomic ground state for the mercury level scheme of Fig. 8.16 but we ignore transitions to other states, giving

$$\rho_{11}+\rho_{22}+\rho_{33} = \text{constant},$$

and it is only necessary to solve the rate equations for two of the density matrix elements. It is not difficult to obtain general solutions of the rate equations in forms analogous to eqn (7.145) and the results are

$$\rho_{33}(t+\tau) = (r/2\gamma_{32})[1-\exp(-2\gamma_{32}\tau)]+\rho_{33}(t)\exp(-2\gamma_{32}\tau) \tag{8.110}$$

and

$$\begin{aligned}\rho_{22}(t+\tau) = {} & (r/2\gamma_{21})[1-\exp(-2\gamma_{21}\tau)]+\rho_{22}(t)\exp(-2\gamma_{21}\tau)\\ & -[2\gamma_{32}\rho_{33}(t)-r][\exp(-2\gamma_{21}\tau)-\exp(-2\gamma_{32}\tau)]/2(\gamma_{21}-\gamma_{32}).\end{aligned} \tag{8.111}$$

The off-diagonal elements of the density matrix decay at much faster rates determined by the Doppler- and collision-broadening.

These solutions for the diagonal matrix elements determine the second-order coherence properties of the emitted light in precisely the same manner as used in §7.10 to treat single-photon emission by a two-level atom. Thus the pairs of transition operators indicated in Fig. 8.16 are defined by

$$\begin{aligned}\hat{\pi}_1^\dagger &= |2\rangle\langle 1| \qquad \hat{\pi}_2^\dagger = |3\rangle\langle 2|\\ \hat{\pi}_1 &= |1\rangle\langle 2| \qquad \hat{\pi}_2 = |2\rangle\langle 3|,\end{aligned} \tag{8.112}$$

similar to eqns (5.121) and (5.122), and their products satisfy relations similar to eqns (5.123) to (5.127). Their expectation values in the interaction representation are given by

$$\langle\hat{\pi}_1^\dagger(t)\hat{\pi}_1(t)\rangle = \rho_{22}(t) \quad \text{and} \quad \langle\hat{\pi}_2^\dagger(t)\hat{\pi}_2(t)\rangle = \rho_{33}(t), \tag{8.113}$$

similar to eqn (7.125). The field $\hat{E}_1^+$ of the light radiated at frequency ω_1 is related to $\hat{\pi}_1$ as in eqn (5.191) and the same relation connects $\hat{\pi}_2$ to the field operator $\hat{E}_2^+$ at frequency ω_2.

With the two distinct frequencies of light emitted in the cascade decay, it is possible to define four degrees of second-order coherence, and a simple generalization of eqn (7.119) gives

$$\begin{aligned}g_{ij}^{(2)}(\tau) &= \frac{\langle\hat{E}_j^-(t)\hat{E}_i^-(t+\tau)\hat{E}_i^+(t+\tau)\hat{E}_j^+(t)\rangle}{\langle\hat{E}_i^-(t)\hat{E}_i^+(t)\rangle\langle\hat{E}_j^-(t)\hat{E}_j^+(t)\rangle}\\ &= \frac{\langle\hat{\pi}_j^\dagger(t)\hat{\pi}_i^\dagger(t+\tau)\hat{\pi}_i(t+\tau)\hat{\pi}_j(t)\rangle}{\langle\hat{\pi}_i^\dagger(t)\hat{\pi}_i(t)\rangle\langle\hat{\pi}_j^\dagger(t)\hat{\pi}_j(t)\rangle} \qquad i,j = 1,2.\end{aligned} \tag{8.114}$$

It is assumed that t is sufficiently large for steady-state conditions to have been reached, and the delay time τ is again taken to be positive. The symmetry property of eqn (3.72) is generalized to

$$g_{ij}^{(2)}(-\tau) = g_{ji}^{(2)}(\tau). \tag{8.115}$$

The light beams 1 and 2 are detected at different positions in the experiment of Fig. 8.17, but the four phototubes are taken to lie at equal linear distances from the source so that the retardation time differences between field and atomic operators in eqn (5.191) can be ignored.

The correlation functions that appear in the numerator of eqn (8.114) are obtained from the preceding equations by use of the quantum regression theorem of eqns (7.135) and (7.136). The procedure is exactly the same as in the calculation for single-photon emission.

Problem 8.8. Prove that the correlation functions

$$\langle ij\rangle = \langle\hat{\pi}_j^\dagger(t)\hat{\pi}_i^\dagger(t+\tau)\hat{\pi}_i(t+\tau)\hat{\pi}_j(t)\rangle$$

are given by the following expressions

$$\begin{aligned}\langle 11\rangle = \frac{r\langle\hat{\pi}_1^\dagger(t)\hat{\pi}_1(t)\rangle}{2\gamma_{21}(\gamma_{21}-\gamma_{32})}\{&\gamma_{21}[1-\exp(-2\gamma_{32}\tau)]\\ &-\gamma_{32}[1-\exp(-2\gamma_{21}\tau)]\}\end{aligned} \tag{8.116}$$

$$\langle 22\rangle = (r/2\gamma_{32})\langle\hat{\pi}_2^\dagger(t)\hat{\pi}_2(t)\rangle[1-\exp(-2\gamma_{32}\tau)] \tag{8.117}$$

$$\langle 21\rangle = (r/2\gamma_{32})\langle\hat{\pi}_1^\dagger(t)\hat{\pi}_1(t)\rangle[1-\exp(-2\gamma_{32}\tau)] \tag{8.118}$$

$$\begin{aligned}\langle 12\rangle = \frac{r\langle\hat{\pi}_2^\dagger(t)\hat{\pi}_2(t)\rangle}{2\gamma_{21}(\gamma_{21}-\gamma_{32})}&\{\gamma_{21}[1-\exp(-2\gamma_{32}\tau)]\\ &-\gamma_{32}[1-\exp(-2\gamma_{21}\tau)]\}\\ &+\langle\hat{\pi}_2^\dagger(t)\hat{\pi}_2(t)\rangle\exp(-2\gamma_{21}\tau).\end{aligned} \tag{8.119}$$

The required degrees of second-order coherence are now obtained from eqn (8.114). With the appropriate steady-state limits inserted for the single-time expectation values, the results are

$$g_{11}^{(2)}(\tau) = \{\gamma_{21}[1-\exp(-2\gamma_{32}\tau)]-\gamma_{32}[1-\exp(-2\gamma_{21}\tau)]\}/(\gamma_{21}-\gamma_{32}) \tag{8.120}$$

$$g_{22}^{(2)}(\tau) = g_{21}^{(2)}(\tau) = 1-\exp(-2\gamma_{32}\tau) \tag{8.121}$$

$$g_{12}^{(2)}(\tau) = g_{11}^{(2)}(\tau)+(2\gamma_{21}/r)\exp(-2\gamma_{21}\tau). \tag{8.122}$$

These degrees of second-order coherence are similar to the expression (7.147) for single-photon emission in that the three in eqns (8.120) and (8.121) vanish at $\tau = 0$ and increase towards unity for long times τ. The two beams individually show photon antibunching.

The main additional feature of the two-photon emission is the possibility of measuring interbeam intensity correlations, and particular interest attaches to the degree of second-order coherence in eqn (8.122). This has a second contribution on the right-hand side that does not vanish at $\tau = 0$. With τ positive, $g_{12}^{(2)}(\tau)$ refers to observations in which photon ω_1 *follows* photon ω_2. The final term in eqn (8.122) is the contribution of observations in which the two photons are produced in the *same* cascade emission; it can be much larger than the first term, which arises from photons produced in *different* cascade emissions, if the excitation rate r is sufficiently small. There is of course no similar contribution to $g_{21}^{(2)}(\tau)$ in eqn (8.121) because, from the nature of a single cascade emission, photon ω_2 must precede photon ω_1.

For comparison with experiment, the single-atom degrees of coherence must be generalized to obtain the properties of the light emitted by a large fluctuating number of similar atoms. The single-atom degrees of first-order coherence can be set equal to zero for times of the order of the radiative lifetimes, where the single-atom degrees of second-order coherence in eqns (8.120)–(8.122) show their main time dependence. The degree of second-order coherence given by eqn (8.64) for radiation emitted by an average number $\bar{\nu}$ of atoms therefore reduces to

$$\bar{G}_{ij}^{(2)}(\tau) = (g_{ij}^{(2)}(\tau)/\bar{\nu})+1. \tag{8.123}$$

Thus for $\bar{\nu} \gg 1$ we find approximately

$$\bar{G}_{11}^{(2)}(\tau) = \bar{G}_{22}^{(2)}(\tau) = \bar{G}_{21}^{(2)}(\tau) = 1 \tag{8.124}$$

and

$$\bar{G}_{12}^{(2)}(\tau) = (2\gamma_{21}/r\bar{\nu})\exp(-2\gamma_{21}\tau)+1. \tag{8.125}$$

The antibunching property is thus removed as before when the multiatom emission is considered but the additional interbeam correlation in $\bar{G}_{12}^{(2)}(\tau)$ remains, and its magnitude is significant when $r\bar{\nu}$ is smaller than or comparable to $2\gamma_{21}$.

Fig. 8.18 shows experimental results[23] for the interbeam correlation in cascade emission from mercury using the energy levels shown in Fig. 8.16. The solid curves are the theoretical predictions from eqns (8.124) and (8.125) with the numerical values

$$2\gamma_{21} = 1{\cdot}19\times 10^8\ \mathrm{s}^{-1} \qquad \text{and} \qquad 2\gamma_{21}/r\bar{\nu} = 1{\cdot}42. \tag{8.126}$$

The radiative lifetime is an independently measured value for the mercury levels concerned, but the excitation rate $r\bar{\nu}$, not available from the experiment, is chosen to give the best fit to the measurements. The agreement between theory and experiment is seen to be very good. Indeed, the observation of

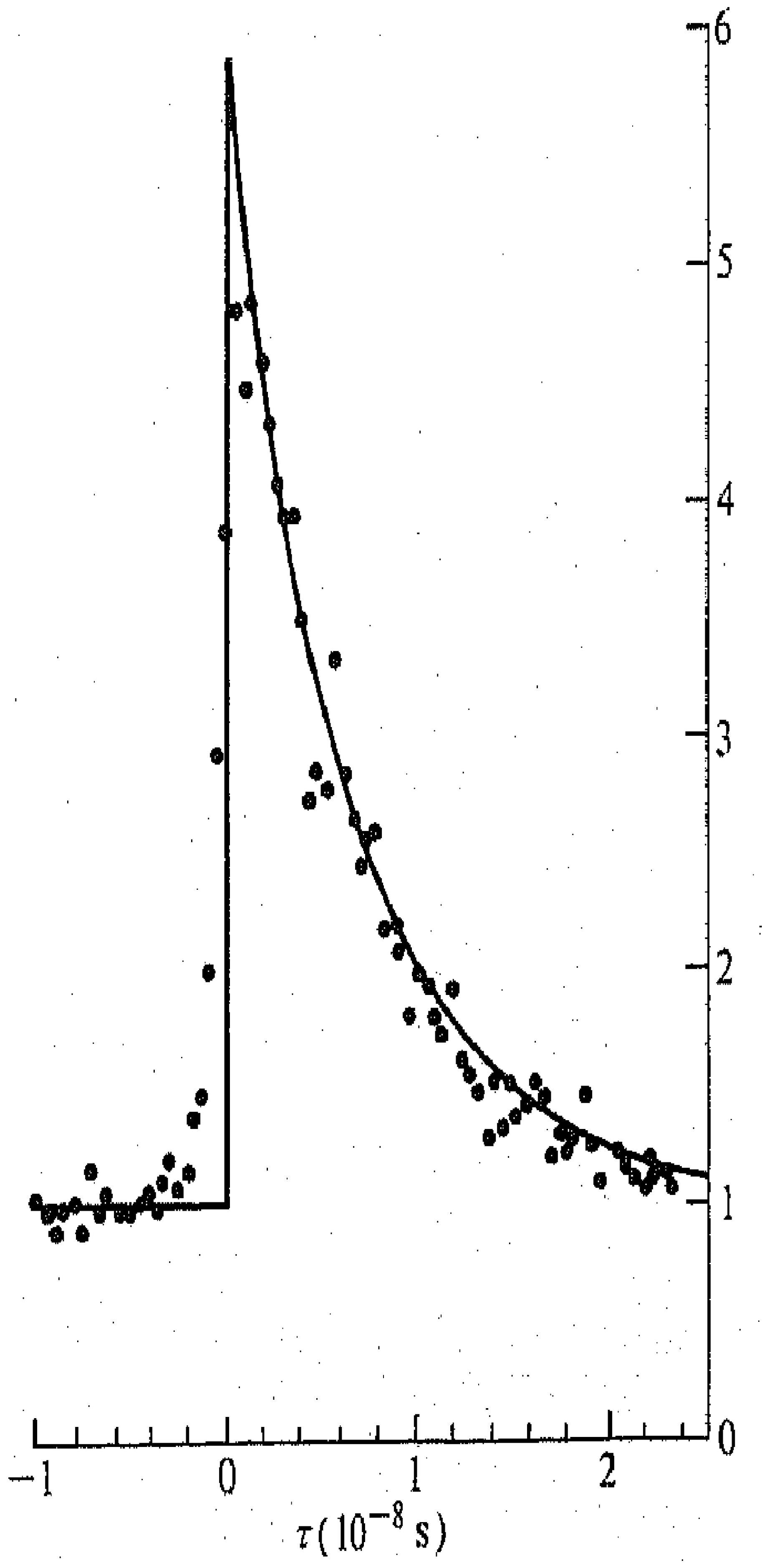

FIG. 8.18. Comparison of experimental points from ref. 23 with the theoretical curve for the interbeam degree of second-order coherence. The function plotted is $\{\bar{G}_{12}^{(2)}(\tau)\}^2$, and its value at negative τ is unity in accordance with eqns (8.115) and (8.124).

correlations between photons emitted in cascade forms a reliable technique for determining radiative lifetimes of the intermediate states.[24]

The physical origin of the interbeam correlation is obvious in the quantum picture of cascade emission, and it is also clear that the interbeam correlation must be enhanced relative to correlations within the beams at low pumping rates r; the intervals between successive photons in the same beam are then lengthy, but emission of the photon pair, one into each beam, always occurs within a time interval of order $1/2\gamma_{21}$. There is however no possibility of a classical description of the correlation effect. If the intensities of the two beams are represented by classical fluctuating quantities $\bar{I}_1(t)$ and $\bar{I}_2(t)$, then use of an inequality similar to (3.79), but including products between intensities in the two beams, leads to

$$\{\bar{G}^{(2)}_{12}(\tau)\}^2 \leqslant \bar{G}^{(2)}_{11}(0)\bar{G}^{(2)}_{22}(0) \qquad \text{(classical)} \qquad (8.127)$$

in the notation of the above calculations. This classical inequality is seriously violated by the quantum results in eqns (8.124) and (8.125). It is also violated by the experimental results for mercury[23], which not only give the points shown in Fig. 8.18 but also confirm the other degrees of coherence in (8.124), and thus agree with all aspects of the quantum theory of two-photon cascade emission.

References

1. Newton, R. G. (1976). *Am. J. Phys.* **44,** 639.
2. Mollow, B. R. (1969). *Phys. Rev.* **188,** 1969.
3. See also the review by Knight, P. L. and Milonni, P. W. (1980). *Phys. Reps.* **66,** 21.
4. Durrant, A. V. (1977). *Am. J. Phys.* **45,** 752.
5. Huber, D. L. (1969). *Phys. Rev.* **178,** 93.
6. Omont, A., Smith, E. W., and Cooper, J. (1972). *Astrophys. J.* **175,** 185.
7. Carlsten, J. L. and Szöke, A. (1976). *Phys. Rev. Lett.* **36,** 667; Carlsten, J. L., Szöke, A., and Raymer, M. G. (1977). *Phys. Rev.* **A15,** 1029.
8. Carmichael, H. J. and Walls, D. F. (1976). *J. Phys.* **B9,** L43; (1976) ibid. **B9,** 1199.
9. Grove, R. E., Wu, F. Y., and Ezekiel, S. (1977). *Phys. Rev.* **A15,** 227.
10. Cohen-Tannoudji, C. and Reynaud, S. (1979). *Phil. Trans. R. Soc.* **A293,** 223.
11. Jakeman, E., Pike, E. R., Pusey, P. N., and Vaughan, J. M. (1977). *J. Phys.* **A10,** L257.
12. Kimble, H. J., Dagenais, M., and Mandel, L. (1978). *Phys. Rev.* **A18,** 201.
13. Kimble, H. J., Dagenais, M., and Mandel, L. (1977). *Phys. Rev. Lett.* **39,** 691.
14. Dagenais, M. and Mandel, L. (1978). *Phys. Rev.* **A18,** 2217.
15. Kimble, H. J. and Mandel, L. (1976). *Phys. Rev.* **A13,** 2123.
16. Bethe, H. A. and Salpeter, E. E. (1957). *Quantum mechanics of one- and two-electron atoms*, §61. Springer-Verlag, Berlin.
17. See, for example, Heitler, W. (1954). *The quantum theory of radiation* (3rd edn.), §22. Clarendon Press, Oxford; or Sakurai, J. J. (1967). *Advanced quantum mechanics*, p. 229. Addison-Wesley, Reading, Massachusetts.
18. Gallagher, T. F. and Cooke, W. E. (1979). *Phys. Rev. Lett.* **42,** 835.
19. Gavrila, M. (1967). *Phys. Rev.* **163,** 147.

20. See, for example, Tinkham, M. (1964). *Group theory and quantum mechanics*, p. 249. McGraw-Hill, New York; or Cracknell, A. P. (1968). *Applied group theory*, p. 148. Pergamon, Oxford.
21. Saslow, W. M. and Mills, D. L. (1969). *Phys. Rev.* **187,** 1025.
22. Shen, Y. R. (1974). *Phys. Rev.* **B9,** 622; Rousseau, D. L., Patterson, G. D., and Williams, P. F. (1975). *Phys. Rev. Lett.* **34,** 1306.
23. Clauser, J. F. (1974). *Phys. Rev.* **D9,** 853.
24. Camhy-Val, C. and Dumont, A. M. (1970). *Astron. Astrophys.* **6,** 27.

9. Nonlinear optics

THE rate of absorption of light by a two-level atom has a component proportional to the beam intensity or energy density, whose size is determined by the Einstein B coefficient. In the derivation of the B coefficient in §§2.3 and 2.4, it was necessary to retain only the part of the transition rate linear in the beam intensity. However, the complete expression for the transition rate also contains terms of higher order in the intensity. The higher-order, or nonlinear terms, are normally much smaller than the linear terms, but this is not necessarily the case for light from a powerful laser source. The present chapter treats the effects of the nonlinear terms on the optical properties of atoms.

The higher-order terms in the absorption rate correspond in quantum language to the excitation of an atom by processes in which two or more photons are absorbed. However, the nonlinear terms in the interaction of light with atoms give rise to a variety of optical processes in addition to multiple-photon absorption. For example, a beam of monochromatic light in interaction with atoms can be partially converted into light whose frequencies are harmonics of the fundamental frequency; alternatively, beams of two or more different frequencies can combine to produce light at the sums and differences of the original frequencies. Again, a strong beam of light can change the refractive index of a medium through which it passes, by an amount that depends on the beam intensity; the scattering of light described in Chapter 8 changes its nature for sufficiently strong incident light, where stimulated scattering becomes important.

The effect of linear absorption and emission in changing the initial statistical properties of light beams is considered in §§7.3 and 7.4. Analogous effects occur for the light beams that participate in nonlinear optical processes. There is now the additional feature that the rates of the nonlinear processes generally depend upon the degrees of coherence of the participating beams. The nonlinear rates thus change with time as the nonlinear process itself changes the photon statistics of the light, leading to time dependences of beam intensities that depend quite sensitively on the initial nature of the light. Some nonlinear processes are capable of producing nonclassical light of the kind defined in §6.5.

Nonlinear optics thus embraces a wide variety of phenomena and is an extensive field of study. The aim of the present chapter is to describe the theory

of some of the simpler processes rather than to give a comprehensive account. The treatment is limited to the nonlinear processes that occur in isotropic media, where the atomic or molecular states have well-defined parity. The atom–radiation Hamiltonian is restricted to the electric-dipole term, and the light beams are assumed to be single-mode excitations of the radiation field.

A greater variety of nonlinear processes occurs for the interaction of light with anisotropic molecules or with atoms at sites in crystals that lack inversion symmetry. The higher-order terms in the multipole expansion of the atom–radiation interaction lead to further nonlinear processes. Extensions of the theory given here are required to treat light beams in which many modes of the radiation field are excited. We do not consider these more general problems, but leave them for specialized textbooks.[1–7]

9.1. Double-beam two-photon absorption

It is convenient to begin the treatment of nonlinear optics with a specific example. We consider first the simultaneous absorption of two photons, and then show how this process fits into the more general theory of nonlinear optics.

The calculation of the two-photon absorption rate parallels the theory of the scattering cross-section in Chapter 8. Both processes result from the interaction of two distinct photons with a single atom. In the scattering of light, one photon is absorbed and one is emitted, whereas both are absorbed in the present calculation. Let the absorbed photons have different frequencies, ω_1, ω_2 and wavevectors $\mathbf{k}_1, \mathbf{k}_2$ corresponding to two single-mode light beams. We suppose that the two-photon absorption excites the atom from its ground state $|1\rangle$ to an excited state $|f\rangle$ of energy $\hbar\omega_f$.

The atom–radiation interaction in the electric-dipole approximation is given in eqn (8.67). Fig. 9.1 shows the diagrams that represent the three possible contributions in the time-dependent perturbation theory of two-photon absorption. The diagrams are similar to those of Fig. 8.10 except that the wavy line for creation of the scattered photon is replaced by a line that represents destruction of the second incident photon. Diagram (a) represents the $\hat{\mathscr{H}}_{\mathrm{NL}}$ part of the absorption matrix element. By arguments similar to those that follow eqn (8.69), it can be shown that $\hat{\mathscr{H}}_{\mathrm{NL}}$ makes a negligible contribution to the transition rate, and this part of the interaction Hamiltonian will therefore be ignored.

The remaining part of the Hamiltonian is

$$\hat{\mathscr{H}}_{\mathrm{ED}} = e\mathbf{D}.(\hat{\mathbf{E}}_1(\mathbf{r})+\hat{\mathbf{E}}_2(\mathbf{r})), \tag{9.1}$$

where $\hat{\mathbf{E}}_1(\mathbf{r})$ and $\hat{\mathbf{E}}_2(\mathbf{r})$ are the transverse electric-field operators for the two light beams at the atomic position $\mathbf{r}$. The two-photon absorption is of second-order in $\hat{\mathscr{H}}_{\mathrm{ED}}$, and there are contributions from the two possible orders of the

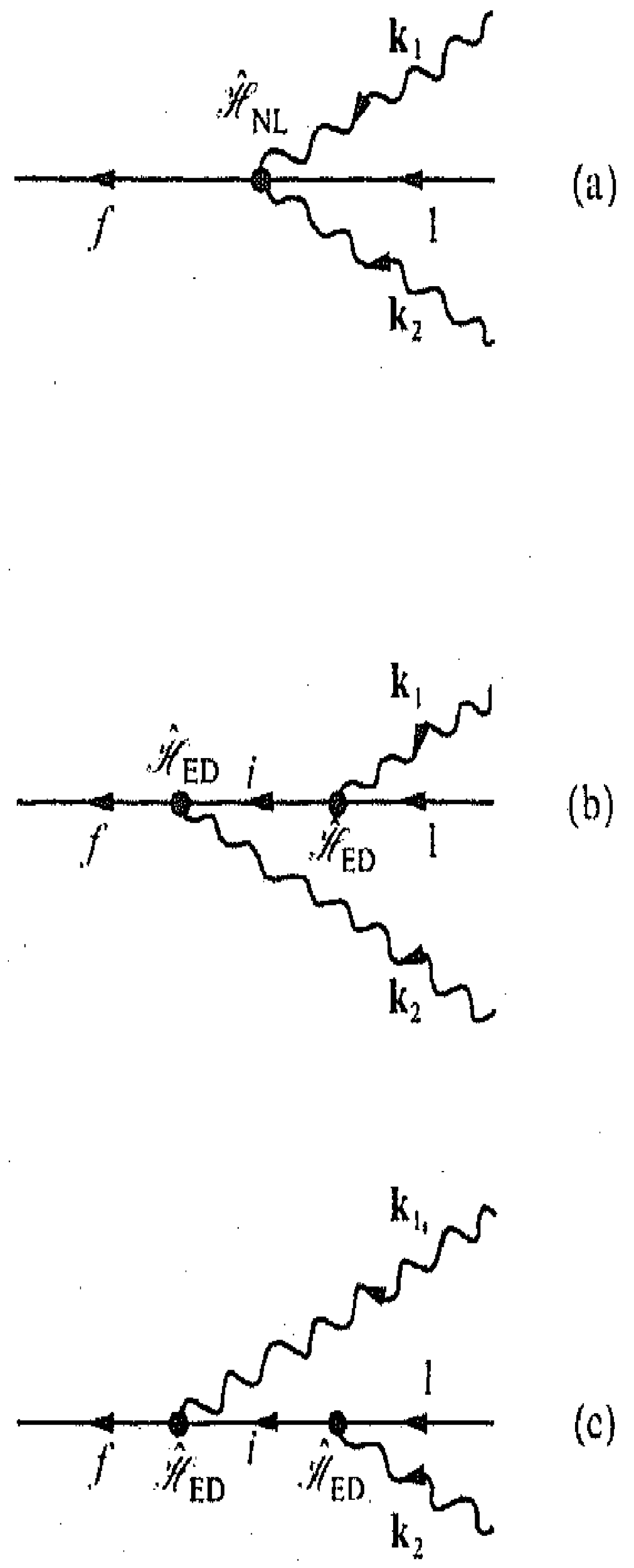
$\mathbf{k}_1$
$\hat{\mathcal{H}}_{\mathrm{NL}}$
f
1
$\mathbf{k}_2$
(a)
$\mathbf{k}_1$
$\hat{\mathcal{H}}_{\mathrm{ED}}$
i
f
$\hat{\mathcal{H}}_{\mathrm{ED}}$
1
$\mathbf{k}_2$
(b)
$\mathbf{k}_1$
1
f
$\hat{\mathcal{H}}_{\mathrm{ED}}$
i
$\hat{\mathcal{H}}_{\mathrm{ED}}$
$\mathbf{k}_2$
(c)

FIG. 9.1. Diagrammatic representations of the three contributions to two-photon absorption in first- and second-order time-dependent perturbation theory. The first-order diagram (a) produces a transition rate that is negligible compared to that of the second-order diagrams (b) and (c).

photon destruction operators, that is $\hat{a}_2\hat{a}_1$ and $\hat{a}_1\hat{a}_2$. These contributions are represented by diagrams (b) and (c) of Fig. 9.1.

The transition rate for two-photon absorption is obtained straightforwardly from the second-order part of eqn (5.152). The matrix element is very similar to eqn (8.69) for light scattering. Let $|R\rangle$ and $|R_f\rangle$ be the states of the radiation field before and after the two-photon absorption, the initial state being a two-mode number state of the kind defined in eqn (4.107). The transition rate is then

$$\frac{1}{\tau} = \frac{2\pi e^4}{\hbar^4}\sum_{R_f}\left|\sum_{R_i}\sum_{i}\left(\frac{\langle R_f, f|\mathbf{D}.\hat{\mathbf{E}}_2^+(\mathbf{r})|R_i, i\rangle\langle R_i, i|\mathbf{D}.\hat{\mathbf{E}}_1^+(\mathbf{r})|R, 1\rangle}{\omega_1-\omega_i} + \frac{\langle R_f, f|\mathbf{D}.\hat{\mathbf{E}}_1^+(\mathbf{r})|R_i, i\rangle\langle R_i, i|\mathbf{D}.\hat{\mathbf{E}}_2^+(\mathbf{r})|R, 1\rangle}{\omega_2-\omega_i}\right)\right|^2 \delta(\omega_1+\omega_2-\omega_f), \quad (9.2)$$

where $\hat{\mathbf{E}}^+$ is the photon-destructive part of the electric-field operator defined in eqn (5.84), $|R_i\rangle$ and $|i\rangle$ are the intermediate states of the radiation and the

atom, and the two terms in the matrix element are the contributions of diagrams (b) and (c) of Fig. 9.1. The final-state summation can be taken over all states of the radiation field, since the physical requirement that $|R_f\rangle$ has two photons fewer than the initial state $|R\rangle$ is automatically enforced by the use in eqn (9.2) of the destructive parts of the field operators. The total two-photon transition rate for the atom could be obtained by a further summation of eqn (9.2) over the atomic states $|f\rangle$, but we consider here the contribution of a particular atomic final state.

The transition rate is simplified by factorization of the radiative and atomic parts. Consider the radiative part; use of the closure relation

$$\sum_{R_i}|R_i\rangle\langle R_i| = 1 \quad (9.3)$$

removes the summation over intermediate states of the radiation field. The squared matrix element from the first term in eqn (9.2) then contains

$$\sum_{R_f}\langle R|\hat{\mathbf{E}}_1^-(\mathbf{r})\hat{\mathbf{E}}_2^-(\mathbf{r})|R_f\rangle\langle R_f|\hat{\mathbf{E}}_2^+(\mathbf{r})\hat{\mathbf{E}}_1^+(\mathbf{r})|R\rangle = \langle R|\hat{\mathbf{E}}_1^-(\mathbf{r})\hat{\mathbf{E}}_2^-(\mathbf{r})\hat{\mathbf{E}}_2^+(\mathbf{r})\hat{\mathbf{E}}_1^+(\mathbf{r})|R\rangle, \quad (9.4)$$

where the closure relation has been used again. The second term in eqn (9.2) contains a similar factor, which can be written in the form (9.4) since $\hat{\mathbf{E}}_1^+$ and $\hat{\mathbf{E}}_2^+$ commute.

The coherence of the two light beams has an important influence on the two-photon absorption, and it is therefore desirable to evaluate the transition rate for light of arbitrary statistical properties. If the initial state of the radiation field is a statistical mixture, it is necessary to sum the transition rates for all the pure-state components of the mixture, each weighted with the appropriate probability. The generalization is analogous to that made in eqn (5.97) for the single-photon transition rate, and the result is conveniently expressed in terms of the density operator. The transition rate (eqn (9.2)) thus becomes

$$1/\tau = (2\pi e^4/\hbar^4)|\mathcal{M}_{\mathrm{TPA}}|^2\,\delta(\omega_1+\omega_2-\omega_f)\mathrm{Tr}\big(\hat{\rho}\hat{E}_1^-(\mathbf{r})\hat{E}_2^-(\mathbf{r})\hat{E}_2^+(\mathbf{r})\hat{E}_1^+(\mathbf{r})\big), \quad (9.5)$$

where

$$\mathcal{M}_{\mathrm{TPA}} = \sum_i\left(\frac{\boldsymbol{\varepsilon}_2.\mathbf{D}_{fi}\boldsymbol{\varepsilon}_1.\mathbf{D}_{i1}}{\omega_1-\omega_i}+\frac{\boldsymbol{\varepsilon}_1.\mathbf{D}_{fi}\boldsymbol{\varepsilon}_2.\mathbf{D}_{i1}}{\omega_2-\omega_i}\right), \quad (9.6)$$

and $\boldsymbol{\varepsilon}_1$ and $\boldsymbol{\varepsilon}_2$ are the unit polarization vectors of the two light beams.

The two-photon transition rate is used to derive the propagation characteristics of the two light beams as they traverse a gas of identical atoms. Suppose that the two beams are propagated parallel to the z-axis, and let $\bar{I}_1$ and $\bar{I}_2$ be their mean intensities at coordinate z. According to eqn (1.96), the spatial rate of change of beam intensity is equal to the time rate of change of its energy density, and hence

$$\partial \bar{I}_1/\partial z = -N\hbar\omega_1/V\tau \tag{9.7}$$

$$\partial \bar{I}_2/\partial z = -N\hbar\omega_2/V\tau, \tag{9.8}$$

where N is the number of identical atoms in volume V. In these expressions τ is given by eqn (9.5), except that an average must be taken to allow for the random atomic or molecular orientations. It is assumed in eqns (9.7) and (9.8) that no linear absorption of the light occurs; the attenuation arises only from the two-photon absorption.

The expectation value of the product of field operators that appears in eqn (9.5) is similar to the correlation function in the numerator of the degree of second-order coherence (8.114) defined for two beams of frequencies ω_1 and ω_2. With space and time coordinates omitted, we have

$$\mathrm{Tr}(\hat{\rho}\hat{E}_1^-\hat{E}_2^-\hat{E}_2^+\hat{E}_1^+) = \langle\hat{E}_1^-\hat{E}_1^+\rangle\langle\hat{E}_2^-\hat{E}_2^+\rangle g_{21}^{(2)}(0). \tag{9.9}$$

The expectation values on the right are proportional to the beam intensities in accordance with eqn (5.100), which in the notation of the present calculation gives

$$\bar{I}_1 = 2\epsilon_0 c\eta_1\langle\hat{E}_1^-\hat{E}_1^+\rangle \tag{9.10}$$

$$\bar{I}_2 = 2\epsilon_0 c\eta_2\langle\hat{E}_2^-\hat{E}_2^+\rangle. \tag{9.11}$$

The refractive indices η_1 and η_2 at frequencies ω_1 and ω_2 are inserted on the right-hand sides of these expressions, as in eqn (1.89). With the assumption of no linear absorption and only a small amount of two-photon absorption, the mode wavevectors are essentially real with magnitudes

$$k_1 = \eta_1\omega_1/c, \qquad k_2 = \eta_2\omega_2/c. \tag{9.12}$$

The trace in eqn (9.9) becomes

$$\mathrm{Tr}(\hat{\rho}\hat{E}_1^-\hat{E}_2^-\hat{E}_2^+\hat{E}_1^+) = \bar{I}_1\bar{I}_2 g_{21}^{(2)}(0)/4\epsilon_0^2c^2\eta_1\eta_2. \tag{9.13}$$

The propagation equations (9.7) and (9.8) are quite difficult to solve in general because the degree of second-order coherence contained in the trace changes as the two-photon absorption proceeds. Light beams obtained from different sources are statistically independent on arrival at the absorbing gas, corresponding to

$$g_{21}^{(2)}(0) = 1 \qquad \text{(independent beams)}. \tag{9.14}$$

However, the two-photon absorption process itself destroys the statistical independence and produces a degree of second-order coherence that deviates progressively from unity. We ignore this feature for the remainder of the present section, and consider it further in §9.7. Thus with substitution of eqns (9.5), (9.13), and (9.14), eqn (9.7) becomes

$$\frac{\partial \bar{I}_1}{\partial z} = -\frac{\pi e^4}{2\epsilon_0^2\hbar^3c^2}\frac{N}{V}\frac{\omega_1}{\eta_1\eta_2}\overline{|\mathcal{M}_{\mathrm{TPA}}|^2}\,\delta(\omega_1+\omega_2-\omega_f)\bar{I}_1\bar{I}_2, \tag{9.15}$$

where the horizontal bar denotes the orientation average mentioned above. Some of the orientation averages that occur in nonlinear optics are quite tedious to carry out, and no explicit evaluations are given here.

Eqn (9.8) can be cast in a form similar to eqn (9.15), to obtain a pair of coupled equations for $\bar{I}_1$ and $\bar{I}_2$. This second equation need not be written out explicitly, however, since we note from eqns (9.7) and (9.8) that

$$\frac{1}{\omega_1}\frac{\partial \bar{I}_1}{\partial z} = \frac{1}{\omega_2}\frac{\partial \bar{I}_2}{\partial z}. \tag{9.16}$$

It follows that

$$(\bar{I}_1/\omega_1)-(\bar{I}_2/\omega_2) = \text{constant} = (\bar{I}_{10}/\omega_1)-(\bar{I}_{20}/\omega_2), \tag{9.17}$$

where $\bar{I}_{10}$ and $\bar{I}_{20}$ are the values of $\bar{I}_1$ and $\bar{I}_2$ at $z = 0$, the start of the absorbing medium. Since $\bar{I}_1/\omega_1$ is proportional to the rate at which photons cross unit area, eqn (9.17) is a consequence of the physical property of the absorption process that one photon is removed from each light beam in each absorption event.

It is now possible, with the help of eqn (9.17), to eliminate $\bar{I}_2$ from eqn (9.15) and obtain a differential equation in which $\bar{I}_1$ is the only unknown. The solution is

$$\bar{I}_1 = \bar{I}_{10}\frac{(\bar{I}_{10}/\omega_1)-(\bar{I}_{20}/\omega_2)}{(\bar{I}_{10}/\omega_1)-(\bar{I}_{20}/\omega_2)\exp(-K_2z)}, \tag{9.18}$$

and hence from eqn (9.17),

$$\bar{I}_2 = \bar{I}_{20}\frac{\{(\bar{I}_{10}/\omega_1)-(\bar{I}_{20}/\omega_2)\}\exp(-K_2z)}{(\bar{I}_{10}/\omega_1)-(\bar{I}_{20}/\omega_2)\exp(-K_2z)}, \tag{9.19}$$

where the two-photon absorption coefficient K_2 is defined by

$$K_2 = \frac{\pi e^4}{2\epsilon_0^2\hbar^3c^2}\frac{N}{V}\frac{\omega_1\omega_2}{\eta_1\eta_2}\overline{|\mathcal{M}_{\mathrm{TPA}}|^2}\,\delta(\omega_1+\omega_2-\omega_f)\left(\frac{\bar{I}_{10}}{\omega_1}-\frac{\bar{I}_{20}}{\omega_2}\right). \tag{9.20}$$

In deriving this result, it has been assumed that beam 1 has the larger flux of photons, so that the constant in eqn (9.17) is positive. Also, it is assumed throughout that the two-photon absorption is sufficiently weak for saturation of the atomic transition to be ignored, and all N atoms are taken to be in their ground states.

The solutions given in eqns (9.18) and (9.19) remain valid in the case of equal fluxes of photons in the two incident beams, but the limit where $\bar{I}_{20}/\omega_2$ tends to $\bar{I}_{10}/\omega_1$ must be evaluated with care. The exponential dependence of eqns (9.18) and (9.19) on the distance z is replaced by an inverse dependence for two beams of equal photon flux.

The spatial dependence of the beam intensities predicted by eqns (9.18) and (9.19) is illustrated in Fig. 9.2. It is convenient to plot the beam intensities divided by their frequencies; the two curves then remain a constant vertical distance apart, according to eqn (9.17). The two-photon absorption ceases when the weaker beam is exhausted. The remnant of the stronger beam then passes through the remainder of the gas without further attenuation.

In some experiments on two-photon absorption, the stronger beam is produced by a laser of fixed frequency and the weaker beam is obtained from a chaotic source, its frequency being varied to examine the details of the two-photon spectrum. In this case, beam 1 is much more intense than beam 2 and the percentage reduction in its intensity is slight, even when beam 2 is completely exhausted. To a good approximation, eqn (9.19) reduces to

$$\bar{I}_2 = \bar{I}_{20} \exp(-K_2 z) \qquad (\bar{I}_1 \gg \bar{I}_2), \tag{9.21}$$

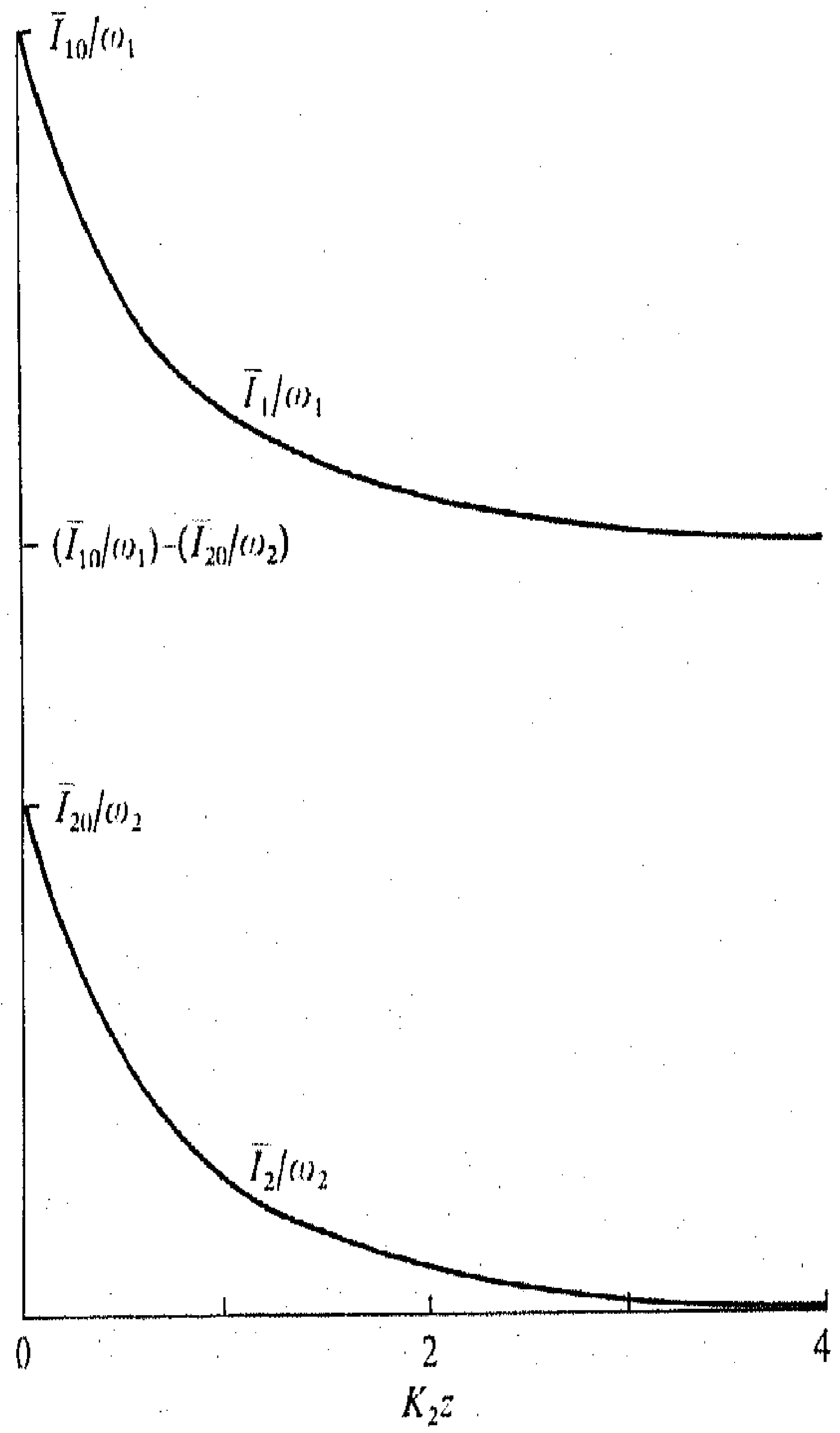

FIG. 9.2. Dependence of the beam intensities on distance in two-photon absorption. The vertical scale is proportional to the beam photon fluxes, the difference between them being a constant independent of z.

and $\bar{I}_{20}$ can be neglected in the expression (9.20) for K_2. The behaviour of the intensity of beam 2 in this limit is similar to that for ordinary linear absorption, as in eqn (1.90).

The selection rules for the atomic states $|f\rangle$ that can be excited by two-photon absorption are the same as those for the atomic final states in inelastic light scattering, discussed in §8.8. Thus the accessible states $|f\rangle$ must have the *same* parity as the ground state, in contrast to single-photon electric-dipole absorption where the final atomic state must have *opposite* parity to the ground state. In addition, it is clear that the magnitude of the matrix element given in eqn (9.6) depends on the directions of the polarization vectors ε_1 and ε_2. Even when the state $|f\rangle$ satisfies the selection rules for two-photon absorption, the matrix element may vanish for certain relative orientations of ε_1 and ε_2.

The calculated[8] frequency dependence of the two-photon absorption coefficient for the 1S to 2S transition of hydrogen is shown in Fig. 9.3. The quantity plotted is the dimensionless factor

$$\omega_1 \omega_2 \overline{|\mathcal{M}_{\mathrm{TPA}}|^2} / a_0^4, \tag{9.22}$$

where a_0 is the Bohr radius given by eqn (2.15). The photon frequencies must

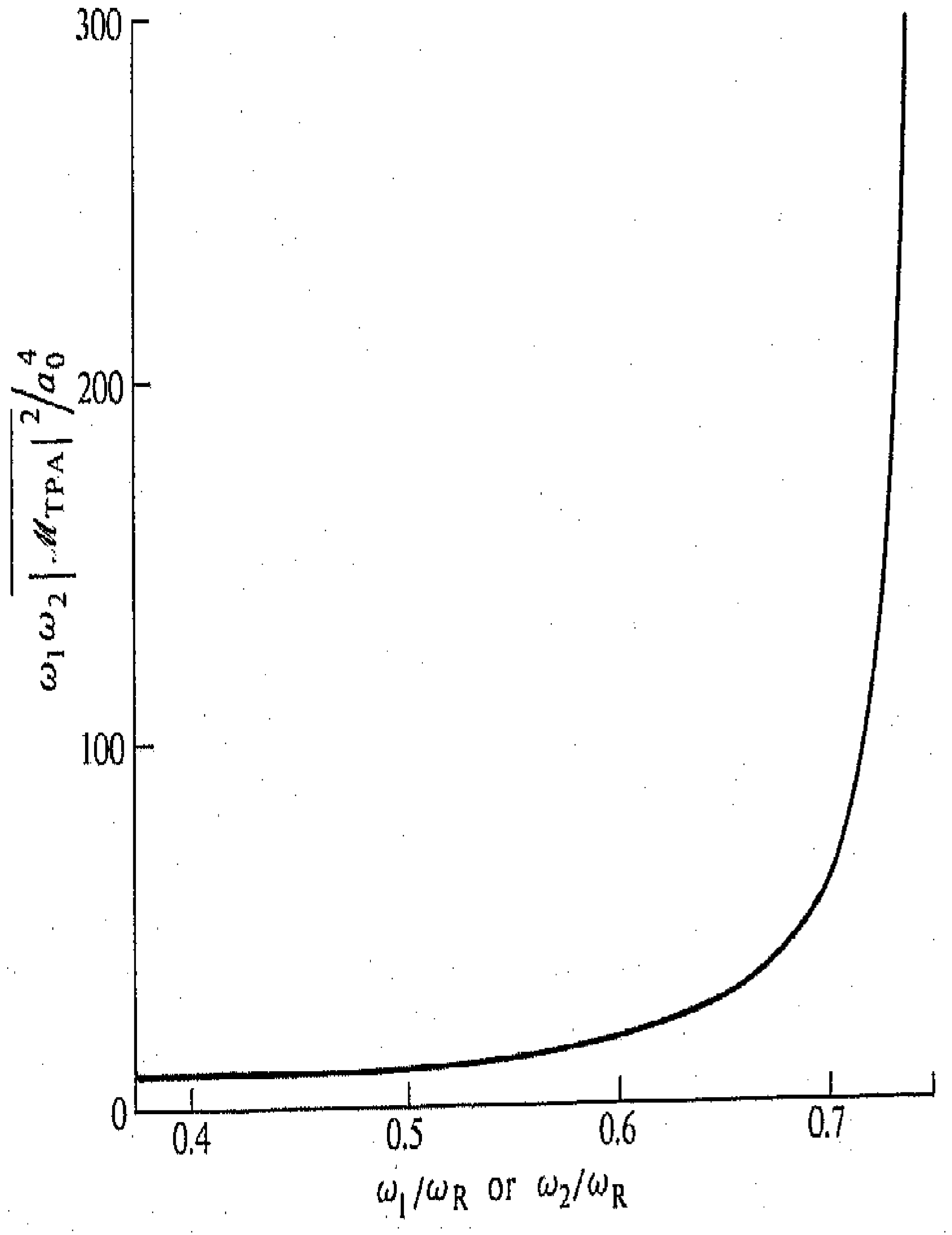

FIG. 9.3. Calculated frequency dependence of the two-photon absorption coefficient for the 1S to 2S transition of hydrogen. (After F. Bassani *et al.*, ref. 8.)

satisfy

$$\omega_1+\omega_2 = \tfrac{3}{4}\omega_R, \qquad (9.23)$$

with the Rydberg frequency defined in eqn (2.29). It is seen from eqn (9.6) that the plotted factor (9.22) is symmetrical in ω_1 and ω_2; the horizontal axis in Fig. 9.3 can accordingly be restricted to values of one of the frequencies between $\frac{3}{8}\omega_R$ and $\frac{3}{4}\omega_R$. Note the resonant behaviour of the absorption coefficient for ω_1 or ω_2 equal to the transition frequency. By contrast, the scattering cross-section for the same hydrogenic transition illustrated in Fig. 8.15 shows no resonance at $\omega = \frac{3}{4}\omega_R$, but has the finite value obtained from eqn (8.105).

Inclusion of the effects of homogeneous broadening of the atomic state $|f\rangle$ in the theory of two-photon absorption leads to the replacement of the delta function in eqn (9.20) by a Lorentzian lineshape,

$$\delta(\omega_1+\omega_2-\omega_f) \to \frac{\gamma'_f/\pi}{(\omega_f-\omega_1-\omega_2)^2+\gamma_f'^2}, \qquad (9.24)$$

where γ'_f includes the usual radiative and collisional contributions considered in Chapter 2. The transition rate theory given above is valid when the collision linewidth is much larger than the radiative linewidth, in accordance with the discussion of §2.14.

The effect of Doppler broadening on the two-photon absorption spectrum depends upon the relative orientation of the light beams at frequencies ω_1 and ω_2. In the special case where the frequencies are the same ($\omega_1 = \omega_2$) but the beams propagate in opposite directions, it is clear from eqn (2.148) that the Doppler shifts in atomic transition frequency with respect to the two beams are equal in magnitude but opposite in sign. Thus the absorption of two photons, one from each beam, occurs at a fixed sum frequency ω_f that is independent of the atomic velocity. It is therefore possible in principle to observe two-photon absorption spectra that are free of the effects of Doppler broadening.[9] For more general values of the beam frequencies and orientations, the expected Doppler width varies between this zero value and the usual magnitude calculated in eqn (2.151).

Problem 9.1. Show that the full width of the Doppler-broadened line for absorption of two photons from beams of mean frequencies ω_1 and ω_2 inclined at a relative angle θ is

$$2\Delta = 2(\omega_1^2+\omega_2^2+2\omega_1\omega_2 \cos\theta)^{\frac{1}{2}}(2k_BT \ln 2/Mc^2)^{\frac{1}{2}}, \qquad (9.25)$$

where the width is assumed very small compared to ω_1 or ω_2.

The narrow linewidths that are obtainable in practice by Doppler-free two-photon absorption spectroscopy permit high-resolution measurements of atomic transition frequencies with somewhat lower-power light sources than would otherwise be needed. Various atomic transitions have been studied by these methods,[6,10] but we restrict attention here to work on the 1S to 2S transition of hydrogen.[11,12] Fig. 9.4 shows the relevant energy levels of the hydrogen atom. The tunable laser light source used in the experiments provided photons at frequencies in the region of $0{\cdot}617\times10^{15}$ Hz and in the region of the second harmonic of this frequency at $1{\cdot}234\times10^{15}$ Hz. A pair of counter-propagating photons at the latter frequency satisfies the energy and momentum conservation requirements for Doppler-free two-photon absorption by the transition from the $1^2S_{\frac{1}{2}}$ ground state to the $2^2S_{\frac{1}{2}}$ excited state. Absorption occurs in accordance with the theory given earlier in the present section and the numerical values shown in Fig. 9.3. The absorption rate was monitored, not by measurement of the depletion of the incident light, but by observation of the photons emitted in subsequent fluorescent decay of the excited atoms to their ground states. The $2^2S_{\frac{1}{2}}$ state cannot itself decay radiatively to the $1^2S_{\frac{1}{2}}$ state (see Fig. 2.4) but collisions transfer the excited atoms to their radiative $2^2P_{\frac{1}{2}}$ states, the hydrogen $n = 2$ levels being separated by the Lamb shift discussed in §5.12.

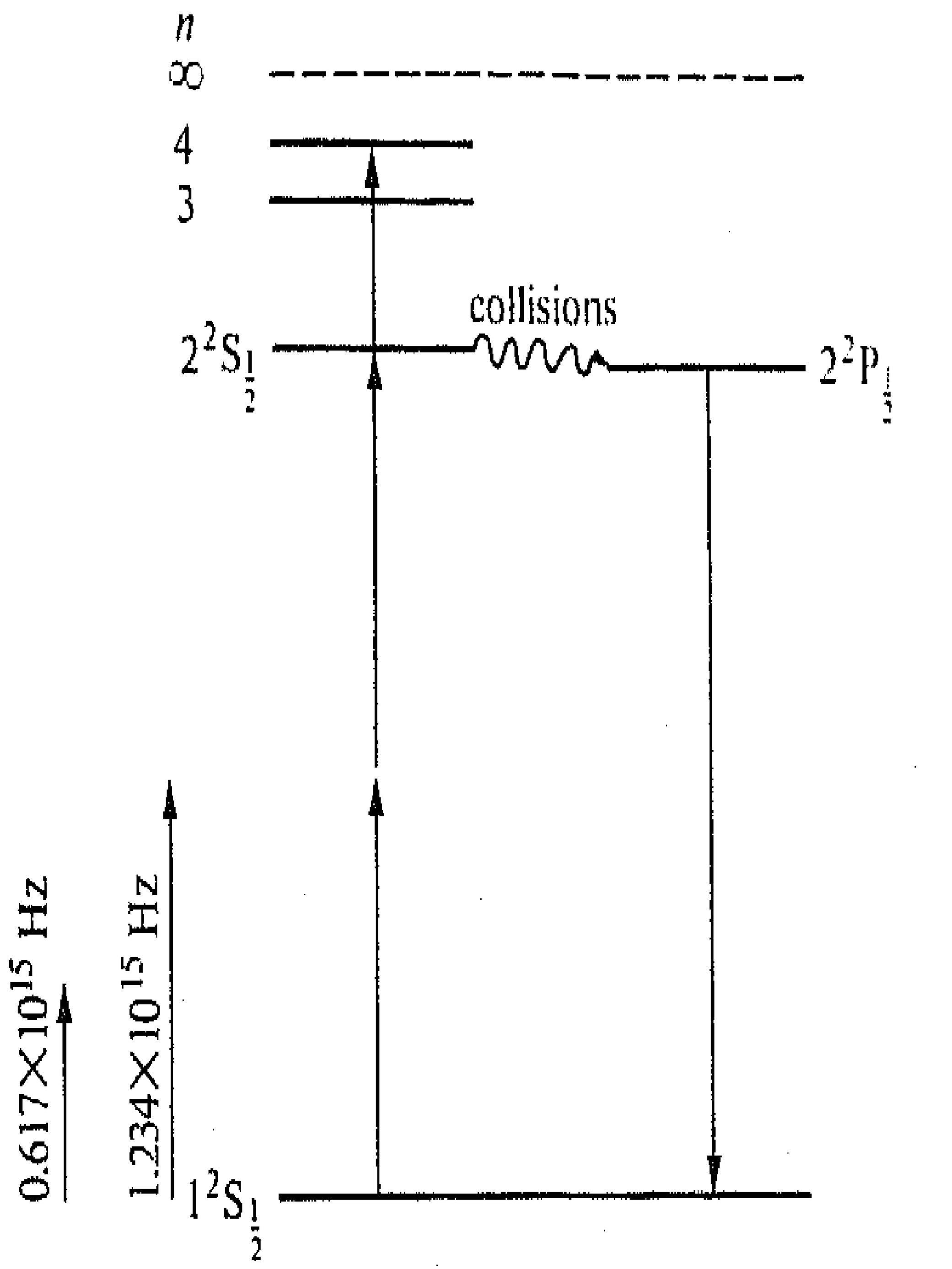

FIG. 9.4. Hydrogen-atom energy-level scheme for the two-photon absorption experiments of refs. 11 and 12. The two arrows on the left show the incident frequencies.

Photons at the fundamental frequency of $0{\cdot}617\times10^{15}$ Hz have the correct energy to cause single-photon absorption for the transition between the $n = 2$ and $n = 4$ states. If the hydrogen state binding energies were exactly proportional to $1/n^2$, then the single-photon absorption of the fundamental and the two-photon absorption of the second harmonic would both occur at exactly the same fundamental frequency. Discrepancies between the frequencies for which the two kinds of absorption in fact occur provide information on various small shifts and splittings of the hydrogen energy levels. The Lamb shift of the ground $1^2S_{\frac{1}{2}}$ state, which is otherwise difficult to determine, has been measured in this way.[11,12]

9.2. Single-beam two-photon absorption

Two-photon absorption can also occur in the presence of a single beam of light. The two absorbed photons are then indistinguishable, and the frequency of the light must be one half that of the atomic excitation under study. The theory of two-beam two-photon absorption requires a few modifications for the single-beam arrangement. With only one beam, the electric-dipole interaction (eqn (9.1)) reduces to a single term, and there is no longer any distinction between diagrams (b) and (c) of Fig. 9.1. There is only a single kind of term in the matrix element for the transition, and the transition rate (eqn (9.5)) is replaced by

$$\frac{1}{\tau} = \frac{2\pi e^4}{\hbar^4}\left|\sum_i \frac{\boldsymbol{\varepsilon}_1 . \mathbf{D}_{fi}\boldsymbol{\varepsilon}_1 . \mathbf{D}_{i1}}{\omega_1 - \omega_i}\right|^2 \delta(2\omega_1 - \omega_f)\mathrm{Tr}(\hat{\rho}\hat{E}_1^-(\mathbf{r})\hat{E}_1^-(\mathbf{r})\hat{E}_1^+(\mathbf{r})\hat{E}_1^+(\mathbf{r})). \qquad (9.26)$$

The trace of electric-field operators is the same function as occurs in the definition, eqn (6.23) or (8.114), of the degree of second-order coherence for a single beam of light evaluated at zero time delay ($\tau = 0$). Thus analogous to eqn (9.13),

$$\mathrm{Tr}(\hat{\rho}\hat{E}_1^-\hat{E}_1^-\hat{E}_1^+\hat{E}_1^+) = \bar{I}_1^2 g_{11}^{(2)}(0)/4\epsilon_0^2 c^2 \eta_1^2, \qquad (9.27)$$

where the electromagnetic field quantities, including the degree of second-order coherence, are evaluated at the position and time of the two-photon absorption event.

It is assumed that the beam is propagated parallel to the z-axis, and its intensity then satisfies an equation similar to eqn (9.7), except that two photons are now removed from the *same* beam each time a two-photon absorption takes place,

$$\partial\bar{I}_1/\partial z = -2N\hbar\omega_1/V\tau. \qquad (9.28)$$

With the help of eqns (9.26) and (9.27), this can be written

$$\partial\bar{I}_1/\partial z = -K_2' g_{11}^{(2)}(0)\bar{I}_1^2/2\bar{I}_{10}, \qquad (9.29)$$

where

$$K_2' = \frac{\pi e^4}{2\epsilon_0^2\hbar^3 c^2}\frac{N}{V}\frac{\omega_1^2}{\eta_1^2}\,4\overline{\left|\sum_i \frac{\boldsymbol{\varepsilon}_1 . \mathbf{D}_{fi}\boldsymbol{\varepsilon}_1 . \mathbf{D}_{i1}}{\omega_1 - \omega_i}\right|^2}\,\delta(2\omega_1 - \omega_f)\frac{\bar{I}_{10}}{\omega_1}. \qquad (9.30)$$

In this expression, the bar again denotes an orientation average, and the delta function should strictly be replaced by a Lorentzian lineshape analogous to eqn (9.24). Note that K_2' is identical to K_2 defined by eqns (9.20) and (9.6) if $\bar{I}_{20}$ is neglected in K_2, and the photons 1 and 2 are made identical.

The propagation eqn (9.29) is difficult to solve rigorously because the degree of second-order coherence is in general a function of z. Let us ignore this complication for the present and assume that $g_{11}^{(2)}(0)$ is a constant. The solution of eqn (9.29) is then

$$\bar{I}_1 = \bar{I}_{10}(1 + \tfrac{1}{2}g_{11}^{(2)}(0)K_2' z)^{-1} \qquad (9.31)$$

or, for small absorption, where the denominator can be expanded,

$$\bar{I}_1 \approx \bar{I}_{10}(1 - \tfrac{1}{2}g_{11}^{(2)}(0)K_2' z). \qquad (9.32)$$

The rate of two-photon absorption from a single beam depends on the statistical properties of the light via the factor $g_{11}^{(2)}(0)$. The degree of second-order coherence for coherent light given by eqn (6.30) is

$$g_{11}^{(2)}(0) = 1, \qquad (9.33)$$

while for single-mode chaotic light from eqn (6.31)

$$g_{11}^{(2)}(0) = 2. \qquad (9.34)$$

Thus for small z, where (9.32) is valid, chaotic light is two-photon absorbed at twice the rate for coherent light.[13,14]

The dependence of the two-photon absorption rate on the magnitude of the degree of second-order coherence can be understood in qualitative terms. As discussed in Chapters 3 and 6, the size of $g_{11}^{(2)}(0)$ is related to the magnitude of the fluctuations in the instantaneous beam-intensity. Since the rate of two-photon absorption is proportional to the square of the intensity at the time of the atom–radiation interaction, enhanced absorption occurs for light beams whose intensities fluctuate to higher values than their long-time averages. For example, a beam whose intensity has a constant value $2\bar{I}$ for intervals that take up one-half of the time axis, but is zero for the remaining time intervals, has a mean intensity $\bar{I}$ and a mean-square instantaneous intensity $2\bar{I}^2$. Such a beam is two-photon absorbed at twice the rate of a beam whose instantaneous intensity is a constant $\bar{I}$ at all times. This conclusion agrees with eqn (9.32) since the degree of second-order coherence of the pulsed beam is shown by eqn (3.115) to be equal to 2 for $f = \frac{1}{2}$.

These features are further illustrated in Fig. 9.5, which shows the results of a calculation of the effect of two-photon absorption on the intensity fluctuations of a chaotic light beam.[15] The calculation is classical and the degree of second-order coherence, defined in terms of intensities or electric fields by eqn (3.71), is restricted to the classical range of eqn (3.77). It is shown in §9.8 that two-photon absorption can produce *nonclassical* light whose degree of second-order coherence lies in the range of eqn (6.26). However, the classical model adopted in Fig. 9.5 provides a useful qualitative understanding of the effect of two-photon absorption. The upper part shows the time dependence of the instantaneous intensity of the original beam, and is similar to Fig. 3.4. The

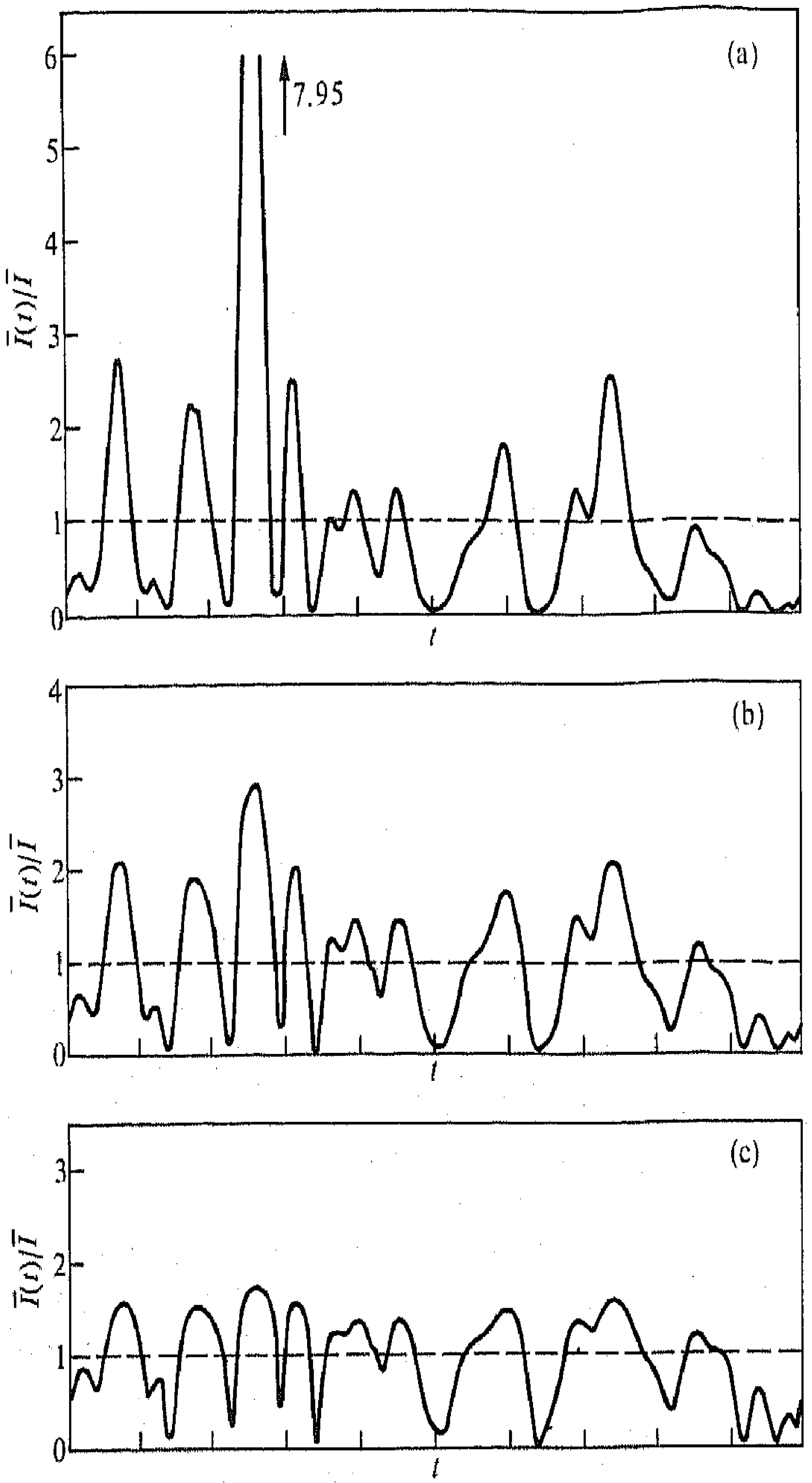

FIG. 9.5. The effect of two-photon absorption on the fluctuations of intensity in a chaotic light beam. The time dependence of the instantaneous intensity in the same section of beam is shown (a) before any absorption takes place, (b) after an absorption path length $(K'_2)^{-1}$, and (c) after a path length $4(K'_2)^{-1}$. The dashed line in each graph shows the long-time average intensity. (After H. P. Weber, ref. 15.)

second and third parts show the intensity fluctuations in the same section of the beam after its passage through increasing thicknesses of two-photon-absorbing medium. It is seen that the two-photon absorption, and consequent attenuation of the beam, occur preferentially at the maxima of the intensity variations. The peaks are progressively eroded in Fig. 9.5, while the troughs are barely changed by the negligibly small two-photon absorption at low intensity. This behaviour contrasts with the effect of single-photon absorption, which reduces the instantaneous intensity by a constant fraction, irrespective of its magnitude.

Two-photon absorption therefore smooths intensity fluctuations and changes the statistical properties of the unabsorbed portion of the beam. In particular, the magnitude of the degree of second-order coherence $g_{11}^{(2)}(0)$ is reduced by a significant amount of two-photon absorption, and the analysis that leads to eqn (9.31) becomes invalid. More generally, in two-photon absorption with distinct beams, the absorption destroys the statistical independence of the beams and the results (9.18) and (9.19) require modification when $K_2 z$ is comparable to, or greater than, unity. The theory of these effects is discussed in §§9.6–9.8.

9.3. The nonlinear susceptibility

Having examined a particular nonlinear process in some detail, we now show how the two-photon absorption is related to the general theory of nonlinear optics. The linear frequency-dependent susceptibility of a medium provides a complete description of the linear propagation of electromagnetic waves in the medium. In a similar way, the propagation of electromagnetic waves through a medium in which nonlinear processes occur is describable in terms of the nonlinear susceptibility of the medium.

The nonlinear susceptibility is calculated by retaining the terms of higher order in the electric field of the radiation that are neglected in the derivation of the linear susceptibility. The expressions given in eqns (2.105) and (2.103) for $C_1(t)$ and $C_2(t)$ are just the first terms of power series in the atom–radiation interaction. The expansion of $C_1(t)$ contains all even powers of the electric field (or equivalently $\mathscr{V}$), while $C_2(t)$ has all the odd powers. The polarization formed from eqns (2.96) and (2.107) thus contains terms proportional to all odd powers of the electric field, and the relation (eqn 1.79) between polarization and field is generalized to

$$P = \epsilon_0(\chi^{(1)}E + \chi^{(3)}E^3 + \chi^{(5)}E^5 + \ldots). \tag{9.35}$$

Here $\chi^{(1)}$ is the same as the linear susceptibility $\chi(\omega)$ calculated in §2.8; $\chi^{(3)}$, $\chi^{(5)}$, etc. are components of the nonlinear susceptibility.

The general forms of the various components of the nonlinear susceptibility are given by quite cumbersome expressions that can be found in books on nonlinear optics.[1,2,7] The treatment here is confined to consideration of the first nonlinear term, that in $\chi^{(3)}$; the form of this component of the nonlinear susceptibility is derived later in two special cases by comparison with the results of calculations of nonlinear processes by time-dependent perturbation theory. We represent the electric fields of the light waves by classical magnitudes for the discussions of the present section. The susceptibility components, being properties of the nonlinear medium alone, are given correctly by a semiclassical theory.

The expansion (9.35) is valid for atoms and those molecules that are invariant under inversion. This symmetry operation changes the signs of both P and E, and it is clear that, with no even powers of E on the right-hand side, eqn (9.35) is correctly invariant under inversion. However, for molecules and for lattice sites in crystals without inversion symmetry, the restrictions on eqn (9.35) are less severe and terms in even powers of E may occur. In order to obtain such terms in the theory, and indeed to obtain correct forms for all components of the nonlinear susceptibility, it is necessary to work with multilevel atoms or molecules, and the two-level calculations of Chapter 2 are inadequate.

The linear susceptibility is of second order in the electric-dipole matrix elements D_{ij}, as for example in eqn (2.108). Each additional order in E in the nonlinear part of the polarization produces an additional dipole matrix element, and $\chi^{(n)}$ is thus of order $n+1$ in the dipole matrix elements. Successive components of the nonlinear susceptibility diminish in accordance with the approximate rule

$$\chi^{(n+2)}/\chi^{(n)} \approx \mathsf{E}_0^{-2}, \tag{9.36}$$

where the electric field E_0 is characteristic of the nonlinear medium, and is typically of order 10^{11} Vm^{-1}. The series on the right of eqn (9.35) converges for fields E that are smaller than E_0; Table 1.1 shows that E satisfies this criterion for almost all light beams, and indeed E is normally *much* smaller than E_0. It is often possible to terminate the series at the third-order term, which is itself much smaller than the linear term. The field E_0 is similar to that determined in problem 2.1.

The frequency dependence of the linear term in eqn (9.35) is straightforward; a field E of frequency ω induces an oscillating polarization at frequency ω, of a magnitude governed by $\chi^{(1)}(\omega)$. If E has components at several different frequencies, then their contributions to the polarization are simply additive. The behaviour of the nonlinear terms is more complicated. Consider the third-order term; if the electric field contains three distinct frequency components

$$\begin{aligned} E(t) = {} & E_1(\exp(-\mathrm{i}\omega_1 t)+\exp(\mathrm{i}\omega_1 t))+E_2(\exp(-\mathrm{i}\omega_2 t)+\exp(\mathrm{i}\omega_2 t)) \\ & +E_3(\exp(-\mathrm{i}\omega_3 t)+\exp(\mathrm{i}\omega_3 t)), \end{aligned} \tag{9.37}$$

then E^3 contains components having the 22 distinct frequencies

$$\begin{array}{llll} \omega_1+\omega_2+\omega_3 & \omega_1+\omega_2-\omega_3 & \omega_1-\omega_2+\omega_3 & -\omega_1+\omega_2+\omega_3 \\ 2\omega_1+\omega_2 & 2\omega_1+\omega_3 & 3\omega_1 & \\ 2\omega_2+\omega_1 & 2\omega_2+\omega_3 & 3\omega_2 & \\ 2\omega_3+\omega_1 & 2\omega_3+\omega_2 & 3\omega_3 & \\ 2\omega_1-\omega_2 & 2\omega_1-\omega_3 & \omega_1 & \\ 2\omega_2-\omega_1 & 2\omega_2-\omega_3 & \omega_2 & \\ 2\omega_3-\omega_1 & 2\omega_3-\omega_2 & \omega_3. & \end{array} \tag{9.38}$$

According to eqn (9.35), the field $E(t)$ induces components of polarization at all these frequencies. The value of the nonlinear susceptibility $\chi^{(3)}$ depends on the frequency components of the electric-field terms that it multiplies. In addition, $\chi^{(3)}$ depends, via its electric-dipole matrix elements, on the polarization vectors of the three field components in eqn (9.37), and also on the direction of the induced polarization P. Thus $\chi^{(3)}$ is a function of three frequencies and four spatial directions.

The physical significance of the nonlinear susceptibility is illustrated by its application to the process of two-photon absorption. The rate of linear or single-photon absorption determined by the Einstein B coefficient is closely related to the imaginary part of the linear susceptibility, as in eqn (1.104). There exist similar relations between the rates of multiple-photon absorption and the imaginary parts of components of the nonlinear susceptibility.

For absorption of two photons from different light beams, the total field E is a sum of contributions E_1 and E_2 of frequencies ω_1 and ω_2. From the linear and third-order terms of eqn (9.35),

$$P = \epsilon_0\chi^{(1)}(E_1+E_2)+\epsilon_0\chi^{(3)}(E_1+E_2)^3. \tag{9.39}$$

It is convenient to separate the fields E and polarization P into their components E^+ and P^+, which have time dependence $\exp(-\mathrm{i}\omega t)$, and components E^- and P^-, which have time dependence $\exp(\mathrm{i}\omega t)$. The division is similar to that made in eqns (5.83), (5.84), and (5.85) for the electric-field operators. The terms on the two sides of eqn (9.39) that oscillate with the same time dependence can be equated separately. The part that has time dependence $\exp(-\mathrm{i}\omega_1 t)$ gives

$$\begin{aligned} P^+(\omega_1) = {} & \epsilon_0\{\chi^{(1)}(\omega_1)E_1^+ + 6\chi^{(3)}(-\omega_2,\omega_2,\omega_1)E_2^- E_2^+ E_1^+ \\ & +3\chi^{(3)}(-\omega_1,\omega_1,\omega_1)E_1^- E_1^+ E_1^+\}, \end{aligned} \tag{9.40}$$

where the frequencies of the susceptibility components are now shown explicitly but the polarization dependence is suppressed in the interests of brevity. In a similar way, the $\exp(-\mathrm{i}\omega_2 t)$ part of eqn (9.39) gives

$$\begin{aligned} P^+(\omega_2) = {} & \epsilon_0\{\chi^{(1)}(\omega_2)E_2^+ + 6\chi^{(3)}(-\omega_1,\omega_1,\omega_2)E_1^- E_1^+ E_2^+ \\ & +3\chi^{(3)}(-\omega_2,\omega_2,\omega_2)E_2^- E_2^+ E_2^+\}. \end{aligned} \tag{9.41}$$

Let us evaluate the magnitude of the two-photon absorption at frequency ω_2 in the limit where beam 1 is much more intense than beam 2. If there is no linear absorption at frequency ω_1 and no two-photon absorption at frequency $2\omega_1$, the cycle-averaged intensity $\bar{I}_{10}$ of beam 1, given by the classical analogue of eqn (9.10), changes by only a small fraction during the two-photon absorption at frequency $\omega_1+\omega_2$. In addition, the final term of eqn (9.41) is much smaller than the middle term, and the equation can be written approximately as

$$P^+(\omega_2) = \epsilon_0\{\chi^{(1)}(\omega_2)+(3/\epsilon_0 c\eta_1)\chi^{(3)}(-\omega_1,\omega_1,\omega_2)\bar{I}_{10}\}E_2^+. \tag{9.42}$$

The second term in the large bracket has the form of an intensity-dependent addition to the linear susceptibility at ω_2.

Let η_2 and κ_2 be the refractive index and extinction coefficient at frequency ω_2 in the presence of two-photon absorption; that is, they are determined by eqns (1.83) and (1.84) with the expression in the large bracket of eqn (9.42) substituted for the susceptibility. Suppose that no linear absorption occurs at frequency ω_2, and the imaginary part of $\chi^{(1)}(\omega_2)$ is therefore zero. Then κ_2 is determined by

$$2\eta_2\kappa_2 = (3/\epsilon_0 c\eta_1)\bar{I}_{10}\,\mathrm{Im}\,\chi^{(3)}(-\omega_1,\omega_1,\omega_2). \tag{9.43}$$

If the real part of $\chi^{(1)}$ is much larger than the real part of the second term in the bracket of eqn (9.42), then η_2 is little changed from its linear value. Thus from eqns (1.91) and (9.43), the absorption coefficient K_2 at frequency ω_2 is

$$K_2 = (3\omega_2/\epsilon_0 c^2\eta_1\eta_2)\bar{I}_{10}\,\mathrm{Im}\,\chi^{(3)}(-\omega_1,\omega_1,\omega_2). \tag{9.44}$$

The cycle-averaged intensity $\bar{I}_2$ at frequency ω_2 therefore falls off exponentially with distance z as in eqn (1.90),

$$\bar{I}_2 = \bar{I}_{20}\exp(-K_2 z). \tag{9.45}$$

It is seen that the propagation characteristics obtained for the weak beam from the calculation in terms of the nonlinear susceptibility are identical to those obtained in eqn (9.21) from time-dependent perturbation theory. Comparison of the expressions (9.20) and (9.44) for the two-photon absorption coefficient K_2 yields

$$\mathrm{Im}\,\chi^{(3)}(-\omega_1,\omega_1,\omega_2) = (\pi N e^4/6\epsilon_0\hbar^3 V)\sum_f \overline{|\mathscr{M}_{\mathrm{TPA}}|^2}\,\delta(\omega_1+\omega_2-\omega_f), \tag{9.46}$$

where the flux of the weaker beam in eqn (9.20) has been neglected, and the summation on the right collects the contributions of all atomic final states $|f\rangle$. This result for the imaginary part of the third-order susceptibility in terms of dipole matrix elements agrees with the expression obtained by direct calculation of $\chi^{(3)}$ for the choice of frequencies appropriate to two-photon absorption.[1,2,7]

If the intensity of beam 1 is sufficiently high, the real part of the second term in the large bracket of eqn (9.42) may no longer be negligible compared to the first, and the result is a change in the refractive index at frequency ω_2. Consider two frequencies ω_1 and ω_2 that do not add to give a frequency close to an atomic resonance. In the absence of any single or two-photon absorption, both $\chi^{(1)}$ and $\chi^{(3)}$ are real, so that κ_2 is zero, and the modified refractive index η_2 is given by

$$\eta_2^2 = 1+\chi^{(1)}(\omega_2)+(3/\epsilon_0 c\eta_1)\bar{I}_{10}\chi^{(3)}(-\omega_1,\omega_1,\omega_2), \tag{9.47}$$

where eqn (1.83) has been used. The refractive index at ω_2 thus depends on the intensity of the beam at frequency ω_1.

Two-photon absorption from a single beam of light can also be treated in the formalism of the nonlinear susceptibility. With only one beam of light, whose frequency is ω_1, eqn (9.40) reduces to

$$P^+(\omega_1) = \epsilon_0\{\chi^{(1)}(\omega_1)E_1^+ + 3\chi^{(3)}(-\omega_1,\omega_1,\omega_1)E_1^-E_1^+E_1^+\}. \tag{9.48}$$

We do not proceed from this equation to calculate the two-photon absorption since a full account of the process has already been given in §9.2.

However, an interesting effect arises from the real parts of the susceptibilities in this case. Away from regions of single or two-photon absorption where $\chi^{(1)}$ and $\chi^{(3)}$ are real, the refractive index η_1 at frequency ω_1 is obtained from

$$\eta_1^2 = 1+\chi^{(1)}(\omega_1)+3\chi^{(3)}(-\omega_1,\omega_1,\omega_1)E_1^-E_1^+. \tag{9.49}$$

The refractive index of an intense light beam is therefore modified by a term proportional to its own intensity. The distribution of intensity in a laser light beam typically has a maximum value at the centre of the beam, and falls off towards the periphery. According to eqn (9.49), if $\chi^{(3)}$ is positive, the beam experiences a higher refractive index at its centre than at its edges, and the velocity at the centre is correspondingly smaller. The result is a self-focusing effect in which the beam converges inwards, and traps itself into a narrower, more intense beam than the original incident light from the laser. This self-focusing, or defocusing in the case of a negative $\chi^{(3)}$, is observed experimentally.[4,7]

The above calculations based on the nonlinear susceptibility are semiclassical in that the fields are represented by classical magnitudes while the susceptibility components are calculated quantum-mechanically. We now revert to a fully quantized theory and examine some further processes associated with the third-order susceptibility $\chi^{(3)}$. We do not consider any of the higher terms, that is $\chi^{(5)}$ and above; they correspond to processes similar in kind to those that result from $\chi^{(3)}$, but involving larger numbers of photons, and they are generally smaller and more difficult to investigate experimentally.

9.4. The stimulated Raman effect

The derivation of the transition rate (eqn (8.70)) for the scattering of light by an atom assumed that the incident beam had a definite number of photons and that no scattered photons were present before the scattering event considered. It is not difficult to carry out a similar calculation for a more general state of the radiation field described by a density operator $\hat{\rho}$, and with operators $\hat{\mathbf{E}}(\mathbf{r})$ and $\hat{\mathbf{E}}_s(\mathbf{r})$ for the electric fields of the incident and scattered beams. The calculation is very similar to that which leads to the transition rate (eqn (9.5)) for two-photon absorption. For a particular atomic final state $|f\rangle$, the scattering transition rate is

$$1/\tau = (2\pi e^4/\hbar^4)\sum_{\mathbf{k}_s} |\mathscr{M}_{\mathrm{SRE}}|^2\ \delta(\omega-\omega_s-\omega_f)\mathrm{Tr}(\hat{\rho}\hat{E}^-(\mathbf{r})\hat{E}_s^+(\mathbf{r})\hat{E}_s^-(\mathbf{r})\hat{E}^+(\mathbf{r})), \tag{9.50}$$

where

$$\mathscr{M}_{\mathrm{SRE}} = \sum_i \left\{\frac{\boldsymbol{\varepsilon}_s.\mathbf{D}_{fi}\boldsymbol{\varepsilon}.\mathbf{D}_{i1}}{\omega_i-\omega}+\frac{\boldsymbol{\varepsilon}.\mathbf{D}_{fi}\boldsymbol{\varepsilon}_s.\mathbf{D}_{i1}}{\omega_i+\omega_s}\right\} \tag{9.51}$$

is the same inelastic scattering matrix element used in Chapter 8. It is assumed that $|f\rangle$ is not the atomic ground state.

The trace over electric field operators is easily evaluated when the incident and scattered fields are statistically independent. It is assumed that the refractive indices η and η_s of the scattering medium at frequencies ω and ω_s are real. The mean intensity $\bar{I}$ of the incident light is related to an expectation value of electric field operators by an expression similar to eqn (9.10), and it is also related to the mean number $\bar{n}$ of incident photons by an expression similar to eqn (5.101). It is necessary in the latter result to accommodate the optical properties of the scattering medium by the replacement of c by the reduced velocity of light c/η. Thus

$$\bar{I} = 2\epsilon_0 c\eta\langle\hat{E}^-\hat{E}^+\rangle = c\hbar\omega\bar{n}/V\eta, \tag{9.52}$$

or

$$\langle\hat{E}^-\hat{E}^+\rangle = \hbar\omega\bar{n}/2\epsilon_0 V\eta^2, \tag{9.53}$$

and a similar result holds for the mean intensity $\bar{I}_s$ and mean photon number $\bar{n}_s$ of the scattered light. The trace in eqn (9.50) is therefore

$$\mathrm{Tr}(\hat{\rho}\hat{E}^-\hat{E}_s^+\hat{E}_s^-\hat{E}^+) = (\hbar/2\epsilon_0 V\eta\eta_s)^2\omega\omega_s\bar{n}(\bar{n}_s+1). \tag{9.54}$$

The factor $(\bar{n}_s+1)$ results from the commutation properties of the scattered-photon creation and destruction operators which occur in the order $\hat{a}_s\hat{a}_s^\dagger$ on the left of eqn (9.54).

The average number of scattered photons in a single mode of the radiation field is always very much smaller than unity for the scattering of ordinary light beams. This can be seen, for example, from Table 1.1 where even the strongest available incident beam has only about 10^{-2} photons per mode for a light source that is not a laser. In this case, it is a good approximation to neglect $\bar{n}_s$ in eqn (9.54), and the transition rate (eqn (9.50)) then reduces to eqn (8.70) if the refractive indices are set equal to unity.

The scattering rate associated with the 1 in the final factor of eqn (9.54) is classified as spontaneous, since the emission of a scattered photon takes place in the absence of any similar photons. The $\bar{n}_s$ in the final factor of eqn (9.54) produces an enhanced rate of scattering in the presence of an initial excitation of scattered photons. This stimulated scattering is known as the stimulated Raman effect; it is observed experimentally with the use of laser light sources of sufficiently high power to generate more than one scattered photon per mode of the radiation field.

The characteristics of the stimulated scattering are investigated most easily if the production of scattered photons in a particular mode $\mathbf{k}_s$ of the radiation field is considered, and the scattering into all other modes is ignored. Retention of the term in $\bar{n}_s$ in eqn (9.54) makes the propagation equations for the incident and scattered beams nonlinear, and the stimulated Raman effect is one of the processes of nonlinear optics. If both beams are propagated parallel to the z-axis, the propagation equations are

$$\partial\bar{I}/\partial z = -N\hbar\omega/V\tau \tag{9.55}$$

and

$$\partial\bar{I}_s/\partial z = N\hbar\omega_s/V\tau, \tag{9.56}$$

where N is the number of scattering atoms in the volume V, and τ is given by eqn (9.50), but with the sum over $\mathbf{k}_s$ removed to give the rate appropriate to a single scattered mode.

The general solution of these equations presents difficulties similar to those encountered in the corresponding eqns (9.7) and (9.8) for two-photon absorption. The transition rate $1/\tau$ depends on the beam characteristics in a complicated way, because even beams that are initially statistically independent do not remain so as the scattering proceeds. The influence of statistical properties of light on the stimulated scattering is discussed in §9.9.

Let us, however, ignore this complication for the present calculation, and assume that the beams remain statistically independent as they propagate through the scattering atoms. The trace in eqn (9.50) is then related to the beam intensities by eqns (9.52) and (9.54), and the propagation eqn (9.56) becomes

$$\frac{\partial\bar{I}_s}{\partial z} = \frac{\pi e^4}{2\epsilon_0^2\hbar^3c^2}\,\frac{N}{V}\,\frac{\omega_s}{\eta\eta_s}\,\overline{|\mathscr{M}_{\mathrm{SRE}}|^2}\ \delta(\omega-\omega_s-\omega_f)\bar{I}\left(\bar{I}_s+\frac{c\hbar\omega_s}{V\eta_s}\right), \tag{9.57}$$

where the horizontal bar denotes the usual orientation average.

It is seen from eqns (9.55) and (9.56) that

$$\frac{1}{\omega}\frac{\partial\bar{I}}{\partial z}+\frac{1}{\omega_s}\frac{\partial\bar{I}_s}{\partial z} = 0, \tag{9.58}$$

and, hence

$$(\bar{I}/\omega)+(\bar{I}_s/\omega_s) = \text{constant} = (\bar{I}_0/\omega)+(\bar{I}_{s0}/\omega_s), \tag{9.59}$$

where the zeros denote the initial values of the mean intensities at $z = 0$. The total flux of photons therefore remains constant; each incident photon removed from the beam is replaced by an additional photon in the scattered beam.

Eqn (9.57) can now be solved if $\bar{I}$ is first removed with the help of eqn (9.59). The solution is

$$\bar{I}_s = \frac{\{(\bar{I}_0/\omega)+(\bar{I}_{s0}/\omega_s)\}\{\bar{I}_{s0}+(\hbar c\omega_s/V\eta_s)\}\exp(Gz)-(\hbar c\omega_s\bar{I}_0/V\omega\eta_s)}{\{(\bar{I}_{s0}/\omega_s)+(\hbar c/V\eta_s)\}\exp(Gz)+(\bar{I}_0/\omega)}, \quad (9.60)$$

where the stimulated Raman gain coefficient G is defined by

$$G = \frac{\pi e^4}{2\epsilon_0^2\hbar^3c^2}\frac{N}{V}\frac{\omega\omega_s}{\eta\eta_s}\overline{|\mathscr{M}_{\mathrm{SRE}}|^2}\,\delta(\omega-\omega_s-\omega_f)\left(\frac{\bar{I}_0}{\omega}+\frac{\bar{I}_{s0}}{\omega_s}+\frac{\hbar c}{V\eta_s}\right). \quad (9.61)$$

This general solution for the intensity of the scattered beam shows three different kinds of dependence on z for different values of Gz. For

$$Gz \ll 1, \quad (9.62)$$

$$\bar{I}_s \approx \bar{I}_{s0}+\frac{(\bar{I}_0/\omega)\{\bar{I}_{s0}+(\hbar c\omega_s/V\eta_s)\}Gz}{(\bar{I}_0/\omega)+(\bar{I}_{s0}/\omega_s)+(\hbar c/V\eta_s)}, \quad (9.63)$$

and the beam intensity initially grows linearly with distance. In the opposite extreme of very large z, where

$$\{(\bar{I}_{s0}/\omega_s)+(\hbar c/V\eta_s)\}\exp(Gz) \gg \bar{I}_0/\omega, \quad (9.64)$$

$$\bar{I}_s/\omega_s \approx (\bar{I}_0/\omega)+(\bar{I}_{s0}/\omega_s), \quad (9.65)$$

and all the photon flux present initially has been converted into light in the scattered beam. Between the two limits represented by eqns (9.62) and (9.64), there is a region of the z-axis where the scattered beam grows exponentially with distance,

$$\bar{I}_s \approx \{1+(\omega\bar{I}_{s0}/\omega_s\bar{I}_0)\}\{\bar{I}_{s0}+(\hbar c\omega_s/V\eta_s)\}\exp(Gz). \quad (9.66)$$

The exponential growth is a direct consequence of the nonlinear term in eqn (9.57) and this solution is characteristic of the stimulated Raman effect.

The scattering of the incident light at frequency ω can be used to amplify a beam of intensity $\bar{I}_{s0}$ at frequency ω_s that is present initially, or it can be used to generate a beam at frequency ω_s, where none is provided externally. With $\bar{I}_{s0}$ set equal to zero, the general solution (eqn (9.60)) reduces to

$$\bar{I}_s = \frac{(\hbar c\omega_s/V\eta_s)(\exp(Gz)-1)}{(\hbar c\omega/V\eta_s\bar{I}_0)\exp(Gz)+1}. \quad (9.67)$$

The z-dependence of the solution in this case is illustrated in Fig. 9.6. The linear, exponential, and saturation regions also occur in the case $\bar{I}_{s0}=0$, where the initial photons of frequency ω_s must be supplied by spontaneous scattering. The exponential region then results from the amplification of these spontaneous photons by the stimulated Raman effect.

The above derivation of the gain coefficient G uses approximate equations (9.55) and (9.56) to relate the spatial dependence of the intensity in an extended medium to the time-dependent transition rate (9.50) for scattering by a single atom. A more accurate treatment[16] of the spatial propagation of the scattered field produces a dependence on z that is qualitatively similar to the form illustrated in Fig. 9.6 but the intensity in the region of exponential growth is reduced.

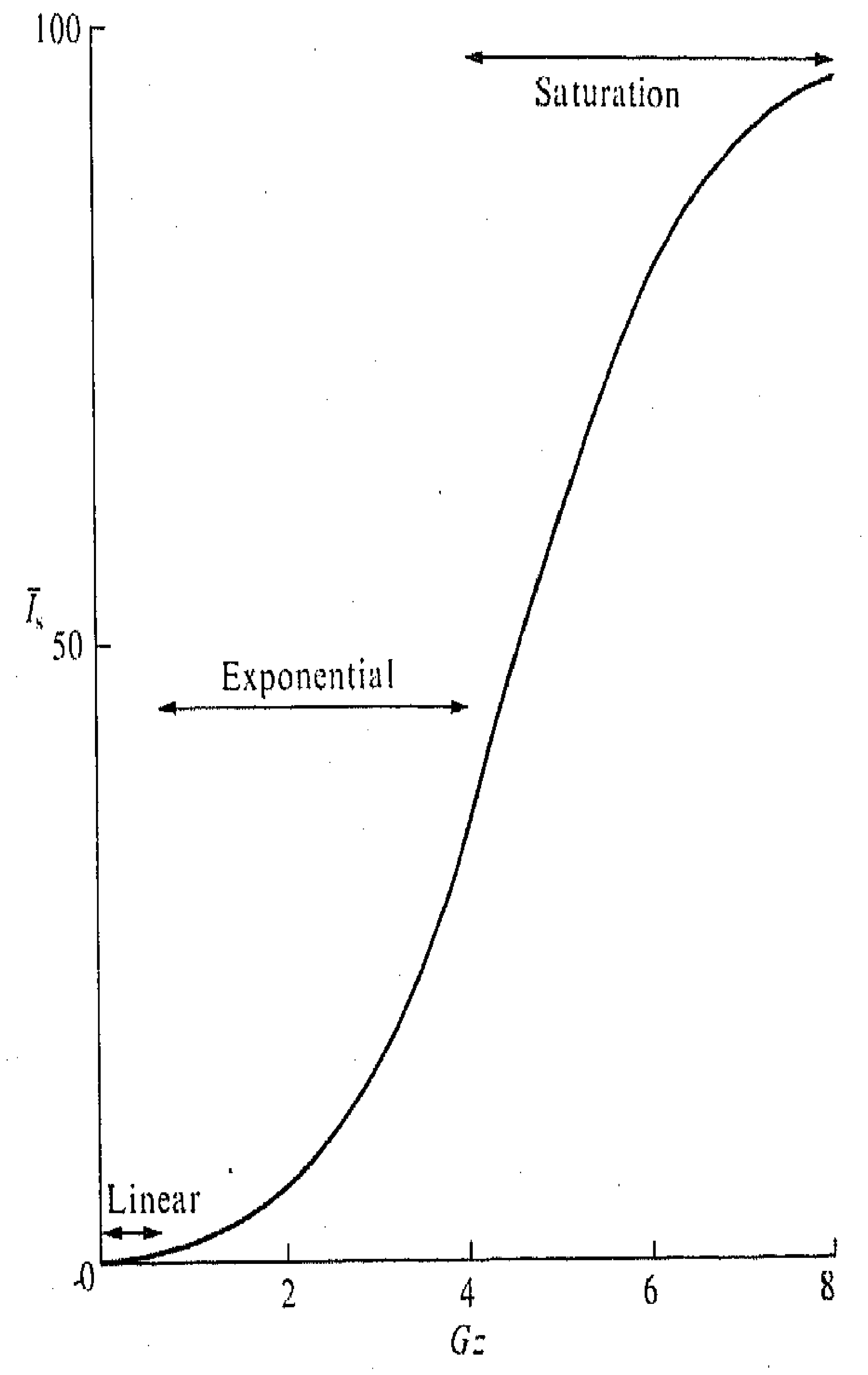

FIG. 9.6. Dependence of the scattered intensity on distance for the stimulated Raman effect, showing the regions of linear and exponential growth and the approach to saturation. The intensity $\bar{I}_s$ is plotted in units of $\hbar c\omega_s/V\eta_s$, and for convenience of drawing the quantity $V\eta_s\bar{I}_0/\hbar c\omega$ is assigned the value 100. A much larger value is normally appropriate, and the region of exponential growth is then correspondingly longer.

In many stimulated scattering experiments, the sample length is sufficiently small that the first term in the denominator of eqn (9.67) is always much smaller than unity, and we can write

$$\bar{I}_s \approx (\hbar c\omega_s/V\eta_s)(\exp(Gz)-1). \quad (9.68)$$

The spontaneous scattering at very small z in the linear region is the same as that treated in Chapter 8, and the methods of the present chapter can be shown as follows to reproduce the spontaneous scattering cross-section $d\sigma/d\Omega$.

Consider a volume V, which contains N atoms and has a length z parallel to the beam propagation direction. The cross-sectional area of the volume is V/z

and the rate at which energy is removed from the incident beam by the scattering is $(\omega/\omega_s)\bar{I}_s(V/z)$. Thus by definition of the single-atom scattering cross-section σ,

$$N\sigma = \sum_{\mathbf{k}_s} \omega \bar{I}_s V/\omega_s \bar{I}_0 z, \tag{9.69}$$

where the summation is introduced to obtain the total spontaneous scattering. Thus, with the use of the linear term from eqn (9.68) and the help of eqn (8.71),

$$\mathrm{d}\sigma/\mathrm{d}\Omega = \left(V/(2\pi)^3\right)\int(\hbar\omega\omega_s^2 G/\bar{I}_0 c^2 N)\,\mathrm{d}\omega_s, \tag{9.70}$$

where the refractive indices have been set equal to unity as in Chapter 8. If only the dominant first term in the final bracket of eqn (9.61) is retained, eqn (9.70) becomes

$$\frac{\mathrm{d}\sigma}{\mathrm{d}\Omega} = \frac{e^4\omega(\omega-\omega_f)^3}{16\pi^2\epsilon_0^2\hbar^2c^4}\overline{|\mathscr{M}_{\mathrm{SRE}}|^2}, \tag{9.71}$$

where ω_s is set equal to $\omega-\omega_f$ in $\mathscr{M}_{\mathrm{SRE}}$. This result is identical to the contribution from state $|f\rangle$ in eqn (8.72), except for the addition of an average over the atomic orientations.

For larger values of z, where the growth of the scattered beam is exponential, the gain coefficient G is experimentally more important than the scattering cross-section. The homogeneous broadening of the atomic final state converts the delta function in eqn (9.61) into a Lorentzian lineshape,

$$\delta(\omega-\omega_s-\omega_f) \to \frac{\gamma'_f/\pi}{(\omega_f-\omega+\omega_s)^2+\gamma_f'^2}, \tag{9.72}$$

similar to eqn (9.24). Since G appears in an exponent in eqn (9.68), the scattered frequency for which G is a maximum is generated with an intensity that at large z greatly exceeds all others. The maximum gain $G_{\max}$ occurs at the peak of the Lorentzian where ω_s is equal to $\omega-\omega_f$ and eqn (9.61) gives

$$G_{\max} = \frac{e^4}{2\epsilon_0^2\hbar^3c^2}\frac{N}{V}\frac{(\omega-\omega_f)}{\eta\eta_s}\overline{|\mathscr{M}_{\mathrm{SRE}}|^2}\frac{\bar{I}_0}{\gamma'_f}, \tag{9.73}$$

where only the dominant term has been retained in the final bracket.

The maximum gain for the stimulated Raman effect in a gas is expressed in terms of the cross-section (9.71) for spontaneous scattering by a single atom as

$$G_{\max} = \frac{\mathrm{d}\sigma}{\mathrm{d}\Omega}\frac{N}{V}\frac{8\pi^2c^2\bar{I}_0}{\hbar\omega(\omega-\omega_f)^2\eta\eta_s\gamma'_f}. \tag{9.74}$$

A numerical estimate for the gain in scattering by potassium vapour gives[7]

$$G_{\max} \approx 10^{-10}\bar{I}_0\,\mathrm{m}^{-1} \tag{9.75}$$

for incident light of frequency $4{\cdot}32\times10^{14}$ Hz and scattered light of frequency $0{\cdot}81\times10^{14}$ Hz. A value of $G_{\max}$ as large as $1000\,\mathrm{m}^{-1}$ is estimated for the scattering of pulsed laser light of the intensity $10^{13}\,\mathrm{W\,m^{-2}}$ quoted in Table 1.1.

The matrix element (9.51) for the stimulated Raman effect is very similar to that for two-photon absorption given by eqn (9.6). Apart from an overall change of sign, the former is obtained from the latter by replacement of ω_1 by ω and of ω_2 by $-\omega_s$. The same modifications are used to convert eqn (9.46) to a relation between the third-order susceptibility and the matrix element for the stimulated Raman effect. Two-photon absorption and the stimulated Raman effect are of course very similar processes in the theory, differing only in the absorption or emission behaviour of the second photon.

The assumption made above that only a single mode of scattered radiation is produced in the stimulated Raman effect is, of course, an approximation to the situation in a real experiment. In general there are contributions to the scattering from several atomic final states $|f\rangle$, and for each final state there is significant excitation of several modes $\mathbf{k}_s$. Nevertheless, it is often the case that a particular atomic final state and a particular scattered field mode have a larger gain coefficient than all others, thus channelling the majority of the scattered light into a single beam.

The brief account of the stimulated Raman effect given above does not do justice to the many facets of the phenomenon that have been investigated both experimentally and theoretically. Fuller details are to be found in the more specialized treatments.[1,4,6,7,17]

9.5. Third-harmonic generation

Two-photon absorption and the stimulated Raman effect are similar nonlinear processes in that they both involve the interaction of two photons with an atom, which is promoted to an excited state. The magnitude of the atomic excitation energy governs the relation between the frequencies of the participating photons.

The atoms play a more passive role in many of the other processes of nonlinear optics. Such processes leave the atoms in the same states as they were found initially, and there is no exchange of energy between the radiation and the atoms. The intensity-dependent contributions to the refractive index that produce the self-focusing or defocusing of light beams described in §9.3 belong to this category. We now consider a more substantial example, the generation of light at the third harmonic of the frequency of an incident monochromatic beam.

Let ω_1 be the frequency of a beam of light incident on an atom. According to the scheme of eqn (9.38), the electric field of the light induces an atomic polarization of frequency $\omega_3 = 3\omega_1$ via the nonlinear third-order susceptibility. This oscillating polarization in turn produces light of frequency ω_3.

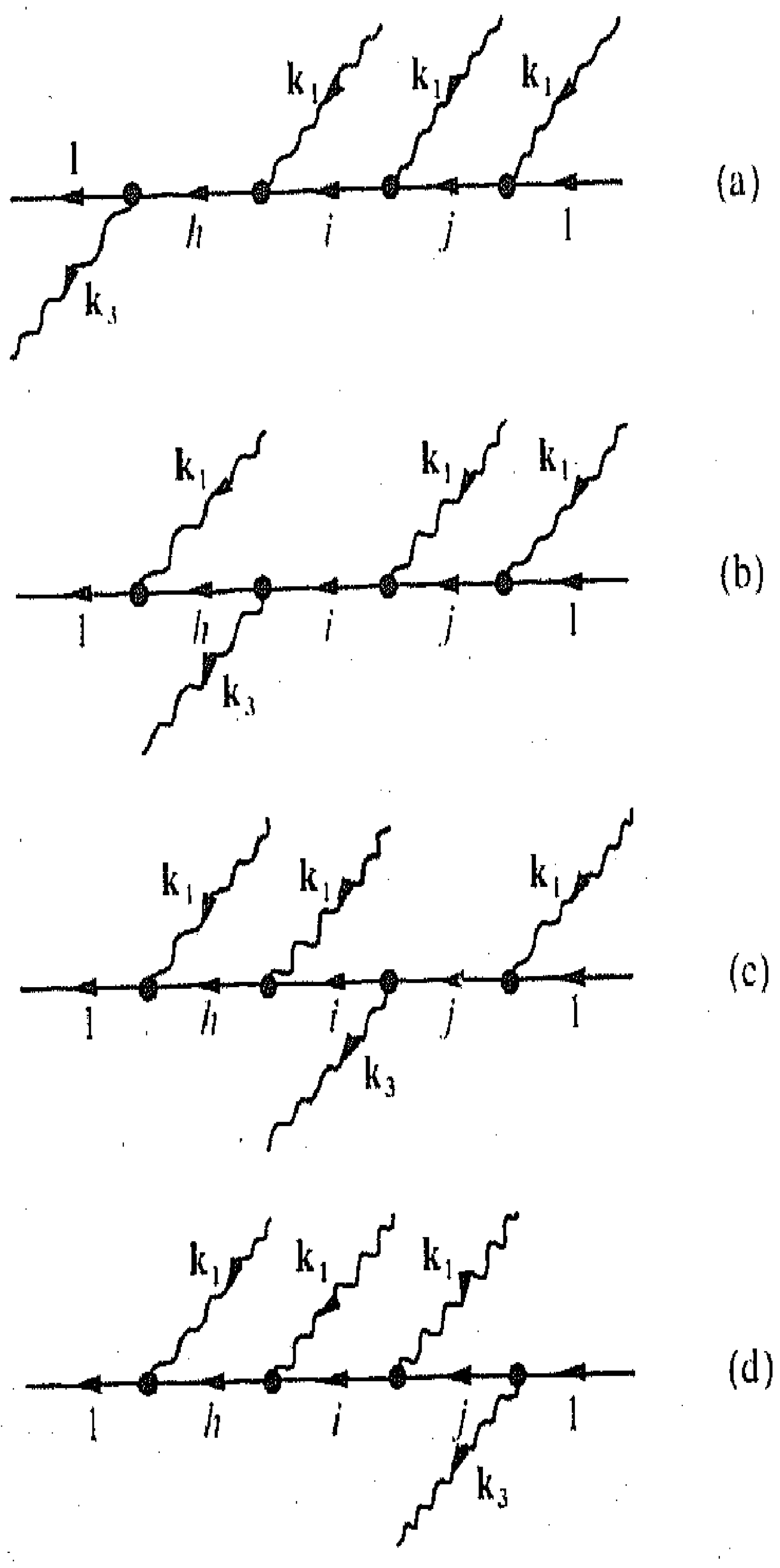

FIG. 9.7. Diagrams for third-harmonic generation. All four interactions in each diagram occur via the electric-dipole Hamiltonian $\mathscr{H}_{ED}$.

The rate of generation of the third-harmonic is calculated by time-dependent perturbation theory. A single event requires the destruction of three photons $\mathbf{k}_1$ of frequency ω_1, and the creation of a single third-harmonic photon, whose wavevector we denote $\mathbf{k}_3$. There are four electric-dipole interactions altogether, and fourth-order perturbation theory is needed. The atom is in its ground state $|1\rangle$ before and after the process, but is excited to virtual intermediate states during the harmonic generation.

The diagrams for the fourth-order perturbation theory are shown in Fig. 9.7. The four different diagrams correspond to the four possible locations of the emission of photon $\mathbf{k}_3$ relative to the absorptions of the three $\mathbf{k}_1$ photons. The transition rate for the four-photon process is obtained straightforwardly from the fourth-order term of eqn (5.152) as

$$1/\tau = (2\pi e^8/\hbar^8)\sum_{\mathbf{k}_3} |\mathscr{M}_{\mathrm{THG}}|^2\ \delta(3\omega_1-\omega_3)\mathrm{Tr}(\hat{\rho}\hat{E}_1^-\hat{E}_1^-\hat{E}_1^-\hat{E}_3^+\hat{E}_3^-\hat{E}_1^+\hat{E}_1^+\hat{E}_1^+), \tag{9.76}$$

where the matrix element for the transition is

$$\mathscr{M}_{\mathrm{THG}} = \sum_{h,i,j}\left\{\frac{\boldsymbol{\varepsilon}_3.\mathbf{D}_{1h}\boldsymbol{\varepsilon}_1.\mathbf{D}_{hi}\boldsymbol{\varepsilon}_1.\mathbf{D}_{ij}\boldsymbol{\varepsilon}_1.\mathbf{D}_{j1}}{(3\omega_1-\omega_h)(2\omega_1-\omega_i)(\omega_1-\omega_j)} + \frac{\boldsymbol{\varepsilon}_1.\mathbf{D}_{1h}\boldsymbol{\varepsilon}_3.\mathbf{D}_{hi}\boldsymbol{\varepsilon}_1.\mathbf{D}_{ij}\boldsymbol{\varepsilon}_1.\mathbf{D}_{j1}}{(-\omega_1-\omega_h)(2\omega_1-\omega_i)(\omega_1-\omega_j)} + \frac{\boldsymbol{\varepsilon}_1.\mathbf{D}_{1h}\boldsymbol{\varepsilon}_1.\mathbf{D}_{hi}\boldsymbol{\varepsilon}_3.\mathbf{D}_{ij}\boldsymbol{\varepsilon}_1.\mathbf{D}_{j1}}{(-\omega_1-\omega_h)(-2\omega_1-\omega_i)(\omega_1-\omega_j)} + \frac{\boldsymbol{\varepsilon}_1.\mathbf{D}_{1h}\boldsymbol{\varepsilon}_1.\mathbf{D}_{hi}\boldsymbol{\varepsilon}_1.\mathbf{D}_{ij}\boldsymbol{\varepsilon}_3.\mathbf{D}_{j1}}{(-\omega_1-\omega_h)(-2\omega_1-\omega_i)(-3\omega_1-\omega_j)}\right\}, \tag{9.77}$$

and $\hat{E}_1$ and $\hat{E}_3$ are the electric-field operators for the incident and harmonic light, respectively.

For harmonic generation by interaction of the light with a single atom, the electric-field operators in eqn (9.76) are all evaluated at the atomic position $\mathbf{r}$. However, the third-harmonic generation transition-rate displays a new feature that is not present in the rates of two-photon absorption and stimulated Raman effect. The two latter processes leave the atom in a particular final state and each single transition excites a definite atom. The total transition rate is thus a sum of the transition rates of the separate atoms, and K_2, K_2', and G in eqns (9.20), (9.30), and (9.61) are all proportional to the number of atoms N.

The harmonic-generation rate has a different behaviour. As far as the atoms are concerned, the final state is the same as the initial state, and there is no distinction between transitions that take place by interaction with different atoms. The matrix element must therefore be summed over the contributions of the different atoms *before* it is squared to obtain the total transition rate. The total rate is then given by eqn (9.76) but with the electric-field term generalized to

$$\sum_{\mathbf{r},\mathbf{r}'}\mathrm{Tr}(\hat{\rho}\hat{E}_1^-(\mathbf{r})\hat{E}_1^-(\mathbf{r})\hat{E}_1^-(\mathbf{r})\hat{E}_3^+(\mathbf{r})\hat{E}_3^-(\mathbf{r}')\hat{E}_1^+(\mathbf{r}')\hat{E}_1^+(\mathbf{r}')\hat{E}_1^+(\mathbf{r}')), \tag{9.78}$$

where $\mathbf{r}$ and $\mathbf{r}'$ are both summed over the locations of all N atoms.

The position-dependent factors of $\hat{E}^+$ and $\hat{E}^-$ given by eqns (5.84) and (5.85) combine in eqn (9.78) to produce a spatial dependence

$$\sum_{\mathbf{r},\mathbf{r}'}\exp\{\mathrm{i}(\mathbf{k}_3-3\mathbf{k}_1).(\mathbf{r}-\mathbf{r}')\} = \left|\sum_{\mathbf{r}}\exp(\mathrm{i}\Delta\mathbf{k}.\mathbf{r})\right|^2, \tag{9.79}$$

where

$$\Delta\mathbf{k} = \mathbf{k}_3-3\mathbf{k}_1. \tag{9.80}$$

The transition rate is thus given by eqn (9.76) with the electric-field operators all evaluated at the same point but with the additional factor shown in eqn (9.79) inserted.

The growth of the mean intensity $\bar{I}_3$ of the third-harmonic beam is described by

$$\partial\bar{I}_3/\partial z = \hbar\omega_3/V\tau, \tag{9.81}$$

similar to propagation equations given previously, except that, in view of the previously discussed modifications, $1/\tau$ is here the total transition rate due to all the atoms.

As in other processes, the growth of the beam intensity is difficult to evaluate in the situation where the beam statistical and correlation properties change significantly with the distance of propagation through the nonlinear medium. We assume here that the path length of the light through the atoms is sufficiently short for the initial intensity $\bar{I}_{10}$ of the incident beam to be only slightly reduced. It is then permissible to retain the initial statistical properties of the incident light in evaluating the electric-field correlation function from eqn (9.78). The third-harmonic light is normally generated with statistical properties that are correlated with those of the incident light. Correlation effects are discussed in subsequent sections and we assume that they can be ignored for the present calculation. With these assumptions, and with the spatial summations treated separately in eqn (9.79), the correlation function (9.78) can be factorized in the form

$$\mathrm{Tr}(\hat{\rho}\hat{E}_1^-\hat{E}_1^-\hat{E}_1^-\hat{E}_1^+\hat{E}_1^+\hat{E}_1^+)\mathrm{Tr}(\hat{\rho}\hat{E}_3^+\hat{E}_3^-). \tag{9.82}$$

Suppose for the moment that there are n_1 photons with the fundamental frequency ω_1 and n_3 photons with the third-harmonic frequency ω_3. The products of creation and destruction operators in (9.82) produce a proportionality of the correlation function to

$$n_1(n_1-1)(n_1-2)(n_3+1), \tag{9.83}$$

analogous to the result (9.54) for the stimulated Raman effect. The two contributions in the final factor correspond to stimulated and spontaneous emission of an additional third-harmonic photon. However, at a position in the nonlinear medium where some third-harmonic light has been generated, the inverse process can occur, in which a photon of frequency ω_3 is destroyed and three photons of frequency ω_1 are created. The theory of the inverse process parallels that of third-harmonic generation and the result for the transition rate is the same except that operators are replaced by their conjugates. Thus in the presence of n_1 photons of frequency ω_1 and n_3 of frequency ω_3, the correlation function for conversion of third harmonic into fundamental is proportional to

$$n_3(n_1+1)(n_1+2)(n_1+3). \tag{9.84}$$

The net rate of generation of third-harmonic light is proportional to the difference of eqns (9.83) and (9.84), which is

$$n_1(n_1-1)(n_1-2)-n_3(9n_1^2+9n_1+6). \tag{9.85}$$

The assumption of the present calculation, that only a small fraction of the incident light is converted to third harmonic, implies that n_3 is always much smaller than n_1. The second term in eqn (9.85) can therefore be neglected. The term that remains is the same as the part of eqn (9.83) that corresponds to spontaneous emission of a third-harmonic photon. The product of field operators in eqn (9.82) that refer to the fundamental beam is the same as occurs in the definition of the degree of third-order coherence at a single space–time point obtained from eqn (6.114). Thus with the fundamental part of the correlation function (9.82) expressed in terms of the fundamental intensity and the third-harmonic part restricted to the spontaneous contribution, using relations similar to eqns (9.27) and (9.53), the propagation eqn (9.81) becomes

$$\frac{\partial\bar{I}_3}{\partial z} = \frac{\pi e^8}{8\epsilon_0^4c^3\hbar^6V^2}\sum_{\mathbf{k}_3}\frac{\omega_3^2}{\eta_1^3\eta_3^2}\overline{|\mathscr{M}_{\mathrm{THG}}|^2}\,\delta(3\omega_1-\omega_3) \tag{9.86}$$
$$\times\left|\sum_{\mathbf{r}}\exp(\mathrm{i}\Delta\mathbf{k}.\mathbf{r})\right|^2 g_{11}^{(3)}(0)\bar{I}_{10}^3,$$

where the spatial factor from eqn (9.79) has been inserted and the bar denotes the usual average over atomic orientations, now carried out before the matrix element is squared. The refractive indices η_1 and η_3 refer to the frequencies of the incident fundamental beam and the generated third-harmonic light respectively.

The derivation of the third-harmonic intensity is completed by evaluation of the two summations in eqn (9.86). The $\mathbf{r}$ summation depends on the shape of the region in which the nonlinear process takes place. We envisage a container of volume V with plane parallel boundaries perpendicular to the propagation direction at $z = 0$ and $z = L$. The cross-sectional area is V/L and we suppose the dimensions in the x- and y-directions to be much larger than L. Then

$$\left|\sum_{\mathbf{r}}\exp(\mathrm{i}\Delta\mathbf{k}.\mathbf{r})\right|^2 \to (N/V)^2\int\mathrm{d}\mathbf{r}\int\exp\{\mathrm{i}\Delta\mathbf{k}.(\mathbf{r}-\mathbf{r}')\}\,\mathrm{d}\mathbf{r}'$$
$$=(N/V)^2(2\pi)^2\,\delta(\Delta k_x)\,\delta(\Delta k_y)\,\frac{V}{L}\left|\frac{\exp(\mathrm{i}\Delta k_zL)-1}{\mathrm{i}\Delta k_z}\right|^2, \tag{9.87}$$

where the limits of integration for the x- and y-axes are assumed sufficiently large to produce delta functions similar to eqn (2.64).

The $\mathbf{k}_3$ summation is also carried out by conversion to an integral,

$$\sum_{\mathbf{k}_3}\left|\sum_{\mathbf{r}}\exp(\mathrm{i}\Delta\mathbf{k}.\mathbf{r})\right|^2\delta(3\omega_1-\omega_3) \to (V/(2\pi)^3)\int\left|\sum_{\mathbf{r}}\exp(\mathrm{i}\Delta\mathbf{k}.\mathbf{r})\right|^2\delta(3\omega_1-\omega_3)\,\mathrm{d}\mathbf{k}_3$$
$$=\frac{4N^2k_3}{2\pi L\omega_3}\frac{\sin^2(\tfrac{1}{2}\Delta kL)}{(\Delta k)^2}, \tag{9.88}$$

where the z subscript has been dropped from Δk because the delta functions in eqn (9.87) force its other components to be zero.

With this substitution, eqn (9.86) is easily integrated to give the third-harmonic intensity at the rear boundary of the gas,

$$\bar{I}_3 = \frac{e^8}{4\epsilon_0^4 c^4 \hbar^6}\left(\frac{N}{V}\right)^2 \frac{\omega_3^2}{\eta_1^3 \eta_3} \overline{|\mathscr{M}_{\mathrm{THG}}|^2} \frac{\sin^2(\frac{1}{2}\Delta kL)}{(\Delta k)^2} g_{11}^{(3)}(0)\bar{I}_{10}^3. \tag{9.89}$$

The harmonic intensity is proportional to the square of the atomic number density, in contrast to the linear dependence of the two-photon absorption and stimulated Raman effect. The intensity is also proportional to the cube of the intensity of the incident beam, and to its degree of third-order coherence $g_{11}^{(3)}(0)$. This factor is equal to unity for a coherent incident beam according to eqns (3.113) or (6.115), but any fluctuations in the beam intensity cause an increase in the third-harmonic output. According to eqn (3.114), $g_{11}^{(3)}(0)$ is equal to 6 for chaotic light.

The dependence of the third-harmonic intensity on the path length is governed by the trigonometric factor in eqn (9.89). The intensity is greatest for

$$\Delta k = 0, \qquad \text{when} \qquad \sin^2(\tfrac{1}{2}\Delta kL)/(\Delta k)^2 = L^2/4. \tag{9.90}$$

The light beams are said to be *phase-matched* when this condition is satisfied. The phase-matching condition can be written from eqn (9.80) as

$$k_3 = 3k_1 \tag{9.91}$$

or, alternatively, since ω_3 is equal to $3\omega_1$,

$$\eta_3 = \eta_1. \tag{9.92}$$

If the phase-matching condition is not satisfied, and in particular if ΔkL is of order unity or larger, the third-harmonic intensity is greatly reduced. The intensity falls to zero when ΔkL is an integral multiple of 2π.

Phase-matching requirements are a general feature of those nonlinear processes that produce no changes in the atomic states. They can be quite difficult to satisfy experimentally and they often severely limit the observable magnitudes of the nonlinear effects. In the case of third-harmonic generation, the refractive indices η_1 at frequency ω_1 and η_3 at frequency $3\omega_1$ are not normally equal, and the phase-matching condition is not generally satisfied.

This problem can be overcome in certain special cases. For example, if either ω_1 or $3\omega_1$ lies close to an atomic transition frequency, where the refractive index varies quite rapidly, it may be possible to equalize η_1 and η_3 for a particular value of ω_1. Proximity of one or more of the fundamental and harmonic frequencies to allowed atomic transition frequencies also has the advantage of producing a resonant enhancement of the matrix element (9.77) for third-harmonic generation. The success of experiments designed to produce significant third-harmonic intensities depends upon the selection of an atom that has energy levels suitably placed to provide resonant enhancement of the matrix element and whose vapour has a refractive index variation appropriate for the phase-matching requirement. An unsuitable refractive index variation can sometimes be adjusted by addition of a second gas to the vapour whose atoms have desirable nonlinear properties. Further details of experimental and theoretical work on third-harmonic generation are to be found in the references.[7,18]

Third-harmonic generation can alternatively be treated by a calculation based on the appropriate component of the third-order susceptibility.[2,7] The harmonic intensity is found to be proportional to the square of $\chi^{(3)}(\omega_1, \omega_1, \omega_1)$, and the expression for $\bar{I}_3$ is identical to eqn (9.89) when the connection

$$\chi^{(3)}(\omega_1, \omega_1, \omega_1) = -(Ne^4/\epsilon_0\hbar^3 V)\overline{\mathscr{M}_{\mathrm{THG}}} \tag{9.93}$$

is made. This expression for $\chi^{(3)}(\omega_1, \omega_1, \omega_1)$ is exactly the same as that found by direct calculation. Both eqns (9.46) and (9.93) are special cases of the general expression for $\chi^{(3)}$ that applies when its three frequencies are all independent.

Each third-harmonic generation event involves a total of four photons. It conforms to a general selection rule valid for media invariant under inversion that only even numbers of photons can participate in electric-dipole transitions that leave the electronic state of the medium unchanged. Rayleigh scattering is another example of such a process. Both even and odd numbers of photons can participate in processes that change the state of the medium, the changes being respectively between states of the same and different parity.

We do not consider here the nonlinear media that are not invariant under inversion, where these selection rules do not apply. The most important additional processes that can occur involve three photons and produce no overall change in the state of the medium. The possibilities are either that one photon is absorbed and two are emitted or that two photons are absorbed and one is emitted. The three-photon nonlinear processes include second-harmonic generation, parametric amplification, and the generation of light at the sums and differences of the frequencies of a pair of incident beams.

9.6. Photon statistics and nonlinear optics

The transition rates for nonlinear optical processes generally depend upon the coherence properties of the participating light beams. The dependence arises from the electric-field operator expectation-value that results from the standard transition-rate formula, typified by the derivation of eqn (9.5) from eqn (9.2). Thus the expectation value (9.13) in the case of double-beam two-photon absorption is proportional to $g_{21}^{(2)}(0)$, the interbeam degree of second-order coherence. The corresponding result (9.27) for single-beam two-photon absorption is proportional to $g_{11}^{(2)}(0)$, the degree of second-order coherence within the beam. The degree of third-order coherence of the incident light occurs in the third-harmonic generation rate derived in the previous section.

The qualitative reasons for the dependence of the single-beam two-photon absorption rate on the degree of second-order coherence have been discussed in §9.2 in connection with the classical calculation illustrated in Fig. 9.5. In quantum terms, the rate of two-photon absorption is enhanced for light beams that are rich in pairs of coincident photons. Thus the twofold increase in absorption rate for chaotic light over that for coherent light reflects the greater availability of photon pairs in the photon bunches of the former, as discussed in §6.5 and illustrated in Fig. 6.4. By contrast, the two-photon absorption rate for incident light that is photon-antibunched, in accordance with eqn (6.48), is diminished below the rate for coherent light. The absorption rate falls to zero for light whose degree of second-order coherence vanishes; a trivial example is provided by an incident beam consisting of a single photon, where there is obviously no possibility of two-photon absorption, and the transition rate indeed vanishes as a consequence of the zero degree of second-order coherence given by eqn (6.29).

Similar remarks apply to the other nonlinear processes. Thus the rate of double-beam two-photon absorption is enhanced for incident beams whose photons are correlated, as in the beams produced by the cascade emission treated in §8.9. Again, the third-harmonic generation requires the removal of three photons from the incident light, and the photon bunches of chaotic light produce a sixfold increase of the generation rate over that for coherent light. In general, for any nonlinear process, the transition rate is enhanced by the coincident availability of whatever photons participate.

It is not difficult to incorporate these coherence effects into the theory, and this is accomplished in the transition rates derived earlier in the chapter. More severe problems are created by the need to take account of the changes produced in the coherence and correlation properties of the light by the nonlinear processes themselves. The results (9.18), (9.19), and (9.31) for two-photon absorption, (9.60) for the stimulated Raman effect, and (9.89) for third-harmonic generation are, in general, correct only to first order in the distance z or L through the nonlinear medium. They are not generally correct for larger distances, where the reaction of the nonlinear process on the beams begins to change the degrees of coherence from their initial values.

The classical calculation shown in Fig. 9.5 has already been discussed in terms of its qualitative explanation for the reduction in the degree of second-order coherence produced by single-beam two-photon absorption. The quantum picture of the effect is best appreciated by consideration of Fig. 6.4. Two-photon absorption preferentially removes pairs of coincident or nearly-coincident photons from the beam. The removal of such photons from the bunched or random distributions in parts (a) and (b) of the figure produces distributions similar to that shown for antibunched light in part (c). The two-photon absorption can in principle continue until all pairs of photons are removed from the light and only one or zero photons remain. The absorption

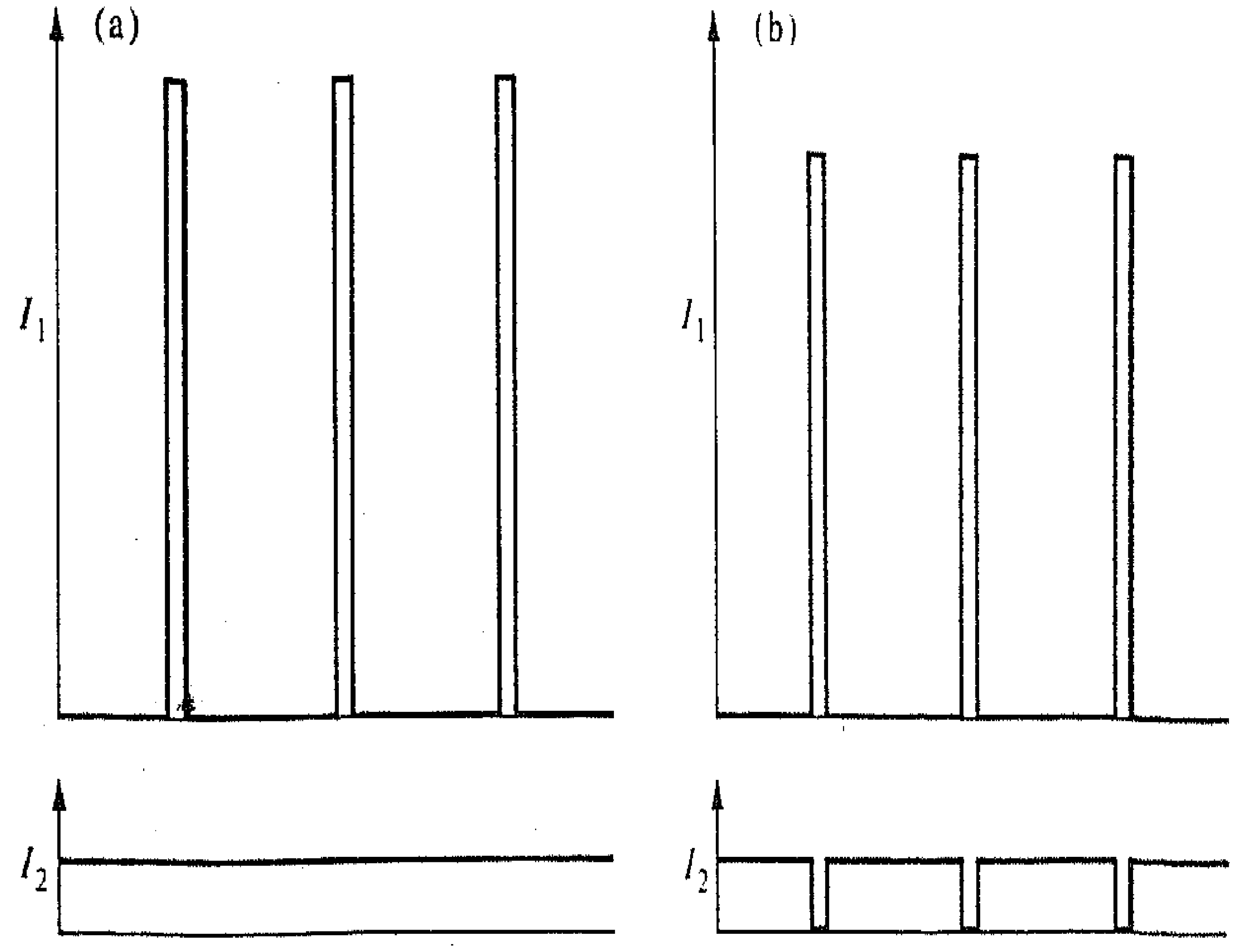

FIG. 9.8. Beam intensities (a) before absorption and (b) after the cessation of absorption for a classical model of two-photon absorption in which one beam is pulsed with $f = 0{\cdot}1$ and the other beam initially has constant intensity. The horizontal axis represents position for a view of the beam at a single time, or vice versa.

then ceases in accordance with the vanishing degree of second-order coherence given by eqn (6.29). It is clear that single-beam two-photon absorption can produce light whose degree of second-order coherence lies in the nonclassical range of eqn (6.48). The classical calculation illustrated in Fig. 9.5 is approximate, and an exact solution of the problem of two-photon absorption must use the quantum theory of light.

However, a similar classical illustration is also useful for a qualitative understanding of the changes in beam coherence properties produced by double-beam two-photon absorption. Fig. 9.8(a) shows the time or space dependence of the intensities of two beams before any two-photon absorption occurs. One of the beams consists of a train of rectangular pulses, the pulse duration being a fraction f of the repeat period of the wave, similar to the intensity variation shown in Fig. 3.11(a). The other, weaker, beam has a constant intensity. Fig. 9.8(b) shows the same sections of the beams after a long period of two-photon absorption. As the beams travel together, (with velocities assumed equal) through the nonlinear medium, absorption can occur only during the pulses of the stronger beam, and the absorption ceases when those sections of the weaker beam coincident with the pulses are exhausted, leaving a fraction $1-f$ of the intensity of the weaker beam unabsorbed. The interbeam degree of second-order coherence $g^{(2)}_{12}(0)$ diminishes in value from 1 to 0 between parts (a) and (b) of Fig. 9.8. It is seen that in this example the strong beam imposes a negative image of its intensity fluctuations on the weak beam. More generally in two-photon absorption, any intensity peaks in one beam tend to generate accompanying troughs in the other beam, the interbeam degree of second-order coherence falls from its initial unit value in eqn (9.14), and the absorption is inhibited.

The effects of several nonlinear optical processes on the statistical and coherence properties of light are treated in more detail in the remainder of the chapter. The method followed is similar to that employed in §§7.1–7.4 to determine the effects of single-photon absorption and emission on the statistical properties of light. We set up rate equations for the changes in the photon probability distribution brought about by the nonlinear process under consideration. As in the single-photon calculations, the method is valid for transitions to collision-broadened atomic states, and we use it to treat two-photon absorption and the stimulated Raman effect. The rate equations are established in a somewhat intuitive fashion, similar to the discussion in §7.1. More rigorous derivations, which use an effective Hamiltonian for the nonlinear transition to obtain the equation of motion for the photon density operator, produce identical rate equations.[19]

9.7. Photon statistics of double-beam two-photon absorption

We treat a slightly more general situation than that assumed in §9.1, by allowing N_2 of the N atoms to be in the upper state of the two-photon transition, the remainder N_1 being in the ground state. Let P_{n_1,n_2} be the probability that at time t there are n_1 photons in mode $\mathbf{k}_1$ and n_2 in mode $\mathbf{k}_2$. The probability distribution is normalized,

$$\sum_{n_1,n_2} P_{n_1,n_2} = 1; \tag{9.94}$$

the existence of the correlations described in the previous section prevents a factorization of the joint probability into a product of probability distributions for the individual beams. The division of atoms between the two active states is also generally dependent on the photon distribution but we assume here that some external influence maintains N_1 and N_2 constant.

A two-photon absorption event reduces the photon numbers from n_1 and n_2 to n_1-1 and n_2-1. The transition rate is given by eqn (9.5), and for definite numbers of photons

$$\mathrm{Tr}(\hat{\rho}\hat{E}_1^-\hat{E}_2^-\hat{E}_2^+\hat{E}_1^+) = (\hbar/2\epsilon_0 V\eta_1\eta_2)^2\omega_1\omega_2 n_1 n_2. \tag{9.95}$$

Thus the probability per unit time that the beam photon numbers are reduced from n_1 and n_2 to n_1-1 and n_2-1 can be written

$$N_1\mathscr{K}n_1n_2, \tag{9.96}$$

where $\mathscr{K}$ includes all the constant factors from eqns (9.5) and (9.95). The N_2 excited atoms can decay to their ground states by emission of two photons.

Such processes change the photon numbers from n_1 and n_2 to n_1+1 and n_2+1. The transition rate is the same as that given by eqn (9.5) except that the field operator expectation value is replaced by

$$\mathrm{Tr}(\hat{\rho}\hat{E}_1^+\hat{E}_2^+\hat{E}_2^-\hat{E}_1^-) = (\hbar/2\epsilon_0 V\eta_1\eta_2)^2\omega_1\omega_2(n_1+1)(n_2+1). \tag{9.97}$$

The probability per unit time that the beam photon numbers are increased from n_1 and n_2 to n_1+1 and n_2+1 is thus

$$N_2\mathscr{K}(n_1+1)(n_2+1). \tag{9.98}$$

These absorption and emission processes reduce P_{n_1,n_2} at a combined rate

$$-N_1\mathscr{K}n_1n_2P_{n_1,n_2} - N_2\mathscr{K}(n_1+1)(n_2+1)P_{n_1,n_2}. \tag{9.99}$$

There are also two positive contributions to the rate of change of P_{n_1,n_2}. If n_1+1 and n_2+1 photons are present in the two beams, absorption of one photon from each beam, at a rate given by eqn (9.96) with appropriate adjustment of the photon numbers, produces a rate of increase

$$N_1\mathscr{K}(n_1+1)(n_2+1)P_{n_1+1,n_2+1}. \tag{9.100}$$

Similarly, if n_1-1 and n_2-1 photons are present, emission of one photon into each beam at a rate obtained by suitable modification of eqn (9.98) produces a rate of increase

$$N_2\mathscr{K}n_1n_2P_{n_1-1,n_2-1}. \tag{9.101}$$

The four kinds of transition that change P_{n_1,n_2} are shown on the two-photon energy-level diagram of Fig. 9.9. The descending arrows represent two-photon

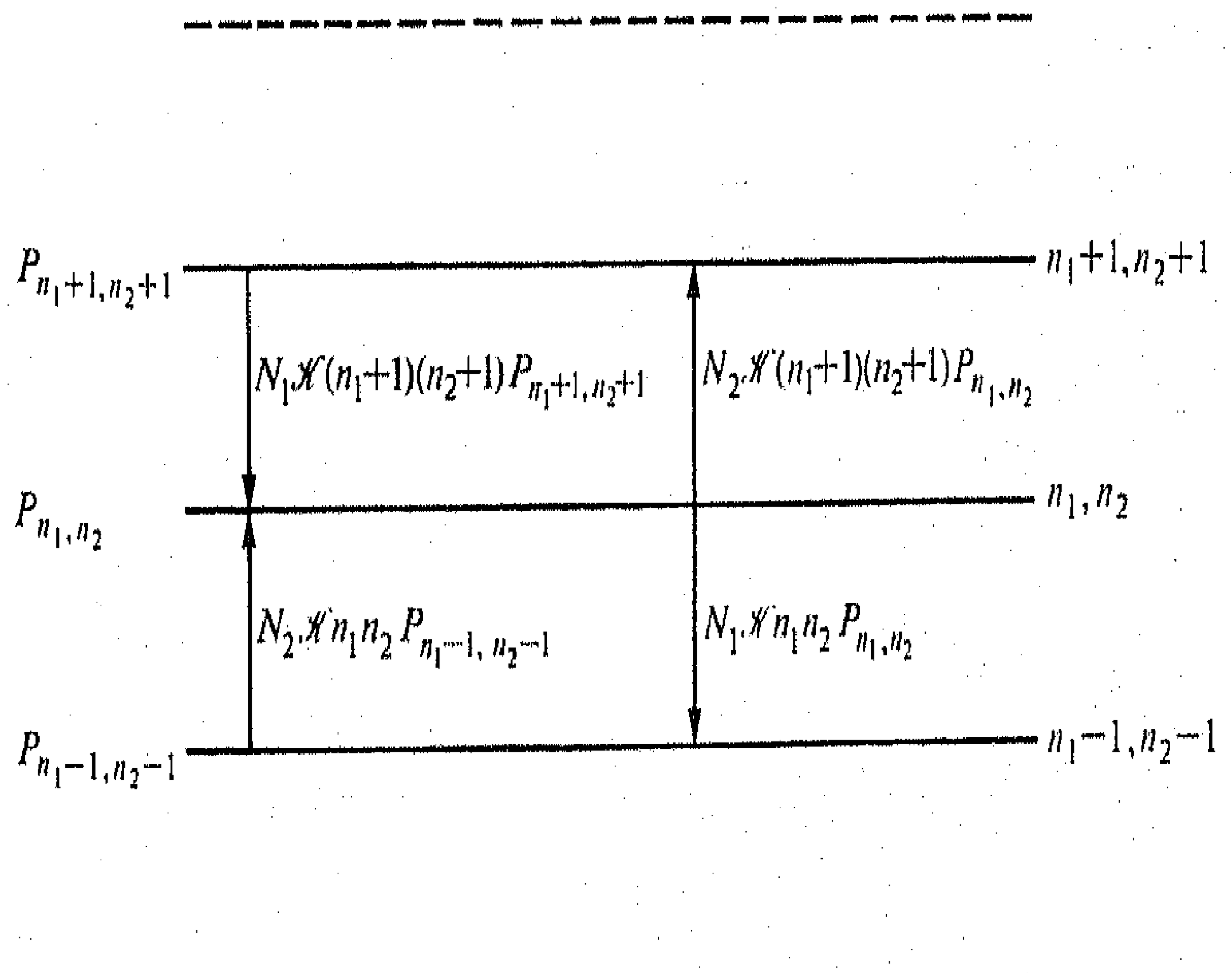
P_{n_1+1,n_2+1}
n_1+1, n_2+1
$N_1\mathscr{K}(n_1+1)(n_2+1)P_{n_1+1,n_2+1}$
$N_2\mathscr{K}(n_1+1)(n_2+1)P_{n_1,n_2}$
P_{n_1,n_2}
n_1, n_2
$N_2\mathscr{K}n_1n_2P_{n_1-1,n_2-1}$
$N_1\mathscr{K}n_1n_2P_{n_1,n_2}$
P_{n_1-1,n_2-1}
n_1-1, n_2-1

FIG. 9.9. Energy-level diagram for the photons in modes $\mathbf{k}_1$ and $\mathbf{k}_2$. The transition rates shown are the contributions to $dP_{n_1,n_2}/dt$. The energy interval is $\hbar(\omega_1+\omega_2)$.

absorption while the ascending arrows represent two-photon emission. The diagram is similar to that in Fig. 7.1 for the case of single-photon absorption and emission. All four transitions combine to produce a rate equation

$$\begin{aligned} \mathrm{d}P_{n_1,n_2}/\mathrm{d}t = {} & -N_1\mathscr{K}n_1n_2P_{n_1,n_2}-N_2\mathscr{K}(n_1+1)(n_2+1)P_{n_1,n_2} \\ & +N_1\mathscr{K}(n_1+1)(n_2+1)P_{n_1+1,n_2+1}+N_2\mathscr{K}n_1n_2P_{n_1-1,n_2-1}. \end{aligned} \tag{9.102}$$

The ladder of energy levels connected by two-photon transitions terminates at a lower end where the photon number in one of the beams falls to zero. The first and last terms on the right-hand side of the rate equation are absent for this lowest level. Note that the rate equation connects only those elements of the probability distribution for which the difference n_1-n_2 of the photon numbers in the two beams has a fixed value.

Consider first the steady-state solution for the photon distribution, where the right-hand side of eqn (9.102) must be set equal to zero. The analysis is similar to that given in §7.2 and it leads to the detailed-balance condition

$$N_2\mathscr{K}n_1n_2P_{n_1-1,n_2-1}-N_1\mathscr{K}n_1n_2\,P_{n_1-1,n_2-1}. \tag{9.103}$$

with the solutions

$$P_{n_1,n_2} = (N_2/N_1)P_{n_1-1,n_2-1} = \begin{cases} (N_2/N_1)^{n_2}P_{n_1-n_2,0} & \text{if} \quad n_1 \geqslant n_2 \\ (N_2/N_1)^{n_1}P_{0,n_2-n_1} & \text{if} \quad n_1 \leqslant n_2. \end{cases} \tag{9.104}$$

It is seen that the subset of probability elements corresponding to a given value of n_1-n_2 has a chaotic type of distribution in the steady state, similar to the result (7.18) found in the case of single-photon absorption and emission. However, the distribution as a whole is not in general chaotic since the relative magnitudes of probability elements in different subsets have arbitrary values determined by the initial conditions.

A simple case is that in which neither mode $\mathbf{k}_1$ nor mode $\mathbf{k}_2$ has any photons excited initially. The natures of the two-photon absorption and emission processes then ensure that at all subsequent times only those elements of the joint probability distribution with $n_1 = n_2$ can be nonzero. Eqn (9.104) gives

$$P_{n_1,n_2} = \delta_{n_1,n_2}(N_2/N_1)^{n_1}P_{0,0}, \tag{9.105}$$

and with $P_{0,0}$ determined from the normalization condition of eqn (9.94), the probability distribution can be written

$$P_{n_1,n_2} = \delta_{n_1,n_2}(\bar{n}_1)^{n_1}/(1+\bar{n}_1)^{1+n_1}; \tag{9.106}$$

the mean photon number for each mode is

$$\bar{n}_1 = \bar{n}_2 = N_2/(N_1-N_2) \tag{9.107}$$

and it is assumed that N_2 is smaller than N_1. This represents a kind of joint chaotic distribution for the two modes but the photon numbers in the modes are correlated and eqn (9.106) cannot be written as a product of two independent distributions.

The probability distribution can be used to evaluate the four degrees of second-order coherence defined by eqn (8.114) for a two-mode excitation.

Problem 9.2. Prove that the steady-state zero-time-delay degrees of second-order coherence for two-mode light generated by two-photon emission into an initial vacuum state are

$$g^{(2)}_{11}(0) = g^{(2)}_{22}(0) = 2 \tag{9.108}$$

and

$$g^{(2)}_{12}(0) = g^{(2)}_{21}(0) = 2+(1/\bar{n}_1) = N/N_2. \tag{9.109}$$

It is seen that the degrees of second-order coherence violate the classical inequality (8.127). The violation is particularly serious when only a small fraction of the atoms are excited, and it occurs for the same qualitative reason as that found in §8.9 for the light generated by two-photon cascade emission. The correlations between the photons produced in individual two-photon emission events are responsible for the violation of the classical inequality.

The degrees of coherence calculated in eqns (9.108) and (9.109) have not been verified experimentally but similar departures from the classical theory are observed in another nonlinear process in which photons are emitted into two distinct modes. This is spontaneous parametric splitting, a three-photon process allowed only in media that are not invariant under spatial inversion, where incident photons at the sum frequency $\omega_1+\omega_2$ are converted into pairs of photons, one each at the frequencies ω_1 and ω_2. Measurements of the various degrees of second-order coherence of the emitted light by photon-coincidence techniques[20] gave results in which the left-hand side of the inequality (8.127) exceeded the right-hand side by a factor of 10^4.

We now return from the steady state to consider the time dependence of the solutions of the two-photon rate equation (9.102). As in the single-photon case treated in §7.3, it is simpler to obtain solutions for the moments of the photon probability distribution rather than the complete distribution itself. The mean photon numbers in the two beams are defined by

$$\bar{n}_1 = \sum_{n_1,n_2} n_1P_{n_1,n_2} \quad \text{and} \quad \bar{n}_2 = \sum_{n_1,n_2} n_2P_{n_1,n_2}, \tag{9.110}$$

and their correlation is

$$\langle n_1n_2\rangle = \sum_{n_1,n_2} n_1n_2P_{n_1,n_2}. \tag{9.111}$$

The equations of motion for $\bar{n}_1$ and $\bar{n}_2$, obtained from the rate equation (9.102) in a manner analogous to the derivation of eqn (7.32), are

$$\mathrm{d}\bar{n}_1/\mathrm{d}t = \mathrm{d}\bar{n}_2/\mathrm{d}t = (N_2-N_1)\mathscr{K}\langle n_1 n_2\rangle + N_2\mathscr{K}(\bar{n}_1+\bar{n}_2+1). \quad (9.112)$$

The rates of change of the first moments thus depend on $\langle n_1 n_2\rangle$, one of the second moments. It is found that the rates of change of the second moments depend on the third moments, and so on. This feature is characteristic of the equations of motion for nonlinear optical processes. By contrast, the corresponding equations for the moments of the photon distribution in linear optics, for example eqns (7.32) and (7.34), involve only moments of the same or lower orders.

Complete solutions of the rate equations are available[21,22] for the case where negligible numbers of atoms are excited, and N_2 can be set equal to zero. The rates of change of the mean photon numbers are then

$$\mathrm{d}\bar{n}_1/\mathrm{d}t = \mathrm{d}\bar{n}_2/\mathrm{d}t = -N\mathscr{K}\langle n_1 n_2\rangle = -N\mathscr{K}\sum_{n_1,n_2} n_1 n_2 P_{n_1,n_2}; \quad (9.113)$$

this is a photon-number version of the intensity eqns (9.7) and (9.8). The assumption of statistical independence of the two beams at the commencement of the two-photon absorption at $t = 0$ implies that the initial probability distribution can be written as a product of distributions for the individual modes,

$$P_{n_1,n_2}(0) = Q_{n_1}(0)R_{n_2}(0). \quad (9.114)$$

The solutions remain quite complicated however, even with the assumptions of initial statistical independence of the light and a low level of atomic excitation. We accordingly consider here only the relatively simple solutions that are found after a further specialization to the case where one of the beams is much stronger than the other.

Let beam 1 be much more intense than beam 2. It is then permissible to neglect the changes in the properties of the first beam brought about by the two-photon absorption and we focus attention on the time dependence of beam 2. According to eqns (9.113) and (9.114), the initial rate of change of the mean photon number $\bar{n}_2$ is

$$(\mathrm{d}\bar{n}_2/\mathrm{d}t)_0 = -N\mathscr{K}\bar{n}_{20}\sum_{n_1} n_1 Q_{n_1}(0), \quad (9.115)$$

where

$$\bar{n}_{20} = \sum_{n_2} n_2 R_{n_2}(0). \quad (9.116)$$

The higher time-derivatives of $\bar{n}_2$ are found by successive differentiations of eqn (9.113) and repeated use of eqn (9.102). Thus

$$\mathrm{d}^2\bar{n}_2/\mathrm{d}t^2 = (N\mathscr{K})^2\sum_{n_1,n_2} n_1 n_2(n_1+n_2-1)P_{n_1,n_2}. \quad (9.117)$$

The assumption that beam 1 is much more intense than beam 2 is now used to approximate the bracketed quantity in the summation of eqn (9.117) simply by n_1. The initial value of the second derivative is then

$$(\mathrm{d}^2\bar{n}_2/\mathrm{d}t^2)_0 = (N\mathscr{K})^2\bar{n}_{20}\sum_{n_1} n_1^2 Q_{n_1}(0), \quad (9.118)$$

and similar approximations in the higher derivatives lead to

$$(\mathrm{d}^r\bar{n}_2/\mathrm{d}t^r)_0 = (-N\mathscr{K})^r\bar{n}_{20}\sum_{n_1} n_1^r Q_{n_1}(0). \quad (9.119)$$

Summation of the Taylor expansion of $\bar{n}_2$ about $t = 0$ now gives

$$\bar{n}_2 = \bar{n}_{20} + \sum_{r=1}^{\infty}(\mathrm{d}^r\bar{n}_2/\mathrm{d}t^r)_0 t^r/r! = \bar{n}_{20}\sum_{n_1=0}^{\infty}\exp(-N\mathscr{K}n_1 t)Q_{n_1}(0). \quad (9.120)$$

The rate of absorption of the weak beam is thus determined by the statistical properties of the strong beam and is independent of its own statistical distribution. The summation in eqn (9.120) is performed without difficulty for the main varieties of strong beam.

Problem 9.3. Prove that the time dependence of the weak-beam photon number is as follows for the kinds of strong beam indicated

$$\frac{\bar{n}_2}{\bar{n}_{20}} = \begin{cases} \exp(-N\mathscr{K}n_1 t) & \text{(number state)} \\ \exp\{\bar{n}_1[\exp(-N\mathscr{K}t)-1]\} & \text{(coherent)} \\ \{1+\bar{n}_1-\bar{n}_1\exp(-N\mathscr{K}t)\}^{-1} & \text{(chaotic).} \end{cases} \quad (9.121)$$

Problem 9.4. Consider a strong beam formed by repeatedly switching a beam of coherent light on and off. If f is the fraction of time for which the beam is turned on and $\bar{n}_1$ is the mean photon number of the resulting pulsed beam, show that

$$Q_{n_1}(0) = \begin{cases} f\{(\bar{n}_1/f)^{n_1}/n_1!\}\exp(-\bar{n}_1/f) & \text{for} \quad n_1 \neq 0 \\ 1-f+f\exp(-\bar{n}_1/f) & \text{for} \quad n_1 = 0 \end{cases} \quad (9.122)$$

and hence that the weak-beam photon number has the time dependence

$$\bar{n}_2/\bar{n}_{20} = 1-f+f\exp\{(\bar{n}_1/f)[\exp(-N\mathscr{K}t)-1]\}. \quad (9.123)$$

Fig. 9.10 shows the calculated forms of time dependence for the weak-beam photon numbers. The rather large steady-state values of $\bar{n}_2$ for the pulsed strong beams result from the absence of any absorption from those parts of the weak beam that coincide with the dark sections of the pulsed beams, as discussed in connection with Fig. 9.8.

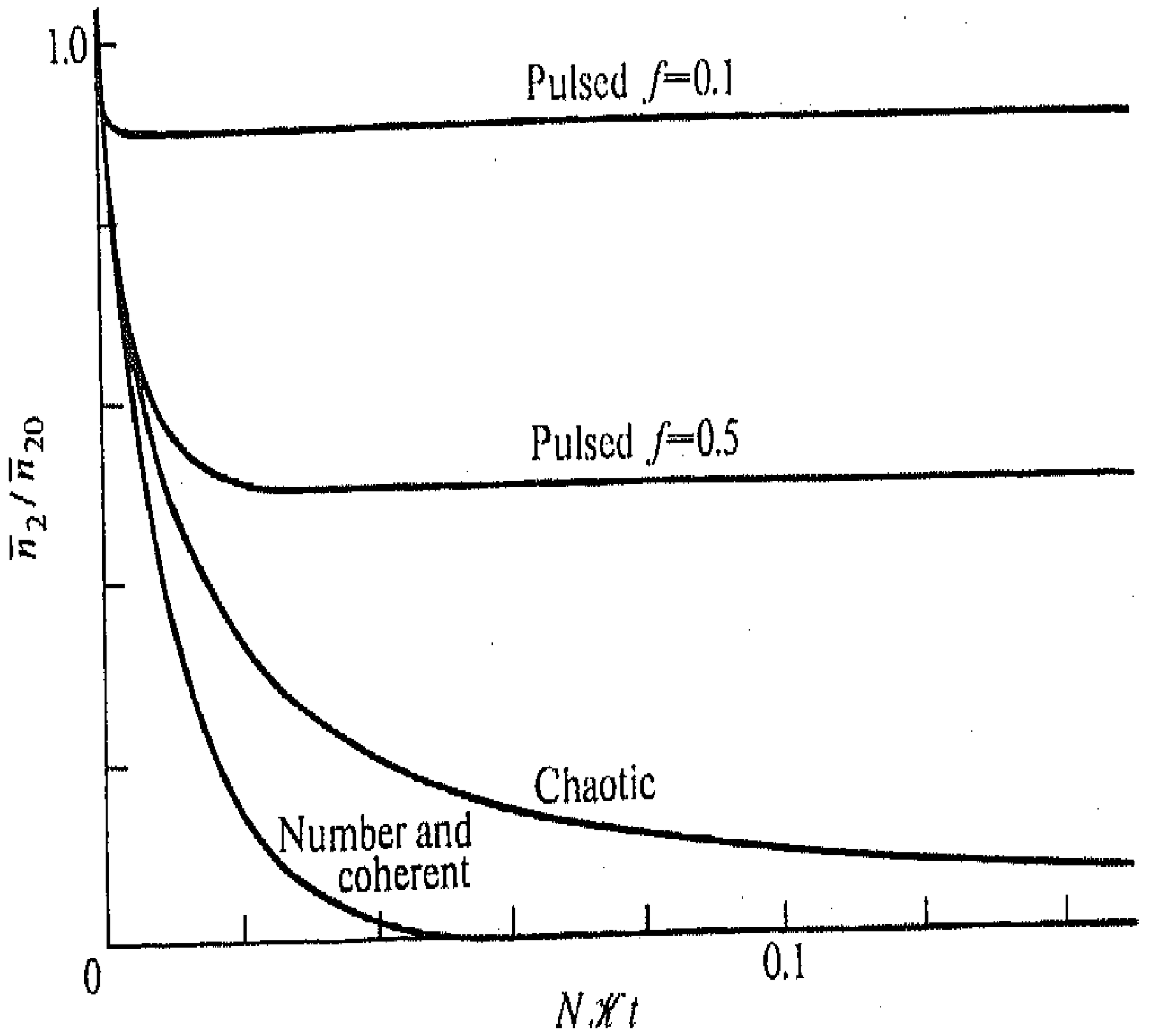

FIG. 9.10. Time dependences of the mean photon numbers in the weak beam for the initial kinds of strong beam indicated. All the strong beams have a mean photon number of 100. (After H. D. Simaan and R. Loudon, ref. 22.)

The method used above to calculate the time dependence of the first moment of the weak-beam photon distribution for various kinds of strong beam can also be employed for the higher-order moments. We consider here only the most important of these, namely the interbeam degree of second-order coherence,

$$g_{12}^{(2)}(0) = g_{21}^{(2)}(0) = \langle n_1 n_2 \rangle / \bar{n}_1 \bar{n}_2, \qquad (9.124)$$

whose magnitude controls the two-photon absorption rate. The equation of motion for $\langle n_1 n_2 \rangle$ is obtained from its definition (9.111) and the rate equation (9.102). The equation is solved by a procedure similar to that which leads from eqn (9.113) to eqn (9.120), and the result is

$$\langle n_1 n_2 \rangle = \bar{n}_{20} \sum_{n_1=0}^{\infty} n_1 \exp(-N\mathscr{K} n_1 t) Q_{n_1}(0). \qquad (9.125)$$

Problem 9.5. Prove that the time dependence of the interbeam degree of second-order coherence is as follows for the kinds of strong beam indicated.

$$g_{12}^{(2)}(0) = \begin{cases} 1 & \text{(number state)} \\ \exp(-N\mathscr{K}t) & \text{(coherent)} \\ \{(1+\bar{n}_1)\exp(N\mathscr{K}t) - \bar{n}_1\}^{-1} & \text{(chaotic)} \\ \exp(-N\mathscr{K}t)/\{(1-f)\exp[(\bar{n}_1/f)(1-\exp(-N\mathscr{K}t))] + f\} & \\ & \text{(pulsed).} \end{cases} \qquad (9.126)$$

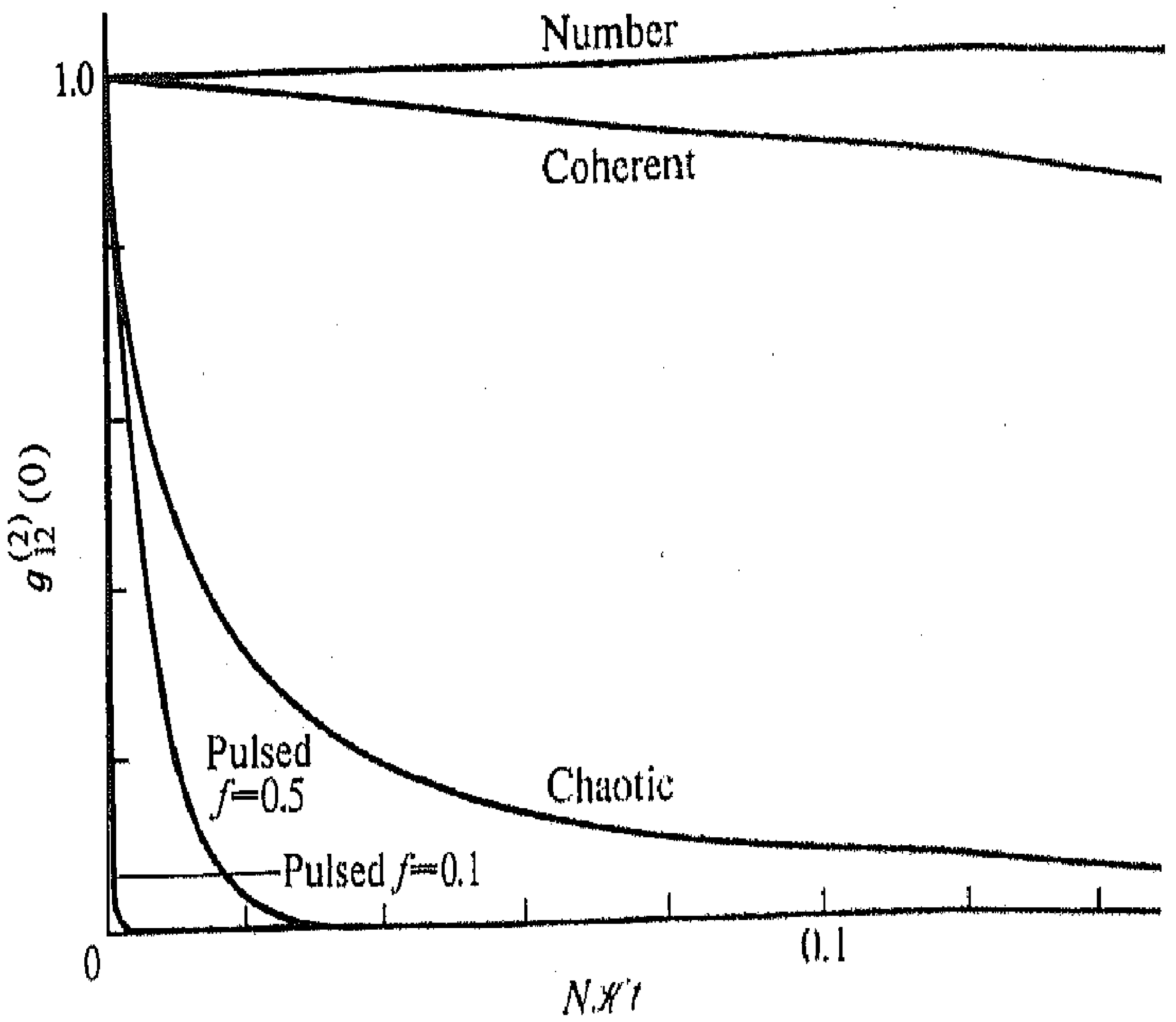

FIG. 9.11. Time dependences of the interbeam degree of second-order coherence for the kinds of strong beam indicated. All the strong beams have a mean photon number of 100. (After H. D. Simaan and R. Loudon, ref. 22.)

Fig. 9.11 shows the forms of these time dependences. The interbeam degree of second-order coherence diminishes with time for all except the number-state strong beam. The fall-off is particularly rapid for the pulsed strong beams, where anticorrelations between the beams develop in the manner illustrated qualitatively in Fig. 9.8.

The effects of the diminishing value of $g_{12}^{(2)}(0)$ on the two-photon absorption rate are seen by comparison of Figs. 9.10 and 9.11. The former figure shows that $\bar{n}_2$ has the same initial rate of decay for all kinds of strong beam. However, the decay rate is subsequently reduced for those strong beams that cause a fall-off in the value of $g_{12}^{(2)}(0)$, and the effect is again particularly marked for the pulsed strong beams. The reversed order of appearance of the curves for the different kinds of strong beam in Figs. 9.10 and 9.11 demonstrates the importance of beam correlation effects in nonlinear optical processes.

9.8. Photon statistics of single-beam two-photon absorption

The treatment of photon-statistical effects in two-photon absorption from a single light beam parallels the corresponding double-beam theory of the previous section. The model used in §9.2 is generalized to allow for a significant population N_2 of atoms in the excited state of the two-photon transition. The normalized photon probability distribution, denoted P_{n_1}, is then influenced by two-photon emission as well as two-photon absorption processes. The first stage in the theory is the derivation of a rate equation for the photon probability distribution.

A two-photon absorption event reduces the photon number from n_1 to n_1-2. The transition rate is given by eqn (9.26), and for a definite number of photons,

$$\mathrm{Tr}(\hat{\rho}\hat{E}_1^-\hat{E}_1^-\hat{E}_1^+\hat{E}_1^+) = (\hbar\omega_1/2\epsilon_0 V\eta_1^2)^2 n_1(n_1-1). \tag{9.127}$$

The probability per unit time that the beam photon number is reduced from n_1 to n_1-2 can be written

$$N_1\mathscr{K}'n_1(n_1-1), \tag{9.128}$$

where $\mathscr{K}'$ includes all the constant factors from eqns (9.26) and (9.127). The corresponding probability that the photon number is increased from n_1 to n_1+2 by two-photon emission is

$$N_2\mathscr{K}'(n_1+1)(n_1+2). \tag{9.129}$$

The two-photon absorption and emission processes produce four kinds of transition that influence P_{n_1}. The corresponding transition rates, shown on the photon energy-level diagram of Fig. 9.12, combine to produce a rate equation

$$\begin{aligned} \mathrm{d}P_{n_1}/\mathrm{d}t = {} & -N_1\mathscr{K}'n_1(n_1-1)P_{n_1} - N_2\mathscr{K}'(n_1+1)(n_1+2)P_{n_1} \\ & + N_1\mathscr{K}'(n_1+2)(n_1+1)P_{n_1+2} + N_2\mathscr{K}'(n_1-1)n_1P_{n_1-2}. \end{aligned} \tag{9.130}$$

The rate equations separate into a set that couples all the even-numbered elements of the photon probability distribution and a set that couples all the odd-numbered elements. The lowest levels in the sets are those for $n_1 = 0$ and $n_1 = 1$ respectively, and the first and last terms on the right-hand side of eqn (9.130) are absent for these two levels.

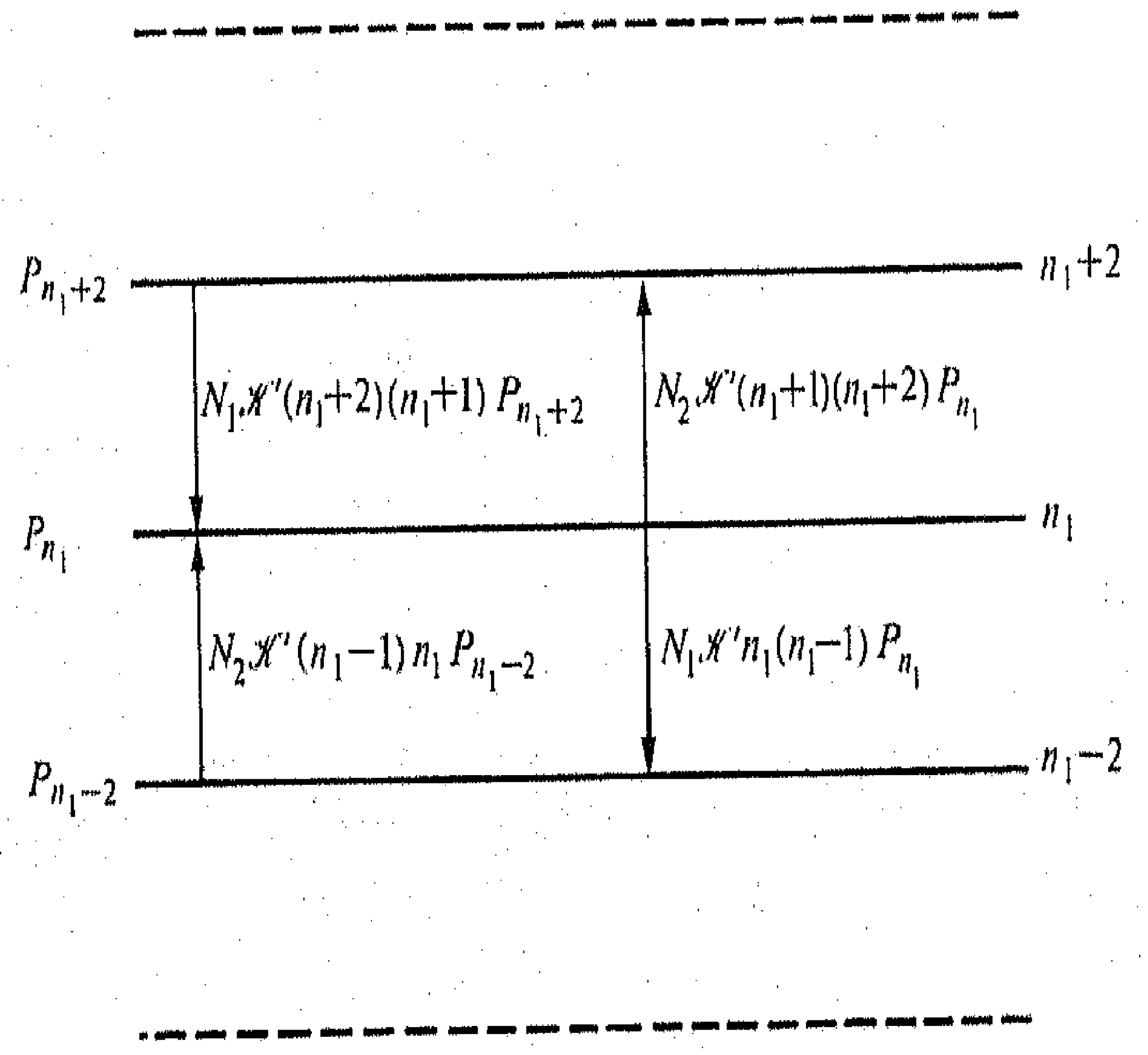
P_{n_1+2}
n_1+2
$N_1\mathscr{K}'(n_1+2)(n_1+1)\,P_{n_1+2}$
$N_2\mathscr{K}'(n_1+1)(n_1+2)\,P_{n_1}$
P_{n_1}
n_1
$N_2\mathscr{K}'(n_1-1)\,n_1\,P_{n_1-2}$
$N_1\mathscr{K}'n_1(n_1-1)\,P_{n_1}$
P_{n_1-2}
n_1-2

FIG. 9.12. Photon energy-level diagram for a single mode subjected to two-photon absorption and emission. The transition rates shown are the contributions to $\mathrm{d}P_{n_1}/\mathrm{d}t$.

The steady-state photon distribution, obtained by setting the right-hand sides of all the rate equations (9.130) equal to zero, has

$$\begin{aligned} P_{n_1} = (N_2/N_1)P_{n_1-2} &= (N_2/N_1)^{n_1/2}P_0 && \text{for} \quad n_1 \text{ even} \\ &= (N_2/N_1)^{(n_1-1)/2}P_1 && \text{for} \quad n_1 \text{ odd}. \end{aligned} \tag{9.131}$$

The sums of the probability elements over all even or all odd values of n_1 are constants of the motion for the rate equations (9.130). It follows that

$$\sum_{n_1}^{\text{even}} P_{n_1} = [1-(N_2/N_1)]^{-1}P_0 = \sum_{n_1}^{\text{even}} P_{n_1}(0) \tag{9.132}$$

$$\sum_{n_1}^{\text{odd}} P_{n_1} = [1-(N_2/N_1)]^{-1}P_1 = \sum_{n_1}^{\text{odd}} P_{n_1}(0), \tag{9.133}$$

where $P_{n_1}(0)$ is the initial probability distribution and N_2 is assumed to be smaller than N_1. The complete steady-state distribution is thus easily found for any given initial conditions.[23,24]

Consider first the case in which no photons are initially excited. The steady-state distribution produced by two-photon emission is then

$$\begin{aligned} P_{n_1} &= \left(\frac{N_2}{N_1}\right)^{n_1/2}\left(1-\frac{N_2}{N_1}\right) && \text{for} \quad n_1 \text{ even} \\ &= 0 && \text{for} \quad n_1 \text{ odd}. \end{aligned} \tag{9.134}$$

Problem 9.6. Prove that the steady-state light generated by two-photon emission into a single mode has a mean photon number and degree of second-order coherence given respectively by

$$\bar{n}_1 = 2N_2/(N_1-N_2) \tag{9.135}$$

$$g_{11}^{(2)}(0) = \frac{N_1+3N_2}{2N_2} = 2+\frac{1}{\bar{n}_1}. \tag{9.136}$$

The light thus has a degree of second-order coherence larger than that of ordinary chaotic light, the enhanced fluctuations being caused by the emission of photons in correlated pairs.

Another simple case is that in which there is initially some intense beam of light whose photon distribution spreads smoothly across a range of even and odd photon numbers, for example chaotic or coherent light with a large mean photon number. The values of the summations over all even or all odd elements of the initial photon distribution on the right-hand sides of eqns (9.132) and (9.133) are then very close to $\frac{1}{2}$.

Problem 9.7. Prove that the steady-state light obtained by interaction of an intense initial beam with two-photon absorbing and emitting atoms has a mean photon number and degree of second-order coherence given respectively by

$$\bar{n}_1 = (N_1+3N_2)/2(N_1-N_2) \qquad (9.137)$$

$$g^{(2)}_{11}(0) = \frac{16N_2(N_1+N_2)}{(N_1+3N_2)^2} = 2 - \frac{1}{2\bar{n}_1^2}. \qquad (9.138)$$

The light now has a degree of second-order coherence smaller than that of chaotic light, and the antibunching condition is satisfied for sufficiently small numbers of excited atoms,

$$g^{(2)}_{11}(0) < 1 \quad \text{for} \quad N_2/N_1 < 0{\cdot}094. \qquad (9.139)$$

The antibunching is produced by the preferential removal of pairs of coincident photons from the light by the two-photon absorption, as described in §9.6.

The complete time dependence of the photon probability distribution can be found[21,23,25,26] in the case where negligible numbers of atoms are excited, and eqn (9.130) reduces to

$$\mathrm{d}P_{n_1}/\mathrm{d}t = -N\mathscr{K}'n_1(n_1-1)P_{n_1} + N\mathscr{K}'(n_1+2)(n_1+1)P_{n_1+2}. \qquad (9.140)$$

The rate of change of the mean photon number is then given by

$$\mathrm{d}\bar{n}_1/\mathrm{d}t = -2N\mathscr{K}'\sum_{n_1} n_1(n_1-1)P_{n_1} = -2N\mathscr{K}'g^{(2)}_{11}(0)\bar{n}_1^2; \qquad (9.141)$$

this is a photon-number version of the intensity eqn (9.29). The rate of change of the second moment of the photon distribution, obtainable from eqn (9.140), depends upon the third moment of the distribution, and so on.

The general solution of eqn (9.140) for the photon probability distribution is somewhat complicated, and we illustrate its properties by showing the forms of time dependence of the mean photon number and degree of second-order coherence in the two cases of initial light beams that are chaotic or coherent. Fig. 9.13 shows the time dependence of $\bar{n}_1$ for beams whose initial mean photon numbers $\bar{n}_{10}$ are equal to 10. The factor of 2 difference between the initial absorption rates in the two cases, previously mentioned in connection with eqns (9.33) and (9.34), is clearly visible. The solution of eqn (9.141) for a constant degree of second-order coherence is

$$\bar{n}_1 = \bar{n}_{10}/(1+2N\mathscr{K}'g^{(2)}_{11}(0)\bar{n}_{10}t), \qquad (9.142)$$

in agreement with the initial behaviours of the curves in Fig. 9.13. It is however clear from Fig. 9.13 that the absorption rates for the two beams tend towards equality at longer times, contrary to the form of solution in eqn (9.142).

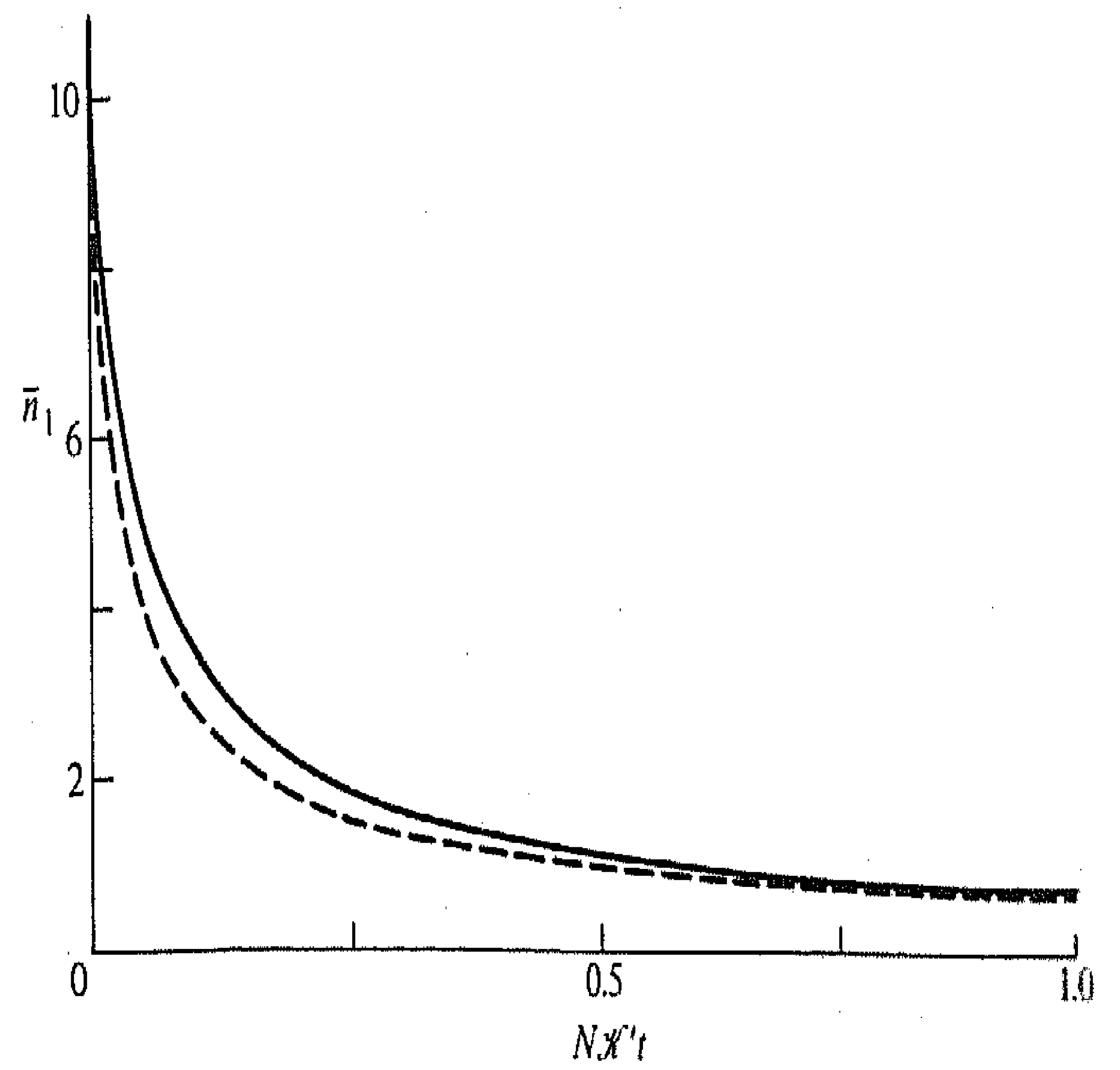

FIG. 9.13. Time dependences of the mean photon numbers for light beams subjected to two-photon absorption. The beams are initially coherent (——) and chaotic (– – – –) with mean photon numbers equal to 10. (After H. D. Simaan and R. Loudon, ref. 23.)

The way in which two-photon absorption reduces the degree of second-order coherence of the unabsorbed portion of the light beam, and hence also reduces the absorption rate, has been discussed in qualitative terms in §§9.2 and 9.6. Quantitative results for the time variation of $g^{(2)}_{11}(0)$ are shown in Fig. 9.14. It is seen that the degree of second-order coherence falls rapidly from its initial value of 2 for chaotic light as two-photon absorption removes the pairs of coincident photons associated with the photon bunches. The nature of initially coherent light is also changed as the random photon coincidences are removed by the two-photon absorption. The values of $g^{(2)}_{11}(0)$ for the two kinds of initial light become very similar after a time corresponding to about 0·5 on the horizontal scale of Fig. 9.14, giving the comparable rates of two-photon absorption seen in Fig. 9.13. For both kinds of light illustrated, and more generally for almost any kind of initial light beam, the degree of second-order coherence eventually falls below unity, corresponding to nonclassical or antibunched light.

It is seen from comparison of Figs. 9.13 and 9.14 that $g^{(2)}_{11}(0)$ falls significantly below the classical lower bound of unity only when the mean photon numbers are reduced to a very low level. Furthermore, the two-photon absorption is a weak effect, and the statistical changes derived above are easily masked by any single-photon absorption and emission that occur at the incident frequency.[27] Thus, while some observations of a reduction in $g^{(2)}_{11}(0)$ brought about by two-photon absorption have been made,[28] this process has proved to be a more difficult technique for the generation of nonclassical light than the resonance

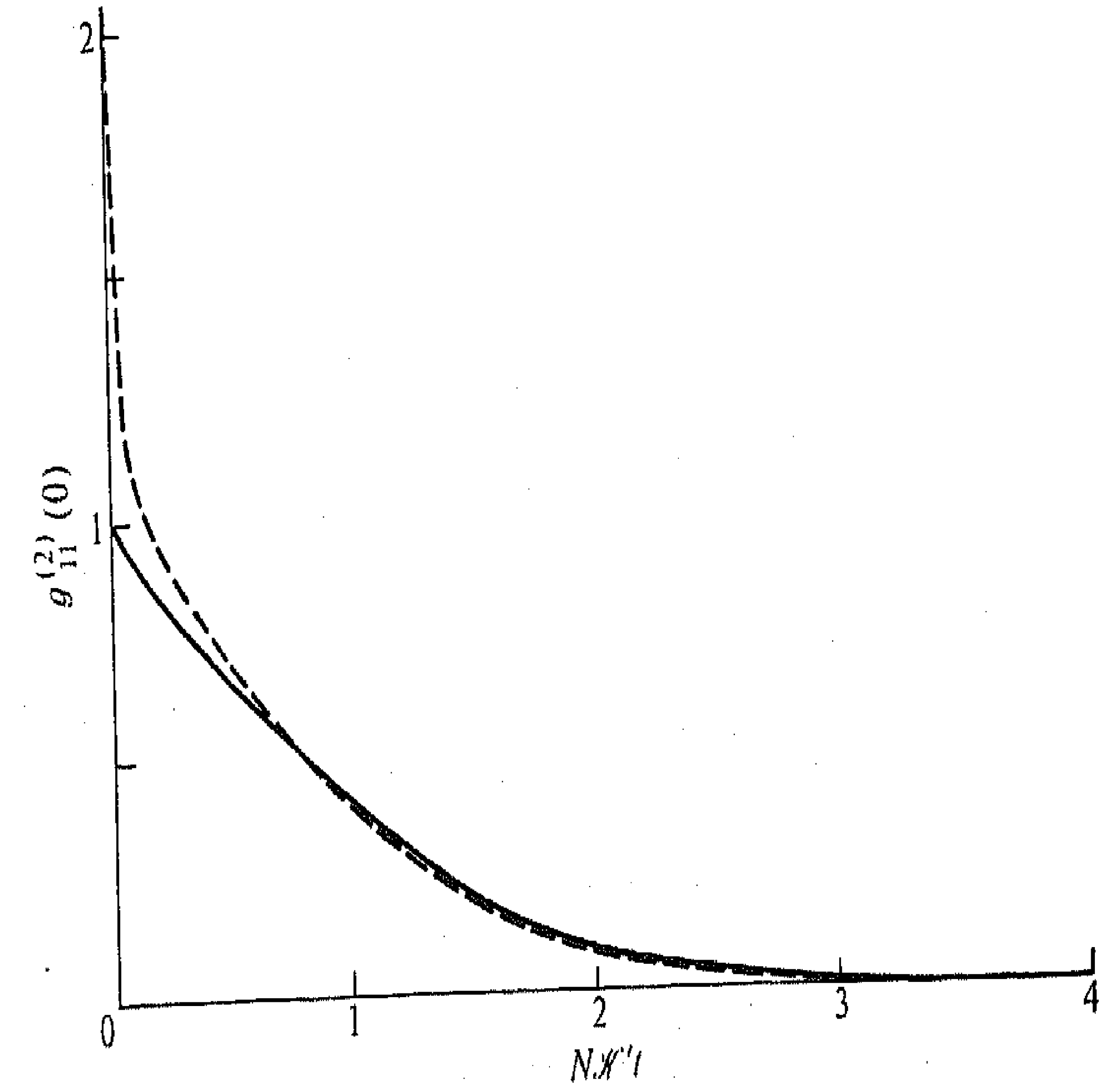

FIG. 9.14. Time dependences of the degrees of second-order coherence for the same light beams as in Fig. 9.13, initially coherent (——) and chaotic (----). (After H. D. Simaan and R. Loudon, ref. 23.)

fluorescence described in Chapter 8. A detailed comparison of theory with experimental results would require a generalization of the single-mode model assumed here to include the effects of optical bandwidths and atomic linewidths.[29] Further generalizations of the theory have been made to cover the replenishment of the absorbed beam by a steady supply of new photons,[30,31] and to allow for the simultaneous absorption of more than two photons;[32] nonclassical light should also be generated under these more general conditions.

9.9. Photon statistics of the stimulated Raman effect

The final nonlinear optical process to be considered in terms of its photon statistical properties is the stimulated Raman effect. Let P_{n,n_s} be the normalized probability that at time t there are n incident photons and n_s scattered photons, with

$$\sum_{n,n_s} P_{n,n_s} = 1. \tag{9.143}$$

It is assumed as in §9.4 that almost all of the N scattering atoms are in their ground states, and that the incident and scattered photons each belong to single modes of the radiation field. The transition rate in the presence of given

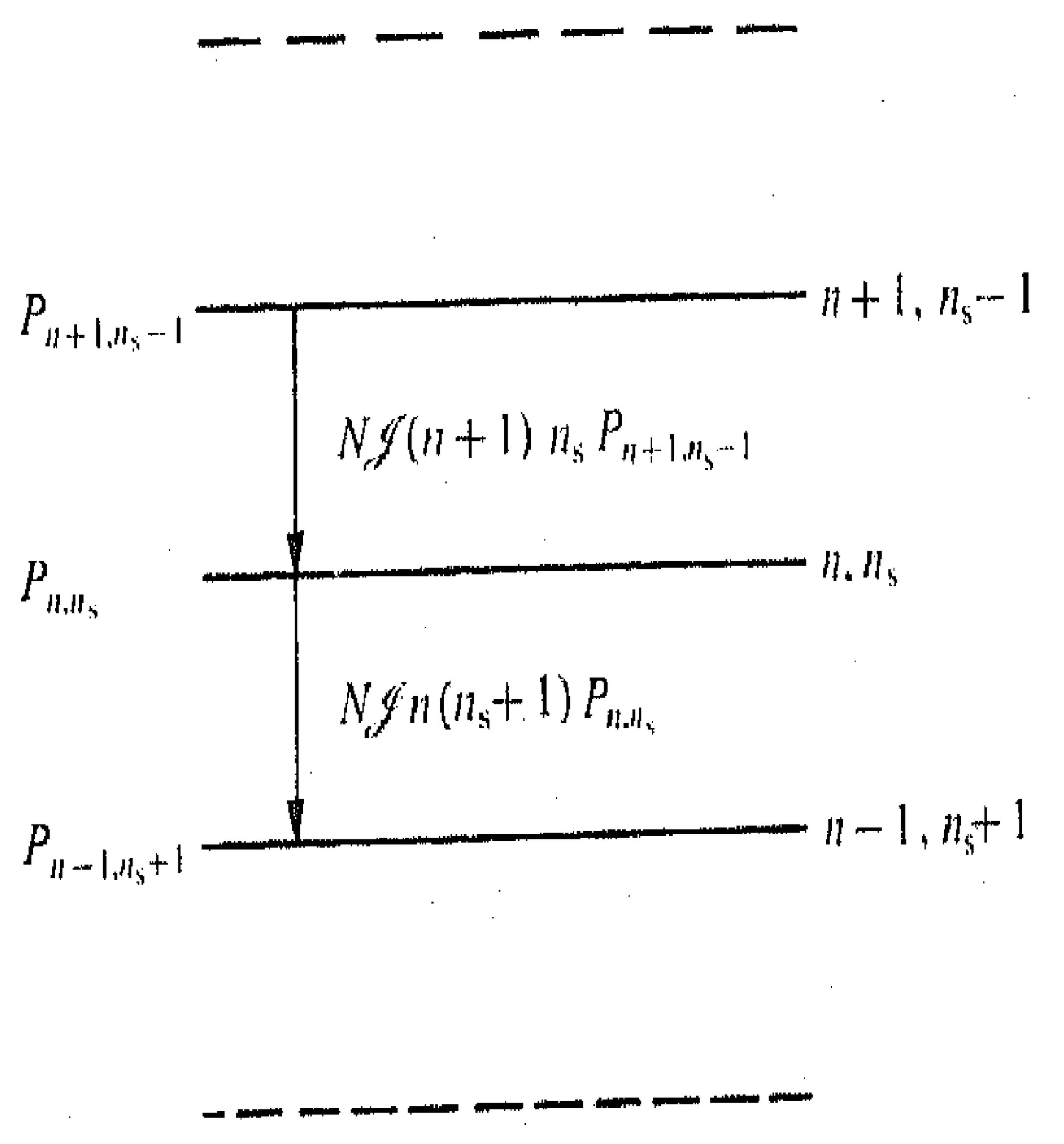

FIG. 9.15. Energy-level diagram for the photons in the two modes that correspond to the incident and scattered light in the Raman process. The transition rates shown are the contributions to $\mathrm{d}P_{n,n_s}/\mathrm{d}t$ under the assumption that the population of the atomic excited state is negligible.

numbers of incident and scattered photons is

$$1/\tau = N\mathcal{J}n(n_s+1), \tag{9.144}$$

where $\mathcal{J}$ includes all the constant factors from eqns (9.50) and (9.54).

The rate equation for the photon probability distribution is derived in the same way as for the two-photon absorption processes. Fig. 9.15 shows the transition rates that affect a given element of the probability distribution; and the corresponding equation of motion is

$$\mathrm{d}P_{n,n_s}/\mathrm{d}t = -N\mathcal{J}n(n_s+1)P_{n,n_s} + N\mathcal{J}(n+1)n_sP_{n+1,n_s-1}. \tag{9.145}$$

The mean photon numbers in the two beams are

$$\bar{n} = \sum_{n,n_s} nP_{n,n_s} \quad \text{and} \quad \bar{n}_s = \sum_{n,n_s} n_sP_{n,n_s}, \tag{9.146}$$

and their correlation is

$$\langle nn_s\rangle = \sum_{n,n_s} nn_sP_{n,n_s}. \tag{9.147}$$

The equations of motion for $\bar{n}$ and $\bar{n}_s$ obtained from the rate equation (9.145) are

$$\mathrm{d}\bar{n}/\mathrm{d}t = -\mathrm{d}\bar{n}_s/\mathrm{d}t = -N\mathcal{J}(\langle nn_s\rangle + \bar{n}) = -N\mathcal{J}\sum_{n,n_s} n(n_s+1)P_{n,n_s}. \tag{9.148}$$

The treatment of stimulated Raman scattering given in §9.4 assumes that $\langle nn_s\rangle$ is equal to the product $\bar{n}\bar{n}_s$, and thus ignores photon-number correlations between the incident and scattered light.

The equations of motion for the joint photon probability distribution and its various moments have been solved[21,33,34] to obtain the general time dependences of these quantities. We do not reproduce these rather complicated general solutions here, but instead consider the simpler special case in which no scattered photons are excited initially and the number of incident photons is always large. Provided that only a small fraction of the photons initially present in the incident beam are scattered, it is safe to neglect the small changes in the statistical distribution of this beam from its initial form $P_n(0)$.

The method of solution for the time dependence of the mean number of scattered photons in this case parallels that given in eqns (9.115)–(9.120) for two-photon absorption in the analogous limit where one beam is much more intense than the other.

Problem 9.8. Prove that the mean number of scattered photons at time t is

$$\bar{n}_s = \sum_{n=0}^{\infty} \exp(N\mathcal{J}nt)P_n(0) - 1 \tag{9.149}$$

for initial conditions in which there are no scattered photons and the incident photons have a distribution $P_n(0)$ with mean number $\bar{n} \gg 1$.

The requirement that only a small fraction of the incident photons are scattered limits the validity of this result to times t such that

$$N\mathcal{J}t \ll 1. \tag{9.150}$$

The summation in eqn (9.149) is easily carried out for the simpler kinds of incident light.

Problem 9.9. Show that the time dependence of the scattered photon number is as follows for the kinds of incident beam indicated,

$$\bar{n}_s = \begin{cases} \exp(N\mathcal{J}nt) - 1 & \text{(number state)} \\ \exp(N\mathcal{J}\bar{n}t) - 1 & \text{(coherent)} \\ N\mathcal{J}\bar{n}t/(1 - N\mathcal{J}\bar{n}t) & \text{(chaotic),} \end{cases} \tag{9.151}$$

where the inequality (9.150) is used to approximate the last two results.

The results for coherent and chaotic light are illustrated in Fig. 9.16. It is seen that the two curves have the same slope at small t, but the chaotic incident light is more strongly scattered than the coherent incident light at longer times.

The time dependences of the mean numbers of scattered photons for number state and coherent incident light in eqn (9.151) are similar to the spatial dependence of eqn (9.68) obtained from a theory that neglects correlation between the two light beams. The more rapid growth of the scattered photon number for chaotic incident light in eqn (9.151) results from the enhanced interbeam correlation that develops in this case. The equation of motion for $\langle nn_s \rangle$ is obtained from its definition (9.147) and the rate equation (9.145). The solution for the same conditions as assumed in problem 9.8 is

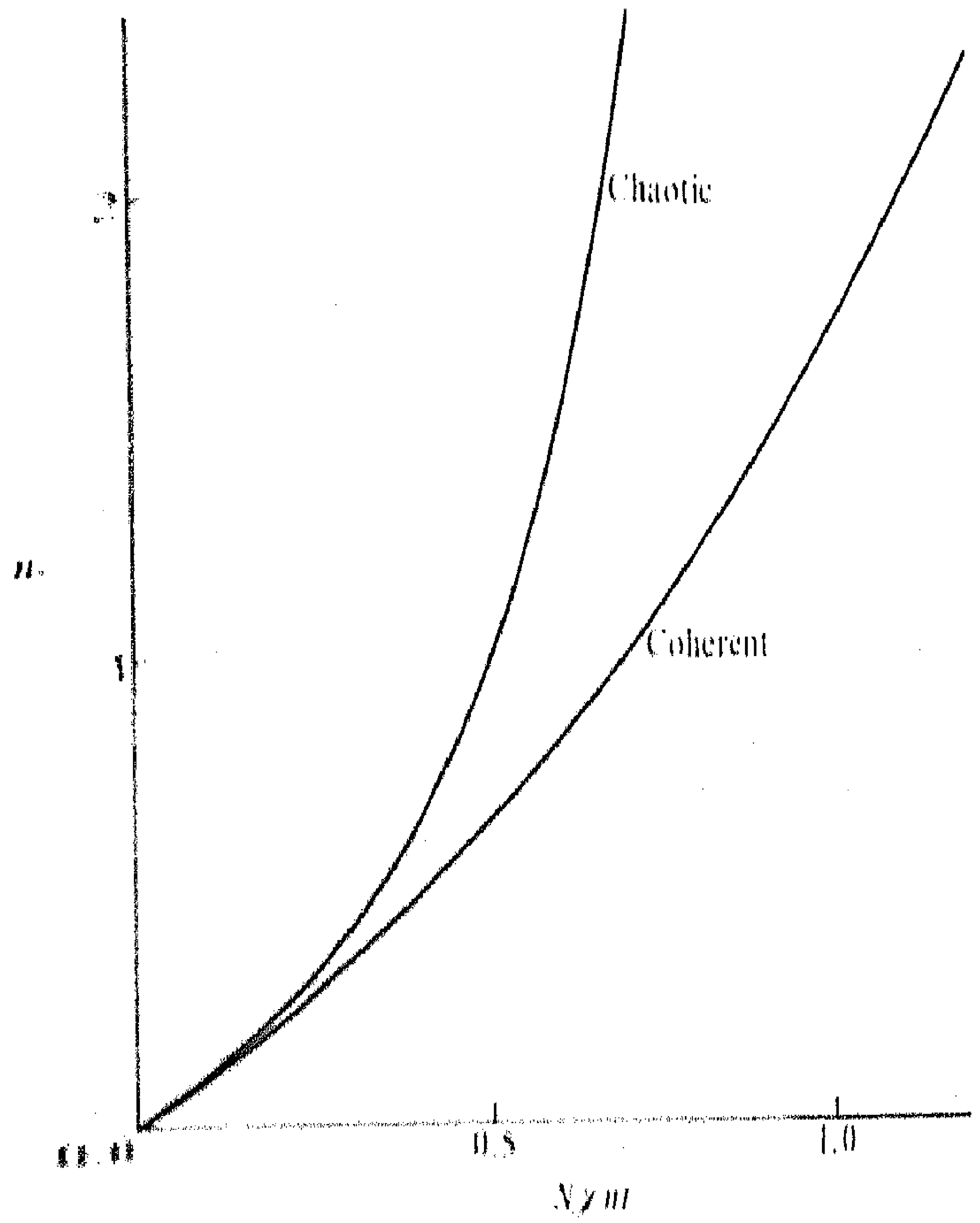

FIG. 9.16. Time dependences of the mean numbers of photons produced by scattering of coherent and chaotic single-mode incident light.

$$\langle nn_s \rangle = \sum_{n=0}^{\infty} n\exp(N\mathcal{J}nt)P_n(0) - \bar{n}. \tag{9.152}$$

The normalized correlation function or interbeam degree of second-order coherence defined by

$$g_s^{(2)}(0) = \langle nn_s \rangle / \bar{n}\bar{n}_s \tag{9.153}$$

has a time dependence determined by eqns (9.149) and (9.152). The initial value of this quantity, obtained from small-time expansions of the exponentials in the latter equations, is

$$g_s^{(2)}(0) = \overline{n^2}/\bar{n}^2 \approx g^{(2)}(0) \qquad (t \to 0), \tag{9.154}$$

where $g^{(2)}(0)$ is the degree of second-order coherence of the incident light, defined by eqn (6.28) and approximately equal to $\overline{n^2}/\bar{n}^2$ in the $\bar{n} \gg 1$ regime assumed here. Thus the initial value of the interbeam correlation for chaotic incident light is about twice that for number state or coherent incident light, and evaluations of eqn (9.153) at finite times show that the disparity increases with t.

The nature of the scattered light is determined by evaluation of the higher moments of the photon probability distribution. Thus the second factorial moment obtained in the same manner as eqns (9.149) and (9.152) is

$$\langle n_s(n_s-1)\rangle = 2\sum_{n=0}^{\infty}\{\exp(2N\mathscr{J}nt)-2\exp(N\mathscr{J}nt)\}P_n(0)+2. \tag{9.155}$$

The degree of second-order coherence of the scattered light,

$$g_{ss}^{(2)}(0) = \langle n_s(n_s-1)\rangle/\bar{n}_s^2 \tag{9.156}$$

has its time dependence determined by eqns (9.149) and (9.155). The small-time expansions of both the numerator and denominator have leading terms proportional to t^2, and the resulting initial value is

$$g_{ss}^{(2)}(0) = 2\overline{n^2}/\bar{n}^2 \approx 2g^{(2)}(0) \qquad (t \rightarrow 0). \tag{9.157}$$

Thus the incident number state and coherent beams generate scattered light with initial degrees of second-order coherence equal to 2; in the former case it can be shown[34] that the scattered photons have a chaotic probability distribution at all times t. Incident chaotic light generates scattered light with much larger photon-number fluctuations, the initial value of the degree of second-order coherence being 4; the scattered light in this case can be described as super-chaotic.[35]

9.10. Conclusion

The calculations outlined in the present chapter show how the nonlinear interactions of light with atoms can change the initial statistical properties of the light. The degrees of second-order coherence of the individual light beams and the photon-number correlations between different light beams may be increased or decreased, depending on the nature of the nonlinear process. The light that is newly created in some processes may have statistical properties quite different from those of the initiating light beams.

Some of the most striking manifestations of the quantum nature of light are found in its statistical and coherence properties. Nonclassical effects can occur in measurements of photon coincidences, or intensity correlations, within a single beam of light or between two light beams of different frequencies. Nonlinear optical processes in principle provide versatile techniques for generating nonclassical light, although linear processes such as resonance fluorescence and two-photon cascade emission have so far proved to be experimentally more fruitful.

The classical and quantum theories differ in their representations of the act of measurement. It is assumed in the classical theory that the intensity of a light beam, represented by a positive single-valued function, can be measured to arbitrary precision, and that repeated measurements do not interfere in any way. By contrast, the quantum theory has separate specifications for the state of the light, represented by a pure state or a density operator, and the act of measurement, represented by an application of the appropriate operator. The measurement process in general changes the state of the light, and successive measurements may register different results, in typical quantum fashion. Intensity measurements involve destruction of photons, and progressively fewer photons remain to give progressively smaller intensities in a series of measurements. In the degrees of coherence, successive intensity or photon-number measurements first occur in second order, and this is the simplest level at which to study nonclassical effects in the theory or in experiments.

The quantum theory appears to provide an accurate description of the properties of all kinds of light, and the results of all optical experiments are in very good agreement with its predictions. The classical theory has a limited range of applicability, within which the fluctuation and coherence properties of light are accurately determined by classical intensity distributions. It is noteworthy that the classical range embraces such important practical cases as the chaotic light from a conventional source and the coherent light available from a single-mode laser.

References

1. Bloembergen, N. (1965). *Nonlinear optics*. Benjamin, New York.
2. Butcher, P. N. (1965). *Nonlinear optical phenomena*. Ohio State University Engineering Publications, Columbus.
3. Zernike, F. and Midwinter, J. E. (1973). *Applied nonlinear optics*. Wiley, New York.
4. Yariv, A. (1975). *Quantum electronics*. Wiley, New York.
5. Bloembergen, N. (Ed.) (1977). *Nonlinear spectroscopy*. North-Holland, Amsterdam.
6. Letokhov, V. S. and Chebotayev, V. P. (1977). *Nonlinear laser spectroscopy*. Springer-Verlag, Berlin.
7. Hanna, D. C., Yuratich, M. A., and Cotter, D. (1979). *Nonlinear optics of free atoms and molecules*. Springer-Verlag, Berlin.
8. Bassani, F., Forney, J. J., and Quattropani, A. (1977). *Phys. Rev. Lett.* **39**, 1070: Quattropani, A., Bassani, F., and Carillo, S. (1982). *Phys. Rev.* **A25**, 3079.
9. Vasilenko, L. S., Chebotayev, V. P., and Shishaev, A. V. (1970). *JETP Lett.* **12**, 113.
10. Hänsch, T. W., ref. 5, p. 17.
11. Hänsch, T. W., Lee, S. A., Wallenstein, R., and Wieman, C. (1975). *Phys. Rev. Lett.* **34**, 307.
12. Lee, S. A., Wallenstein, R., and Hänsch, T. W. (1975). *Phys. Rev. Lett.* **35**, 1262.

13. This was first pointed out by Teich, M. C. and Wolga, G. J. (1966). *Phys. Rev. Lett.* **16,** 625, and Lambropoulos, P., Kikuchi, C., and Osborn, R. K. (1966). *Phys. Rev.* **144,** 1081.
14. For a discussion of the experimental verifications of this prediction, see Armstrong, L., Lambropoulos, P., and Rahman, N. K. (1976). *Phys. Rev. Lett.* **36,** 952.
15. Weber, H. P. (1971). *I.E.E.E. J. Quantum Electron.* **QE-7,** 189.
16. Raymer, M. G. and Mostowski, J. (1981). *Phys. Rev.* **A24,** 1980.
17. Bloembergen, N. (1967). *Am. J. Phys.* **35,** 989.
18. Ward, J. F. and New, G. H. C. (1969). *Phys. Rev.* **185,** 57.
19. Shen, Y. R. (1967). *Phys. Rev.* **155,** 921.
20. Burnham, D. C. and Weinberg, D. L. (1970). *Phys. Rev. Lett.* **25,** 84.
21. McNeil, K. J. and Walls, D. F. (1974). *J. Phys.* **A7,** 617.
22. Simaan, H. D. and Loudon, R. (1975). *J. Phys.* **A8,** 1140.
23. Simaan, H. D. and Loudon, R. (1975). *J. Phys.* **A8,** 539.
24. McNeil, K. J. and Walls, D. F. (1975). *Phys. Lett.* **51A,** 233.
25. Agarwal, G. S. (1970). *Phys. Rev.* **A1,** 1445.
26. Tornau, N. and Bach, A. (1974). *Optics Commun.* **11,** 46.
27. Bandilla, A. (1977). *Optics Commun.* **23,** 299.
28. Krasinski, J. and Dinev, S. (1976). *Optics Commun.* **18,** 424.
29. Mollow, B. R. (1968). *Phys. Rev.* **175,** 1555; (1971). ibid. **A4,** 1666.
30. Bandilla, A. and Ritze, H. H. (1976). *Optics Commun.* **19,** 169.
31. Chaturvedi, S., Drummond, P., and Walls, D. F. (1977). *J. Phys.* **A10,** L187.
32. Voigt, H., Bandilla, A., and Ritze, H. H. (1980). *Z. Physik* **B36,** 295.
33. Walls, D. F. (1973). *J. Phys.* **A6,** 496.
34. Simaan, H. D. (1975). *J. Phys.* **A8,** 1620.
35. Georges, A. T. (1982). *Optics Commun.* **41,** 61.

Index

A coefficient, *see* Einstein *A* coefficient
absorption coefficient 26, 62
  related to *B* coefficient 29
  related to scattering cross-section 295, 318, 325
absorption of photons, *see* Einstein *B* coefficient; photon
adiabatic approximation 267
allowed transition 171–2
atomic
  angular momentum 165
    operator 170
  density matrix
    definition 55
    properties 55, 297
    related to transition operators 208, 285, 329
    solutions with collision broadening 79
    solutions with radiative damping 66–9
    steady-state solutions 64, 71
    three-level atom 327–8
  electric dipole moment 43, 60–2, 165
    second quantization 173, 190
  electric quadrupole moment 165
  energy eigenstates 40
  fluorescence, *see* fluorescent emission; resonance fluorescence
  Hamiltonian 40, 170
    second quantization 172–5, 190
  hydrogen, *see* hydrogen atom
  level degeneracy 14, 16–17, 28, 30
  level population 14, 17
    laser 267–70
    optical excitation 22–4
  magnetic dipole moment 165
  magnetic quadrupole moment 165
  multipole moments 162–6
  orientation 19, 50–1, 61–2
  potential energy 164–5
  rate equation, *see* rate equation
  relaxation times 78
  stored energy 23
  transition
    operator 190, 198, 207–8, 329
    rate, *see* transition rate
    saturation 23, 30, 65, 270, 277
  velocity distribution 73
  wavefunction parity 44, 172, 321, 341
attenuation coefficient, *see* absorption coefficient

B coefficient, *see* Einstein *B* coefficient
Bernoulli distribution 240, 245, 257
black-body radiation 2
Bloch equations, *see* optical Bloch equations
Bohr radius 43
Boltzmann distribution 8, 16, 30
boundary conditions 2–3
Brownian motion 105, 235

cascade emission, *see* two-photon cascade emission
Cauchy's inequality 106
cavity, *see* optical cavity
chaotic light
  amplitude distribution 103–4
  coherence length 90, 97
  coherence time 90, 96–7, 101, 105, 235–6, 256
  density operator 158–60
  electric field 86–7
  first-order coherence 90–2, 97, 217–18
  intensity distribution 103–5
  intensity fluctuations 88–90, 101–5, 112–14, 233
    effect of two-photon absorption 345–7
  interaction with two-level atom 255–63
  laser below threshold 274–5
  long-time average intensity 101–2
  partially polarized 117–19, 248–9
  phase 86–90
    distribution 102–4
    fluctuations 87–90
  photon-count distribution 233–9, 241
  *r*th-order coherence 117, 248
  second-order coherence 107–11, 221, 255–6
  stimulated Raman effect 380–2
  time dependence 85–90
  two-photon absorption 345–7, 364, 371–3, 375–8
charge density 121, 163

- classical electron radius 315
- classical stable wave
  - definition 98
  - first-order coherence 98
  - photon-count distribution 232–3
  - rth-order coherence 117
  - second-order coherence 107, 111
- closure theorem 153, 195, 337
- coherence
  - degree of first-order
    - classical definition 84, 96
    - classical stable wave 98
    - coherent state 216
    - collision-broadened chaotic light 90–2
    - composite chaotic light 100
    - emission by driven atom 284–7
    - Gaussian chaotic light 99–101
    - general properties 85, 92, 96, 216–17
    - Lorentzian chaotic light 97, 217–18
    - multimode coherent state 216
    - number state 216
    - quantum definition 216
    - related to spectral distribution 84–5
    - resonance fluorescence 297–302, 304, 308
    - single-mode chaotic light 99
    - single-mode statistical mixture 216
    - two cavity modes 99, 217
    - two-mode number state 217
  - degree of rth-order
    - chaotic beam 117, 248
    - classical definition 116
    - classical stable wave 117
    - multimode coherent state 248
    - pulsed beam 117
    - quantum definition 247
  - degree of second-order
    - chaotic and coherent superposition 259–60
    - chaotic light 107–11, 221, 253, 255–6
    - classical definition 106, 111
    - classical inequalities 106–7, 332, 369
    - classical stable wave 107, 111
    - coherent state 221, 253
    - double-beam two-photon absorption 338, 364–6, 369, 372–3
    - emission by driven atom 284–8, 329–31
    - Gaussian chaotic light 110
    - general properties 106–8, 219, 329
    - laser 277–8
    - Lorentzian chaotic light 109
    - multimode coherent state 221
    - number state 220
    - partially polarized light 119, 249
    - pulsed beam 107–8, 345
    - quantum definition 219
    - quantum inequalities 219–20, 222
    - related to first-order coherence 109, 221
    - related to photon correlation 223–6
    - related to photon-count distribution 242
    - resonance fluorescence 298, 301–2, 306–11
    - single-beam two-photon absorption 344–7, 364–5, 375–8
    - single-mode chaotic light 111, 221, 309
    - single-mode state 220
    - stimulated Raman effect 381–2
    - time dependence 258–61
    - two-photon cascade emission 329–31
  - degree of third-order, third-harmonic generation 361–2
  - length 90, 97
  - spatial 95, 114–16
  - time 90, 96–7, 101, 105
    - measurement 235–6
- coherent light
  - conditions for 97, 111
  - interaction with two-level atom 259–63
  - laser above threshold 275–8
  - stimulated Raman effect 380–2
  - two-photon absorption 345, 364, 371–3, 375–8
  - *see also* quantized radiation field, coherent state
- coherent state, *see* quantized radiation field, coherent state
- collision broadening 70–2, 85–8, 90–2
- composite lineshape 74–8
- Compton scattering 34, 316
- confluent hypergeometric function 273–5
- continuity equation 124
- correlation function
  - first order
    - classical stable wave 98
    - definition 83, 94
    - evaluation 90–2, 100
    - laser light 282
    - related to first-order coherence 84, 92, 96, 216
  - photon number 223–9
    - stimulated Raman effect 379–81
    - two-photon absorption 369, 372
  - second-order
    - definition 106
    - Lorentzian beam 108–9
    - related to first-order correlation function 109, 308
    - related to second-order coherence 106, 219
    - two-photon cascade emission 329–30
- Coulomb gauge 123–6, 163, 166
- creation operator, *see* harmonic oscillator; photon

- cross-section
  - light scattering 292–5, 311–26
    - related to absorption coefficient 295, 318, 325
  - photoelectric effect 183
  - resonance fluorescence 297
- current density 121, 124–6, 163
- cycle-average theorem 6

- de Broglie relation 33
- degeneracy of atomic levels 14, 16–17, 28, 30
- degree of coherence, *see* coherence
- degree of polarization 117, 249
- density matrix, *see* atomic density matrix
- density of modes in a cavity 2–5
  - numerical estimate 21
- density operator 152–61
  - definition 153
  - general properties 154–5
  - Heisenberg representation 198
  - interaction representation 207
  - multimode chaotic light 158–60
  - multimode pure state 157
  - pure states 155–7
  - Schrödinger representation 189–90
  - single-mode thermal excitation 158
- destruction operator, *see* harmonic oscillator; photon
- dielectric constant 25
- differential cross-section
  - light scattering 293
    - elastic scattering 315–20
    - inelastic scattering 320–5, 356
    - Kramers–Heisenberg formula 314
    - Thomson scattering 315
  - photoelectric effect 183–4
  - resonance fluorescence 297
- diffusion equation 282
- Dirac delta-function
  - definition 52–3
  - homogeneous broadening 342, 356
  - properties 53–4
  - representations 53–4, 201
- Doppler broadening 72–4, 342
- Doppler-free two-photon absorption 342–3
- dynamic Stark effect 57, 305–7

- Einstein
  - A coefficient
    - definition 14–15
    - fluorescent emission 24
    - multilevel atom 317
    - numerical values 52
    - quantized field calculation 178
    - quantum-mechanical expression 51
    - related to B coefficient 16
    - related to radiative lifetime 24, 61
  - B coefficient
    - definition 14–15
    - orientation average 19, 50–1
    - quantum-mechanical expression 51, 177
    - related to A coefficient 16
    - related to absorption coefficient 29
    - related to electric susceptibility 29
- elastic light scattering 290–1
  - hydrogen atom 316, 319–20
  - quantum theory 314–20
  - resonant cross-section 299–301, 316–19
  - Thomson scattering 315
- electric
  - dipole moment of atom 43, 60–2, 165, 205
  - permittivity 5
  - quadrupole moment of atom 165
  - susceptibility, *see* frequency-dependent susceptibility; nonlinear susceptibility;
- electric-dipole approximation 169–72, 180, 311, 335
- electromagnetic field, classical theory
  - Coulomb gauge 123–6, 166
  - energy 5–6, 128
  - energy density 10–11
  - field equations 122–4
  - gauge transformation 122
  - harmonic oscillator coordinates 128
  - in dielectric 24–6
  - interaction with atom
    - Hamiltonian 166–9
    - multipole expansion 169–72
  - longitudinal part 124–6
  - Maxwell's equations 3, 6, 121, 126
  - mode 3
  - neglect of thermal excitation 17–18
  - potential theory 121–6
  - transition to quantum theory 135
  - transverse part 124–6
- electromagnetic wave
  - absorption coefficient 26, 29, 62
  - classical harmonic oscillator coordinates 128
  - classical stable wave 98
  - energy density 10–11
    - related to intensity 28
  - equation 3, 126
  - extinction coefficient 25
  - in dielectric 24–6
  - intensity 25
    - numerical estimate 21
    - related to energy density 28
  - Poynting vector 25, 292–3
  - refractive index 25, 350–1
  - relation between electric and magnetic vectors 6, 25

- electromagnetic wave *cont'd*
  - vector potential 126–8
  - *see also* quantized radiation field
- emission of photons, *see* Einstein; photon
- ensemble
  - average 11, 153, 216, 219
    - related to time average 11–12, 84, 102, 234
  - chaotic light beams 105
  - definition 11
- ergodic theorem 11–12, 84, 102, 234, 279
- extinction coefficient 25

- Fabry–Perot spectroscopy 228
- Fermi's golden rule 178
- fine-structure constant 171
- first-order
  - coherence, *see* coherence, degree of first-order
  - correlation function, *see* correlation function, first order
- fluorescent emission 24, 61, 291
  - lifetime 24
  - *see also* resonance fluorescence
- forbidden transition 171–2
- frequency-dependent susceptibility
  - definition 24, 59
  - inclusion of collision broadening 71
  - inclusion of power broadening 65
  - inclusion of spontaneous emission 60–1
  - related to B coefficient 29
  - semiclassical theory 59–63, 65
  - *see also* nonlinear susceptibility

- gauge transformation 122
- Gaussian
  - light 104
  - lineshape 73–4

- Hanbury Brown and Twiss experiment
  - classical treatment 111–16
  - quantum treatment 222–6
  - scatter of readings 247
- harmonic oscillator
  - creation operator 129, 133
  - destruction operator 129, 133
  - energy 6–7, 132
  - ground-state condition 131
  - normalization 132
  - number operator 129
  - quantum mechanics 129–33
- Heisenberg representation 188, 197–9
- Helmholtz theorem 124
- Hermitian operator 133
- homogeneous line broadening 77–8
- hydrogen atom
  - Bohr radius 43
  - elastic light scattering 316, 319–20
  - inelastic light scattering 323–5
  - matrix element for 1S–2P transition 44
  - photoelectric effect 179–84
  - radiative frequency shift
    - $1^2S_{1/2}$ state 344
    - $2^2S_{1/2}$ state 202, 343
  - radiative lifetime of 2P state 51
  - spontaneous emission rates 52
  - two-photon absorption 341–4
  - wavefunctions
    - 1S state 44
    - 2S state 324
    - 2P state 44

- induced emission, *see* Einstein *B* coefficient; photon
- inelastic light scattering 290–1
  - Compton scattering 34, 316
  - hydrogen atom 323–5
  - quantum theory 320–6
  - resonant cross-section 321–2
- inhomogeneous line broadening 76–7
- integration related to summation
  - one dimension 218
  - three dimensions 5, 138, 182, 314
- intensity-fluctuation spectroscopy 116, 228
- intensity interference, *see* Hanbury Brown and Twiss experiment
- interaction Hamiltonian
  - diagrammatic representation 174–5
  - electric-dipole 42–4, 59, 170–2, 311–14, 335
  - electric-quadrupole 170–2
  - Heisenberg representation 198
  - interaction representation 208
  - magnetic dipole 170–2
  - minimal-coupling form 166–7
  - multipolar form 166–9
  - multipole expansion 170–2
  - nonlinear 171, 311–14, 335
  - parity 43
  - perturbation theory 193–7
  - rotating-wave approximation 175, 190, 198
  - Schrödinger representation 188–91
  - second quantization 174–5, 190–1
  - unitary transformation 167–9
- interaction representation 188, 206–9
- interference
  - fringe visibility 95
  - Hanbury Brown and Twiss experiment 111–16, 222–6
  - independent light beams 215

  - Michelson experiment 242–7
  - Young's experiment 92–6, 211–15
- intermediate state 196
- isotope separation 37

- Kramers–Heisenberg formula 311–14

- Lamb shift, *see* radiative frequency shift
- laser
  - adiabatic approximation 267
  - atomic rate equations 267–70
  - cavity loss rate 265–6, 281
  - comparison with coherent light 280
  - condition for inversion 31–2, 264
  - electric-field fluctuation 278–83
  - gain coefficient 32
  - mean photon number 273–7
  - numerical values of parameters 266, 269
  - phase diffusion 282–3
  - photon
    - count distribution 277–8
    - probability distribution 273–8
    - rate equations 271–3
  - pumping rate 31, 264–6
  - saturation effects 32–3, 270, 277
  - second-order coherence 277–8
  - three-level theory 30–3, 263–70
  - threshold condition 263–6
- light
  - amplification 32–3, 261–3
    - *see also* laser
  - scattering, *see* scattering of light
  - source
    - chaotic 82
    - numerical data 21
    - stationary 84
  - velocity 3, 5
  - wavevector 3
- lineshape function 26–7
  - composite 74–8
  - Gaussian form 73–4
  - homogeneous 77–8
  - inhomogeneous 76–7
  - Lorentzian form 62–3, 71, 73–4
  - related to first-order coherence 84
  - Voigt 76–7
- linewidth of spectral line
  - collision 71–2, 92
  - Doppler 74
  - Gaussian case 73–4
  - Lorentzian case 62–3, 71
  - natural 63
  - numerical estimate 21, 62–3, 72
  - power 65
  - radiative 59–63
- longitudinal part of vector field 138–9, 164
- longitudinal relaxation time 78
- Lorentzian lineshape 62–3, 71, 304–5

- magnetic permeability 5
- magnetization 163
- mass renormalization 202
- Maxwell
  - equations 3, 6, 121, 126
  - velocity distribution 73
- Michelson interferometer 242–7
- mode of radiation field 3
  - density of states 2–5
  - polarization 3
  - wavevector 3

- negative temperature condition 30
- nonclassical light 220, 228–9, 332, 369, 382
  - *see also* photon antibunching
- nonlinear susceptibility
  - definition 347
  - frequency components 348–9
  - intensity-dependent refractive index 350–1
  - numerical estimate 348
  - self-focusing 351
  - third-harmonic generation 363
  - two-photon absorption 349–51
- normal ordering 187, 203, 205
  - operator 238
- number state, *see* quantized radiation field
- nutation 66–8

- optical
  - Bloch equations 39
    - comparison with rate equations 78–81
    - derivation 54–6, 208–9
    - inclusion of collision broadening 71, 78, 296
    - inclusion of spontaneous emission 64, 303
    - rotating-wave approximation 55–6
  - cavity 2
    - density of modes 2–5
    - loss rate 265–6, 281
    - quality factor 266
  - coherence, *see* coherence
  - excitation of atoms 22–4
  - nutation 66–8
  - theorem 295, 318, 325
- orientation average 19, 50–1, 61–2, 318

- parity
  - interaction Hamiltonian 43, 172
  - wavefunction 44, 172, 321, 341
- partial coherence 96
- partially-polarized chaotic light
  - degree of polarization 117, 249
  - degree of second-order coherence 119, 249

partially-polarized chaotic light *cont'd*
  intensity distribution 118
  photon probability distribution 249
particle fluctuations 233
phase
  diffusion 282–3
  matching 362
photoelectric effect 1, 179–86
photon
  absorption 14–15
    influence of atomic saturation 29–30
    macroscopic theory 24–6
    microscopic theory 26–30
    momentum properties 34
    photoelectric effect 179–84
    transition rate 45–50, 175–6, 252
  antibunching 228–9
    resonance fluorescence 288, 302, 308–11
    two-photon absorption 364–5, 376–8
    two-photon cascade emission 330
    see also nonclassical light
  bunching 226–8, 364, 377
  coherence, *see* coherence
  correlation 223–9, 369, 372, 379–81
  creation operator 134, 199, 207
    mode superposition 213, 243–4
  destruction operator 134, 199, 207
    mode superposition 213, 243–4
  energy density 10–11
  energy-level diagram 7–8, 254, 271, 367, 374, 379
  intensity operator 184–7, 238
  interference experiments
    Hanbury Brown and Twiss 222–6
    independent sources 215
    Michelson 242–7
    Young 211–15
  mean-square number
    chaotic light 13
    coherent light 148
    thermal equilibrium 13
    time dependence 258
  momentum 33–7, 72
    see also radiation pressure
  name 1
  neglect of thermal excitation 17–18
  number
    fluctuations 11–13
    laser 273–7
    numerical estimate 21
    operator 134
    stimulated Raman effect 379–81
    thermal equilibrium 9
    time dependence 257–63, 370–3, 376–7, 379–81
    two-photon absorption 369–72, 375–7
  number–phase uncertainty relations 144, 150
  phase operators 141–4
  polarization vectors 137, 203
  probability distribution
    chaotic light 8–13, 241, 253
    coherent state 149, 241, 253
    divided beam 215, 222
    factorial moment 13
    interaction with two-level atom 255, 257
    laser 273–8
    partially-polarized chaotic light 249
    pulsed beam 371
    related to photon-count distribution 240–2
    second moment 13, 148, 258
    stimulated Raman effect 378–80
    thermal equilibrium 8–13
    two-photon absorption 366–70, 373–6
  rate-equations
    interaction with two-level atom 251–63
    laser 271–3
    steady-state solutions 255–6
    stimulated Raman effect 379
    two-photon absorption 368, 374
  scattering, *see* scattering of light; stimulated Raman effect
  spontaneous emission 14–15, 178–9
    compared with stimulated emission 16–17, 19–20
    directional properties 19–20
    effect on laser light 279–83
    Heisenberg representation calculation 199–201
    linewidth 61–3
    momentum properties 34
    radiative damping 59–63
    related to scattering of light 20
  statistics and nonlinear optics 363–6
  stimulated emission 14–15, 177
    by thermal photons 16–17
    directional properties 19–20, 178
    effect on laser light 279
    momentum properties 34
  two-photon absorption
    double beam 335–44, 349–50, 364–73
    single beam 344–7, 351, 364–5
  two-photon cascade emission 326–32
photon counting
  distribution 229–32, 238–42
    chaotic light 233–8, 241
    coherent light 232–3, 239, 241
    laser 277–8
    Michelson interferometer 242–7
    related to photon distribution 240–2

  experiments 13, 229, 235–6, 277
  particle fluctuations 233
  wave fluctuations 236
phototube 179, 185, 229
Planck
  constant 1
  distribution 9–10, 12
  quantization hypothesis 6
  radiation law 2, 8–11, 16
Poisson
  distribution 149, 232–3, 239, 294, 309
  equation 123
polarization 24
  nonlinear 347–51
  quantum-mechanical treatment 59–62
population
  atomic level, *see* atomic level population
  inversion 30, 261–3
power broadening 63–5
Poynting vector 25, 185, 292–3
pressure broadening, *see* collision broadening
principal value 201
probability distribution, *see* chaotic light; photon probability distribution
pulsed light beam
  photon distribution 371
  *r*th-order coherence 117
  second-order coherence 107–8, 345
  two-photon absorption 345, 365, 371–3
pump 31
pumping rate 31, 264–6
pure state 152

quantized radiation field
  coherent state
    comparison with classical stable wave 209, 218, 221, 248
    definition 146
    density operator 156–7
    electric-field expectation value 150–2, 156–7
    first-order coherence 216
    interaction with two-level atom 259–63
    number uncertainty 148
    overlap 147
    phase uncertainty 149–50
    photon-count distribution 241
    second-order coherence 220–1
    stimulated Raman effect 380–2
    two-photon absorption 371–3, 375–8
  creation operator 134, 199, 207
  destruction operator 134, 199, 207
  electric field operator 135, 141, 169, 181, 186
    source-field expression 202–6
    superposition 212, 243
  energy 136
  field commutation properties 137–9
  Hamiltonian 136–7, 170
  intensity 184–7, 212, 238
  magnetic field operator 135
  multimode coherent state 157
    density operator 157
    electric-field eigenvalue 186
    first-order coherence 216
    intensity expectation value 186
    photon-count distribution 239
    *r*th-order coherence 248
    second-order coherence 221
  multimode number state 134
    density operator 157
  number operator 134
  number state
    density operator 155
    electric-field expectation value 145–6
    first-order coherence 216–17
    phase properties 144–5
    second-order coherence 220
    stimulated Raman effect 380, 382
    two-photon absorption 371–3
  Planck's hypothesis 6–7
  Poynting vector 185
  transition from classical theory 135
  vector potential operator 135
  zero-point energy 7–9, 139–41, 187
quantum efficiency 239
quantum regression theorem 286, 329

Rabi
  frequency 58, 66–7, 296, 304–6
  oscillations 56–9, 78
    radiative damping 65–9
radiation
  field, *see* electromagnetic field; quantized radiation field
  pressure 33–7
    force 35
    isotope separation 37
    saturation effects 35, 37
radiative
  broadening 59–63, 317
  damping 59–63, 317, 320
  frequency shift
    Lamb and Retherford experiment 202
    quantized field calculation 201–2
    two-photon absorption 343–4
  lifetime
    hydrogen atom 51–2
    quantized field calculation 178–9
    related to *A* coefficient 24
  linewidth
    multilevel atom 317
    partial contributions 317
  transition rate, *see* transition rate

Raman scattering 291
  see also inelastic light scattering; stimulated Raman effect
random-walk theory 103, 105, 281
rate equation
  atoms in laser 267–70
  comparison with optical Bloch equations 78–81
  photon 251–63, 271–3
  three-level atom 30–1, 327
  two-level atom 15, 18, 22–4, 80, 287
Rayleigh
  radiation law 10
  scattering 290–1
    see also elastic light scattering
rectangular pulse beam, *see* pulsed light beam
refractive index 25
  intensity-dependent 350–1
relaxation times 78
representation 187–8
  Heisenberg 188, 197–9
  interaction 188, 206–9
  Schrödinger 187–91
resonance fluorescence 291
  cross-section 297
  emitted light
    coherent fraction 297–9, 303
    first-order coherence 297–302, 304, 308
    photon antibunching 288, 302, 308–11
    second-order coherence 298, 301–2, 306–11
    spectrum 298–300, 304–6, 326
  exactly-resonant incident beam 303–8
  experiments 305, 310–11
  general method of calculation 284–7, 295–9
  multiatom effects 308–11
  rate-equation treatment 287–8
  two-level atom theory 295–311
  weak incident beam 299–303
response time of detector 113–14, 225
retarded time 125, 205
rotating-wave approximation 47, 55–6, 175, 190, 198

saturation
  broadening 63–5
  influence on absorption 30
  influence on radiation pressure 35, 37
  laser 32–3, 270, 277
  stimulated Raman effect 354–5
  two-level atom 23, 65
scalar potential 121–5
  gauge transformation 122
scattering of light
  by distribution of atoms 293

GOA UNIVERSITY LIBRARY
TALEIGAO - GOA

  cross-section 292–5
  diagrammatic representation 312–13
  Kramers–Heisenberg formula 314
  optical theorem 295, 318, 325
  quantum theory 311–26
  source of absorption coefficient 20, 26, 295
  see also elastic light scattering; inelastic light scattering; stimulated Raman effect
Schrödinger representation 187–91
second-order
  coherence, *see* coherence
  correlation function, *see* correlation function
  phase transition 283–4
second quantization of atomic Hamiltonian 172–5
secondary waves 93
selection rule
  absorption and emission 172
  inelastic light scattering 321
  nonlinear processes 363
  two-photon absorption 341
self-focusing 351
source-field expression 202–6
spatial coherence 95, 114–16
spontaneous
  emission, *see* Einstein *A* coefficient; photon
  parametric splitting 369
stationary
  light source 84
  state 40
statistical mixture 152
Stefan–Boltzmann radiation law 11
stimulated emission, *see* Einstein *B* coefficient; photon
stimulated Raman effect 351–7, 378–82
  gain coefficient 354
    numerical estimate 356–7
    related to differential cross-section 356
  photon-number time dependence 379–81
  photon rate equation 379
  photon statistics 378–82
  second-order coherence 381–2
  spatial growth of intensity 353–5
summation related to integration
  one dimension 218
  three dimensions 5, 138, 182, 314
super-chaotic light 382
susceptibility, *see* frequency-dependent susceptibility; nonlinear susceptibility

temporal coherence, *see* coherence
thermal equilibrium
  mode excitation probability 8–9
  photon distribution 9–13
  photon emission 16–17

third-harmonic generation 357–63
  dependence on third-order coherence 361–2, 364
  diagrammatic representation 358
  nonlinear susceptibility 363
  phase-matching condition 362
  spatial dependence of intensity 360–2
Thomson scattering 315
three-level laser, *see* laser
time average, related to ensemble average 11–12, 84
time-dependent
  perturbation theory 45–50, 193–7
  wave equation 40
  wavefunction 40, 60
    boundary conditions 45
    linear superposition state 41
    normalization 41, 45, 61
time-development operator 189
time-domain spectroscopy 116, 228
transition operator 190, 198, 207–8
transition rate
  absorption 45–50, 175–6
  emission 177–9
  Fermi's golden rule 178, 191, 194
  general expression 191–7
  light scattering 311–14
  oscillatory applied field 45–50, 54
  photoelectric effect 182–3
  rotating-wave approximation 47
  static applied field 45
  stimulated Raman effect 352
  third-harmonic generation 358
  two-photon absorption 336–7, 344
transverse part of vector field 138–9, 164
transverse relaxation time 78
two-photon absorption
  double-beam
    absorption coefficient 339, 350
    diagrammatic representation 336
    Doppler broadening 342–3
    hydrogen 1S–2S transition 341–4
    nonlinear susceptibility 349–50
    photon-number time dependence 370–2
    photon rate equations 368
    photon statistics 366–73
    pulsed beam 365
    second-order coherence 338, 364–6, 372–3
    spatial dependence of intensity 338–41
  single-beam
    effect on intensity fluctuations 345–7
    nonlinear susceptibility 351
    photon-number time dependence 376–7
    photon rate equations 374
    photon statistics 373–8
    second-order coherence 344–7, 364–5, 375–8
    spatial dependence of intensity 344–5
two-photon cascade emission 326–32
  nonclassical effects 330–2

uncertainty relation
  frequency-time 78
  photon number and phase 144–5, 150

van der Waals forces 141
vector potential
  classical radiation field 121–8
  Fourier coefficients 127–8
  gauge transformation 122
  operator 135
virtual intermediate state 196
visibility of interference fringes 95
Voigt lineshape 76–7

wave fluctuations 236
Wien
  displacement law 11
  formula 10
Wiener–Khintchine theorem 84–5

Young's interference experiment
  classical treatment 92–96
  quantum treatment 211–15

zero-point energy 7–9, 139–41, 187